

Shigley's

Mechanical Engineering Design

Ninth Edition¹³



Richard G. Budynas and J. Keith Nisbett

| Conversion Factors A to Convert Input X to Output Y Using the Formula $Y = AX^*$

Multiply Input X	By Factor A	To Get Output Y	Multiply Input X	By Factor A	To Get Output Y
British thermal unit, Btu	1055	joule, J	mile/hour, mi/h	1.61	kilometer/hour, km/h
Btu/second, Btu/s	1.05	kilowatt, kW	mile/hour, mi/h	0.447	meter/second, m/s
calorie	4.19	joule, J	moment of inertia, lbm · ft ²	0.0421	kilogram-meter ² , kg · m ²
centimeter of mercury (0°C)	1.333	kilopascal, kPa	moment of inertia, lbm · in ²	293	kilogram-millimeter ² , kg · mm ²
centipoise, cP	0.001	pascal-second, Pa · s	moment of section (second moment of area), in ⁴	41.6	centimeter ⁴ , cm ⁴
degree (angle)	0.0174	radian, rad	ounce-force, oz	0.278	newton, N
foot, ft	0.305	meter, m	ounce-mass	0.0311	kilogram, kg
foot ² , ft ²	0.0929	meter ² , m ²	pound, lbf [†]	4.45	newton, N
foot/minute, ft/min	0.0051	meter/second, m/s	pound-foot, lbf · ft	1.36	newton-meter, N · m
foot-pound, ft · lbf	1.35	joule, J	pound/foot ² , lbf/ft ²	47.9	pascal, Pa
foot-pound/ second, ft · lbf/s	1.35	watt, W	pound-inch, lbf · in	0.113	joule, J
foot/second, ft/s	0.305	meter/second, m/s	pound-inch, lbf · in	0.113	newton-meter, N · m
gallon (U.S.), gal	3.785	liter, L			
horsepower, hp	0.746	kilowatt, kW	pound/inch, lbf/in	175	newton/meter, N/m
inch, in	0.0254	meter, m	pound/inch ² , psi (lbf/in ²)	6.89	kilopascal, kPa
inch, in	25.4	millimeter, mm	pound-mass, lbm	0.454	kilogram, kg
inch ² , in ²	645	millimeter ² , mm ²	pound-mass/ second, lbm/s	0.454	kilogram/second, kg/s
inch of mercury (32°F)	3.386	kilopascal, kPa	quart (U.S. liquid), qt	946	milliliter, mL
kilopound, kip	4.45	kilonewton, kN	section modulus, in ³	16.4	centimeter ³ , cm ³
kilopound/inch ² , kpsi (ksi)	6.89	megapascal, MPa (N/mm ²)	slug	14.6	kilogram, kg
mass, lbf · s ² /in	175	kilogram, kg	ton (short 2000 lbm)	907	kilogram, kg
mile, mi	1.610	kilometer, km	yard, yd	0.914	meter, m

*Approximate.

†The U.S. Customary system unit of the pound-force is often abbreviated as lbf to distinguish it from the pound-mass, which is abbreviated as lbm.

| Physical Constants of Materials

Material	Modulus of Elasticity E		Modulus of Rigidity G		Poisson's Ratio ν	Unit Weight w		
	Mpsi	GPa	Mpsi	GPa				
Aluminum (all alloys)	10.4	71.7	3.9	26.9	0.333	0.098	169	26.6
Beryllium copper	18.0	124.0	7.0	48.3	0.285	0.297	513	80.6
Brass	15.4	106.0	5.82	40.1	0.324	0.309	534	83.8
Carbon steel	30.0	207.0	11.5	79.3	0.292	0.282	487	76.5
Cast iron (gray)	14.5	100.0	6.0	41.4	0.211	0.260	450	70.6
Copper	17.2	119.0	6.49	44.7	0.326	0.322	556	87.3
Douglas fir	1.6	11.0	0.6	4.1	0.33	0.016	28	4.3
Glass	6.7	46.2	2.7	18.6	0.245	0.094	162	25.4
Inconel	31.0	214.0	11.0	75.8	0.290	0.307	530	83.3
Lead	5.3	36.5	1.9	13.1	0.425	0.411	710	111.5
Magnesium	6.5	44.8	2.4	16.5	0.350	0.065	112	17.6
Molybdenum	48.0	331.0	17.0	117.0	0.307	0.368	636	100.0
Monel metal	26.0	179.0	9.5	65.5	0.320	0.319	551	86.6
Nickel silver	18.5	127.0	7.0	48.3	0.322	0.316	546	85.8
Nickel steel	30.0	207.0	11.5	79.3	0.291	0.280	484	76.0
Phosphor bronze	16.1	111.0	6.0	41.4	0.349	0.295	510	80.1
Stainless steel (18-8)	27.6	190.0	10.6	73.1	0.305	0.280	484	76.0
Titanium alloys	16.5	114.0	6.2	42.4	0.340	0.160	276	43.4

Shigley's Mechanical Engineering Design

McGRAW-HILL SERIES IN MECHANICAL ENGINEERING

Alciatore/Histand:	<i>Introduction to Mechatronics and Measurement Systems</i>
Anderson:	<i>Computational Fluid Dynamics: The Basics with Applications</i>
Anderson:	<i>Fundamentals of Aerodynamics</i>
Anderson:	<i>Introduction to Flight</i>
Anderson:	<i>Modern Compressible Flow</i>
Barber:	<i>Intermediate Mechanics of Materials</i>
Beer/Johnston:	<i>Vector Mechanics for Engineers: Statics and Dynamics</i>
Beer/Johnston:	<i>Mechanics of Materials</i>
Budynas:	<i>Advanced Strength and Applied Stress Analysis</i>
Budynas/Nisbett:	<i>Shigley's Mechanical Engineering Design</i>
Byers/Dorf:	<i>Technology Ventures: From Idea to Enterprise</i>
Çengel:	<i>Heat and Mass Transfer: A Practical Approach</i>
Çengel:	<i>Introduction to Thermodynamics & Heat Transfer</i>
Çengel/Boles:	<i>Thermodynamics: An Engineering Approach</i>
Çengel/Cimbala:	<i>Fluid Mechanics: Fundamentals and Applications</i>
Çengel/Turner:	<i>Fundamentals of Thermal-Fluid Sciences</i>
Crespo da Silva:	<i>Intermediate Dynamics</i>
Dieter:	<i>Engineering Design: A Materials & Processing Approach</i>
Dieter:	<i>Mechanical Metallurgy</i>
Doebelin:	<i>Measurement Systems: Application & Design</i>
Dunn:	<i>Measurement & Data Analysis for Engineering & Science</i>
EDS, Inc.:	<i>I-DEAS Student Guide</i>
Finnemore/Franzini:	<i>Fluid Mechanics with Engineering Applications</i>
Hamrock/Schmid/Jacobson:	<i>Fundamentals of Machine Elements</i>
Heywood:	<i>Internal Combustion Engine Fundamentals</i>
Holman:	<i>Experimental Methods for Engineers</i>
Holman:	<i>Heat Transfer</i>
Hutton:	<i>Fundamentals of Finite Element Analysis</i>
Kays/Crawford/Weigand:	<i>Convective Heat and Mass Transfer</i>
Meirovitch:	<i>Fundamentals of Vibrations</i>
Norton:	<i>Design of Machinery</i>
Palm:	<i>System Dynamics</i>
Reddy:	<i>An Introduction to Finite Element Method</i>
Schaffer et al.:	<i>The Science and Design of Engineering Materials</i>
Schey:	<i>Introduction to Manufacturing Processes</i>
Smith/Hashemi:	<i>Foundations of Materials Science and Engineering</i>
Turns:	<i>An Introduction to Combustion: Concepts and Applications</i>
Ugural:	<i>Mechanical Design: An Integrated Approach</i>
Ullman:	<i>The Mechanical Design Process</i>
White:	<i>Fluid Mechanics</i>
White:	<i>Viscous Fluid Flow</i>
Zeid:	<i>CAD/CAM Theory and Practice</i>
Zeid:	<i>Mastering CAD/CAM</i>

Shigley's Mechanical Engineering Design

Ninth Edition

Richard G. Budynas

Professor Emeritus, Kate Gleason College of Engineering, Rochester Institute of Technology

J. Keith Nisbett

Associate Professor of Mechanical Engineering, Missouri University of Science and Technology





SHIGLEY'S MECHANICAL ENGINEERING DESIGN, NINTH EDITION

Published by McGraw-Hill, a business unit of The McGraw-Hill Companies, Inc., 1221 Avenue of the Americas, New York, NY 10020. Copyright © 2011 by The McGraw-Hill Companies, Inc. All rights reserved. Previous edition © 2008. No part of this publication may be reproduced or distributed in any form or by any means, or stored in a database or retrieval system, without the prior written consent of The McGraw-Hill Companies, Inc., including, but not limited to, in any network or other electronic storage or transmission, or broadcast for distance learning.

Some ancillaries, including electronic and print components, may not be available to customers outside the United States.

This book is printed on acid-free paper.

1 2 3 4 5 6 7 8 9 0 RJE/RJE 10 9 8 7 6 5 4 3 2 1 0

ISBN 978-0-07-352928-8

MHID 0-07-352928-1

Vice President & Editor-in-Chief: *Marty Lange*

Vice President, EDP/Central Publishing Services: *Kimberly Meriwether-David*

Global Publisher: *Raghothaman Srinivasan*

Senior Sponsoring Editor: *Bill Stenquist*

Director of Development: *Kristine Tibbets*

Developmental Editor: *Lora Neyens*

Senior Marketing Manager: *Curt Reynolds*

Project Manager: *Melissa Leick*

Senior Production Supervisor: *Kara Kudronowicz*

Design Coordinator: *Margarite Reynolds*

Cover Designer: *J. Adam Nisbett*

Senior Photo Research Coordinator: *John C. Leland*

Compositor: *Aptara®, Inc.*

Typeface: *10/12 Times Roman*

Printer: *R. R. Donnelley*

All credits appearing on page or at the end of the book are considered to be an extension of the copyright page.

Library of Congress Cataloging-in-Publication Data

Budynas, Richard G. (Richard Gordon)

Shigley's mechanical engineering design / Richard G. Budynas, J. Keith Nisbett. —9th ed.

p. cm. — (McGraw-Hill series in mechanical engineering)

Includes bibliographical references and index.

ISBN 978-0-07-352928-8 (alk. paper)

1. Machine design. I. Nisbett, J. Keith. II. Title. III. Series.

TJ230.S5 2011

621.8'15—dc22

2009049802

Dedication

**To my wife Joanne, my children and grandchildren, and
to good friends, especially Sally and Peter.**

Richard G. Budynas

**To Professor T. J. Lawley, who first introduced me to
Shigley's text, and who instigated in me a fascination
for the details of machine design.**

J. Keith Nisbett

Dedication to Joseph Edward Shigley

Joseph Edward Shigley (1909–1994) is undoubtedly one of the most known and respected contributors in machine design education. He authored or co-authored eight books, including *Theory of Machines and Mechanisms* (with John J. Uicker, Jr.), and *Applied Mechanics of Materials*. He was Coeditor-in-Chief of the well-known *Standard Handbook of Machine Design*. He began *Machine Design* as sole author in 1956, and it evolved into *Mechanical Engineering Design*, setting the model for such textbooks. He contributed to the first five editions of this text, along with co-authors Larry Mitchell and Charles Mischke. Uncounted numbers of students across the world got their first taste of machine design with Shigley's textbook, which has literally become a classic. Practically every mechanical engineer for the past half century has referenced terminology, equations, or procedures as being from "Shigley." McGraw-Hill is honored to have worked with Professor Shigley for over 40 years, and as a tribute to his lasting contribution to this textbook, its title officially reflects what many have already come to call it—*Shigley's Mechanical Engineering Design*.

Having received a Bachelor's Degree in Electrical and Mechanical Engineering from Purdue University and a Master of Science in Engineering Mechanics from The University of Michigan, Professor Shigley pursued an academic career at Clemson College from 1936 through 1954. This lead to his position as Professor and Head of Mechanical Design and Drawing at Clemson College. He joined the faculty of the Department of Mechanical Engineering of The University of Michigan in 1956, where he remained for 22 years until his retirement in 1978.

Professor Shigley was granted the rank of Fellow of the American Society of Mechanical Engineers in 1968. He received the ASME Mechanisms Committee Award in 1974, the Worcester Reed Warner Medal for outstanding contribution to the permanent literature of engineering in 1977, and the ASME Machine Design Award in 1985.

Joseph Edward Shigley indeed made a difference. His legacy shall continue.

About the Authors

Richard G. Budynas is Professor Emeritus of the Kate Gleason College of Engineering at Rochester Institute of Technology. He has over 40 years experience in teaching and practicing mechanical engineering design. He is the author of a McGraw-Hill textbook, *Advanced Strength and Applied Stress Analysis*, Second Edition; and co-author of a McGraw-Hill reference book, *Roark's Formulas for Stress and Strain*, Seventh Edition. He was awarded the BME of Union College, MSME of the University of Rochester, and the Ph.D. of the University of Massachusetts. He is a licensed Professional Engineer in the state of New York.

J. Keith Nisbett is an Associate Professor and Associate Chair of Mechanical Engineering at the Missouri University of Science and Technology. He has over 25 years of experience with using and teaching from this classic textbook. As demonstrated by a steady stream of teaching awards, including the Governor's Award for Teaching Excellence, he is devoted to finding ways of communicating concepts to the students. He was awarded the BS, MS, and Ph.D. of the University of Texas at Arlington.

Brief Contents

Preface xv

Part 1 Basics 2

- 1 Introduction to Mechanical Engineering Design 3**
- 2 Materials 31**
- 3 Load and Stress Analysis 71**
- 4 Deflection and Stiffness 147**

Part 2 Failure Prevention 212

- 5 Failures Resulting from Static Loading 213**
- 6 Fatigue Failure Resulting from Variable Loading 265**

Part 3 Design of Mechanical Elements 358

- 7 Shafts and Shaft Components 359**
- 8 Screws, Fasteners, and the Design of Nonpermanent Joints 409**
- 9 Welding, Bonding, and the Design of Permanent Joints 475**
- 10 Mechanical Springs 517**
- 11 Rolling-Contact Bearings 569**
- 12 Lubrication and Journal Bearings 617**
- 13 Gears—General 673**
- 14 Spur and Helical Gears 733**
- 15 Bevel and Worm Gears 785**
- 16 Clutches, Brakes, Couplings, and Flywheels 825**
- 17 Flexible Mechanical Elements 879**
- 18 Power Transmission Case Study 933**

Part 4 Analysis Tools 952**19 Finite-Element Analysis 953****20 Statistical Considerations 977****Appendices****A Useful Tables 1003****B Answers to Selected Problems 1059***Index* 1065

Contents

<i>Preface</i>	xv
Part 1 Basics	2
1 Introduction to Mechanical Engineering Design	3
1-1	Design 4
1-2	Mechanical Engineering Design 5
1-3	Phases and Interactions of the Design Process 5
1-4	Design Tools and Resources 8
1-5	The Design Engineer's Professional Responsibilities 10
1-6	Standards and Codes 12
1-7	Economics 12
1-8	Safety and Product Liability 15
1-9	Stress and Strength 15
1-10	Uncertainty 16
1-11	Design Factor and Factor of Safety 17
1-12	Reliability 18
1-13	Dimensions and Tolerances 19
1-14	Units 21
1-15	Calculations and Significant Figures 22
1-16	Design Topic Interdependencies 23
1-17	Power Transmission Case Study Specifications 24
	Problems 26
2 Materials	31
2-1	Material Strength and Stiffness 32
2-2	The Statistical Significance of Material Properties 36
2-3	Strength and Cold Work 38
2-4	Hardness 41
2-5	Impact Properties 42
2-6	Temperature Effects 43
2-7	Numbering Systems 45
2-8	Sand Casting 46
2-9	Shell Molding 47
2-10	Investment Casting 47
2-11	Powder-Metallurgy Process 47
2-12	Hot-Working Processes 47
2-13	Cold-Working Processes 48
2-14	The Heat Treatment of Steel 49
2-15	Alloy Steels 52
2-16	Corrosion-Resistant Steels 53
2-17	Casting Materials 54
2-18	Nonferrous Metals 55
2-19	Plastics 58
2-20	Composite Materials 60
2-21	Materials Selection 61
	Problems 67
3 Load and Stress Analysis	71
3-1	Equilibrium and Free-Body Diagrams 72
3-2	Shear Force and Bending Moments in Beams 77
3-3	Singularity Functions 79
3-4	Stress 79
3-5	Cartesian Stress Components 79
3-6	Mohr's Circle for Plane Stress 80
3-7	General Three-Dimensional Stress 86
3-8	Elastic Strain 87
3-9	Uniformly Distributed Stresses 88
3-10	Normal Stresses for Beams in Bending 89
3-11	Shear Stresses for Beams in Bending 94
3-12	Torsion 101
3-13	Stress Concentration 110
3-14	Stresses in Pressurized Cylinders 113
3-15	Stresses in Rotating Rings 115

3-16	Press and Shrink Fits 116	5-6	Coulomb-Mohr Theory for Ductile Materials 228
3-17	Temperature Effects 117	5-7	Failure of Ductile Materials Summary 231
3-18	Curved Beams in Bending 118	5-8	Maximum-Normal-Stress Theory for Brittle Materials 235
3-19	Contact Stresses 122	5-9	Modifications of the Mohr Theory for Brittle Materials 235
3-20	Summary 126	5-10	Failure of Brittle Materials Summary 238
	Problems 127	5-11	Selection of Failure Criteria 238
4	Deflection and Stiffness 147	5-12	Introduction to Fracture Mechanics 239
4-1	Spring Rates 148	5-13	Stochastic Analysis 248
4-2	Tension, Compression, and Torsion 149	5-14	Important Design Equations 254
4-3	Deflection Due to Bending 150		Problems 256
4-4	Beam Deflection Methods 152	6	Fatigue Failure Resulting from Variable Loading 265
4-5	Beam Deflections by Superposition 153	6-1	Introduction to Fatigue in Metals 266
4-6	Beam Deflections by Singularity Functions 156	6-2	Approach to Fatigue Failure in Analysis and Design 272
4-7	Strain Energy 162	6-3	Fatigue-Life Methods 273
4-8	Castigliano's Theorem 164	6-4	The Stress-Life Method 273
4-9	Deflection of Curved Members 169	6-5	The Strain-Life Method 276
4-10	Statically Indeterminate Problems 175	6-6	The Linear-Elastic Fracture Mechanics Method 278
4-11	Compression Members—General 181	6-7	The Endurance Limit 282
4-12	Long Columns with Central Loading 181	6-8	Fatigue Strength 283
4-13	Intermediate-Length Columns with Central Loading 184	6-9	Endurance Limit Modifying Factors 286
4-14	Columns with Eccentric Loading 184	6-10	Stress Concentration and Notch Sensitivity 295
4-15	Struts or Short Compression Members 188	6-11	Characterizing Fluctuating Stresses 300
4-16	Elastic Stability 190	6-12	Fatigue Failure Criteria for Fluctuating Stress 303
4-17	Shock and Impact 191	6-13	Torsional Fatigue Strength under Fluctuating Stresses 317
	Problems 192	6-14	Combinations of Loading Modes 317
Part 2	Failure Prevention 212	6-15	Varying, Fluctuating Stresses; Cumulative Fatigue Damage 321
5	Failures Resulting from Static Loading 213	6-16	Surface Fatigue Strength 327
5-1	Static Strength 216	6-17	Stochastic Analysis 330
5-2	Stress Concentration 217	6-18	Road Maps and Important Design Equations for the Stress-Life Method 344
5-3	Failure Theories 219		Problems 348
5-4	Maximum-Shear-Stress Theory for Ductile Materials 219		
5-5	Distortion-Energy Theory for Ductile Materials 221		

Part 3 Design of Mechanical Elements 358**7 Shafts and Shaft Components** 359

- 7-1** Introduction 360
7-2 Shaft Materials 360
7-3 Shaft Layout 361
7-4 Shaft Design for Stress 366
7-5 Deflection Considerations 379
7-6 Critical Speeds for Shafts 383
7-7 Miscellaneous Shaft Components 388
7-8 Limits and Fits 395
Problems 400

8 Screws, Fasteners, and the Design of Nonpermanent Joints 409

- 8-1** Thread Standards and Definitions 410
8-2 The Mechanics of Power Screws 414
8-3 Threaded Fasteners 422
8-4 Joints—Fastener Stiffness 424
8-5 Joints—Member Stiffness 427
8-6 Bolt Strength 432
8-7 Tension Joints—The External Load 435
8-8 Relating Bolt Torque to Bolt Tension 437
8-9 Statically Loaded Tension Joint with Preload 440
8-10 Gasketed Joints 444
8-11 Fatigue Loading of Tension Joints 444
8-12 Bolted and Riveted Joints Loaded in Shear 451
Problems 459

9 Welding, Bonding, and the Design of Permanent Joints 475

- 9-1** Welding Symbols 476
9-2 Butt and Fillet Welds 478
9-3 Stresses in Welded Joints in Torsion 482
9-4 Stresses in Welded Joints in Bending 487

- 9-5** The Strength of Welded Joints 489
9-6 Static Loading 492
9-7 Fatigue Loading 496
9-8 Resistance Welding 498
9-9 Adhesive Bonding 498
Problems 507

10 Mechanical Springs 517

- 10-1** Stresses in Helical Springs 518
10-2 The Curvature Effect 519
10-3 Deflection of Helical Springs 520
10-4 Compression Springs 520
10-5 Stability 522
10-6 Spring Materials 523
10-7 Helical Compression Spring Design for Static Service 528
10-8 Critical Frequency of Helical Springs 534
10-9 Fatigue Loading of Helical Compression Springs 536
10-10 Helical Compression Spring Design for Fatigue Loading 539
10-11 Extension Springs 542
10-12 Helical Coil Torsion Springs 550
10-13 Belleville Springs 557
10-14 Miscellaneous Springs 558
10-15 Summary 560
Problems 560

11 Rolling-Contact Bearings 569

- 11-1** Bearing Types 570
11-2 Bearing Life 573
11-3 Bearing Load Life at Rated Reliability 574
11-4 Bearing Survival: Reliability versus Life 576
11-5 Relating Load, Life, and Reliability 577
11-6 Combined Radial and Thrust Loading 579
11-7 Variable Loading 584
11-8 Selection of Ball and Cylindrical Roller Bearings 588
11-9 Selection of Tapered Roller Bearings 590
11-10 Design Assessment for Selected Rolling-Contact Bearings 599

11-11	Lubrication 603	13-17	Force Analysis—Worm Gearing 714
11-12	Mounting and Enclosure 604	Problems	720
	Problems 608		
12	Lubrication and Journal Bearings 617		
12-1	Types of Lubrication 618	14	Spur and Helical Gears 733
12-2	Viscosity 619	14-1	The Lewis Bending Equation 734
12-3	Petroff's Equation 621	14-2	Surface Durability 743
12-4	Stable Lubrication 623	14-3	AGMA Stress Equations 745
12-5	Thick-Film Lubrication 624	14-4	AGMA Strength Equations 747
12-6	Hydrodynamic Theory 625	14-5	Geometry Factors I and J (Z_I and Y_J) 751
12-7	Design Considerations 629	14-6	The Elastic Coefficient C_p (Z_E) 756
12-8	The Relations of the Variables 631	14-7	Dynamic Factor K_v 756
12-9	Steady-State Conditions in Self-Contained Bearings 645	14-8	Overload Factor K_o 758
12-10	Clearance 648	14-9	Surface Condition Factor C_f (Z_R) 758
12-11	Pressure-Fed Bearings 650	14-10	Size Factor K_s 759
12-12	Loads and Materials 656	14-11	Load-Distribution Factor K_m (K_H) 759
12-13	Bearing Types 658	14-12	Hardness-Ratio Factor C_H 761
12-14	Thrust Bearings 659	14-13	Stress Cycle Life Factors Y_N and Z_N 762
12-15	Boundary-Lubricated Bearings 660	14-14	Reliability Factor K_R (Y_Z) 763
	Problems 669	14-15	Temperature Factor K_T (Y_θ) 764
13	Gears—General 673	14-16	Rim-Thickness Factor K_B 764
13-1	Types of Gear 674	14-17	Safety Factors S_F and S_H 765
13-2	Nomenclature 675	14-18	Analysis 765
13-3	Conjugate Action 677	14-19	Design of a Gear Mesh 775
13-4	Involute Properties 678	Problems	780
13-5	Fundamentals 678		
13-6	Contact Ratio 684		
13-7	Interference 685		
13-8	The Forming of Gear Teeth 687	15	Bevel and Worm Gears 785
13-9	Straight Bevel Gears 690	15-1	Bevel Gearing—General 786
13-10	Parallel Helical Gears 691	15-2	Bevel-Gear Stresses and Strengths 788
13-11	Worm Gears 695	15-3	AGMA Equation Factors 791
13-12	Tooth Systems 696	15-4	Straight-Bevel Gear Analysis 803
13-13	Gear Trains 698	15-5	Design of a Straight-Bevel Gear Mesh 806
13-14	Force Analysis—Spur Gearing 705	15-6	Worm Gearing—AGMA Equation 809
13-15	Force Analysis—Bevel Gearing 709	15-7	Worm-Gear Analysis 813
13-16	Force Analysis—Helical Gearing 712	15-8	Designing a Worm-Gear Mesh 817
		15-9	Buckingham Wear Load 820
		Problems	821
16	Clutches, Brakes, Couplings, and Flywheels 825		
16-1	Static Analysis of Clutches and Brakes 827		
16-2	Internal Expanding Rim Clutches and Brakes 832		

16-3	External Contracting Rim Clutches and Brakes 840
16-4	Band-Type Clutches and Brakes 844
16-5	Frictional-Contact Axial Clutches 845
16-6	Disk Brakes 849
16-7	Cone Clutches and Brakes 853
16-8	Energy Considerations 856
16-9	Temperature Rise 857
16-10	Friction Materials 861
16-11	Miscellaneous Clutches and Couplings 864
16-12	Flywheels 866
	Problems 871
17	Flexible Mechanical Elements 879
17-1	Belts 880
17-2	Flat- and Round-Belt Drives 883
17-3	V Belts 898
17-4	Timing Belts 906
17-5	Roller Chain 907
17-6	Wire Rope 916
17-7	Flexible Shafts 924
	Problems 925
18	Power Transmission Case Study 933
18-1	Design Sequence for Power Transmission 935
18-2	Power and Torque Requirements 936
18-3	Gear Specification 936
18-4	Shaft Layout 943
18-5	Force Analysis 945
18-6	Shaft Material Selection 945
18-7	Shaft Design for Stress 946
18-8	Shaft Design for Deflection 946
18-9	Bearing Selection 947
18-11	Key and Retaining Ring Selection 948
18-12	Final Analysis 951
	Problems 951

Part 4 Analysis Tools 952**19 Finite-Element Analysis** 953

19-1	The Finite-Element Method 955
19-2	Element Geometries 957
19-3	The Finite-Element Solution Process 959
19-4	Mesh Generation 962
19-5	Load Application 964
19-6	Boundary Conditions 965
19-7	Modeling Techniques 966
19-8	Thermal Stresses 969
19-9	Critical Buckling Load 969
19-10	Vibration Analysis 971
19-11	Summary 972
	Problems 974

20 Statistical Considerations 977

20-1	Random Variables 978
20-2	Arithmetic Mean, Variance, and Standard Deviation 980
20-3	Probability Distributions 985
20-4	Propagation of Error 992
20-5	Linear Regression 994
	Problems 997

Appendices**A Useful Tables** 1003**B Answers to Selected Problems** 1059

Index 1065

Objectives

This text is intended for students beginning the study of mechanical engineering design. The focus is on blending fundamental development of concepts with practical specification of components. Students of this text should find that it inherently directs them into familiarity with both the basis for decisions and the standards of industrial components. For this reason, as students transition to practicing engineers, they will find that this text is indispensable as a reference text. The objectives of the text are to:

- Cover the basics of machine design, including the design process, engineering mechanics and materials, failure prevention under static and variable loading, and characteristics of the principal types of mechanical elements
- Offer a practical approach to the subject through a wide range of real-world applications and examples
- Encourage readers to link design and analysis
- Encourage readers to link fundamental concepts with practical component specification.

New to This Edition

Enhancements and modifications to the ninth edition are described in the following summaries:

- *New and revised end-of-chapter problems.* This edition includes 1017 end-of-chapter problems, a 43 percent increase from the previous edition. Of these problems, 671 are new or revised, providing a fresh slate of problems that do not have years of previous circulation. Particular attention has been given to adding problems that provide more practice with the fundamental concepts. With an eye toward both the instructor and the students, the problems assist in the process of acquiring knowledge and practice. Multiple problems with variations are available for the basic concepts, allowing for extra practice and for a rotation of similar problems between semesters.
- *Problems linked across multiple chapters.* To assist in demonstrating the linkage of topics between chapters, a series of multichapter linked problems is introduced. Table 1–1 on p. 24 provides a guide to these problems. Instructors are encouraged to select several of these linked problem series each semester to use in homework assignments that continue to build upon the background knowledge gained in previous assignments. Some problems directly build upon the results of previous problems, which can either be provided by the instructor or by the students’ results from working the previous problems. Other problems simply build upon the background context of previous problems. In all cases, the students are encouraged to see the connectivity of a whole process. By the time a student has worked through

a series of linked problems, a substantial analysis has been achieved, addressing such things as deflection, stress, static failure, dynamic failure, and multiple component selection. Since it comes one assignment at a time, it is no more daunting than regular homework assignments. Many of the linked problems blend very nicely with the transmission case study developed throughout the book, and detailed in Chap. 18.

- *Content changes.* The bulk of the content changes in this edition falls into categories of pedagogy and keeping current. These changes include improved examples, clarified presentations, improved notations, and updated references. A detailed list of content changes is available on the resource website, www.mhhe.com/shigley.

A few content changes warrant particular mention for the benefit of instructors familiar with previous editions.

- Transverse shear stress is covered in greater depth (Sec. 3–11 and Ex. 3–7).
- The sections on strain energy and Castigliano’s method are modified in presentation of equations and examples, particularly in the deflections of curved members (Secs. 4–7 through 4–9).
- The coverage of shock and impact loading is mathematically simplified by using an energy approach (Sec. 4–17).
- The variable σ_{rev} is introduced to denote a completely reversed stress, avoiding confusion with σ_a , which is the amplitude of alternating stress about a mean stress (Sec. 6–8).
- The method for determining notch sensitivity for shear loading is modified to be more consistent with currently available data (Sec. 6–10).
- For tension-loaded bolts, the yielding factor of safety is defined and distinguished from the load factor (Sec. 8–9).
- The presentation of fatigue loading of bolted joints now handles general fluctuating stresses, treating repeated loading as a special case (Sec. 8–11).
- The notation for bearing life now distinguishes more clearly and consistently between life in revolutions versus life in hours (Sec. 11–3).
- The material on tapered roller bearings is generalized to emphasize the concepts and processes, and to be less dependent on specific manufacturer’s terminology (Sec. 11–9).
- *Streamlining for clarity to the student.* There is a fine line between being comprehensive and being cumbersome and confusing. It is a continual process to refine and maintain focus on the needs of the student. This text is first and foremost an educational tool for the initial presentation of its topics to the developing engineering student. Accordingly, the presentation has been examined with attentiveness to how the beginning student would likely understand it. Also recognizing that this text is a valued reference for practicing engineers, the authors have endeavored to keep the presentation complete, accurate, properly referenced, and straightforward.



Connect Engineering

The 9th edition also features McGraw-Hill Connect Engineering, a Web-based assignment and assessment platform that allows instructors to deliver assignments, quizzes, and tests easily online. Students can practice important skills at their own pace and on their own schedule.

Additional media offerings available at www.mhhe.com/shigley include:

Student Supplements

- *Tutorials*—Presentation of major concepts, with visuals. Among the topics covered are pressure vessel design, press and shrink fits, contact stresses, and design for static failure.
- *MATLAB® for machine design*. Includes visual simulations and accompanying source code. The simulations are linked to examples and problems in the text and demonstrate the ways computational software can be used in mechanical design and analysis.
- *Fundamentals of Engineering (FE) exam questions for machine design*. Interactive problems and solutions serve as effective, self-testing problems as well as excellent preparation for the FE exam.

Instructor Supplements (under password protection)

- *Solutions manual*. The instructor's manual contains solutions to most end-of-chapter nondesign problems.
- *PowerPoint® slides*. Slides of important figures and tables from the text are provided in PowerPoint format for use in lectures.
- *C.O.S.M.O.S.* A complete online solutions manual organization system that allows instructors to create custom homework, quizzes, and tests using end-of-chapter problems from the text.

Electronic Textbooks

Ebooks are an innovative way for students to save money and create a greener environment at the same time. An ebook can save students about half the cost of a traditional textbook and offers unique features like a powerful search engine, highlighting, and the ability to share notes with classmates using ebooks.

McGraw-Hill offers this text as an ebook. To talk about the ebook options, contact your McGraw-Hill sales rep or visit the site www.coursesmart.com to learn more.

Acknowledgments

The authors would like to acknowledge the many reviewers who have contributed to this text over the past 40 years and eight editions. We are especially grateful to those who provided input to this ninth edition:

Amanda Brenner, *Missouri University of Science and Technology*
C. Andrew Campbell, *Conestoga College*
Gloria Starns, *Iowa State University*
Jonathon Blotter, *Brigham Young University*
Michael Latcha, *Oakland University*
Om P. Agrawal, *Southern Illinois University*
Pal Molian, *Iowa State University*
Pierre Larochelle, *Florida Institute of Technology*
Shaoping Xiao, *University of Iowa*
Steve Yurgartis, *Clarkson University*
Timothy Van Rhein, *Missouri University of Science and Technology*

This page intentionally left blank

List of Symbols

This is a list of common symbols used in machine design and in this book. Specialized use in a subject-matter area often attracts fore and post subscripts and superscripts. To make the table brief enough to be useful, the symbol kernels are listed. See Table 14–1, pp. 735–736 for spur and helical gearing symbols, and Table 15–1, pp. 789–790 for bevel-gear symbols.

A	Area, coefficient
A	Area variate
a	Distance, regression constant
\hat{a}	Regression constant estimate
a	Distance variate
B	Coefficient
Bhn	Brinell hardness
B	Variate
b	Distance, Weibull shape parameter, range number, regression constant, width
\hat{b}	Regression constant estimate
b	Distance variate
C	Basic load rating, bolted-joint constant, center distance, coefficient of variation, column end condition, correction factor, specific heat capacity, spring index
c	Distance, viscous damping, velocity coefficient
CDF	Cumulative distribution function
COV	Coefficient of variation
c	Distance variate
D	Helix diameter
d	Diameter, distance
E	Modulus of elasticity, energy, error
e	Distance, eccentricity, efficiency, Naperian logarithmic base
F	Force, fundamental dimension force
f	Coefficient of friction, frequency, function
fom	Figure of merit
G	Torsional modulus of elasticity
g	Acceleration due to gravity, function
H	Heat, power
H_B	Brinell hardness
HRC	Rockwell C-scale hardness
h	Distance, film thickness
\hbar_{CR}	Combined overall coefficient of convection and radiation heat transfer
I	Integral, linear impulse, mass moment of inertia, second moment of area
i	Index
i	Unit vector in x -direction

J	Mechanical equivalent of heat, polar second moment of area, geometry factor
j	Unit vector in the y -direction
K	Service factor, stress-concentration factor, stress-augmentation factor, torque coefficient
<i>k</i>	Marin endurance limit modifying factor, spring rate
k	k variate, unit vector in the z -direction
L	Length, life, fundamental dimension length
L	Life in hours
LN	Lognormal distribution
<i>l</i>	Length
M	Fundamental dimension mass, moment
M	Moment vector, moment variate
<i>m</i>	Mass, slope, strain-strengthening exponent
<i>N</i>	Normal force, number, rotational speed
N	Normal distribution
<i>n</i>	Load factor, rotational speed, safety factor
<i>n_d</i>	Design factor
P	Force, pressure, diametral pitch
PDF	Probability density function
<i>p</i>	Pitch, pressure, probability
Q	First moment of area, imaginary force, volume
<i>q</i>	Distributed load, notch sensitivity
R	Radius, reaction force, reliability, Rockwell hardness, stress ratio
R	Vector reaction force
<i>r</i>	Correlation coefficient, radius
r	Distance vector
S	Sommerfeld number, strength
S	S variate
<i>s</i>	Distance, sample standard deviation, stress
T	Temperature, tolerance, torque, fundamental dimension time
T	Torque vector, torque variate
<i>t</i>	Distance, Student's t-statistic, time, tolerance
U	Strain energy
U	Uniform distribution
<i>u</i>	Strain energy per unit volume
V	Linear velocity, shear force
<i>v</i>	Linear velocity
W	Cold-work factor, load, weight
W	Weibull distribution
<i>w</i>	Distance, gap, load intensity
w	Vector distance
X	Coordinate, truncated number
<i>x</i>	Coordinate, true value of a number, Weibull parameter
x	x variate
Y	Coordinate
<i>y</i>	Coordinate, deflection
y	y variate
Z	Coordinate, section modulus, viscosity
<i>z</i>	Standard deviation of the unit normal distribution
z	Variate of z

α	Coefficient, coefficient of linear thermal expansion, end-condition for springs, thread angle
β	Bearing angle, coefficient
Δ	Change, deflection
δ	Deviation, elongation
ϵ	Eccentricity ratio, engineering (normal) strain
ϵ	Normal distribution with a mean of 0 and a standard deviation of s
ε	True or logarithmic normal strain
Γ	Gamma function
γ	Pitch angle, shear strain, specific weight
λ	Slenderness ratio for springs
λ	Unit lognormal with a mean of 1 and a standard deviation equal to COV
μ	Absolute viscosity, population mean
ν	Poisson ratio
ω	Angular velocity, circular frequency
ϕ	Angle, wave length
ψ	Slope integral
ρ	Radius of curvature
σ	Normal stress
σ'	Von Mises stress
σ	Normal stress variate
$\hat{\sigma}$	Standard deviation
τ	Shear stress
τ	Shear stress variate
θ	Angle, Weibull characteristic parameter
ϱ	Cost per unit weight
$\$$	Cost

This page intentionally left blank

Shigley's Mechanical Engineering Design

PART

1

Basics

1

Introduction to Mechanical Engineering Design

Chapter Outline

1-1	Design	4
1-2	Mechanical Engineering Design	5
1-3	Phases and Interactions of the Design Process	5
1-4	Design Tools and Resources	8
1-5	The Design Engineer's Professional Responsibilities	10
1-6	Standards and Codes	12
1-7	Economics	12
1-8	Safety and Product Liability	15
1-9	Stress and Strength	15
1-10	Uncertainty	16
1-11	Design Factor and Factor of Safety	17
1-12	Reliability	18
1-13	Dimensions and Tolerances	19
1-14	Units	21
1-15	Calculations and Significant Figures	22
1-16	Design Topic Interdependencies	23
1-17	Power Transmission Case Study Specifications	24

Mechanical design is a complex process, requiring many skills. Extensive relationships need to be subdivided into a series of simple tasks. The complexity of the process requires a sequence in which ideas are introduced and iterated.

We first address the nature of design in general, and then mechanical engineering design in particular. Design is an iterative process with many interactive phases. Many resources exist to support the designer, including many sources of information and an abundance of computational design tools. Design engineers need not only develop competence in their field but they must also cultivate a strong sense of responsibility and professional work ethic.

There are roles to be played by codes and standards, ever-present economics, safety, and considerations of product liability. The survival of a mechanical component is often related through stress and strength. Matters of uncertainty are ever-present in engineering design and are typically addressed by the design factor and factor of safety, either in the form of a deterministic (absolute) or statistical sense. The latter, statistical approach, deals with a design's *reliability* and requires good statistical data.

In mechanical design, other considerations include dimensions and tolerances, units, and calculations.

The book consists of four parts. Part 1, *Basics*, begins by explaining some differences between design and analysis and introducing some fundamental notions and approaches to design. It continues with three chapters reviewing material properties, stress analysis, and stiffness and deflection analysis, which are the principles necessary for the remainder of the book.

Part 2, *Failure Prevention*, consists of two chapters on the prevention of failure of mechanical parts. Why machine parts fail and how they can be designed to prevent failure are difficult questions, and so we take two chapters to answer them, one on preventing failure due to static loads, and the other on preventing fatigue failure due to time-varying cyclic loads.

In Part 3, *Design of Mechanical Elements*, the concepts of Parts 1 and 2 are applied to the analysis, selection, and design of specific mechanical elements such as shafts, fasteners, weldments, springs, rolling contact bearings, film bearings, gears, belts, chains, and wire ropes.

Part 4, *Analysis Tools*, provides introductions to two important methods used in mechanical design, finite element analysis and statistical analysis. This is optional study material, but some sections and examples in Parts 1 to 3 demonstrate the use of these tools.

There are two appendixes at the end of the book. Appendix A contains many useful tables referenced throughout the book. Appendix B contains answers to selected end-of-chapter problems.

1–1 Design

To design is either to formulate a plan for the satisfaction of a specified need or to solve a specific problem. If the plan results in the creation of something having a physical reality, then the product must be functional, safe, reliable, competitive, usable, manufacturable, and marketable.

Design is an innovative and highly iterative process. It is also a decision-making process. Decisions sometimes have to be made with too little information, occasionally with just the right amount of information, or with an excess of partially contradictory information. Decisions are sometimes made tentatively, with the right reserved to adjust as more becomes known. The point is that the engineering designer has to be personally comfortable with a decision-making, problem-solving role.

Design is a communication-intensive activity in which both words and pictures are used, and written and oral forms are employed. Engineers have to communicate effectively and work with people of many disciplines. These are important skills, and an engineer's success depends on them.

A designer's personal resources of creativeness, communicative ability, and problem-solving skill are intertwined with the knowledge of technology and first principles. Engineering tools (such as mathematics, statistics, computers, graphics, and languages) are combined to produce a plan that, when carried out, produces a product that is *functional, safe, reliable, competitive, usable, manufacturable, and marketable*, regardless of who builds it or who uses it.

1–2

Mechanical Engineering Design

Mechanical engineers are associated with the production and processing of energy and with providing the means of production, the tools of transportation, and the techniques of automation. The skill and knowledge base are extensive. Among the disciplinary bases are mechanics of solids and fluids, mass and momentum transport, manufacturing processes, and electrical and information theory. Mechanical engineering design involves all the disciplines of mechanical engineering.

Real problems resist compartmentalization. A simple journal bearing involves fluid flow, heat transfer, friction, energy transport, material selection, thermomechanical treatments, statistical descriptions, and so on. A building is environmentally controlled. The heating, ventilation, and air-conditioning considerations are sufficiently specialized that some speak of heating, ventilating, and air-conditioning design as if it is separate and distinct from mechanical engineering design. Similarly, internal-combustion engine design, turbomachinery design, and jet-engine design are sometimes considered discrete entities. Here, the leading string of words preceding the word design is merely a product descriptor. Similarly, there are phrases such as machine design, machine-element design, machine-component design, systems design, and fluid-power design. All of these phrases are somewhat more focused *examples* of mechanical engineering design. They all draw on the same bodies of knowledge, are similarly organized, and require similar skills.

1–3

Phases and Interactions of the Design Process

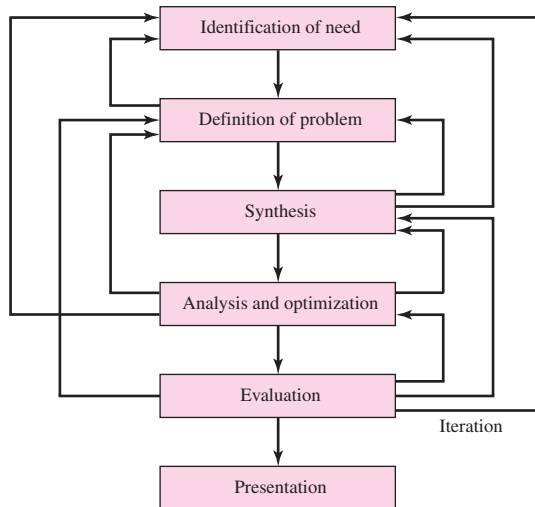
What is the design process? How does it begin? Does the engineer simply sit down at a desk with a blank sheet of paper and jot down some ideas? What happens next? What factors influence or control the decisions that have to be made? Finally, how does the design process end?

The complete design process, from start to finish, is often outlined as in Fig. 1–1. The process begins with an identification of a need and a decision to do something about it. After many iterations, the process ends with the presentation of the plans for satisfying the need. Depending on the nature of the design task, several design phases may be repeated throughout the life of the product, from inception to termination. In the next several subsections, we shall examine these steps in the design process in detail.

Identification of need generally starts the design process. Recognition of the need and phrasing the need often constitute a highly creative act, because the need may be only a vague discontent, a feeling of uneasiness, or a sensing that something is not right. The need is often not evident at all; recognition can be triggered by a particular adverse

Figure 1-1

The phases in design,
acknowledging the many
feedbacks and iterations.



circumstance or a set of random circumstances that arises almost simultaneously. For example, the need to do something about a food-packaging machine may be indicated by the noise level, by a variation in package weight, and by slight but perceptible variations in the quality of the packaging or wrap.

There is a distinct difference between the statement of the need and the definition of the problem. The *definition of problem* is more specific and must include all the specifications for the object that is to be designed. The specifications are the input and output quantities, the characteristics and dimensions of the space the object must occupy, and all the limitations on these quantities. We can regard the object to be designed as something in a black box. In this case we must specify the inputs and outputs of the box, together with their characteristics and limitations. The specifications define the cost, the number to be manufactured, the expected life, the range, the operating temperature, and the reliability. Specified characteristics can include the speeds, feeds, temperature limitations, maximum range, expected variations in the variables, dimensional and weight limitations, etc.

There are many implied specifications that result either from the designer's particular environment or from the nature of the problem itself. The manufacturing processes that are available, together with the facilities of a certain plant, constitute restrictions on a designer's freedom, and hence are a part of the implied specifications. It may be that a small plant, for instance, does not own cold-working machinery. Knowing this, the designer might select other metal-processing methods that can be performed in the plant. The labor skills available and the competitive situation also constitute implied constraints. Anything that limits the designer's freedom of choice is a constraint. Many materials and sizes are listed in supplier's catalogs, for instance, but these are not all easily available and shortages frequently occur. Furthermore, inventory economics requires that a manufacturer stock a minimum number of materials and sizes. An example of a specification is given in Sec. 1-17. This example is for a case study of a power transmission that is presented throughout this text.

The *synthesis* of a scheme connecting possible system elements is sometimes called the *invention of the concept* or *concept design*. This is the first and most important step in the synthesis task. Various schemes must be proposed, investigated, and

quantified in terms of established metrics.¹ As the fleshing out of the scheme progresses, analyses must be performed to assess whether the system performance is satisfactory or better, and, if satisfactory, just how well it will perform. System schemes that do not survive analysis are revised, improved, or discarded. Those with potential are optimized to determine the best performance of which the scheme is capable. Competing schemes are compared so that the path leading to the most competitive product can be chosen. Figure 1–1 shows that synthesis and *analysis and optimization* are intimately and iteratively related.

We have noted, and we emphasize, that design is an iterative process in which we proceed through several steps, evaluate the results, and then return to an earlier phase of the procedure. Thus, we may synthesize several components of a system, analyze and optimize them, and return to synthesis to see what effect this has on the remaining parts of the system. For example, the design of a system to transmit power requires attention to the design and selection of individual components (e.g., gears, bearings, shaft). However, as is often the case in design, these components are not independent. In order to design the shaft for stress and deflection, it is necessary to know the applied forces. If the forces are transmitted through gears, it is necessary to know the gear specifications in order to determine the forces that will be transmitted to the shaft. But stock gears come with certain bore sizes, requiring knowledge of the necessary shaft diameter. Clearly, rough estimates will need to be made in order to proceed through the process, refining and iterating until a final design is obtained that is satisfactory for each individual component as well as for the overall design specifications. Throughout the text we will elaborate on this process for the case study of a power transmission design.

Both analysis and optimization require that we construct or devise abstract models of the system that will admit some form of mathematical analysis. We call these models mathematical models. In creating them it is our hope that we can find one that will simulate the real physical system very well. As indicated in Fig. 1–1, *evaluation* is a significant phase of the total design process. Evaluation is the final proof of a successful design and usually involves the testing of a prototype in the laboratory. Here we wish to discover if the design really satisfies the needs. Is it reliable? Will it compete successfully with similar products? Is it economical to manufacture and to use? Is it easily maintained and adjusted? Can a profit be made from its sale or use? How likely is it to result in product-liability lawsuits? And is insurance easily and cheaply obtained? Is it likely that recalls will be needed to replace defective parts or systems? The project designer or design team will need to address a myriad of engineering and non-engineering questions.

Communicating the design to others is the final, vital *presentation* step in the design process. Undoubtedly, many great designs, inventions, and creative works have been lost to posterity simply because the originators were unable or unwilling to properly explain their accomplishments to others. Presentation is a selling job. The engineer, when presenting a new solution to administrative, management, or supervisory persons, is attempting to sell or to prove to them that their solution is a better one. Unless this can be done successfully, the time and effort spent on obtaining the solution have been largely wasted. When designers sell a new idea, they also sell themselves. If they are repeatedly successful in selling ideas, designs, and new solutions to management, they begin to receive salary increases and promotions; in fact, this is how anyone succeeds in his or her profession.

¹An excellent reference for this topic is presented by Stuart Pugh, *Total Design—Integrated Methods for Successful Product Engineering*, Addison-Wesley, 1991. A description of the *Pugh method* is also provided in Chap. 8, David G. Ullman, *The Mechanical Design Process*, 3rd ed., McGraw-Hill, 2003.

Design Considerations

Sometimes the strength required of an element in a system is an important factor in the determination of the geometry and the dimensions of the element. In such a situation we say that strength is an important *design consideration*. When we use the expression design consideration, we are referring to some characteristic that influences the design of the element or, perhaps, the entire system. Usually quite a number of such characteristics must be considered and prioritized in a given design situation. Many of the important ones are as follows (not necessarily in order of importance):

- | | | | |
|----|---------------------------------|----|-----------------------------------|
| 1 | Functionality | 14 | Noise |
| 2 | Strength/stress | 15 | Styling |
| 3 | Distortion/deflection/stiffness | 16 | Shape |
| 4 | Wear | 17 | Size |
| 5 | Corrosion | 18 | Control |
| 6 | Safety | 19 | Thermal properties |
| 7 | Reliability | 20 | Surface |
| 8 | Manufacturability | 21 | Lubrication |
| 9 | Utility | 22 | Marketability |
| 10 | Cost | 23 | Maintenance |
| 11 | Friction | 24 | Volume |
| 12 | Weight | 25 | Liability |
| 13 | Life | 26 | Remanufacturing/resource recovery |

Some of these characteristics have to do directly with the dimensions, the material, the processing, and the joining of the elements of the system. Several characteristics may be interrelated, which affects the configuration of the total system.

1–4

Design Tools and Resources

Today, the engineer has a great variety of tools and resources available to assist in the solution of design problems. Inexpensive microcomputers and robust computer software packages provide tools of immense capability for the design, analysis, and simulation of mechanical components. In addition to these tools, the engineer always needs technical information, either in the form of basic science/engineering behavior or the characteristics of specific off-the-shelf components. Here, the resources can range from science/engineering textbooks to manufacturers' brochures or catalogs. Here too, the computer can play a major role in gathering information.²

Computational Tools

Computer-aided design (CAD) software allows the development of three-dimensional (3-D) designs from which conventional two-dimensional orthographic views with automatic dimensioning can be produced. Manufacturing tool paths can be generated from the 3-D models, and in some cases, parts can be created directly from a 3-D database by using a rapid prototyping and manufacturing method (stereolithography)—*paperless manufacturing!* Another advantage of a 3-D database is that it allows rapid and accurate calculations of mass properties such as mass, location of the center of gravity, and mass moments of inertia. Other geometric properties such as areas and distances between points are likewise easily obtained. There are a great many CAD software packages available such

²An excellent and comprehensive discussion of the process of “gathering information” can be found in Chap. 4, George E. Dieter, *Engineering Design, A Materials and Processing Approach*, 3rd ed., McGraw-Hill, New York, 2000.

as Aries, AutoCAD, CadKey, I-Deas, Unigraphics, Solid Works, and ProEngineer, to name a few.

The term *computer-aided engineering* (CAE) generally applies to all computer-related engineering applications. With this definition, CAD can be considered as a subset of CAE. Some computer software packages perform specific engineering analysis and/or simulation tasks that assist the designer, but they are not considered a tool for the creation of the design that CAD is. Such software fits into two categories: engineering-based and non-engineering-specific. Some examples of engineering-based software for mechanical engineering applications—software that might also be integrated within a CAD system—include finite-element analysis (FEA) programs for analysis of stress and deflection (see Chap. 19), vibration, and heat transfer (e.g., Algor, ANSYS, and MSC/NASTRAN); computational fluid dynamics (CFD) programs for fluid-flow analysis and simulation (e.g., CFD++, FIDAP, and Fluent); and programs for simulation of dynamic force and motion in mechanisms (e.g., ADAMS, DADS, and Working Model).

Examples of non-engineering-specific computer-aided applications include software for word processing, spreadsheet software (e.g., Excel, Lotus, and Quattro-Pro), and mathematical solvers (e.g., Maple, MathCad, MATLAB,³ Mathematica, and TKsolver).

Your instructor is the best source of information about programs that may be available to you and can recommend those that are useful for specific tasks. One caution, however: Computer software is no substitute for the human thought process. *You* are the driver here; the computer is the vehicle to assist you on your journey to a solution. Numbers generated by a computer can be far from the truth if you entered incorrect input, if you misinterpreted the application or the output of the program, if the program contained bugs, etc. It is your responsibility to assure the validity of the results, so be careful to check the application and results carefully, perform benchmark testing by submitting problems with known solutions, and monitor the software company and user-group newsletters.

Acquiring Technical Information

We currently live in what is referred to as the *information age*, where information is generated at an astounding pace. It is difficult, but extremely important, to keep abreast of past and current developments in one's field of study and occupation. The reference in Footnote 2 provides an excellent description of the informational resources available and is highly recommended reading for the serious design engineer. Some sources of information are:

- *Libraries (community, university, and private)*. Engineering dictionaries and encyclopedias, textbooks, monographs, handbooks, indexing and abstract services, journals, translations, technical reports, patents, and business sources/brochures/catalogs.
- *Government sources*. Departments of Defense, Commerce, Energy, and Transportation; NASA; Government Printing Office; U.S. Patent and Trademark Office; National Technical Information Service; and National Institute for Standards and Technology.
- *Professional societies*. American Society of Mechanical Engineers, Society of Manufacturing Engineers, Society of Automotive Engineers, American Society for Testing and Materials, and American Welding Society.
- *Commercial vendors*. Catalogs, technical literature, test data, samples, and cost information.
- *Internet*. The computer network gateway to websites associated with most of the categories listed above.⁴

³MATLAB is a registered trademark of The MathWorks, Inc.

⁴Some helpful Web resources, to name a few, include www.globalspec.com, www.engnetglobal.com, www.efunda.com, www.thomasnet.com, and www.uspto.gov.

This list is not complete. The reader is urged to explore the various sources of information on a regular basis and keep records of the knowledge gained.

1-5 **The Design Engineer's Professional Responsibilities**

In general, the design engineer is required to satisfy the needs of *customers* (management, clients, consumers, etc.) and is expected to do so in a competent, responsible, ethical, and professional manner. Much of engineering course work and practical experience focuses on competence, but when does one begin to develop engineering responsibility and professionalism? To start on the road to success, you should start to develop these characteristics early in your educational program. You need to cultivate your professional work ethic and process skills before graduation, so that when you begin your formal engineering career, you will be prepared to meet the challenges.

It is not obvious to some students, but communication skills play a large role here, and it is the wise student who continuously works to improve these skills—*even if it is not a direct requirement of a course assignment!* Success in engineering (achievements, promotions, raises, etc.) may in large part be due to competence but if you cannot communicate your ideas clearly and concisely, your technical proficiency may be compromised.

You can start to develop your communication skills by keeping a neat and clear journal/logbook of your activities, entering dated entries frequently. (Many companies require their engineers to keep a journal for patent and liability concerns.) Separate journals should be used for each design project (or course subject). When starting a project or problem, in the definition stage, make journal entries quite frequently. Others, as well as yourself, may later question why you made certain decisions. Good chronological records will make it easier to explain your decisions at a later date.

Many engineering students see themselves after graduation as practicing engineers designing, developing, and analyzing products and processes and consider the need of good communication skills, either oral or writing, as secondary. This is far from the truth. Most practicing engineers spend a good deal of time communicating with others, writing proposals and technical reports, and giving presentations and interacting with engineering and nonengineering support personnel. You have the time now to sharpen your communication skills. When given an assignment to write or make any presentation, technical *or* nontechnical, accept it enthusiastically, and work on improving your communication skills. It will be time well spent to learn the skills now rather than on the job.

When you are working on a design problem, it is important that you develop a systematic approach. Careful attention to the following action steps will help you to organize your solution processing technique.

- *Understand the problem.* Problem definition is probably the most significant step in the engineering design process. Carefully read, understand, and refine the problem statement.
- *Identify the knowns.* From the refined problem statement, describe concisely what information is known and relevant.
- *Identify the unknowns and formulate the solution strategy.* State what must be determined, in what order, so as to arrive at a solution to the problem. Sketch the component or system under investigation, identifying known and unknown parameters. Create a flowchart of the steps necessary to reach the final solution. The steps may require the use of free-body diagrams; material properties from tables; equations

from first principles, textbooks, or handbooks relating the known and unknown parameters; experimentally or numerically based charts; specific computational tools as discussed in Sec. 1–4; etc.

- *State all assumptions and decisions.* Real design problems generally do not have unique, ideal, closed-form solutions. Selections, such as the choice of materials, and heat treatments, require decisions. Analyses require assumptions related to the modeling of the real components or system. All assumptions and decisions should be identified and recorded.
- *Analyze the problem.* Using your solution strategy in conjunction with your decisions and assumptions, execute the analysis of the problem. Reference the sources of all equations, tables, charts, software results, etc. Check the credibility of your results. Check the order of magnitude, dimensionality, trends, signs, etc.
- *Evaluate your solution.* Evaluate each step in the solution, noting how changes in strategy, decisions, assumptions, and execution might change the results, in positive or negative ways. Whenever possible, incorporate the positive changes in your final solution.
- *Present your solution.* Here is where your communication skills are important. At this point, you are selling yourself and your technical abilities. If you cannot skillfully explain what you have done, some or all of your work may be misunderstood and unaccepted. Know your audience.

As stated earlier, all design processes are interactive and iterative. Thus, it may be necessary to repeat some or all of the above steps more than once if less than satisfactory results are obtained.

In order to be effective, all professionals must keep current in their fields of endeavor. The design engineer can satisfy this in a number of ways by: being an active member of a professional society such as the American Society of Mechanical Engineers (ASME), the Society of Automotive Engineers (SAE), and the Society of Manufacturing Engineers (SME); attending meetings, conferences, and seminars of societies, manufacturers, universities, etc.; taking specific graduate courses or programs at universities; regularly reading technical and professional journals; etc. An engineer's education does not end at graduation.

The design engineer's professional obligations include conducting activities in an ethical manner. Reproduced here is the *Engineers' Creed* from the National Society of Professional Engineers (NSPE)⁵:

As a Professional Engineer I dedicate my professional knowledge and skill to the advancement and betterment of human welfare.

I pledge:

To give the utmost of performance;
To participate in none but honest enterprise;
To live and work according to the laws of man and the highest standards of professional conduct;
To place service before profit, the honor and standing of the profession before personal advantage, and the public welfare above all other considerations.
In humility and with need for Divine Guidance, I make this pledge.

⁵Adopted by the National Society of Professional Engineers, June 1954. "The Engineer's Creed." Reprinted by permission of the National Society of Professional Engineers. NSPE also publishes a much more extensive *Code of Ethics for Engineers* with rules of practice and professional obligations. For the current revision, July 2007 (at the time of this book's printing), see the website www.nspe.org/Ethics/CodeofEthics/index.html.

1–6 Standards and Codes

A *standard* is a set of specifications for parts, materials, or processes intended to achieve uniformity, efficiency, and a specified quality. One of the important purposes of a standard is to limit the multitude of variations that can arise from the arbitrary creation of a part, material, or process.

A *code* is a set of specifications for the analysis, design, manufacture, and construction of something. The purpose of a code is to achieve a specified degree of safety, efficiency, and performance or quality. It is important to observe that safety codes *do not imply absolute safety*. In fact, absolute safety is impossible to obtain. Sometimes the unexpected event really does happen. Designing a building to withstand a 120 mi/h wind does not mean that the designers think a 140 mi/h wind is impossible; it simply means that they think it is highly improbable.

All of the organizations and societies listed below have established specifications for standards and safety or design codes. The name of the organization provides a clue to the nature of the standard or code. Some of the standards and codes, as well as addresses, can be obtained in most technical libraries or on the Internet. The organizations of interest to mechanical engineers are:

- Aluminum Association (AA)
- American Bearing Manufacturers Association (ABMA)
- American Gear Manufacturers Association (AGMA)
- American Institute of Steel Construction (AISC)
- American Iron and Steel Institute (AISI)
- American National Standards Institute (ANSI)
- American Society of Heating, Refrigerating and Air-Conditioning Engineers (ASHRAE)
- American Society of Mechanical Engineers (ASME)
- American Society of Testing and Materials (ASTM)
- American Welding Society (AWS)
- ASM International
- British Standards Institution (BSI)
- Industrial Fasteners Institute (IFI)
- Institute of Transportation Engineers (ITE)
- Institution of Mechanical Engineers (IMechE)
- International Bureau of Weights and Measures (BIPM)
- International Federation of Robotics (IFR)
- International Standards Organization (ISO)
- National Association of Power Engineers (NAPE)
- National Institute for Standards and Technology (NIST)
- Society of Automotive Engineers (SAE)

1–7 Economics

The consideration of cost plays such an important role in the design decision process that we could easily spend as much time in studying the cost factor as in the study of the entire subject of design. Here we introduce only a few general concepts and simple rules.

First, observe that nothing can be said in an absolute sense concerning costs. Materials and labor usually show an increasing cost from year to year. But the costs

of processing the materials can be expected to exhibit a decreasing trend because of the use of automated machine tools and robots. The cost of manufacturing a single product will vary from city to city and from one plant to another because of overhead, labor, taxes, and freight differentials and the inevitable slight manufacturing variations.

Standard Sizes

The use of standard or stock sizes is a first principle of cost reduction. An engineer who specifies an AISI 1020 bar of hot-rolled steel 53 mm square has added cost to the product, provided that a bar 50 or 60 mm square, both of which are preferred sizes, would do equally well. The 53-mm size can be obtained by special order or by rolling or machining a 60-mm square, but these approaches add cost to the product. To ensure that standard or preferred sizes are specified, designers must have access to stock lists of the materials they employ.

A further word of caution regarding the selection of preferred sizes is necessary. Although a great many sizes are usually listed in catalogs, they are not all readily available. Some sizes are used so infrequently that they are not stocked. A rush order for such sizes may add to the expense and delay. Thus you should also have access to a list such as those in Table A-17 for preferred inch and millimeter sizes.

There are many purchased parts, such as motors, pumps, bearings, and fasteners, that are specified by designers. In the case of these, too, you should make a special effort to specify parts that are readily available. Parts that are made and sold in large quantities usually cost somewhat less than the odd sizes. The cost of rolling bearings, for example, depends more on the quantity of production by the bearing manufacturer than on the size of the bearing.

Large Tolerances

Among the effects of design specifications on costs, tolerances are perhaps most significant. Tolerances, manufacturing processes, and surface finish are interrelated and influence the producibility of the end product in many ways. Close tolerances may necessitate additional steps in processing and inspection or even render a part completely impractical to produce economically. Tolerances cover dimensional variation and surface-roughness range and also the variation in mechanical properties resulting from heat treatment and other processing operations.

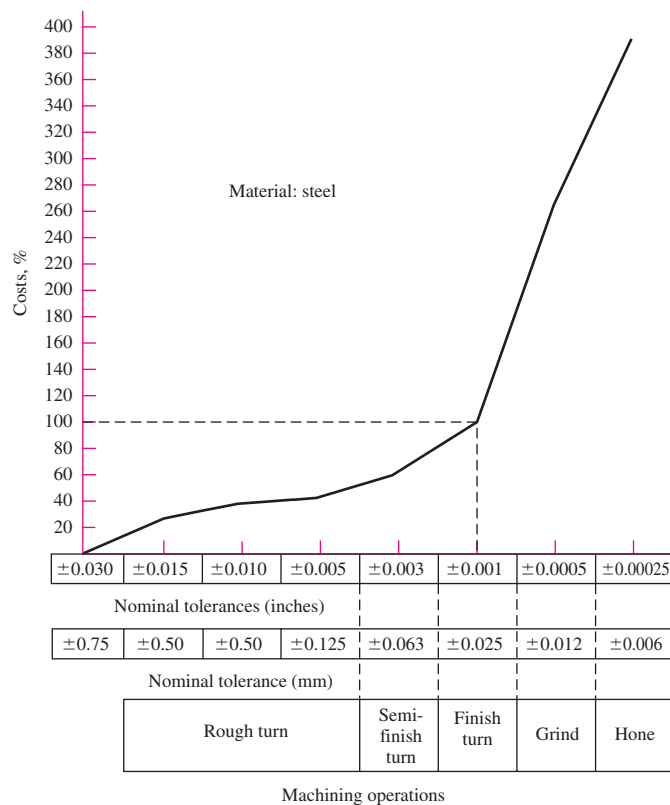
Since parts having large tolerances can often be produced by machines with higher production rates, costs will be significantly smaller. Also, fewer such parts will be rejected in the inspection process, and they are usually easier to assemble. A plot of cost versus tolerance/machining process is shown in Fig. 1-2, and illustrates the drastic increase in manufacturing cost as tolerance diminishes with finer machining processing.

Breakeven Points

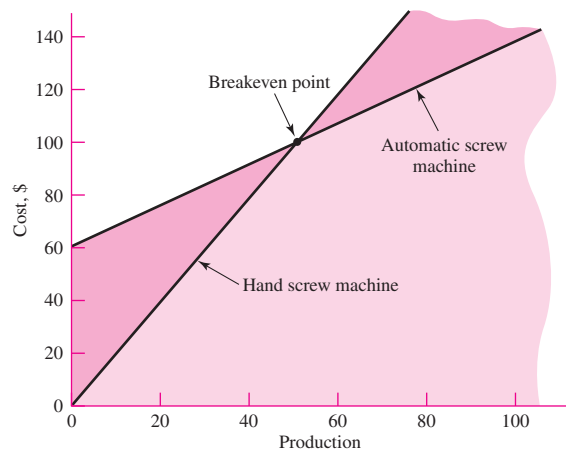
Sometimes it happens that, when two or more design approaches are compared for cost, the choice between the two depends on a set of conditions such as the quantity of production, the speed of the assembly lines, or some other condition. There then occurs a point corresponding to equal cost, which is called the *break-even point*.

Figure 1–2

Cost versus tolerance/machining process.
(From David G. Ullman, The Mechanical Design Process, 3rd ed., McGraw-Hill, New York, 2003.)

**Figure 1–3**

A breakeven point.



As an example, consider a situation in which a certain part can be manufactured at the rate of 25 parts per hour on an automatic screw machine or 10 parts per hour on a hand screw machine. Let us suppose, too, that the setup time for the automatic is 3 h and that the labor cost for either machine is \$20 per hour, including overhead. Figure 1–3 is a graph of cost versus production by the two methods. The breakeven point for this example corresponds to 50 parts. If the desired production is greater than 50 parts, the automatic machine should be used.

Cost Estimates

There are many ways of obtaining relative cost figures so that two or more designs can be roughly compared. A certain amount of judgment may be required in some instances. For example, we can compare the relative value of two automobiles by comparing the dollar cost per pound of weight. Another way to compare the cost of one design with another is simply to count the number of parts. The design having the smaller number of parts is likely to cost less. Many other cost estimators can be used, depending upon the application, such as area, volume, horsepower, torque, capacity, speed, and various performance ratios.⁶

1-8 Safety and Product Liability

The *strict liability* concept of product liability generally prevails in the United States. This concept states that the manufacturer of an article is liable for any damage or harm that results because of a defect. And it doesn't matter whether the manufacturer knew about the defect, or even could have known about it. For example, suppose an article was manufactured, say, 10 years ago. And suppose at that time the article could not have been considered defective on the basis of all technological knowledge then available. Ten years later, according to the concept of strict liability, the manufacturer is still liable. Thus, under this concept, the plaintiff needs only to prove that the article was defective and that the defect caused some damage or harm. Negligence of the manufacturer need not be proved.

The best approaches to the prevention of product liability are good engineering in analysis and design, quality control, and comprehensive testing procedures. Advertising managers often make glowing promises in the warranties and sales literature for a product. These statements should be reviewed carefully by the engineering staff to eliminate excessive promises and to insert adequate warnings and instructions for use.

1-9 Stress and Strength

The survival of many products depends on how the designer adjusts the maximum stresses in a component to be less than the component's strength at critical locations. The designer must allow the maximum stress to be less than the strength by a sufficient margin so that despite the uncertainties, failure is rare.

In focusing on the stress-strength comparison at a critical (controlling) location, we often look for "strength in the geometry and condition of use." Strengths are the magnitudes of stresses at which something of interest occurs, such as the proportional limit, 0.2 percent-offset yielding, or fracture (see Sec. 2-1). In many cases, such events represent the stress level at which loss of function occurs.

Strength is a property of a material or of a mechanical element. The strength of an element depends on the choice, the treatment, and the processing of the material. Consider, for example, a shipment of springs. We can associate a strength with a specific spring. When this spring is incorporated into a machine, external forces are applied that result in load-induced stresses in the spring, the magnitudes of which depend on its geometry and are independent of the material and its processing. If the spring is removed from the machine unharmed, the stress due to the external forces will return

⁶For an overview of estimating manufacturing costs, see Chap. 11, Karl T. Ulrich and Steven D. Eppinger, *Product Design and Development*, 3rd ed., McGraw-Hill, New York, 2004.

to zero. But the strength remains as one of the properties of the spring. Remember, then, that *strength is an inherent property of a part*, a property built into the part because of the use of a particular material and process.

Various metalworking and heat-treating processes, such as forging, rolling, and cold forming, cause variations in the strength from point to point throughout a part. The spring cited above is quite likely to have a strength on the outside of the coils different from its strength on the inside because the spring has been formed by a cold winding process, and the two sides may not have been deformed by the same amount. Remember, too, therefore, that a strength value given for a part may apply to only a particular point or set of points on the part.

In this book we shall use the capital letter S to denote *strength*, with appropriate subscripts to denote the type of strength. Thus, S_y is a yield strength, S_u an ultimate strength, S_{sy} a shear yield strength, and S_e an endurance strength.

In accordance with accepted engineering practice, we shall employ the Greek letters σ (sigma) and τ (tau) to designate normal and shear *stresses*, respectively. Again, various subscripts will indicate some special characteristic. For example, σ_1 is a principal normal stress, σ_y a normal stress component in the y direction, and σ_r a normal stress component in the radial direction.

Stress is a state property at a specific point within a body, which is a function of load, geometry, temperature, and manufacturing processing. In an elementary course in mechanics of materials, stress related to load and geometry is emphasized with some discussion of thermal stresses. However, stresses due to heat treatments, molding, assembly, etc. are also important and are sometimes neglected. A review of stress analysis for basic load states and geometry is given in Chap. 3.

1-10

Uncertainty

Uncertainties in machinery design abound. Examples of uncertainties concerning stress and strength include

- Composition of material and the effect of variation on properties.
- Variations in properties from place to place within a bar of stock.
- Effect of processing locally, or nearby, on properties.
- Effect of nearby assemblies such as weldments and shrink fits on stress conditions.
- Effect of thermomechanical treatment on properties.
- Intensity and distribution of loading.
- Validity of mathematical models used to represent reality.
- Intensity of stress concentrations.
- Influence of time on strength and geometry.
- Effect of corrosion.
- Effect of wear.
- Uncertainty as to the length of any list of uncertainties.

Engineers must accommodate uncertainty. Uncertainty always accompanies change. Material properties, load variability, fabrication fidelity, and validity of mathematical models are among concerns to designers.

There are mathematical methods to address uncertainties. The primary techniques are the deterministic and stochastic methods. The deterministic method establishes a *design factor* based on the absolute uncertainties of a loss-of-function parameter and a

maximum allowable parameter. Here the parameter can be load, stress, deflection, etc. Thus, the design factor n_d is defined as

$$n_d = \frac{\text{loss-of-function parameter}}{\text{maximum allowable parameter}} \quad (1-1)$$

If the parameter is load, then the maximum allowable load can be found from

$$\text{Maximum allowable load} = \frac{\text{loss-of-function load}}{n_d} \quad (1-2)$$

EXAMPLE 1-1

Consider that the maximum load on a structure is known with an uncertainty of ± 20 percent, and the load causing failure is known within ± 15 percent. If the load causing failure is *nominally* 2000 lbf, determine the design factor and the maximum allowable load that will offset the absolute uncertainties.

Solution

To account for its uncertainty, the loss-of-function load must increase to $1/0.85$, whereas the maximum allowable load must decrease to $1/1.2$. Thus to offset the absolute uncertainties the design factor, from Eq. (1-1), should be

Answer

$$n_d = \frac{1/0.85}{1/1.2} = 1.4$$

From Eq. (1-2), the maximum allowable load is found to be

Answer

$$\text{Maximum allowable load} = \frac{2000}{1.4} = 1400 \text{ lbf}$$

Stochastic methods (see Chap. 20) are based on the statistical nature of the design parameters and focus on the probability of survival of the design's function (that is, on reliability). Sections 5–13 and 6–17 demonstrate how this is accomplished.

1-11

Design Factor and Factor of Safety

A general approach to the allowable load versus loss-of-function load problem is the deterministic design factor method, and sometimes called the classical method of design. The fundamental equation is Eq. (1-1) where n_d is called the *design factor*. All loss-of-function modes must be analyzed, and the mode leading to the smallest design factor governs. After the design is completed, the *actual* design factor may change as a result of changes such as rounding up to a standard size for a cross section or using off-the-shelf components with higher ratings instead of employing what is calculated by using the design factor. The factor is then referred to as the *factor of safety*, n . The factor of safety has the same definition as the design factor, but it generally differs numerically.

Since stress may not vary linearly with load (see Sec. 3–19), using load as the loss-of-function parameter may not be acceptable. It is more common then to express the design factor in terms of a stress and a relevant strength. Thus Eq. (1-1) can be rewritten as

$$n_d = \frac{\text{loss-of-function strength}}{\text{allowable stress}} = \frac{S}{\sigma(\text{or } \tau)} \quad (1-3)$$

The stress and strength terms in Eq. (1–3) must be of the same type and units. Also, the stress and strength must apply to the same critical location in the part.

EXAMPLE 1–2

A rod with a cross-sectional area of A and loaded in tension with an axial force of $P = 2000$ lbf undergoes a stress of $\sigma = P/A$. Using a material strength of 24 kpsi and a *design factor* of 3.0, determine the minimum diameter of a solid circular rod. Using Table A–17, select a preferred fractional diameter and determine the rod's *factor of safety*.

Solution

Since $A = \pi d^2/4$, $\sigma = P/A$, and from Eq. (1–3), $\sigma = S/n_d$, then

$$\sigma = \frac{P}{A} = \frac{P}{\pi d^2/4} = \frac{S}{n_d}$$

Solving for d yields

Answer

$$d = \left(\frac{4Pn_d}{\pi S} \right)^{1/2} = \left(\frac{4(2000)3}{\pi(24\,000)} \right)^{1/2} = 0.564 \text{ in}$$

From Table A–17, the next higher preferred size is $\frac{5}{8}$ in = 0.625 in. Thus, when n_d is replaced with n in the equation developed above, the factor of safety n is

Answer

$$n = \frac{\pi S d^2}{4P} = \frac{\pi(24\,000)(0.625)^2}{4(2000)} = 3.68$$

Thus rounding the diameter has increased the actual design factor.

1–12 Reliability

In these days of greatly increasing numbers of liability lawsuits and the need to conform to regulations issued by governmental agencies such as EPA and OSHA, it is very important for the designer and the manufacturer to know the reliability of their product. The reliability method of design is one in which we obtain the distribution of stresses and the distribution of strengths and then relate these two in order to achieve an acceptable success rate.

The statistical measure of the probability that a mechanical element will not fail in use is called the *reliability* of that element. The reliability R can be expressed by

$$R = 1 - p_f \quad (1-4)$$

where p_f is the *probability of failure*, given by the number of instances of failures per total number of possible instances. The value of R falls in the range $0 \leq R \leq 1$. A reliability of $R = 0.90$ means that there is a 90 percent chance that the part will perform its proper function without failure. The failure of 6 parts out of every 1000 manufactured might be considered an acceptable failure rate for a certain class of products. This represents a reliability of

$$R = 1 - \frac{6}{1000} = 0.994$$

or 99.4 percent.

In the *reliability method of design*, the designer's task is to make a judicious selection of materials, processes, and geometry (size) so as to achieve a specific reliability

goal. Thus, if the objective reliability is to be 99.4 percent, as above, what combination of materials, processing, and dimensions is needed to meet this goal? If a mechanical system fails when any one component fails, the system is said to be a *series system*. If the reliability of component i is R_i in a series system of n components, then the reliability of the system is given by

$$R = \prod_{i=1}^n R_i \quad (1-5)$$

For example, consider a shaft with two bearings having reliabilities of 95 percent and 98 percent. From Eq. (1-5), the overall reliability of the shaft system is then

$$R = R_1 R_2 = 0.95 (0.98) = 0.93$$

or 93 percent.

Analyses that lead to an assessment of reliability address uncertainties, or their estimates, in parameters that describe the situation. Stochastic variables such as stress, strength, load, or size are described in terms of their means, standard deviations, and distributions. If bearing balls are produced by a manufacturing process in which a diameter distribution is created, we can say upon choosing a ball that there is uncertainty as to size. If we wish to consider weight or moment of inertia in rolling, this size uncertainty can be considered to be *propagated* to our knowledge of weight or inertia. There are ways of estimating the statistical parameters describing weight and inertia from those describing size and density. These methods are variously called *propagation of error*, *propagation of uncertainty*, or *propagation of dispersion*. These methods are integral parts of analysis or synthesis tasks when probability of failure is involved.

It is important to note that good statistical data and estimates are essential to perform an acceptable reliability analysis. This requires a good deal of testing and validation of the data. In many cases, this is not practical and a deterministic approach to the design must be undertaken.

1-13 Dimensions and Tolerances

The following terms are used generally in dimensioning:

- *Nominal size*. The size we use in speaking of an element. For example, we may specify a $1\frac{1}{2}$ -in pipe or a $\frac{1}{2}$ -in bolt. Either the theoretical size or the actual measured size may be quite different. The theoretical size of a $1\frac{1}{2}$ -in pipe is 1.900 in for the outside diameter. And the diameter of the $\frac{1}{2}$ -in bolt, say, may actually measure 0.492 in.
- *Limits*. The stated maximum and minimum dimensions.
- *Tolerance*. The difference between the two limits.
- *Bilateral tolerance*. The variation in both directions from the basic dimension. That is, the basic size is between the two limits, for example, 1.005 ± 0.002 in. The two parts of the tolerance need not be equal.
- *Unilateral tolerance*. The basic dimension is taken as one of the limits, and variation is permitted in only one direction, for example,

$$1.005^{+0.004}_{-0.000} \text{ in}$$

- *Clearance*. A general term that refers to the mating of cylindrical parts such as a bolt and a hole. The word clearance is used only when the internal member is smaller than the external member. The *diametral clearance* is the measured difference in the two diameters. The *radial clearance* is the difference in the two radii.

- **Interference.** The opposite of clearance, for mating cylindrical parts in which the internal member is larger than the external member (e.g., press-fits).
- **Allowance.** The minimum stated clearance or the maximum stated interference for mating parts.

When several parts are assembled, the gap (or interference) depends on the dimensions and tolerances of the individual parts.

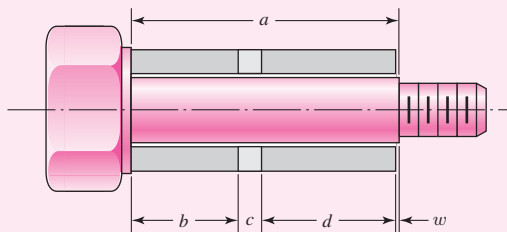
EXAMPLE 1-3

A shouldered screw contains three hollow right circular cylindrical parts on the screw before a nut is tightened against the shoulder. To sustain the function, the gap w must equal or exceed 0.003 in. The parts in the assembly depicted in Fig. 1-4 have dimensions and tolerances as follows:

$$\begin{aligned} a &= 1.750 \pm 0.003 \text{ in} & b &= 0.750 \pm 0.001 \text{ in} \\ c &= 0.120 \pm 0.005 \text{ in} & d &= 0.875 \pm 0.001 \text{ in} \end{aligned}$$

Figure 1-4

An assembly of three cylindrical sleeves of lengths a , b , and c on a shoulder bolt shank of length a . The gap w is of interest.



All parts except the part with the dimension d are supplied by vendors. The part containing the dimension d is made in-house.

- Estimate the mean and tolerance on the gap w .
- What basic value of d will assure that $w \geq 0.003$ in?

Solution

- The mean value of w is given by

Answer

$$\bar{w} = \bar{a} - \bar{b} - \bar{c} - \bar{d} = 1.750 - 0.750 - 0.120 - 0.875 = 0.005 \text{ in}$$

For equal bilateral tolerances, the tolerance of the gap is

Answer

$$t_w = \sum_{\text{all}} t = 0.003 + 0.001 + 0.005 + 0.001 = 0.010 \text{ in}$$

Then, $w = 0.005 \pm 0.010$ in, and

$$w_{\max} = \bar{w} + t_w = 0.005 + 0.010 = 0.015 \text{ in}$$

$$w_{\min} = \bar{w} - t_w = 0.005 - 0.010 = -0.005 \text{ in}$$

Thus, both clearance and interference are possible.

- If w_{\min} is to be 0.003 in, then, $\bar{w} = w_{\min} + t_w = 0.003 + 0.010 = 0.013$ in. Thus,

Answer

$$\bar{d} = \bar{a} - \bar{b} - \bar{c} - \bar{w} = 1.750 - 0.750 - 0.120 - 0.013 = 0.867 \text{ in}$$

The previous example represented an *absolute tolerance system*. Statistically, gap dimensions near the gap limits are rare events. Using a *statistical tolerance system*, the probability that the gap falls within a given limit is determined.⁷ This probability deals with the statistical distributions of the individual dimensions. For example, if the distributions of the dimensions in the previous example were normal and the tolerances, t , were given in terms of standard deviations of the dimension distribution, the standard deviation of the gap \bar{w} would be $t_w = \sqrt{\sum_{\text{all}} t^2}$. However, this assumes a normal distribution for the individual dimensions, a rare occurrence. To find the distribution of w and/or the probability of observing values of w within certain limits requires a computer simulation in most cases. *Monte Carlo* computer simulations are used to determine the distribution of w by the following approach:

- 1 Generate an instance for each dimension in the problem by selecting the value of each dimension based on its probability distribution.
- 2 Calculate w using the values of the dimensions obtained in step 1.
- 3 Repeat steps 1 and 2 N times to generate the distribution of w . As the number of trials increases, the reliability of the distribution increases.

1-14 Units

In the symbolic units equation for Newton's second law, $F = ma$,

$$F = MLT^{-2} \quad (1-6)$$

F stands for force, M for mass, L for length, and T for time. Units chosen for *any* three of these quantities are called *base* units. The first three having been chosen, the fourth unit is called a *derived* unit. When force, length, and time are chosen as base units, the mass is the derived unit and the system that results is called a *gravitational system of units*. When mass, length, and time are chosen as base units, force is the derived unit and the system that results is called an *absolute system of units*.

In some English-speaking countries, the *U.S. customary foot-pound-second system* (fps) and the *inch-pound-second system* (ips) are the two standard gravitational systems most used by engineers. In the fps system the unit of mass is

$$M = \frac{FT^2}{L} = \frac{(\text{pound-force})(\text{second})^2}{\text{foot}} = \text{lbf} \cdot \text{s}^2/\text{ft} = \text{slug} \quad (1-7)$$

Thus, length, time, and force are the three base units in the fps gravitational system.

The unit of force in the fps system is the pound, more properly the *pound-force*. We shall often abbreviate this unit as lbf; the abbreviation lb is permissible however, since we shall be dealing only with the U.S. customary gravitational system. In some branches of engineering it is useful to represent 1000 lbf as a kilopound and to abbreviate it as kip. *Note:* In Eq. (1-7) the derived unit of mass in the fps gravitational system is the $\text{lbf} \cdot \text{s}^2/\text{ft}$ and is called a *slug*; there is no abbreviation for slug.

The unit of mass in the ips gravitational system is

$$M = \frac{FT^2}{L} = \frac{(\text{pound-force})(\text{second})^2}{\text{inch}} = \text{lbf} \cdot \text{s}^2/\text{in} \quad (1-8)$$

The mass unit $\text{lbf} \cdot \text{s}^2/\text{in}$ has no official name.

⁷See Chapter 20 for a description of the statistical terminology.

The *International System of Units* (SI) is an absolute system. The base units are the meter, the kilogram (for mass), and the second. The unit of force is derived by using Newton's second law and is called the *newton*. The units constituting the newton (N) are

$$F = \frac{ML}{T^2} = \frac{(\text{kilogram})(\text{meter})}{(\text{second})^2} = \text{kg} \cdot \text{m/s}^2 = \text{N} \quad (1-9)$$

The weight of an object is the force exerted upon it by gravity. Designating the weight as W and the acceleration due to gravity as g , we have

$$W = mg \quad (1-10)$$

In the fps system, standard gravity is $g = 32.1740 \text{ ft/s}^2$. For most cases this is rounded off to 32.2. Thus the weight of a mass of 1 slug in the fps system is

$$W = mg = (1 \text{ slug})(32.2 \text{ ft/s}^2) = 32.2 \text{ lbf}$$

In the ips system, standard gravity is 386.088 or about 386 in/s^2 . Thus, in this system, a unit mass weighs

$$W = (1 \text{ lbf} \cdot \text{s}^2/\text{in})(386 \text{ in/s}^2) = 386 \text{ lbf}$$

With SI units, standard gravity is 9.806 or about 9.81 m/s. Thus, the weight of a 1-kg mass is

$$W = (1 \text{ kg})(9.81 \text{ m/s}^2) = 9.81 \text{ N}$$

A series of names and symbols to form multiples and submultiples of SI units has been established to provide an alternative to the writing of powers of 10. Table A-1 includes these prefixes and symbols.

Numbers having four or more digits are placed in groups of three and separated by a space instead of a comma. However, the space may be omitted for the special case of numbers having four digits. A period is used as a decimal point. These recommendations avoid the confusion caused by certain European countries in which a comma is used as a decimal point, and by the English use of a centered period. Examples of correct and incorrect usage are as follows:

- 1924 or 1 924 but not 1,924
- 0.1924 or 0.192 4 but not 0.192,4
- 192 423.618 50 but not 192,423.61850

The decimal point should always be preceded by a zero for numbers less than unity.

1-15 Calculations and Significant Figures

The discussion in this section applies to real numbers, not integers. The accuracy of a real number depends on the number of significant figures describing the number. Usually, but not always, three or four significant figures are necessary for engineering accuracy. Unless otherwise stated, *no less* than three significant figures should be used in your calculations. The number of significant figures is usually inferred by the number of figures given (except for leading zeros). For example, 706, 3.14, and 0.002 19 are assumed to be

numbers with three significant figures. For trailing zeros, a little more clarification is necessary. To display 706 to four significant figures insert a trailing zero and display either 706.0 , 7.060×10^2 , or 0.7060×10^3 . Also, consider a number such as 91 600. Scientific notation should be used to clarify the accuracy. For three significant figures express the number as 91.6×10^3 . For four significant figures express it as 91.60×10^3 .

Computers and calculators display calculations to many significant figures. However, you should never report a number of significant figures of a calculation any greater than the smallest number of significant figures of the numbers used for the calculation. Of course, you should use the greatest accuracy possible when performing a calculation. For example, determine the circumference of a solid shaft with a diameter of $d = 0.40$ in. The circumference is given by $C = \pi d$. Since d is given with two significant figures, C should be reported with only two significant figures. Now if we used only two significant figures for π our calculator would give $C = 3.1(0.40) = 1.24$ in. This rounds off to two significant figures as $C = 1.2$ in. However, using $\pi = 3.141\ 592\ 654$ as programmed in the calculator, $C = 3.141\ 592\ 654(0.40) = 1.256\ 637\ 061$ in. This rounds off to $C = 1.3$ in, which is 8.3 percent higher than the first calculation. Note, however, since d is given with two significant figures, it is implied that the range of d is 0.40 ± 0.005 . This means that the calculation of C is only accurate to within $\pm 0.005/0.40 = \pm 0.0125 = \pm 1.25\%$. The calculation could also be one in a series of calculations, and rounding each calculation separately may lead to an accumulation of greater inaccuracy. Thus, it is considered good engineering practice to make all calculations to the greatest accuracy possible and report the results within the accuracy of the given input.

1-16

Design Topic Interdependencies

One of the characteristics of machine design problems is the interdependencies of the various elements of a given mechanical system. For example, a change from a spur gear to a helical gear on a drive shaft would add axial components of force, which would have implications on the layout and size of the shaft, and the type and size of the bearings. Further, even within a single component, it is necessary to consider many different facets of mechanics and failure modes, such as excessive deflection, static yielding, fatigue failure, contact stress, and material characteristics. However, in order to provide significant attention to the details of each topic, most machine design textbooks focus on these topics separately and give end-of-chapter problems that relate only to that specific topic.

To help the reader see the interdependence between the various design topics, this textbook presents many ongoing and interdependent problems in the end-of-chapter problem sections. Each row of Table 1-1 shows the problem numbers that apply to the same mechanical system that is being analyzed according to the topics being presented in that particular chapter. For example, in the second row, Probs. 3-40, 5-65, and 5-66 correspond to a pin in a knuckle joint that is to be analyzed for stresses in Chap. 3 and then for static failure in Chap. 5. This is a simple example of interdependencies, but as can be seen in the table, other systems are analyzed with as many as 10 separate problems. It may be beneficial to work through some of these continuing sequences as the topics are covered to increase your awareness of the various interdependencies.

In addition to the problems given in Table 1-1, Sec. 1-17 describes a power transmission case study where various interdependent analyses are performed throughout the book, when appropriate in the presentation of the topics. The final results of the case study are then presented in Chap. 18.

Table 1-1

Problem Numbers for Linked End-of-Chapter Problems*

3-1	4-50	4-74
3-40	5-65	5-66
3-68	4-23	4-29
3-69	4-24	4-30
3-70	4-25	4-31
3-71	4-26	4-32
3-72	4-27	4-33
3-73	4-28	4-34
3-74	5-45	6-43
3-76	5-46	6-44
3-77	5-47	6-45
3-79	5-48	6-46
3-80	4-41	4-71
3-81	5-50	6-48
3-82	5-51	6-49
3-83	5-52	6-50
3-84	4-43	4-73
3-85	5-54	6-52
3-86	5-55	6-53
3-87	5-56	

*Each row corresponds to the same mechanical component repeated for a different design concept.

1-17 Power Transmission Case Study Specifications

A case study incorporating the many facets of the design process for a power transmission speed reducer will be considered throughout this textbook. The problem will be introduced here with the definition and specification for the product to be designed. Further details and component analysis will be presented in subsequent chapters. Chapter 18 provides an overview of the entire process, focusing on the design sequence, the interaction between the component designs, and other details pertinent to transmission of power. It also contains a complete case study of the power transmission speed reducer introduced here.

Many industrial applications require machinery to be powered by engines or electric motors. The power source usually runs most efficiently at a narrow range of rotational speed. When the application requires power to be delivered at a slower speed than supplied by the motor, a speed reducer is introduced. The speed reducer should transmit the power from the motor to the application with as little energy loss as practical, while reducing the speed and consequently increasing the torque. For example, assume that a company wishes to provide off-the-shelf speed reducers in various capacities and speed ratios to sell to a wide variety of target applications. The marketing team has

determined a need for one of these speed reducers to satisfy the following customer requirements.

Design Requirements

- Power to be delivered: 20 hp
- Input speed: 1750 rev/min
- Output speed: 85 rev/min
- Targeted for uniformly loaded applications, such as conveyor belts, blowers, and generators
- Output shaft and input shaft in-line
- Base mounted with 4 bolts
- Continuous operation
- 6-year life, with 8 hours/day, 5 days/wk
- Low maintenance
- Competitive cost
- Nominal operating conditions of industrialized locations
- Input and output shafts standard size for typical couplings

In reality, the company would likely design for a whole range of speed ratios for each power capacity, obtainable by interchanging gear sizes within the same overall design. For simplicity, in this case study only one speed ratio will be considered.

Notice that the list of customer requirements includes some numerical specifics, but also includes some generalized requirements, e.g., low maintenance and competitive cost. These general requirements give some guidance on what needs to be considered in the design process, but are difficult to achieve with any certainty. In order to pin down these nebulous requirements, it is best to further develop the customer requirements into a set of product specifications that are measurable. This task is usually achieved through the work of a team including engineering, marketing, management, and customers. Various tools may be used (see footnote 1, p. 7) to prioritize the requirements, determine suitable metrics to be achieved, and to establish target values for each metric. The goal of this process is to obtain a product specification that identifies precisely what the product must satisfy. The following product specifications provide an appropriate framework for this design task.

Design Specifications

- Power to be delivered: 20 hp
- Power efficiency: >95%
- Steady state input speed: 1750 rev/min
- Maximum input speed: 2400 rev/min
- Steady-state output speed: 82–88 rev/min
- Usually low shock levels, occasional moderate shock
- Input and output shafts extend 4 in outside gearbox
- Input and output shaft diameter tolerance: ± 0.001 in
- Input and output shafts in-line: concentricity ± 0.005 in, alignment ± 0.001 rad
- Maximum allowable loads on input shaft: axial, 50 lbf; transverse, 100 lbf
- Maximum allowable loads on output shaft: axial, 50 lbf; transverse, 500 lbf
- Maximum gearbox size: 14-in \times 14-in base, 22-in height
- Base mounted with 4 bolts
- Mounting orientation only with base on bottom
- 100% duty cycle

Maintenance schedule: lubrication check every 2000 hours; change of lubrication every 8000 hours of operation; gears and bearing life >12,000 hours; infinite shaft life; gears, bearings, and shafts replaceable

Access to check, drain, and refill lubrication without disassembly or opening of gasketed joints.

Manufacturing cost per unit: <\$300

Production: 10,000 units per year

Operating temperature range: -10° to 120°F

Sealed against water and dust from typical weather

Noise: <85 dB from 1 meter

PROBLEMS

- 1-1** Select a mechanical component from Part 3 of this book (roller bearings, springs, etc.), go to your university's library or the appropriate internet website, and, using the *Thomas Register of American Manufacturers* (www.thomasnet.com), report on the information obtained on five manufacturers or suppliers.
- 1-2** Select a mechanical component from Part 3 of this book (roller bearings, springs, etc.), go to the Internet, and, using a search engine, report on the information obtained on five manufacturers or suppliers.
- 1-3** Select an organization listed in Sec. 1-6, go to the Internet, and list what information is available on the organization.
- 1-4** Go to the Internet and connect to the NSPE website (www.nspe.org/ethics). Read the history of the *Code of Ethics* and briefly discuss your reading.
- 1-5** Go to the Internet and connect to the NSPE website (www.nspe.org/ethics). Read the complete *NSPE Code of Ethics for Engineers* and briefly discuss your reading.
- 1-6** Go to the Internet and connect to the NSPE website (www.nspe.org/ethics). Go to *Ethics Resources* and review one or more of the topics given. A sample of some of the topics may be:
- (a) Education Publications
 - (b) Ethics Case Search
 - (c) Ethics Exam
 - (d) FAQ
 - (e) Milton Lunch Contest
 - (f) Other Resources
 - (g) You Be the Judge
- Briefly discuss your reading.
- 1-7** Estimate the relative cost of grinding a steel part to a tolerance of ± 0.0005 in versus turning it to a tolerance of ± 0.003 in.
- 1-8** The costs to manufacture a part using methods *A* and *B* are estimated by $C_A = 10 + 0.8 P$ and $C_B = 60 + 0.8 P - 0.005 P^2$ respectively, where the cost *C* is in dollars and *P* is the number of parts. Estimate the break-even point.
- 1-9** A cylindrical part of diameter *d* is loaded by an axial force *P*. This causes a stress of *P/A*, where $A = \pi d^2/4$. If the load is known with an uncertainty of ± 10 percent, the diameter is known within ± 5 percent (tolerances), and the stress that causes failure (strength) is known within ± 15 percent, determine the minimum design factor that will guarantee that the part will not fail.

- 1-10** When one knows the true values x_1 and x_2 and has approximations X_1 and X_2 at hand, one can see where errors may arise. By viewing error as something to be added to an approximation to attain a true value, it follows that the error e_i , is related to X_i , and x_i as $x_i = X_i + e_i$
- (a) Show that the error in a sum $X_1 + X_2$ is

$$(x_1 + x_2) - (X_1 + X_2) = e_1 + e_2$$

- (b) Show that the error in a difference $X_1 - X_2$ is

$$(x_1 - x_2) - (X_1 - X_2) = e_1 - e_2$$

- (c) Show that the error in a product $X_1 X_2$ is

$$x_1 x_2 - X_1 X_2 = X_1 X_2 \left(\frac{e_1}{X_1} + \frac{e_2}{X_2} \right)$$

- (d) Show that in a quotient X_1/X_2 the error is

$$\frac{x_1}{x_2} - \frac{X_1}{X_2} = \frac{X_1}{X_2} \left(\frac{e_1}{X_1} - \frac{e_2}{X_2} \right)$$

- 1-11** Use the true values $x_1 = \sqrt{7}$ and $x_2 = \sqrt{8}$
- (a) Demonstrate the correctness of the error equation from Prob. 1-10 for addition if three correct digits are used for X_1 and X_2 .
- (b) Demonstrate the correctness of the error equation for addition using three-digit significant numbers for X_1 and X_2 .

- 1-12** A solid circular rod of diameter d undergoes a bending moment $M = 1000$ lbf · in inducing a stress $\sigma = 16M/(\pi d^3)$. Using a material strength of 25 kpsi and a *design factor* of 2.5, determine the minimum diameter of the rod. Using Table A-17 select a preferred fractional diameter and determine the resulting *factor of safety*.

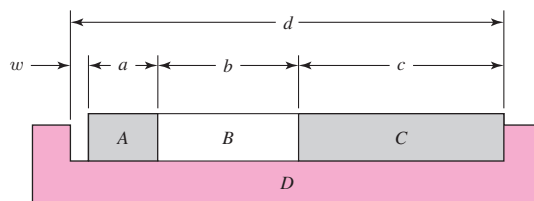
- 1-13** A mechanical system comprises three subsystems in series with reliabilities of 98, 96, and 94 percent. What is the overall reliability of the system?

- 1-14** Three blocks A , B , and C and a grooved block D have dimensions a , b , c , and d as follows:

$$a = 1.500 \pm 0.001 \text{ in} \quad b = 2.000 \pm 0.003 \text{ in}$$

$$c = 3.000 \pm 0.004 \text{ in} \quad d = 6.520 \pm 0.010 \text{ in}$$

Problem 1-14



- (a) Determine the mean gap \bar{w} and its tolerance.
 (b) Determine the mean size of d that will assure that $w \geq 0.010$ in.

- 1-15** The volume of a rectangular parallelepiped is given by $V = xyz$. If $x = a \pm \Delta a$, $y = b \pm \Delta b$, $z = c \pm \Delta c$, show that

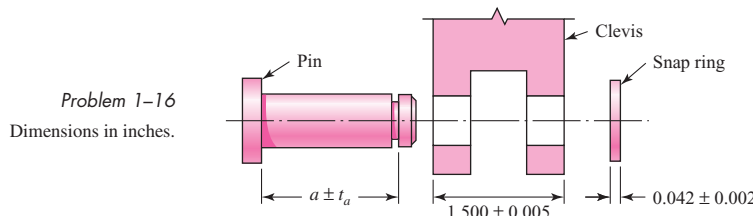
$$\frac{\Delta V}{\bar{V}} = \frac{\Delta a}{\bar{a}} + \frac{\Delta b}{\bar{b}} + \frac{\Delta c}{\bar{c}}$$

Use this result to determine the bilateral tolerance on the volume of a rectangular parallelepiped with dimensions

$$a = 1.500 \pm 0.002 \text{ in} \quad b = 1.875 \pm 0.003 \text{ in} \quad c = 3.000 \pm 0.004 \text{ in}$$

1-16

A pivot in a linkage has a pin in the figure whose dimension $a \pm t_a$ is to be established. The thickness of the link clevis is 1.500 ± 0.005 in. The designer has concluded that a gap of between 0.004 and 0.05 in will satisfactorily sustain the function of the linkage pivot. Determine the dimension a and its tolerance.



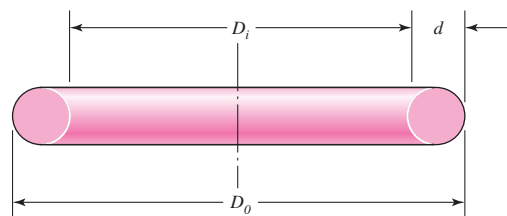
1-17

A circular cross section O ring has the dimensions shown in the figure. In particular, an AS 568A standard No. 240 O ring has an inside diameter D_i and a cross-section diameter d of

$$D_i = 3.734 \pm 0.028 \text{ in} \quad d = 0.139 \pm 0.004 \text{ in}$$

Estimate the mean outside diameter \bar{D}_o and its bilateral tolerance.

Problem 1-17



1-18 to 1-21

For the table given, repeat Prob. 1-17 for the following O rings, given the AS 568A standard number. Solve Problems 1-18 and 1-19 using SI units. Solve Problems 1-20 and 1-21 using ips units. *Note:* The solutions require research.

Problem number	1-18	1-19	1-20	1-21
AS 568A No.	110	220	160	320

1-22

Convert the following to appropriate ips units:

- (a) A stress, $\sigma = 150 \text{ MPa}$.
- (b) A force, $F = 2 \text{ kN}$.
- (c) A moment, $M = 150 \text{ N} \cdot \text{m}$.
- (d) An area, $A = 1500 \text{ mm}^2$.
- (e) A second moment of area, $I = 750 \text{ cm}^4$.
- (f) A modulus of elasticity, $E = 145 \text{ GPa}$.
- (g) A speed, $v = 75 \text{ km/h}$.
- (h) A volume, $V = 1 \text{ liter}$.

1-23 Convert the following to appropriate SI units:

- (a) A length, $l = 5 \text{ ft}$.
- (b) A stress, $\sigma = 90 \text{ kpsi}$.
- (c) A pressure, $p = 25 \text{ psi}$.
- (d) A section modulus, $Z = 12 \text{ in}^3$.
- (e) A unit weight, $w = 0.208 \text{ lbf/in}$.
- (f) A deflection, $\delta = 0.001\ 89 \text{ in}$.
- (g) A velocity, $v = 1\ 200 \text{ ft/min}$.
- (h) A unit strain, $\epsilon = 0.002\ 15 \text{ in/in}$.
- (i) A volume, $V = 1830 \text{ in}^3$.

1-24 Generally, final design results are rounded to or fixed to three digits because the given data cannot justify a greater display. In addition, prefixes should be selected so as to limit number strings to no more than four digits to the left of the decimal point. Using these rules, as well as those for the choice of prefixes, solve the following relations:

- (a) $\sigma = M/Z$, where $M = 1770 \text{ lbf} \cdot \text{in}$ and $Z = 0.934 \text{ in}^3$.
- (b) $\sigma = F/A$, where $F = 9440 \text{ lbf}$ and $A = 23.8 \text{ in}^2$.
- (c) $y = Fl^3/3EI$, where $F = 270 \text{ lbf}$, $l = 31.5 \text{ in}$, $E = 30 \text{ Mpsi}$, and $I = 0.154 \text{ in}^4$.
- (d) $\theta = Tl/GJ$, where $T = 9\ 740 \text{ lbf} \cdot \text{in}$, $l = 9.85 \text{ in}$, $G = 11.3 \text{ Mpsi}$, and $d = 1.00 \text{ in}$.

1-25 Repeat Prob. 1-24 for the following:

- (a) $\sigma = F/wt$, where $F = 1 \text{ kN}$, $w = 25 \text{ mm}$, and $t = 5 \text{ mm}$.
- (b) $I = bh^3/12$, where $b = 10 \text{ mm}$ and $h = 25 \text{ mm}$.
- (c) $I = \pi d^4/64$, where $d = 25.4 \text{ mm}$.
- (d) $\tau = 16 T/\pi d^3$, where $T = 25 \text{ N} \cdot \text{m}$, and $d = 12.7 \text{ mm}$.

1-26 Repeat Prob. 1-24 for:

- (a) $\tau = F/A$, where $A = \pi d^2/4$, $F = 2\ 700 \text{ lbf}$, and $d = 0.750 \text{ in}$.
- (b) $\sigma = 32 Fa/\pi d^3$, where $F = 180 \text{ lbf}$, $a = 31.5 \text{ in}$, and $d = 1.25 \text{ in}$.
- (c) $Z = \pi(d_o^4 - d_i^4)/(32 d_o)$ for $d_o = 1.50 \text{ in}$ and $d_i = 1.00 \text{ in}$.
- (d) $k = (d^4 G)/(8 D^3 N)$, where $d = 0.062\ 5 \text{ in}$, $G = 11.3 \text{ Mpsi}$, $D = 0.760 \text{ in}$, and $N = 32$
(a dimensionless number).

This page intentionally left blank

2 Materials

Chapter Outline

2-1	Material Strength and Stiffness	32
2-2	The Statistical Significance of Material Properties	36
2-3	Strength and Cold Work	38
2-4	Hardness	41
2-5	Impact Properties	42
2-6	Temperature Effects	43
2-7	Numbering Systems	45
2-8	Sand Casting	46
2-9	Shell Molding	47
2-10	Investment Casting	47
2-11	Powder-Metallurgy Process	47
2-12	Hot-Working Processes	47
2-13	Cold-Working Processes	48
2-14	The Heat Treatment of Steel	49
2-15	Alloy Steels	52
2-16	Corrosion-Resistant Steels	53
2-17	Casting Materials	54
2-18	Nonferrous Metals	55
2-19	Plastics	58
2-20	Composite Materials	60
2-21	Materials Selection	61

The selection of a material for a machine part or a structural member is one of the most important decisions the designer is called on to make. The decision is usually made before the dimensions of the part are established. After choosing the process of creating the desired geometry and the material (the two cannot be divorced), the designer can proportion the member so that loss of function can be avoided or the chance of loss of function can be held to an acceptable risk.

In Chaps. 3 and 4, methods for estimating stresses and deflections of machine members are presented. These estimates are based on the properties of the material from which the member will be made. For deflections and stability evaluations, for example, the elastic (stiffness) properties of the material are required, and evaluations of stress at a critical location in a machine member require a comparison with the strength of the material at that location in the geometry and condition of use. This strength is a material property found by testing and is adjusted to the geometry and condition of use as necessary.

As important as stress and deflection are in the design of mechanical parts, the selection of a material is not always based on these factors. Many parts carry no loads on them whatever. Parts may be designed merely to fill up space or for aesthetic qualities. Members must frequently be designed to also resist corrosion. Sometimes temperature effects are more important in design than stress and strain. So many other factors besides stress and strain may govern the design of parts that the designer must have the versatility that comes only with a broad background in materials and processes.

2-1

Material Strength and Stiffness

The standard tensile test is used to obtain a variety of material characteristics and strengths that are used in design. Figure 2-1 illustrates a typical tension-test specimen and its characteristic dimensions.¹ The original diameter d_0 and the gauge length l_0 , used to measure the deflections, are recorded before the test is begun. The specimen is then mounted in the test machine and slowly loaded in tension while the load P and deflection are observed. The load is converted to stress by the calculation

$$\sigma = \frac{P}{A_0} \quad (2-1)$$

where $A_0 = \frac{1}{4}\pi d_0^2$ is the original area of the specimen.

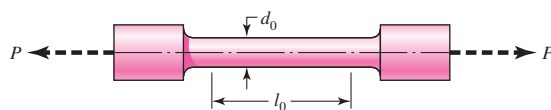


Figure 2-1

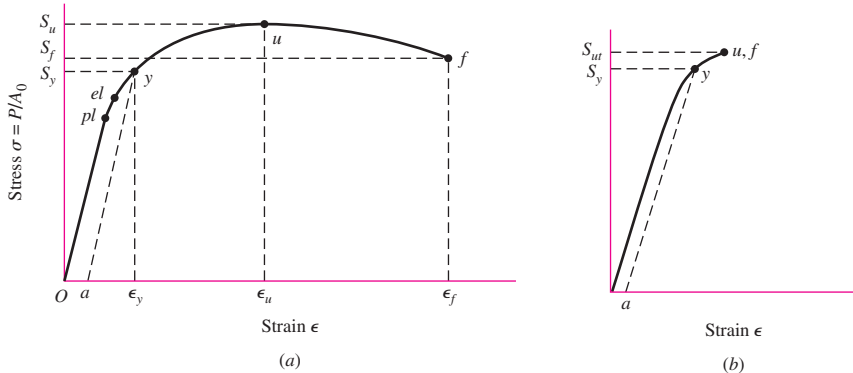
A typical tension-test specimen. Some of the standard dimensions used for d_0 are 2.5, 6.25, and 12.5 mm and 0.505 in, but other sections and sizes are in use. Common gauge lengths l_0 used are 10, 25, and 50 mm and 1 and 2 in.

¹See ASTM standards E8 and E-8 m for standard dimensions.

Figure 2–2

Stress-strain diagram obtained from the standard tensile test
(a) Ductile material; (b) brittle material.

pl marks the proportional limit; *el*, the elastic limit; *y*, the offset-yield strength as defined by offset strain *a*; *u*, the maximum or ultimate strength; and *f*, the fracture strength.



The deflection, or extension of the gauge length, is given by $l - l_0$ where l is the gauge length corresponding to the load P . The normal strain is calculated from

$$\epsilon = \frac{l - l_0}{l_0} \quad (2-2)$$

The results are plotted as a *stress-strain diagram*. Figure 2–2 depicts typical stress-strain diagrams for ductile and brittle materials. Ductile materials deform much more than brittle materials.

Point *pl* in Fig. 2–2a is called the *proportional limit*. This is the point at which the curve first begins to deviate from a straight line. No permanent set will be observable in the specimen if the load is removed at this point. In the linear range, the uniaxial stress-strain relation is given by *Hooke's law* as

$$\sigma = E\epsilon \quad (2-3)$$

where the constant of proportionality E , the slope of the linear part of the stress-strain curve, is called *Young's modulus* or the *modulus of elasticity*. E is a measure of the stiffness of a material, and since strain is dimensionless, the units of E are the same as stress. Steel, for example, has a modulus of elasticity of about 30 Mpsi (207 GPa) *regardless of heat treatment, carbon content, or alloying*. Stainless steel is about 27.5 Mpsi (190 GPa).

Point *el* in Fig. 2–2 is called the *elastic limit*. If the specimen is loaded beyond this point, the deformation is said to be plastic and the material will take on a permanent set when the load is removed. Between *pl* and *el* the diagram is not a perfectly straight line, even though the specimen is elastic.

During the tension test, many materials reach a point at which the strain begins to increase very rapidly without a corresponding increase in stress. This point is called the *yield point*. Not all materials have an obvious yield point, especially for brittle materials. For this reason, *yield strength* S_y is often defined by an *offset method* as shown in Fig. 2–2, where line *ay* is drawn at slope E . Point *a* corresponds to a definite or stated amount of permanent set, usually 0.2 percent of the original gauge length ($\epsilon = 0.002$), although 0.01, 0.1, and 0.5 percent are sometimes used.

The *ultimate*, or *tensile*, *strength* S_u or S_{ut} corresponds to point *u* in Fig. 2–2 and is the maximum stress reached on the stress-strain diagram.² As shown in Fig. 2–2a,

²Usage varies. For a long time engineers used the term *ultimate strength*, hence the subscript *u* in S_u or S_{ut} . However, in material science and metallurgy the term *tensile strength* is used.

some materials exhibit a downward trend after the maximum stress is reached and fracture at point *f* on the diagram. Others, such as some of the cast irons and high-strength steels, fracture while the stress-strain trace is still rising, as shown in Fig. 2-2*b*, where points *u* and *f* are identical.

As noted in Sec. 1-9, *strength*, as used in this book, is a built-in property of a material, or of a mechanical element, because of the selection of a particular material or process or both. The strength of a connecting rod at the critical location in the geometry and condition of use, for example, is the same no matter whether it is already an element in an operating machine or whether it is lying on a workbench awaiting assembly with other parts. On the other hand, *stress* is something that occurs in a part, usually as a result of its being assembled into a machine and loaded. However, stresses may be built into a part by processing or handling. For example, shot peening produces a compressive *stress* in the outer surface of a part, and also improves the fatigue strength of the part. Thus, in this book we will be very careful in distinguishing between *strength*, designated by *S*, and *stress*, designated by σ or τ .

The diagrams in Fig. 2-2 are called *engineering stress-strain diagrams* because the stresses and strains calculated in Eqs. (2-1) and (2-2) are not *true* values. The stress calculated in Eq. (2-1) is based on the original area *before* the load is applied. In reality, as the load is applied the area reduces so that the *actual* or *true stress* is larger than the *engineering stress*. To obtain the true stress for the diagram the load and the cross-sectional area must be measured simultaneously during the test. Figure 2-2*a* represents a ductile material where the stress appears to decrease from points *u* to *f*. Typically, beyond point *u* the specimen begins to “neck” at a location of weakness where the area reduces dramatically, as shown in Fig. 2-3. For this reason, the true stress is much higher than the engineering stress at the necked section.

The engineering strain given by Eq. (2-2) is based on net change in length from the *original* length. In plotting the *true stress-strain diagram*, it is customary to use a term called *true strain* or, sometimes, *logarithmic strain*. True strain is the sum of the incremental elongations divided by the *current gauge length* at load *P*, or

$$\varepsilon = \int_{l_0}^l \frac{dl}{l} = \ln \frac{l}{l_0} \quad (2-4)$$

where the symbol ε is used to represent true strain. The most important characteristic of a true stress-strain diagram (Fig. 2-4) is that the true stress continually increases all the way to fracture. Thus, as shown in Fig. 2-4, the true fracture stress σ_f is greater than the true ultimate stress σ_u . Contrast this with Fig. 2-2*a*, where the engineering fracture strength S_f is less than the engineering ultimate strength S_u .

Compression tests are more difficult to conduct, and the geometry of the test specimens differs from the geometry of those used in tension tests. The reason for this is that the specimen may buckle during testing or it may be difficult to distribute the stresses evenly. Other difficulties occur because ductile materials will bulge after yielding. However, the results can be plotted on a stress-strain diagram also, and the same strength definitions can be applied as used in tensile testing. For most ductile materials the compressive strengths are about the same as the tensile strengths. When substantial differences occur between tensile and compressive strengths, however, as is the case with

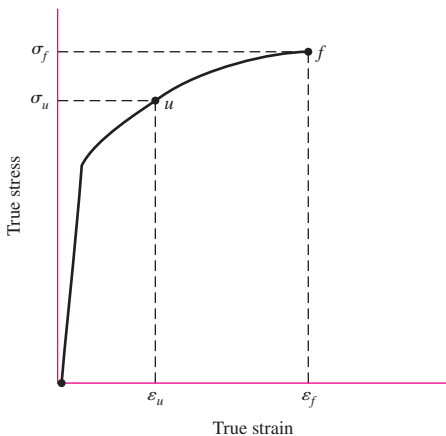
Figure 2-3

Tension specimen after necking.



Figure 2–4

True stress-strain diagram plotted in Cartesian coordinates.



the cast irons, the tensile and compressive strengths should be stated separately, S_{ut} , S_{uc} , where S_{uc} is reported as a *positive* quantity.

Torsional strengths are found by twisting solid circular bars and recording the torque and the twist angle. The results are then plotted as a *torque-twist diagram*. The shear stresses in the specimen are linear with respect to radial location, being zero at the center of the specimen and maximum at the outer radius r (see Chap. 3). The maximum shear stress τ_{\max} is related to the angle of twist θ by

$$\tau_{\max} = \frac{Gr}{l_0}\theta \quad (2-5)$$

where θ is in radians, r is the radius of the specimen, l_0 is the gauge length, and G is the material stiffness property called the *shear modulus* or the *modulus of rigidity*. The maximum shear stress is also related to the applied torque T as

$$\tau_{\max} = \frac{Tr}{J} \quad (2-6)$$

where $J = \frac{1}{2}\pi r^4$ is the polar second moment of area of the cross section.

The torque-twist diagram will be similar to Fig. 2–2, and, using Eqs. (2–5) and (2–6), the modulus of rigidity can be found as well as the elastic limit and the *torsional yield strength* S_{sy} . The maximum point on a torque-twist diagram, corresponding to point u on Fig. 2–2, is T_u . The equation

$$S_{su} = \frac{T_u r}{J} \quad (2-7)$$

defines the *modulus of rupture* for the torsion test. Note that it is incorrect to call S_{su} the ultimate torsional strength, as the outermost region of the bar is in a plastic state at the torque T_u and the stress distribution is no longer linear.

All of the stresses and strengths defined by the stress-strain diagram of Fig. 2–2 and similar diagrams are specifically known as *engineering stresses* and *strengths* or *nominal stresses* and *strengths*. These are the values normally used in all engineering design calculations. The adjectives *engineering* and *nominal* are used here to emphasize that the stresses are computed by using the *original* or *unstressed cross-sectional area* of the specimen. In this book we shall use these modifiers only when we specifically wish to call attention to this distinction.

In addition to providing strength values for a material, the stress-strain diagram provides insight into the energy-absorbing characteristics of a material. This is because the stress-strain diagram involves both loads and deflections, which are directly related to energy. The capacity of a material to absorb energy within its elastic range is called *resilience*. The *modulus of resilience* u_R of a material is defined as the energy absorbed per unit volume without permanent deformation, and is equal to the area under the stress-strain curve up to the elastic limit. The elastic limit is often approximated by the yield point, since it is more readily determined, giving

$$u_R \cong \int_0^{\epsilon_y} \sigma d\epsilon \quad (2-8)$$

where ϵ_y is the strain at the yield point. If the stress-strain is linear to the yield point, then the area under the curve is simply a triangular area; thus

$$u_R \cong \frac{1}{2} S_y \epsilon_y = \frac{1}{2} (S_y)(S_y/E) = \frac{S_y^2}{2E} \quad (2-9)$$

This relationship indicates that for two materials with the same yield strength, the less stiff material (lower E), will have a greater resilience, that is, an ability to absorb more energy without yielding.

The capacity of a material to absorb energy without fracture is called *toughness*. The *modulus of toughness* u_T of a material is defined as the energy absorbed per unit volume without fracture, which is equal to the total area under the stress-strain curve up to the fracture point, or

$$u_T = \int_0^{\epsilon_f} \sigma d\epsilon \quad (2-10)$$

where ϵ_f is the strain at the fracture point. This integration is often performed graphically from the stress-strain data, or a rough approximation can be obtained by using the average of the yield and ultimate strengths and the strain at fracture to calculate an area; that is,

$$u_T \cong \left(\frac{S_y + S_{ut}}{2} \right) \epsilon_f \quad (2-11)$$

The units of toughness and resilience are energy per unit volume ($\text{lbf} \cdot \text{in}/\text{in}^3$ or J/m^3), which are numerically equivalent to psi or Pa. These definitions of toughness and resilience assume the low strain rates that are suitable for obtaining the stress-strain diagram. For higher strain rates, see Sec. 2–5 for impact properties.

2–2 The Statistical Significance of Material Properties

There is some subtlety in the ideas presented in the previous section that should be pondered carefully before continuing. Figure 2–2 depicts the result of a *single* tension test (*one* specimen, now fractured). It is common for engineers to consider these important stress values (at points pl , el , y , u , and f) as properties and to denote them as strengths with a special notation, uppercase S , in lieu of lowercase sigma σ , with subscripts added: S_{pl} for proportional limit, S_y for yield strength, S_u for ultimate tensile strength (S_{ut} or S_{uc} , if tensile or compressive sense is important).

If there were 1000 nominally identical specimens, the values of strength obtained would be distributed between some minimum and maximum values. It follows that the

description of strength, a material property, is distributional and thus is statistical in nature. Chapter 20 provides more detail on statistical considerations in design. Here we will simply describe the results of one example, Ex. 20–4. Consider the following table, which is a histographic report containing the maximum stresses of 1000 tensile tests on a 1020 steel from a single heat. Here we are seeking the ultimate tensile strength S_{ut} . The class frequency is the number of occurrences within a 1 kpsi range given by the class midpoint. For example, 18 maximum stress values occurred in the range of 57 to 58 kpsi.

Class Frequency f_i	2	18	23	31	83	109	138	151	139	130	82	49	28	11	4	2
Class Midpoint x_i , kpsi	56.5	57.5	58.5	59.5	60.5	61.5	62.5	63.5	64.5	65.5	66.5	67.5	68.5	69.5	70.5	71.5

The *probability density* is defined as the number of occurrences divided by the total sample number. The bar chart in Fig. 2–5 depicts the histogram of the probability density. If the data is in the form of a *Gaussian* or *normal distribution*, the *probability density function* determined in Ex. 20–4 is

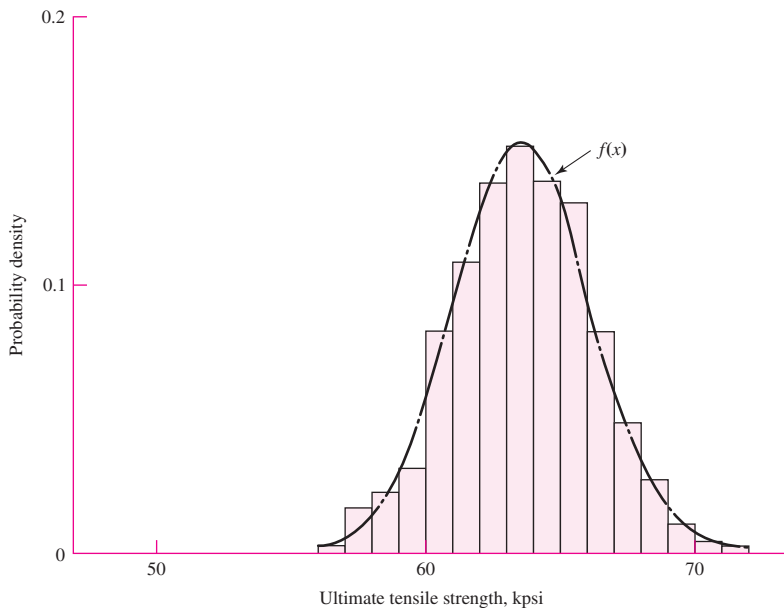
$$f(x) = \frac{1}{2.594\sqrt{2\pi}} \exp\left[-\frac{1}{2}\left(\frac{x - 63.62}{2.594}\right)^2\right]$$

where the mean stress is 63.62 kpsi and the standard deviation is 2.594 kpsi. A plot of $f(x)$ is also included in Fig. 2–5. The description of the strength S_{ut} is then expressed in terms of its statistical parameters and its distribution type. In this case $S_{ut} = N(63.62, 2.594)$ kpsi, indicating a normal distribution with a mean stress of 63.62 kpsi and a standard deviation of 2.594 kpsi.

Note that the test program has described 1020 property S_{ut} , for only one heat of one supplier. Testing is an involved and expensive process. Tables of properties are often prepared to be helpful to other persons. A statistical quantity is described by its

Figure 2–5

Histogram for 1000 tensile tests on a 1020 steel from a single heat.



mean, standard deviation, and distribution type. Many tables display a single number, which is often the mean, minimum, or some percentile, such as the 99th percentile. Always read the footnotes to the table. If no qualification is made in a single-entry table, the table is subject to serious doubt.

Since it is no surprise that useful descriptions of a property are statistical in nature, engineers, when ordering property tests, should couch the instructions so the data generated are enough for them to observe the statistical parameters and to identify the distributional characteristic. The tensile test program on 1000 specimens of 1020 steel is a large one. If you were faced with putting something in a table of ultimate tensile strengths and constrained to a single number, what would it be and just how would your footnote read?

2–3

Strength and Cold Work

Cold working is the process of plastic straining below the recrystallization temperature in the plastic region of the stress-strain diagram. Materials can be deformed plastically by the application of heat, as in forging or hot rolling, but the resulting mechanical properties are quite different from those obtained by cold working. The purpose of this section is to explain what happens to the significant mechanical properties of a material when that material is cold worked.

Consider the stress-strain diagram of Fig. 2–6a. Here a material has been stressed beyond the yield strength at y to some point i , in the plastic region, and then the load removed. At this point the material has a permanent plastic deformation ϵ_p . If the load corresponding to point i is now reapplied, the material will be elastically deformed by the amount ϵ_e . Thus at point i the total unit strain consists of the two components ϵ_p and ϵ_e and is given by the equation

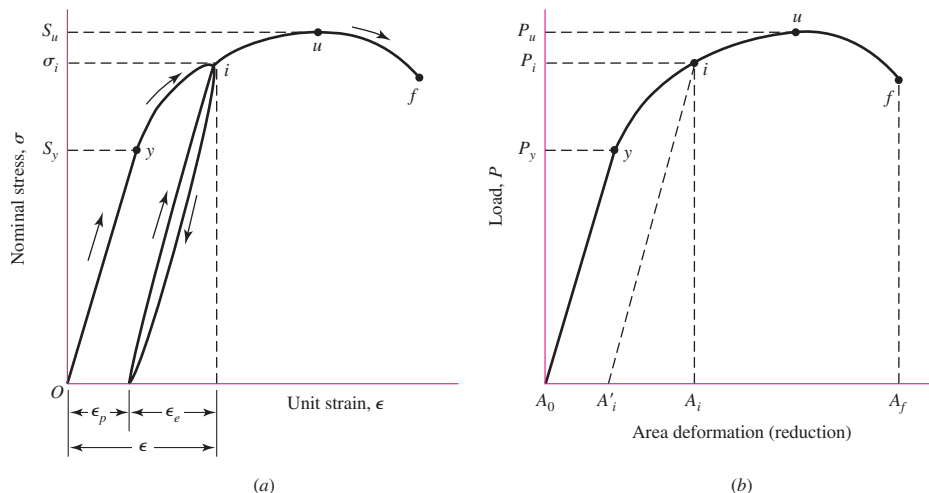
$$\epsilon = \epsilon_p + \epsilon_e \quad (a)$$

This material can be unloaded and reloaded any number of times from and to point i , and it is found that the action always occurs along the straight line that is approximately parallel to the initial elastic line Oy . Thus

$$\epsilon_e = \frac{\sigma_i}{E} \quad (b)$$

Figure 2–6

(a) Stress-strain diagram showing unloading and reloading at point i in the plastic region; (b) analogous load-deformation diagram.



The material now has a higher yield point, is less ductile as a result of a reduction in strain capacity, and is said to be *strain-hardened*. If the process is continued, increasing ϵ_p , the material can become brittle and exhibit sudden fracture.

It is possible to construct a similar diagram, as in Fig. 2–6b, where the abscissa is the area deformation and the ordinate is the applied load. The *reduction in area* corresponding to the load P_f , at fracture, is defined as

$$R = \frac{A_0 - A_f}{A_0} = 1 - \frac{A_f}{A_0} \quad (2-12)$$

where A_0 is the original area. The quantity R in Eq. (2–12) is usually expressed in percent and tabulated in lists of mechanical properties as a measure of *ductility*. See Appendix Table A–20, for example. Ductility is an important property because it measures the ability of a material to absorb overloads and to be cold-worked. Thus such operations as bending, drawing, heading, and stretch forming are metal-processing operations that require ductile materials.

Figure 2–6b can also be used to define the quantity of cold work. The *cold-work factor* W is defined as

$$W = \frac{A_0 - A'_i}{A_0} \approx \frac{A_0 - A_i}{A_0} \quad (2-13)$$

where A'_i corresponds to the area after the load P_i has been released. The approximation in Eq. (2–13) results because of the difficulty of measuring the small diametral changes in the elastic region. If the amount of cold work is known, then Eq. (2–13) can be solved for the area A'_i . The result is

$$A'_i = A_0(1 - W) \quad (2-14)$$

Cold working a material produces a new set of values for the strengths, as can be seen from stress-strain diagrams. Datsko³ describes the plastic region of the true stress–true strain diagram by the equation

$$\sigma = \sigma_0 \varepsilon^m \quad (2-15)$$

where σ = true stress

σ_0 = a strength coefficient, or strain-strengthening coefficient

ε = true plastic strain

m = strain-strengthening exponent

It can be shown⁴ that

$$m = \varepsilon_u \quad (2-16)$$

provided that the load-deformation curve exhibits a stationary point (a place of zero slope).

³Joseph Datsko, "Solid Materials," Chap. 32 in Joseph E. Shigley, Charles R. Mischke, and Thomas H. Brown, Jr. (eds.), *Standard Handbook of Machine Design*, 3rd ed., McGraw-Hill, New York, 2004. See also Joseph Datsko, "New Look at Material Strength," *Machine Design*, vol. 58, no. 3, Feb. 6, 1986, pp. 81–85.

⁴See Sec. 5–2, J. E. Shigley and C. R. Mischke, *Mechanical Engineering Design*, 6th ed., McGraw-Hill, New York, 2001.

Difficulties arise when using the gauge length to evaluate the true strain in the plastic range, since necking causes the strain to be nonuniform. A more satisfactory relation can be obtained by using the area at the neck. Assuming that the change in volume of the material is small, $Al = A_0 l_0$. Thus, $l/l_0 = A_0/A$, and the true strain is given by

$$\varepsilon = \ln \frac{l}{l_0} = \ln \frac{A_0}{A} \quad (2-17)$$

Returning to Fig. 2-6b, if point i is to the left of point u , that is, $P_i < P_u$, then the new yield strength is

$$S'_y = \frac{P_i}{A'_i} = \sigma_0 \varepsilon_i^m \quad P_i \leq P_u \quad (2-18)$$

Because of the reduced area, that is, because $A'_i < A_0$, the ultimate strength also changes, and is

$$S'_u = \frac{P_u}{A'_i} \quad (c)$$

Since $P_u = S_u A_0$, we find, with Eq. (2-14), that

$$S'_u = \frac{S_u A_0}{A_0(1-W)} = \frac{S_u}{1-W} \quad \varepsilon_i \leq \varepsilon_u \quad (2-19)$$

which is valid only when point i is to the left of point u .

For points to the right of u , the yield strength is approaching the ultimate strength, and, with small loss in accuracy,

$$S'_u \doteq S'_y \doteq \sigma_0 \varepsilon_i^m \quad \varepsilon_i > \varepsilon_u \quad (2-20)$$

A little thought will reveal that a bar will have the same ultimate load in tension after being strain-strengthened in tension as it had before. The new strength is of interest to us not because the static ultimate load increases, but—since fatigue strengths are correlated with the local ultimate strengths—because the fatigue strength improves. Also the yield strength increases, giving a larger range of sustainable *elastic* loading.

EXAMPLE 2-1

An annealed AISI 1018 steel (see Table A-22) has $S_y = 32.0$ kpsi, $S_u = 49.5$ kpsi, $\sigma_f = 91.1$ kpsi, $\sigma_0 = 90$ kpsi, $m = 0.25$, and $\varepsilon_f = 1.05$ in/in. Find the new values of the strengths if the material is given 15 percent cold work.

Solution

From Eq. (2-16), we find the true strain corresponding to the ultimate strength to be

$$\varepsilon_u = m = 0.25$$

The ratio A_0/A_i is, from Eq. (2-13),

$$\frac{A_0}{A_i} = \frac{1}{1-W} = \frac{1}{1-0.15} = 1.176$$

The true strain corresponding to 15 percent cold work is obtained from Eq. (2–17). Thus

$$\varepsilon_i = \ln \frac{A_0}{A_i} = \ln 1.176 = 0.1625$$

Since $\varepsilon_i < \varepsilon_u$, Eqs. (2–18) and (2–19) apply. Therefore,

Answer

$$S'_y = \sigma_0 \varepsilon_i^m = 90(0.1625)^{0.25} = 57.1 \text{ kpsi}$$

Answer

$$S'_u = \frac{S_u}{1 - W} = \frac{49.5}{1 - 0.15} = 58.2 \text{ kpsi}$$

2–4 Hardness

The resistance of a material to penetration by a pointed tool is called *hardness*. Though there are many hardness-measuring systems, we shall consider here only the two in greatest use.

Rockwell hardness tests are described by ASTM standard hardness method E–18 and measurements are quickly and easily made, they have good reproducibility, and the test machine for them is easy to use. In fact, the hardness number is read directly from a dial. Rockwell hardness scales are designated as *A*, *B*, *C*, . . . , etc. The indenters are described as a diamond, a $\frac{1}{16}$ -in-diameter ball, and a diamond for scales *A*, *B*, and *C*, respectively, where the load applied is either 60, 100, or 150 kg. Thus the Rockwell *B* scale, designated R_B , uses a 100-kg load and a No. 2 indenter, which is a $\frac{1}{16}$ -in-diameter ball. The Rockwell *C* scale R_C uses a diamond cone, which is the No. 1 indenter, and a load of 150 kg. Hardness numbers so obtained are relative. Therefore a hardness $R_C = 50$ has meaning only in relation to another hardness number using the same scale.

The *Brinell hardness* is another test in very general use. In testing, the indenting tool through which force is applied is a ball and the hardness number H_B is found as a number equal to the applied load divided by the spherical surface area of the indentation. Thus the units of H_B are the same as those of stress, though they are seldom used. Brinell hardness testing takes more time, since H_B must be computed from the test data. The primary advantage of both methods is that they are nondestructive in most cases. Both are empirically and directly related to the ultimate strength of the material tested. This means that the strength of parts could, if desired, be tested part by part during manufacture.

Hardness testing provides a convenient and nondestructive means of estimating the strength properties of materials. The Brinell hardness test is particularly well known for this estimation, since for many materials the relationship between the minimum ultimate strength and the Brinell hardness number is roughly linear. The constant of proportionality varies between classes of materials, and is also dependent on the load used to determine the hardness. There is a wide scatter in the data, but for rough approximations for *steels*, the relationship is generally accepted as

$$S_u = \begin{cases} 0.5H_B & \text{kpsi} \\ 3.4H_B & \text{MPa} \end{cases} \quad (2-21)$$

Similar relationships for *cast iron* can be derived from data supplied by Krause.⁵ The minimum strength, as defined by the ASTM, is found from these data to be

$$S_u = \begin{cases} 0.23H_B - 12.5 \text{ kpsi} \\ 1.58H_B - 86 \text{ MPa} \end{cases} \quad (2-22)$$

Walton⁶ shows a chart from which the SAE minimum strength can be obtained, which is more conservative than the values obtained from Eq. (2-22).

EXAMPLE 2-2

It is necessary to ensure that a certain part supplied by a foundry always meets or exceeds ASTM No. 20 specifications for cast iron (see Table A-24). What hardness should be specified?

Solution

From Eq. (2-22), with $(S_u)_{\min} = 20$ kpsi, we have

Answer

$$H_B = \frac{S_u + 12.5}{0.23} = \frac{20 + 12.5}{0.23} = 141$$

If the foundry can control the hardness within 20 points, routinely, then specify $145 < H_B < 165$. This imposes no hardship on the foundry and assures the designer that ASTM grade 20 will always be supplied at a predictable cost.

2-5

Impact Properties

An external force applied to a structure or part is called an *impact load* if the time of application is less than one-third the lowest natural period of vibration of the part or structure. Otherwise it is called simply a *static load*.

The *Charpy* (commonly used) and *Izod* (rarely used) *notched-bar tests* utilize bars of specified geometries to determine brittleness and impact strength. These tests are helpful in comparing several materials and in the determination of low-temperature brittleness. In both tests the specimen is struck by a pendulum released from a fixed height, and the energy absorbed by the specimen, called the *impact value*, can be computed from the height of swing after fracture, but is read from a dial that essentially “computes” the result.

The effect of temperature on impact values is shown in Fig. 2-7 for a material showing a ductile-brittle transition. Not all materials show this transition. Notice the narrow region of critical temperatures where the impact value increases very rapidly. In the low-temperature region the fracture appears as a brittle, shattering type, whereas the appearance is a tough, tearing type above the critical-temperature region. The critical temperature seems to be dependent on both the material and the geometry of the notch. For this reason designers should not rely too heavily on the results of notched-bar tests.

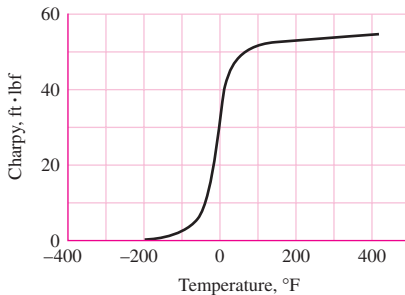
The average strain rate used in obtaining the stress-strain diagram is about 0.001 in/(in · s) or less. When the strain rate is increased, as it is under impact conditions,

⁵D. E. Krause, “Gray Iron—A Unique Engineering Material,” ASTM Special Publication 455, 1969, pp. 3–29, as reported in Charles F. Walton (ed.), *Iron Castings Handbook*, Iron Founders Society, Inc., Cleveland, 1971, pp. 204, 205.

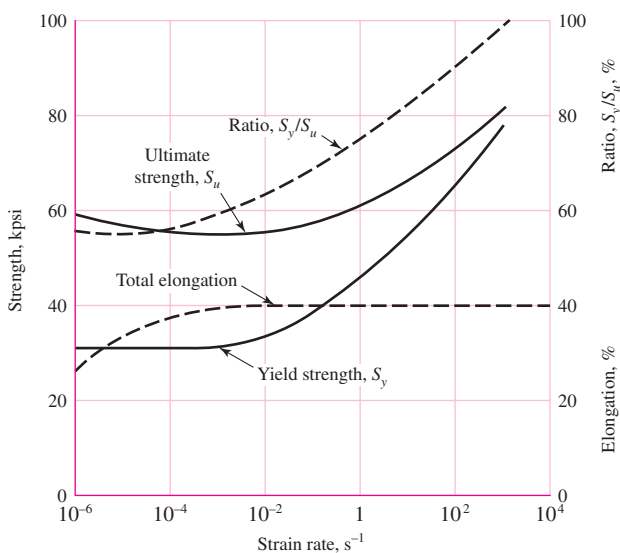
⁶Ibid.

Figure 2–7

A mean trace shows the effect of temperature on impact values. The result of interest is the brittle-ductile transition temperature, often defined as the temperature at which the mean trace passes through the 15 ft · lbf level. The critical temperature is dependent on the geometry of the notch, which is why the Charpy V notch is closely defined.

**Figure 2–8**

Influence of strain rate on tensile properties.



the strengths increase, as shown in Fig. 2–8. In fact, at very high strain rates the yield strength seems to approach the ultimate strength as a limit. But note that the curves show little change in the elongation. This means that the ductility remains about the same. Also, in view of the sharp increase in yield strength, a mild steel could be expected to behave elastically throughout practically its entire strength range under impact conditions.

The Charpy and Izod tests really provide toughness data under dynamic, rather than static, conditions. It may well be that impact data obtained from these tests are as dependent on the notch geometry as they are on the strain rate. For these reasons it may be better to use the concepts of notch sensitivity, fracture toughness, and fracture mechanics, discussed in Chaps. 5 and 6, to assess the possibility of cracking or fracture.

2–6

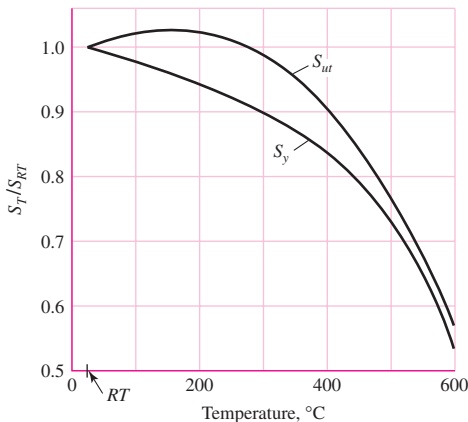
Temperature Effects

Strength and ductility, or brittleness, are properties affected by the temperature of the operating environment.

The effect of temperature on the static properties of steels is typified by the strength versus temperature chart of Fig. 2–9. Note that the tensile strength changes

Figure 2-9

A plot of the results of 145 tests of 21 carbon and alloy steels showing the effect of operating temperature on the yield strength S_y and the ultimate strength S_{ut} . The ordinate is the ratio of the strength at the operating temperature to the strength at room temperature. The standard deviations were $0.0442 \leq \hat{\sigma}_{S_y} \leq 0.152$ for S_y and $0.099 \leq \hat{\sigma}_{S_{ut}} \leq 0.11$ for S_{ut} . (Data source: E. A. Brandes (ed.), Smithells Metal Reference Book, 6th ed., Butterworth, London, 1983 pp. 22-128 to 22-131.)



only a small amount until a certain temperature is reached. At that point it falls off rapidly. The yield strength, however, decreases continuously as the environmental temperature is increased. There is a substantial increase in ductility, as might be expected, at the higher temperatures.

Many tests have been made of ferrous metals subjected to constant loads for long periods of time at elevated temperatures. The specimens were found to be permanently deformed during the tests, even though at times the actual stresses were less than the yield strength of the material obtained from short-time tests made at the same temperature. This continuous deformation under load is called *creep*.

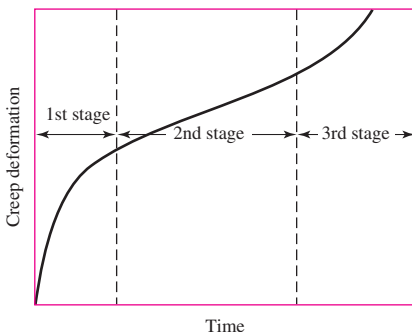
One of the most useful tests to have been devised is the long-time creep test under constant load. Figure 2-10 illustrates a curve that is typical of this kind of test. The curve is obtained at a constant stated temperature. A number of tests are usually run simultaneously at different stress intensities. The curve exhibits three distinct regions. In the first stage are included both the elastic and the plastic deformation. This stage shows a decreasing creep rate, which is due to the strain hardening. The second stage shows a constant minimum creep rate caused by the annealing effect. In the third stage the specimen shows a considerable reduction in area, the true stress is increased, and a higher creep eventually leads to fracture.

When the operating temperatures are lower than the transition temperature (Fig. 2-7), the possibility arises that a part could fail by a brittle fracture. This subject will be discussed in Chap. 5.

Of course, heat treatment, as will be shown, is used to make substantial changes in the mechanical properties of a material.

Figure 2-10

Creep-time curve.



Heating due to electric and gas welding also changes the mechanical properties. Such changes may be due to clamping during the welding process, as well as heating; the resulting stresses then remain when the parts have cooled and the clamps have been removed. Hardness tests can be used to learn whether the strength has been changed by welding, but such tests will not reveal the presence of residual stresses.

2-7 Numbering Systems

The Society of Automotive Engineers (SAE) was the first to recognize the need, and to adopt a system, for the numbering of steels. Later the American Iron and Steel Institute (AISI) adopted a similar system. In 1975 the SAE published the Unified Numbering System for Metals and Alloys (UNS); this system also contains cross-reference numbers for other material specifications.⁷ The UNS uses a letter prefix to designate the material, as, for example, G for the carbon and alloy steels, A for the aluminum alloys, C for the copper-base alloys, and S for the stainless or corrosion-resistant steels. For some materials, not enough agreement has as yet developed in the industry to warrant the establishment of a designation.

For the steels, the first two numbers following the letter prefix indicate the composition, excluding the carbon content. The various compositions used are as follows:

G10	Plain carbon	G46	Nickel-molybdenum
G11	Free-cutting carbon steel with more sulfur or phosphorus	G48	Nickel-molybdenum
G13	Manganese	G50	Chromium
G23	Nickel	G51	Chromium
G25	Nickel	G52	Chromium
G31	Nickel-chromium	G61	Chromium-vanadium
G33	Nickel-chromium	G86	Chromium-nickel-molybdenum
G40	Molybdenum	G87	Chromium-nickel-molybdenum
G41	Chromium-molybdenum	G92	Manganese-silicon
G43	Nickel-chromium-molybdenum	G94	Nickel-chromium-molybdenum

The second number pair refers to the approximate carbon content. Thus, G10400 is a plain carbon steel with a nominal carbon content of 0.40 percent (0.37 to 0.44 percent). The fifth number following the prefix is used for special situations. For example, the old designation AISI 52100 represents a chromium alloy with about 100 points of carbon. The UNS designation is G52986.

The UNS designations for the stainless steels, prefix S, utilize the older AISI designations for the first three numbers following the prefix. The next two numbers are reserved for special purposes. The first number of the group indicates the approximate composition. Thus 2 is a chromium-nickel-manganese steel, 3 is a chromium-nickel steel, and 4 is a chromium alloy steel. Sometimes stainless steels are referred to by their alloy content. Thus S30200 is often called an 18-8 stainless steel, meaning 18 percent chromium and 8 percent nickel.

⁷Many of the materials discussed in the balance of this chapter are listed in the Appendix tables. Be sure to review these.

Table 2-1

Aluminum Alloy Designations	Aluminum 99.00% pure and greater Copper alloys Manganese alloys Silicon alloys Magnesium alloys Magnesium-silicon alloys Zinc alloys	Ax1xxx Ax2xxx Ax3xxx Ax4xxx Ax5xxx Ax6xxx Ax7xxx
-----------------------------	--	--

The prefix for the aluminum group is the letter A. The first number following the prefix indicates the processing. For example, A9 is a wrought aluminum, while A0 is a casting alloy. The second number designates the main alloy group as shown in Table 2-1. The third number in the group is used to modify the original alloy or to designate the impurity limits. The last two numbers refer to other alloys used with the basic group.

The American Society for Testing and Materials (ASTM) numbering system for cast iron is in widespread use. This system is based on the tensile strength. Thus ASTM A18 speaks of classes; e.g., 30 cast iron has a minimum tensile strength of 30 kpsi. Note from Appendix A-24, however, that the *typical* tensile strength is 31 kpsi. You should be careful to designate which of the two values is used in design and problem work because of the significance of factor of safety.

2-8 Sand Casting

Sand casting is a basic low-cost process, and it lends itself to economical production in large quantities with practically no limit to the size, shape, or complexity of the part produced.

In sand casting, the casting is made by pouring molten metal into sand molds. A pattern, constructed of metal or wood, is used to form the cavity into which the molten metal is poured. Recesses or holes in the casting are produced by sand cores introduced into the mold. The designer should make an effort to visualize the pattern and casting in the mold. In this way the problems of core setting, pattern removal, draft, and solidification can be studied. Castings to be used as test bars of cast iron are cast separately and properties may vary.

Steel castings are the most difficult of all to produce, because steel has the highest melting temperature of all materials normally used for casting. This high temperature aggravates all casting problems.

The following rules will be found quite useful in the design of any sand casting:

- 1 All sections should be designed with a uniform thickness.
- 2 The casting should be designed so as to produce a gradual change from section to section where this is necessary.
- 3 Adjoining sections should be designed with generous fillets or radii.
- 4 A complicated part should be designed as two or more simple castings to be assembled by fasteners or by welding.

Steel, gray iron, brass, bronze, and aluminum are most often used in castings. The minimum wall thickness for any of these materials is about 5 mm, though with particular care, thinner sections can be obtained with some materials.

2-9 Shell Molding

The shell-molding process employs a heated metal pattern, usually made of cast iron, aluminum, or brass, which is placed in a shell-molding machine containing a mixture of dry sand and thermosetting resin. The hot pattern melts the plastic, which, together with the sand, forms a shell about 5 to 10 mm thick around the pattern. The shell is then baked at from 400 to 700°F for a short time while still on the pattern. It is then stripped from the pattern and placed in storage for use in casting.

In the next step the shells are assembled by clamping, bolting, or pasting; they are placed in a backup material, such as steel shot; and the molten metal is poured into the cavity. The thin shell permits the heat to be conducted away so that solidification takes place rapidly. As solidification takes place, the plastic bond is burned and the mold collapses. The permeability of the backup material allows the gases to escape and the casting to air-cool. All this aids in obtaining a fine-grain, stress-free casting.

Shell-mold castings feature a smooth surface, a draft that is quite small, and close tolerances. In general, the rules governing sand casting also apply to shell-mold casting.

2-10 Investment Casting

Investment casting uses a pattern that may be made from wax, plastic, or other material. After the mold is made, the pattern is melted out. Thus a mechanized method of casting a great many patterns is necessary. The mold material is dependent upon the melting point of the cast metal. Thus a plaster mold can be used for some materials while others would require a ceramic mold. After the pattern is melted out, the mold is baked or fired; when firing is completed, the molten metal may be poured into the hot mold and allowed to cool.

If a number of castings are to be made, then metal or permanent molds may be suitable. Such molds have the advantage that the surfaces are smooth, bright, and accurate, so that little, if any, machining is required. *Metal-mold castings* are also known as *die castings* and *centrifugal castings*.

2-11 Powder-Metallurgy Process

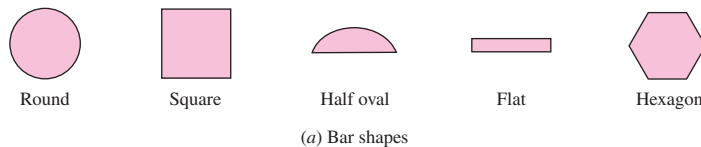
The powder-metallurgy process is a quantity-production process that uses powders from a single metal, several metals, or a mixture of metals and nonmetals. It consists essentially of mechanically mixing the powders, compacting them in dies at high pressures, and heating the compacted part at a temperature less than the melting point of the major ingredient. The particles are united into a single strong part similar to what would be obtained by melting the same ingredients together. The advantages are (1) the elimination of scrap or waste material, (2) the elimination of machining operations, (3) the low unit cost when mass-produced, and (4) the exact control of composition. Some of the disadvantages are (1) the high cost of dies, (2) the lower physical properties, (3) the higher cost of materials, (4) the limitations on the design, and (5) the limited range of materials that can be used. Parts commonly made by this process are oil-impregnated bearings, incandescent lamp filaments, cemented-carbide tips for tools, and permanent magnets. Some products can be made only by powder metallurgy: surgical implants, for example. The structure is different from what can be obtained by melting the same ingredients.

2-12 Hot-Working Processes

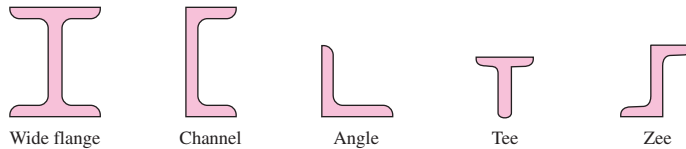
By *hot working* are meant such processes as rolling, forging, hot extrusion, and hot pressing, in which the metal is heated above its recrystallization temperature.

Figure 2-11

Common shapes available through hot rolling.



(a) Bar shapes



(b) Structural shapes

Hot rolling is usually used to create a bar of material of a particular shape and dimension. Figure 2–11 shows some of the various shapes that are commonly produced by the hot-rolling process. All of them are available in many different sizes as well as in different materials. The materials most available in the hot-rolled bar sizes are steel, aluminum, magnesium, and copper alloys.

Tubing can be manufactured by hot-rolling strip or plate. The edges of the strip are rolled together, creating seams that are either butt-welded or lap-welded. Seamless tubing is manufactured by roll-piercing a solid heated rod with a piercing mandrel.

Extrusion is the process by which great pressure is applied to a heated metal billet or blank, causing it to flow through a restricted orifice. This process is more common with materials of low melting point, such as aluminum, copper, magnesium, lead, tin, and zinc. Stainless steel extrusions are available on a more limited basis.

Forging is the hot working of metal by hammers, presses, or forging machines. In common with other hot-working processes, forging produces a refined grain structure that results in increased strength and ductility. Compared with castings, forgings have greater strength for the same weight. In addition, drop forgings can be made smoother and more accurate than sand castings, so that less machining is necessary. However, the initial cost of the forging dies is usually greater than the cost of patterns for castings, although the greater unit strength rather than the cost is usually the deciding factor between these two processes.

2-13

Cold-Working Processes

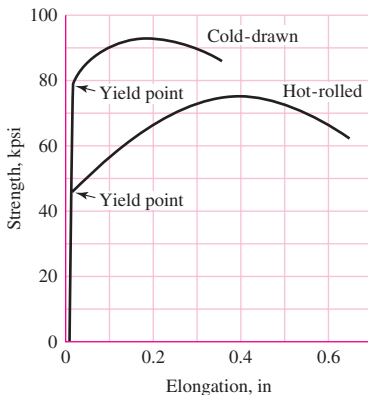
By *cold working* is meant the forming of the metal while at a low temperature (usually room temperature). In contrast to parts produced by hot working, cold-worked parts have a bright new finish, are more accurate, and require less machining.

Cold-finished bars and shafts are produced by rolling, drawing, turning, grinding, and polishing. Of these methods, by far the largest percentage of products are made by the cold-rolling and cold-drawing processes. Cold rolling is now used mostly for the production of wide flats and sheets. Practically all cold-finished bars are made by cold drawing but even so are sometimes mistakenly called “cold-rolled bars.” In the drawing process, the hot-rolled bars are first cleaned of scale and then drawn by pulling them through a die that reduces the size about $\frac{1}{32}$ to $\frac{1}{16}$ in. This process does not remove material from the bar but reduces, or “draws” down, the size. Many different shapes of hot-rolled bars may be used for cold drawing.

Cold rolling and cold drawing have the same effect upon the mechanical properties. The cold-working process does not change the grain size but merely distorts it. Cold working results in a large increase in yield strength, an increase in ultimate

Figure 2-12

Stress-strain diagram for hot-rolled and cold-drawn UNS G10350 steel.



strength and hardness, and a decrease in ductility. In Fig. 2–12 the properties of a cold-drawn bar are compared with those of a hot-rolled bar of the same material.

Heading is a cold-working process in which the metal is gathered, or upset. This operation is commonly used to make screw and rivet heads and is capable of producing a wide variety of shapes. *Roll threading* is the process of rolling threads by squeezing and rolling a blank between two serrated dies. *Spinning* is the operation of working sheet material around a rotating form into a circular shape. *Stamping* is the term used to describe punch-press operations such as *blanking*, *coining*, *forming*, and *shallow drawing*.

2-14

The Heat Treatment of Steel

Heat treatment of steel refers to time- and temperature-controlled processes that relieve residual stresses and/or modifies material properties such as hardness (strength), ductility, and toughness. Other mechanical or chemical operations are sometimes grouped under the heading of heat treatment. The common heat-treating operations are annealing, quenching, tempering, and case hardening.

Annealing

When a material is cold- or hot-worked, residual stresses are built in, and, in addition, the material usually has a higher hardness as a result of these working operations. These operations change the structure of the material so that it is no longer represented by the equilibrium diagram. Full annealing and normalizing is a heating operation that permits the material to transform according to the equilibrium diagram. The material to be annealed is heated to a temperature that is approximately 100°F above the critical temperature. It is held at this temperature for a time that is sufficient for the carbon to become dissolved and diffused through the material. The object being treated is then allowed to cool slowly, usually in the furnace in which it was treated. If the transformation is complete, then it is said to have a full anneal. Annealing is used to soften a material and make it more ductile, to relieve residual stresses, and to refine the grain structure.

The term *annealing* includes the process called *normalizing*. Parts to be normalized may be heated to a slightly higher temperature than in full annealing. This produces a coarser grain structure, which is more easily machined if the material is a low-carbon steel. In the normalizing process the part is cooled in still air at room temperature. Since this cooling is more rapid than the slow cooling used in full annealing, less time is available for equilibrium, and the material is harder than fully annealed steel. Normalizing is often used as the final treating operation for steel. The cooling in still air amounts to a slow quench.

Quenching

Eutectoid steel that is fully annealed consists entirely of pearlite, which is obtained from austenite under conditions of equilibrium. A fully annealed hypoeutectoid steel would consist of pearlite plus ferrite, while hypereutectoid steel in the fully annealed condition would consist of pearlite plus cementite. The hardness of steel of a given carbon content depends upon the structure that replaces the pearlite when full annealing is not carried out.

The absence of full annealing indicates a more rapid rate of cooling. The rate of cooling is the factor that determines the hardness. A controlled cooling rate is called *quenching*. A mild quench is obtained by cooling in still air, which, as we have seen, is obtained by the normalizing process. The two most widely used media for quenching are water and oil. The oil quench is quite slow but prevents quenching cracks caused by rapid expansion of the object being treated. Quenching in water is used for carbon steels and for medium-carbon, low-alloy steels.

The effectiveness of quenching depends upon the fact that when austenite is cooled it does not transform into pearlite instantaneously but requires time to initiate and complete the process. Since the transformation ceases at about 800°F, it can be prevented by rapidly cooling the material to a lower temperature. When the material is cooled rapidly to 400°F or less, the austenite is transformed into a structure called *martensite*. Martensite is a supersaturated solid solution of carbon in ferrite and is the hardest and strongest form of steel.

If steel is rapidly cooled to a temperature between 400 and 800°F and held there for a sufficient length of time, the austenite is transformed into a material that is generally called *bainite*. Bainite is a structure intermediate between pearlite and martensite. Although there are several structures that can be identified between the temperatures given, depending upon the temperature used, they are collectively known as bainite. By the choice of this transformation temperature, almost any variation of structure may be obtained. These range all the way from coarse pearlite to fine martensite.

Tempering

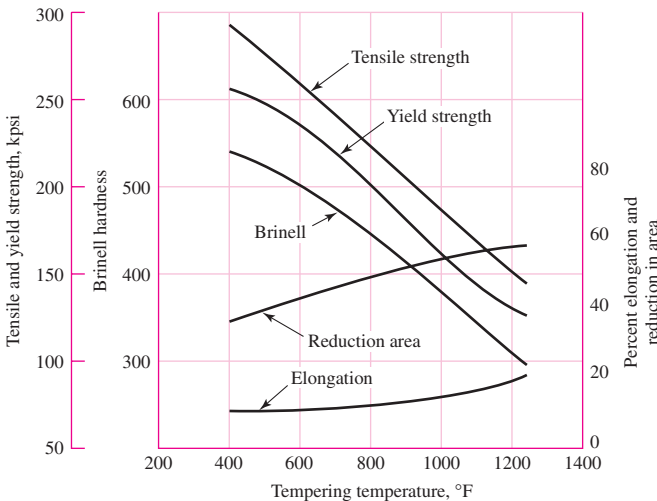
When a steel specimen has been fully hardened, it is very hard and brittle and has high residual stresses. The steel is unstable and tends to contract on aging. This tendency is increased when the specimen is subjected to externally applied loads, because the resultant stresses contribute still more to the instability. These internal stresses can be relieved by a modest heating process called *stress relieving*, or a combination of stress relieving and softening called *tempering* or *drawing*. After the specimen has been fully hardened by being quenched from above the critical temperature, it is reheated to some temperature below the critical temperature for a certain period of time and then allowed to cool in still air. The temperature to which it is reheated depends upon the composition and the degree of hardness or toughness desired.⁸ This reheating operation releases the carbon held in the martensite, forming carbide crystals. The structure obtained is called *tempered martensite*. It is now essentially a superfine dispersion of iron carbide(s) in fine-grained ferrite.

The effect of heat-treating operations upon the various mechanical properties of a low alloy steel is shown graphically in Fig. 2–13.

⁸For the quantitative aspects of tempering in plain carbon and low-alloy steels, see Charles R. Mischke, "The Strength of Cold-Worked and Heat-Treated Steels," Chap. 33 in Joseph E. Shigley, Charles R. Mischke, and Thomas H. Brown, Jr. (eds.), *Standard Handbook of Machine Design*, 3rd ed., McGraw-Hill, New York, 2004.

Figure 2-13

The effect of thermal-mechanical history on the mechanical properties of AISI 4340 steel. (Prepared by the International Nickel Company.)



Condition	Tensile strength, kpsi	Yield strength, kpsi	Reduction in area, %	Elongation in 2 in., %	Brinell hardness, Bhn
Normalized	200	147	20	10	410
As rolled	190	144	18	9	380
Annealed	120	99	43	18	228

Case Hardening

The purpose of case hardening is to produce a hard outer surface on a specimen of low-carbon steel while at the same time retaining the ductility and toughness in the core. This is done by increasing the carbon content at the surface. Either solid, liquid, or gaseous carburizing materials may be used. The process consists of introducing the part to be carburized into the carburizing material for a stated time and at a stated temperature, depending upon the depth of case desired and the composition of the part. The part may then be quenched directly from the carburization temperature and tempered, or in some cases it must undergo a double heat treatment in order to ensure that both the core and the case are in proper condition. Some of the more useful case-hardening processes are pack carburizing, gas carburizing, nitriding, cyaniding, induction hardening, and flame hardening. In the last two cases carbon is not added to the steel in question, generally a medium carbon steel, for example SAE/AISI 1144.

Quantitative Estimation of Properties of Heat-Treated Steels

Courses in metallurgy (or material science) for mechanical engineers usually present the addition method of Crafts and Lamont for the prediction of heat-treated properties from the Jominy test for plain carbon steels.⁹ If this has not been in your prerequisite experience, then refer to the *Standard Handbook of Machine Design*, where the addition method is covered with examples.¹⁰ If this book is a textbook for a machine

⁹W. Crafts and J. L. Lamont, *Hardenability and Steel Selection*, Pitman and Sons, London, 1949.

¹⁰Charles R. Mischke, Chap. 33 in Joseph E. Shigley, Charles R. Mischke, and Thomas H. Brown, Jr. (eds.), *Standard Handbook of Machine Design*, 3rd ed., McGraw-Hill, New York, 2004, p. 33.9.

elements course, it is a good class project (many hands make light work) to study the method and report to the class.

For low-alloy steels, the multiplication method of Grossman¹¹ and Field¹² is explained in the *Standard Handbook of Machine Design* (Secs. 29.6 and 33.6).

Modern Steels and Their Properties Handbook explains how to predict the Jominy curve by the method of Grossman and Field from a ladle analysis and grain size.¹³ Bethlehem Steel has developed a circular plastic slide rule that is convenient to the purpose.

2-15

Alloy Steels

Although a plain carbon steel is an alloy of iron and carbon with small amounts of manganese, silicon, sulfur, and phosphorus, the term *alloy steel* is applied when one or more elements other than carbon are introduced in sufficient quantities to modify its properties substantially. The alloy steels not only possess more desirable physical properties but also permit a greater latitude in the heat-treating process.

Chromium

The addition of chromium results in the formation of various carbides of chromium that are very hard, yet the resulting steel is more ductile than a steel of the same hardness produced by a simple increase in carbon content. Chromium also refines the grain structure so that these two combined effects result in both increased toughness and increased hardness. The addition of chromium increases the critical range of temperatures and moves the eutectoid point to the left. Chromium is thus a very useful alloying element.

Nickel

The addition of nickel to steel also causes the eutectoid point to move to the left and increases the critical range of temperatures. Nickel is soluble in ferrite and does not form carbides or oxides. This increases the strength without decreasing the ductility. Case hardening of nickel steels results in a better core than can be obtained with plain carbon steels. Chromium is frequently used in combination with nickel to obtain the toughness and ductility provided by the nickel and the wear resistance and hardness contributed by the chromium.

Manganese

Manganese is added to all steels as a deoxidizing and desulfurizing agent, but if the sulfur content is low and the manganese content is over 1 percent, the steel is classified as a manganese alloy. Manganese dissolves in the ferrite and also forms carbides. It causes the eutectoid point to move to the left and lowers the critical range of temperatures. It increases the time required for transformation so that oil quenching becomes practicable.

Silicon

Silicon is added to all steels as a deoxidizing agent. When added to very-low-carbon steels, it produces a brittle material with a low hysteresis loss and a high magnetic permeability. The principal use of silicon is with other alloying elements, such as manganese, chromium, and vanadium, to stabilize the carbides.

¹¹M. A. Grossman, *AIME*, February 1942.

¹²J. Field, *Metals Progress*, March 1943.

¹³*Modern Steels and Their Properties*, 7th ed., Handbook 2757, Bethlehem Steel, 1972, pp. 46–50.

Molybdenum

While molybdenum is used alone in a few steels, it finds its greatest use when combined with other alloying elements, such as nickel, chromium, or both. Molybdenum forms carbides and also dissolves in ferrite to some extent, so that it adds both hardness and toughness. Molybdenum increases the critical range of temperatures and substantially lowers the transformation point. Because of this lowering of the transformation point, molybdenum is most effective in producing desirable oil-hardening and air-hardening properties. Except for carbon, it has the greatest hardening effect, and because it also contributes to a fine grain size, this results in the retention of a great deal of toughness.

Vanadium

Vanadium has a very strong tendency to form carbides; hence it is used only in small amounts. It is a strong deoxidizing agent and promotes a fine grain size. Since some vanadium is dissolved in the ferrite, it also toughens the steel. Vanadium gives a wide hardening range to steel, and the alloy can be hardened from a higher temperature. It is very difficult to soften vanadium steel by tempering; hence, it is widely used in tool steels.

Tungsten

Tungsten is widely used in tool steels because the tool will maintain its hardness even at red heat. Tungsten produces a fine, dense structure and adds both toughness and hardness. Its effect is similar to that of molybdenum, except that it must be added in greater quantities.

2-16

Corrosion-Resistant Steels

Iron-base alloys containing at least 12 percent chromium are called *stainless steels*. The most important characteristic of these steels is their resistance to many, but not all, corrosive conditions. The four types available are the ferritic chromium steels, the austenitic chromium-nickel steels, and the martensitic and precipitation-hardenable stainless steels.

The ferritic chromium steels have a chromium content ranging from 12 to 27 percent. Their corrosion resistance is a function of the chromium content, so that alloys containing less than 12 percent still exhibit some corrosion resistance, although they may rust. The quench-hardenability of these steels is a function of both the chromium and the carbon content. The very high carbon steels have good quench hardenability up to about 18 percent chromium, while in the lower carbon ranges it ceases at about 13 percent. If a little nickel is added, these steels retain some degree of hardenability up to 20 percent chromium. If the chromium content exceeds 18 percent, they become difficult to weld, and at the very high chromium levels the hardness becomes so great that very careful attention must be paid to the service conditions. Since chromium is expensive, the designer will choose the lowest chromium content consistent with the corrosive conditions.

The chromium-nickel stainless steels retain the austenitic structure at room temperature; hence, they are not amenable to heat treatment. The strength of these steels can be greatly improved by cold working. They are not magnetic unless cold-worked. Their work hardenability properties also cause them to be difficult to machine. All the chromium-nickel steels may be welded. They have greater corrosion-resistant properties than the plain chromium steels. When more chromium is added for greater corrosion resistance, more nickel must also be added if the austenitic properties are to be retained.

2-17 Casting Materials

Gray Cast Iron

Of all the cast materials, gray cast iron is the most widely used. This is because it has a very low cost, is easily cast in large quantities, and is easy to machine. The principal objections to the use of gray cast iron are that it is brittle and that it is weak in tension. In addition to a high carbon content (over 1.7 percent and usually greater than 2 percent), cast iron also has a high silicon content, with low percentages of sulfur, manganese, and phosphorus. The resultant alloy is composed of pearlite, ferrite, and graphite, and under certain conditions the pearlite may decompose into graphite and ferrite. The resulting product then contains all ferrite and graphite. The graphite, in the form of thin flakes distributed evenly throughout the structure, darkens it; hence, the name *gray cast iron*.

Gray cast iron is not readily welded, because it may crack, but this tendency may be reduced if the part is carefully preheated. Although the castings are generally used in the as-cast condition, a mild anneal reduces cooling stresses and improves the machinability. The tensile strength of gray cast iron varies from 100 to 400 MPa (15 to 60 kpsi), and the compressive strengths are 3 to 4 times the tensile strengths. The modulus of elasticity varies widely, with values extending all the way from 75 to 150 GPa (11 to 22 Mpsi).

Ductile and Nodular Cast Iron

Because of the lengthy heat treatment required to produce malleable cast iron, engineers have long desired a cast iron that would combine the ductile properties of malleable iron with the ease of casting and machining of gray iron and at the same time would possess these properties in the as-cast conditions. A process for producing such a material using magnesium-containing material seems to fulfill these requirements.

Ductile cast iron, or *nodular cast iron*, as it is sometimes called, is essentially the same as malleable cast iron, because both contain graphite in the form of spheroids. However, ductile cast iron in the as-cast condition exhibits properties very close to those of malleable iron, and if a simple 1-h anneal is given and is followed by a slow cool, it exhibits even more ductility than the malleable product. Ductile iron is made by adding MgFeSi to the melt; since magnesium boils at this temperature, it is necessary to alloy it with other elements before it is introduced.

Ductile iron has a high modulus of elasticity (172 GPa or 25 Mpsi) as compared with gray cast iron, and it is elastic in the sense that a portion of the stress-strain curve is a straight line. Gray cast iron, on the other hand, does not obey Hooke's law, because the modulus of elasticity steadily decreases with increase in stress. Like gray cast iron, however, nodular iron has a compressive strength that is higher than the tensile strength, although the difference is not as great. In 40 years it has become extensively used.

White Cast Iron

If all the carbon in cast iron is in the form of cementite and pearlite, with no graphite present, the resulting structure is white and is known as *white cast iron*. This may be produced in two ways. The composition may be adjusted by keeping the carbon and silicon content low, or the gray-cast-iron composition may be cast against chills in order to promote rapid cooling. By either method, a casting with large amounts of cementite is produced, and as a result the product is very brittle and hard to machine but also very resistant to wear. A chill is usually used in the production of gray-iron castings in order

to provide a very hard surface within a particular area of the casting, while at the same time retaining the more desirable gray structure within the remaining portion. This produces a relatively tough casting with a wear-resistant area.

Malleable Cast Iron

If white cast iron within a certain composition range is annealed, a product called *malleable cast iron* is formed. The annealing process frees the carbon so that it is present as graphite, just as in gray cast iron but in a different form. In gray cast iron the graphite is present in a thin flake form, while in malleable cast iron it has a nodular form and is known as *temper carbon*. A good grade of malleable cast iron may have a tensile strength of over 350 MPa (50 kpsi), with an elongation of as much as 18 percent. The percentage elongation of a gray cast iron, on the other hand, is seldom over 1 percent. Because of the time required for annealing (up to 6 days for large and heavy castings), malleable iron is necessarily somewhat more expensive than gray cast iron.

Alloy Cast Irons

Nickel, chromium, and molybdenum are the most common alloying elements used in cast iron. Nickel is a general-purpose alloying element, usually added in amounts up to 5 percent. Nickel increases the strength and density, improves the wearing qualities, and raises the machinability. If the nickel content is raised to 10 to 18 percent, an austenitic structure with valuable heat- and corrosion-resistant properties results. Chromium increases the hardness and wear resistance and, when used with a chill, increases the tendency to form white iron. When chromium and nickel are both added, the hardness and strength are improved without a reduction in the machinability rating. Molybdenum added in quantities up to 1.25 percent increases the stiffness, hardness, tensile strength, and impact resistance. It is a widely used alloying element.

Cast Steels

The advantage of the casting process is that parts having complex shapes can be manufactured at costs less than fabrication by other means, such as welding. Thus the choice of steel castings is logical when the part is complex and when it must also have a high strength. The higher melting temperatures for steels do aggravate the casting problems and require closer attention to such details as core design, section thicknesses, fillets, and the progress of cooling. The same alloying elements used for the wrought steels can be used for cast steels to improve the strength and other mechanical properties. Cast-steel parts can also be heat-treated to alter the mechanical properties, and, unlike the cast irons, they can be welded.

2-18 Nonferrous Metals

Aluminum

The outstanding characteristics of aluminum and its alloys are their strength-weight ratio, their resistance to corrosion, and their high thermal and electrical conductivity. The density of aluminum is about 2770 kg/m^3 (0.10 lbf/in^3), compared with 7750 kg/m^3 (0.28 lbf/in^3) for steel. Pure aluminum has a tensile strength of about 90 MPa (13 kpsi), but this can be improved considerably by cold working and also by alloying with other materials. The modulus of elasticity of aluminum, as well as of its alloys, is 71.7 GPa (10.4 Mpsi), which means that it has about one-third the stiffness of steel.

Considering the cost and strength of aluminum and its alloys, they are among the most versatile materials from the standpoint of fabrication. Aluminum can be processed by sand casting, die casting, hot or cold working, or extruding. Its alloys can be machined, press-worked, soldered, brazed, or welded. Pure aluminum melts at 660°C (1215°F), which makes it very desirable for the production of either permanent or sand-mold castings. It is commercially available in the form of plate, bar, sheet, foil, rod, and tube and in structural and extruded shapes. Certain precautions must be taken in joining aluminum by soldering, brazing, or welding; these joining methods are not recommended for all alloys.

The corrosion resistance of the aluminum alloys depends upon the formation of a thin oxide coating. This film forms spontaneously because aluminum is inherently very reactive. Constant erosion or abrasion removes this film and allows corrosion to take place. An extra-heavy oxide film may be produced by the process called *anodizing*. In this process the specimen is made to become the anode in an electrolyte, which may be chromic acid, oxalic acid, or sulfuric acid. It is possible in this process to control the color of the resulting film very accurately.

The most useful alloying elements for aluminum are copper, silicon, manganese, magnesium, and zinc. Aluminum alloys are classified as *casting alloys* or *wrought alloys*. The casting alloys have greater percentages of alloying elements to facilitate casting, but this makes cold working difficult. Many of the casting alloys, and some of the wrought alloys, cannot be hardened by heat treatment. The alloys that are heat-treatable use an alloying element that dissolves in the aluminum. The heat treatment consists of heating the specimen to a temperature that permits the alloying element to pass into solution, then quenching so rapidly that the alloying element is not precipitated. The aging process may be accelerated by heating slightly, which results in even greater hardness and strength. One of the better-known heat-treatable alloys is duraluminum, or 2017 (4 percent Cu, 0.5 percent Mg, 0.5 percent Mn). This alloy hardens in 4 days at room temperature. Because of this rapid aging, the alloy must be stored under refrigeration after quenching and before forming, or it must be formed immediately after quenching. Other alloys (such as 5053) have been developed that age-harden much more slowly, so that only mild refrigeration is required before forming. After forming, they are artificially aged in a furnace and possess approximately the same strength and hardness as the 2024 alloys. Those alloys of aluminum that cannot be heat-treated can be hardened only by cold working. Both work hardening and the hardening produced by heat treatment may be removed by an annealing process.

Magnesium

The density of magnesium is about 1800 kg/m³ (0.065 lb/in³), which is two-thirds that of aluminum and one-fourth that of steel. Since it is the lightest of all commercial metals, its greatest use is in the aircraft and automotive industries, but other uses are now being found for it. Although the magnesium alloys do not have great strength, because of their light weight the strength-weight ratio compares favorably with the stronger aluminum and steel alloys. Even so, magnesium alloys find their greatest use in applications where strength is not an important consideration. Magnesium will not withstand elevated temperatures; the yield point is definitely reduced when the temperature is raised to that of boiling water.

Magnesium and its alloys have a modulus of elasticity of 45 GPa (6.5 Mpsi) in tension and in compression, although some alloys are not as strong in compression as in tension. Curiously enough, cold working reduces the modulus of elasticity. A range of cast magnesium alloys are also available.

Titanium

Titanium and its alloys are similar in strength to moderate-strength steel but weigh half as much as steel. The material exhibits very good resistance to corrosion, has low thermal conductivity, is nonmagnetic, and has high-temperature strength. Its modulus of elasticity is between those of steel and aluminum at 16.5 Mpsi (114 GPa). Because of its many advantages over steel and aluminum, applications include: aerospace and military aircraft structures and components, marine hardware, chemical tanks and processing equipment, fluid handling systems, and human internal replacement devices. The disadvantages of titanium are its high cost compared to steel and aluminum and the difficulty of machining it.

Copper-Base Alloys

When copper is alloyed with zinc, it is usually called *brass*. If it is alloyed with another element, it is often called *bronze*. Sometimes the other element is specified too, as, for example, *tin bronze* or *phosphor bronze*. There are hundreds of variations in each category.

Brass with 5 to 15 Percent Zinc

The low-zinc brasses are easy to cold work, especially those with the higher zinc content. They are ductile but often hard to machine. The corrosion resistance is good. Alloys included in this group are *gilding brass* (5 percent Zn), *commercial bronze* (10 percent Zn), and *red brass* (15 percent Zn). Gilding brass is used mostly for jewelry and articles to be gold-plated; it has the same ductility as copper but greater strength, accompanied by poor machining characteristics. Commercial bronze is used for jewelry and for forgings and stampings, because of its ductility. Its machining properties are poor, but it has excellent cold-working properties. Red brass has good corrosion resistance as well as high-temperature strength. Because of this it is used a great deal in the form of tubing or piping to carry hot water in such applications as radiators or condensers.

Brass with 20 to 36 Percent Zinc

Included in the intermediate-zinc group are *low brass* (20 percent Zn), *cartridge brass* (30 percent Zn), and *yellow brass* (35 percent Zn). Since zinc is cheaper than copper, these alloys cost less than those with more copper and less zinc. They also have better machinability and slightly greater strength; this is offset, however, by poor corrosion resistance and the possibility of cracking at points of residual stresses. Low brass is very similar to red brass and is used for articles requiring deep-drawing operations. Of the copper-zinc alloys, cartridge brass has the best combination of ductility and strength. Cartridge cases were originally manufactured entirely by cold working; the process consisted of a series of deep draws, each draw being followed by an anneal to place the material in condition for the next draw, hence the name cartridge brass. Although the hot-working ability of yellow brass is poor, it can be used in practically any other fabricating process and is therefore employed in a large variety of products.

When small amounts of lead are added to the brasses, their machinability is greatly improved and there is some improvement in their abilities to be hot-worked. The addition of lead impairs both the cold-working and welding properties. In this group are *low-leaded brass* ($32\frac{1}{2}$ percent Zn, $\frac{1}{2}$ percent Pb), *high-leaded brass* (34 percent Zn, 2 percent Pb), and *free-cutting brass* ($35\frac{1}{2}$ percent Zn, 3 percent Pb). The low-leaded brass is not only easy to machine but has good cold-working properties. It is used for various screw-machine parts. High-leaded brass, sometimes called *engraver's brass*, is used for instrument, lock, and watch parts. Free-cutting brass is also used for screw-machine parts and has good corrosion resistance with excellent mechanical properties.

Admiralty metal (28 percent Zn) contains 1 percent tin, which imparts excellent corrosion resistance, especially to saltwater. It has good strength and ductility but only fair machining and working characteristics. Because of its corrosion resistance it is used in power-plant and chemical equipment. *Aluminum brass* (22 percent Zn) contains 2 percent aluminum and is used for the same purposes as admiralty metal, because it has nearly the same properties and characteristics. In the form of tubing or piping, it is favored over admiralty metal, because it has better resistance to erosion caused by high-velocity water.

Brass with 36 to 40 Percent Zinc

Brasses with more than 38 percent zinc are less ductile than cartridge brass and cannot be cold-worked as severely. They are frequently hot-worked and extruded. *Muntz metal* (40 percent Zn) is low in cost and mildly corrosion-resistant. *Naval brass* has the same composition as Muntz metal except for the addition of 0.75 percent tin, which contributes to the corrosion resistance.

Bronze

Silicon bronze, containing 3 percent silicon and 1 percent manganese in addition to the copper, has mechanical properties equal to those of mild steel, as well as good corrosion resistance. It can be hot- or cold-worked, machined, or welded. It is useful wherever corrosion resistance combined with strength is required.

Phosphor bronze, made with up to 11 percent tin and containing small amounts of phosphorus, is especially resistant to fatigue and corrosion. It has a high tensile strength and a high capacity to absorb energy, and it is also resistant to wear. These properties make it very useful as a spring material.

Aluminum bronze is a heat-treatable alloy containing up to 12 percent aluminum. This alloy has strength and corrosion-resistance properties that are better than those of brass, and in addition, its properties may be varied over a wide range by cold working, heat treating, or changing the composition. When iron is added in amounts up to 4 percent, the alloy has a high endurance limit, a high shock resistance, and excellent wear resistance.

Beryllium bronze is another heat-treatable alloy, containing about 2 percent beryllium. This alloy is very corrosion resistant and has high strength, hardness, and resistance to wear. Although it is expensive, it is used for springs and other parts subjected to fatigue loading where corrosion resistance is required.

With slight modification most copper-based alloys are available in cast form.

2-19

Plastics

The term *thermoplastics* is used to mean any plastic that flows or is moldable when heat is applied to it; the term is sometimes applied to plastics moldable under pressure. Such plastics can be remolded when heated.

A *thermoset* is a plastic for which the polymerization process is finished in a hot molding press where the plastic is liquefied under pressure. Thermoset plastics cannot be remolded.

Table 2-2 lists some of the most widely used thermoplastics, together with some of their characteristics and the range of their properties. Table 2-3, listing some of the thermosets, is similar. These tables are presented for information only and should not be used to make a final design decision. The range of properties and characteristics that can be obtained with plastics is very great. The influence of many factors, such as cost, moldability, coefficient of friction, weathering, impact strength, and the effect of fillers and reinforcements, must be considered. Manufacturers' catalogs will be found quite helpful in making possible selections.

Table 2–2

The Thermoplastics *Source:* These data have been obtained from the *Machine Design Materials Reference Issue*, published by Penton/IPC, Cleveland. These reference issues are published about every 2 years and constitute an excellent source of data on a great variety of materials.

Name	<i>S_u</i> kpsi	<i>E</i> Mpsi	Hardness Rockwell	Elongation %	Dimensional Stability	Heat Resistance	Chemical Resistance	Processing
ABS group	2–8	0.10–0.37	60–110R	3–50	Good	*	Fair	EMST
Acetal group	8–10	0.41–0.52	80–94M	40–60	Excellent	Good	High	M
Acrylic	5–10	0.20–0.47	92–110M	3–75	High	*	Fair	EMS
Fluoroplastic group	0.50–7	...	50–80D	100–300	High	Excellent	Excellent	MPR [†]
Nylon	8–14	0.18–0.45	112–120R	10–200	Poor	Poor	Good	CEM
Phenylene oxide	7–18	0.35–0.92	115R, 106L	5–60	Excellent	Good	Fair	EFM
Polycarbonate	8–16	0.34–0.86	62–91M	10–125	Excellent	Excellent	Fair	EMS
Polyester	8–18	0.28–1.6	65–90M	1–300	Excellent	Poor	Excellent	CLMR
Polyimide	6–50	...	88–120M	Very low	Excellent	Excellent	Excellent [†]	CLMP
Polyphenylene sulfide	14–19	0.11	122R	1.0	Good	Excellent	Excellent	M
Polystyrene group	1.5–12	0.14–0.60	10–90M	0.5–60	...	Poor	Poor	EM
Polysulfone	10	0.36	120R	50–100	Excellent	Excellent	Excellent [†]	EFM
Polyvinyl chloride	1.5–7.5	0.35–0.60	65–85D	40–450	...	Poor	Poor	EFM

*Heat-resistant grades available.

[†]With exceptions.

C Coatings L Laminates R Resins E Extrusions M Moldings S Sheet F Foams P Press and sinter methods T Tubing

Table 2–3

The Thermosets *Source:* These data have been obtained from the *Machine Design Materials Reference Issue*, published by Penton/IPC, Cleveland. These reference issues are published about every 2 years and constitute an excellent source of data on a great variety of materials.

Name	<i>S_u</i> kpsi	<i>E</i> Mpsi	Hardness Rockwell	Elongation %	Dimensional Stability	Heat Resistance	Chemical Resistance	Processing
Alkyd	3–9	0.05–0.30	99M*	...	Excellent	Good	Fair	M
Allylic	4–10	...	105–120M	...	Excellent	Excellent	Excellent	CM
Amino group	5–8	0.13–0.24	110–120M	0.30–0.90	Good	Excellent*	Excellent*	LR
Epoxy	5–20	0.03–0.30*	80–120M	1–10	Excellent	Excellent	Excellent	CMR
Phenolics	5–9	0.10–0.25	70–95E	...	Excellent	Excellent	Good	EMR
Silicones	5–6	...	80–90M	Excellent	Excellent	CLMR

*With exceptions.

C Coatings L Laminates R Resins E Extrusions M Moldings S Sheet F Foams P Press and sinter methods T Tubing

2-20 Composite Materials¹⁴

Composite materials are formed from two or more dissimilar materials, each of which contributes to the final properties. Unlike metallic alloys, the materials in a composite remain distinct from each other at the macroscopic level.

Most engineering composites consist of two materials: a reinforcement called a *filler* and a *matrix*. The filler provides stiffness and strength; the matrix holds the material together and serves to transfer load among the discontinuous reinforcements. The most common reinforcements, illustrated in Fig. 2-14, are continuous fibers, either straight or woven, short chopped fibers, and particulates. The most common matrices are various plastic resins although other materials including metals are used.

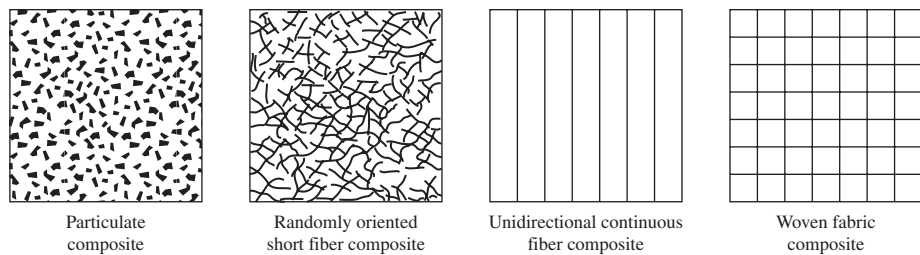
Metals and other traditional engineering materials are uniform, or isotropic, in nature. This means that material properties, such as strength, stiffness, and thermal conductivity, are independent of both position within the material and the choice of coordinate system. The discontinuous nature of composite reinforcements, though, means that material properties can vary with both position and direction. For example, an epoxy resin reinforced with continuous graphite fibers will have very high strength and stiffness in the direction of the fibers, but very low properties normal or transverse to the fibers. For this reason, structures of composite materials are normally constructed of multiple plies (laminates) where each ply is oriented to achieve optimal structural stiffness and strength performance.

High strength-to-weight ratios, up to 5 times greater than those of high-strength steels, can be achieved. High stiffness-to-weight ratios can also be obtained, as much as 8 times greater than those of structural metals. For this reason, composite materials are becoming very popular in automotive, marine, aircraft, and spacecraft applications where weight is a premium.

The directionality of properties of composite materials increases the complexity of structural analyses. Isotropic materials are fully defined by two engineering constants: Young's modulus E and Poisson's ratio ν . A single ply of a composite material, however, requires four constants, defined with respect to the ply coordinate system. The constants are two Young's moduli (the longitudinal modulus in the direction of the fibers, E_1 , and the transverse modulus normal to the fibers, E_2), one Poisson's ratio (ν_{12} , called the major Poisson's ratio), and one shear modulus (G_{12}). A fifth constant, the minor Poisson's ratio, ν_{21} , is determined through the reciprocity relation, $\nu_{21}/E_2 = \nu_{12}/E_1$. Combining this with multiple plies oriented at different angles makes structural analysis of complex structures unapproachable by manual techniques. For this reason, computer software is available to calculate the properties of a laminated composite construction.¹⁵

Figure 2-14

Composites categorized by type of reinforcement.



¹⁴For references see I. M. Daniel and O. Ishai, *Engineering Mechanics of Composite Materials*, Oxford University Press, 1994, and *ASM Engineered Materials Handbook: Composites*, ASM International, Materials Park, OH, 1988.

¹⁵About Composite Materials Software listing, <http://composite.about.com/cs/software/index.htm>.

2-21 Materials Selection

As stated earlier, the selection of a material for a machine part or structural member is one of the most important decisions the designer is called on to make. Up to this point in this chapter we have discussed many important material physical properties, various characteristics of typical engineering materials, and various material production processes. The actual selection of a material for a particular design application can be an easy one, say, based on previous applications (1020 steel is always a good candidate because of its many positive attributes), or the selection process can be as involved and daunting as any design problem with the evaluation of the many material physical, economical, and processing parameters. There are systematic and optimizing approaches to material selection. Here, for illustration, we will only look at how to approach some material properties. One basic technique is to list all the important material properties associated with the design, e.g., strength, stiffness, and cost. This can be prioritized by using a weighting measure depending on what properties are more important than others. Next, for each property, list all available materials and rank them in order beginning with the best material; e.g., for strength, high-strength steel such as 4340 steel should be near the top of the list. For completeness of available materials, this might require a large source of material data. Once the lists are formed, select a manageable amount of materials from the top of each list. From each reduced list select the materials that are contained within every list for further review. The materials in the reduced lists can be graded within the list and then weighted according to the importance of each property.

M. F. Ashby has developed a powerful systematic method using *materials selection charts*.¹⁶ This method has also been implemented in a software package called CES Edupack.¹⁷ The charts display data of various properties for the families and classes of materials listed in Table 2-4. For example, considering material stiffness properties, a simple bar chart plotting Young's modulus E on the y axis is shown

Table 2-4

Material Families and Classes

Family	Classes	Short Name
Metals (the metals and alloys of engineering)	Aluminum alloys Copper alloys Lead alloys Magnesium alloys Nickel alloys Carbon steels Stainless steels Tin alloys Titanium alloys Tungsten alloys Lead alloys Zinc alloys	Al alloys Cu alloys Lead alloys Mg alloys Ni alloys Steels Stainless steels Tin alloys Ti alloys W alloys Pb alloys Zn alloys

(continued)

¹⁶M. F. Ashby, *Materials Selection in Mechanical Design*, 3rd ed., Elsevier Butterworth-Heinemann, Oxford, 2005.

¹⁷Produced by Granta Design Limited. See www.grantadesign.com.

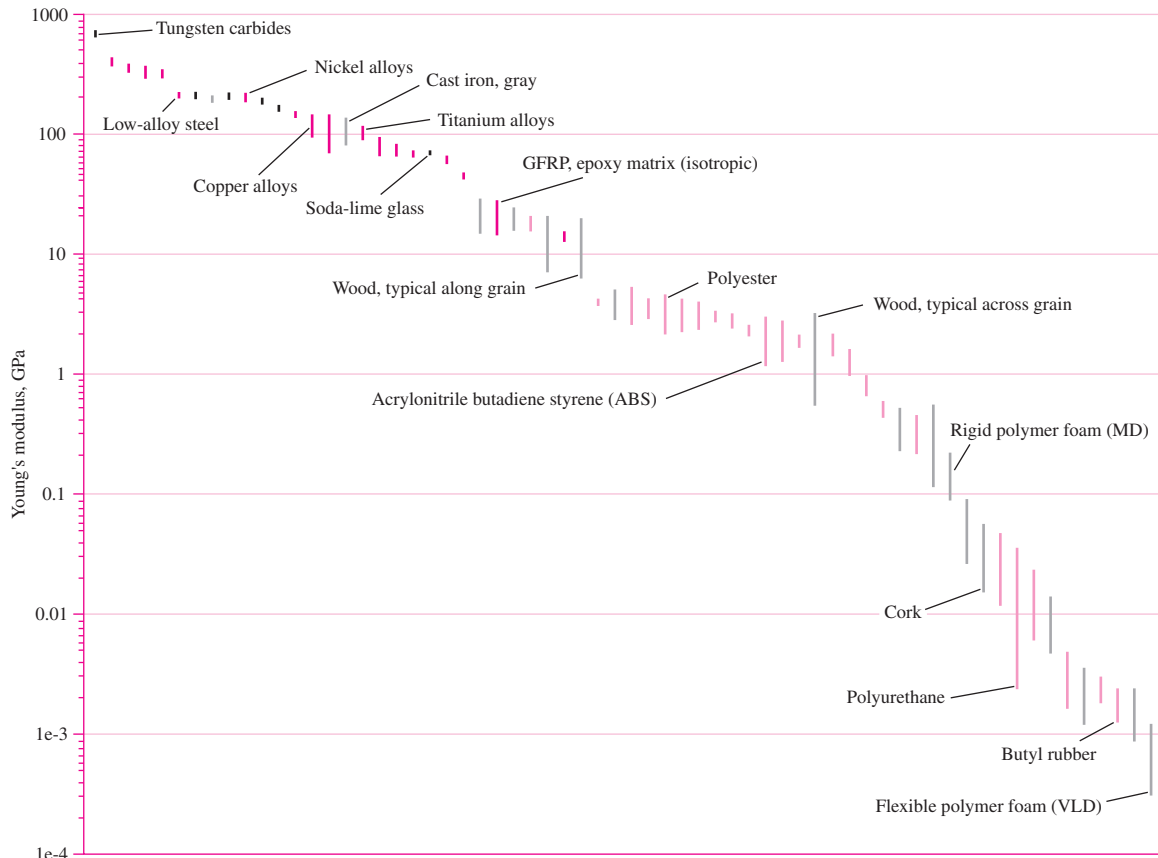
| **Table 2-4** (continued)

Family	Classes	Short Name
Ceramics Technical ceramics (fine ceramics capable of load-bearing application)	Alumina Aluminum nitride Boron carbide Silicon carbide Silicon nitride Tungsten carbide	Al_2O_3 AlN B_4C SiC Si_3N_4 WC
Nontechnical ceramics (porous ceramics of construction)	Brick Concrete Stone	Brick Concrete Stone
Glasses	Soda-lime glass Borosilicate glass Silica glass Glass ceramic	Soda-lime glass Borosilicate glass Silica glass Glass ceramic
Polymers (the thermoplastics and thermosets of engineering)	Acrylonitrile butadiene styrene Cellulose polymers Ionomers Epoxies Phenolics Polyamides (nylons) Polycarbonate Polyesters Polyetheretherketone Polyethylene Polyethylene terephalate Polymethylmethacrylate Polyoxymethylene(Acetal) Polypropylene Polystyrene Polytetrafluoroethylene Polyvinylchloride	ABS CA Ionomers Epoxy Phenolics PA PC Polyester PEEK PE PET or PETE PMMA POM PP PS PTFE PVC
Elastomers (engineering rubbers, natural and synthetic)	Butyl rubber EVA Isoprene Natural rubber Polychloroprene (Neoprene) Polyurethane Silicon elastomers	Butyl rubber EVA Isoprene Natural rubber Neoprene PU Silicones
Hybrids	Carbon-fiber reinforced polymers Glass-fiber reinforced polymers SiC reinforced aluminum	CFRP GFRP Al-SiC
Composites	Flexible polymer foams Rigid polymer foams	Flexible foams Rigid foams
Foams	Cork Bamboo	Cork Bamboo
Natural materials	Wood	Wood

From M. F. Ashby, *Materials Selection in Mechanical Design*, 3rd ed., Elsevier Butterworth-Heinemann, Oxford, 2005. Table 4-1, pp. 49–50.

Figure 2-15

Young's modulus E for various materials. (Figure courtesy of Prof. Mike Ashby, Granta Design, Cambridge, U.K.)

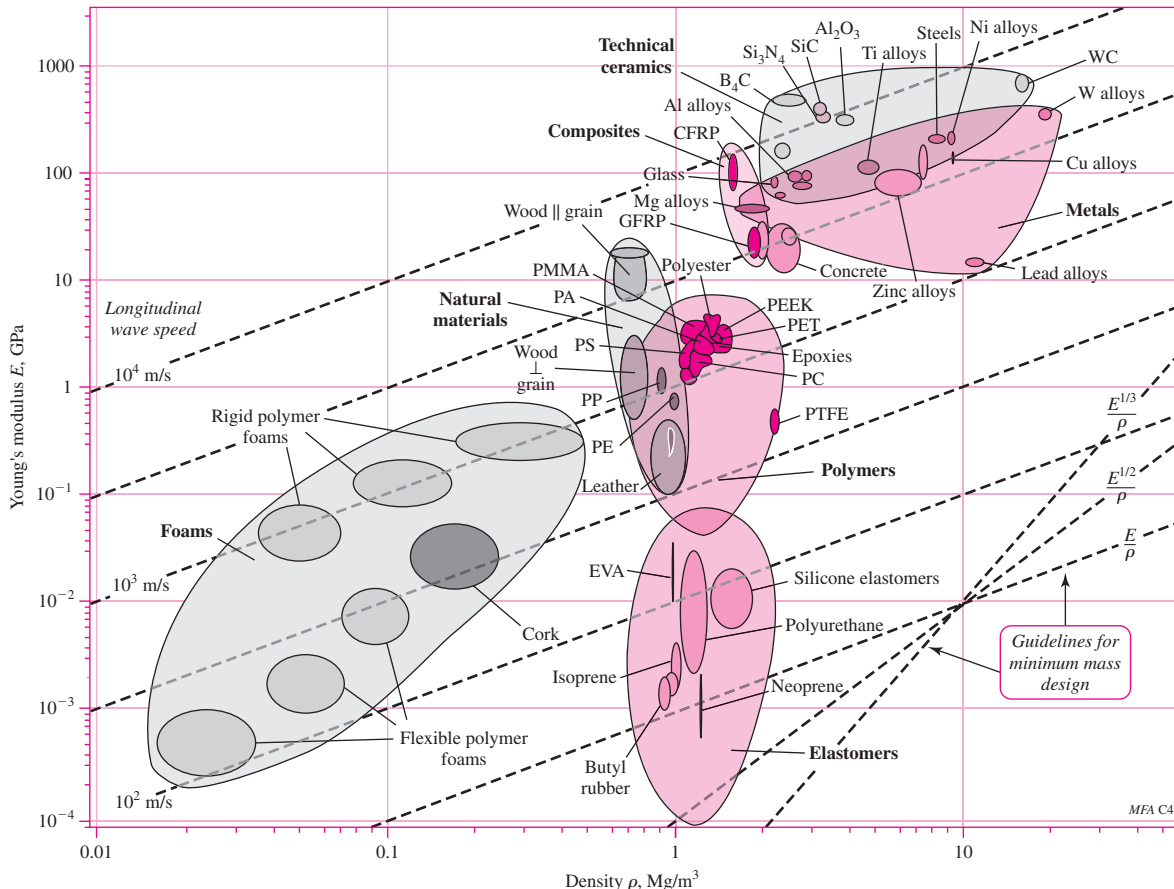


in Fig. 2-15. Each vertical line represents the range of values of E for a particular material. Only some of the materials are labeled. Now, more material information can be displayed if the x axis represents another material property, say density. Figure 2-16, called a “bubble” chart, represents Young's modulus E plotted against density ρ . The line ranges for each material property plotted two-dimensionally now form ellipses, or bubbles. Groups of bubbles outlined according to the material families of Table 2-4 are also shown. This plot is more useful than the two separate bar charts of each property. Now, we also see how stiffness/weight for various materials relate. The ratio of Young's modulus to density, E/ρ , is known as the *specific modulus*, or *specific stiffness*. This ratio is of particular interest when it is desired to minimize weight where the primary design limitation is deflection, stiffness, or natural frequency, rather than strength. Machine parts made from materials with higher specific modulus will exhibit lower deflection, higher stiffness, and higher natural frequency.

In the lower right corner of the chart in Figure 2-16, dotted lines indicate ratios of E^{β}/ρ . Several parallel dotted lines are shown for $\beta = 1$ that represent different values of the specific modulus E/ρ . This allows simple comparison of the specific modulus between materials. It can be seen, for example, that some woods and aluminum alloys have about the same specific modulus as steels. Different values of β allow comparisons for

Figure 2-16

Young's modulus E versus density ρ for various materials. (Figure courtesy of Prof. Mike Ashby, Granta Design, Cambridge, U.K.)



various relationships between stiffness and weight, such as in different loading conditions. The relationship is linear ($\beta = 1$) for axial loading, but nonlinear ($\beta = 1/2$) for bending loading [see Eq. (2-31) and its development]. Since the plot is on a log-log scale, the exponential functions still plot as straight lines. The $\beta = 1$ lines can also be used to represent constant values of the speed of sound in a material, since the relationship between E and ρ is linear in the equation for the speed of sound in a material, $c = (E/\rho)^{1/2}$. The same can be shown for natural frequency, which is a function of the ratio of stiffness to mass.

To see how β fits into the mix, consider the following. The performance metric P of a structural element depends on (1) the functional requirements, (2) the geometry, and (3) the material properties of the structure. That is,

$$P = \left[\begin{pmatrix} \text{functional requirements } F \\ \text{geometric parameters } G \\ \text{material properties } M \end{pmatrix} \right]$$

or, symbolically,

$$P = f(F, G, M) \quad (2-23)$$

If the function is *separable*, which it often is, we can write Eq. (2–23) as

$$P = f_1(F) \cdot f_2(G) \cdot f_3(M) \quad (2-24)$$

For optimum design, we desire to maximize or minimize P . With regards to material properties alone, this is done by maximizing or minimizing $f_3(M)$, called the *material efficiency coefficient*.

For illustration, say we want to design a light, stiff, end-loaded cantilever beam with a circular cross section. For this we will use the mass m of the beam for the performance metric to minimize. The stiffness of the beam is related to its material and geometry. The stiffness of a beam is given by $k = F/\delta$, where F and δ are the end load and deflection, respectively (see Chap. 4). The end deflection of an end-loaded cantilever beam is given in Table A–9, beam 1, as $\delta = y_{\max} = (Fl^3)/(3EI)$, where E is Young's modulus, I the second moment of the area, and l the length of the beam. Thus, the stiffness is given by

$$k = \frac{F}{\delta} = \frac{3EI}{l^3} \quad (2-25)$$

From Table A–18, the second moment of the area of a circular cross section is

$$I = \frac{\pi D^4}{64} = \frac{A^2}{4\pi} \quad (2-26)$$

where D and A are the diameter and area of the cross section, respectively. Substituting Eq. (2–26) in (2–25) and solving for A , we obtain

$$A = \left(\frac{4\pi kl^3}{3E} \right)^{1/2} \quad (2-27)$$

The mass of the beam is given by

$$m = Al\rho \quad (2-28)$$

Substituting Eq. (2–27) into (2–28) and rearranging yields

$$m = 2\sqrt{\frac{\pi}{3}}(k^{1/2})(l^{5/2})\left(\frac{\rho}{E^{1/2}}\right) \quad (2-29)$$

Equation (2–29) is of the form of Eq. (2–24). The term $2\sqrt{\pi/3}$ is simply a constant and can be associated with any function, say $f_1(F)$. Thus, $f_1(F) = 2\sqrt{\pi/3}(k^{1/2})$ is the functional requirement, stiffness; $f_2(G) = (l^{5/2})$, the geometric parameter, length; and the material efficiency coefficient

$$f_3(M) = \frac{\rho}{E^{1/2}} \quad (2-30)$$

is the material property in terms of density and Young's modulus. To minimize m we want to minimize $f_3(M)$, or maximize

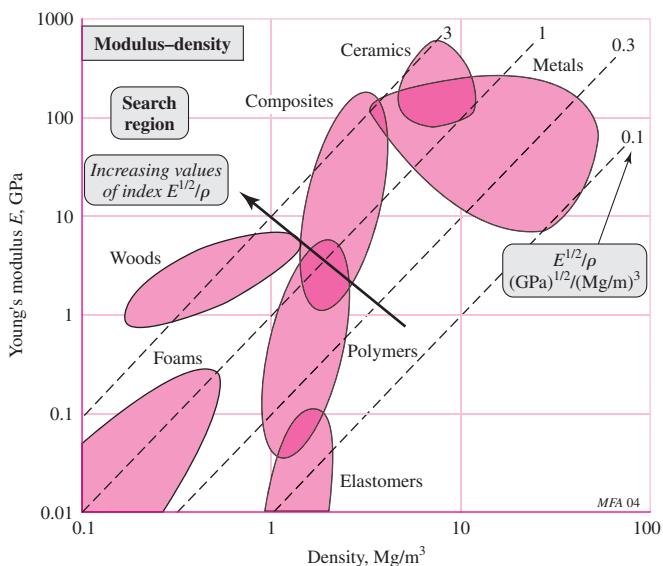
$$M = \frac{E^{1/2}}{\rho} \quad (2-31)$$

where M is called the *material index*, and $\beta = \frac{1}{2}$. Returning to Fig. 2–16, draw lines of various values of $E^{1/2}/\rho$ as shown in Fig. 2–17. Lines of increasing M move up and to the left as shown. Thus, we see that good candidates for a light, stiff, end-loaded cantilever beam with a circular cross section are certain woods, composites, and ceramics.

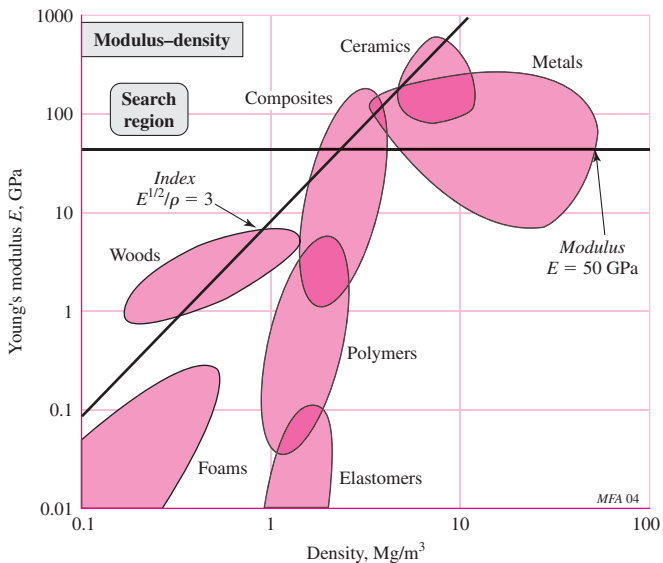
Other limits/constraints may warrant further investigation. Say, for further illustration, the design requirements indicate that we need a Young's modulus greater than

Figure 2–17

A schematic E versus ρ chart showing a grid of lines for various values the material index $M = E^{1/2}/\rho$. (From M. F. Ashby, *Materials Selection in Mechanical Design*, 3rd ed., Elsevier Butterworth-Heinemann, Oxford, 2005.)

**Figure 2–18**

The search region of Fig. 2–16 further reduced by restricting $E \geq 50$ GPa. (From M. F. Ashby, *Materials Selection in Mechanical Design*, 3rd ed., Elsevier Butterworth-Heinemann, Oxford, 2005.)



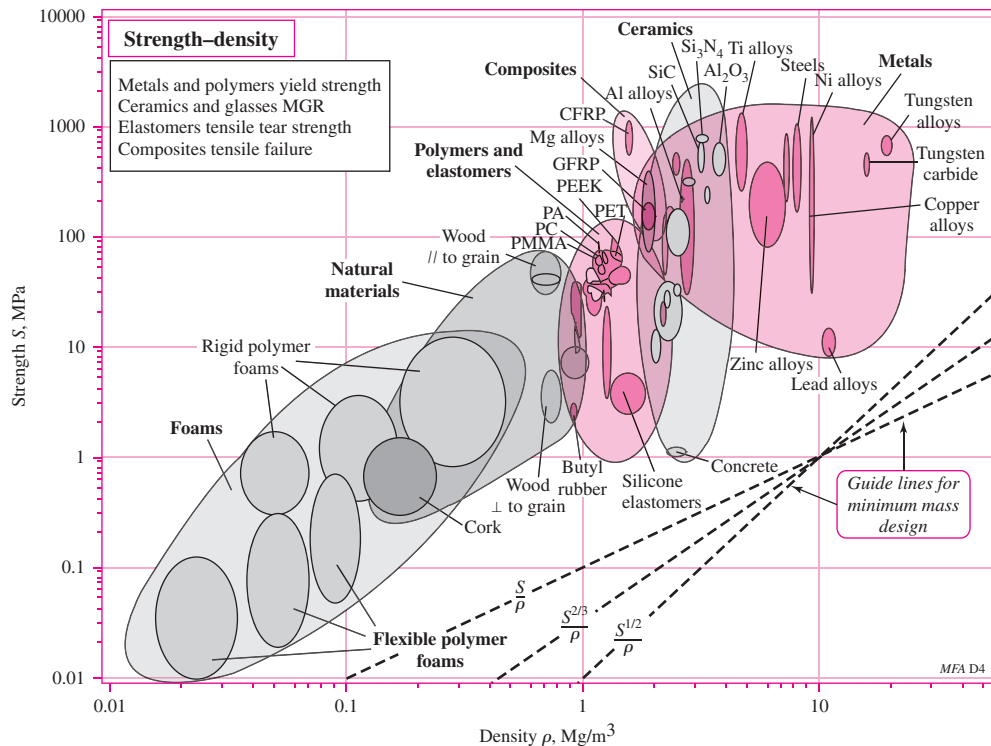
50 GPa. Figure 2–18 shows how this further restricts the search region. This eliminates woods as a possible material.

Another commonly useful chart, shown in Fig. 2–19, represents strength versus density for the material families. The ratio of strength to density is known as *specific strength*, and is particularly useful when it is desired to minimize weight where the primary design limitation is strength, rather than deflection. The guidelines in the lower right corner represent different relationships between strength and density, in the form of S^β/ρ . Following an approach similar to that used before, it can be shown that for axial loading, $\beta = 1$, and for bending loading, $\beta = 2/3$.

Certainly, in a given design exercise, there will be other considerations such as environment, cost, availability, and machinability, and other charts may be necessary to investigate. Also, we have not brought in the material process selection part of the picture. If done properly, material selection can result in a good deal of bookkeeping. This is where software packages such as CES Edupack become very effective.

Figure 2-19

Strength S versus density ρ for various materials. For metals, S is the 0.2 percent offset yield strength. For polymers, S is the 1 percent yield strength. For ceramics and glasses, S is the compressive crushing strength. For composites, S is the tensile strength. For elastomers, S is the tear strength. (Figure courtesy of Prof. Mike Ashby, Granta Design, Cambridge, U.K.)



PROBLEMS

2-1

Determine the tensile and yield strengths for the following materials:

- UNS G10200 hot-rolled steel.
- SAE 1050 cold-drawn steel.
- AISI 1141 steel quenched and tempered at 540°C.
- 2024-T4 aluminum alloy.
- Ti-6Al-4V annealed titanium alloy.

2-2

Assume you were specifying an AISI 1060 steel for an application. Using Table A-21,

- how would you specify it if you desired to maximize the yield strength?
- how would you specify it if you desired to maximize the ductility?

2-3

Determine the yield strength-to-weight density ratios (specific strength) in units of kN · m/kg for AISI 1018 CD steel, 2011-T6 aluminum, Ti-6Al-4V titanium alloy, and ASTM No. 40 gray cast iron.

2-4

Determine the stiffness-to-weight density ratios (specific modulus) in units of inches for AISI 1018 CD steel, 2011-T6 aluminum, Ti-6Al-4V titanium alloy, and ASTM No. 40 gray cast iron.

2-5

Poisson's ratio ν is a material property and is the ratio of the lateral strain and the longitudinal strain for a member in tension. For a homogeneous, isotropic material, the modulus of rigidity G is related to Young's modulus as

$$G = \frac{E}{2(1 + \nu)}$$

Using the tabulated values of G and E in Table A–5, calculate Poisson's ratio for steel, aluminum, beryllium copper, and gray cast iron. Determine the percent difference between the calculated values and the values tabulated in Table A–5.

- 2–6** A specimen of steel having an initial diameter of 0.503 in was tested in tension using a gauge length of 2 in. The following data were obtained for the elastic and plastic states:

Elastic State		Plastic State	
Load P lbf	Elongation in	Load P lbf	Area A , in 2
1 000	0.0004	8 800	0.1984
2 000	0.0006	9 200	0.1978
3 000	0.0010	9 100	0.1963
4 000	0.0013	13 200	0.1924
7 000	0.0023	15 200	0.1875
8 400	0.0028	17 000	0.1563
8 800	0.0036	16 400	0.1307
9 200	0.0089	14 800	0.1077

Note that there is some overlap in the data.

- (a) Plot the engineering or nominal stress-strain diagram using two scales for the unit strain ϵ , one scale from zero to about 0.02 in/in and the other scale from zero to maximum strain.
- (b) From this diagram find the modulus of elasticity, the 0.2 percent offset yield strength, the ultimate strength, and the percent reduction in area.
- (c) Characterize the material as ductile or brittle. Explain your reasoning.
- (d) Identify a material specification from Table A–20 that has a reasonable match to the data.

- 2–7** Compute the true stress and the logarithmic strain using the data of Prob. 2–6 and plot the results on log-log paper. Then find the plastic strength coefficient σ_0 and the strain-strengthening exponent m . Find also the yield strength and the ultimate strength after the specimen has had 20 percent cold work.

- 2–8** The stress-strain data from a tensile test on a cast-iron specimen are

Engineering stress, kpsi	5	10	16	19	26	32	40	46	49	54
Engineering strain, $\epsilon \cdot 10^{-3}$ in/in	0.20	0.44	0.80	1.0	1.5	2.0	2.8	3.4	4.0	5.0

Plot the stress-strain locus and find the 0.1 percent offset yield strength, and the tangent modulus of elasticity at zero stress and at 20 kpsi.

- 2–9** A part made from annealed AISI 1018 steel undergoes a 20 percent cold-work operation.
- (a) Obtain the yield strength and ultimate strength before and after the cold-work operation. Determine the percent increase in each strength.
 - (b) Determine the ratios of ultimate strength to yield strength before and after the cold-work operation. What does the result indicate about the change of ductility of the part?

- 2–10** Repeat Prob. 2–9 for a part made from hot-rolled AISI 1212 steel.

- 2–11** Repeat Prob. 2–9 for a part made from 2024-T4 aluminum alloy.

- 2–12** A steel member has a Brinell of $H_B = 275$. Estimate the ultimate strength of the steel in MPa.

- 2-13** A gray cast iron part has a Brinell hardness number of $H_B = 200$. Estimate the ultimate strength of the part in kpsi. Make a reasonable assessment of the likely grade of cast iron by comparing both hardness and strength to material options in Table A-24.
- 2-14** A part made from 1040 hot-rolled steel is to be heat treated to increase its strength to approximately 100 kpsi. What Brinell hardness number should be expected from the heat-treated part?
- 2-15** Brinell hardness tests were made on a random sample of 10 steel parts during processing. The results were H_B values of 230, 232(2), 234, 235(3), 236(2), and 239. Estimate the mean and standard deviation of the ultimate strength in kpsi.
- 2-16** Repeat Prob. 2-15 assuming the material to be cast iron.
- 2-17** For the material in Prob. 2-6: (a) Determine the modulus of resilience, and (b) Estimate the modulus of toughness, assuming that the last data point corresponds to fracture.
- 2-18** Some commonly used plain carbon steels are AISI 1010, 1018, and 1040. Research these steels and provide a comparative summary of their characteristics, focusing on aspects that make each one unique for certain types of application. Product application guides provided on the Internet by steel manufacturers and distributors are one source of information.
- 2-19** Repeat Prob. 2-18 for the commonly used alloy steels, AISI 4130 and 4340.
- 2-20** An application requires the support of an axial load of 100 kips with a round rod without exceeding the yield strength of the material. Assume the current cost per pound for round stock is given in the table below for several materials that are being considered. Material properties are available in Tables A-5, A-20, A-21, and A-24. Select one of the materials for each of the following additional design goals.
- Minimize diameter.
 - Minimize weight.
 - Minimize cost.
 - Minimize axial deflection.

Material	Cost/lbf
1020 HR	\$0.27
1020 CD	\$0.30
1040 Q&T @800°F	\$0.35
4140 Q&T @800°F	\$0.80
Wrought Al 2024 T3	\$1.10
Titanium alloy (Ti-6Al-4V)	\$7.00

- 2-21 to
2-23** A 1-in-diameter rod, 3 ft long, of unknown material is found in a machine shop. A variety of inexpensive nondestructive tests are readily available to help determine the material, as described below:
- Visual inspection.
 - Scratch test: Scratch the surface with a file; observe color of underlying material and depth of scratch.
 - Check if it is attracted to a magnet.
 - Measure weight (± 0.05 lbf).
 - Inexpensive bending deflection test: Clamp one end in a vise, leaving 24 in cantilevered. Apply a force of 100 lbf (± 1 lbf). Measure deflection of the free end (within $\pm 1/32$ in).
 - Brinell hardness test.

Choose which tests you would actually perform, and in what sequence, to minimize time and cost, but to determine the material with a reasonable level of confidence. The table below provides results that would be available to you if you choose to perform a given test. Explain your process, and include any calculations. You may assume the material is one listed in Table A–5. If it is carbon steel, try to determine an approximate specification from Table A–20.

Test	Results if test were made		
	Prob. 2–21	Prob. 2–22	Prob. 2–23
(a)	Dark gray, rough surface finish, moderate scale	Silvery gray, smooth surface finish, slightly tarnished	Reddish-brown, tarnished, smooth surface finish
(b)	Metallic gray, moderate scratch	Silvery gray, deep scratch	Shiny brassy color, deep scratch
(c)	Magnetic	Not magnetic	Not magnetic
(d)	$W = 7.95 \text{ lbf}$	$W = 2.90 \text{ lbf}$	$W = 9.00 \text{ lbf}$
(e)	$\delta = 5/16 \text{ in}$	$\delta = 7/8 \text{ in}$	$\delta = 17/32 \text{ in}$
(f)	$H_B = 200$	$H_B = 95$	$H_B = 70$

- 2–24** Search the website noted in Sec. 2–20 (<http://composite.about.com/cs/software/>) and report your findings. Your instructor may wish to elaborate on the level of this report. The website contains a large variety of resources. The activity for this problem can be divided among the class.
- 2–25** Research the material Inconel, briefly described in Table A–5. Compare it to various carbon and alloy steels in stiffness, strength, ductility, and toughness. What makes this material so special?
- 2–26** Consider a rod transmitting a tensile force. The following materials are being considered: tungsten carbide, high-carbon heat-treated steel, polycarbonate polymer, aluminum alloy. Using the Ashby charts, recommend one or two of the materials for a design situation in which failure is by exceeding the strength of the material, and it is desired to minimize the weight.
- 2–27** Repeat Prob. 2–26, except that the design situation is failure by excessive deflection, and it is desired to minimize the weight.
- 2–28** Consider a cantilever beam that is loaded with a transverse force at its tip. The following materials are being considered: tungsten carbide, high-carbon heat-treated steel, polycarbonate polymer, aluminum alloy. Using the Ashby charts, recommend one or two of the materials for a design situation in which failure is by exceeding the strength of the material and it is desired to minimize the weight.
- 2–29** Repeat Prob. 2–28, except that the design situation is failure by excessive deflection, and it is desired to minimize the weight.
- 2–30** For an axially loaded rod, prove that $\beta = 1$ for the E^β/ρ guidelines in Fig. 2–16.
- 2–31** For an axially loaded rod, prove that $\beta = 1$ for the S^β/ρ guidelines in Fig. 2–19.
- 2–32** For a cantilever beam loaded in bending, prove that $\beta = 1/2$ for the E^β/ρ guidelines in Fig. 2–16.
- 2–33** For a cantilever beam loaded in bending, prove that $\beta = 2/3$ for the S^β/ρ guidelines in Fig. 2–19.
- 2–34** Consider a tie rod transmitting a tensile force F . The corresponding tensile stress is given by $\sigma = F/A$, where A is the area of the cross section. The deflection of the rod is given by Eq. (4–3), which is $\delta = (Fl)/(AE)$, where l is the length of the rod. Using the Ashby charts of Figs. 2–16 and 2–19, explore what ductile materials are best suited for a light, stiff, and strong tie rod.
Hint: Consider stiffness and strength separately.

3

Load and Stress Analysis

Chapter Outline

3-1	Equilibrium and Free-Body Diagrams	72
3-2	Shear Force and Bending Moments in Beams	75
3-3	Singularity Functions	77
3-4	Stress	79
3-5	Cartesian Stress Components	79
3-6	Mohr's Circle for Plane Stress	80
3-7	General Three-Dimensional Stress	86
3-8	Elastic Strain	87
3-9	Uniformly Distributed Stresses	88
3-10	Normal Stresses for Beams in Bending	89
3-11	Shear Stresses for Beams in Bending	94
3-12	Torsion	101
3-13	Stress Concentration	110
3-14	Stresses in Pressurized Cylinders	113
3-15	Stresses in Rotating Rings	115
3-16	Press and Shrink Fits	116
3-17	Temperature Effects	117
3-18	Curved Beams in Bending	118
3-19	Contact Stresses	122
3-20	Summary	126

One of the main objectives of this book is to describe how specific machine components function and how to design or specify them so that they function safely without failing structurally. Although earlier discussion has described structural strength in terms of load or stress versus strength, failure of function for structural reasons may arise from other factors such as excessive deformations or deflections.

Here it is assumed that the reader has completed basic courses in statics of rigid bodies and mechanics of materials and is quite familiar with the analysis of loads, and the stresses and deformations associated with the basic load states of simple prismatic elements. In this chapter and Chap. 4 we will review and extend these topics briefly. Complete derivations will not be presented here, and the reader is urged to return to basic textbooks and notes on these subjects.

This chapter begins with a review of equilibrium and free-body diagrams associated with load-carrying components. One must understand the nature of forces before attempting to perform an extensive stress or deflection analysis of a mechanical component. An extremely useful tool in handling discontinuous loading of structures employs *Macaulay* or *singularity functions*. Singularity functions are described in Sec. 3–3 as applied to the shear forces and bending moments in beams. In Chap. 4, the use of singularity functions will be expanded to show their real power in handling deflections of complex geometry and statically indeterminate problems.

Machine components transmit forces and motion from one point to another. The transmission of force can be envisioned as a flow or force distribution that can be further visualized by isolating internal surfaces within the component. Force distributed over a surface leads to the concept of stress, stress components, and stress transformations (Mohr's circle) for all possible surfaces at a point.

The remainder of the chapter is devoted to the stresses associated with the basic loading of prismatic elements, such as uniform loading, bending, and torsion, and topics with major design ramifications such as stress concentrations, thin- and thick-walled pressurized cylinders, rotating rings, press and shrink fits, thermal stresses, curved beams, and contact stresses.

3–1 Equilibrium and Free-Body Diagrams

Equilibrium

The word *system* will be used to denote any *isolated* part or portion of a machine or structure—including all of it if desired—that we wish to study. A system, under this definition, may consist of a particle, several particles, a part of a rigid body, an entire rigid body, or even several rigid bodies.

If we assume that the system to be studied is motionless or, at most, has constant velocity, then the system has zero acceleration. Under this condition the system is said to be in *equilibrium*. The phrase *static equilibrium* is also used to imply that the system is *at rest*. For equilibrium, the forces and moments acting on the system balance such that

$$\sum \mathbf{F} = 0 \quad (3-1)$$

$$\sum \mathbf{M} = 0 \quad (3-2)$$

which states that *the sum of all force* and the *sum of all moment vectors* acting upon a system in equilibrium is zero.

Free-Body Diagrams

We can greatly simplify the analysis of a very complex structure or machine by successively isolating each element and studying and analyzing it by the use of *free-body diagrams*. When all the members have been treated in this manner, the knowledge obtained can be assembled to yield information concerning the behavior of the total system. Thus, free-body diagramming is essentially a means of breaking a complicated problem into manageable segments, analyzing these simple problems, and then, usually, putting the information together again.

Using free-body diagrams for force analysis serves the following important purposes:

- The diagram establishes the directions of reference axes, provides a place to record the dimensions of the subsystem and the magnitudes and directions of the known forces, and helps in assuming the directions of unknown forces.
- The diagram simplifies your thinking because it provides a place to store one thought while proceeding to the next.
- The diagram provides a means of communicating your thoughts clearly and unambiguously to other people.
- Careful and complete construction of the diagram clarifies fuzzy thinking by bringing out various points that are not always apparent in the statement or in the geometry of the total problem. Thus, the diagram aids in understanding all facets of the problem.
- The diagram helps in the planning of a logical attack on the problem and in setting up the mathematical relations.
- The diagram helps in recording progress in the solution and in illustrating the methods used.
- The diagram allows others to follow your reasoning, showing *all* forces.

EXAMPLE 3-1

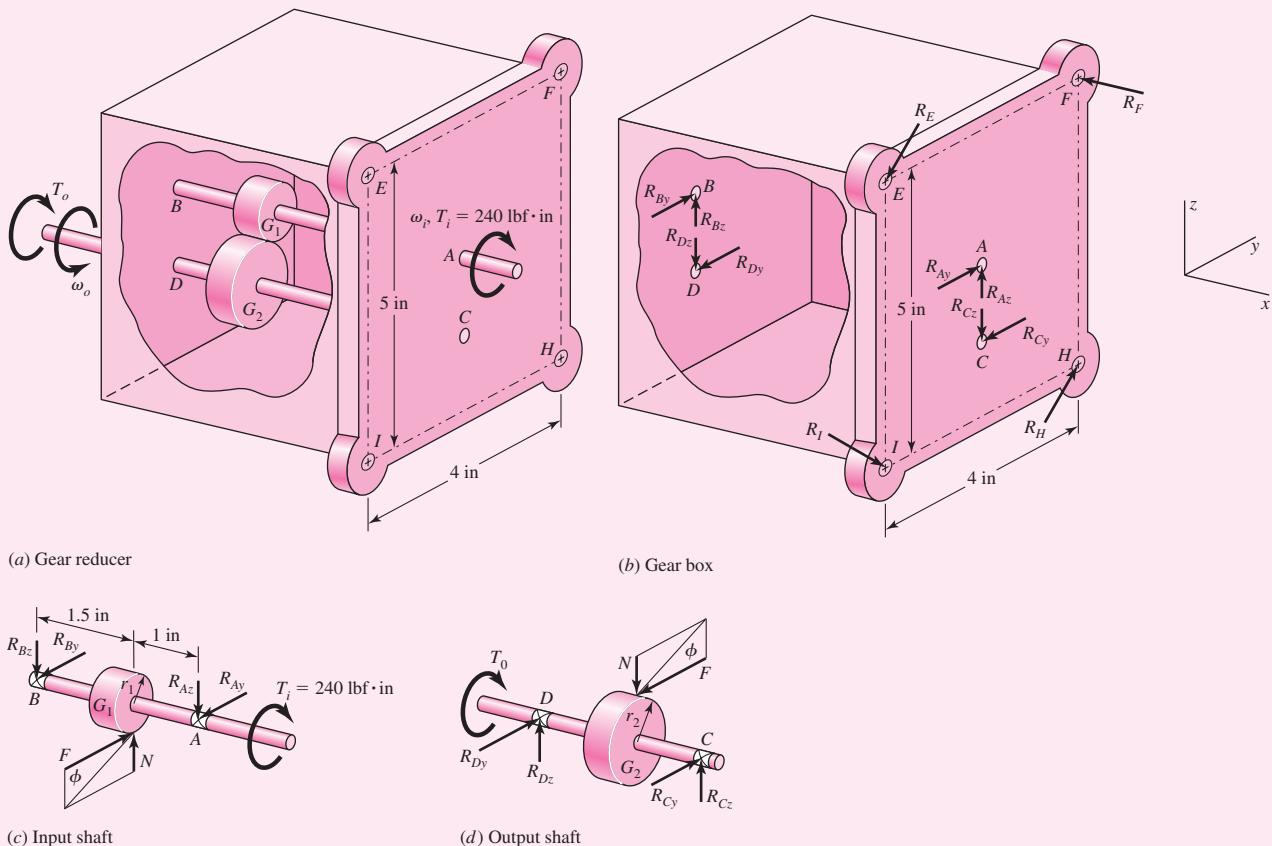
Figure 3–1a shows a simplified rendition of a gear reducer where the input and output shafts AB and CD are rotating at constant speeds ω_i and ω_o , respectively. The input and output torques (torsional moments) are $T_i = 240 \text{ lbf} \cdot \text{in}$ and T_o , respectively. The shafts are supported in the housing by bearings at A , B , C , and D . The pitch radii of gears G_1 and G_2 are $r_1 = 0.75 \text{ in}$ and $r_2 = 1.5 \text{ in}$, respectively. Draw the free-body diagrams of each member and determine the net reaction forces and moments at all points.

Solution

First, we will list all simplifying assumptions.

- 1 Gears G_1 and G_2 are simple spur gears with a standard pressure angle $\phi = 20^\circ$ (see Sec. 13–5).
- 2 The bearings are self-aligning and the shafts can be considered to be simply supported.
- 3 The weight of each member is negligible.
- 4 Friction is negligible.
- 5 The mounting bolts at E , F , H , and I are the same size.

The separate free-body diagrams of the members are shown in Figs. 3–1b–d. Note that Newton's third law, called the *law of action and reaction*, is used extensively where each member mates. The force transmitted between the spur gears is not tangential but at the pressure angle ϕ . Thus, $N = F \tan \phi$.

**Figure 3-1**

(a) Gear reducer; (b-d) free-body diagrams. Diagrams are not drawn to scale.

Summing moments about the x axis of shaft AB in Fig. 3-1d gives

$$\sum M_x = F(0.75) - 240 = 0$$

$$F = 320 \text{ lbf}$$

The normal force is $N = 320 \tan 20^\circ = 116.5 \text{ lbf}$.Using the equilibrium equations for Figs. 3-1c and d, the reader should verify that: $R_{Ay} = 192 \text{ lbf}$, $R_{Az} = 69.9 \text{ lbf}$, $R_{By} = 128 \text{ lbf}$, $R_{Bz} = 46.6 \text{ lbf}$, $R_{Cy} = 192 \text{ lbf}$, $R_{Cz} = 69.9 \text{ lbf}$, $R_{Dy} = 128 \text{ lbf}$, $R_{Dz} = 46.6 \text{ lbf}$, and $T_o = 480 \text{ lbf}\cdot\text{in}$. The direction of the output torque T_o is opposite ω_o because it is the resistive load on the system opposing the motion ω_o .Note in Fig. 3-1b the net force from the bearing reactions is zero whereas the net moment about the x axis is $(1.5 + 0.75)(192) + (1.5 + 0.75)(128) = 720 \text{ lbf}\cdot\text{in}$. This value is the same as $T_i + T_o = 240 + 480 = 720 \text{ lbf}\cdot\text{in}$, as shown in Fig. 3-1a. The reaction forces R_E , R_F , R_H , and R_I , from the mounting bolts cannot be determined from the equilibrium equations as there are too many unknowns. Only three equations are available, $\sum F_y = \sum F_z = \sum M_x = 0$. In case you were wondering about assumption 5, here is where we will use it (see Sec. 8-12). The gear box tends to rotate about the x axis because of a pure torsional moment of $720 \text{ lbf}\cdot\text{in}$. The bolt forces must provide

an equal but opposite torsional moment. The center of rotation relative to the bolts lies at the centroid of the bolt cross-sectional areas. Thus if the bolt areas are equal: the center of rotation is at the center of the four bolts, a distance of $\sqrt{(4/2)^2 + (5/2)^2} = 3.202$ in from each bolt; the bolt forces are equal ($R_E = R_F = R_H = R_I = R$), and each bolt force is perpendicular to the line from the bolt to the center of rotation. This gives a net torque from the four bolts of $4R(3.202) = 720$. Thus, $R_E = R_F = R_H = R_I = 56.22$ lbf.

3-2

Shear Force and Bending Moments in Beams

Figure 3-2a shows a beam supported by reactions R_1 and R_2 and loaded by the concentrated forces F_1 , F_2 , and F_3 . If the beam is cut at some section located at $x = x_1$ and the left-hand portion is removed as a free body, an *internal shear force* V and *bending moment* M must act on the cut surface to ensure equilibrium (see Fig. 3-2b). The shear force is obtained by summing the forces on the isolated section. The bending moment is the sum of the moments of the forces to the left of the section taken about an axis through the isolated section. The sign conventions used for bending moment and shear force in this book are shown in Fig. 3-3. Shear force and bending moment are related by the equation

$$V = \frac{dM}{dx} \quad (3-3)$$

Sometimes the bending is caused by a distributed load $q(x)$, as shown in Fig. 3-4; $q(x)$ is called the *load intensity* with units of force per unit length and is positive in the

Figure 3-2

Free-body diagram of simply-supported beam with V and M shown in positive directions.

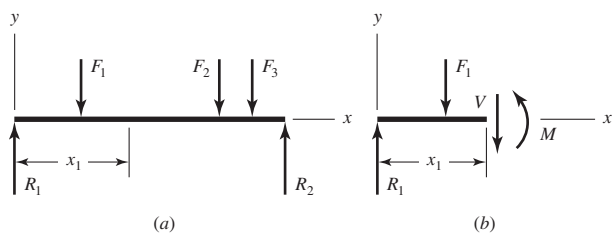


Figure 3-3

Sign conventions for bending and shear.

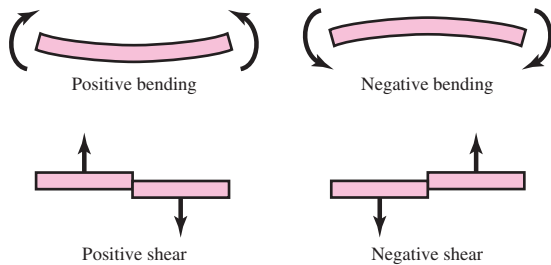
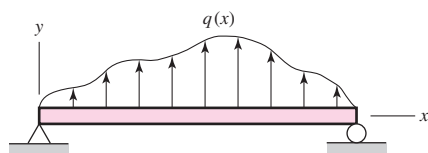


Figure 3-4

Distributed load on beam.



positive y direction. It can be shown that differentiating Eq. (3–3) results in

$$\frac{dV}{dx} = \frac{d^2M}{dx^2} = q \quad (3-4)$$

Normally the applied distributed load is directed downward and labeled w (e.g., see Fig. 3–6). In this case, $w = -q$.

Equations (3–3) and (3–4) reveal additional relations if they are integrated. Thus, if we integrate between, say, x_A and x_B , we obtain

$$\int_{V_A}^{V_B} dV = V_B - V_A = \int_{x_A}^{x_B} q dx \quad (3-5)$$

which states that *the change in shear force from A to B is equal to the area of the loading diagram between x_A and x_B* .

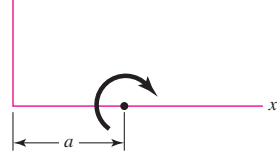
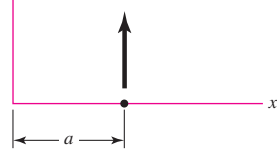
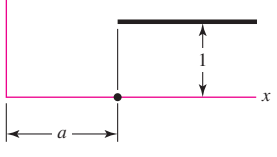
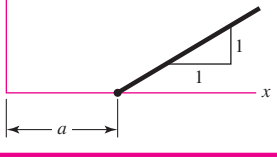
In a similar manner,

$$\int_{M_A}^{M_B} dM = M_B - M_A = \int_{x_A}^{x_B} V dx \quad (3-6)$$

which states that *the change in moment from A to B is equal to the area of the shear-force diagram between x_A and x_B* .

Table 3-1

Singularity (Macaulay)[†] Functions

Function	Graph of $f_n(x)$	Meaning
Concentrated moment (unit doublet)	$\langle x - a \rangle^{-2}$ 	$\langle x - a \rangle^{-2} = 0 \quad x \neq a$ $\langle x - a \rangle^{-2} = \pm\infty \quad x = a$ $\int \langle x - a \rangle^{-2} dx = \langle x - a \rangle^{-1}$
Concentrated force (unit impulse)	$\langle x - a \rangle^{-1}$ 	$\langle x - a \rangle^{-1} = 0 \quad x \neq a$ $\langle x - a \rangle^{-1} = +\infty \quad x = a$ $\int \langle x - a \rangle^{-1} dx = \langle x - a \rangle^0$
Unit step	$\langle x - a \rangle^0$ 	$\langle x - a \rangle^0 = \begin{cases} 0 & x < a \\ 1 & x \geq a \end{cases}$ $\int \langle x - a \rangle^0 dx = \langle x - a \rangle^1$
Ramp	$\langle x - a \rangle^1$ 	$\langle x - a \rangle^1 = \begin{cases} 0 & x < a \\ x - a & x \geq a \end{cases}$ $\int \langle x - a \rangle^1 dx = \frac{(x - a)^2}{2}$

[†]W. H. Macaulay, "Note on the deflection of beams," *Messenger of Mathematics*, vol. 48, pp. 129–130, 1919.

3–3 Singularity Functions

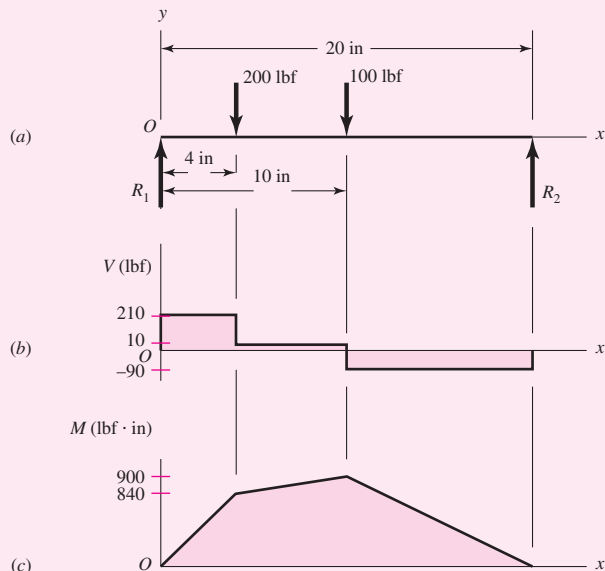
The four singularity functions defined in Table 3–1, using the *angle brackets* $\langle \rangle$, constitute a useful and easy means of integrating across discontinuities. By their use, general expressions for shear force and bending moment in beams can be written when the beam is loaded by concentrated moments or forces. As shown in the table, the concentrated moment and force functions are zero for all values of x not equal to a . The functions are undefined for values of $x = a$. Note that the unit step and ramp functions are zero only for values of x that are less than a . The integration properties shown in the table constitute a part of the mathematical definition too. The first two integrations of $q(x)$ for $V(x)$ and $M(x)$ do not require constants of integration provided *all* loads on the beam are accounted for in $q(x)$. The examples that follow show how these functions are used.

EXAMPLE 3–2

Derive the loading, shear-force, and bending-moment relations for the beam of Fig. 3–5a.

Figure 3–5

- (a) Loading diagram for a simply-supported beam.
- (b) Shear-force diagram.
- (c) Bending-moment diagram.



Solution

Using Table 3–1 and $q(x)$ for the loading function, we find

$$q = R_1\langle x \rangle^{-1} - 200\langle x - 4 \rangle^{-1} - 100\langle x - 10 \rangle^{-1} + R_2\langle x - 20 \rangle^{-1} \quad (1)$$

Integrating successively gives

$$V = \int q \, dx = R_1\langle x \rangle^0 - 200\langle x - 4 \rangle^0 - 100\langle x - 10 \rangle^0 + R_2\langle x - 20 \rangle^0 \quad (2)$$

$$M = \int V \, dx = R_1\langle x \rangle^1 - 200\langle x - 4 \rangle^1 - 100\langle x - 10 \rangle^1 + R_2\langle x - 20 \rangle^1 \quad (3)$$

Note that $V = M = 0$ at $x = 0^-$.

The reactions R_1 and R_2 can be found by taking a summation of moments and forces as usual, *or* they can be found by noting that the shear force and bending moment must be zero everywhere except in the region $0 \leq x \leq 20$ in. This means that Eq. (2)

should give $V = 0$ at x slightly larger than 20 in. Thus

$$R_1 - 200 - 100 + R_2 = 0 \quad (4)$$

Since the bending moment should also be zero in the same region, we have, from Eq. (3),

$$R_1(20) - 200(20 - 4) - 100(20 - 10) = 0 \quad (5)$$

Equations (4) and (5) yield the reactions $R_1 = 210$ lbf and $R_2 = 90$ lbf.

The reader should verify that substitution of the values of R_1 and R_2 into Eqs. (2) and (3) yield Figs. 3-5b and c.

EXAMPLE 3-3

Figure 3-6a shows the loading diagram for a beam cantilevered at A with a uniform load of 20 lbf/in acting on the portion $3 \text{ in} \leq x \leq 7$ in, and a concentrated clockwise moment of 240 lbf · in at $x = 10$ in. Derive the shear-force and bending-moment relations, and the support reactions M_1 and R_1 .

Solution

Following the procedure of Example 3-2, we find the load intensity function to be

$$q = -M_1(x)^{-2} + R_1(x)^{-1} - 20(x - 3)^0 + 20(x - 7)^0 - 240(x - 10)^{-2} \quad (1)$$

Note that the $20(x - 7)^0$ term was necessary to “turn off” the uniform load at C . Integrating successively gives

Answers

$$V = -M_1(x)^{-1} + R_1(x)^0 - 20(x - 3)^1 + 20(x - 7)^1 - 240(x - 10)^{-1} \quad (2)$$

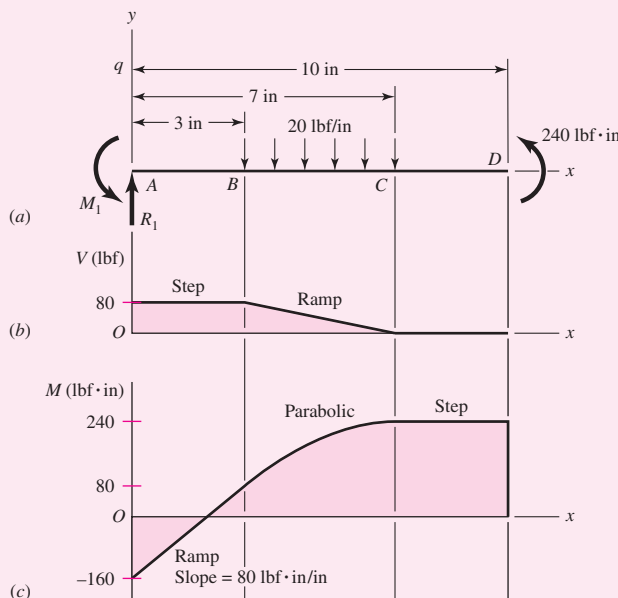
$$M = -M_1(x)^0 + R_1(x)^1 - 10(x - 3)^2 + 10(x - 7)^2 - 240(x - 10)^0 \quad (3)$$

The reactions are found by making x slightly larger than 10 in, where both V and M are zero in this region. Noting that $(10)^{-1} = 0$, Eq. (2) will then give

$$-M_1(0) + R_1(1) - 20(10 - 3) + 20(10 - 7) - 240(0) = 0$$

Figure 3-6

- (a) Loading diagram for a beam cantilevered at A .
- (b) Shear-force diagram.
- (c) Bending-moment diagram.



Answer which yields $R_1 = 80 \text{ lbf}$.

From Eq. (3) we get

$$-M_1(1) + 80(10) - 10(10 - 3)^2 + 10(10 - 7)^2 - 240(1) = 0$$

Answer which yields $M_1 = 160 \text{ lbf} \cdot \text{in}$.

Figures 3–6b and c show the shear-force and bending-moment diagrams. Note that the impulse terms in Eq. (2), $-M_1 \langle x \rangle^{-1}$ and $-240 \langle x - 10 \rangle^{-1}$, are physically not forces and are not shown in the V diagram. Also note that both the M_1 and 240 lbf · in moments are counterclockwise and negative singularity functions; however, by the convention shown in Fig. 3–2 the M_1 and 240 lbf · in are negative and positive bending moments, respectively, which is reflected in Fig. 3–6c.

3–4 Stress

When an internal surface is isolated as in Fig. 3–2b, the net force and moment acting on the surface manifest themselves as force distributions across the entire area. The force distribution acting at a point on the surface is unique and will have components in the normal and tangential directions called *normal stress* and *tangential shear stress*, respectively. Normal and shear stresses are labeled by the Greek symbols σ and τ , respectively. If the direction of σ is outward from the surface it is considered to be a *tensile stress* and is a positive normal stress. If σ is into the surface it is a *compressive stress* and commonly considered to be a negative quantity. The units of stress in U.S. Customary units are pounds per square inch (psi). For SI units, stress is in newtons per square meter (N/m^2); $1 \text{ N}/\text{m}^2 = 1 \text{ pascal (Pa)}$.

3–5 Cartesian Stress Components

The Cartesian stress components are established by defining three mutually orthogonal surfaces at a point within the body. The normals to each surface will establish the x , y , z Cartesian axes. In general, each surface will have a normal and shear stress. The shear stress may have components along two Cartesian axes. For example, Fig. 3–7 shows an infinitesimal surface area isolation at a point Q within a body where the surface normal is the x direction. The normal stress is labeled σ_x . The symbol σ indicates a normal stress and the subscript x indicates the direction of the surface normal. The net shear stress acting on the surface is $(\tau_x)_{\text{net}}$ which can be resolved into components in the y and z directions, labeled as τ_{xy} and τ_{xz} , respectively (see Fig. 3–7).

Figure 3–7

Stress components on surface normal to x direction.

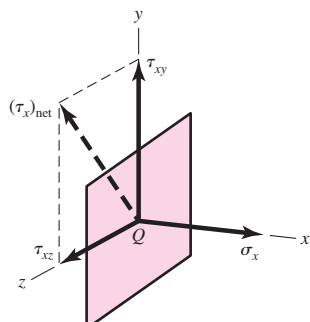
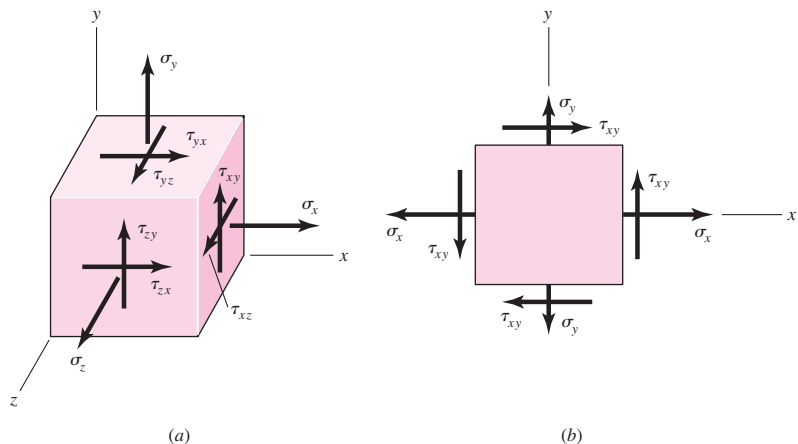


Figure 3-8

(a) General three-dimensional stress. (b) Plane stress with “cross-shears” equal.



Note that double subscripts are necessary for the shear. The first subscript indicates the direction of the surface normal whereas the second subscript is the direction of the shear stress.

The state of stress at a point described by three mutually perpendicular surfaces is shown in Fig. 3-8a. It can be shown through coordinate transformation that this is sufficient to determine the state of stress on *any* surface intersecting the point. As the dimensions of the cube in Fig. 3-8a approach zero, the stresses on the hidden faces become equal and opposite to those on the opposing visible faces. Thus, in general, a complete state of stress is defined by nine stress components, σ_x , σ_y , σ_z , τ_{xy} , τ_{xz} , τ_{yx} , τ_{yz} , τ_{zx} , and τ_{zy} .

For equilibrium, in most cases, “cross-shears” are equal, hence

$$\tau_{yx} = \tau_{xy} \quad \tau_{zy} = \tau_{yz} \quad \tau_{xz} = \tau_{zx} \quad (3-7)$$

This reduces the number of stress components for most three-dimensional states of stress from nine to six quantities, σ_x , σ_y , σ_z , τ_{xy} , τ_{yz} , and τ_{zx} .

A very common state of stress occurs when the stresses on one surface are zero. When this occurs the state of stress is called *plane stress*. Figure 3-8b shows a state of plane stress, arbitrarily assuming that the normal for the stress-free surface is the z direction such that $\sigma_z = \tau_{zx} = \tau_{zy} = 0$. It is important to note that the element in Fig. 3-8b is still a three-dimensional cube. Also, here it is assumed that the cross-shears are equal such that $\tau_{yx} = \tau_{xy}$, and $\tau_{yz} = \tau_{zy} = \tau_{xz} = \tau_{zx} = 0$.

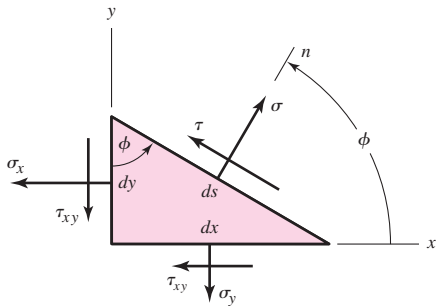
3-6 Mohr's Circle for Plane Stress

Suppose the $dx dy dz$ element of Fig. 3-8b is cut by an oblique plane with a normal n at an arbitrary angle ϕ counterclockwise from the x axis as shown in Fig. 3-9. Here, we are concerned with the stresses σ and τ that act upon this oblique plane. By summing the forces caused by all the stress components to zero, the stresses σ and τ are found to be

$$\sigma = \frac{\sigma_x + \sigma_y}{2} + \frac{\sigma_x - \sigma_y}{2} \cos 2\phi + \tau_{xy} \sin 2\phi \quad (3-8)$$

$$\tau = -\frac{\sigma_x - \sigma_y}{2} \sin 2\phi + \tau_{xy} \cos 2\phi \quad (3-9)$$

Equations (3-8) and (3-9) are called the *plane-stress transformation equations*.

| Figure 3–9

Differentiating Eq. (3–8) with respect to ϕ and setting the result equal to zero maximizes σ and gives

$$\tan 2\phi_p = \frac{2\tau_{xy}}{\sigma_x - \sigma_y} \quad (3-10)$$

Equation (3–10) defines two particular values for the angle $2\phi_p$, one of which defines the maximum normal stress σ_1 and the other, the minimum normal stress σ_2 . These two stresses are called the *principal stresses*, and their corresponding directions, the *principal directions*. The angle between the two principal directions is 90° . It is important to note that Eq. (3–10) can be written in the form

$$\frac{\sigma_x - \sigma_y}{2} \sin 2\phi_p - \tau_{xy} \cos 2\phi_p = 0 \quad (a)$$

Comparing this with Eq. (3–9), we see that $\tau = 0$, meaning that the perpendicular *surfaces containing principal stresses have zero shear stresses*.

In a similar manner, we differentiate Eq. (3–9), set the result equal to zero, and obtain

$$\tan 2\phi_s = -\frac{\sigma_x - \sigma_y}{2\tau_{xy}} \quad (3-11)$$

Equation (3–11) defines the two values of $2\phi_s$ at which the shear stress τ reaches an extreme value. The angle between the two surfaces containing the maximum shear stresses is 90° . Equation (3–11) can also be written as

$$\frac{\sigma_x - \sigma_y}{2} \cos 2\phi_p + \tau_{xy} \sin 2\phi_p = 0 \quad (b)$$

Substituting this into Eq. (3–8) yields

$$\sigma = \frac{\sigma_x + \sigma_y}{2} \quad (3-12)$$

Equation (3–12) tells us that the two surfaces containing the maximum shear stresses also contain equal normal stresses of $(\sigma_x + \sigma_y)/2$.

Comparing Eqs. (3–10) and (3–11), we see that $\tan 2\phi_s$ is the negative reciprocal of $\tan 2\phi_p$. This means that $2\phi_s$ and $2\phi_p$ are angles 90° apart, and thus the angles between the surfaces containing the maximum shear stresses and the surfaces containing the principal stresses are $\pm 45^\circ$.

Formulas for the two principal stresses can be obtained by substituting the angle $2\phi_p$ from Eq. (3–10) in Eq. (3–8). The result is

$$\sigma_1, \sigma_2 = \frac{\sigma_x + \sigma_y}{2} \pm \sqrt{\left(\frac{\sigma_x - \sigma_y}{2}\right)^2 + \tau_{xy}^2} \quad (3-13)$$

In a similar manner the two extreme-value shear stresses are found to be

$$\tau_1, \tau_2 = \pm \sqrt{\left(\frac{\sigma_x - \sigma_y}{2}\right)^2 + \tau_{xy}^2} \quad (3-14)$$

Your particular attention is called to the fact that an extreme value of the shear stress *may not be the same as the actual maximum value*. See Sec. 3-7.

It is important to note that the equations given to this point are quite sufficient for performing any plane stress transformation. However, extreme care must be exercised when applying them. For example, say you are attempting to determine the principal state of stress for a problem where $\sigma_x = 14$ MPa, $\sigma_y = -10$ MPa, and $\tau_{xy} = -16$ MPa. Equation (3-10) yields $\phi_p = -26.57^\circ$ and 63.43° , which locate the principal stress surfaces, whereas, Eq. (3-13) gives $\sigma_1 = 22$ MPa and $\sigma_2 = -18$ MPa for the principal stresses. If all we wanted was the principal stresses, we would be finished. However, what if we wanted to draw the element containing the principal stresses properly oriented relative to the x, y axes? Well, we have two values of ϕ_p and two values for the principal stresses. How do we know which value of ϕ_p corresponds to which value of the principal stress? To clear this up we would need to substitute one of the values of ϕ_p into Eq. (3-8) to determine the normal stress corresponding to that angle.

A graphical method for expressing the relations developed in this section, called *Mohr's circle diagram*, is a very effective means of visualizing the stress state at a point and keeping track of the directions of the various components associated with plane stress. Equations (3-8) and (3-9) can be shown to be a set of parametric equations for σ and τ , where the parameter is 2ϕ . The parametric relationship between σ and τ is that of a circle plotted in the σ, τ plane, where the center of the circle is located at $C = (\sigma, \tau) = [(\sigma_x + \sigma_y)/2, 0]$ and has a radius of $R = \sqrt{[(\sigma_x - \sigma_y)/2]^2 + \tau_{xy}^2}$. A problem arises in the sign of the shear stress. The transformation equations are based on a positive ϕ being counterclockwise, as shown in Fig. 3-9. If a positive τ were plotted above the σ axis, points would rotate clockwise on the circle 2ϕ in the opposite direction of rotation on the element. It would be convenient if the rotations were in the same direction. One could solve the problem easily by plotting positive τ below the axis. However, the classical approach to Mohr's circle uses a different convention for the shear stress.

Mohr's Circle Shear Convention

This convention is followed in drawing Mohr's circle:

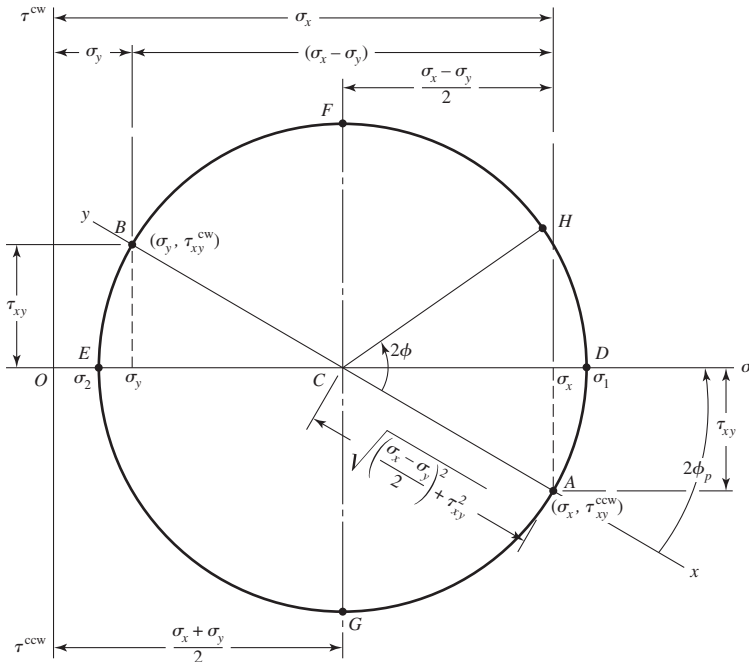
- Shear stresses tending to rotate the element clockwise (cw) are plotted *above* the σ axis.
- Shear stresses tending to rotate the element counterclockwise (ccw) are plotted *below* the σ axis.

For example, consider the right face of the element in Fig. 3-8b. By Mohr's circle convention the shear stress shown is plotted *below* the σ axis because it tends to rotate the element counterclockwise. The shear stress on the top face of the element is plotted *above* the σ axis because it tends to rotate the element clockwise.

In Fig. 3-10 we create a coordinate system with normal stresses plotted along the abscissa and shear stresses plotted as the ordinates. On the abscissa, tensile (positive) normal stresses are plotted to the right of the origin O and compressive (negative) normal stresses to the left. On the ordinate, clockwise (cw) shear stresses are plotted up; counterclockwise (ccw) shear stresses are plotted down.

Figure 3-10

Mohr's circle diagram.



Using the stress state of Fig. 3-8b, we plot Mohr's circle, Fig. 3-10, by first looking at the right surface of the element containing σ_x to establish the sign of σ_x and the cw or ccw direction of the shear stress. The right face is called the *x face* where $\phi = 0^\circ$. If σ_x is positive and the shear stress τ_{xy} is ccw as shown in Fig. 3-8b, we can establish point A with coordinates $(\sigma_x, \tau_{xy}^{ccw})$ in Fig. 3-10. Next, we look at the top *y face*, where $\phi = 90^\circ$, which contains σ_y , and repeat the process to obtain point B with coordinates $(\sigma_y, \tau_{xy}^{cw})$ as shown in Fig. 3-10. The two states of stress for the element are $\Delta\phi = 90^\circ$ from each other on the element so they will be $2\Delta\phi = 180^\circ$ from each other on Mohr's circle. Points A and B are the same vertical distance from the σ axis. Thus, AB must be on the diameter of the circle, and the center of the circle C is where AB intersects the σ axis. With points A and B on the circle, and center C, the complete circle can then be drawn. Note that the extended ends of line AB are labeled *x* and *y* as references to the normals to the surfaces for which points A and B represent the stresses.

The entire Mohr's circle represents the state of stress at a *single* point in a structure. Each point on the circle represents the stress state for a *specific* surface intersecting the point in the structure. Each pair of points on the circle 180° apart represent the state of stress on an element whose surfaces are 90° apart. Once the circle is drawn, the states of stress can be visualized for various surfaces intersecting the point being analyzed. For example, the principal stresses σ_1 and σ_2 are points D and E, respectively, and their values obviously agree with Eq. (3-13). We also see that the shear stresses are zero on the surfaces containing σ_1 and σ_2 . The two extreme-value shear stresses, one clockwise and one counterclockwise, occur at F and G with magnitudes equal to the radius of the circle. The surfaces at F and G each also contain normal stresses of $(\sigma_x + \sigma_y)/2$ as noted earlier in Eq. (3-12). Finally, the state of stress on an arbitrary surface located at an angle ϕ counterclockwise from the *x* face is point H.

At one time, Mohr's circle was used graphically where it was drawn to scale very accurately and values were measured by using a scale and protractor. Here, we are strictly using Mohr's circle as a visualization aid and will use a semigraphical approach, calculating values from the properties of the circle. This is illustrated by the following example.

EXAMPLE 3-4

A stress element has $\sigma_x = 80$ MPa and $\tau_{xy} = 50$ MPa cw, as shown in Fig. 3-11a.

(a) Using Mohr's circle, find the principal stresses and directions, and show these on a stress element correctly aligned with respect to the xy coordinates. Draw another stress element to show τ_1 and τ_2 , find the corresponding normal stresses, and label the drawing completely.

(b) Repeat part *a* using the transformation equations only.

Solution

(a) In the semigraphical approach used here, we first make an approximate freehand sketch of Mohr's circle and then use the geometry of the figure to obtain the desired information.

Draw the σ and τ axes first (Fig. 3-11b) and from the x face locate $\sigma_x = 80$ MPa along the σ axis. On the x face of the element, we see that the shear stress is 50 MPa in the cw direction. Thus, for the x face, this establishes point A (80, 50^{cw}) MPa. Corresponding to the y face, the stress is $\sigma = 0$ and $\tau = 50$ MPa in the ccw direction. This locates point B (0, 50^{ccw}) MPa. The line AB forms the diameter of the required circle, which can now be drawn. The intersection of the circle with the σ axis defines σ_1 and σ_2 as shown. Now, noting the triangle ACD , indicate on the sketch the length of the legs AD and CD as 50 and 40 MPa, respectively. The length of the hypotenuse AC is

Answer

$$\tau_1 = \sqrt{(50)^2 + (40)^2} = 64.0 \text{ MPa}$$

and this should be labeled on the sketch too. Since intersection C is 40 MPa from the origin, the principal stresses are now found to be

Answer

$$\sigma_1 = 40 + 64 = 104 \text{ MPa} \quad \text{and} \quad \sigma_2 = 40 - 64 = -24 \text{ MPa}$$

The angle 2ϕ from the x axis cw to σ_1 is

Answer

$$2\phi_p = \tan^{-1} \frac{50}{40} = 51.3^\circ$$

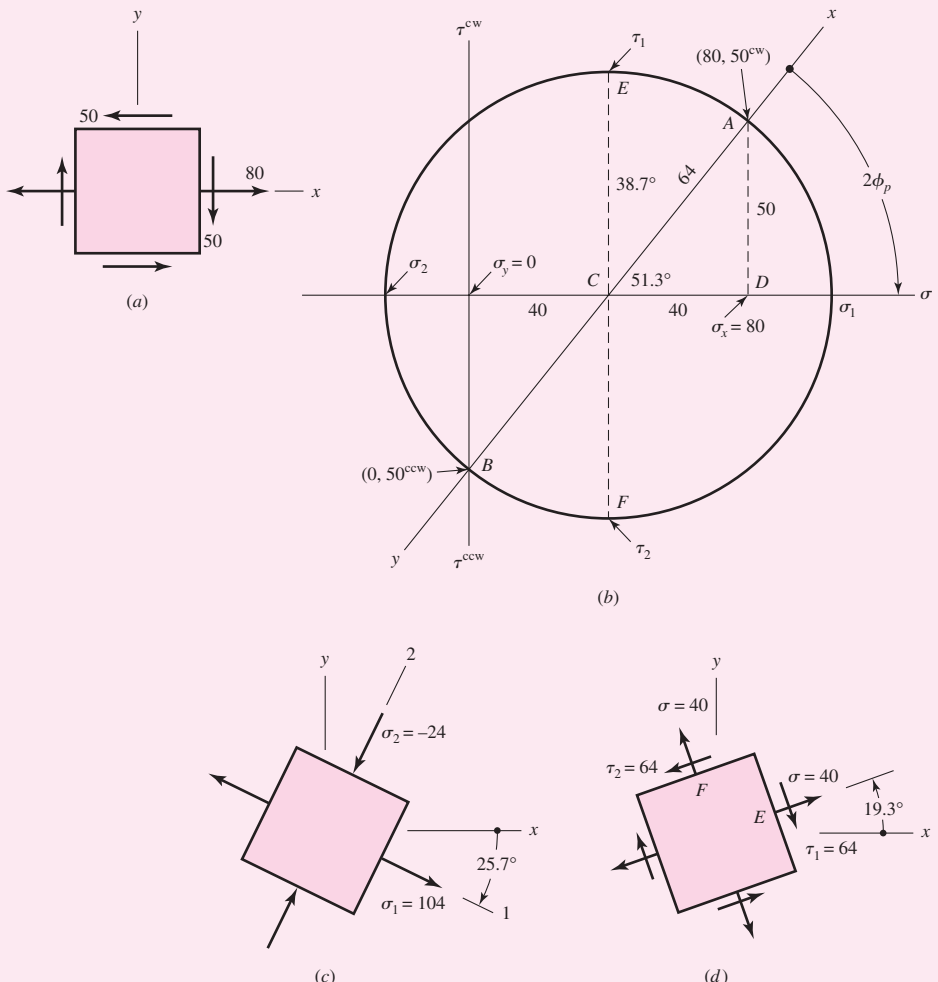
To draw the principal stress element (Fig. 3-11c), sketch the x and y axes parallel to the original axes. The angle ϕ_p on the stress element must be measured in the *same* direction as is the angle $2\phi_p$ on the Mohr circle. Thus, from x measure 25.7° (half of 51.3°) clockwise to locate the σ_1 axis. The σ_2 axis is 90° from the σ_1 axis and the stress element can now be completed and labeled as shown. Note that there are *no* shear stresses on this element.

The two maximum shear stresses occur at points E and F in Fig. 3-11b. The two normal stresses corresponding to these shear stresses are each 40 MPa, as indicated. Point E is 38.7° ccw from point A on Mohr's circle. Therefore, in Fig. 3-11d, draw a stress element oriented 19.3° (half of 38.7°) ccw from x . The element should then be labeled with magnitudes and directions as shown.

In constructing these stress elements it is important to indicate the x and y directions of the original reference system. This completes the link between the original machine element and the orientation of its principal stresses.

Figure 3-11

All stresses in MPa.

**Answer**

(b) The transformation equations are programmable. From Eq. (3-10),

$$\phi_p = \frac{1}{2} \tan^{-1} \left(\frac{2\tau_{xy}}{\sigma_x - \sigma_y} \right) = \frac{1}{2} \tan^{-1} \left(\frac{2(-50)}{80} \right) = -25.7^\circ, 64.3^\circ$$

From Eq. (3-8), for the first angle \$\phi_p = -25.7^\circ\$,

$$\sigma = \frac{80 + 0}{2} + \frac{80 - 0}{2} \cos[2(-25.7)] + (-50) \sin[2(-25.7)] = 104.03 \text{ MPa}$$

The shear on this surface is obtained from Eq. (3-9) as

$$\tau = -\frac{80 - 0}{2} \sin[2(-25.7)] + (-50) \cos[2(-25.7)] = 0 \text{ MPa}$$

which confirms that 104.03 MPa is a principal stress. From Eq. (3-8), for \$\phi_p = 64.3^\circ\$,

$$\sigma = \frac{80 + 0}{2} + \frac{80 - 0}{2} \cos[2(64.3)] + (-50) \sin[2(64.3)] = -24.03 \text{ MPa}$$

Answer Substituting $\phi_p = 64.3^\circ$ into Eq. (3–9) again yields $\tau = 0$, indicating that -24.03 MPa is also a principal stress. Once the principal stresses are calculated they can be ordered such that $\sigma_1 \geq \sigma_2$. Thus, $\sigma_1 = 104.03 \text{ MPa}$ and $\sigma_2 = -24.03 \text{ MPa}$.

Since for $\sigma_1 = 104.03 \text{ MPa}$, $\phi_p = -25.7^\circ$, and since ϕ is defined positive ccw in the transformation equations, we rotate *clockwise* 25.7° for the surface containing σ_1 . We see in Fig. 3–11c that this totally agrees with the semigraphical method.

To determine τ_1 and τ_2 , we first use Eq. (3–11) to calculate ϕ_s :

$$\phi_s = \frac{1}{2} \tan^{-1} \left(-\frac{\sigma_x - \sigma_y}{2\tau_{xy}} \right) = \frac{1}{2} \tan^{-1} \left(-\frac{80}{2(-50)} \right) = 19.3^\circ, 109.3^\circ$$

For $\phi_s = 19.3^\circ$, Eqs. (3–8) and (3–9) yield

Answer $\sigma = \frac{80+0}{2} + \frac{80-0}{2} \cos[2(19.3)] + (-50) \sin[2(19.3)] = 40.0 \text{ MPa}$

$$\tau = -\frac{80-0}{2} \sin[2(19.3)] + (-50) \cos[2(19.3)] = -64.0 \text{ MPa}$$

Remember that Eqs. (3–8) and (3–9) are *coordinate* transformation equations. Imagine that we are rotating the x , y axes 19.3° counterclockwise and y will now point up and to the left. So a negative shear stress on the rotated x face will point down and to the right as shown in Fig. 3–11d. Thus again, results agree with the semigraphical method.

For $\phi_s = 109.3^\circ$, Eqs. (3–8) and (3–9) give $\sigma = 40.0 \text{ MPa}$ and $\tau = +64.0 \text{ MPa}$. Using the same logic for the coordinate transformation we find that results again agree with Fig. 3–11d.

3–7

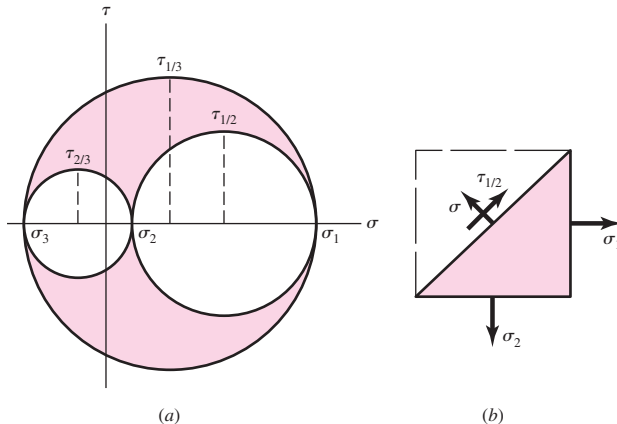
General Three-Dimensional Stress

As in the case of plane stress, a particular orientation of a stress element occurs in space for which all shear-stress components are zero. When an element has this particular orientation, the normals to the faces are mutually orthogonal and correspond to the principal directions, and the normal stresses associated with these faces are the principal stresses. Since there are three faces, there are three principal directions and three principal stresses σ_1 , σ_2 , and σ_3 . For plane stress, the stress-free surface contains the third principal stress which is zero.

In our studies of plane stress we were able to specify any stress state σ_x , σ_y , and τ_{xy} and find the principal stresses and principal directions. But six components of stress are required to specify a general state of stress in three dimensions, and the problem of determining the principal stresses and directions is more difficult. In design, three-dimensional transformations are rarely performed since most maximum stress states occur under plane stress conditions. One notable exception is contact stress, which is not a case of plane stress, where the three principal stresses are given in Sec. 3–19. In fact, *all* states of stress are truly three-dimensional, where they might be described one- or two-dimensionally with respect to *specific* coordinate axes. Here it is most important to understand the relationship among the *three* principal stresses. The process in finding the three principal stresses from the six

Figure 3-12

Mohr's circles for three-dimensional stress.



stress components σ_x , σ_y , σ_z , τ_{xy} , τ_{yz} , and τ_{zx} , involves finding the roots of the cubic equation¹

$$\begin{aligned}\sigma^3 - (\sigma_x + \sigma_y + \sigma_z)\sigma^2 + (\sigma_x\sigma_y + \sigma_x\sigma_z + \sigma_y\sigma_z - \tau_{xy}^2 - \tau_{yz}^2 - \tau_{zx}^2)\sigma \\ - (\sigma_x\sigma_y\sigma_z + 2\tau_{xy}\tau_{yz}\tau_{zx} - \sigma_x\tau_{yz}^2 - \sigma_y\tau_{zx}^2 - \sigma_z\tau_{xy}^2) = 0\end{aligned}\quad (3-15)$$

In plotting Mohr's circles for three-dimensional stress, the principal normal stresses are ordered so that $\sigma_1 \geq \sigma_2 \geq \sigma_3$. Then the result appears as in Fig. 3-12a. The stress coordinates σ , τ for any arbitrarily located plane will always lie on the boundaries or within the shaded area.

Figure 3-12a also shows the three *principal shear stresses* $\tau_{1/2}$, $\tau_{2/3}$, and $\tau_{1/3}$.² Each of these occurs on the two planes, one of which is shown in Fig. 3-12b. The figure shows that the principal shear stresses are given by the equations

$$\tau_{1/2} = \frac{\sigma_1 - \sigma_2}{2} \quad \tau_{2/3} = \frac{\sigma_2 - \sigma_3}{2} \quad \tau_{1/3} = \frac{\sigma_1 - \sigma_3}{2} \quad (3-16)$$

Of course, $\tau_{\max} = \tau_{1/3}$ when the normal principal stresses are ordered ($\sigma_1 > \sigma_2 > \sigma_3$), so always order your principal stresses. Do this in any computer code you generate and you'll always generate τ_{\max} .

3-8 Elastic Strain

Normal strain ϵ is defined and discussed in Sec. 2-1 for the tensile specimen and is given by Eq. (2-2) as $\epsilon = \delta/l$, where δ is the total elongation of the bar within the length l . Hooke's law for the tensile specimen is given by Eq. (2-3) as

$$\sigma = E\epsilon \quad (3-17)$$

where the constant E is called *Young's modulus* or the *modulus of elasticity*.

¹For development of this equation and further elaboration of three-dimensional stress transformations see: Richard G. Budynas, *Advanced Strength and Applied Stress Analysis*, 2nd ed., McGraw-Hill, New York, 1999, pp. 46–78.

²Note the difference between this notation and that for a shear stress, say, τ_{xy} . The use of the shilling mark is not accepted practice, but it is used here to emphasize the distinction.

When a material is placed in tension, there exists not only an axial strain, but also negative strain (contraction) perpendicular to the axial strain. Assuming a linear, homogeneous, isotropic material, this lateral strain is proportional to the axial strain. If the axial direction is x , then the lateral strains are $\epsilon_y = \epsilon_z = -\nu\epsilon_x$. The constant of proportionality ν is called *Poisson's ratio*, which is about 0.3 for most structural metals. See Table A-5 for values of ν for common materials.

If the axial stress is in the x direction, then from Eq. (3-17)

$$\epsilon_x = \frac{\sigma_x}{E} \quad \epsilon_y = \epsilon_z = -\nu \frac{\sigma_x}{E} \quad (3-18)$$

For a stress element undergoing σ_x , σ_y , and σ_z simultaneously, the normal strains are given by

$$\begin{aligned}\epsilon_x &= \frac{1}{E} [\sigma_x - \nu(\sigma_y + \sigma_z)] \\ \epsilon_y &= \frac{1}{E} [\sigma_y - \nu(\sigma_x + \sigma_z)] \\ \epsilon_z &= \frac{1}{E} [\sigma_z - \nu(\sigma_x + \sigma_y)]\end{aligned}\quad (3-19)$$

Shear strain γ is the change in a right angle of a stress element when subjected to pure shear stress, and Hooke's law for shear is given by

$$\tau = G\gamma \quad (3-20)$$

where the constant G is the *shear modulus of elasticity* or *modulus of rigidity*.

It can be shown for a linear, isotropic, homogeneous material, the three elastic constants are related to each other by

$$E = 2G(1 + \nu) \quad (3-21)$$

3-9 Uniformly Distributed Stresses

The assumption of a uniform distribution of stress is frequently made in design. The result is then often called *pure tension*, *pure compression*, or *pure shear*, depending upon how the external load is applied to the body under study. The word *simple* is sometimes used instead of *pure* to indicate that there are no other complicating effects. The tension rod is typical. Here a tension load F is applied through pins at the ends of the bar. The assumption of uniform stress means that if we cut the bar at a section remote from the ends and remove one piece, we can replace its effect by applying a uniformly distributed force of magnitude σA to the cut end. So the stress σ is said to be uniformly distributed. It is calculated from the equation

$$\sigma = \frac{F}{A} \quad (3-22)$$

This assumption of uniform stress distribution requires that:

- The bar be straight and of a homogeneous material
- The line of action of the force contains the centroid of the section
- The section be taken remote from the ends and from any discontinuity or abrupt change in cross section

For simple compression, Eq. (3–22) is applicable with F normally being considered a negative quantity. Also, a slender bar in compression may fail by buckling, and this possibility must be eliminated from consideration before Eq. (3–22) is used.³

Another type of loading that assumes a uniformly distributed stress is known as *direct shear*. This occurs when there is a shearing action with no bending. An example is the action on a piece of sheet metal caused by the two blades of tin snips. Bolts and pins that are loaded in shear often have direct shear. Think of a cantilever beam with a force pushing down on it. Now move the force all the way up to the wall so there is no bending moment, just a force trying to shear the beam off the wall. This is direct shear. Direct shear is usually assumed to be uniform across the cross section, and is given by

$$\tau = \frac{V}{A} \quad (3-23)$$

where V is the shear force and A is the area of the cross section that is being sheared. The assumption of uniform stress is not accurate, particularly in the vicinity where the force is applied, but the assumption generally gives acceptable results.

3-10 Normal Stresses for Beams in Bending

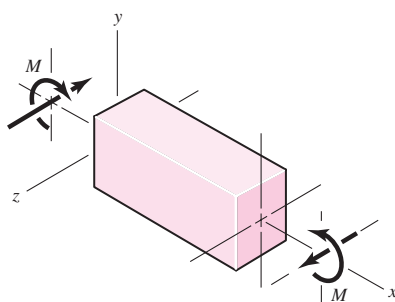
The equations for the normal bending stresses in straight beams are based on the following assumptions.

- The beam is subjected to pure bending. This means that the shear force is zero, and that no torsion or axial loads are present (for most engineering applications it is assumed that these loads affect the bending stresses minimally).
- The material is isotropic and homogeneous.
- The material obeys Hooke's law.
- The beam is initially straight with a cross section that is constant throughout the beam length.
- The beam has an axis of symmetry in the plane of bending.
- The proportions of the beam are such that it would fail by bending rather than by crushing, wrinkling, or sidewise buckling.
- Plane cross sections of the beam remain plane during bending.

In Fig. 3–13 we visualize a portion of a straight beam acted upon by a positive bending moment M shown by the curved arrow showing the physical action of the moment together with a straight arrow indicating the moment vector. The x axis is coincident with the *neutral axis* of the section, and the xz plane, which contains the

Figure 3-13

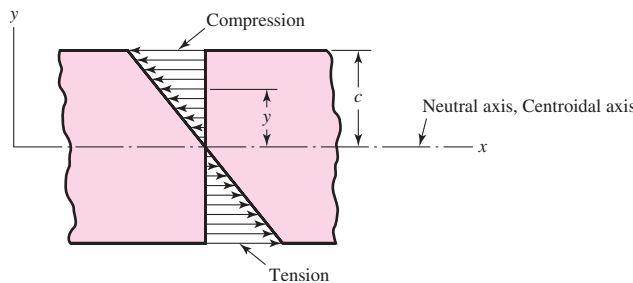
Straight beam in positive bending.



³See Sec. 4–11.

Figure 3-14

Bending stresses according to Eq. (3-24).



neutral axes of all cross sections, is called the *neutral plane*. Elements of the beam coincident with this plane have zero stress. The location of the neutral axis with respect to the cross section is coincident with the *centroidal axis* of the cross section.

The bending stress varies linearly with the distance from the neutral axis, y , and is given by

$$\sigma_x = -\frac{My}{I} \quad (3-24)$$

where I is the *second-area moment* about the z axis. That is,

$$I = \int y^2 dA \quad (3-25)$$

The stress distribution given by Eq. (3-24) is shown in Fig. 3-14. The maximum magnitude of the bending stress will occur where y has the greatest magnitude. Designating σ_{\max} as the maximum *magnitude* of the bending stress, and c as the maximum *magnitude* of y

$$\sigma_{\max} = \frac{Mc}{I} \quad (3-26a)$$

Equation (3-24) can still be used to ascertain whether σ_{\max} is tensile or compressive.

Equation (3-26a) is often written as

$$\sigma_{\max} = \frac{M}{Z} \quad (3-26b)$$

where $Z = I/c$ is called the *section modulus*.

EXAMPLE 3-5

A beam having a T section with the dimensions shown in Fig. 3-15 is subjected to a bending moment of 1600 N · m, about the negative z axis, that causes tension at the top surface. Locate the neutral axis and find the maximum tensile and compressive bending stresses.

Solution

Dividing the T section into two rectangles, numbered 1 and 2, the total area is $A = 12(75) + 12(88) = 1956 \text{ mm}^2$. Summing the area moments of these rectangles about the top edge, where the moment arms of areas 1 and 2 are 6 mm and $(12 + 88)/2 = 56$ mm respectively, we have

$$1956c_1 = 12(75)(6) + 12(88)(56)$$

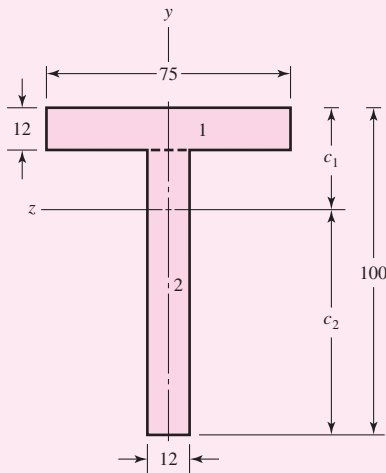
and hence $c_1 = 32.99 \text{ mm}$. Therefore $c_2 = 100 - 32.99 = 67.01 \text{ mm}$.

Next we calculate the second moment of area of each rectangle about its own centroidal axis. Using Table A-18, we find for the top rectangle

$$I_1 = \frac{1}{12}bh^3 = \frac{1}{12}(75)12^3 = 1.080 \times 10^4 \text{ mm}^4$$

Figure 3-15

Dimensions in millimeters.



For the bottom rectangle, we have

$$I_2 = \frac{1}{12}(12)88^3 = 6.815 \times 10^5 \text{ mm}^4$$

We now employ the *parallel-axis theorem* to obtain the second moment of area of the composite figure about its own centroidal axis. This theorem states

$$I_z = I_{ca} + Ad^2$$

where I_{ca} is the second moment of area about its own centroidal axis and I_z is the second moment of area about any parallel axis a distance d removed. For the top rectangle, the distance is

$$d_1 = 32.99 - 6 = 26.99 \text{ mm}$$

and for the bottom rectangle,

$$d_2 = 67.01 - \frac{88}{2} = 23.01 \text{ mm}$$

Using the parallel-axis theorem for both rectangles, we now find that

$$\begin{aligned} I &= [1.080 \times 10^4 + 12(75)26.99^2] + [6.815 \times 10^5 + 12(88)23.01^2] \\ &= 1.907 \times 10^6 \text{ mm}^4 \end{aligned}$$

Finally, the maximum tensile stress, which occurs at the top surface, is found to be

Answer

$$\sigma = \frac{Mc_1}{I} = \frac{1600(32.99)10^{-3}}{1.907(10^{-6})} = 27.68(10^6) \text{ Pa} = 27.68 \text{ MPa}$$

Similarly, the maximum compressive stress at the lower surface is found to be

Answer

$$\sigma = -\frac{Mc_2}{I} = -\frac{1600(67.01)10^{-3}}{1.907(10^{-6})} = -56.22(10^6) \text{ Pa} = -56.22 \text{ MPa}$$

Two-Plane Bending

Quite often, in mechanical design, bending occurs in both xy and xz planes. Considering cross sections with one or two planes of symmetry only, the bending stresses are given by

$$\sigma_x = -\frac{M_z y}{I_z} + \frac{M_y z}{I_y} \quad (3-27)$$

where the first term on the right side of the equation is identical to Eq. (3-24), M_y is the bending moment in the xz plane (moment vector in y direction), z is the distance from the neutral y axis, and I_y is the second area moment about the y axis.

For *noncircular* cross sections, Eq. (3-27) is the superposition of stresses caused by the two bending moment components. The maximum tensile and compressive bending stresses occur where the summation gives the greatest positive and negative stresses, respectively. For solid *circular* cross sections, all lateral axes are the same and the plane containing the moment corresponding to the vector sum of M_z and M_y contains the maximum bending stresses. For a beam of diameter d the maximum distance from the neutral axis is $d/2$, and from Table A-18, $I = \pi d^4/64$. The maximum bending stress for a solid circular cross section is then

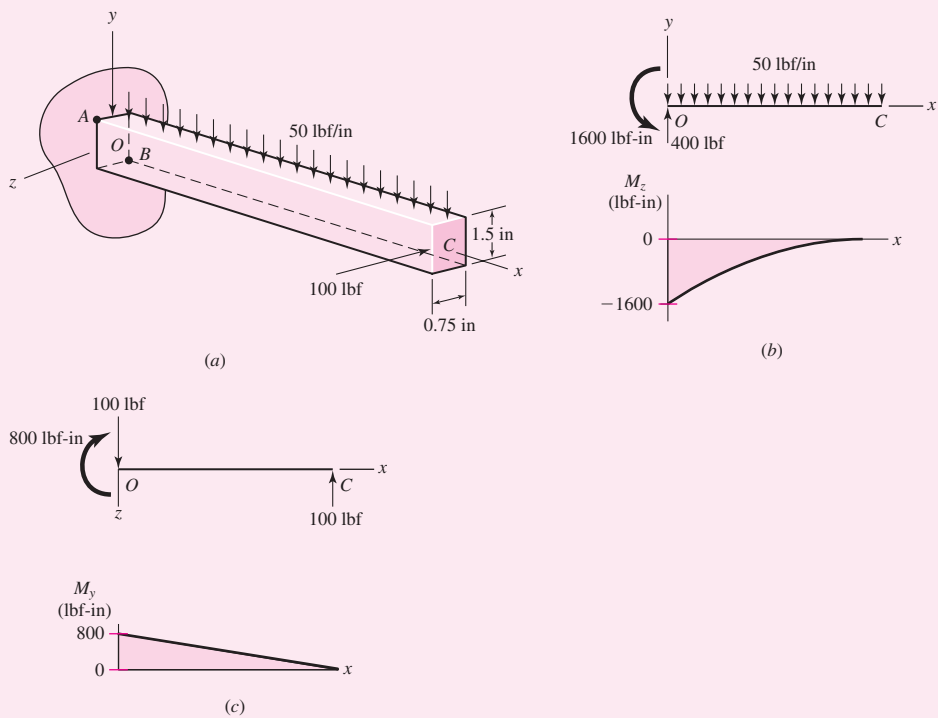
$$\sigma_m = \frac{Mc}{I} = \frac{(M_y^2 + M_z^2)^{1/2}(d/2)}{\pi d^4/64} = \frac{32}{\pi d^3} (M_y^2 + M_z^2)^{1/2} \quad (3-28)$$

EXAMPLE 3-6

As shown in Fig. 3-16a, beam OC is loaded in the xy plane by a uniform load of 50 lbf/in, and in the xz plane by a concentrated force of 100 lbf at end C . The beam is 8 in long.

Figure 3-16

- (a) Beam loaded in two planes; (b) loading and bending-moment diagrams in xy plane; (c) loading and bending-moment diagrams in xz plane.



(a) For the cross section shown determine the maximum tensile and compressive bending stresses and where they act.

(b) If the cross section was a solid circular rod of diameter, $d = 1.25$ in, determine the magnitude of the maximum bending stress.

Solution

(a) The reactions at O and the bending-moment diagrams in the xy and xz planes are shown in Figs. 3–16b and c, respectively. The maximum moments in both planes occur at O where

$$(M_z)_O = -\frac{1}{2}(50)8^2 = -1600 \text{ lbf-in} \quad (M_y)_O = 100(8) = 800 \text{ lbf-in}$$

The second moments of area in both planes are

$$I_z = \frac{1}{12}(0.75)1.5^3 = 0.2109 \text{ in}^4 \quad I_y = \frac{1}{12}(1.5)0.75^3 = 0.05273 \text{ in}^4$$

The maximum tensile stress occurs at point A , shown in Fig. 3–16a, where the maximum tensile stress is due to both moments. At A , $y_A = 0.75$ in and $z_A = 0.375$ in. Thus, from Eq. (3–27)

$$\text{Answer} \quad (\sigma_x)_A = -\frac{-1600(0.75)}{0.2109} + \frac{800(0.375)}{0.05273} = 11,380 \text{ psi} = 11.38 \text{ kpsi}$$

The maximum compressive bending stress occurs at point B where, $y_B = -0.75$ in and $z_B = -0.375$ in. Thus

$$\text{Answer} \quad (\sigma_x)_B = -\frac{-1600(-0.75)}{0.2109} + \frac{800(-0.375)}{0.05273} = -11,380 \text{ psi} = -11.38 \text{ kpsi}$$

(b) For a solid circular cross section of diameter, $d = 1.25$ in, the maximum bending stress at end O is given by Eq. (3–28) as

$$\text{Answer} \quad \sigma_m = \frac{32}{\pi(1.25)^3} [800^2 + (-1600)^2]^{1/2} = 9329 \text{ psi} = 9.329 \text{ kpsi}$$

Beams with Asymmetrical Sections⁴

The bending stress equations, given by Eqs. (3–24) and (3–27), can also be applied to beams having asymmetrical cross sections, provided the planes of bending coincide with the *area principal axes* of the section. The method for determining the orientation of the area principal axes and the values of the corresponding *principal second-area moments* can be found in any statics book. If a section has an axis of symmetry, that axis and its perpendicular axis are the area principal axes.

For example, consider a beam in bending, using an equal leg angle as shown in Table A–6. Equation (3–27) cannot be used if the bending moments are resolved about axis 1–1 and/or axis 2–2. However, Eq. (3–27) can be used if the moments are resolved

⁴For further discussion, see Sec. 5.3, Richard G. Budynas, *Advanced Strength and Applied Stress Analysis*, 2nd ed., McGraw-Hill, New York, 1999.

about axis 3–3 and its perpendicular axis (let us call it, say, axis 4–4). Note, for this cross section, axis 4–4 is an axis of symmetry. Table A–6 is a standard table, and for brevity, does not directly give all the information needed to use it. The orientation of the area principal axes and the values of I_{2-2} , I_{3-3} , and I_{4-4} are not given because they can be determined as follows. Since the legs are equal, the principal axes are oriented $\pm 45^\circ$ from axis 1–1, and $I_{2-2} = I_{1-1}$. The second-area moment I_{3-3} is given by

$$I_{3-3} = A(k_{3-3})^2 \quad (a)$$

where k_{3-3} is called the *radius of gyration*. The sum of the second-area moments for a cross section is invariant, so $I_{1-1} + I_{2-2} = I_{3-3} + I_{4-4}$. Thus, I_{4-4} is given by

$$I_{4-4} = 2 I_{1-1} - I_{3-3} \quad (b)$$

where $I_{2-2} = I_{1-1}$. For example, consider a $3 \times 3 \times \frac{1}{4}$ angle. Using Table A–6 and Eqs. (a) and (b), $I_{3-3} = 1.44 (0.592)^2 = 0.505 \text{ in}^4$, and $I_{4-4} = 2(1.24) - 0.505 = 1.98 \text{ in}^4$.

3-11

Shear Stresses for Beams in Bending

Most beams have both shear forces and bending moments present. It is only occasionally that we encounter beams subjected to pure bending, that is to say, beams having zero shear force. The flexure formula is developed on the assumption of pure bending. This is done, however, to eliminate the complicating effects of shear force in the development. For engineering purposes, the flexure formula is valid no matter whether a shear force is present or not. For this reason, we shall utilize the same normal bending-stress distribution [Eqs. (3–24) and (3–26)] when shear forces are also present.

In Fig. 3–17a we show a beam segment of constant cross section subjected to a shear force V and a bending moment M at x . Because of external loading and V , the shear force and bending moment change with respect to x . At $x + dx$ the shear force and bending moment are $V + dV$ and $M + dM$, respectively. Considering forces in the x direction only, Fig. 3–17b shows the stress distribution σ_x due to the bending moments. If dM is positive, with the bending moment increasing, the stresses on the right face, for a given value of y , are larger in magnitude than the stresses on the left face. If we further isolate the element by making a slice at $y = y_1$ (see Fig. 3–17b), the net force in the x direction will be directed to the left with a value of

$$\int_{y_1}^c \frac{(dM)y}{I} dA$$

as shown in the rotated view of Fig. 3–17c. For equilibrium, a shear force on the bottom face, directed to the right, is required. This shear force gives rise to a shear stress τ , where, if assumed uniform, the force is $\tau b dx$. Thus

$$\tau b dx = \int_{y_1}^c \frac{(dM)y}{I} dA \quad (a)$$

The term dM/I can be removed from within the integral and $b dx$ placed on the right side of the equation; then, from Eq. (3–3) with $V = dM/dx$, Eq. (a) becomes

$$\tau = \frac{V}{Ib} \int_{y_1}^c y dA \quad (3-29)$$

In this equation, the integral is the first moment of the area A' with respect to the neutral axis (see Fig. 3–17c). This integral is usually designated as Q . Thus

$$Q = \int_{y_1}^c y dA = \bar{y}' A' \quad (3-30)$$

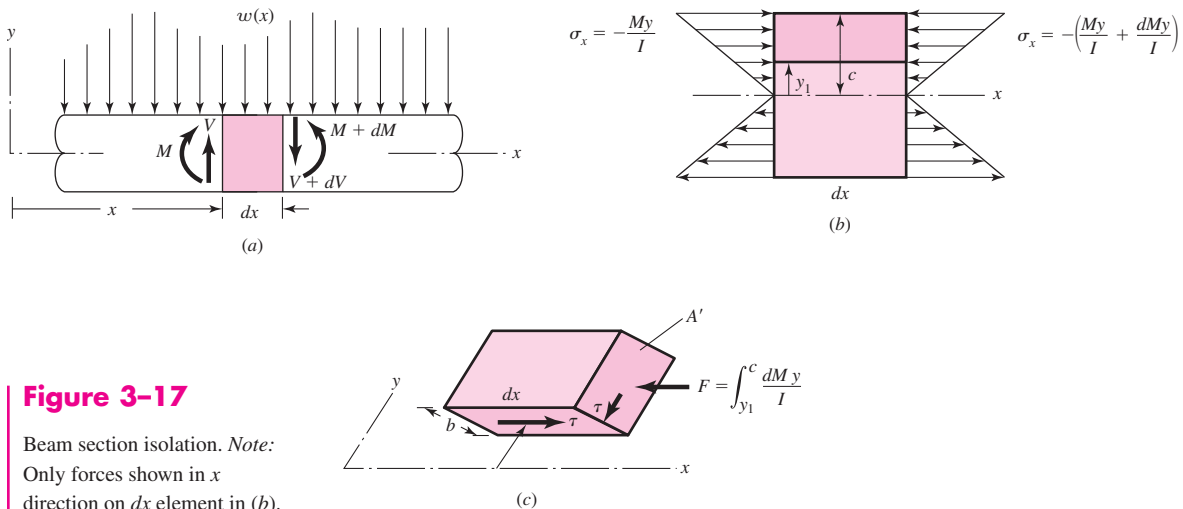


Figure 3-17

Beam section isolation. Note:
Only forces shown in x direction on dx element in (b).

where, for the isolated area y_1 to c , \bar{y}' is the distance in the y direction from the neutral plane to the centroid of the area A' . With this, Eq. (3-29) can be written as

$$\tau = \frac{VQ}{Ib} \quad (3-31)$$

This stress is known as the *transverse shear stress*. It is always accompanied with bending stress.

In using this equation, note that b is the width of the section at $y = y_1$. Also, I is the second moment of area of the entire section about the neutral axis.

Because cross shears are equal, and area A' is finite, the shear stress τ given by Eq. (3-31) and shown on area A' in Fig. 3-17c occurs only at $y = y_1$. The shear stress on the lateral area varies with y , normally maximum at $y = 0$ (where $\bar{y}'A'$ is maximum) and zero at the outer fibers of the beam where $A' = 0$.

The shear stress distribution in a beam depends on how Q/b varies as a function of y_1 . Here we will show how to determine the shear stress distribution for a beam with a rectangular cross section and provide results of maximum values of shear stress for other standard cross sections. Figure 3-18 shows a portion of a beam with a rectangular cross section, subjected to a shear force V and a bending moment M . As a result of the bending moment, a normal stress σ is developed on a cross section such as $A-A$, which is in compression above the neutral axis and in tension below. To investigate the shear stress at a distance y_1 above the neutral axis, we select an element of area dA at a distance y above the neutral axis. Then, $dA = b dy$, and so Eq. (3-30) becomes

$$Q = \int_{y_1}^c y dA = b \int_{y_1}^c y dy = \frac{by^2}{2} \Big|_{y_1}^c = \frac{b}{2} (c^2 - y_1^2) \quad (b)$$

Substituting this value for Q into Eq. (3-31) gives

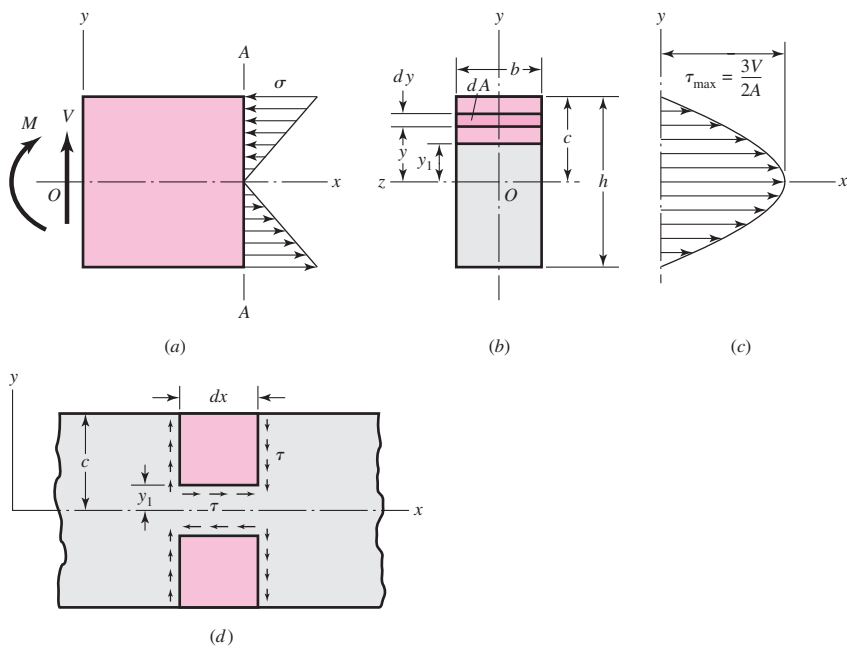
$$\tau = \frac{V}{2I} (c^2 - y_1^2) \quad (3-32)$$

This is the general equation for shear stress in a rectangular beam. To learn something about it, let us make some substitutions. From Table A-18, the second moment of area for a rectangular section is $I = bh^3/12$; substituting $h = 2c$ and $A = bh = 2bc$ gives

$$I = \frac{Ac^2}{3} \quad (c)$$

Figure 3-18

Transverse shear stresses in a rectangular beam.



If we now use this value of I for Eq. (3-32) and rearrange, we get

$$\tau = \frac{3V}{2A} \left(1 - \frac{y_1^2}{c^2} \right) \quad (3-33)$$

We note that the maximum shear stress exists when $y_1 = 0$, which is at the bending neutral axis. Thus

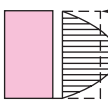
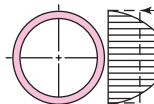
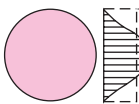
$$\tau_{\max} = \frac{3V}{2A} \quad (3-34)$$

for a rectangular section. As we move away from the neutral axis, the shear stress decreases parabolically until it is zero at the outer surfaces where $y_1 = \pm c$, as shown in Fig. 3-18c. Horizontal shear stress is always accompanied by vertical shear stress of the same magnitude, and so the distribution can be diagrammed as shown in Fig. 3-18d. Figure 3-18c shows that the shear τ on the vertical surfaces varies with y . We are almost always interested in the horizontal shear, τ in Fig. 3-18d, which is nearly uniform over dx with constant $y = y_1$. The maximum horizontal shear occurs where the vertical shear is largest. This is usually at the neutral axis but may not be if the width b is smaller somewhere else. Furthermore, if the section is such that b can be minimized on a plane not horizontal, then the horizontal shear stress occurs on an inclined plane. For example, with tubing, the horizontal shear stress occurs on a radial plane and the corresponding “vertical shear” is not vertical, but tangential.

The distributions of transverse shear stresses for several commonly used cross sections are shown in Table 3-2. The profiles represent the VQ/Ib relationship, which is a function of the distance y from the neutral axis. For each profile, the formula for the maximum value at the neutral axis is given. Note that the expression given for the I beam is a commonly used approximation that is reasonable for a standard I beam with a thin web. Also, the profile for the I beam is idealized. In reality the transition from the web to the flange is quite complex locally, and not simply a step change.

Table 3–2

Formulas for Maximum Transverse Shear Stress from VQ/Ib

Beam Shape	Formula	Beam Shape	Formula
 Rectangular	$\tau_{\text{avc}} = \frac{V}{A}$ $\tau_{\text{max}} = \frac{3V}{2A}$	 Hollow, thin-walled round	$\tau_{\text{avc}} = \frac{V}{A}$ $\tau_{\text{max}} = \frac{2V}{A}$
 Circular	$\tau_{\text{avc}} = \frac{V}{A}$ $\tau_{\text{max}} = \frac{4V}{3A}$	 Structural I beam (thin-walled)	$\tau_{\text{max}} = \frac{V}{A_{\text{web}}}$

It is significant to observe that the transverse shear stress in each of these common cross sections is maximum on the neutral axis, and zero on the outer surfaces. Since this is exactly the opposite of where the bending and torsional stresses have their maximum and minimum values, the transverse shear stress is often not critical from a design perspective.

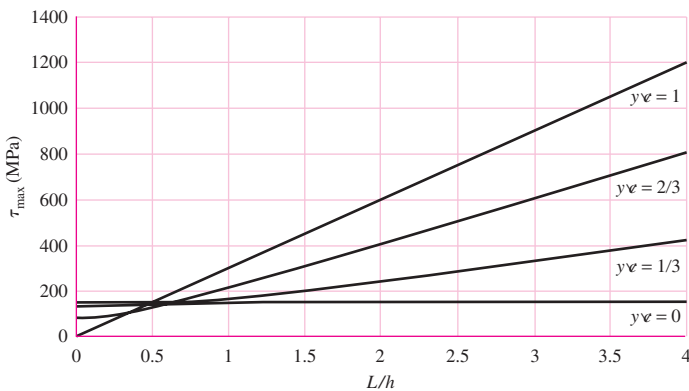
Let us examine the significance of the transverse shear stress, using as an example a cantilever beam of length L , with rectangular cross section $b \times h$, loaded at the free end with a transverse force F . At the wall, where the bending moment is the largest, at a distance y from the neutral axis, a stress element will include both bending stress and transverse shear stress. In Sec. 5–4 it will be shown that a good measure of the combined effects of multiple stresses on a stress element is the maximum shear stress. Inserting the bending stress (My/I) and the transverse shear stress (VQ/Ib) into the maximum shear stress equation, Eq. (3–14), we obtain a general equation for the maximum shear stress in a cantilever beam with a rectangular cross section. This equation can then be normalized with respect to L/h and y/c , where c is the distance from the neutral axis to the outer surface ($h/2$), to give

$$\tau_{\text{max}} = \sqrt{\left(\frac{\sigma}{2}\right)^2 + \tau^2} = \frac{3F}{2bh} \sqrt{4(L/h)^2(y/c)^2 + [1 - (y/c)^2]^2} \quad (d)$$

To investigate the significance of transverse shear stress, we plot τ_{max} as a function of L/h for several values of y/c , as shown in Fig. 3–19. Since F and b appear only as linear multipliers outside the radical, they will only serve to scale the plot in the vertical direction without changing any of the relationships. Notice that at the neutral axis where $y/c = 0$, τ_{max} is constant for any length beam, since the bending stress is zero at the neutral axis and the transverse shear stress is independent of L . On the other hand, on the outer surface where $y/c = 1$, τ_{max} increases linearly with L/h because of the bending moment. For y/c between zero and one, τ_{max} is nonlinear for low values of L/h , but behaves linearly as L/h increases, displaying the dominance of the bending stress as the moment arm increases. We can see from the graph that the critical stress element (the largest value of τ_{max}) will always be either on the outer surface ($y/c = 1$) or at the neutral axis ($y/c = 0$), and never between. Thus, for the rectangular cross section, the transition between these two locations occurs at $L/h = 0.5$ where the line for $y/c = 1$ crosses the horizontal line for $y/c = 0$. The critical stress element is either on the outer

Figure 3-19

Plot of maximum shear stress for a cantilever beam, combining the effects of bending and transverse shear stresses.



surface where the transverse shear is zero, or if L/h is small enough, it is on the neutral axis where the bending stress is zero.

The conclusions drawn from Fig. 3-19 are generally similar for any cross section that does not increase in width farther away from the neutral axis. This notably includes solid round cross sections, but not I beams or channels. Care must be taken with I beams and channels that have thin webs that extend far enough from the neutral axis that the bending and shear may both be significant on the same stress element (See Ex. 3-7). For any common cross section beam, if the beam length to height ratio is greater than 10, the transverse shear stress is generally considered negligible compared to the bending stress at any point within the cross section.

EXAMPLE 3-7

A beam 12 in long is to support a load of 488 lbf acting 3 in from the left support, as shown in Fig. 3-20a. The beam is an I beam with the cross-sectional dimensions shown. To simplify the calculations, assume a cross section with square corners, as shown in Fig. 3-20c. Points of interest are labeled (*a*, *b*, *c*, and *d*) at distances *y* from the neutral axis of 0 in, 1.240⁻ in, 1.240⁺ in, and 1.5 in (Fig. 3-20c). At the critical axial location along the beam, find the following information.

- (a) Determine the profile of the distribution of the transverse shear stress, obtaining values at each of the points of interest.
- (b) Determine the bending stresses at the points of interest.
- (c) Determine the maximum shear stresses at the points of interest, and compare them.

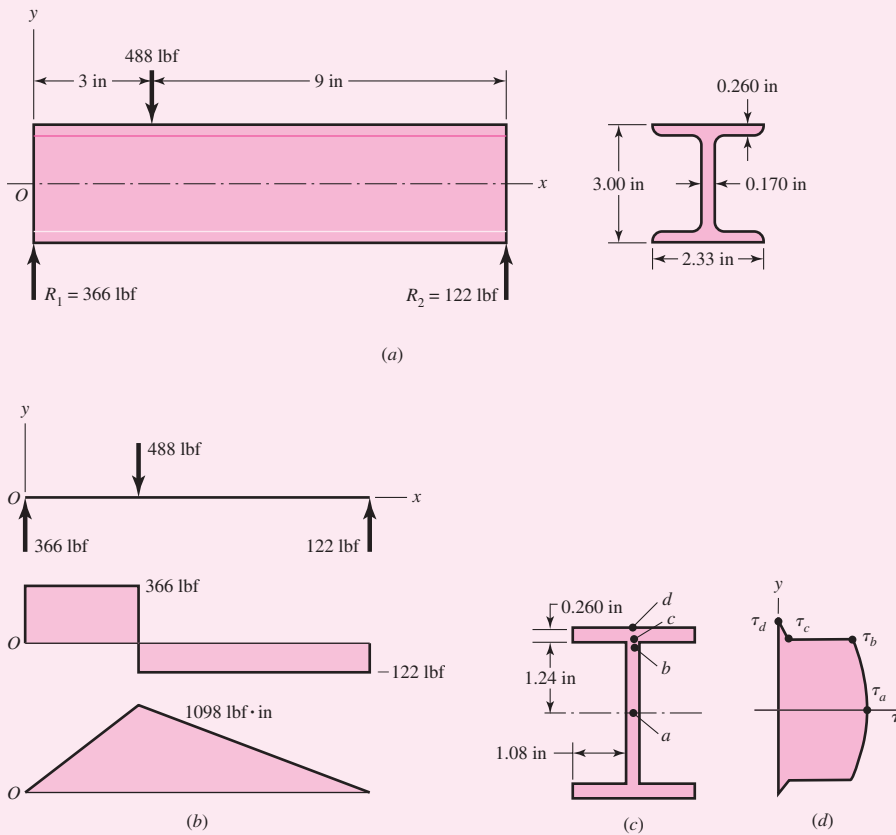
Solution

First, we note that the transverse shear stress is not likely to be negligible in this case since the beam length to height ratio is much less than 10, and since the thin web and wide flange will allow the transverse shear to be large. The loading, shear-force, and bending-moment diagrams are shown in Fig. 3-20b. The critical axial location is at $x = 3^-$ where the shear force and the bending moment are both maximum.

- (a) We obtain the area moment of inertia I by evaluating I for a solid 3.0-in \times 2.33-in rectangular area, and then subtracting the two rectangular areas that are not part of the cross section.

$$I = \frac{(2.33)(3.00)^3}{12} - 2 \left[\frac{(1.08)(2.48)^3}{12} \right] = 2.50 \text{ in}^4$$

| Figure 3–20



Finding Q at each point of interest using Eq. (3–30) gives

$$Q_a = \left(1.24 + \frac{0.260}{2}\right)[(2.33)(0.260)] + \left(\frac{1.24}{2}\right)[(1.24)(0.170)] = 0.961 \text{ in}^3$$

$$Q_b = Q_c = \left(1.24 + \frac{0.260}{2}\right)[(2.33)(0.260)] = 0.830 \text{ in}^3$$

$$Q_d = (1.5)(0) = 0 \text{ in}^3$$

Applying Eq. (3–31) at each point of interest, with V and I constant for each point, and b equal to the width of the cross section at each point, shows that the magnitudes of the transverse shear stresses are

Answer $\tau_a = \frac{VQ_a}{Ib_a} = \frac{(366)(0.961)}{(2.50)(0.170)} = 828 \text{ psi}$

$$\tau_b = \frac{VQ_b}{Ib_b} = \frac{(366)(0.830)}{(2.50)(0.170)} = 715 \text{ psi}$$

$$\tau_c = \frac{VQ_c}{Ib_c} = \frac{(366)(0.830)}{(2.50)(2.33)} = 52.2 \text{ psi}$$

$$\tau_d = \frac{VQ_d}{Ib_d} = \frac{(366)(0)}{(2.50)(2.33)} = 0 \text{ psi}$$

The magnitude of the idealized transverse shear stress profile through the beam depth will be as shown in Fig. 3–20d.

(b) The bending stresses at each point of interest are

Answer

$$\sigma_a = \frac{My_a}{I} = \frac{(1098)(0)}{2.50} = 0 \text{ psi}$$

$$\sigma_b = \sigma_c = -\frac{My_b}{I} = -\frac{(1098)(1.24)}{2.50} = -545 \text{ psi}$$

$$\sigma_d = -\frac{My_d}{I} = -\frac{(1098)(1.50)}{2.50} = -659 \text{ psi}$$

(c) Now at each point of interest, consider a stress element that includes the bending stress and the transverse shear stress. The maximum shear stress for each stress element can be determined by Mohr's circle, or analytically by Eq. (3–14) with $\sigma_y = 0$,

$$\tau_{\max} = \sqrt{\left(\frac{\sigma}{2}\right)^2 + \tau^2}$$

Thus, at each point

$$\tau_{\max,a} = \sqrt{0 + (828)^2} = 828 \text{ psi}$$

$$\tau_{\max,b} = \sqrt{\left(\frac{-545}{2}\right)^2 + (715)^2} = 765 \text{ psi}$$

$$\tau_{\max,c} = \sqrt{\left(\frac{-545}{2}\right)^2 + (52.2)^2} = 277 \text{ psi}$$

$$\tau_{\max,d} = \sqrt{\left(\frac{-659}{2}\right)^2 + 0} = 330 \text{ psi}$$

Answer

Interestingly, the critical location is at point *a* where the maximum shear stress is the largest, even though the bending stress is zero. The next critical location is at point *b* in the web, where the thin web thickness dramatically increases the transverse shear stress compared to points *c* or *d*. These results are counterintuitive, since both points *a* and *b* turn out to be more critical than point *d*, even though the bending stress is maximum at point *d*. The thin web and wide flange increase the impact of the transverse shear stress. If the beam length to height ratio were increased, the critical point would move from point *a* to point *b*, since the transverse shear stress at point *a* would remain constant, but the bending stress at point *b* would increase. The designer should be particularly alert to the possibility of the critical stress element not being on the outer surface with cross sections that get wider farther from the neutral axis, particularly in cases with thin web sections and wide flanges. For rectangular and circular cross sections, however, the maximum bending stresses at the outer surfaces will dominate, as was shown in Fig. 3–19.

3-12 Torsion

Any moment vector that is collinear with an axis of a mechanical element is called a *torque vector*, because the moment causes the element to be twisted about that axis. A bar subjected to such a moment is also said to be in *torsion*.

As shown in Fig. 3-21, the torque T applied to a bar can be designated by drawing arrows on the surface of the bar to indicate direction or by drawing torque-vector arrows along the axes of twist of the bar. Torque vectors are the hollow arrows shown on the x axis in Fig. 3-21. Note that they conform to the right-hand rule for vectors.

The *angle of twist*, in radians, for a solid round bar is

$$\theta = \frac{Tl}{GJ} \quad (3-35)$$

where T = torque

l = length

G = modulus of rigidity

J = polar second moment of area

Shear stresses develop throughout the cross section. For a round bar in torsion, these stresses are proportional to the radius ρ and are given by

$$\tau = \frac{Tr}{J} \quad (3-36)$$

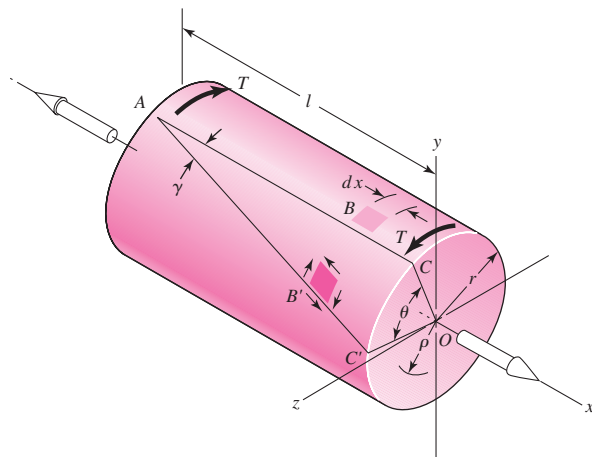
Designating r as the radius to the outer surface, we have

$$\tau_{\max} = \frac{Tr}{J} \quad (3-37)$$

The assumptions used in the analysis are:

- The bar is acted upon by a pure torque, and the sections under consideration are remote from the point of application of the load and from a change in diameter.
- The material obeys Hooke's law.
- Adjacent cross sections originally plane and parallel remain plane and parallel after twisting, and any radial line remains straight.

| Figure 3-21



The last assumption depends upon the axisymmetry of the member, so it does not hold true for noncircular cross sections. Consequently, Eqs. (3–35) through (3–37) apply *only* to circular sections. For a solid round section,

$$J = \frac{\pi d^4}{32} \quad (3-38)$$

where d is the diameter of the bar. For a hollow round section,

$$J = \frac{\pi}{32} (d_o^4 - d_i^4) \quad (3-39)$$

where the subscripts o and i refer to the outside and inside diameters, respectively.

There are some applications in machinery for noncircular cross section members and shafts where a regular polygonal cross section is useful in transmitting torque to a gear or pulley that can have an axial change in position. Because no key or keyway is needed, the possibility of a lost key is avoided. The development of equations for stress and deflection for torsional loading of noncircular cross sections can be obtained from the mathematical theory of elasticity. In general, the shear stress does not vary linearly with the distance from the axis, and depends on the specific cross section. In fact, for a rectangular section bar the shear stress is zero at the corners where the distance from the axis is the largest. The maximum shearing stress in a rectangular $b \times c$ section bar occurs in the middle of the *longest* side b and is of the magnitude

$$\tau_{\max} = \frac{T}{\alpha bc^2} \doteq \frac{T}{bc^2} \left(3 + \frac{1.8}{b/c} \right) \quad (3-40)$$

where b is the width (longer side) and c is the thickness (shorter side). They can *not* be interchanged. The parameter α is a factor that is a function of the ratio b/c as shown in the following table.⁵ The angle of twist is given by

$$\theta = \frac{Tl}{\beta bc^3 G} \quad (3-41)$$

where β is a function of b/c , as shown in the table.

b/c	1.00	1.50	1.75	2.00	2.50	3.00	4.00	6.00	8.00	10	∞
α	0.208	0.231	0.239	0.246	0.258	0.267	0.282	0.299	0.307	0.313	0.333
β	0.141	0.196	0.214	0.228	0.249	0.263	0.281	0.299	0.307	0.313	0.333

Equation (3–40) is also approximately valid for equal-sided angles; these can be considered as two rectangles, each of which is capable of carrying half the torque.⁶

It is often necessary to obtain the torque T from a consideration of the power and speed of a rotating shaft. For convenience when U. S. Customary units are used, three forms of this relation are

$$H = \frac{FV}{33\,000} = \frac{2\pi Tn}{33\,000(12)} = \frac{Tn}{63\,025} \quad (3-42)$$

⁵S. Timoshenko, *Strength of Materials*, Part I, 3rd ed., D. Van Nostrand Company, New York, 1955, p. 290.

⁶For other sections see W. C. Young and R. G. Budynas, *Roark's Formulas for Stress and Strain*, 7th ed., McGraw-Hill, New York, 2002.

where H = power, hp
 T = torque, lbf · in
 n = shaft speed, rev/min
 F = force, lbf
 V = velocity, ft/min

When SI units are used, the equation is

$$H = T\omega \quad (3-43)$$

where H = power, W
 T = torque, N · m
 ω = angular velocity, rad/s

The torque T corresponding to the power in watts is given approximately by

$$T = 9.55 \frac{H}{n} \quad (3-44)$$

where n is in revolutions per minute.

EXAMPLE 3-8

Figure 3-22 shows a crank loaded by a force $F = 300$ lbf that causes twisting and bending of a $\frac{3}{4}$ -in-diameter shaft fixed to a support at the origin of the reference system. In actuality, the support may be an inertia that we wish to rotate, but for the purposes of a stress analysis we can consider this a statics problem.

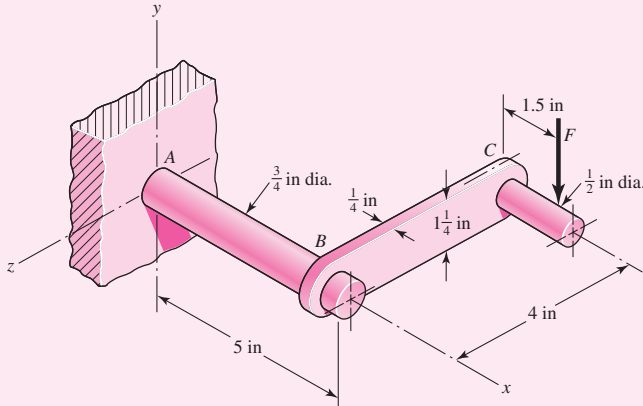
(a) Draw separate free-body diagrams of the shaft AB and the arm BC , and compute the values of all forces, moments, and torques that act. Label the directions of the coordinate axes on these diagrams.

(b) Compute the maxima of the torsional stress and the bending stress in the arm BC and indicate where these act.

(c) Locate a stress element on the top surface of the shaft at A , and calculate all the stress components that act upon this element.

(d) Determine the maximum normal and shear stresses at A .

| Figure 3-22



Solution

(a) The two free-body diagrams are shown in Fig. 3–23. The results are

At end *C* of arm *BC*:

$$\mathbf{F} = -300\mathbf{j} \text{ lbf}, \mathbf{T}_C = -450\mathbf{k} \text{ lbf} \cdot \text{in}$$

At end *B* of arm *BC*:

$$\mathbf{F} = 300\mathbf{j} \text{ lbf}, \mathbf{M}_1 = 1200\mathbf{i} \text{ lbf} \cdot \text{in}, \mathbf{T}_1 = 450\mathbf{k} \text{ lbf} \cdot \text{in}$$

At end *B* of shaft *AB*:

$$\mathbf{F} = -300\mathbf{j} \text{ lbf}, \mathbf{T}_2 = -1200\mathbf{i} \text{ lbf} \cdot \text{in}, \mathbf{M}_2 = -450\mathbf{k} \text{ lbf} \cdot \text{in}$$

At end *A* of shaft *AB*:

$$\mathbf{F} = 300\mathbf{j} \text{ lbf}, \mathbf{M}_A = 1950\mathbf{k} \text{ lbf} \cdot \text{in}, \mathbf{T}_A = 1200\mathbf{i} \text{ lbf} \cdot \text{in}$$

(b) For arm *BC*, the bending moment will reach a maximum near the shaft at *B*. If we assume this is 1200 lbf · in, then the bending stress for a rectangular section will be

Answer

$$\sigma = \frac{M}{I/c} = \frac{6M}{bh^2} = \frac{6(1200)}{0.25(1.25)^2} = 18\,400 \text{ psi} = 18.4 \text{ kpsi}$$

Of course, this is not exactly correct, because at *B* the moment is actually being transferred into the shaft, probably through a weldment.

For the torsional stress, use Eq. (3–43). Thus

Answer

$$\tau_{\max} = \frac{T}{bc^2} \left(3 + \frac{1.8}{b/c} \right) = \frac{450}{1.25(0.25^2)} \left(3 + \frac{1.8}{1.25/0.25} \right) = 19\,400 \text{ psi} = 19.4 \text{ kpsi}$$

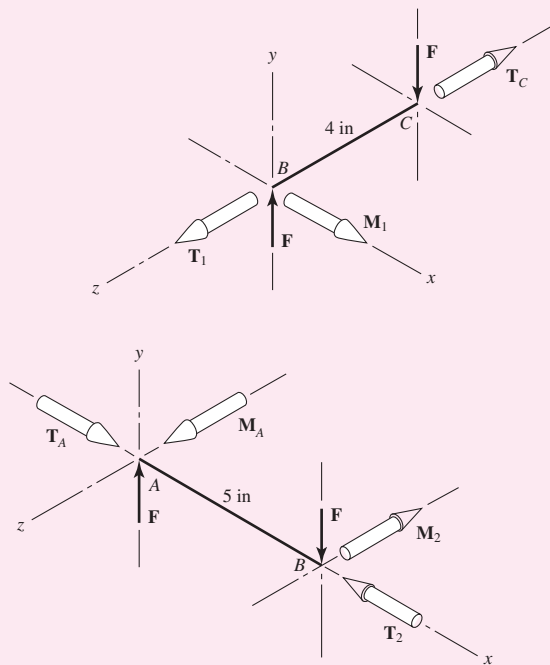
This stress occurs at the middle of the $1\frac{1}{4}$ -in side.

(c) For a stress element at *A*, the bending stress is tensile and is

Answer

$$\sigma_x = \frac{M}{I/c} = \frac{32M}{\pi d^3} = \frac{32(1950)}{\pi (0.75)^3} = 47\,100 \text{ psi} = 47.1 \text{ kpsi}$$

| **Figure 3–23**



The torsional stress is

Answer

$$\tau_{xz} = \frac{-T}{J/c} = \frac{-16T}{\pi d^3} = \frac{-16(1200)}{\pi(0.75)^3} = -14500 \text{ psi} = -14.5 \text{ kpsi}$$

where the reader should verify that the negative sign accounts for the direction of τ_{xz} .

(d) Point A is in a state of plane stress where the stresses are in the xz plane. Thus the principal stresses are given by Eq. (3–13) with subscripts corresponding to the x, z axes.

Answer The maximum normal stress is then given by

$$\begin{aligned}\sigma_1 &= \frac{\sigma_x + \sigma_z}{2} + \sqrt{\left(\frac{\sigma_x - \sigma_z}{2}\right)^2 + \tau_{xz}^2} \\ &= \frac{47.1 + 0}{2} + \sqrt{\left(\frac{47.1 - 0}{2}\right)^2 + (-14.5)^2} = 51.2 \text{ kpsi}\end{aligned}$$

Answer The maximum shear stress at A occurs on surfaces different than the surfaces containing the principal stresses or the surfaces containing the bending and torsional shear stresses. The maximum shear stress is given by Eq. (3–14), again with modified subscripts, and is given by

$$\tau_1 = \sqrt{\left(\frac{\sigma_x - \sigma_z}{2}\right)^2 + \tau_{xz}^2} = \sqrt{\left(\frac{47.1 - 0}{2}\right)^2 + (-14.5)^2} = 27.7 \text{ kpsi}$$

EXAMPLE 3–9

The 1.5-in-diameter solid steel shaft shown in Fig. 3–24a is simply supported at the ends. Two pulleys are keyed to the shaft where pulley B is of diameter 4.0 in and pulley C is of diameter 8.0 in. Considering bending and torsional stresses only, determine the locations and magnitudes of the greatest tensile, compressive, and shear stresses in the shaft.

Solution

Figure 3–24b shows the net forces, reactions, and torsional moments on the shaft. Although this is a three-dimensional problem and vectors might seem appropriate, we will look at the components of the moment vector by performing a two-plane analysis. Figure 3–24c shows the loading in the xy plane, as viewed down the z axis, where bending moments are actually vectors in the z direction. Thus we label the moment diagram as M_z versus x . For the xz plane, we look down the y axis, and the moment diagram is M_y versus x as shown in Fig. 3–24d.

The net moment on a section is the vector sum of the components. That is,

$$M = \sqrt{M_y^2 + M_z^2} \quad (1)$$

At point B,

$$M_B = \sqrt{2000^2 + 8000^2} = 8246 \text{ lbf} \cdot \text{in}$$

At point C,

$$M_C = \sqrt{4000^2 + 4000^2} = 5657 \text{ lbf} \cdot \text{in}$$

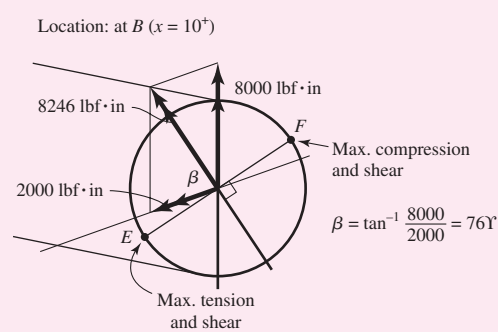
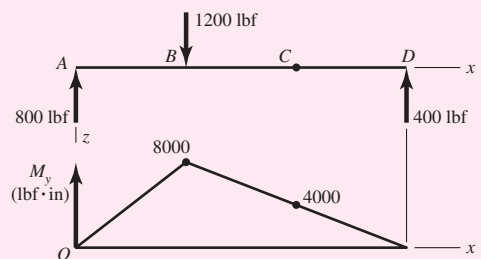
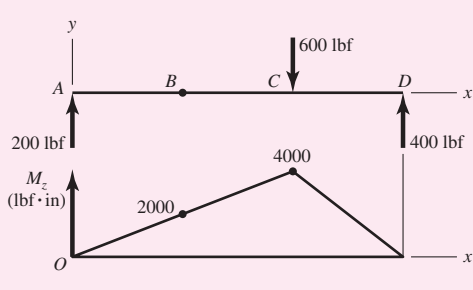
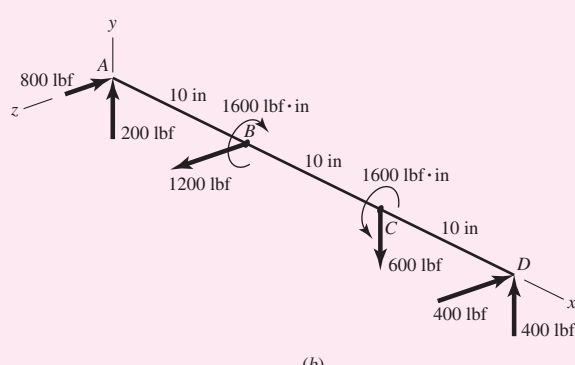
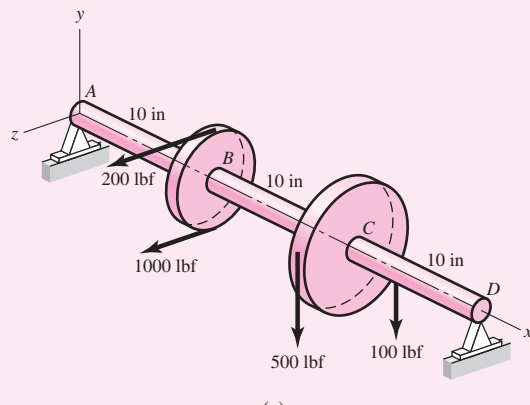


| Figure 3-24

Thus the maximum bending moment is 8246 lbf · in and the maximum bending stress at pulley *B* is

$$\sigma = \frac{M d/2}{\pi d^4/64} = \frac{32M}{\pi d^3} = \frac{32(8246)}{\pi(1.5^3)} = 24,890 \text{ psi} = 24.89 \text{ kpsi}$$

The maximum torsional shear stress occurs between *B* and *C* and is

$$\tau = \frac{T d/2}{\pi d^4/32} = \frac{16T}{\pi d^3} = \frac{16(1600)}{\pi(1.5^3)} = 2414 \text{ psi} = 2.414 \text{ kpsi}$$

The maximum bending and torsional shear stresses occur just to the right of pulley *B* at points *E* and *F* as shown in Fig. 3–24e. At point *E*, the maximum tensile stress will be σ_1 given by

Answer

$$\sigma_1 = \frac{\sigma}{2} + \sqrt{\left(\frac{\sigma}{2}\right)^2 + \tau^2} = \frac{24.89}{2} + \sqrt{\left(\frac{24.89}{2}\right)^2 + 2.414^2} = 25.12 \text{ kpsi}$$

At point *F*, the maximum compressive stress will be σ_2 given by

Answer

$$\sigma_2 = \frac{-\sigma}{2} - \sqrt{\left(\frac{-\sigma}{2}\right)^2 + \tau^2} = \frac{-24.89}{2} - \sqrt{\left(\frac{-24.89}{2}\right)^2 + 2.414^2} = -25.12 \text{ kpsi}$$

The extreme shear stress also occurs at *E* and *F* and is

Answer

$$\tau_1 = \sqrt{\left(\frac{\pm\sigma}{2}\right)^2 + \tau^2} = \sqrt{\left(\frac{\pm24.89}{2}\right)^2 + 2.414^2} = 12.68 \text{ kpsi}$$

Closed Thin-Walled Tubes ($t \ll r$)⁷

In closed thin-walled tubes, it can be shown that the product of shear stress times thickness of the wall τt is constant, meaning that the shear stress τ is inversely proportional to the wall thickness t . The total torque T on a tube such as depicted in Fig. 3–25 is given by

$$T = \int \tau r dr ds = (\tau t) \int r dr = \tau t (2A_m) = 2A_m t \tau$$

where A_m is the *area enclosed by the section median line*. Solving for τ gives

$$\tau = \frac{T}{2A_m t} \quad (3-45)$$

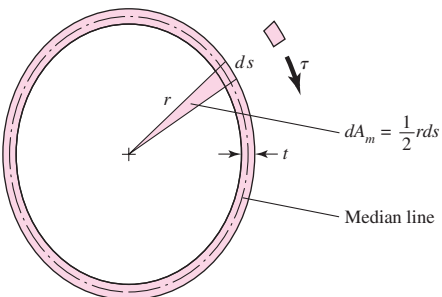
For constant wall thickness t , the angular twist (radians) per unit of length of the tube θ_1 is given by

$$\theta_1 = \frac{TL_m}{4GA_m^2 t} \quad (3-46)$$

⁷See Sec. 3–13, F. P. Beer, E. R. Johnston, and J. T. De Wolf, *Mechanics of Materials*, 5th ed., McGraw-Hill, New York, 2009.

Figure 3–25

The depicted cross section is elliptical, but the section need not be symmetrical nor of constant thickness.



where L_m is the *length of the section median line*. These equations presume the buckling of the tube is prevented by ribs, stiffeners, bulkheads, and so on, and that the stresses are below the proportional limit.

EXAMPLE 3–10

A welded steel tube is 40 in long, has a $\frac{1}{8}$ -in wall thickness, and a 2.5-in by 3.6-in rectangular cross section as shown in Fig. 3–26. Assume an allowable shear stress of 11 500 psi and a shear modulus of $11.5(10^6)$ psi.

- Estimate the allowable torque T .
- Estimate the angle of twist due to the torque.

Solution

(a) Within the section median line, the area enclosed is

$$A_m = (2.5 - 0.125)(3.6 - 0.125) = 8.253 \text{ in}^2$$

and the length of the median perimeter is

$$L_m = 2[(2.5 - 0.125) + (3.6 - 0.125)] = 11.70 \text{ in}$$

Answer

From Eq. (3–45) the torque T is

$$T = 2A_m t \tau = 2(8.253)0.125(11\,500) = 23\,730 \text{ lbf} \cdot \text{in}$$

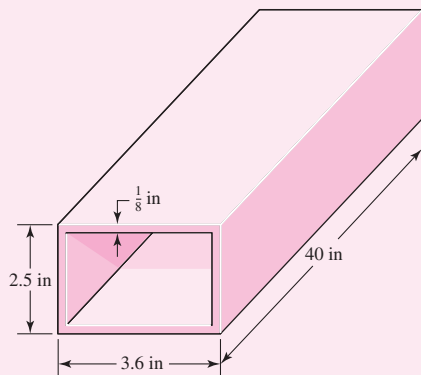
Answer

(b) The angle of twist θ from Eq. (3–46) is

$$\theta = \theta_1 l = \frac{TL_m}{4GA_m^2 t} l = \frac{23\,730(11.70)}{4(11.5 \times 10^6)(8.253^2)(0.125)}(40) = 0.0284 \text{ rad} = 1.62^\circ$$

Figure 3–26

A rectangular steel tube produced by welding.



EXAMPLE 3-11

Compare the shear stress on a circular cylindrical tube with an outside diameter of 1 in and an inside diameter of 0.9 in, predicted by Eq. (3-37), to that estimated by Eq. (3-45).

Solution

From Eq. (3-37),

$$\tau_{\max} = \frac{Tr}{J} = \frac{Tr}{(\pi/32)(d_o^4 - d_i^4)} = \frac{T(0.5)}{(\pi/32)(1^4 - 0.9^4)} = 14.809T$$

From Eq. (3-45),

$$\tau = \frac{T}{2A_m t} = \frac{T}{2(\pi 0.95^2/4)0.05} = 14.108T$$

Taking Eq. (3-37) as correct, the error in the thin-wall estimate is -4.7 percent.

Open Thin-Walled Sections

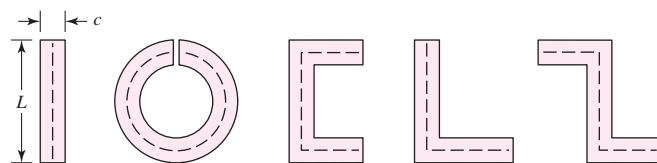
When the median wall line is not closed, the section is said to be an *open section*. Figure 3-27 presents some examples. Open sections in torsion, where the wall is thin, have relations derived from the membrane analogy theory⁸ resulting in:

$$\tau = G\theta_1 c = \frac{3T}{Lc^2} \quad (3-47)$$

where τ is the shear stress, G is the shear modulus, θ_1 is the angle of twist per unit length, T is torque, and L is the length of the median line. The wall thickness is designated c (rather than t) to remind you that you are in open sections. By studying the table that follows Eq. (3-41) you will discover that membrane theory presumes $b/c \rightarrow \infty$. Note that open thin-walled sections in torsion should be avoided in design. As indicated in Eq. (3-47), the shear stress and the angle of twist are inversely proportional to c^2 and c^3 , respectively. Thus, for small wall thickness, stress and twist can become quite large. For example, consider the thin round tube with a slit in Fig. 3-27. For a ratio of wall thickness of outside diameter of $c/d_o = 0.1$, the open section has greater magnitudes of stress and angle of twist by factors of 12.3 and 61.5, respectively, compared to a closed section of the same dimensions.

Figure 3-27

Some open thin-wall sections.



⁸See S. P. Timoshenko and J. N. Goodier, *Theory of Elasticity*, 3rd ed., McGraw-Hill, New York, 1970, Sec. 109.

EXAMPLE 3-12

A 12-in-long strip of steel is $\frac{1}{8}$ in thick and 1 in wide, as shown in Fig. 3-28. If the allowable shear stress is 11 500 psi and the shear modulus is $11.5(10^6)$ psi, find the torque corresponding to the allowable shear stress and the angle of twist, in degrees, (a) using Eq. (3-47) and (b) using Eqs. (3-40) and (3-41).

Solution

(a) The length of the median line is 1 in. From Eq. (3-47),

$$T = \frac{Lc^2\tau}{3} = \frac{(1)(1/8)^2 11500}{3} = 59.90 \text{ lbf} \cdot \text{in}$$

$$\theta = \theta_1 l = \frac{\tau l}{Gc} = \frac{11500(12)}{11.5(10^6)(1/8)} = 0.0960 \text{ rad} = 5.5^\circ$$

A torsional spring rate k_t can be expressed as T/θ :

$$k_t = 59.90/0.0960 = 624 \text{ lbf} \cdot \text{in/rad}$$

(b) From Eq. (3-40),

$$T = \frac{\tau_{\max} bc^2}{3 + 1.8/(b/c)} = \frac{11500(1)(0.125)^2}{3 + 1.8/(1/0.125)} = 55.72 \text{ lbf} \cdot \text{in}$$

From Eq. (3-41), with $b/c = 1/0.125 = 8$,

$$\theta = \frac{Tl}{\beta bc^3 G} = \frac{55.72(12)}{0.307(1)0.125^3(11.5)10^6} = 0.0970 \text{ rad} = 5.6^\circ$$

$$k_t = 55.72/0.0970 = 574 \text{ lbf} \cdot \text{in/rad}$$

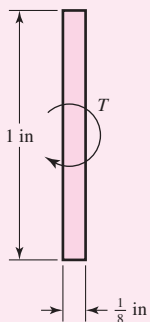


Figure 3-28

The cross-section of a thin strip of steel subjected to a torsional moment T .

The cross section is not thin, where b should be greater than c by at least a factor of 10. In estimating the torque, Eq. (3-47) provides a value of 7.5 percent higher than Eq. (3-40), and is 8.5 percent higher than when the table on page 102 is used.

3-13**Stress Concentration**

In the development of the basic stress equations for tension, compression, bending, and torsion, it was assumed that no geometric irregularities occurred in the member under consideration. But it is quite difficult to design a machine without permitting some changes in the cross sections of the members. Rotating shafts must have shoulders designed on them so that the bearings can be properly seated and so that they will take thrust loads; and the shafts must have key slots machined into them for securing pulleys and gears. A bolt has a head on one end and screw threads on the other end, both of which account for abrupt changes in the cross section. Other parts require holes, oil grooves, and notches of various kinds. Any discontinuity in a machine part alters the stress distribution in the neighborhood of the discontinuity so that the elementary stress equations no longer describe the state of stress in the part at these locations. Such discontinuities are called *stress raisers*, and the regions in which they occur are called areas of *stress concentration*. Stress concentrations can also arise from some irregularity not inherent in the member, such as tool marks, holes, notches, grooves, or threads.

A theoretical, or geometric, stress-concentration factor K_t or K_{ts} is used to relate the actual maximum stress at the discontinuity to the nominal stress. The factors are defined by the equations

$$K_t = \frac{\sigma_{\max}}{\sigma_0} \quad K_{ts} = \frac{\tau_{\max}}{\tau_0} \quad (3-48)$$

where K_t is used for normal stresses and K_{ts} for shear stresses. The nominal stress σ_0 or τ_0 is the stress calculated by using the elementary stress equations and the net area, or net cross section. Sometimes the gross cross section is used instead, and so it is always wise to double check the source of K_t or K_{ts} before calculating the maximum stress.

The stress-concentration factor depends for its value only on the geometry of the part. That is, the particular material used has no effect on the value of K_t . This is why it is called a *theoretical* stress-concentration factor.

The analysis of geometric shapes to determine stress-concentration factors is a difficult problem, and not many solutions can be found. Most stress-concentration factors are found by using experimental techniques.⁹ Though the finite-element method has been used, the fact that the elements are indeed finite prevents finding the true maximum stress. Experimental approaches generally used include photoelasticity, grid methods, brittle-coating methods, and electrical strain-gauge methods. Of course, the grid and strain-gauge methods both suffer from the same drawback as the finite-element method.

Stress-concentration factors for a variety of geometries may be found in Tables A-15 and A-16.

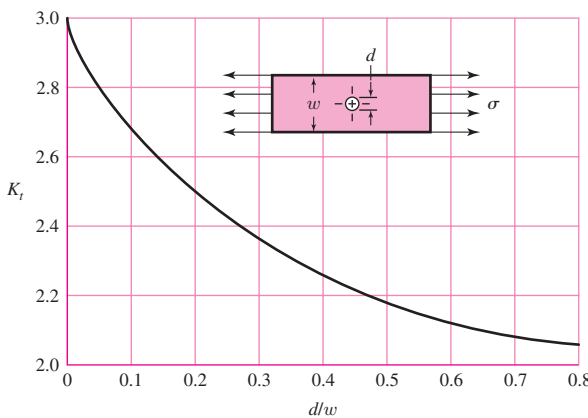
An example is shown in Fig. 3-29, that of a thin plate loaded in tension where the plate contains a centrally located hole.

In static loading, stress-concentration factors are applied as follows. In ductile materials ($\epsilon_f \geq 0.05$), the stress-concentration factor is not usually applied to predict the critical stress, because plastic strain in the region of the stress is localized and has a strengthening effect. In brittle materials ($\epsilon_f < 0.05$), the geometric stress-concentration factor K_t is applied to the nominal stress before comparing it with strength. Gray cast iron has so many inherent stress raisers that the stress raisers introduced by the designer have only a modest (but additive) effect.

Figure 3-29

Thin plate in tension or simple compression with a transverse central hole. The net tensile force is $F = \sigma wt$, where t is the thickness of the plate. The nominal stress is given by

$$\sigma_0 = \frac{F}{(w-d)t} = \frac{w}{(w-d)}\sigma$$



⁹The best source book is W. D. Pilkey and D. F. Pilkey, *Peterson's Stress Concentration Factors*, 3rd ed., John Wiley & Sons, New York, 2008.

Consider a part made of a ductile material and loaded by a gradually applied static load such that the stress in an area of a stress concentration goes beyond the yield strength. The yielding will be restricted to a very small region, and the permanent deformation as well as the residual stresses after the load is released will be insignificant and normally can be tolerated. If yielding does occur, the stress distribution changes and tends toward a more uniform distribution. In the region where yielding occurs, there is little danger of fracture of a ductile material, but if the possibility of a brittle fracture exists, the stress concentration must be taken seriously. Brittle fracture is not just limited to brittle materials. Materials often thought of as being ductile can fail in a brittle manner under certain conditions, e.g., any single application or combination of cyclic loading, rapid application of static loads, loading at low temperatures, and parts containing defects in their material structures (see Sec. 5–12). The effects on a ductile material of processing, such as hardening, hydrogen embrittlement, and welding, may also accelerate failure. Thus, care should always be exercised when dealing with stress concentrations.

For *dynamic loading*, the stress concentration effect is significant for *both* ductile and brittle materials and must always be taken into account (see Sec. 6–10).

EXAMPLE 3–13

The 2-mm-thick bar shown in Fig. 3–30 is loaded axially with a constant force of 10 kN. The bar material has been heat treated and quenched to raise its strength, but as a consequence it has lost most of its ductility. It is desired to drill a hole through the center of the 40-mm face of the plate to allow a cable to pass through it. A 4-mm hole is sufficient for the cable to fit, but an 8-mm drill is readily available. Will a crack be more likely to initiate at the larger hole, the smaller hole, or at the fillet?

Solution

Since the material is brittle, the effect of stress concentrations near the discontinuities must be considered. Dealing with the hole first, for a 4-mm hole, the nominal stress is

$$\sigma_0 = \frac{F}{A} = \frac{F}{(w-d)t} = \frac{10\,000}{(40-4)2} = 139 \text{ MPa}$$

The theoretical stress concentration factor, from Fig. A–15–1, with $d/w = 4/40 = 0.1$, is $K_t = 2.7$. The maximum stress is

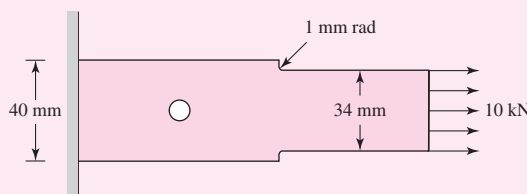
Answer $\sigma_{\max} = K_t \sigma_0 = 2.7(139) = 380 \text{ MPa}$

Similarly, for an 8-mm hole,

$$\sigma_0 = \frac{F}{A} = \frac{F}{(w-d)t} = \frac{10\,000}{(40-8)2} = 156 \text{ MPa}$$

With $d/w = 8/40 = 0.2$, then $K_t = 2.5$, and the maximum stress is

| **Figure 3–30**



Answer

$$\sigma_{\max} = K_t \sigma_0 = 2.5(156) = 390 \text{ MPa}$$

Though the stress concentration is higher with the 4-mm hole, in this case the increased nominal stress with the 8-mm hole has more effect on the maximum stress.

For the fillet,

$$\sigma_0 = \frac{F}{A} = \frac{10\,000}{(34)2} = 147 \text{ MPa}$$

From Table A-15-5, $D/d = 40/34 = 1.18$, and $r/d = 1/34 = 0.026$. Then $K_t = 2.5$.

Answer

$$\sigma_{\max} = K_t \sigma_0 = 2.5(147) = 368 \text{ MPa}$$

Answer

The crack will most likely occur with the 8-mm hole, next likely would be the 4-mm hole, and least likely at the fillet.

3-14**Stresses in Pressurized Cylinders**

Cylindrical pressure vessels, hydraulic cylinders, gun barrels, and pipes carrying fluids at high pressures develop both radial and tangential stresses with values that depend upon the radius of the element under consideration. In determining the radial stress σ_r and the tangential stress σ_t , we make use of the assumption that the longitudinal elongation is constant around the circumference of the cylinder. In other words, a right section of the cylinder remains plane after stressing.

Referring to Fig. 3-31, we designate the inside radius of the cylinder by r_i , the outside radius by r_o , the internal pressure by p_i , and the external pressure by p_o . Then it can be shown that tangential and radial stresses exist whose magnitudes are¹⁰

$$\sigma_t = \frac{p_i r_i^2 - p_o r_o^2 - r_i^2 r_o^2 (p_o - p_i)/r^2}{r_o^2 - r_i^2} \quad (3-49)$$

$$\sigma_r = \frac{p_i r_i^2 - p_o r_o^2 + r_i^2 r_o^2 (p_o - p_i)/r^2}{r_o^2 - r_i^2}$$

As usual, positive values indicate tension and negative values, compression.

For the special case of $p_o = 0$, Eq. (3-49) gives

$$\sigma_t = \frac{r_i^2 p_i}{r_o^2 - r_i^2} \left(1 + \frac{r_o^2}{r^2} \right) \quad (3-50)$$

$$\sigma_r = \frac{r_i^2 p_i}{r_o^2 - r_i^2} \left(1 - \frac{r_o^2}{r^2} \right)$$

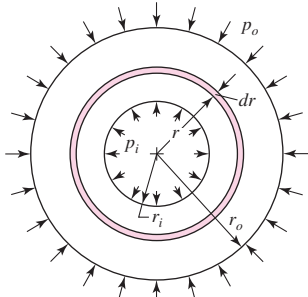


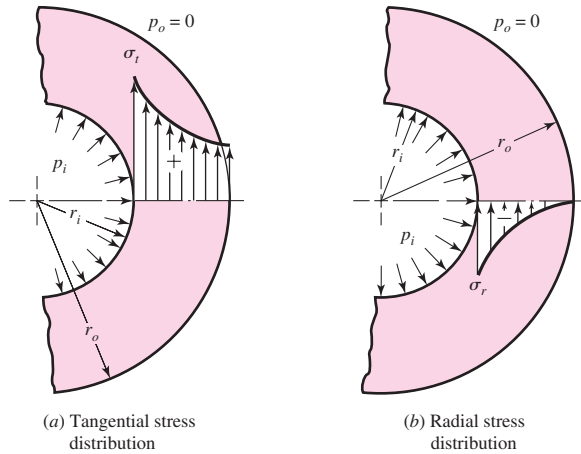
Figure 3-31

A cylinder subjected to both internal and external pressure.

¹⁰See Richard G. Budynas, *Advanced Strength and Applied Stress Analysis*, 2nd ed., McGraw-Hill, New York, 1999, pp. 348–352.

Figure 3-32

Distribution of stresses in a thick-walled cylinder subjected to internal pressure.



The equations of set (3-50) are plotted in Fig. 3-32 to show the distribution of stresses over the wall thickness. It should be realized that longitudinal stresses exist when the end reactions to the internal pressure are taken by the pressure vessel itself. This stress is found to be

$$\sigma_l = \frac{p_i r_i^2}{r_o^2 - r_i^2} \quad (3-51)$$

We further note that Eqs. (3-49), (3-50), and (3-51) apply only to sections taken a significant distance from the ends and away from any areas of stress concentration.

Thin-Walled Vessels

When the wall thickness of a cylindrical pressure vessel is about one-tenth, or less, of its radius, the radial stress that results from pressurizing the vessel is quite small compared with the tangential stress. Under these conditions the tangential stress can be obtained as follows: Let an internal pressure p be exerted on the wall of a cylinder of thickness t and inside diameter d_i . The force tending to separate two halves of a unit length of the cylinder is pd_i . This force is resisted by the tangential stress, also called the *hoop stress*, acting uniformly over the stressed area. We then have $pd_i = 2t\sigma_t$, or

$$(\sigma_t)_{av} = \frac{pd_i}{2t} \quad (3-52)$$

This equation gives the *average* tangential stress and is valid regardless of the wall thickness. For a thin-walled vessel an approximation to the maximum tangential stress is

$$(\sigma_t)_{max} = \frac{p(d_i + t)}{2t} \quad (3-53)$$

where $d_i + t$ is the average diameter.

In a closed cylinder, the longitudinal stress σ_l exists because of the pressure upon the ends of the vessel. If we assume this stress is also distributed uniformly over the wall thickness, we can easily find it to be

$$\sigma_l = \frac{pd_i}{4t} \quad (3-54)$$

EXAMPLE 3-14

An aluminum-alloy pressure vessel is made of tubing having an outside diameter of 8 in and a wall thickness of $\frac{1}{4}$ in.

(a) What pressure can the cylinder carry if the permissible tangential stress is 12 kpsi and the theory for thin-walled vessels is assumed to apply?

(b) On the basis of the pressure found in part (a), compute the stress components using the theory for thick-walled cylinders.

Solution

(a) Here $d_i = 8 - 2(0.25) = 7.5$ in, $r_i = 7.5/2 = 3.75$ in, and $r_o = 8/2 = 4$ in. Then $t/r_i = 0.25/3.75 = 0.067$. Since this ratio is less than 0.1, the theory for thin-walled vessels should yield safe results.

We first solve Eq. (3-53) to obtain the allowable pressure. This gives

Answer

$$p = \frac{2t(\sigma_t)_{\max}}{d_i + t} = \frac{2(0.25)(12)(10)^3}{7.5 + 0.25} = 774 \text{ psi}$$

Answer

(b) The maximum tangential stress will occur at the inside radius, and so we use $r = r_i$ in the first equation of Eq. (3-50). This gives

$$(\sigma_t)_{\max} = \frac{r_i^2 p_i}{r_o^2 - r_i^2} \left(1 + \frac{r_o^2}{r_i^2} \right) = p_i \frac{r_o^2 + r_i^2}{r_o^2 - r_i^2} = 774 \frac{4^2 + 3.75^2}{4^2 - 3.75^2} = 12\,000 \text{ psi}$$

Similarly, the maximum radial stress is found, from the second equation of Eq. (3-50) to be

Answer

$$\sigma_r = -p_i = -774 \text{ psi}$$

The stresses σ_t and σ_r are principal stresses, since there is no shear on these surfaces. Note that there is no significant difference in the stresses in parts (a) and (b), and so the thin-wall theory can be considered satisfactory for this problem.

3-15**Stresses in Rotating Rings**

Many rotating elements, such as flywheels and blowers, can be simplified to a rotating ring to determine the stresses. When this is done it is found that the same tangential and radial stresses exist as in the theory for thick-walled cylinders except that they are caused by inertial forces acting on all the particles of the ring. The tangential and radial stresses so found are subject to the following restrictions:

- The outside radius of the ring, or disk, is large compared with the thickness $r_o \geq 10t$.
- The thickness of the ring or disk is constant.
- The stresses are constant over the thickness.

The stresses are¹¹

$$\begin{aligned} \sigma_t &= \rho \omega^2 \left(\frac{3+\nu}{8} \right) \left(r_i^2 + r_o^2 + \frac{r_i^2 r_o^2}{r^2} - \frac{1+3\nu}{3+\nu} r^2 \right) \\ \sigma_r &= \rho \omega^2 \left(\frac{3+\nu}{8} \right) \left(r_i^2 + r_o^2 - \frac{r_i^2 r_o^2}{r^2} - r^2 \right) \end{aligned} \quad (3-55)$$

¹¹Ibid, pp. 348–357.

where r is the radius to the stress element under consideration, ρ is the mass density, and ω is the angular velocity of the ring in radians per second. For a rotating disk, use $r_i = 0$ in these equations.

3-16 Press and Shrink Fits

When two cylindrical parts are assembled by shrinking or press fitting one part upon another, a contact pressure is created between the two parts. The stresses resulting from this pressure may easily be determined with the equations of the preceding sections.

Figure 3-33 shows two cylindrical members that have been assembled with a shrink fit. Prior to assembly, the outer radius of the inner member was larger than the inner radius of the outer member by the *radial interference* δ . After assembly, an interference contact pressure p develops between the members at the nominal radius R , causing radial stresses $\sigma_r = -p$ in each member at the contacting surfaces. This pressure is given by¹²

$$p = \frac{\delta}{R \left[\frac{1}{E_o} \left(\frac{r_o^2 + R^2}{r_o^2 - R^2} + v_o \right) + \frac{1}{E_i} \left(\frac{R^2 + r_i^2}{R^2 - r_i^2} - v_i \right) \right]} \quad (3-56)$$

where the subscripts o and i on the material properties correspond to the outer and inner members, respectively. If the two members are of the same material with $E_o = E_i = E$, $v_o = v_i$, the relation simplifies to

$$p = \frac{E\delta}{2R^3} \left[\frac{(r_o^2 - R^2)(R^2 - r_i^2)}{r_o^2 - r_i^2} \right] \quad (3-57)$$

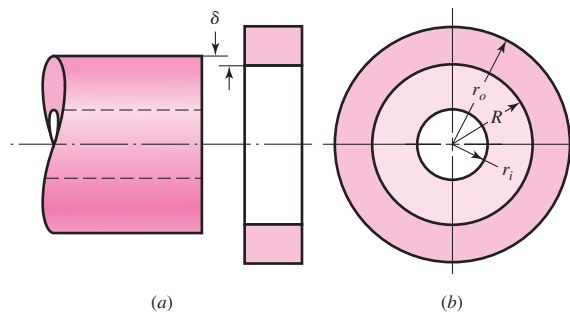
For Eqs. (3-56) or (3-57), diameters can be used in place of R , r_i , and r_o , provided δ is the diametral interference (twice the radial interference).

With p , Eq. (3-49) can be used to determine the radial and tangential stresses in each member. For the inner member, $p_o = p$ and $p_i = 0$. For the outer member, $p_o = 0$ and $p_i = p$. For example, the magnitudes of the tangential stresses at the transition radius R are maximum for both members. For the inner member

$$(\sigma_t)_i \Big|_{r=R} = -p \frac{R^2 + r_i^2}{R^2 - r_i^2} \quad (3-58)$$

Figure 3-33

Notation for press and shrink fits. (a) Unassembled parts; (b) after assembly.



¹²Ibid, pp. 348–354.

and, for the outer member

$$(\sigma_t)_o \Big|_{r=R} = p \frac{r_o^2 + R^2}{r_o^2 - R^2} \quad (3-59)$$

Assumptions

It is assumed that both members have the same length. In the case of a hub that has been press-fitted onto a shaft, this assumption would not be true, and there would be an increased pressure at each end of the hub. It is customary to allow for this condition by employing a stress-concentration factor. The value of this factor depends upon the contact pressure and the design of the female member, but its theoretical value is seldom greater than 2.

3-17

Temperature Effects

When the temperature of an unrestrained body is uniformly increased, the body expands, and the normal strain is

$$\epsilon_x = \epsilon_y = \epsilon_z = \alpha(\Delta T) \quad (3-60)$$

where α is the coefficient of thermal expansion and ΔT is the temperature change, in degrees. In this action the body experiences a simple volume increase with the components of shear strain all zero.

If a straight bar is restrained at the ends so as to prevent lengthwise expansion and then is subjected to a uniform increase in temperature, a compressive stress will develop because of the axial constraint. The stress is

$$\sigma = -\epsilon E = -\alpha(\Delta T)E \quad (3-61)$$

In a similar manner, if a uniform flat plate is restrained at the edges and also subjected to a uniform temperature rise, the compressive stress developed is given by the equation

$$\sigma = -\frac{\alpha(\Delta T)E}{1-\nu} \quad (3-62)$$

The stresses expressed by Eqs. (3-61) and (3-62) are called *thermal stresses*. They arise because of a temperature change in a clamped or restrained member. Such stresses, for example, occur during welding, since parts to be welded must be clamped before welding. Table 3-3 lists approximate values of the coefficients of thermal expansion.

Table 3-3

Coefficients of Thermal Expansion (Linear Mean Coefficients for the Temperature Range 0–100°C)

Material	Celsius Scale ($^{\circ}\text{C}^{-1}$)	Fahrenheit Scale ($^{\circ}\text{F}^{-1}$)
Aluminum	$23.9(10)^{-6}$	$13.3(10)^{-6}$
Brass, cast	$18.7(10)^{-6}$	$10.4(10)^{-6}$
Carbon steel	$10.8(10)^{-6}$	$6.0(10)^{-6}$
Cast iron	$10.6(10)^{-6}$	$5.9(10)^{-6}$
Magnesium	$25.2(10)^{-6}$	$14.0(10)^{-6}$
Nickel steel	$13.1(10)^{-6}$	$7.3(10)^{-6}$
Stainless steel	$17.3(10)^{-6}$	$9.6(10)^{-6}$
Tungsten	$4.3(10)^{-6}$	$2.4(10)^{-6}$

3-18 Curved Beams in Bending¹³

The distribution of stress in a curved flexural member is determined by using the following assumptions:

- The cross section has an axis of symmetry in the plane of bending.
- Plane cross sections remain plane after bending.
- The modulus of elasticity is the same in tension as in compression.

We shall find that the neutral axis and the centroidal axis of a curved beam, unlike the axes of a straight beam, are not coincident and also that the stress does not vary linearly from the neutral axis. The notation shown in Fig. 3-34 is defined as follows:

r_o = radius of outer fiber

r_i = radius of inner fiber

h = depth of section

c_o = distance from neutral axis to outer fiber

c_i = distance from neutral axis to inner fiber

r_n = radius of neutral axis

r_c = radius of centroidal axis

e = distance from centroidal axis to neutral axis

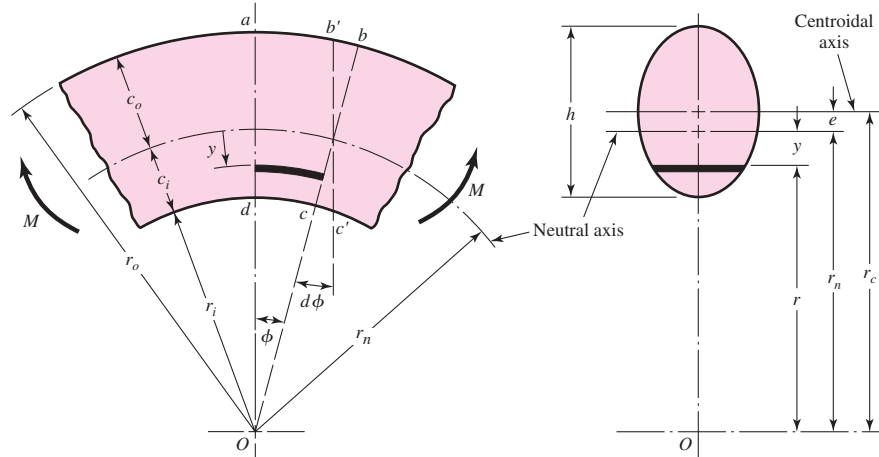
M = bending moment; positive M decreases curvature

Figure 3-34 shows that the neutral and centroidal axes are not coincident. The location of the neutral axis with respect to the center of curvature O is given by the equation

$$r_n = \frac{A}{\int \frac{dA}{r}} \quad (3-63)$$

Figure 3-34

Note that y is positive in the direction toward the center of curvature, point O .



¹³For a complete development of the relations in this section, see Richard G. Budynas, *Advanced Strength and Applied Stress Analysis*, 2nd ed., McGraw-Hill, New York, 1999, pp. 309–317.

Furthermore, it can be shown that the stress distribution is given by

$$\sigma = \frac{My}{Ae(r_n - y)} \quad (3-64)$$

where M is positive in the direction shown in Fig. 3–34. The stress distribution given by Eq. (3–64) is *hyperbolic* and not linear as is the case for straight beams. The critical stresses occur at the inner and outer surfaces where $y = c_i$ and $y = -c_o$, respectively, and are

$$\sigma_i = \frac{Mc_i}{Aer_i} \quad \sigma_o = -\frac{Mc_o}{Aer_o} \quad (3-65)$$

These equations are valid for pure bending. In the usual and more general case, such as a crane hook, the U frame of a press, or the frame of a C clamp, the bending moment is due to a force acting at a distance from the cross section under consideration. Thus, the cross section transmits a bending moment *and* an axial force. The axial force is located at the *centroidal axis* of the section and the bending moment is then computed at this location. The tensile or compressive stress due to the axial force, from Eq. (3–22), is then added to the bending stresses given by Eqs. (3–64) and (3–65) to obtain the resultant stresses acting on the section.

EXAMPLE 3–15

Plot the distribution of stresses across section A–A of the crane hook shown in Fig. 3–35a. The cross section is rectangular, with $b = 0.75$ in and $h = 4$ in, and the load is $F = 5000$ lbf.

Solution

Since $A = bh$, we have $dA = b dr$ and, from Eq. (3–63),

$$r_n = \frac{A}{\int \frac{dA}{r}} = \frac{bh}{\int_{r_i}^{r_o} \frac{b}{r} dr} = \frac{h}{\ln \frac{r_o}{r_i}} \quad (1)$$

From Fig. 3–35b, we see that $r_i = 2$ in, $r_o = 6$ in, $r_c = 4$ in, and $A = 3$ in². Thus, from Eq. (1),

$$r_n = \frac{h}{\ln(r_o/r_i)} = \frac{4}{\ln \frac{6}{2}} = 3.641 \text{ in}$$

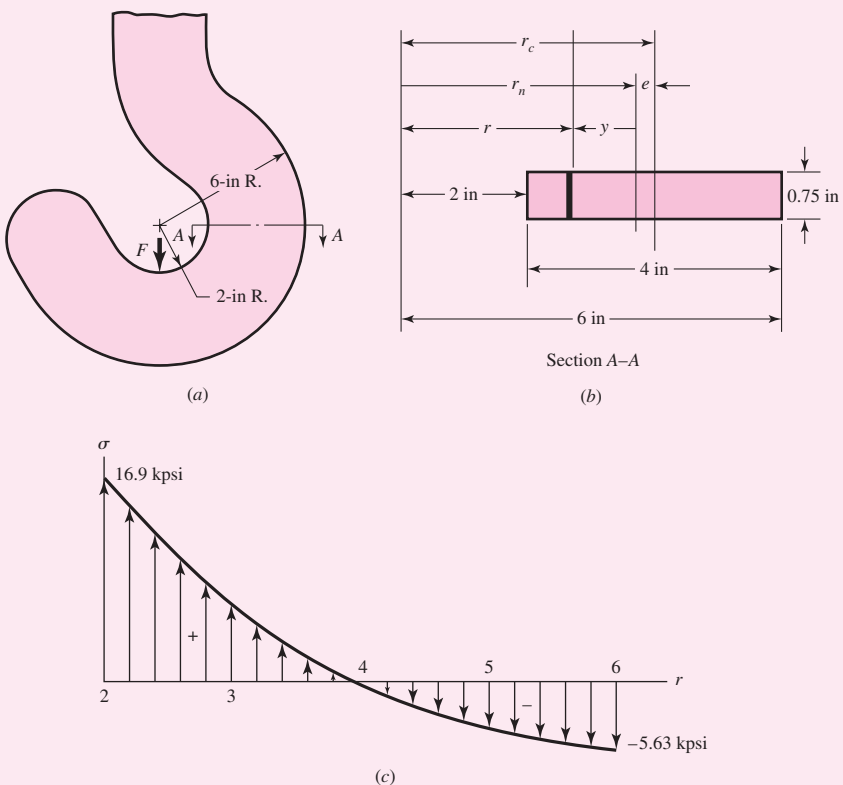
and the eccentricity is $e = r_c - r_n = 4 - 3.641 = 0.359$ in. The moment M is positive and is $M = Fr_c = 5000(4) = 20\,000$ lbf · in. Adding the axial component of stress to Eq. (3–64) gives

$$\sigma = \frac{F}{A} + \frac{My}{Ae(r_n - y)} = \frac{5000}{3} + \frac{(20\,000)(3.641 - r)}{3(0.359)r} \quad (2)$$

Substituting values of r from 2 to 6 in results in the stress distribution shown in Fig. 3–35c. The stresses at the inner and outer radii are found to be 16.9 and -5.63 kpsi, respectively, as shown.

Figure 3–35

- (a) Plan view of crane hook;
 (b) cross section and notation;
 (c) resulting stress distribution.
 There is no stress concentration.



Note in the hook example, the symmetrical rectangular cross section causes the maximum tensile stress to be 3 times greater than the maximum compressive stress. If we wanted to design the hook to use material more effectively we would use more material at the inner radius and less material at the outer radius. For this reason, trapezoidal, T, or unsymmetric I, cross sections are commonly used. Sections most frequently encountered in the stress analysis of curved beams are shown in Table 3–4.

Alternative Calculations for e

Calculating r_n and r_c mathematically and subtracting the difference can lead to large errors if not done carefully, since r_n and r_c are typically large values compared to e . Since e is in the denominator of Eqs. (3–64) and (3–65), a large error in e can lead to an inaccurate stress calculation. Furthermore, if you have a complex cross section that the tables do not handle, alternative methods for determining e are needed. For a quick and simple approximation of e , it can be shown that¹⁴

$$e \doteq \frac{I}{r_c A} \quad (3-66)$$

¹⁴Ibid., pp. 317–321. Also presents a numerical method.

Table 3–4

Formulas for Sections
of Curved Beams

	$r_c = r_i + \frac{h}{2}$ $r_n = \frac{h}{\ln(r_o/r_i)}$
	$r_c = r_i + \frac{h}{3} \frac{b_i + 2b_o}{b_i + b_o}$ $r_n = \frac{A}{b_o - b_i + [(b_i r_o - b_o r_i)/h] \ln(r_o/r_i)}$
	$r_c = r_i + \frac{b_i c_1^2 + 2b_o c_1 c_2 + b_o c_2^2}{2(b_o c_2 + b_i c_1)}$ $r_n = \frac{b_i c_1 + b_o c_2}{b_i \ln[(r_i + c_1)/r_i] + b_o \ln[r_o/(r_i + c_1)]}$
	$r_c = r_i + R$ $r_n = \frac{R^2}{2 \left(r_c - \sqrt{r_c^2 - R^2} \right)}$
	$r_c = r_i + \frac{\frac{1}{2}h^2t + \frac{1}{2}t_i^2(b_i - t) + t_o(b_o - t)(h - t_o/2)}{t_i(b_i - t) + t_o(b_o - t) + ht}$ $r_n = \frac{t_i(b_i - t) + t_o(b_o - t) + ht_o}{b_i \ln \frac{r_i + t}{r_i} + t \ln \frac{r_o - t_o}{r_i + t_i} + b_o \ln \frac{r_o}{r_o - t_o}}$
	$r_c = r_i + \frac{\frac{1}{2}h^2t + \frac{1}{2}t_i^2(b - t) + t_o(b - t)(h - t_o/2)}{ht + (b - t)(t_i + t_o)}$ $r_n = \frac{(b - t)(t_i + t_o) + ht}{b \left(\ln \frac{r_i + t_i}{r_i} + \ln \frac{r_o}{r_o - t_o} \right) + t \ln \frac{r_o - t_o}{r_i + t_i}}$

This approximation is good for a large curvature where e is small with $r_n \doteq r_c$. Substituting Eq. (3–66) into Eq. (3–64), with $r_n - y = r$, gives

$$\sigma \doteq \frac{My}{I} \frac{r_c}{r} \quad (3-67)$$

If $r_n \doteq r_c$, which it should be to use Eq. (3–67), then it is only necessary to calculate r_c , and to measure y from this axis. Determining r_c for a complex cross section can be done easily by most CAD programs or numerically as shown in the before-mentioned reference. Observe that as the curvature increases, $r \rightarrow r_c$, and Eq. (3–67) becomes the straight-beam formulation, Eq. (3–24). Note that the negative sign is missing because y in Fig. 3–34 is vertically downward, opposite that for the straight-beam equation.

EXAMPLE 3–16

Consider the circular section in Table 3–4 with $r_c = 3$ in and $R = 1$ in. Determine e by using the formula from the table and approximately by using Eq. (3–66). Compare the results of the two solutions.

Solution

Using the formula from Table 3–4 gives

$$r_n = \frac{R^2}{2(r_c - \sqrt{r_c^2 - R^2})} = \frac{1^2}{2(3 - \sqrt{3^2 - 1})} = 2.914\ 21 \text{ in}$$

This gives an eccentricity of

Answer

$$e = r_c - r_n = 3 - 2.914\ 21 = 0.085\ 79 \text{ in}$$

The approximate method, using Eq. (3–66), yields

Answer

$$e \doteq \frac{I}{r_c A} = \frac{\pi R^4/4}{r_c(\pi R^2)} = \frac{R^2}{4r_c} = \frac{1^2}{4(3)} = 0.083\ 33 \text{ in}$$

This differs from the exact solution by –2.9 percent.

3–19

Contact Stresses

When two bodies having curved surfaces are pressed together, point or line contact changes to area contact, and the stresses developed in the two bodies are three-dimensional. Contact-stress problems arise in the contact of a wheel and a rail, in automotive valve cams and tappets, in mating gear teeth, and in the action of rolling bearings. Typical failures are seen as cracks, pits, or flaking in the surface material.

The most general case of contact stress occurs when each contacting body has a double radius of curvature; that is, when the radius in the plane of rolling is different from the radius in a perpendicular plane, both planes taken through the axis of the contacting force. Here we shall consider only the two special cases of contacting spheres and contacting cylinders.¹⁵ The results presented here are due to Hertz and so are frequently known as *Hertzian stresses*.

¹⁵A more comprehensive presentation of contact stresses may be found in Arthur P. Boresi and Richard J. Schmidt, *Advanced Mechanics of Materials*, 6th ed., Wiley, New York, 2003, pp. 589–623.

Spherical Contact

When two solid spheres of diameters d_1 and d_2 are pressed together with a force F , a circular area of contact of radius a is obtained. Specifying E_1, ν_1 and E_2, ν_2 as the respective elastic constants of the two spheres, the radius a is given by the equation

$$a = \sqrt[3]{\frac{3F}{8} \frac{(1 - \nu_1^2)/E_1 + (1 - \nu_2^2)/E_2}{1/d_1 + 1/d_2}} \quad (3-68)$$

The pressure distribution within the contact area of each sphere is hemispherical, as shown in Fig. 3-36b. The maximum pressure occurs at the center of the contact area and is

$$p_{\max} = \frac{3F}{2\pi a^2} \quad (3-69)$$

Equations (3-68) and (3-69) are perfectly general and also apply to the contact of a sphere and a plane surface or of a sphere and an internal spherical surface. For a plane surface, use $d = \infty$. For an internal surface, the diameter is expressed as a negative quantity.

The maximum stresses occur on the z axis, and these are principal stresses. Their values are

$$\sigma_1 = \sigma_2 = \sigma_x = \sigma_y = -p_{\max} \left[\left(1 - \left| \frac{z}{a} \right| \tan^{-1} \frac{1}{|z/a|} \right) (1 + \nu) - \frac{1}{2 \left(1 + \frac{z^2}{a^2} \right)} \right] \quad (3-70)$$

$$\sigma_3 = \sigma_z = \frac{-p_{\max}}{1 + \frac{z^2}{a^2}} \quad (3-71)$$

Figure 3-36

(a) Two spheres held in contact by force F ; (b) contact stress has a hemispherical distribution across contact zone diameter $2a$.

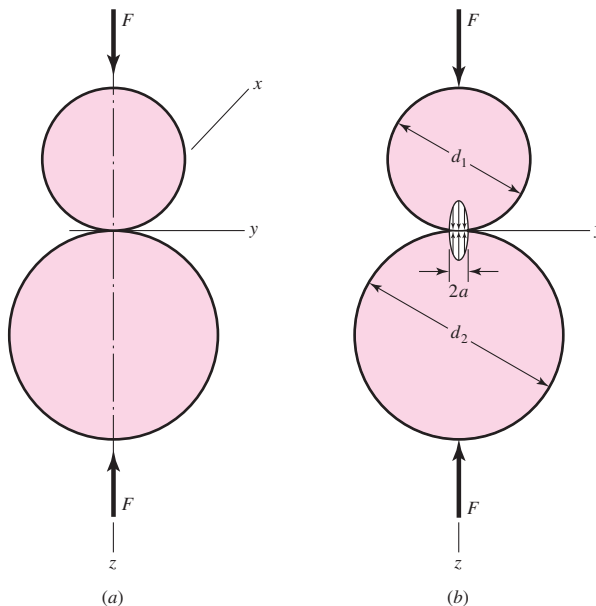
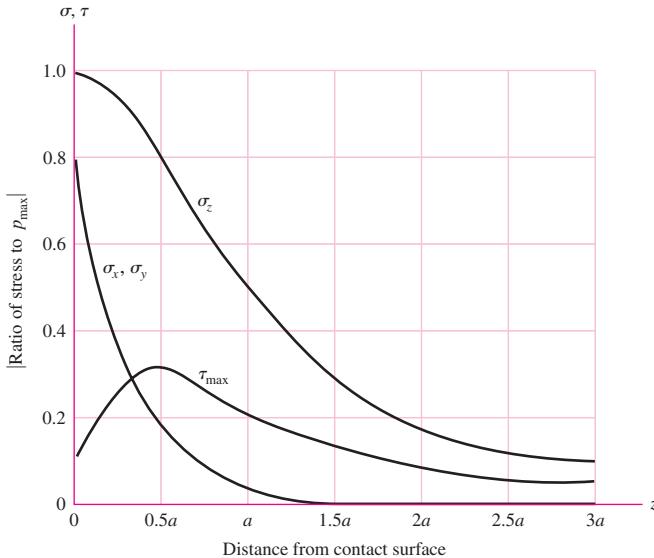


Figure 3-37

Magnitude of the stress components below the surface as a function of the maximum pressure of contacting spheres. Note that the maximum shear stress is slightly below the surface at $z = 0.48a$ and is approximately $0.3p_{\max}$. The chart is based on a Poisson ratio of 0.30. Note that the normal stresses are all compressive stresses.



These equations are valid for either sphere, but the value used for Poisson's ratio must correspond with the sphere under consideration. The equations are even more complicated when stress states off the z axis are to be determined, because here the x and y coordinates must also be included. But these are not required for design purposes, because the maxima occur on the z axis.

Mohr's circles for the stress state described by Eqs. (3-70) and (3-71) are a point and two coincident circles. Since $\sigma_1 = \sigma_2$, we have $\tau_{1/2} = 0$ and

$$\tau_{\max} = \tau_{1/3} = \tau_{2/3} = \frac{\sigma_1 - \sigma_3}{2} = \frac{\sigma_2 - \sigma_3}{2} \quad (3-72)$$

Figure 3-37 is a plot of Eqs. (3-70), (3-71), and (3-72) for a distance to $3a$ below the surface. Note that the shear stress reaches a maximum value slightly below the surface. It is the opinion of many authorities that this maximum shear stress is responsible for the surface fatigue failure of contacting elements. The explanation is that a crack originates at the point of maximum shear stress below the surface and progresses to the surface and that the pressure of the lubricant wedges the chip loose.

Cylindrical Contact

Figure 3-38 illustrates a similar situation in which the contacting elements are two cylinders of length l and diameters d_1 and d_2 . As shown in Fig. 3-38b, the area of contact is a narrow rectangle of width $2b$ and length l , and the pressure distribution is elliptical. The half-width b is given by the equation

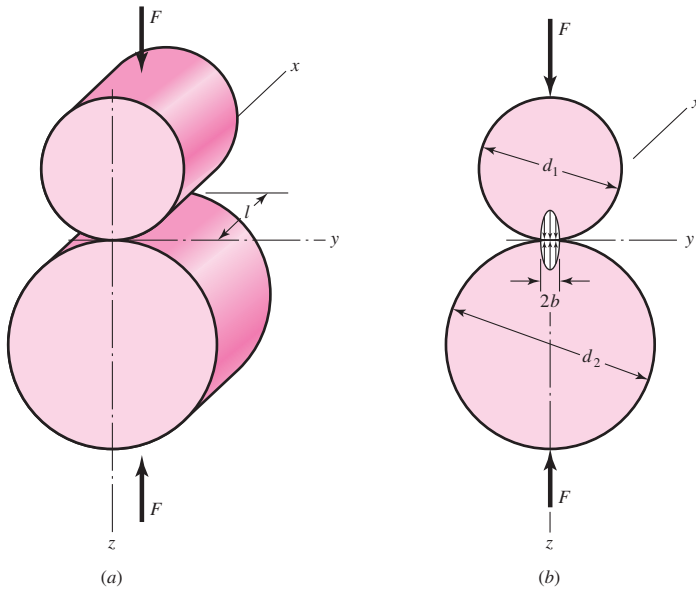
$$b = \sqrt{\frac{2F(1 - v_1^2)/E_1 + (1 - v_2^2)/E_2}{\pi l}} \quad (3-73)$$

The maximum pressure is

$$p_{\max} = \frac{2F}{\pi bl} \quad (3-74)$$

Figure 3–38

(a) Two right circular cylinders held in contact by forces F uniformly distributed along cylinder length l . (b) Contact stress has an elliptical distribution across the contact zone width $2b$.



Equations (3–73) and (3–74) apply to a cylinder and a plane surface, such as a rail, by making $d = \infty$ for the plane surface. The equations also apply to the contact of a cylinder and an internal cylindrical surface; in this case d is made negative for the internal surface.

The stress state along the z axis is given by the equations

$$\sigma_x = -2\nu p_{\max} \left(\sqrt{1 + \frac{z^2}{b^2}} - \left| \frac{z}{b} \right| \right) \quad (3-75)$$

$$\sigma_y = -p_{\max} \left(\frac{1 + 2\frac{z^2}{b^2}}{\sqrt{1 + \frac{z^2}{b^2}}} - 2 \left| \frac{z}{b} \right| \right) \quad (3-76)$$

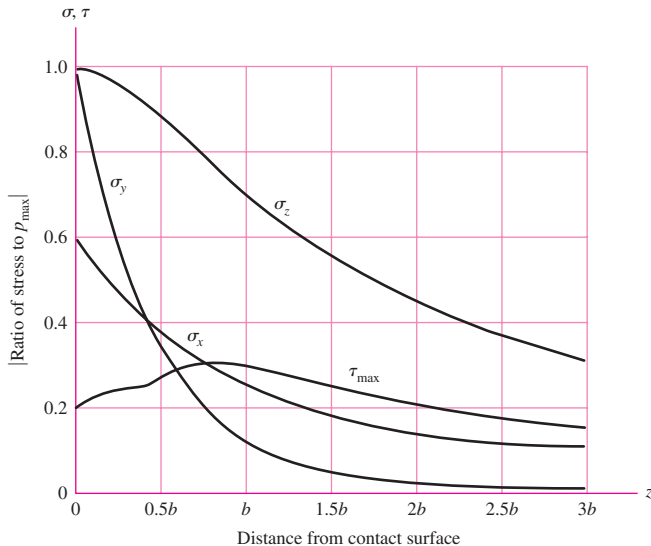
$$\sigma_3 = \sigma_z = \frac{-p_{\max}}{\sqrt{1 + z^2/b^2}} \quad (3-77)$$

These three equations are plotted in Fig. 3–39 up to a distance of $3b$ below the surface. For $0 \leq z \leq 0.436b$, $\sigma_1 = \sigma_x$, and $\tau_{\max} = (\sigma_1 - \sigma_3)/2 = (\sigma_x - \sigma_z)/2$. For $z \geq 0.436b$, $\sigma_1 = \sigma_y$, and $\tau_{\max} = (\sigma_y - \sigma_z)/2$. A plot of τ_{\max} is also included in Fig. 3–39, where the greatest value occurs at $z/b = 0.786$ with a value of $0.300 p_{\max}$.

Hertz (1881) provided the preceding mathematical models of the stress field when the contact zone is free of shear stress. Another important contact stress case is *line of contact* with friction providing the shearing stress on the contact zone. Such shearing stresses are small with cams and rollers, but in cams with flat-faced followers, wheel-rail contact, and gear teeth, the stresses are elevated above the Hertzian field. Investigations of the effect on the stress field due to normal and shear stresses in the contact zone were begun theoretically by Lundberg (1939), and continued by Mindlin (1949), Smith-Liu (1949), and Poritsky (1949) independently. For further detail, see the reference cited in Footnote 15, p. 122.

Figure 3-39

Magnitude of the stress components below the surface as a function of the maximum pressure for contacting cylinders. The largest value of τ_{\max} occurs at $z/b = 0.786$. Its maximum value is $0.30p_{\max}$. The chart is based on a Poisson ratio of 0.30. Note that all normal stresses are compressive stresses.

**3-20****Summary**

The ability to quantify the stress condition at a critical location in a machine element is an important skill of the engineer. Why? Whether the member fails or not is assessed by comparing the (damaging) stress at a critical location with the corresponding material strength at this location. This chapter has addressed the description of stress.

Stresses can be estimated with great precision where the geometry is sufficiently simple that theory easily provides the necessary quantitative relationships. In other cases, approximations are used. There are numerical approximations such as finite element analysis (FEA, see Chap. 19), whose results tend to converge on the true values. There are experimental measurements, strain gauging, for example, allowing *inference* of stresses from the measured strain conditions. Whatever the method(s), the goal is a robust description of the stress condition at a critical location.

The nature of research results and understanding in any field is that the longer we work on it, the more involved things seem to be, and new approaches are sought to help with the complications. As newer schemes are introduced, engineers, hungry for the improvement the new approach *promises*, begin to use the approach. Optimism usually recedes, as further experience adds concerns. Tasks that promised to extend the capabilities of the nonexpert eventually show that expertise is not optional.

In stress analysis, the computer can be helpful if the necessary equations are available. Spreadsheet analysis can quickly reduce complicated calculations for parametric studies, easily handling “what if” questions relating trade-offs (e.g., less of a costly material or more of a cheaper material). It can even give insight into optimization opportunities.

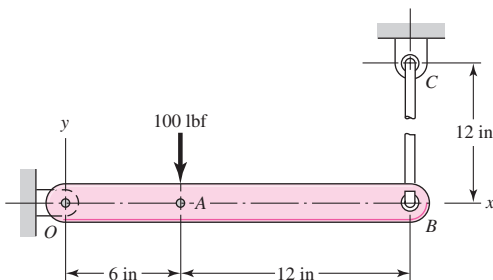
When the necessary equations are not available, then methods such as FEA are attractive, but cautions are in order. Even when you have access to a powerful FEA code, you should be near an expert while you are learning. There are nagging questions of convergence at discontinuities. Elastic analysis is much easier than elastic-plastic analysis. The results are no better than the modeling of reality that was used to formulate the problem. Chapter 19 provides an idea of what finite-element analysis is and how it can be used in design. The chapter is by no means comprehensive in finite-element theory and the application of finite elements in practice. Both skill sets require much exposure and experience to be adept.

PROBLEMS

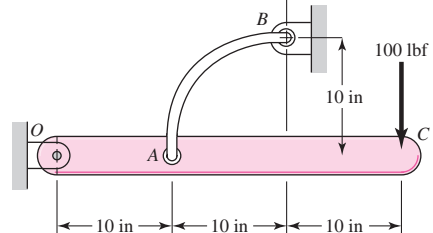
Problems marked with an asterisk (*) are linked with problems in other chapters, as summarized in Table 1–1 of Sec. 1–16, p. 24.

3-1* to 3-4

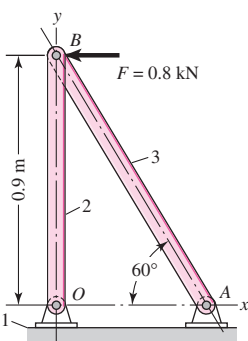
Sketch a free-body diagram of each element in the figure. Compute the magnitude and direction of each force using an algebraic or vector method, as specified.



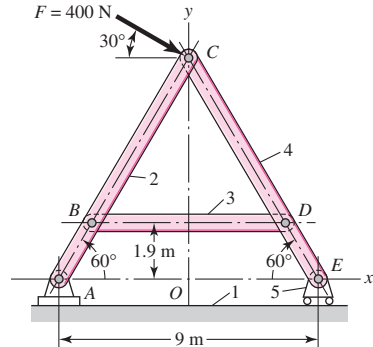
Problem 3-1*



Problem 3-2



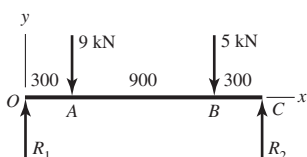
Problem 3-3



Problem 3-4

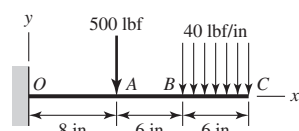
3-5 to 3-8

For the beam shown, find the reactions at the supports and plot the shear-force and bending-moment diagrams. Label the diagrams properly and provide values at all key points.

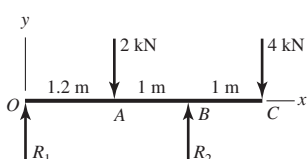


Problem 3-5

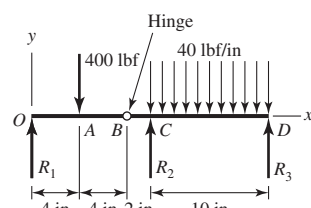
Dimensions in millimeters



Problem 3-6



Problem 3-7



Problem 3-8

- 3-9** Repeat Prob. 3-5 using singularity functions exclusively (including reactions).
- 3-10** Repeat Prob. 3-6 using singularity functions exclusively (including reactions).
- 3-11** Repeat Prob. 3-7 using singularity functions exclusively (including reactions).
- 3-12** Repeat Prob. 3-8 using singularity functions exclusively (including reactions).
- 3-13** For a beam from Table A-9, as specified by your instructor, find general expressions for the loading, shear-force, bending-moment, and support reactions. Use the method specified by your instructor.
- 3-14** A beam carrying a uniform load is simply supported with the supports set back a distance a from the ends as shown in the figure. The bending moment at x can be found from summing moments to zero at section x :

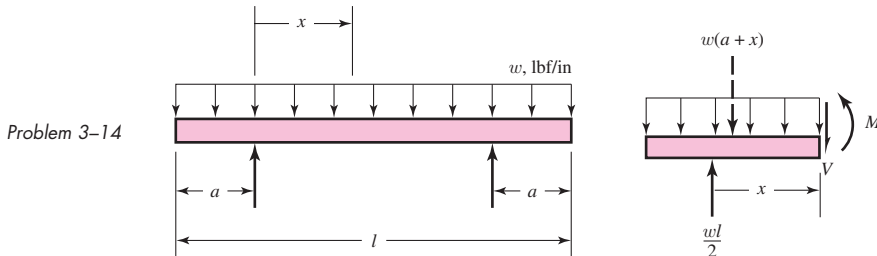
$$\sum M = M + \frac{1}{2}w(a+x)^2 - \frac{1}{2}wlx = 0$$

or

$$M = \frac{w}{2}[lx - (a+x)^2]$$

where w is the loading intensity in lbf/in. The designer wishes to minimize the necessary weight of the supporting beam by choosing a setback resulting in the smallest possible maximum bending stress.

- (a) If the beam is configured with $a = 2.25$ in, $l = 10$ in, and $w = 100$ lbf/in, find the magnitude of the severest bending moment in the beam.
- (b) Since the configuration in part (a) is not optimal, find the optimal setback a that will result in the lightest-weight beam.



- 3-15** For each of the plane stress states listed below, draw a Mohr's circle diagram properly labeled, find the principal normal and shear stresses, and determine the angle from the x axis to σ_1 . Draw stress elements as in Fig. 3-11c and d and label all details.

- (a) $\sigma_x = 20$ kpsi, $\sigma_y = -10$ kpsi, $\tau_{xy} = 8$ kpsi cw
 (b) $\sigma_x = 16$ kpsi, $\sigma_y = 9$ kpsi, $\tau_{xy} = 5$ kpsi ccw
 (c) $\sigma_x = 10$ kpsi, $\sigma_y = 24$ kpsi, $\tau_{xy} = 6$ kpsi ccw
 (d) $\sigma_x = -12$ kpsi, $\sigma_y = 22$ kpsi, $\tau_{xy} = 12$ kpsi cw

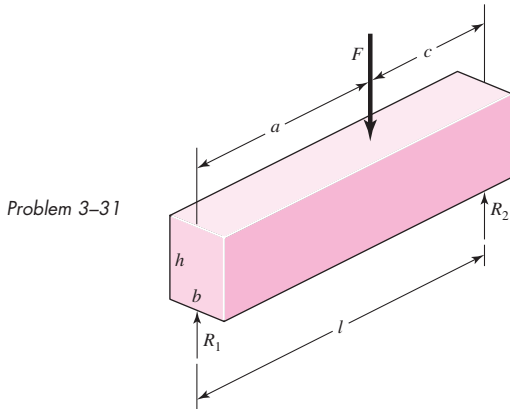
- 3-16** Repeat Prob. 3-15 for:

- (a) $\sigma_x = -8$ MPa, $\sigma_y = 7$ MPa, $\tau_{xy} = 6$ MPa cw
 (b) $\sigma_x = 9$ MPa, $\sigma_y = -6$ MPa, $\tau_{xy} = 3$ MPa cw
 (c) $\sigma_x = -4$ MPa, $\sigma_y = 12$ MPa, $\tau_{xy} = 7$ MPa ccw
 (d) $\sigma_x = 6$ MPa, $\sigma_y = -5$ MPa, $\tau_{xy} = 8$ MPa ccw

- 3-17** Repeat Prob. 3–15 for:
- $\sigma_x = 12 \text{ kpsi}$, $\sigma_y = 6 \text{ kpsi}$, $\tau_{xy} = 4 \text{ kpsi cw}$
 - $\sigma_x = 30 \text{ kpsi}$, $\sigma_y = -10 \text{ kpsi}$, $\tau_{xy} = 10 \text{ kpsi ccw}$
 - $\sigma_x = -10 \text{ kpsi}$, $\sigma_y = 18 \text{ kpsi}$, $\tau_{xy} = 9 \text{ kpsi cw}$
 - $\sigma_x = 9 \text{ kpsi}$, $\sigma_y = 19 \text{ kpsi}$, $\tau_{xy} = 8 \text{ kpsi cw}$
- 3-18** For each of the stress states listed below, find all three principal normal and shear stresses. Draw a complete Mohr's three-circle diagram and label all points of interest.
- $\sigma_x = -80 \text{ MPa}$, $\sigma_y = -30 \text{ MPa}$, $\tau_{xy} = 20 \text{ MPa cw}$
 - $\sigma_x = 30 \text{ MPa}$, $\sigma_y = -60 \text{ MPa}$, $\tau_{xy} = 30 \text{ MPa cw}$
 - $\sigma_x = 40 \text{ MPa}$, $\sigma_z = -30 \text{ MPa}$, $\tau_{xy} = 20 \text{ MPa ccw}$
 - $\sigma_x = 50 \text{ MPa}$, $\sigma_z = -20 \text{ MPa}$, $\tau_{xy} = 30 \text{ MPa cw}$
- 3-19** Repeat Prob. 3–18 for:
- $\sigma_x = 10 \text{ kpsi}$, $\sigma_y = -4 \text{ kpsi}$
 - $\sigma_x = 10 \text{ kpsi}$, $\tau_{xy} = 4 \text{ kpsi ccw}$
 - $\sigma_x = -2 \text{ kpsi}$, $\sigma_y = -8 \text{ kpsi}$, $\tau_{xy} = 4 \text{ kpsi cw}$
 - $\sigma_x = 10 \text{ kpsi}$, $\sigma_y = -30 \text{ kpsi}$, $\tau_{xy} = 10 \text{ kpsi ccw}$
- 3-20** The state of stress at a point is $\sigma_x = -6$, $\sigma_y = 18$, $\sigma_z = -12$, $\tau_{xy} = 9$, $\tau_{yz} = 6$, and $\tau_{zx} = -15 \text{ kpsi}$. Determine the principal stresses, draw a complete Mohr's three-circle diagram, labeling all points of interest, and report the maximum shear stress for this case.
- 3-21** Repeat Prob. 3–20 with $\sigma_x = 20$, $\sigma_y = 0$, $\sigma_z = 20$, $\tau_{xy} = 40$, $\tau_{yz} = -20\sqrt{2}$, and $\tau_{zx} = 0 \text{ kpsi}$.
- 3-22** Repeat Prob. 3–20 with $\sigma_x = 10$, $\sigma_y = 40$, $\sigma_z = 40$, $\tau_{xy} = 20$, $\tau_{yz} = -40$, and $\tau_{zx} = -20 \text{ MPa}$.
- 3-23** A $\frac{3}{4}$ -in-diameter steel tension rod is 5 ft long and carries a load of 15 kip. Find the tensile stress, the total deformation, the unit strains, and the change in the rod diameter.
- 3-24** Repeat Prob. 3–23 except change the rod to aluminum and the load to 3000 lbf.
- 3-25** A 30-mm-diameter copper rod is 1 m long with a yield strength of 70 MPa. Determine the axial force necessary to cause the diameter of the rod to reduce by 0.01 percent, assuming elastic deformation. Check that the elastic deformation assumption is valid by comparing the axial stress to the yield strength.
- 3-26** A diagonal aluminum alloy tension rod of diameter d and initial length l is used in a rectangular frame to prevent collapse. The rod can safely support a tensile stress of σ_{allow} . If $d = 0.5 \text{ in}$, $l = 8 \text{ ft}$, and $\sigma_{\text{allow}} = 20 \text{ kpsi}$, determine how much the rod must be stretched to develop this allowable stress.
- 3-27** Repeat Prob. 3–26 with $d = 16 \text{ mm}$, $l = 3 \text{ m}$, and $\sigma_{\text{allow}} = 140 \text{ MPa}$.
- 3-28** Repeat Prob. 3–26 with $d = \frac{5}{8} \text{ in}$, $l = 10 \text{ ft}$, and $\sigma_{\text{allow}} = 15 \text{ kpsi}$.
- 3-29** Electrical strain gauges were applied to a notched specimen to determine the stresses in the notch. The results were $\epsilon_x = 0.0019$ and $\epsilon_y = -0.00072$. Find σ_x and σ_y if the material is carbon steel.
- 3-30** Repeat Prob. 3–29 for a material of aluminum.
- 3-31** The Roman method for addressing uncertainty in design was to build a copy of a design that was satisfactory and had proven durable. Although the early Romans did not have the intellectual tools to deal with scaling size up or down, you do. Consider a simply supported, rectangular-cross-section beam with a concentrated load F , as depicted in the figure.
- (a) Show that the stress-to-load equation is

$$F = \frac{\sigma b h^2 l}{6ac}$$

(b) Subscript every parameter with m (for model) and divide into the above equation. Introduce a scale factor, $s = a_m/a = b_m/b = c_m/c$ etc. Since the Roman method was to not "lean on" the material any more than the proven design, set $\sigma_m/\sigma = 1$. Express F_m in terms of the scale factors and F , and comment on what you have learned.



3-32 Using our experience with concentrated loading on a simple beam, Prob. 3-31, consider a uniformly loaded simple beam (Table A-9-7).

(a) Show that the stress-to-load equation for a rectangular-cross-section beam is given by

$$W = \frac{4}{3} \frac{\sigma b h^2}{l}$$

where $W = wl$.

(b) Subscript every parameter with m (for model) and divide the model equation into the prototype equation. Introduce the scale factor s as in Prob. 3-31, setting $\sigma_m/\sigma = 1$. Express W_m and w_m in terms of the scale factor, and comment on what you have learned.

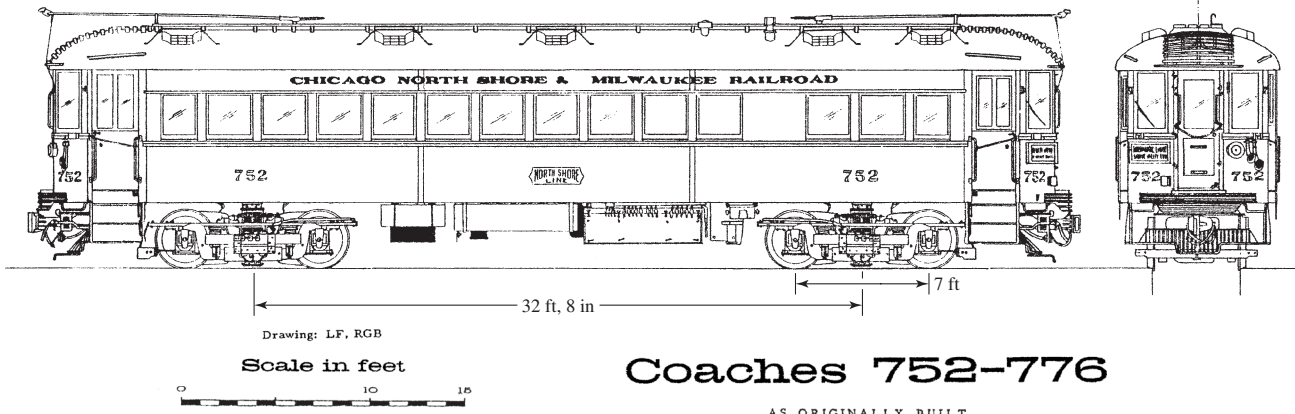
3-33 The Chicago North Shore & Milwaukee Railroad was an electric railway running between the cities in its corporate title. It had passenger cars as shown in the figure, which weighed 104.4 kip, had 32-ft, 8-in truck centers, 7-ft-wheelbase trucks, and a coupled length of 55 ft, $3\frac{1}{4}$ in. Consider the case of a single car on a 100-ft-long, simply supported deck plate girder bridge.

(a) What was the largest bending moment in the bridge?

(b) Where on the bridge was the moment located?

(c) What was the position of the car on the bridge?

(d) Under which axle is the bending moment?

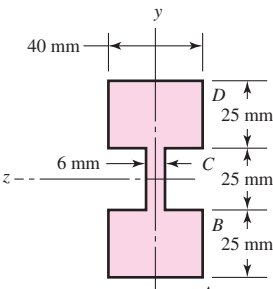


Problem 3-33

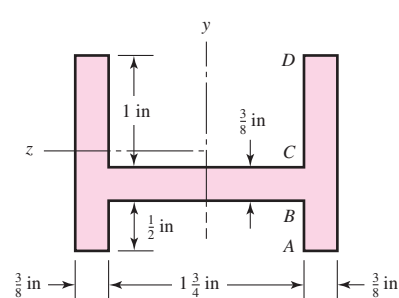
Copyright 1963 by Central Electric Railfans Association, Bull. 107, p. 145, reproduced by permission.

3-34

For each section illustrated, find the second moment of area, the location of the neutral axis, and the distances from the neutral axis to the top and bottom surfaces. Consider that the section is transmitting a positive bending moment about the z axis, M_z , where $M_z = 10 \text{ kip} \cdot \text{in}$ if the dimensions are given in ips units, or $M_z = 1.13 \text{ kN} \cdot \text{m}$ if the dimensions are in SI units. Determine the resulting stresses at the top and bottom surfaces and at every abrupt change in the cross section.

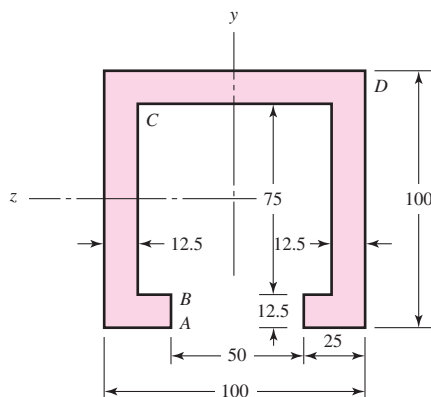


(a)

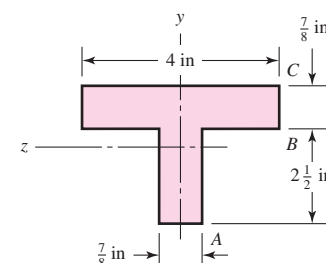


(b)

Problem 3-34



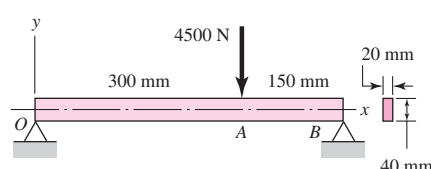
(c) Dimensions in mm



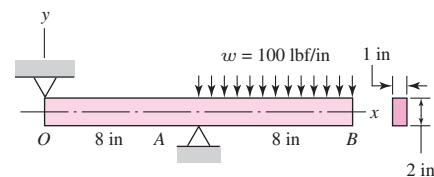
(d)

**3-35 to
3-38**

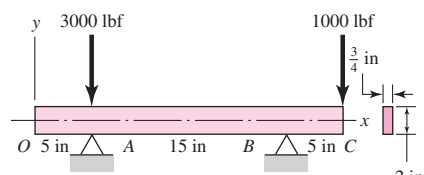
For the beam illustrated in the figure, find the locations and magnitudes of the maximum tensile bending stress due to M and the maximum shear stress due to V .



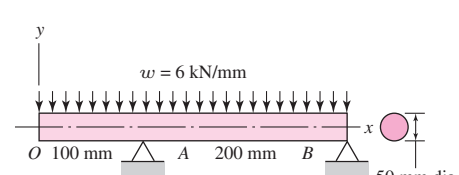
Problem 3-35



Problem 3-36



Problem 3-37



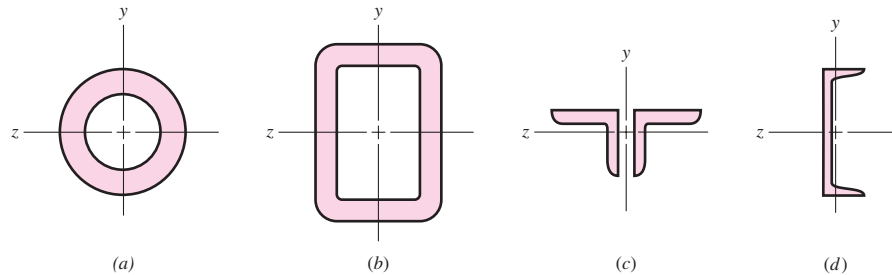
Problem 3-38

3-39

The figure illustrates a number of beam sections. Use an allowable bending stress of 12 kpsi for steel and find the maximum safe uniformly distributed load that each beam can carry if the given lengths are between simple supports.

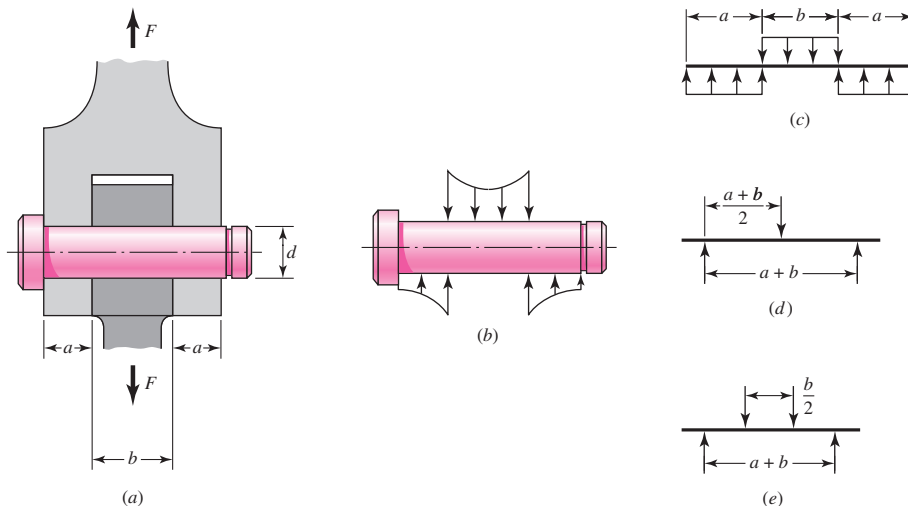
- Standard 2-in $\times \frac{1}{4}$ -in tube, 48 in long
- Hollow steel tube 3 by 2 in, outside dimensions, formed from $\frac{3}{16}$ -in material and welded, 60 in long
- Steel angles $2\frac{1}{2} \times 2\frac{1}{2} \times \frac{1}{4}$ in and 60 in long
- A 6.0 lbf/in, 3-in steel channel, 60 in long

Problem 3-39

**3-40***

A pin in a knuckle joint carrying a tensile load F deflects somewhat on account of this loading, making the distribution of reaction and load as shown in part (b) of the figure. A common simplification is to assume uniform load distributions, as shown in part (c). To further simplify, designers may consider replacing the distributed loads with point loads, such as in the two models shown in parts (d) and (e). If $a = 0.5$ in, $b = 0.75$ in, $d = 0.5$ in, and $F = 1000$ lbf, estimate the maximum bending stress and the maximum shear stress due to V for the three simplified models. Compare the three models from a designer's perspective in terms of accuracy, safety, and modeling time.

Problem 3-40*

**3-41**

Repeat Prob. 3-40 for $a = 6$ mm, $b = 18$ mm, $d = 12$ mm, and $F = 4$ kN.

3-42

For the knuckle joint described in Prob. 3-40, assume the maximum allowable tensile stress in the pin is 30 kpsi and the maximum allowable shearing stress in the pin is 15 kpsi. Use the model

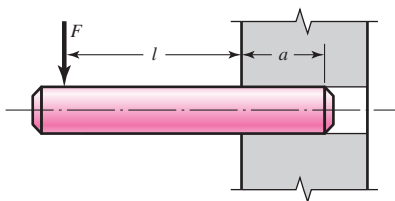
shown in part *c* of the figure to determine a minimum pin diameter for each of the following potential failure modes.

- Consider failure based on bending at the point of maximum bending stress in the pin.
- Consider failure based on the average shear stress on the pin cross section at the interface plane of the knuckle and clevis.
- Consider failure based on shear at the point of the maximum transverse shear stress in the pin.

3-43

The figure illustrates a pin tightly fitted into a hole of a substantial member. A usual analysis is one that assumes concentrated reactions R and M at distance l from F . Suppose the reaction is distributed linearly along distance a . Is the resulting moment reaction larger or smaller than the concentrated reaction? What is the loading intensity q ? What do you think of using the usual assumption?

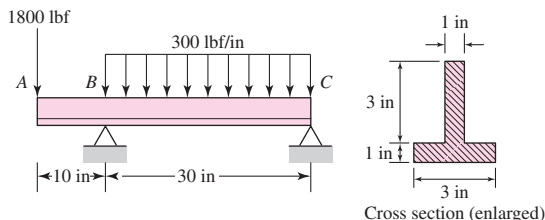
Problem 3-43



3-44

For the beam shown, determine (a) the maximum tensile and compressive bending stresses, (b) the maximum shear stress due to V , and (c) the maximum shear stress in the beam.

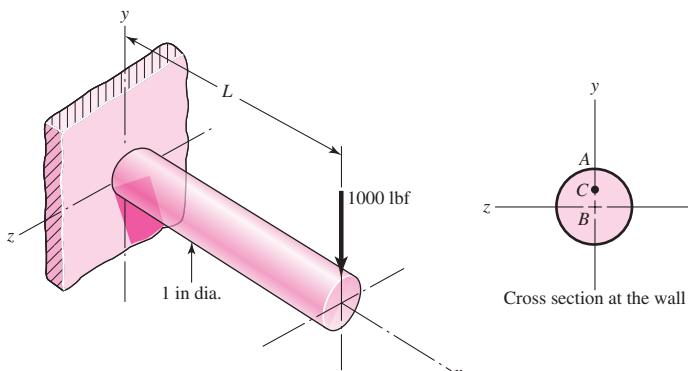
Problem 3-44



3-45

A cantilever beam with a 1-in-diameter round cross section is loaded at the tip with a transverse force of 1000 lbf, as shown in the figure. The cross section at the wall is also shown, with labeled points *A* at the top, *B* at the center, and *C* at the midpoint between *A* and *B*. Study the

Problem 3-45



significance of the transverse shear stress in combination with bending by performing the following steps.

- Assume $L = 10$ in. For points A , B , and C , sketch three-dimensional stress elements, labeling the coordinate directions and showing all stresses. Calculate magnitudes of the stresses on the stress elements. Do not neglect transverse shear stress. Calculate the maximum shear stress for each stress element.
- For each stress element in part (a), calculate the maximum shear stress if the transverse shear stress is neglected. Determine the percent error for each stress element from neglecting the transverse shear stress.
- Repeat the problem for $L = 4$, 1 , and 0.1 in. Compare the results and state any conclusions regarding the significance of the transverse shear stress in combination with bending.

3-46

Consider a simply supported beam of rectangular cross section of constant width b and variable depth h , so proportioned that the maximum stress σ_x at the outer surface due to bending is constant, when subjected to a load F at a distance a from the left support and a distance c from the right support. Show that the depth h at location x is given by

$$h = \sqrt{\frac{6Fcx}{lb\sigma_{\max}}} \quad 0 \leq x \leq a$$

3-47

In Prob. 3-46, $h \rightarrow 0$ as $x \rightarrow 0$, which cannot occur. If the maximum shear stress τ_{\max} due to direct shear is to be constant in this region, show that the depth h at location x is given by

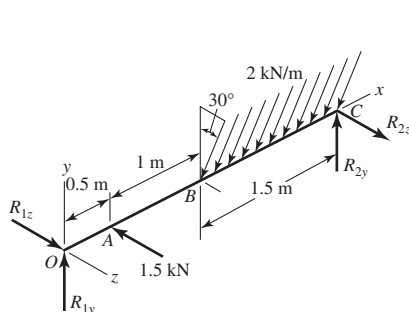
$$h = \frac{3}{2} \frac{Fc}{lb\tau_{\max}} \quad 0 \leq x \leq \frac{3}{8} \frac{Fc\sigma_{\max}}{lb\tau_{\max}^2}$$

3-48 and

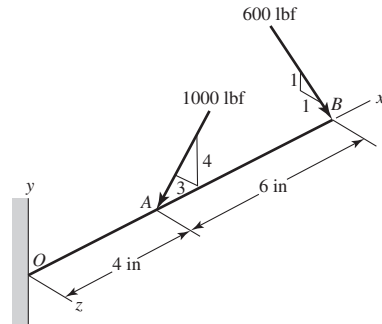
3-49

The beam shown is loaded in the xy and xz planes.

- Find the y_z components of the reactions at the supports.
- Plot the shear-force and bending-moment diagrams for the xy and xz planes. Label the diagrams properly and provide the values at key points.
- Determine the net shear-force and bending-moment at the key points of part (b).
- Determine the maximum tensile bending stress. For Prob. 3-48, use the cross section given in Prob. 3-34, part (a). For Prob. 3-49, use the cross section given in Prob. 3-39, part (b).



Problem 3-48



Problem 3-49

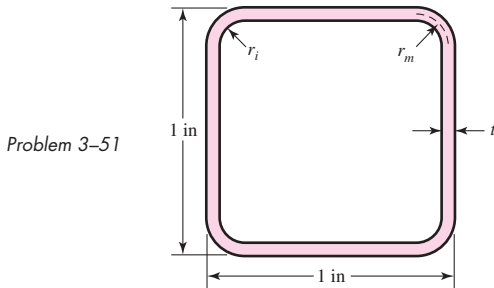
3-50

Two steel thin-wall tubes in torsion of equal length are to be compared. The first is of square cross section, side length b , and wall thickness t . The second is a round of diameter b and wall thickness t . The largest allowable shear stress is τ_{all} and is to be the same in both cases. How does the angle of twist per unit length compare in each case?

- 3-51** Consider a 1-in-square steel thin-walled tube loaded in torsion. The tube has a wall thickness $t = \frac{1}{16}$ in, is 36 in long, and has a maximum allowable shear stress of 12 kpsi. Determine the maximum torque that can be applied and the corresponding angle of twist of the tube.

(a) Assume that the internal radius at the corners $r_i = 0$.

(b) Assume that the internal radius at the corners is more realistically $r_i = \frac{1}{8}$ in.

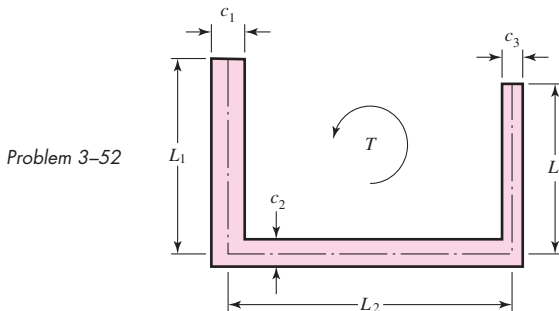


- 3-52** The thin-walled open cross-section shown is transmitting torque T . The angle of twist per unit length of each leg can be determined separately using Eq. (3-47) and is given by

$$\theta_i = \frac{3T_i}{GL_i c_i^3}$$

where for this case, $i = 1, 2, 3$, and T_i represents the torque in leg i . Assuming that the angle of twist per unit length for each leg is the same, show that

$$T = \frac{G\theta_1}{3} \sum_{i=1}^3 L_i c_i^3 \quad \text{and} \quad \tau_{\max} = G\theta_1 c_{\max}$$



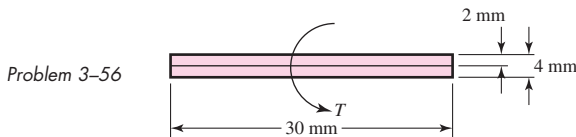
- 3-53 to 3-55** Using the results from Prob. 3-52, consider a steel section with $\tau_{\text{allow}} = 12$ kpsi.

- (a) Determine the torque transmitted by each leg and the torque transmitted by the entire section.
 (b) Determine the angle of twist per unit length.

Problem Number	c_1	L_1	c_2	L_2	c_3	L_3
3-53	2 mm	20 mm	3 mm	30 mm	0	0
3-54	$\frac{1}{16}$ in	$\frac{3}{4}$ in	$\frac{1}{8}$ in	1 in	$\frac{1}{16}$ in	$\frac{5}{8}$ in
3-55	2 mm	20 mm	3 mm	30 mm	2 mm	25 mm

- 3-56** Two 300-mm-long rectangular steel strips are placed together as shown. Using a maximum allowable shear stress of 80 MPa, determine the maximum torque and angular twist, and the torsional

spring rate. Compare these with a single strip of cross section 30 mm by 4 mm. Solve the problem two ways: (a) using Eqs. (3–40) and (3–41), and (b) using Eq. (3–47). Compare and discuss your results



3-57 Using a maximum allowable shear stress of 70 MPa, find the shaft diameter needed to transmit 40 kW when

- (a) The shaft speed is 2500 rev/min.
- (b) The shaft speed is 250 rev/min.

3-58 Repeat Prob. 3-57 with an allowable shear stress of 20 kpsi and a power of 50 hp.

3-59 Using an allowable shear stress of 50 MPa, determine the power that can be transmitted at 2000 rpm through a shaft with a 30-mm diameter.

3-60 A 20-mm-diameter steel bar is to be used as a torsion spring. If the torsional stress in the bar is not to exceed 110 MPa when one end is twisted through an angle of 15° , what must be the length of the bar?

3-61 A 2-ft-long steel bar with a $\frac{3}{4}$ -in diameter is to be used as a torsion spring. If the torsional stress in the bar is not to exceed 30 kpsi, what is the maximum angle of twist of the bar?

3-62 A 40-mm-diameter solid steel shaft, used as a torque transmitter, is replaced with a hollow shaft having a 40-mm OD and a 36-mm ID. If both materials have the same strength, what is the percentage reduction in torque transmission? What is the percentage reduction in shaft weight?

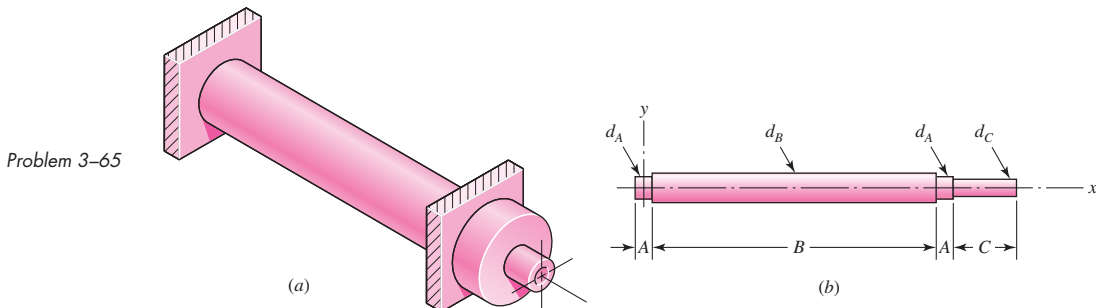
3-63 Generalize Prob. 3-62 for a solid shaft of diameter d replaced with a hollow shaft of the same material with an outside diameter d , and an inside diameter that is a fraction of the outside diameter, $x \times d$, where x is any fraction between zero and one. Obtain expressions for percentage reduction in torque transmission and percentage reduction in weight in terms of only x . Notice that the length and diameter of the shaft, and the material, are not needed for this comparison. Plot both results on the same axis for the range $0 < x < 1$. From the plot, what is the approximate value of x to obtain the greatest difference between the percent decrease in weight and the percent decrease in torque?

3-64 A hollow steel shaft is to transmit 4200 N · m of torque and is to be sized so that the torsional stress does not exceed 120 MPa.

- (a) If the inside diameter is 70 percent of the outside diameter, what size shaft should be used?
Use preferred sizes.
- (b) What is the stress on the inside of the shaft when full torque is applied?

3-65 The figure shows an endless-belt conveyor drive roll. The roll has a diameter 120 mm and is driven at 10 rev/min by a geared-motor source rated at 1.5 kW. Determine a suitable shaft diameter d_C for an allowable torsional stress of 80 MPa.

- (a) What would be the stress in the shaft you have sized if the motor starting torque is twice the running torque?
- (b) Is bending stress likely to be a problem? What is the effect of different roll lengths B on bending?



Problem 3-65

3-66

The conveyor drive roll in the figure for Prob. 3-65 is 5 in in diameter and is driven at 8 rev/min by a geared-motor source rated at 1 hp. Find a suitable shaft diameter d_C based on an allowable torsional stress of 15 kpsi.

3-67

Consider two shafts in torsion, each of the same material, length, and cross-sectional area. One shaft has a solid square cross section and the other shaft has a solid circular section.

(a) Which shaft has the greater maximum shear stress and by what percentage?

(b) Which shaft has the greater angular twist θ and by what percentage?

3-68* to**3-71***

A countershaft carrying two V-belt pulleys is shown in the figure. Pulley A receives power from a motor through a belt with the belt tensions shown. The power is transmitted through the shaft and delivered to the belt on pulley B. Assume the belt tension on the loose side at B is 15 percent of the tension on the tight side.

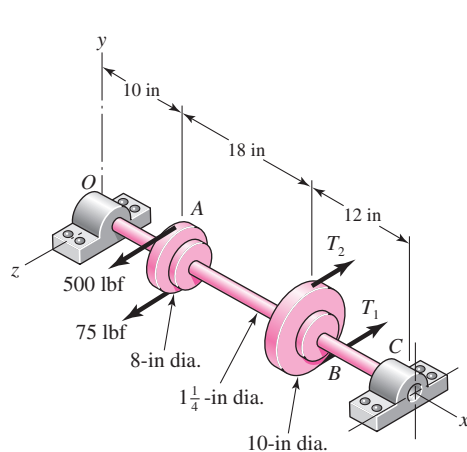
(a) Determine the tensions in the belt on pulley B, assuming the shaft is running at a constant speed.

(b) Find the magnitudes of the bearing reaction forces, assuming the bearings act as simple supports.

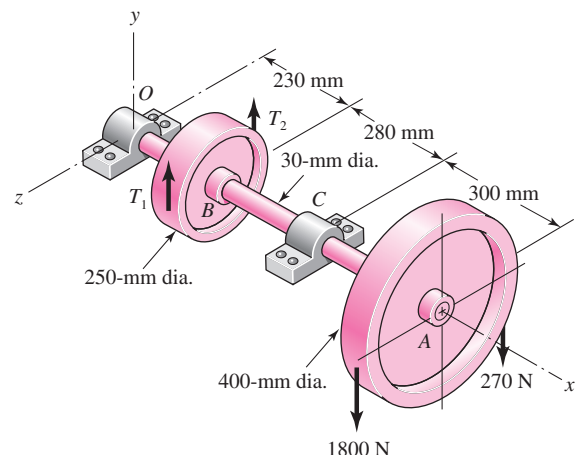
(c) Draw shear-force and bending-moment diagrams for the shaft. If needed, make one set for the horizontal plane and another set for the vertical plane.

(d) At the point of maximum bending moment, determine the bending stress and the torsional shear stress.

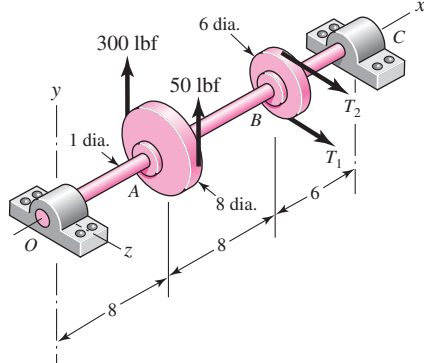
(e) At the point of maximum bending moment, determine the principal stresses and the maximum shear stress.



Problem 3-68*

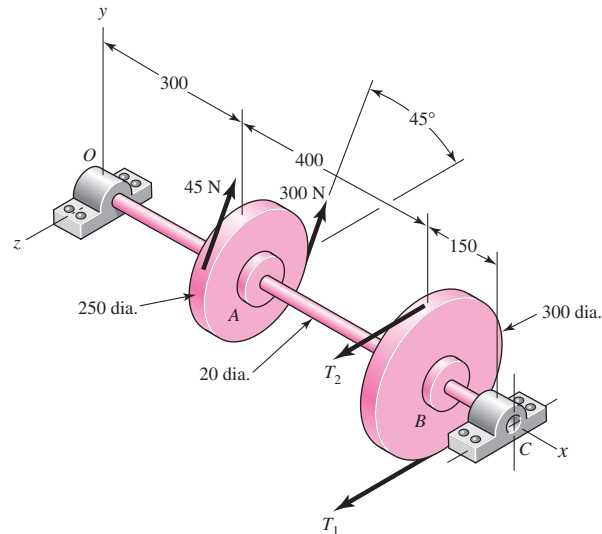


Problem 3-69*



Problem 3-70*

Dimensions in inches.



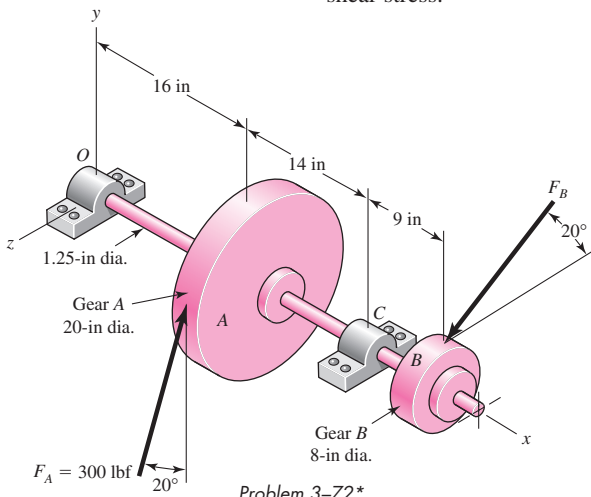
Problem 3-71*

Dimensions in millimeters.

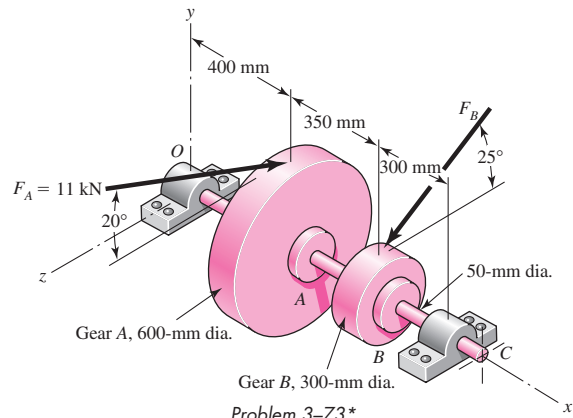
**3-72* to
3-73***

A gear reduction unit uses the countershaft shown in the figure. Gear A receives power from another gear with the transmitted force F_A applied at the 20° pressure angle as shown. The power is transmitted through the shaft and delivered through gear B through a transmitted force F_B at the pressure angle shown.

- Determine the force F_B , assuming the shaft is running at a constant speed.
- Find the magnitudes of the bearing reaction forces, assuming the bearings act as simple supports.
- Draw shear-force and bending-moment diagrams for the shaft. If needed, make one set for the horizontal plane and another set for the vertical plane.
- At the point of maximum bending moment, determine the bending stress and the torsional shear stress.
- At the point of maximum bending moment, determine the principal stresses and the maximum shear stress.



Problem 3-72*

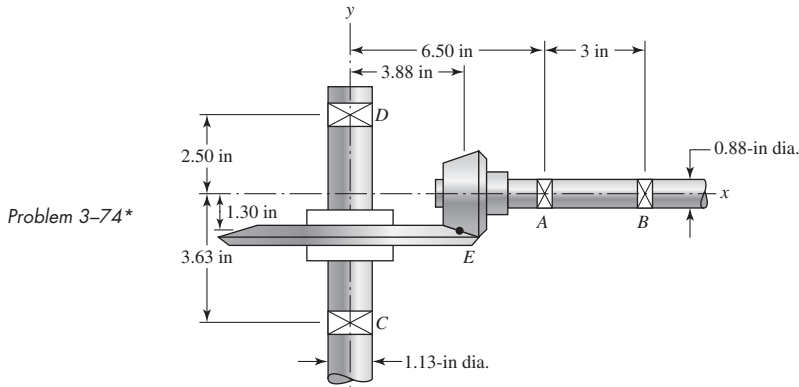


Problem 3-73*

3-74*

In the figure, shaft AB transmits power to shaft CD through a set of bevel gears contacting at point E. The contact force at E on the gear of shaft CD is determined to be $(F_E)_{CD} = -92.8\mathbf{i} - 362.8\mathbf{j} + 808.0\mathbf{k}$ lbf. For shaft CD: (a) draw a free-body diagram and determine the reactions at C and D

assuming simple supports (assume also that bearing *C* carries the thrust load), (b) draw the shear-force and bending-moment diagrams, (c) for the critical stress element, determine the torsional shear stress, the bending stress, and the axial stress, and (d) for the critical stress element, determine the principal stresses and the maximum shear stress.

**3-75**

Repeat Prob. 3-74 except for a contact force at *E* of $(\mathbf{F}_E)_{CD} = -46.6\mathbf{i} - 140\mathbf{j} + 406\mathbf{k}$ lbf and a shaft diameter of 1.0 in.

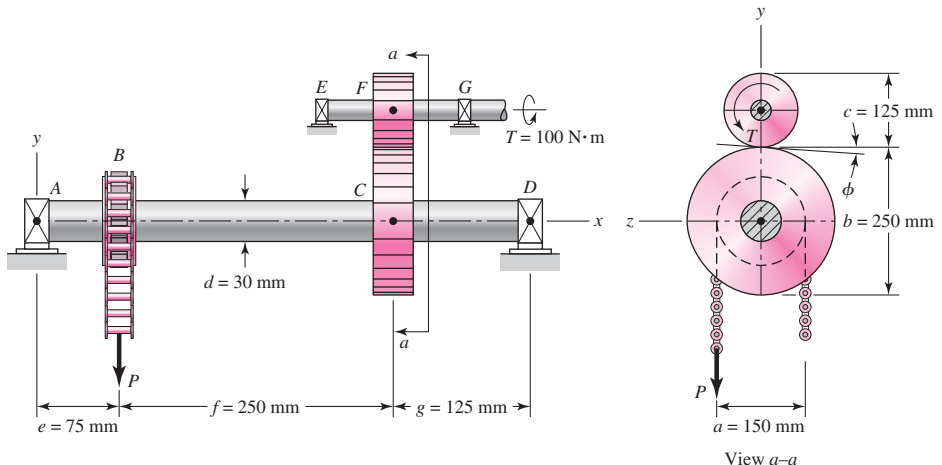
3-76*

Repeat the analysis of Prob. 3-74 for shaft *AB*. Assume that bearing *A* carries the thrust load.

3-77*

A torque $T = 100 \text{ N}\cdot\text{m}$ is applied to the shaft *EFG*, which is running at constant speed and contains gear *F*. Gear *F* transmits torque to shaft *ABCD* through gear *C*, which drives the chain sprocket at *B*, transmitting a force *P* as shown. Sprocket *B*, gear *C*, and gear *F* have pitch diameters of $a = 150$, $b = 250$, and $c = 125$ mm, respectively. The contact force between the gears is transmitted through the pressure angle $\phi = 20^\circ$. Assuming no frictional losses and considering the bearings at *A*, *D*, *E*, and *G* to be simple supports, locate the point on shaft *ABCD* that contains the maximum tensile bending and maximum torsional shear stresses. Combine these stresses and determine the maximum principal normal and shear stresses in the shaft.

Problem 3-77*

**3-78**

Repeat Prob. 3-77 with the chain parallel to the *z* axis with *P* in the positive *z* direction.

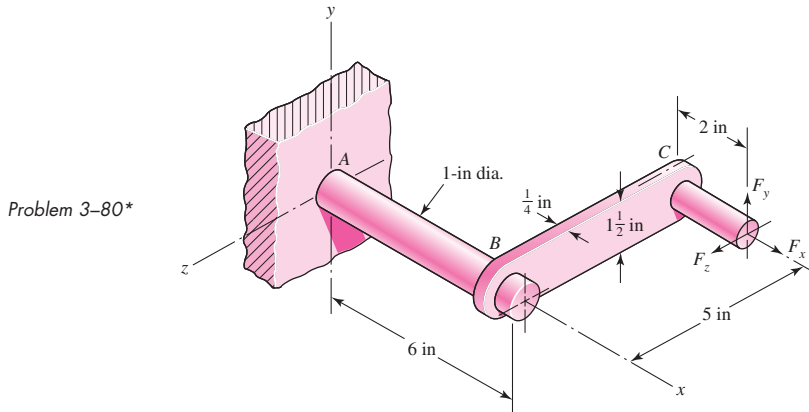
3-79*

Repeat Prob. 3-77 with $T = 900 \text{ lbf}\cdot\text{in}$, $a = 6 \text{ in}$, $b = 5 \text{ in}$, $c = 10 \text{ in}$, $d = 1.375 \text{ in}$, $e = 4 \text{ in}$, $f = 10 \text{ in}$, and $g = 6 \text{ in}$.

3-80*

The cantilevered bar in the figure is made from a ductile material and is statically loaded with $F_y = 200 \text{ lbf}$ and $F_x = F_z = 0$. Analyze the stress situation in rod *AB* by obtaining the following information.

- (a) Determine the precise location of the critical stress element.
 (b) Sketch the critical stress element and determine magnitudes and directions for all stresses acting on it. (Transverse shear may only be neglected if you can justify this decision.)
 (c) For the critical stress element, determine the principal stresses and the maximum shear stress.

**3-81***

Repeat Prob. 3-80 with $F_x = 0$, $F_y = 175$ lbf, and $F_z = 100$ lbf.

3-82*

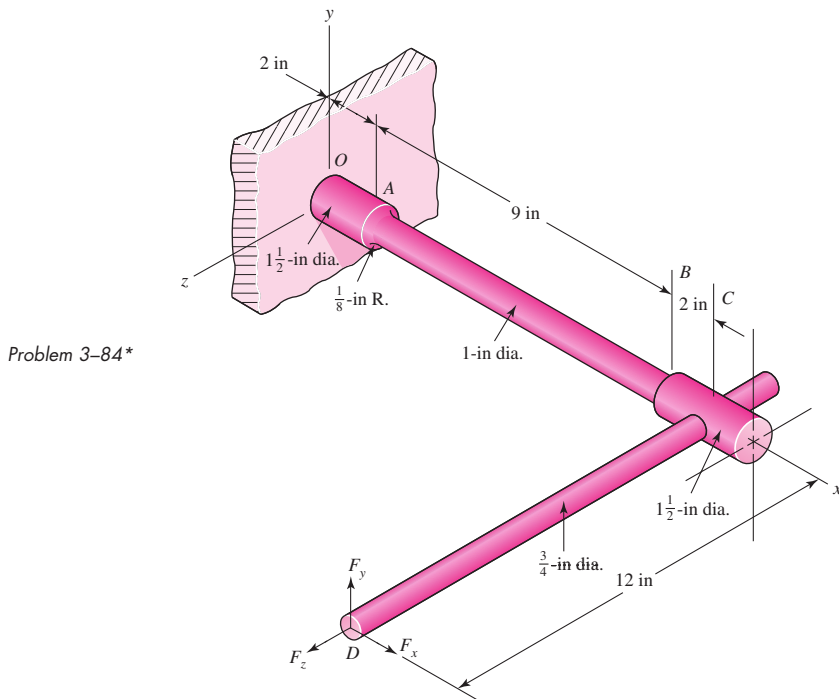
Repeat Prob. 3-80 with $F_x = 75$ lbf, $F_y = -200$ lbf, and $F_z = 100$ lbf.

3-83*

For the handle in Prob. 3-80, one potential failure mode is twisting of the flat plate BC. Determine the maximum value of the shear stress due to torsion in the main section of the plate, ignoring the complexities of the interfaces at B and C.

3-84*

The cantilevered bar in the figure is made from a ductile material and is statically loaded with $F_y = 250$ lbf and $F_x = F_z = 0$. Analyze the stress situation in the small diameter at the shoulder at A by obtaining the following information.



- (a) Determine the precise location of the critical stress element at the cross section at A.
 (b) Sketch the critical stress element and determine magnitudes and directions for all stresses acting on it. (Transverse shear may be neglected if you can justify this decision.)
 (c) For the critical stress element, determine the principal stresses and the maximum shear stress.

3-85*

Repeat Prob. 3-84 with $F_x = 300 \text{ lbf}$, $F_y = 250 \text{ lbf}$, and $F_z = 0$.

3-86*

Repeat Prob. 3-84 with $F_x = 300 \text{ lbf}$, $F_y = 250 \text{ lbf}$, and $F_z = -100 \text{ lbf}$.

3-87*

Repeat Prob. 3-84 for a brittle material, requiring the inclusion of stress concentration in the fillet radius.

3-88

Repeat Prob. 3-84 with $F_x = 300 \text{ lbf}$, $F_y = 250 \text{ lbf}$, and $F_z = 0$, and for a brittle material, requiring the inclusion of stress concentration in the fillet radius.

3-89

Repeat Prob. 3-84 with $F_x = 300 \text{ lbf}$, $F_y = 250 \text{ lbf}$, and $F_z = -100 \text{ lbf}$, and for a brittle material, requiring the inclusion of stress concentration in the fillet radius.

3-90

The figure shows a simple model of the loading of a square thread of a power screw transmitting an axial load F with an application of torque T . The torque is balanced by the frictional force F_f acting along the top surface of the thread. The forces on the thread are considered to be distributed along the circumference of the *mean diameter* d_m over the number of engaged threads, n_t . From the figure, $d_m = d_r + p/2$, where d_r is the *root diameter* of the thread and p is the pitch of the thread.

(a) Considering the thread to be a cantilever beam as shown in the cutaway view, show that the bending stress at the root of the thread can be approximated by

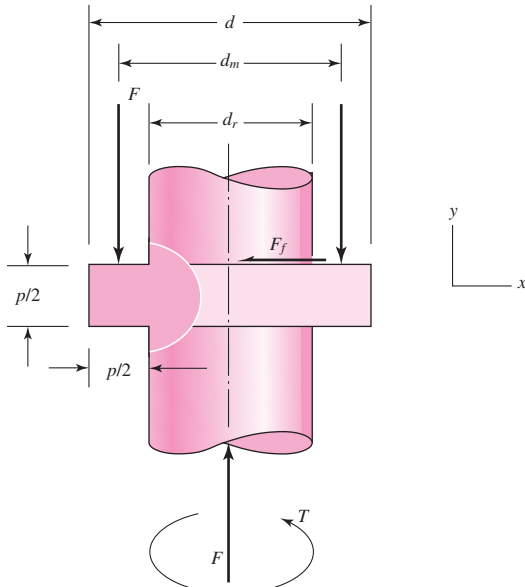
$$\sigma_b = \pm \frac{6F}{\pi d_r n_t p}$$

(b) Show that the axial and maximum torsional shear stresses in the body of the shaft can be approximated by

$$\sigma_a = -\frac{4F}{\pi d_r^2} \quad \text{and} \quad \tau_t = \frac{16T}{\pi d_r^3}$$

(c) For the stresses of parts (a) and (b) show a three-dimensional representation of the state of stress on an element located at the intersection of the lower thread root base and the

Problem 3-90



thread body. Using the given coordinate system label the stresses using the notation given in Fig. 3–8a.

- (d) A square-thread power screw has an outside diameter $d = 1.5$ in, pitch $p = 0.25$ in, and transmits a load $F = 1\,500$ lbf through the application of a torque $T = 235$ lbf · in. If $n_t = 2$, determine the key stresses and the corresponding *principal stresses* (normal and shear).

3–91 Develop the formulas for the maximum radial and tangential stresses in a thick-walled cylinder due to internal pressure only.

3–92 Repeat Prob. 3–91 where the cylinder is subject to external pressure only. At what radii do the maximum stresses occur?

3–93 Develop the equations for the principal stresses in a thin-walled spherical pressure vessel of inside diameter d_i , thickness t , and with an internal pressure p_i . You may wish to follow a process similar to that used for a thin-walled cylindrical pressure vessel on p. 114.

**3–94 to
3–96** A pressure cylinder has an outer diameter d_o , wall thickness t , internal pressure p_i , and maximum allowable shear stress τ_{\max} . In the table given, determine the appropriate value of x .

Problem Number	d_o	t	p_i	τ_{\max}
3–94	6 in	0.25 in	x_{\max}	10 ksi
3–95	200 mm	x_{\min}	4 MPa	25 MPa
3–96	8 in	0.25 in	500 psi	x

**3–97 to
3–99** A pressure cylinder has an outer diameter d_o , wall thickness t , external pressure p_o , and maximum allowable shear stress τ_{\max} . In the table given, determine the appropriate value of x .

Problem Number	d_o	t	p_o	τ_{\max}
3–97	6 in	0.25 in	x_{\max}	10 ksi
3–98	200 mm	x_{\min}	4 MPa	25 MPa
3–99	8 in	0.25 in	500 psi	x

3–100 An AISI 1040 cold-drawn steel tube has an OD = 50 mm and wall thickness 6 mm. What maximum external pressure can this tube withstand if the largest principal normal stress is not to exceed 80 percent of the minimum yield strength of the material?

3–101 Repeat Prob. 3–100 with an OD of 2 in and wall thickness of 0.25 in.

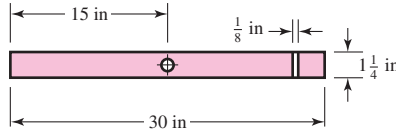
3–102 Repeat Prob. 3–100 with an internal pressure.

3–103 Repeat Prob. 3–101 with an internal pressure.

3–104 A thin-walled cylindrical steel water storage tank 30 ft in diameter and 60 ft long is oriented with its longitudinal axis vertical. The tank is topped with a hemispherical steel dome. The wall thickness of the tank and dome is 0.75 in. If the tank is unpressurized and contains water 55 ft above its base, and considering the weight of the tank, determine the maximum state of stress in the tank and the corresponding principal stresses (normal and shear). The weight density of water is 62.4 lbf/ft³.

- 3-105** Repeat Prob. 3-104 with the tank being pressurized to 50 psig.
- 3-106** Find the maximum shear stress in a $5\frac{1}{2}$ -in-diameter circular saw blade if it runs idle at 5000 rev/min. The saw is 14 gauge (0.0747 in) steel and is used on a $\frac{5}{8}$ -in-diameter arbor. The thickness is uniform. What is the maximum radial component of stress?
- 3-107** The maximum recommended speed for a 250-mm-diameter abrasive grinding wheel is 2000 rev/min. Assume that the material is isotropic; use a bore of 20 mm, $v = 0.24$, and a mass density of 3320 kg/m^3 , and find the maximum tensile stress at this speed.
- 3-108** An abrasive cutoff wheel has a diameter of 5 in, is $\frac{1}{16}$ in thick, and has a $\frac{3}{4}$ -in bore. It weighs 5 oz and is designed to run at 12 000 rev/min. If the material is isotropic and $v = 0.20$, find the maximum shear stress at the design speed.
- 3-109** A rotary lawnmower blade rotates at 3500 rev/min. The steel blade has a uniform cross section $\frac{1}{8}$ in thick by $1\frac{1}{4}$ in wide, and has a $\frac{1}{2}$ -in-diameter hole in the center as shown in the figure. Estimate the nominal tensile stress at the central section due to rotation.

Problem 3-109

**3-110 to
3-115**

The table lists the maximum and minimum hole and shaft dimensions for a variety of standard press and shrink fits. The materials are both hot-rolled steel. Find the maximum and minimum values of the radial interference and the corresponding interface pressure. Use a collar diameter of 100 mm for the metric sizes and 4 in for those in inch units.

Problem Number	Fit Designation [†]	Basic Size	Hole	Shaft		
			D_{\max}	D_{\min}	d_{\max}	d_{\min}
3-110	50H7/p6	50 mm	50.025	50.000	50.042	50.026
3-111	(2 in)H7/p6	2 in	2.0010	2.0000	2.0016	2.0010
3-112	50H7/s6	50 mm	50.025	50.000	50.059	50.043
3-113	(2 in)H7/s6	2 in	2.0010	2.0000	2.0023	2.0017
3-114	50H7/u6	50 mm	50.025	50.000	50.086	50.070
3-115	(2 in)H7/u6	2 in	2.0010	2.0000	2.0034	2.0028

[†]Note: See Table 7-9 for description of fits.

**3-116 to
3-119**

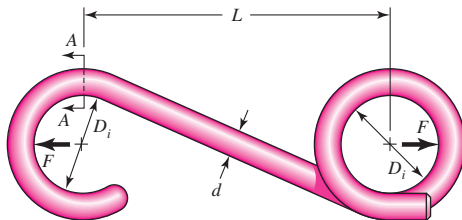
The table gives data concerning the shrink fit of two cylinders of differing materials and dimensional specification in inches. Elastic constants for different materials may be found in Table A-5. Identify the radial interference δ , then find the interference pressure p , and the tangential normal stress on both sides of the fit surface. If dimensional tolerances are given at fit surfaces, repeat the problem for the highest and lowest stress levels.

Problem Number	Inner Cylinder			Outer Cylinder		
	Material	d_i	d_o	Material	D_i	D_o
3-116	Steel	0	2.002	Steel	2.000	3.00
3-117	Steel	0	2.002	Cast iron	2.000	3.00
3-118	Steel	0	1.002/1.003	Steel	1.001/1.002	2.00
3-119	Aluminum	0	2.003/2.006	Steel	2.000/2.002	3.00

3-120

A utility hook was formed from a round rod of diameter $d = 20$ mm into the geometry shown in the figure. What are the stresses at the inner and outer surfaces at section A–A if $F = 4$ kN, $L = 250$ mm, and $D_i = 75$ mm?

Problem 3-120

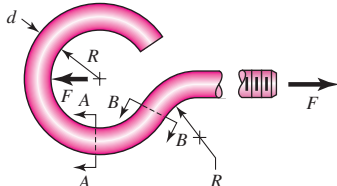
**3-121**

Repeat Prob. 3-120 with $d = 0.75$ in, $F = 750$ lbf, $L = 10$ in, and $D_i = 2.5$ in.

3-122

The steel eyebolt shown in the figure is loaded with a force $F = 300$ N. The bolt is formed from wire of diameter $d = 6$ mm to a radius $R = 10$ mm in the eye and at the shank. Estimate the stresses at the inner and outer surfaces at section A–A.

Problem 3-122

**3-123**

For Prob. 3-122 estimate the stresses at the inner and outer surfaces at section B–B.

3-124

Repeat Prob. 3-122 with $d = \frac{1}{4}$ in, $R = \frac{1}{2}$ in, and $F = 75$ lbf.

3-125

Repeat Prob. 3-123 with $d = \frac{1}{4}$ in, $R = \frac{1}{2}$ in, and $F = 75$ lbf.

3-126

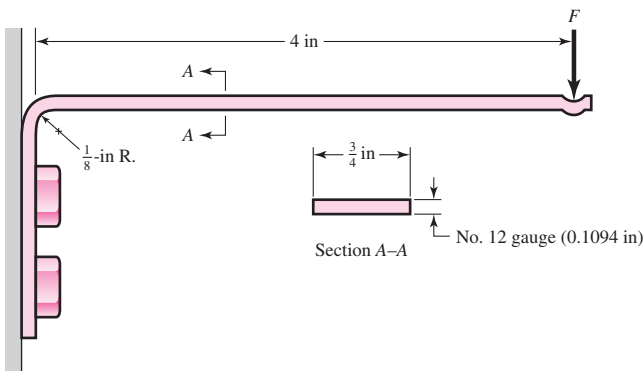
Shown in the figure is a 12-gauge (0.1094-in) by $\frac{3}{4}$ -in latching spring that supports a load of $F = 3$ lbf. The inside radius of the bend is $\frac{1}{8}$ in.

(a) Using straight-beam theory, determine the stresses at the top and bottom surfaces immediately to the right of the bend.

(b) Using curved-beam theory, determine the stresses at the inner and outer surfaces at the bend.

(c) By comparing the stresses at the bend with the nominal stresses before the bend, estimate effective stress concentration factors for the inner and outer surfaces.

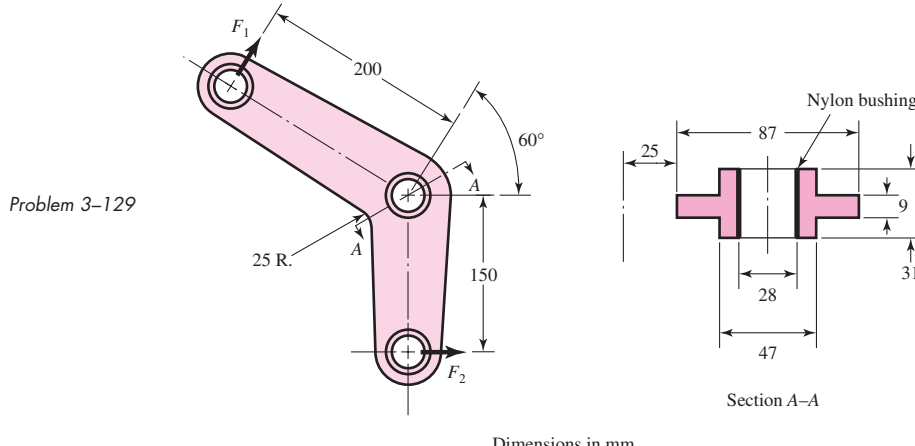
Problem 3-126

**3-127**

Repeat Prob. 3-126 with a 10-gauge (0.1406-in) material thickness.

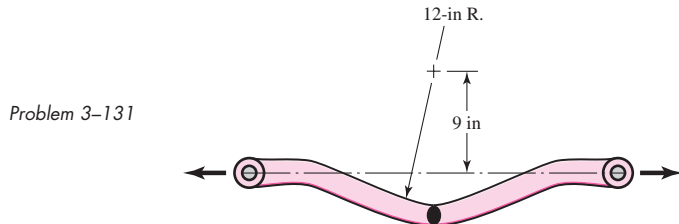
3-128 Repeat Prob. 3-126 with a bend radius of $\frac{1}{4}$ in.

3-129 The cast-iron bell-crank lever depicted in the figure is acted upon by forces F_1 of 2.4 kN and F_2 of 3.2 kN. The section A-A at the central pivot has a curved inner surface with a radius of $r_i = 25$ mm. Estimate the stresses at the inner and outer surfaces of the curved portion of the lever.

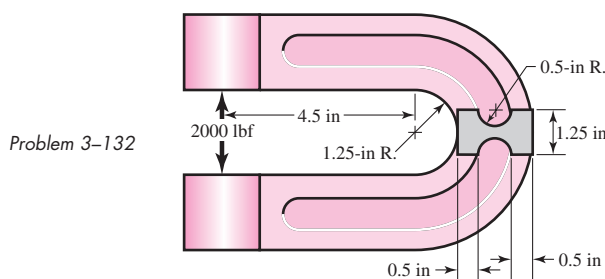


3-130 The crane hook depicted in Fig. 3-35 has a $\frac{3}{4}$ -in-diameter hole in the center of the critical section. For a load of 6 kip, estimate the bending stresses at the inner and outer surfaces at the critical section.

3-131 An offset tensile link is shaped to clear an obstruction with a geometry as shown in the figure. The cross section at the critical location is elliptical, with a major axis of 3 in and a minor axis of 1.5 in. For a load of 20 kip, estimate the stresses at the inner and outer surfaces of the critical section.



3-132 A cast-steel C frame as shown in the figure has a rectangular cross section of 1.25 in by 2 in, with a 0.5-in-radius semicircular notch on both sides that forms midflank fluting as shown. Estimate A , r_c , r_n , and e , and for a load of 2000 lbf, estimate the inner and outer surface stresses at the throat C. Note: Table 3-4 can be used to determine r_n for this section. From the table, the integral $\int dA/r$ can be evaluated for a rectangle and a circle by evaluating A/r_n for each shape [see Eq. (3-64)]. Subtracting A/r_n of the circle from that of the rectangle yields $\int dA/r$ for the C frame, and r_n can then be evaluated.



3-133

Two carbon steel balls, each 30 mm in diameter, are pressed together by a force F . In terms of the force F , find the maximum values of the principal stress, and the maximum shear stress, in MPa.

3-134

A carbon steel ball with 25-mm diameter is pressed together with an aluminum ball with a 40-mm diameter by a force of 10 N. Determine the maximum shear stress, and the depth at which it will occur for the aluminum ball. Assume Fig. 3-37, which is based on a typical Poisson's ratio of 0.3, is applicable to estimate the depth at which the maximum shear stress occurs for these materials.

3-135

Repeat Prob. 3-134 but determine the maximum shear stress and depth for the steel ball.

3-136

A carbon steel ball with a 30-mm diameter is pressed against a flat carbon steel plate with a force of 20 N. Determine the maximum shear stress, and the depth in the plate at which it will occur.

3-137

An AISI 1018 steel ball with 1-in diameter is used as a roller between a flat plate made from 2024 T3 aluminum and a flat table surface made from ASTM No. 30 gray cast iron. Determine the maximum amount of weight that can be stacked on the aluminum plate without exceeding a maximum shear stress of 20 kpsi in any of the three pieces. Assume Fig. 3-37, which is based on a typical Poisson's ratio of 0.3, is applicable to estimate the depth at which the maximum shear stress occurs for these materials.

3-138

An aluminum alloy cylindrical roller with diameter 1.25 in and length 2 in rolls on the inside of a cast-iron ring having an inside radius of 6 in, which is 2 in thick. Find the maximum contact force F that can be used if the shear stress is not to exceed 4000 psi.

3-139

A pair of mating steel spur gears with a 0.75-in face width transmits a load of 40 lbf. For estimating the contact stresses, make the simplifying assumption that the teeth profiles can be treated as cylindrical with instantaneous radii at the contact point of interest of 0.47 in and 0.62 in, respectively. Estimate the maximum contact pressure and the maximum shear stress experienced by either gear.

3-140 to**3-142**

A wheel of diameter d and width w carrying a load F rolls on a flat rail.

Assume that Fig. 3-39, which is based on a Poisson's ratio of 0.3, is applicable to estimate the depth at which the maximum shear stress occurs for these materials. At this critical depth, calculate the Hertzian stresses σ_x , σ_y , σ_z , and τ_{\max} for the wheel.

Problem Number	d	w	F	Wheel Material	Rail Material
3-140	5 in	2 in	600 lbf	Steel	Steel
3-141	150 mm	40 mm	2 kN	Steel	Cast iron
3-142	3 in	1.25 mm	250 lbf	Cast iron	Cast iron

4

Deflection and Stiffness

Chapter Outline

4-1	Spring Rates	148
4-2	Tension, Compression, and Torsion	149
4-3	Deflection Due to Bending	150
4-4	Beam Deflection Methods	152
4-5	Beam Deflections by Superposition	153
4-6	Beam Deflections by Singularity Functions	156
4-7	Strain Energy	162
4-8	Castigliano's Theorem	164
4-9	Deflection of Curved Members	169
4-10	Statically Indeterminate Problems	175
4-11	Compression Members—General	181
4-12	Long Columns with Central Loading	181
4-13	Intermediate-Length Columns with Central Loading	184
4-14	Columns with Eccentric Loading	184
4-15	Struts or Short Compression Members	188
4-16	Elastic Stability	190
4-17	Shock and Impact	191

All real bodies deform under load, either elastically or plastically. A body can be sufficiently insensitive to deformation that a presumption of rigidity does not affect an analysis enough to warrant a nonrigid treatment. If the body deformation later proves to be not negligible, then declaring rigidity was a poor decision, not a poor assumption. A wire rope is flexible, but in tension it can be robustly rigid and it distorts enormously under attempts at compressive loading. The same body can be both rigid and nonrigid.

Deflection analysis enters into design situations in many ways. A snap ring, or retaining ring, must be flexible enough to be bent without permanent deformation and assembled with other parts, and then it must be rigid enough to hold the assembled parts together. In a transmission, the gears must be supported by a rigid shaft. If the shaft bends too much, that is, if it is too flexible, the teeth will not mesh properly, and the result will be excessive impact, noise, wear, and early failure. In rolling sheet or strip steel to prescribed thicknesses, the rolls must be crowned, that is, curved, so that the finished product will be of uniform thickness. Thus, to design the rolls it is necessary to know exactly how much they will bend when a sheet of steel is rolled between them. Sometimes mechanical elements must be designed to have a particular force-deflection characteristic. The suspension system of an automobile, for example, must be designed within a very narrow range to achieve an optimum vibration frequency for all conditions of vehicle loading, because the human body is comfortable only within a limited range of frequencies.

The size of a load-bearing component is often determined on deflections, rather than limits on stress.

This chapter considers distortion of single bodies due to geometry (shape) and loading, then, briefly, the behavior of groups of bodies.

4-1 Spring Rates

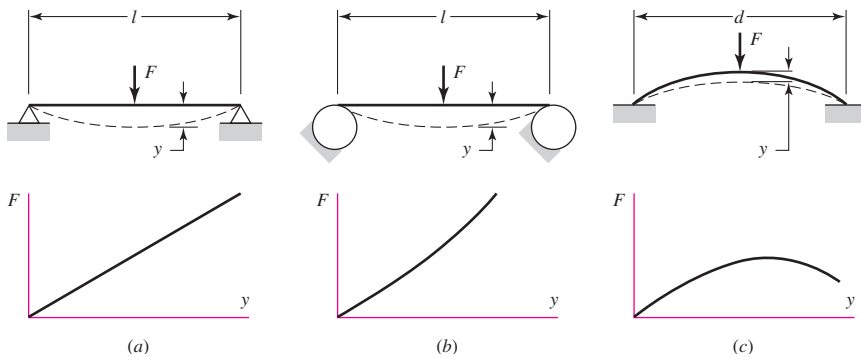
Elasticity is that property of a material that enables it to regain its original configuration after having been deformed. A *spring* is a mechanical element that exerts a force when deformed. Figure 4-1a shows a straight beam of length l simply supported at the ends and loaded by the transverse force F . The deflection y is linearly related to the force, as long as the elastic limit of the material is not exceeded, as indicated by the graph. This beam can be described as a *linear spring*.

In Fig. 4-1b a straight beam is supported on two cylinders such that the length between supports decreases as the beam is deflected by the force F . A larger force is required to deflect a short beam than a long one, and hence the more this beam is deflected, the stiffer it becomes. Also, the force is not linearly related to the deflection, and hence this beam can be described as a *nonlinear stiffening spring*.

Figure 4-1c is an edge-view of a dish-shaped round disk. The force necessary to flatten the disk increases at first and then decreases as the disk approaches a flat configuration,

Figure 4-1

- (a) A linear spring;
- (b) a stiffening spring;
- (c) a softening spring.



as shown by the graph. Any mechanical element having such a characteristic is called a *nonlinear softening spring*.

If we designate the general relationship between force and deflection by the equation

$$F = F(y) \quad (a)$$

then *spring rate* is defined as

$$k(y) = \lim_{\Delta y \rightarrow 0} \frac{\Delta F}{\Delta y} = \frac{dF}{dy} \quad (4-1)$$

where y must be measured in the direction of F and at the point of application of F . Most of the force-deflection problems encountered in this book are linear, as in Fig. 4-1a. For these, k is a constant, also called the *spring constant*; consequently Eq. (4-1) is written

$$k = \frac{F}{y} \quad (4-2)$$

We might note that Eqs. (4-1) and (4-2) are quite general and apply equally well for torques and moments, provided angular measurements are used for y . For linear displacements, the units of k are often pounds per inch or newtons per meter, and for angular displacements, pound-inches per radian or newton-meters per radian.

4-2 Tension, Compression, and Torsion

The total extension or contraction of a uniform bar in pure tension or compression, respectively, is given by

$$\delta = \frac{Fl}{AE} \quad (4-3)$$

This equation does not apply to a *long* bar loaded in compression if there is a possibility of buckling (see Secs. 4-11 to 4-15). Using Eqs. (4-2) and (4-3) with $\delta = y$, we see that the spring constant of an axially loaded bar is

$$k = \frac{AE}{l} \quad (4-4)$$

The angular deflection of a uniform solid or hollow round bar subjected to a twisting moment T was given in Eq. (3-35), and is

$$\theta = \frac{Tl}{GJ} \quad (4-5)$$

where θ is in radians. If we multiply Eq. (4-5) by $180/\pi$ and substitute $J = \pi d^4/32$ for a solid round bar, we obtain

$$\theta = \frac{583.6Tl}{Gd^4} \quad (4-6)$$

where θ is in degrees.

Equation (4-5) can be rearranged to give the torsional spring rate as

$$k = \frac{T}{\theta} = \frac{GJ}{l} \quad (4-7)$$

Equations (4-5), (4-6), and (4-7) apply *only* to circular cross sections. Torsional loading for bars with noncircular cross sections is discussed in Sec. 3-12 (p. 101). For the angular twist of rectangular cross sections, closed thin-walled tubes, and open thin-walled sections, refer to Eqs. (3-41), (3-46), and (3-47), respectively.

4-3 Deflection Due to Bending

The problem of bending of beams probably occurs more often than any other loading problem in mechanical design. Shafts, axles, cranks, levers, springs, brackets, and wheels, as well as many other elements, must often be treated as beams in the design and analysis of mechanical structures and systems. The subject of bending, however, is one that you should have studied as preparation for reading this book. It is for this reason that we include here only a brief review to establish the nomenclature and conventions to be used throughout this book.

The curvature of a beam subjected to a bending moment M is given by

$$\frac{1}{\rho} = \frac{M}{EI} \quad (4-8)$$

where ρ is the radius of curvature. From studies in mathematics we also learn that the curvature of a plane curve is given by the equation

$$\frac{1}{\rho} = \frac{d^2y/dx^2}{[1 + (dy/dx)^2]^{3/2}} \quad (4-9)$$

where the interpretation here is that y is the lateral deflection of the centroidal axis of the beam at any point x along its length. The slope of the beam at any point x is

$$\theta = \frac{dy}{dx} \quad (a)$$

For many problems in bending, the slope is very small, and for these the denominator of Eq. (4-9) can be taken as unity. Equation (4-8) can then be written

$$\frac{M}{EI} = \frac{d^2y}{dx^2} \quad (b)$$

Noting Eqs. (3-3) and (3-4) and successively differentiating Eq. (b) yields

$$\frac{V}{EI} = \frac{d^3y}{dx^3} \quad (c)$$

$$\frac{q}{EI} = \frac{d^4y}{dx^4} \quad (d)$$

It is convenient to display these relations in a group as follows:

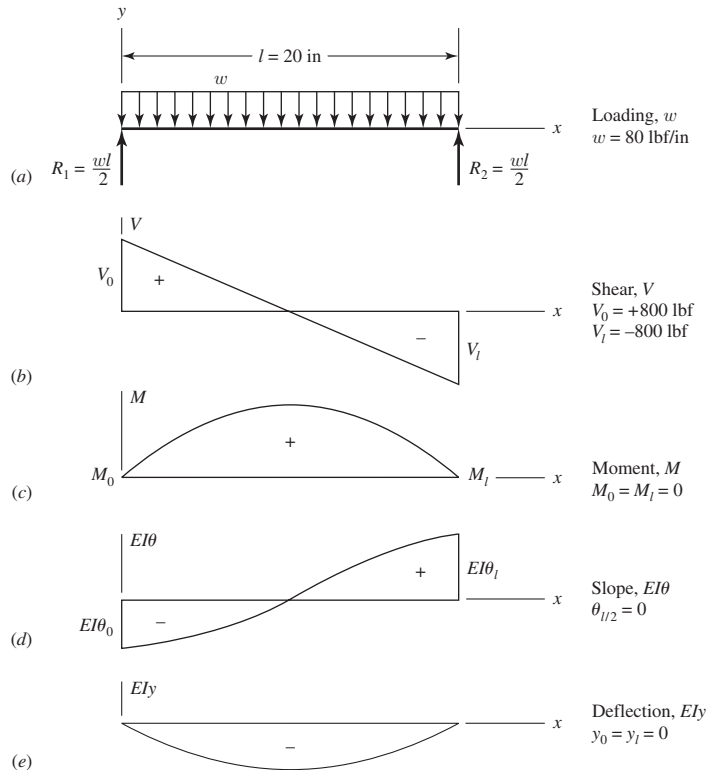
$$\frac{q}{EI} = \frac{d^4y}{dx^4} \quad (4-10)$$

$$\frac{V}{EI} = \frac{d^3y}{dx^3} \quad (4-11)$$

$$\frac{M}{EI} = \frac{d^2y}{dx^2} \quad (4-12)$$

$$\theta = \frac{dy}{dx} \quad (4-13)$$

$$y = f(x) \quad (4-14)$$

| Figure 4–2

The nomenclature and conventions are illustrated by the beam of Fig. 4–2. Here, a beam of length $l = 20$ in is loaded by the uniform load $w = 80$ lbf per inch of beam length. The x axis is positive to the right, and the y axis positive upward. All quantities—loading, shear, moment, slope, and deflection—have the same sense as y ; they are positive if upward, negative if downward.

The reactions $R_1 = R_2 = +800$ lbf and the shear forces $V_0 = +800$ lbf and $V_l = -800$ lbf are easily computed by using the methods of Chap. 3. The bending moment is zero at each end because the beam is simply supported. For a simply-supported beam, the deflections are also zero at each end.

EXAMPLE 4–1 For the beam in Fig. 4–2, the bending moment equation, for $0 \leq x \leq l$, is

$$M = \frac{wl}{2}x - \frac{w}{2}x^2$$

Using Eq. (4–12), determine the equations for the slope and deflection of the beam, the slopes at the ends, and the maximum deflection.

Solution Integrating Eq. (4–12) as an indefinite integral we have

$$EI \frac{dy}{dx} = \int M dx = \frac{wl}{4}x^2 - \frac{w}{6}x^3 + C_1 \quad (1)$$

where C_1 is a constant of integration that is evaluated from geometric boundary conditions. We could impose that the slope is zero at the midspan of the beam, since the beam and

loading are symmetric relative to the midspan. However, we will use the given boundary conditions of the problem and verify that the slope is zero at the midspan. Integrating Eq. (1) gives

$$EIy = \iint M dx = \frac{wl}{12}x^3 - \frac{w}{24}x^4 + C_1x + C_2 \quad (2)$$

The boundary conditions for the simply supported beam are $y = 0$ at $x = 0$ and l . Applying the first condition, $y = 0$ at $x = 0$, to Eq. (2) results in $C_2 = 0$. Applying the second condition to Eq. (2) with $C_2 = 0$,

$$EIy(l) = \frac{wl}{12}l^3 - \frac{w}{24}l^4 + C_1l = 0$$

Solving for C_1 yields $C_1 = -wl^3/24$. Substituting the constants back into Eqs. (1) and (2) and solving for the deflection and slope results in

$$y = \frac{wx}{24EI}(2lx^2 - x^3 - l^3) \quad (3)$$

$$\theta = \frac{dy}{dx} = \frac{w}{24EI}(6lx^2 - 4x^3 - l^3) \quad (4)$$

Comparing Eq. (3) with that given in Table A-9, beam 7, we see complete agreement. For the slope at the left end, substituting $x = 0$ into Eq. (4) yields

$$\theta|_{x=0} = -\frac{wl^3}{24EI}$$

and at $x = l$,

$$\theta|_{x=l} = \frac{wl^3}{24EI}$$

At the midspan, substituting $x = l/2$ gives $dy/dx = 0$, as earlier suspected.

The maximum deflection occurs where $dy/dx = 0$. Substituting $x = l/2$ into Eq. (3) yields

$$y_{\max} = -\frac{5wl^4}{384EI}$$

which again agrees with Table A-9-7.

The approach used in the example is fine for simple beams with continuous loading. However, for beams with discontinuous loading and/or geometry such as a step shaft with multiple gears, flywheels, pulleys, etc., the approach becomes unwieldy. The following section discusses bending deflections in general and the techniques that are provided in this chapter.

4-4 Beam Deflection Methods

Equations (4-10) through (4-14) are the basis for relating the intensity of loading q , vertical shear V , bending moment M , slope of the neutral surface θ , and the transverse deflection y . Beams have intensities of loading that range from $q = \text{constant}$

(uniform loading), variable intensity $q(x)$, to Dirac delta functions (concentrated loads).

The intensity of loading usually consists of piecewise contiguous zones, the expressions for which are integrated through Eqs. (4–10) to (4–14) with varying degrees of difficulty. Another approach is to represent the deflection $y(x)$ as a Fourier series, which is capable of representing single-valued functions with a finite number of finite discontinuities, then differentiating through Eqs. (4–14) to (4–10), and stopping at some level where the Fourier coefficients can be evaluated. A complication is the piecewise continuous nature of some beams (shafts) that are stepped-diameter bodies.

All of the above constitute, in one form or another, formal integration methods, which, with properly selected problems, result in solutions for q , V , M , θ , and y . These solutions may be

- 1 Closed-form, or
- 2 Represented by infinite series, which amount to closed form if the series are rapidly convergent, or
- 3 Approximations obtained by evaluating the first or the first and second terms.

The series solutions can be made equivalent to the closed-form solution by the use of a computer. Roark's¹ formulas are committed to commercial software and can be used on a personal computer.

There are many techniques employed to solve the integration problem for beam deflection. Some of the popular methods include:

- Superposition (see Sec. 4–5)
- The moment-area method²
- Singularity functions (see Sec. 4–6)
- Numerical integration³

The two methods described in this chapter are easy to implement and can handle a large array of problems.

There are methods that do not deal with Eqs. (4–10) to (4–14) directly. An energy method, based on Castigliano's theorem, is quite powerful for problems not suitable for the methods mentioned earlier and is discussed in Secs. 4–7 to 4–10. Finite element programs are also quite useful for determining beam deflections.

4–5 Beam Deflections by Superposition

The results of many simple load cases and boundary conditions have been solved and are available. Table A–9 provides a limited number of cases. Roark's⁴ provides a much more comprehensive listing. *Superposition* resolves the effect of combined loading on a structure by determining the effects of each load separately and adding

¹Warren C. Young and Richard G. Budynas, *Roark's Formulas for Stress and Strain*, 7th ed., McGraw-Hill, New York, 2002.

²See Chap. 9, F. P. Beer, E. R. Johnston Jr., and J. T. DeWolf, *Mechanics of Materials*, 5th ed., McGraw-Hill, New York, 2009.

³See Sec. 4–4, J. E. Shigley and C. R. Mischke, *Mechanical Engineering Design*, 6th ed., McGraw-Hill, New York, 2001.

⁴Warren C. Young and Richard G. Budynas, *Roark's Formulas for Stress and Strain*, 7th ed., McGraw-Hill, New York, 2002.

the results algebraically. Superposition may be applied provided: (1) each effect is linearly related to the load that produces it, (2) a load does not create a condition that affects the result of another load, and (3) the deformations resulting from any specific load are not large enough to appreciably alter the geometric relations of the parts of the structural system.

The following examples are illustrations of the use of superposition.

EXAMPLE 4-2

Consider the uniformly loaded beam with a concentrated force as shown in Fig. 4-3. Using superposition, determine the reactions and the deflection as a function of x .

Solution

Considering each load state separately, we can superpose beams 6 and 7 of Table A-9. For the reactions we find

Answer

$$R_1 = \frac{Fb}{l} + \frac{wl}{2}$$

Answer

$$R_2 = \frac{Fa}{l} + \frac{wl}{2}$$

The loading of beam 6 is discontinuous and separate deflection equations are given for regions AB and BC . Beam 7 loading is not discontinuous so there is only one equation. Superposition yields

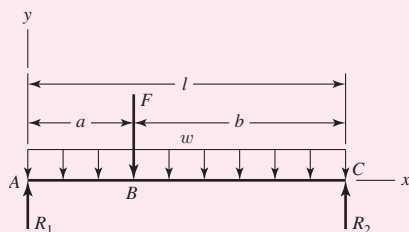
Answer

$$y_{AB} = \frac{Fbx}{6EIl}(x^2 + b^2 - l^2) + \frac{wx}{24EI}(2lx^2 - x^3 - l^3)$$

Answer

$$y_{BC} = \frac{Fa(l-x)}{6EIl}(x^2 + a^2 - 2lx) + \frac{wx}{24EI}(2lx^2 - x^3 - l^3)$$

| Figure 4-3



If the maximum deflection of a beam is desired, it will occur either where the slope is zero or at the end of the overhang if the beam has a free end. In the previous example, there is no overhang, so setting $dy/dx = 0$ will yield the equation for x that locates where the maximum deflection occurs. In the example there are two equations for y where only one will yield a solution. If $a = l/2$, the maximum deflection would obviously occur at $x = l/2$ because of symmetry. However, if $a < l/2$, where would the maximum deflection occur? It can be shown that as F moves toward the left support, the maximum deflection moves toward the left support also, but not as much as F (see Prob. 4-34). Thus, we would set $dy_{BC}/dx = 0$ and solve for x . If $a > l/2$, then we would set $dy_{AB}/dx = 0$. For more complicated problems, plotting the equations using numerical data is the simplest approach to finding the maximum deflection.

Sometimes it may not be obvious that we can use superposition with the tables at hand, as demonstrated in the next example.

EXAMPLE 4-3

Consider the beam in Fig. 4-4a and determine the deflection equations using superposition.

Solution

For region *AB* we can superpose beams 7 and 10 of Table A-9 to obtain

Answer

$$y_{AB} = \frac{wx}{24EI} (2lx^2 - x^3 - l^3) + \frac{Fax}{6EI} (l^2 - x^2)$$

For region *BC*, how do we represent the uniform load? Considering the uniform load *only*, the beam deflects as shown in Fig. 4-4b. Region *BC* is straight since there is no bending moment due to *w*. The slope of the beam at *B* is θ_B and is obtained by taking the derivative of *y* given in the table with respect to *x* and setting *x* = *l*. Thus,

$$\frac{dy}{dx} = \frac{d}{dx} \left[\frac{wx}{24EI} (2lx^2 - x^3 - l^3) \right] = \frac{w}{24EI} (6lx^2 - 4x^3 - l^3)$$

Substituting *x* = *l* gives

$$\theta_B = \frac{w}{24EI} (6l^2 - 4l^3 - l^3) = \frac{wl^3}{24EI}$$

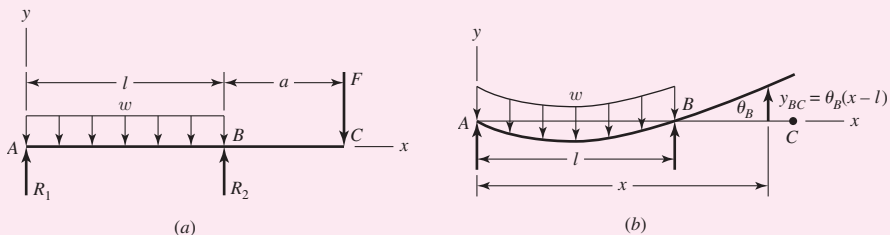
The deflection in region *BC* due to *w* is $\theta_B(x - l)$, and adding this to the deflection due to *F*, in *BC*, yields

Answer

$$y_{BC} = \frac{wl^3}{24EI} (x - l) + \frac{F(x - l)}{6EI} [(x - l)^2 - a(3x - l)]$$

Figure 4-4

(a) Beam with uniformly distributed load and overhang force; (b) deflections due to uniform load only.



EXAMPLE 4-4

Figure 4-5a shows a cantilever beam with an end load. Normally we model this problem by considering the left support as rigid. After testing the rigidity of the wall it was found that the translational stiffness of the wall was k_t force per unit vertical deflection, and the rotational stiffness was k_r moment per unit angular (radian) deflection (see Fig. 4-5b). Determine the deflection equation for the beam under the load *F*.

Solution

Here we will superpose the *modes* of deflection. They are: (1) translation due to the compression of spring k_t , (2) rotation of the spring k_r , and (3) the elastic deformation of beam 1 given in Table A-9. The force in spring k_t is $R_1 = F$, giving a deflection from Eq. (4-2) of

$$y_1 = -\frac{F}{k_t} \quad (1)$$

The moment in spring k_r is $M_1 = Fl$. This gives a clockwise rotation of $\theta = Fl/k_r$. Considering this mode of deflection only, the beam rotates rigidly clockwise, leading to a deflection equation of

$$y_2 = -\frac{Fl}{k_r}x \quad (2)$$

Finally, the elastic deformation of beam 1 from Table A-9 is

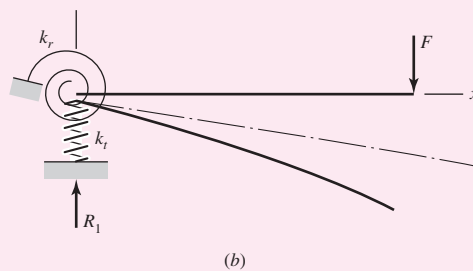
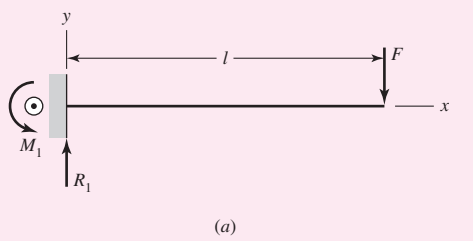
$$y_3 = \frac{Fx^2}{6EI}(x - 3l) \quad (3)$$

Adding the deflections from each mode yields

Answer

$$y = \frac{Fx^2}{6EI}(x - 3l) - \frac{F}{k_t} - \frac{Fl}{k_r}x$$

| **Figure 4-5**



4-6

Beam Deflections by Singularity Functions

Introduced in Sec. 3-3, singularity functions are excellent for managing discontinuities, and their application to beam deflection is a simple extension of what was presented in the earlier section. They are easy to program, and as will be seen later, they can greatly simplify the solution of statically indeterminate problems. The following examples illustrate the use of singularity functions to evaluate deflections of statically determinate beam problems.

EXAMPLE 4-5

Consider beam 6 of Table A-9, which is a simply supported beam having a concentrated load F not in the center. Develop the deflection equations using singularity functions.

Solution

First, write the load intensity equation from the free-body diagram,

$$q = R_1 \langle x \rangle^{-1} - F \langle x - a \rangle^{-1} + R_2 \langle x - l \rangle^{-1} \quad (1)$$

Integrating Eq. (1) twice results in

$$V = R_1 \langle x \rangle^0 - F \langle x - a \rangle^0 + R_2 \langle x - l \rangle^0 \quad (2)$$

$$M = R_1 \langle x \rangle^1 - F \langle x - a \rangle^1 + R_2 \langle x - l \rangle^1 \quad (3)$$

Recall that as long as the q equation is complete, integration constants are unnecessary for V and M ; therefore, they are not included up to this point. From statics, setting $V = M = 0$ for x slightly greater than l yields $R_1 = Fb/l$ and $R_2 = Fa/l$. Thus Eq. (3) becomes

$$M = \frac{Fb}{l} \langle x \rangle^1 - F \langle x - a \rangle^1 + \frac{Fa}{l} \langle x - l \rangle^1$$

Integrating Eqs. (4-12) and (4-13) as indefinite integrals gives

$$EI \frac{dy}{dx} = \frac{Fb}{2l} \langle x \rangle^2 - \frac{F}{2} \langle x - a \rangle^2 + \frac{Fa}{2l} \langle x - l \rangle^2 + C_1$$

$$EIy = \frac{Fb}{6l} \langle x \rangle^3 - \frac{F}{6} \langle x - a \rangle^3 + \frac{Fa}{6l} \langle x - l \rangle^3 + C_1x + C_2$$

Note that the first singularity term in both equations always exists, so $\langle x \rangle^2 = x^2$ and $\langle x \rangle^3 = x^3$. Also, the last singularity term in both equations does not exist until $x = l$, where it is zero, and since there is no beam for $x > l$ we can drop the last term. Thus

$$EI \frac{dy}{dx} = \frac{Fb}{2l} x^2 - \frac{F}{2} \langle x - a \rangle^2 + C_1 \quad (4)$$

$$EIy = \frac{Fb}{6l} x^3 - \frac{F}{6} \langle x - a \rangle^3 + C_1x + C_2 \quad (5)$$

The constants of integration C_1 and C_2 are evaluated by using the two boundary conditions $y = 0$ at $x = 0$ and $y = 0$ at $x = l$. The first condition, substituted into Eq. (5), gives $C_2 = 0$ (recall that $\langle 0 - a \rangle^3 = 0$). The second condition, substituted into Eq. (5), yields

$$0 = \frac{Fb}{6l} l^3 - \frac{F}{6} (l - a)^3 + C_1 l = \frac{Fbl^2}{6} - \frac{Fb^3}{6} + C_1 l$$

Solving for C_1 gives

$$C_1 = -\frac{Fb}{6l} (l^2 - b^2)$$

Finally, substituting C_1 and C_2 in Eq. (5) and simplifying produces

$$y = \frac{F}{6EIl} [bx(x^2 + b^2 - l^2) - l(x - a)^3] \quad (6)$$

Comparing Eq. (6) with the two deflection equations for beam 6 in Table A-9, we note that the use of singularity functions enables us to express the deflection equation with a single equation.

EXAMPLE 4-6

Determine the deflection equation for the simply supported beam with the load distribution shown in Fig. 4-6.

Solution

This is a good beam to add to our table for later use with superposition. The load intensity equation for the beam is

$$q = R_1\langle x \rangle^{-1} - w\langle x \rangle^0 + w\langle x - a \rangle^0 + R_2\langle x - l \rangle^{-1} \quad (1)$$

where the $w\langle x - a \rangle^0$ is necessary to “turn off” the uniform load at $x = a$.

From statics, the reactions are

$$R_1 = \frac{wa}{2l}(2l - a) \quad R_2 = \frac{wa^2}{2l} \quad (2)$$

For simplicity, we will retain the form of Eq. (1) for integration and substitute the values of the reactions in later.

Two integrations of Eq. (1) reveal

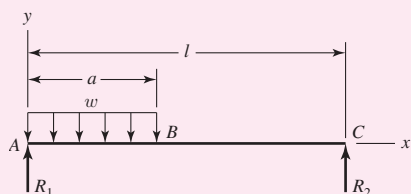
$$V = R_1\langle x \rangle^0 - w\langle x \rangle^1 + w\langle x - a \rangle^1 + R_2\langle x - l \rangle^0 \quad (3)$$

$$M = R_1\langle x \rangle^1 - \frac{w}{2}\langle x \rangle^2 + \frac{w}{2}\langle x - a \rangle^2 + R_2\langle x - l \rangle^1 \quad (4)$$

As in the previous example, singularity functions of order zero or greater starting at $x = 0$ can be replaced by normal polynomial functions. Also, once the reactions are determined, singularity functions starting at the extreme right end of the beam can be omitted. Thus, Eq. (4) can be rewritten as

$$M = R_1x - \frac{w}{2}x^2 + \frac{w}{2}\langle x - a \rangle^2 \quad (5)$$

| Figure 4-6



Integrating two more times for slope and deflection gives

$$EI \frac{dy}{dx} = \frac{R_1}{2}x^2 - \frac{w}{6}x^3 + \frac{w}{6}(x-a)^3 + C_1 \quad (6)$$

$$EIy = \frac{R_1}{6}x^3 - \frac{w}{24}x^4 + \frac{w}{24}(x-a)^4 + C_1x + C_2 \quad (7)$$

The boundary conditions are $y = 0$ at $x = 0$ and $y = 0$ at $x = l$. Substituting the first condition in Eq. (7) shows $C_2 = 0$. For the second condition

$$0 = \frac{R_1}{6}l^3 - \frac{w}{24}l^4 + \frac{w}{24}(l-a)^4 + C_1l$$

Solving for C_1 and substituting into Eq. (7) yields

$$EIy = \frac{R_1}{6}x(x^2 - l^2) - \frac{w}{24}x(x^3 - l^3) - \frac{w}{24l}x(l-a)^4 + \frac{w}{24}(x-a)^4$$

Finally, substitution of R_1 from Eq. (2) and simplifying results gives

Answer $y = \frac{w}{24EIl}[2ax(2l-a)(x^2 - l^2) - xl(x^3 - l^3) - x(l-a)^4 + l(x-a)^4]$

As stated earlier, singularity functions are relatively simple to program, as they are omitted when their arguments are negative, and the $\langle \rangle$ brackets are replaced with $()$ parentheses when the arguments are positive.

EXAMPLE 4-7

The steel step shaft shown in Fig. 4-7a is mounted in bearings at A and F . A pulley is centered at C where a total radial force of 600 lbf is applied. Using singularity functions evaluate the shaft displacements at $\frac{1}{2}$ -in increments. Assume the shaft is simply supported.

Solution

The reactions are found to be $R_1 = 360$ lbf and $R_2 = 240$ lbf. Ignoring R_2 , using singularity functions, the moment equation is

$$M = 360x - 600(x-8)^1 \quad (1)$$

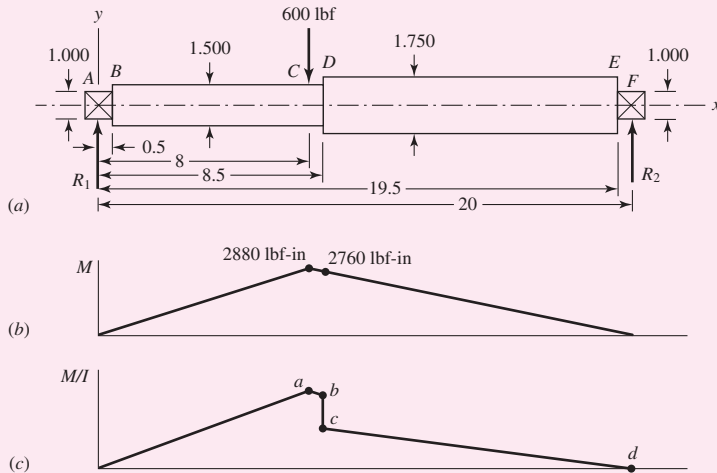
This is plotted in Fig. 4-7b.

For simplification, we will consider only the step at D . That is, we will assume section AB has the same diameter as BC and section EF has the same diameter as DE . Since these sections are short and at the supports, the size reduction will not add much to the deformation. We will examine this simplification later. The second area moments for BC and DE are

$$I_{BC} = \frac{\pi}{64}1.5^4 = 0.2485 \text{ in}^4 \quad I_{DE} = \frac{\pi}{64}1.75^4 = 0.4604 \text{ in}^4$$

Figure 4-7

Dimensions in inches.



A plot of M/I is shown in Fig. 4-7c. The values at points *b* and *c*, and the step change are

$$\left(\frac{M}{I}\right)_b = \frac{2760}{0.2485} = 11\ 106.6 \text{ lbf/in}^3 \quad \left(\frac{M}{I}\right)_c = \frac{2760}{0.4604} = 5\ 994.8 \text{ lbf/in}^3$$

$$\Delta \left(\frac{M}{I}\right) = 5\ 994.8 - 11\ 106.6 = -5\ 111.8 \text{ lbf/in}^3$$

The slopes for *ab* and *cd*, and the change are

$$m_{ab} = \frac{2760 - 2880}{0.2485(0.5)} = -965.8 \text{ lbf/in}^4 \quad m_{cd} = \frac{-5\ 994.8}{11.5} = -521.3 \text{ lbf/in}^4$$

$$\Delta m = -521.3 - (-965.8) = 444.5 \text{ lbf/in}^4$$

Dividing Eq. (1) by I_{BC} and, at $x = 8.5$ in, adding a step of $-5\ 111.8 \text{ lbf/in}^3$ and a ramp of slope 444.5 lbf/in^4 , gives

$$\frac{M}{I} = 1\ 448.7x - 2\ 414.5(x - 8)^1 - 5\ 111.8(x - 8.5)^0 + 444.5(x - 8.5)^1 \quad (2)$$

Integration gives

$$E \frac{dy}{dx} = 724.35x^2 - 1207.3(x - 8)^2 - 5\ 111.8(x - 8.5)^1 + 222.3(x - 8.5)^2 + C_1 \quad (3)$$

Integrating again yields

$$Ey = 241.5x^3 - 402.4(x - 8)^3 - 2\ 555.9(x - 8.5)^2 + 74.08(x - 8.5)^3 + C_1x + C_2 \quad (4)$$

At $x = 0$, $y = 0$. This gives $C_2 = 0$ (remember, singularity functions do not exist until the argument is positive). At $x = 20$ in, $y = 0$, and

$$0 = 241.5(20)^3 - 402.4(20 - 8)^3 - 2\ 555.9(20 - 8.5)^2 + 74.08(20 - 8.5)^3 + C_1(20)$$

Solving, gives $C_1 = -50\ 565 \text{ lbf/in}^2$. Thus, Eq. (4) becomes, with $E = 30(10)^6 \text{ psi}$,

$$\begin{aligned} y &= \frac{1}{30(10^6)} (241.5x^3 - 402.4(x-8)^3 - 2\ 555.9(x-8.5)^2 \\ &\quad + 74.08(x-8.5)^3 - 50\ 565x) \end{aligned} \quad (5)$$

When using a spreadsheet, program the following equations:

$$\begin{aligned} y &= \frac{1}{30(10^6)} (241.5x^3 - 50\ 565x) & 0 \leq x \leq 8 \text{ in} \\ y &= \frac{1}{30(10^6)} [241.5x^3 - 402.4(x-8)^3 - 50\ 565x] & 8 \leq x \leq 8.5 \text{ in} \\ y &= \frac{1}{30(10^6)} [241.5x^3 - 402.4(x-8)^3 - 2\ 555.9(x-8.5)^2 \\ &\quad + 74.08(x-8.5)^3 - 50\ 565x] & 8.5 \leq x \leq 20 \text{ in} \end{aligned}$$

The following table results.

x	y								
0	0.000000	4.5	-0.006851	9	-0.009335	13.5	-0.007001	18	-0.002377
0.5	-0.000842	5	-0.007421	9.5	-0.009238	14	-0.006571	18.5	-0.001790
1	-0.001677	5.5	-0.007931	10	-0.009096	14.5	-0.006116	19	-0.001197
1.5	-0.002501	6	-0.008374	10.5	-0.008909	15	-0.005636	19.5	-0.000600
2	-0.003307	6.5	-0.008745	11	-0.008682	15.5	-0.005134	20	0.000000
2.5	-0.004088	7	-0.009037	11.5	-0.008415	16	-0.004613		
3	-0.004839	7.5	-0.009245	12	-0.008112	16.5	-0.004075		
3.5	-0.005554	8	-0.009362	12.5	-0.007773	17	-0.003521		
4	-0.006227	8.5	-0.009385	13	-0.007403	17.5	-0.002954		

where x and y are in inches. We see that the greatest deflection is at $x = 8.5$ in, where $y = -0.009385$ in.

Substituting C_1 into Eq. (3) the slopes at the supports are found to be $\theta_A = 1.686(10^{-3})$ rad = 0.09657 deg, and $\theta_F = 1.198(10^{-3})$ rad = 0.06864 deg. You might think these to be insignificant deflections, but as you will see in Chap. 7, on shafts, they are not.

A finite-element analysis was performed for the same model and resulted in

$$y|_{x=8.5 \text{ in}} = -0.009380 \text{ in} \quad \theta_A = -0.09653^\circ \quad \theta_F = 0.06868^\circ$$

Virtually the same answer save some round-off error in the equations.

If the steps of the bearings were incorporated into the model, more equations result, but the process is the same. The solution to this model is

$$y|_{x=8.5 \text{ in}} = -0.009387 \text{ in} \quad \theta_A = -0.09763^\circ \quad \theta_F = 0.06973^\circ$$

The largest difference between the models is of the order of 1.5 percent. Thus the simplification was justified.

In Sec. 4–9, we will demonstrate the usefulness of singularity functions in solving statically indeterminate problems.

4-7 Strain Energy

The external work done on an elastic member in deforming it is transformed into *strain*, or *potential energy*. If the member is deformed a distance y , and if the force-deflection relationship is linear, this energy is equal to the product of the average force and the deflection, or

$$U = \frac{F}{2}y = \frac{F^2}{2k} \quad (4-15)$$

This equation is general in the sense that the force F can also mean torque, or moment, provided, of course, that consistent units are used for k . By substituting appropriate expressions for k , strain-energy formulas for various simple loadings may be obtained. For tension and compression, for example, we employ Eq. (4-4) and obtain

$$\text{or } U = \frac{F^2 l}{2AE} \quad (4-16)$$

tension and compression

$$U = \int \frac{F^2}{2AE} dx \quad (4-17)$$

where the first equation applies when all the terms are constant throughout the length, and the more general integral equation allows for any of the terms to vary through the length.

Similarly, from Eq. (4-7), the strain energy for torsion is given by

$$\text{or } U = \frac{T^2 l}{2GJ} \quad (4-18)$$

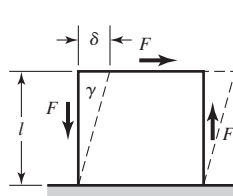
$$U = \int \frac{T^2}{2GJ} dx \quad (4-19)$$

To obtain an expression for the strain energy due to direct shear, consider the element with one side fixed in Fig. 4-8a. The force F places the element in pure shear, and the work done is $U = F\delta/2$. Since the shear strain is $\gamma = \delta/l = \tau/G = F/AG$, we have

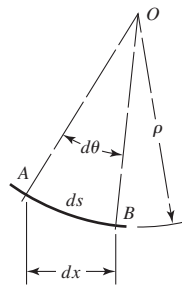
$$\text{or } U = \frac{F^2 l}{2AG} \quad (4-20)$$

$$U = \int \frac{F^2}{2AG} dx \quad (4-21)$$

| **Figure 4-8**



(a) Pure shear element



(b) Beam bending element

The strain energy stored in a beam or lever by bending may be obtained by referring to Fig. 4–8b. Here AB is a section of the elastic curve of length ds having a radius of curvature ρ . The strain energy stored in this element of the beam is $dU = (M/2)d\theta$. Since $\rho d\theta = ds$, we have

$$dU = \frac{M ds}{2\rho} \quad (a)$$

We can eliminate ρ by using Eq. (4–8), $\rho = EI/M$. Thus

$$dU = \frac{M^2 ds}{2EI} \quad (b)$$

For small deflections, $ds \doteq dx$. Then, for the entire beam

$$U = \int dU = \int \frac{M^2}{2EI} dx \quad (c)$$

The integral equation is commonly needed for bending, where the moment is typically a function of x . Summarized to include both the integral and nonintegral form, the strain energy for bending is

$$U = \frac{M^2 l}{2EI} \quad (4-22)$$

or

$$U = \int \frac{M^2}{2EI} dx \quad (4-23)$$

Equations (4–22) and (4–23) are exact only when a beam is subject to pure bending. Even when transverse shear is present, these equations continue to give quite good results, except for very short beams. The strain energy due to shear loading of a beam is a complicated problem. An approximate solution can be obtained by using Eq. (4–20) with a correction factor whose value depends upon the shape of the cross section. If we use C for the correction factor and V for the shear force, then the strain energy due to shear in bending is

$$U = \frac{CV^2 l}{2AG} \quad (4-24)$$

or

$$U = \int \frac{CV^2}{2AG} dx \quad (4-25)$$

Values of the factor C are listed in Table 4–1.

Table 4–1

Strain-Energy Correction Factors for Transverse Shear

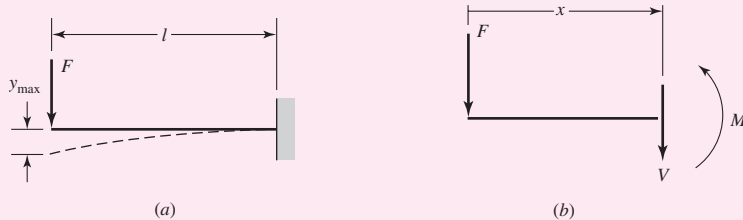
Source: Richard G. Budynas, *Advanced Strength and Applied Stress Analysis*, 2nd ed., McGraw-Hill, New York, 1999. Copyright © 1999 The McGraw-Hill Companies.

Beam Cross-Sectional Shape	Factor C
Rectangular	1.2
Circular	1.11
Thin-walled tubular, round	2.00
Box sections [†]	1.00
Structural sections [†]	1.00

[†]Use area of web only.

EXAMPLE 4-8

A cantilever beam with a round cross section has a concentrated load F at the end, as shown in Fig. 4-9a. Find the strain energy in the beam.

Figure 4-9**Solution**

To determine what forms of strain energy are involved with the deflection of the beam, we break into the beam and draw a free-body diagram to see the forces and moments being carried within the beam. Figure 4-9b shows such a diagram in which the transverse shear is $V = -F$, and the bending moment is $M = -Fx$. The variable x is simply a variable of integration and can be defined to be measured from any convenient point. The same results will be obtained from a free-body diagram of the right-hand portion of the beam with x measured from the wall. Using the free end of the beam usually results in reduced effort since the ground reaction forces do not need to be determined.

For the transverse shear, using Eq. (4-24) with the correction factor $C = 1.11$ from Table 4-2, and noting that V is constant through the length of the beam,

$$U_{\text{shear}} = \frac{CV^2l}{2AG} = \frac{1.11F^2l}{2AG}$$

For the bending, since M is a function of x , Eq. (4-23) gives

$$U_{\text{bend}} = \int \frac{M^2dx}{2EI} = \frac{1}{2EI} \int_0^l (-Fx)^2 dx = \frac{F^2l^3}{6EI}$$

The total strain energy is

Answer

$$U = U_{\text{bend}} + U_{\text{shear}} = \frac{F^2l^3}{6EI} + \frac{1.11F^2l}{2AG}$$

Note, except for very short beams, the shear term (of order l) is typically small compared to the bending term (of order l^3). This will be demonstrated in the next example.

4-8**Castigliano's Theorem**

A most unusual, powerful, and often surprisingly simple approach to deflection analysis is afforded by an energy method called *Castigliano's theorem*. It is a unique way of analyzing deflections and is even useful for finding the reactions of indeterminate structures. Castigliano's theorem states that *when forces act on elastic systems subject to small displacements, the displacement corresponding to any force, in the direction of the force, is equal to the partial derivative of the total strain energy with respect to that force*. The

terms *force* and *displacement* in this statement are broadly interpreted to apply equally to moments and angular displacements. Mathematically, the theorem of Castigiano is

$$\delta_i = \frac{\partial U}{\partial F_i} \quad (4-26)$$

where δ_i is the displacement of the point of application of the force F_i in the direction of F_i . For rotational displacement Eq. (4-26) can be written as

$$\theta_i = \frac{\partial U}{\partial M_i} \quad (4-27)$$

where θ_i is the rotational displacement, in radians, of the beam where the moment M_i exists and in the direction of M_i .

As an example, apply Castigiano's theorem using Eqs. (4-16) and (4-18) to get the axial and torsional deflections. The results are

$$\delta = \frac{\partial}{\partial F} \left(\frac{F^2 l}{2AE} \right) = \frac{Fl}{AE} \quad (a)$$

$$\theta = \frac{\partial}{\partial T} \left(\frac{T^2 l}{2GJ} \right) = \frac{Tl}{GJ} \quad (b)$$

Compare Eqs. (a) and (b) with Eqs. (4-3) and (4-5).

EXAMPLE 4-9

The cantilever of Ex. 4-8 is a carbon steel bar 10 in long with a 1-in diameter and is loaded by a force $F = 100$ lbf.

- (a) Find the maximum deflection using Castigiano's theorem, including that due to shear.
- (b) What error is introduced if shear is neglected?

Solution

- (a) From Ex. 4-8, the total energy of the beam is

$$U = \frac{F^2 l^3}{6EI} + \frac{1.11F^2 l}{2AG} \quad (1)$$

Then, according to Castigiano's theorem, the deflection of the end is

$$y_{\max} = \frac{\partial U}{\partial F} = \frac{Fl^3}{3EI} + \frac{1.11Fl}{AG} \quad (2)$$

We also find that

$$I = \frac{\pi d^4}{64} = \frac{\pi (1)^4}{64} = 0.0491 \text{ in}^4$$

$$A = \frac{\pi d^2}{4} = \frac{\pi (1)^2}{4} = 0.7854 \text{ in}^2$$

Substituting these values, together with $F = 100$ lbf, $l = 10$ in, $E = 30$ Mpsi, and $G = 11.5$ Mpsi, in Eq. (3) gives

Answer

$$y_{\max} = 0.02263 + 0.00012 = 0.02275 \text{ in}$$

Note that the result is positive because it is in the *same* direction as the force F .

Answer

- (b) The error in neglecting shear for this problem is $(0.02275 - 0.02263)/0.02275 = 0.0053 = 0.53$ percent.

The relative contribution of transverse shear to beam deflection decreases as the length-to-height ratio of the beam increases, and is generally considered negligible for $l/d > 10$. Note that the deflection equations for the beams in Table A-9 do not include the effects of transverse shear.

Castigiano's theorem can be used to find the deflection at a point even though no force or moment acts there. The procedure is:

- 1 Set up the equation for the total strain energy U by including the energy due to a fictitious force or moment Q acting at the point whose deflection is to be found.
- 2 Find an expression for the desired deflection δ , in the direction of Q , by taking the derivative of the total strain energy with respect to Q .
- 3 Since Q is a fictitious force, solve the expression obtained in step 2 by setting Q equal to zero. Thus, the displacement at the point of application of the fictitious force Q is

$$\delta = \left. \frac{\partial U}{\partial Q} \right|_{Q=0} \quad (4-28)$$

In cases where integration is necessary to obtain the strain energy, it is more efficient to obtain the deflection directly without explicitly finding the strain energy, by moving the partial derivative inside the integral. For the example of the bending case,

$$\begin{aligned} \delta_i = \frac{\partial U}{\partial F_i} &= \frac{\partial}{\partial F_i} \left(\int \frac{M^2}{2EI} dx \right) = \int \frac{\partial}{\partial F_i} \left(\frac{M^2}{2EI} \right) dx = \int \frac{2M \frac{\partial M}{\partial F_i}}{2EI} dx \\ &= \int \frac{1}{EI} \left(M \frac{\partial M}{\partial F_i} \right) dx \end{aligned}$$

This allows the derivative to be taken before integration, simplifying the mathematics. This method is especially helpful if the force is a fictitious force Q , since it can be set to zero as soon as the derivative is taken. The expressions for the common cases in Eqs. (4-17), (4-19), and (4-23) are rewritten as

$$\delta_i = \frac{\partial U}{\partial F_i} = \int \frac{1}{AE} \left(F \frac{\partial F}{\partial F_i} \right) dx \quad \text{tension and compression} \quad (4-29)$$

$$\theta_i = \frac{\partial U}{\partial M_i} = \int \frac{1}{GJ} \left(T \frac{\partial T}{\partial M_i} \right) dx \quad \text{torsion} \quad (4-30)$$

$$\delta_i = \frac{\partial U}{\partial F_i} = \int \frac{1}{EI} \left(M \frac{\partial M}{\partial F_i} \right) dx \quad \text{bending} \quad (4-31)$$

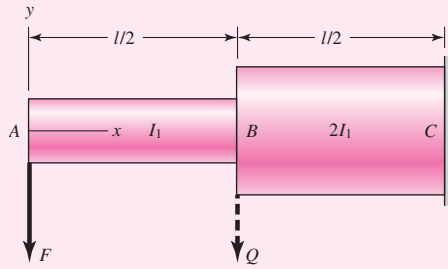
EXAMPLE 4-10

Using Castigiano's method, determine the deflections of points A and B due to the force F applied at the end of the step shaft shown in Fig. 4-10. The second area moments for sections AB and BC are I_1 and $2I_1$, respectively.

Solution

To avoid the need to determine the ground reaction forces, define the origin of x at the left end of the beam as shown. For $0 \leq x \leq l$, the bending moment is

$$M = -Fx \quad (1)$$

Figure 4-10

Since F is at A and in the direction of the desired deflection, the deflection at A from Eq. (4-31) is

$$\delta_A = \frac{\partial U}{\partial F} = \int_0^l \frac{1}{EI} \left(M \frac{\partial M}{\partial F} \right) dx \quad (2)$$

Substituting Eq. (1) into Eq. (2), noting that $I = I_1$ for $0 \leq x \leq l/2$, and $I = 2I_1$ for $l/2 \leq x \leq l$, we get

$$\begin{aligned} \delta_A &= \frac{1}{E} \left[\int_0^{l/2} \frac{1}{I_1} (-Fx)(-x) dx + \int_{l/2}^l \frac{1}{2I_1} (-Fx)(-x) dx \right] \\ &= \frac{1}{E} \left[\frac{Fl^3}{24I_1} + \frac{7Fl^3}{48I_1} \right] = \frac{3}{16} \frac{Fl^3}{EI_1} \end{aligned}$$

Answer

which is positive, as it is in the direction of F .

For B , a fictitious force Q is necessary at the point. Assuming Q acts down at B , and x is as before, the moment equation is

$$\begin{aligned} M &= -Fx & 0 \leq x \leq l/2 \\ M &= -Fx - Q \left(x - \frac{l}{2} \right) & l/2 \leq x \leq l \end{aligned} \quad (3)$$

For Eq. (4-31), we need $\partial M / \partial Q$. From Eq. (3),

$$\begin{aligned} \frac{\partial M}{\partial Q} &= 0 & 0 \leq x \leq l/2 \\ \frac{\partial M}{\partial Q} &= - \left(x - \frac{l}{2} \right) & l/2 \leq x \leq l \end{aligned} \quad (4)$$

Once the derivative is taken, Q can be set to zero, so Eq. (4-31) becomes

$$\begin{aligned} \delta_B &= \left[\int_0^l \frac{1}{EI} \left(M \frac{\partial M}{\partial Q} \right) dx \right]_{Q=0} \\ &= \frac{1}{EI_1} \int_0^{l/2} (-Fx)(0) dx + \frac{1}{E(2I_1)} \int_{l/2}^l (-Fx) \left[- \left(x - \frac{l}{2} \right) \right] dx \end{aligned}$$

Evaluating the last integral gives

$$\delta_B = \frac{F}{2EI_1} \left(\frac{x^3}{3} - \frac{lx^2}{4} \right) \Big|_{l/2}^l = \frac{5}{96} \frac{Fl^3}{EI_1}$$

which again is positive, in the direction of Q .

Answer

EXAMPLE 4-11

For the wire form of diameter d shown in Fig. 4-11a, determine the deflection of point B in the direction of the applied force F (neglect the effect of transverse shear).

Solution

Figure 4-11b shows free body diagrams where the body has been broken in each section, and internal balancing forces and moments are shown. The sign convention for the force and moment variables is positive in the directions shown. With energy methods, sign conventions are arbitrary, so use a convenient one. In each section, the variable x is defined with its origin as shown. The variable x is used as a variable of integration for each section independently, so it is acceptable to reuse the same variable for each section. For completeness, the transverse shear forces are included, but the effects of transverse shear on the strain energy (and deflection) will be neglected.

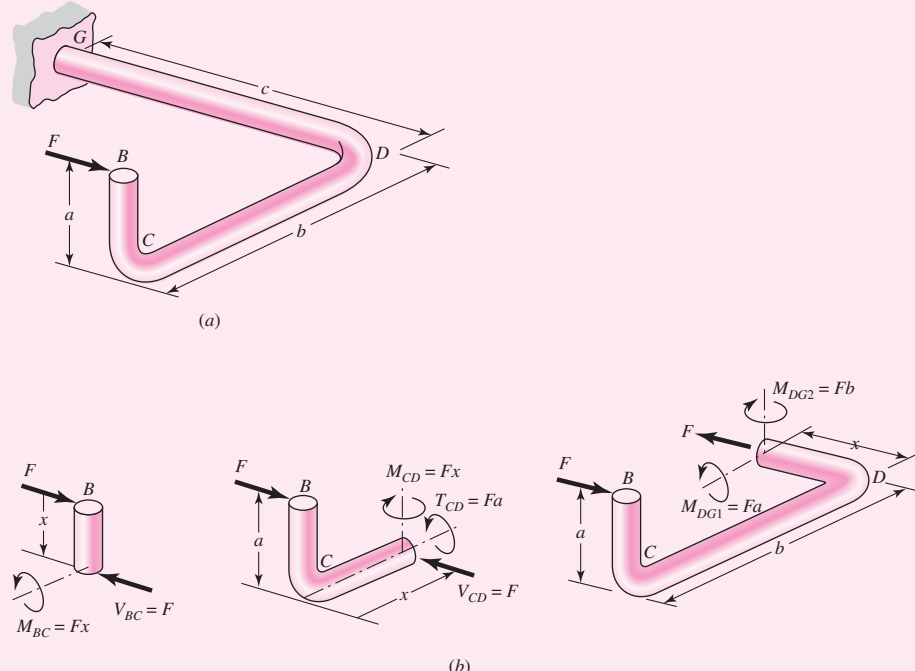
Element BC is in bending only so from Eq. (4-31),⁵

$$\frac{\partial U_{BC}}{\partial F} = \frac{1}{EI} \int_0^a (Fx)(x) dx = \frac{Fa^3}{3EI} \quad (1)$$

Element CD is in bending and in torsion. The torsion is constant so Eq. (4-30) can be written as

$$\frac{\partial U}{\partial F_i} = \left(T \frac{\partial T}{\partial F_i} \right) \frac{l}{GJ}$$

| **Figure 4-11**



⁵It is very tempting to mix techniques and try to use superposition also, for example. However, some subtle things can occur that you may visually miss. It is highly recommended that if you are using Castiglione's theorem on a problem, you use it for all parts of the problem.

where l is the length of the member. So for the torsion in member CD , $F_i = F$, $T = Fa$, and $l = b$. Thus,

$$\left(\frac{\partial U_{CD}}{\partial F} \right)_{\text{torsion}} = (Fa)(a) \frac{b}{GJ} = \frac{Fa^2 b}{GJ} \quad (2)$$

For the bending in CD ,

$$\left(\frac{\partial U_{CD}}{\partial F} \right)_{\text{bending}} = \frac{1}{EI} \int_0^b (Fx)(x) dx = \frac{Fb^3}{3EI} \quad (3)$$

Member DG is axially loaded and is bending in two planes. The axial loading is constant, so Eq. (4–29) can be written as

$$\frac{\partial U}{\partial F_i} = \left(F \frac{\partial F}{\partial F_i} \right) \frac{l}{AE}$$

where l is the length of the member. Thus, for the axial loading of DG , $F_i = F$, $l = c$, and

$$\left(\frac{\partial U_{DG}}{\partial F} \right)_{\text{axial}} = \frac{Fc}{AE} \quad (4)$$

The bending moments in each plane of DG are constant along the length, with $M_{DG2} = Fb$ and $M_{DG1} = Fa$. Considering each one separately in the form of Eq. (4–31) gives

$$\begin{aligned} \left(\frac{\partial U_{DG}}{\partial F} \right)_{\text{bending}} &= \frac{1}{EI} \int_0^c (Fb)(b) dx + \frac{1}{EI} \int_0^c (Fa)(a) dx \\ &= \frac{Fc(a^2 + b^2)}{EI} \end{aligned} \quad (5)$$

Adding Eqs. (1) to (5), noting that $I = \pi d^4/64$, $J = 2I$, $A = \pi d^2/4$, and $G = E/[2(1 + \nu)]$, we find that the deflection of B in the direction of F is

Answer $(\delta_B)_F = \frac{4F}{3\pi Ed^4} [16(a^3 + b^3) + 48c(a^2 + b^2) + 48(1 + \nu)a^2b + 3cd^2]$

Now that we have completed the solution, see if you can physically account for each term in the result using an independent method such as superposition.

4–9

Deflection of Curved Members

Machine frames, springs, clips, fasteners, and the like frequently occur as curved shapes. The determination of stresses in curved members has already been described in Sec. 3–18. Castigliano's theorem is particularly useful for the analysis of deflections in curved parts too.⁶ Consider, for example, the curved frame of Fig. 4–12a. We are

⁶For more solutions than are included here, see Joseph E. Shigley, "Curved Beams and Rings," Chap. 38 in Joseph E. Shigley, Charles R. Mischke, and Thomas H. Brown, Jr. (eds.), *Standard Handbook of Machine Design*, 3rd ed., McGraw-Hill, New York, 2004.

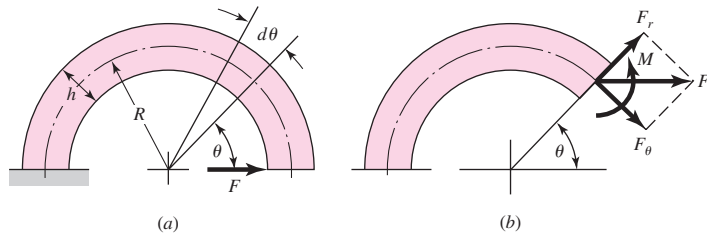


Figure 4-12

(a) Curved bar loaded by force F . R = radius to centroidal axis of section; h = section thickness. (b) Diagram showing forces acting on section taken at angle θ . F_r = V = shear component of F ; F_θ is component of F normal to section; M is moment caused by force F .

interested in finding the deflection of the frame due to F and in the direction of F . The total strain energy consists of four terms, and we shall consider each separately. The first is due to the bending moment and is⁷

$$U_1 = \int \frac{M^2 d\theta}{2AeE} \quad (4-32)$$

In this equation, the eccentricity e is

$$e = R - r_n \quad (4-33)$$

where r_n is the radius of the neutral axis as defined in Sec. 3-18 and shown in Fig. 3-34.

The strain energy component due to the normal force F_θ consists of two parts, one of which is axial and analogous to Eq. (4-17). This part is

$$U_2 = \int \frac{F_\theta^2 R d\theta}{2AE} \quad (4-34)$$

The force F_θ also produces a moment, which opposes the moment M in Fig. 4-12b. The resulting strain energy will be subtractive and is

$$U_3 = - \int \frac{MF_\theta d\theta}{AE} \quad (4-35)$$

The negative sign of Eq. (4-35) can be appreciated by referring to both parts of Fig. 4-12. Note that the moment M tends to decrease the angle $d\theta$. On the other hand, the moment due to F_θ tends to increase $d\theta$. Thus U_3 is negative. If F_θ had been acting in the opposite direction, then both M and F_θ would tend to decrease the angle $d\theta$.

The fourth and last term is the transverse shear energy due to F_r . Adapting Eq. (4-25) gives

$$U_4 = \int \frac{CF_r^2 R d\theta}{2AG} \quad (4-36)$$

where C is the correction factor of Table 4-1.

⁷See Richard G. Budynas, *Advanced Strength and Applied Stress Analysis*, 2nd ed., Sec. 6.7, McGraw-Hill, New York, 1999.

Combining the four terms gives the total strain energy

$$U = \int \frac{M^2 d\theta}{2AeE} + \int \frac{F_\theta^2 R d\theta}{2AE} - \int \frac{MF_\theta d\theta}{AE} + \int \frac{CF_r^2 R d\theta}{2AG} \quad (4-37)$$

The deflection produced by the force F can now be found. It is

$$\begin{aligned} \delta = \frac{\partial U}{\partial F} &= \int \frac{M}{AeE} \left(\frac{\partial M}{\partial F} \right) d\theta + \int \frac{F_\theta R}{AE} \left(\frac{\partial F_\theta}{\partial F} \right) d\theta \\ &\quad - \int \frac{1}{AE} \frac{\partial(MF_\theta)}{\partial F} d\theta + \int \frac{CF_r R}{AG} \left(\frac{\partial F_r}{\partial F} \right) d\theta \end{aligned} \quad (4-38)$$

This equation is general and may be applied to any section of a thick-walled circular curved beam with application of appropriate limits of integration.

For the specific curved beam in Fig. 4-12b, the integrals are evaluated from 0 to π . Also, for this case we find

$$\begin{aligned} M &= FR \sin \theta & \frac{\partial M}{\partial F} &= R \sin \theta \\ F_\theta &= F \sin \theta & \frac{\partial F_\theta}{\partial F} &= \sin \theta \\ MF_\theta &= F^2 R \sin^2 \theta & \frac{\partial(MF_\theta)}{\partial F} &= 2FR \sin^2 \theta \\ F_r &= F \cos \theta & \frac{\partial F_r}{\partial F} &= \cos \theta \end{aligned}$$

Substituting these into Eq. (4-38) and factoring yields

$$\begin{aligned} \delta &= \frac{FR^2}{AeE} \int_0^\pi \sin^2 \theta d\theta + \frac{FR}{AE} \int_0^\pi \sin^2 \theta d\theta - \frac{2FR}{AE} \int_0^\pi \sin^2 \theta d\theta \\ &\quad + \frac{CFR}{AG} \int_0^\pi \cos^2 \theta d\theta \\ &= \frac{\pi FR^2}{2AeE} + \frac{\pi FR}{2AE} - \frac{\pi FR}{AE} + \frac{\pi CFR}{2AG} = \frac{\pi FR^2}{2AeE} - \frac{\pi FR}{2AE} + \frac{\pi CFR}{2AG} \end{aligned} \quad (4-39)$$

Because the first term contains the square of the radius, the second two terms will be small if the frame has a large radius.

For curved sections in which the radius is significantly larger than the thickness, say $R/h > 10$, the effect of the eccentricity is negligible, so that the strain energies can be approximated directly from Eqs. (4-17), (4-23), and (4-25) with a substitution of $R d\theta$ for dx . Further, as R increases, the contributions to deflection from the normal force and tangential force becomes negligibly small compared to the bending component. Therefore, an approximate result can be obtained for a thin circular curved member as

$$U \doteq \int \frac{M^2}{2EI} R d\theta \quad R/h > 10 \quad (4-40)$$

$$\delta = \frac{\partial U}{\partial F} \doteq \int \frac{1}{EI} \left(M \frac{\partial M}{\partial F} \right) R d\theta \quad R/h > 10 \quad (4-41)$$

EXAMPLE 4-12

The cantilevered hook shown in Fig. 4-13a is formed from a round steel wire with a diameter of 2 mm. The hook dimensions are $l = 40$ and $R = 50$ mm. A force P of 1 N is applied at point C . Use Castiglione's theorem to estimate the deflection at point D at the tip.

Solution

Since l/d and R/d are significantly greater than 10, only the contributions due to bending will be considered. To obtain the vertical deflection at D , a fictitious force Q will be applied there. Free-body diagrams are shown in Figs. 4-13b, c, and d, with breaks in sections AB , BC , and CD , respectively. The normal and shear forces, N and V respectively, are shown but are considered negligible in the deflection analysis.

For section AB , with the variable of integration x defined as shown in Fig. 4-13b, summing moments about the break gives an equation for the moment in section AB ,

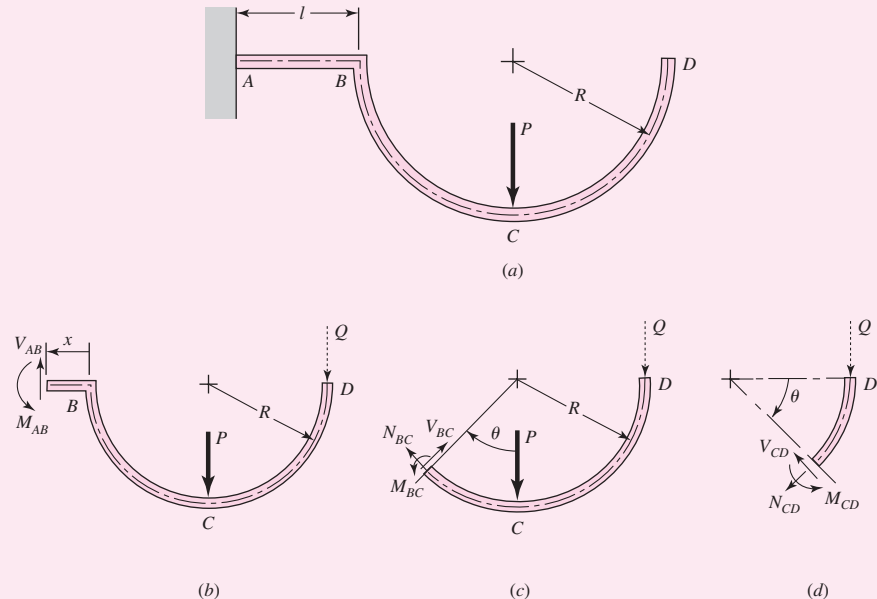
$$M_{AB} = P(R + x) + Q(2R + x) \quad (1)$$

$$\partial M_{AB}/\partial Q = 2R + x \quad (2)$$

Since the derivative with respect to Q has been taken, we can set Q equal to zero. From Eq. (4-31), inserting Eqs. (1) and (2),

$$\begin{aligned} (\delta_D)_{AB} &= \int_0^l \frac{1}{EI} \left(M_{AB} \frac{\partial M_{AB}}{\partial Q} \right) dx = \frac{1}{EI} \int_0^l P(R + x)(2R + x) dx \\ &= \frac{P}{EI} \int_0^l (2R^2 + 3Rx + x^2) dx = \frac{P}{EI} (2R^2 l + \frac{3}{2}l^2 R + \frac{1}{3}l^3) \end{aligned} \quad (3)$$

| **Figure 4-13**



For section BC , with the variable of integration θ defined as shown in Fig. 4–13c, summing moments about the break gives the moment equation for section BC .

$$M_{BC} = Q(R + R \sin \theta) + PR \sin \theta \quad (4)$$

$$\partial M_{BC} / \partial Q = R(1 + \sin \theta) \quad (5)$$

From Eq. (4–41), inserting Eqs. (4) and (5) and setting $Q = 0$, we get

$$\begin{aligned} (\delta_D)_{BC} &= \int_0^{\pi/2} \frac{1}{EI} \left(M_{BC} \frac{\partial M_{BC}}{\partial Q} \right) R d\theta = \frac{R}{EI} \int_0^{\pi/2} (PR \sin \theta)[R(1 + \sin \theta)] dx \\ &= \frac{PR^3}{EI} \left(1 + \frac{\pi}{4} \right) \end{aligned} \quad (6)$$

Noting that the break in section CD contains nothing but Q , and after setting $Q = 0$, we can conclude that there is no actual strain energy contribution in this section. Combining terms from Eqs. (3) and (6) to get the total vertical deflection at D ,

$$\begin{aligned} \delta_D &= (\delta_D)_{AB} + (\delta_D)_{BC} = \frac{P}{EI} (2R^2l + \frac{3}{2}l^2R + \frac{1}{3}l^3) + \frac{PR^3}{EI} \left(1 + \frac{\pi}{4} \right) \\ &= \frac{P}{EI} (1.785R^3 + 2R^2l + 1.5Rl^2 + 0.333l^3) \end{aligned} \quad (7)$$

Substituting values, and noting $I = \pi d^4/64$, and $E = 207$ GPa for steel, we get

Answer

$$\begin{aligned} \delta_D &= \frac{1}{207(10^9)[\pi(0.002^4)/64]} [1.785(0.05^3) + 2(0.05^2)0.04 \\ &\quad + 1.5(0.05)0.04^2 + 0.333(0.04^3)] \\ &= 3.47(10^{-3}) \text{ m} = 3.47 \text{ mm} \end{aligned}$$

EXAMPLE 4–13 Deflection in a Variable-Cross-Section Punch-Press Frame

The general result expressed in Eq. (4–39),

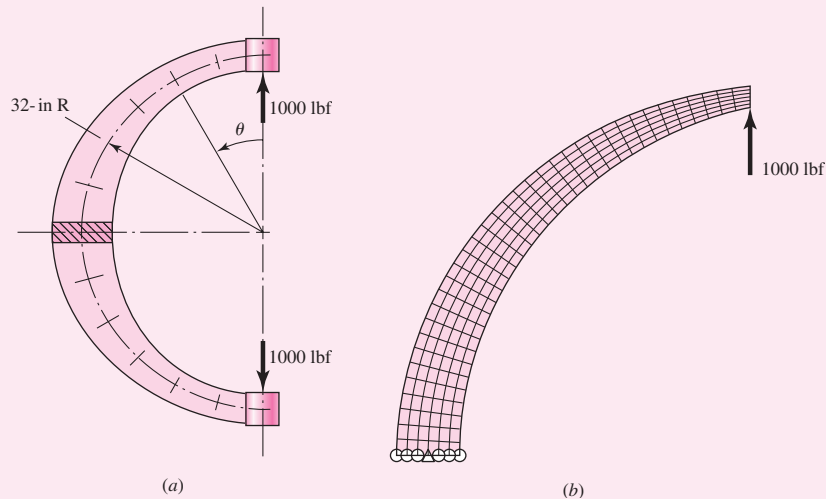
$$\delta = \frac{\pi FR^2}{2AeE} - \frac{\pi FR}{2AE} + \frac{\pi CFR}{2AG}$$

is useful in sections that are uniform and in which the centroidal locus is circular. The bending moment is largest where the material is farthest from the load axis. Strengthening requires a larger second area moment I . A variable-depth cross section is attractive, but it makes the integration to a closed form very difficult. However, if you are seeking results, numerical integration with computer assistance is helpful.

Consider the steel C frame depicted in Fig. 4–14a in which the centroidal radius is 32 in, the cross section at the ends is 2 in \times 2 in, and the depth varies sinusoidally with

Figure 4-14

(a) A steel punch press has a C frame with a varying-depth rectangular cross section depicted. The cross section varies sinusoidally from $2 \text{ in} \times 2 \text{ in}$ at $\theta = 0^\circ$ to $2 \text{ in} \times 6 \text{ in}$ at $\theta = 90^\circ$, and back to $2 \text{ in} \times 2 \text{ in}$ at $\theta = 180^\circ$. Of immediate interest to the designer is the deflection in the load axis direction under the load. (b) Finite-element model.



an amplitude of 2 in. The load is 1000 lbf. It follows that $C = 1.2$, $G = 11.5(10^6)$ psi, $E = 30(10^6)$ psi. The outer and inner radii are

$$R_{\text{out}} = 33 + 2 \sin \theta \quad R_{\text{in}} = 31 - 2 \sin \theta$$

The remaining geometrical terms are

$$h = R_{\text{out}} - R_{\text{in}} = 2(1 + 2 \sin \theta)$$

$$A = bh = 4(1 + 2 \sin \theta)$$

$$r_n = \frac{h}{\ln(R_{\text{out}}/R_{\text{in}})} = \frac{2(1 + 2 \sin \theta)}{\ln[(33 + 2 \sin \theta)/(31 - 2 \sin \theta)]}$$

$$e = R - r_n = 32 - r_n$$

Note that

$$M = FR \sin \theta \quad \partial M / \partial F = R \sin \theta$$

$$F_\theta = F \sin \theta \quad \partial F_\theta / \partial F = \sin \theta$$

$$MF_\theta = F^2 R \sin^2 \theta \quad \partial MF_\theta / \partial F = 2FR \sin^2 \theta$$

$$F_r = F \cos \theta \quad \partial F_r / \partial F = \cos \theta$$

Substitution of the terms into Eq. (4-38) yields three integrals

$$\delta = I_1 + I_2 + I_3 \quad (1)$$

where the integrals are

$$I_1 = 8.5333(10^{-3}) \int_0^\pi \frac{\sin^2 \theta d\theta}{(1 + 2 \sin \theta) \left[32 - \frac{2(1 + 2 \sin \theta)}{\ln \left(\frac{33 + 2 \sin \theta}{31 - 2 \sin \theta} \right)} \right]} \quad (2)$$

$$I_2 = -2.6667(10^{-4}) \int_0^\pi \frac{\sin^2 \theta d\theta}{1 + 2 \sin \theta} \quad (3)$$

$$I_3 = 8.3478(10^{-4}) \int_0^\pi \frac{\cos^2 \theta d\theta}{1 + 2 \sin \theta} \quad (4)$$

The integrals may be evaluated in a number of ways: by a program using Simpson's rule integration,⁸ by a program using a spreadsheet, or by mathematics software. Using MathCad and checking the results with Excel gives the integrals as $I_1 = 0.076\ 615$, $I_2 = -0.000\ 159$, and $I_3 = 0.000\ 773$. Substituting these into Eq. (1) gives

Answer

$$\delta = 0.077\ 23 \text{ in}$$

Finite-element (FE) programs are also very accessible. Figure 4–14b shows a simple half-model, using symmetry, of the press consisting of 216 plane-stress (2-D) elements. Creating the model and analyzing it to obtain a solution took minutes. Doubling the results from the FE analysis yielded $\delta = 0.07790$ in, a less than 1 percent variation from the results of the numerical integration.

4–10 **Statically Indeterminate Problems**

A system is *overconstrained* when it has more unknown support (reaction) forces and/or moments than static equilibrium equations. Such a system is said to be *statically indeterminate* and the extra constraint supports are called *redundant supports*. In addition to the static equilibrium equations, a deflection equation is required for *each* redundant support reaction in order to obtain a solution. For example, consider a beam in bending with a wall support on one end and a simple support on the other, such as beam 12 of Table A–9. There are three support reactions and only two static equilibrium equations are available. This beam has *one* redundant support. To solve for the three unknown support reactions we use the two equilibrium equations and *one* additional deflection equation. For another example, consider beam 15 of Table A–9. This beam has a wall on both ends, giving rise to *two* redundant supports requiring *two* deflection equations in addition to the equations from statics. The purpose of redundant supports is to provide safety and reduce deflection.

A simple example of a statically indeterminate problem is furnished by the nested helical springs in Fig. 4–15a. When this assembly is loaded by the compressive force F , it deforms through the distance δ . What is the compressive force in each spring?

Only one equation of static equilibrium can be written. It is

$$\sum F = F - F_1 - F_2 = 0 \quad (a)$$

which simply says that the total force F is resisted by a force F_1 in spring 1 plus the force F_2 in spring 2. Since there are two unknowns and only one static equilibrium equation, the system is statically indeterminate.

To write another equation, note the deformation relation in Fig. 4–15b. The two springs have the same deformation. Thus, we obtain the second equation as

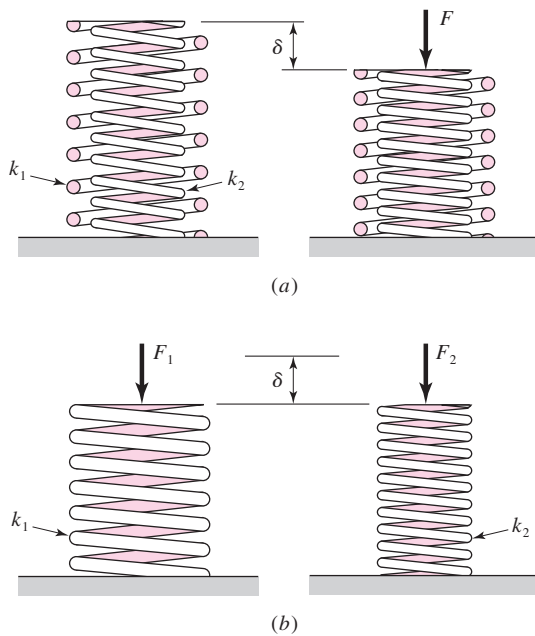
$$\delta_1 = \delta_2 = \delta \quad (b)$$

If we now substitute Eq. (4–2) in Eq. (b), we have

$$\frac{F_1}{k_1} = \frac{F_2}{k_2} \quad (c)$$

⁸See Case Study 4, p. 203, J. E. Shigley and C. R. Mischke, *Mechanical Engineering Design*, 6th ed., McGraw-Hill, New York, 2001.

| Figure 4-15



Now we solve Eq. (c) for F_1 and substitute the result in Eq. (a). This gives

$$F - \frac{k_1}{k_2} F_2 - F_2 = 0 \quad \text{or} \quad F_2 = \frac{k_2 F}{k_1 + k_2} \quad (d)$$

Substituting F_2 into Eq. (c) gives $F_1 = k_1 F / (k_1 + k_2)$ and so $\delta = \delta_1 = \delta_2 = F / (k_1 + k_2)$. Thus, for two springs in parallel, the overall spring constant is $k = F / \delta = k_1 + k_2$.

In the spring example, obtaining the necessary deformation equation was very straightforward. However, for other situations, the deformation relations may not be as easy. A more structured approach may be necessary. Here we will show two basic procedures for general statically indeterminate problems.

Procedure 1

- 1 Choose the redundant reaction(s). There may be alternative choices (See Example 4-14).
- 2 Write the equations of static equilibrium for the remaining reactions in terms of the applied loads and the redundant reaction(s) of step 1.
- 3 Write the deflection equation(s) for the point(s) at the locations of the redundant reaction(s) of step 1 in terms of the applied loads and the redundant reaction(s) of step 1. Normally the deflection(s) is (are) zero. If a redundant reaction is a moment, the corresponding deflection equation is a rotational deflection equation.
- 4 The equations from steps 2 and 3 can now be solved to determine the reactions.

In step 3 the deflection equations can be solved in any of the standard ways. Here we will demonstrate the use of superposition and Castigiano's theorem on a beam problem.

EXAMPLE 4-14

The indeterminate beam 11 of Appendix Table A-9 is reproduced in Fig. 4-16. Determine the reactions using procedure 1.

Solution

The reactions are shown in Fig. 4-16b. Without R_2 the beam is a statically determinate cantilever beam. Without M_1 the beam is a statically determinate simply supported beam. In either case, the beam has only *one* redundant support. We will first solve this problem using superposition, choosing R_2 as the redundant reaction. For the second solution, we will use Castigliano's theorem with M_1 as the redundant reaction.

Solution 1

- 1 Choose R_2 at B to be the redundant reaction.
- 2 Using static equilibrium equations solve for R_1 and M_1 in terms of F and R_2 . This results in

$$R_1 = F - R_2 \quad M_1 = \frac{Fl}{2} - R_2 l \quad (1)$$

- 3 Write the deflection equation for point B in terms of F and R_2 . Using superposition of beam 1 of Table A-9 with $F = -R_2$, and beam 2 of Table A-9 with $a = l/2$, the deflection of B , at $x = l$, is

$$\delta_B = -\frac{R_2 l^2}{6EI}(l - 3l) + \frac{F(l/2)^2}{6EI}\left(\frac{l}{2} - 3l\right) = \frac{R_2 l^3}{3EI} - \frac{5Fl^3}{48EI} = 0 \quad (2)$$

- 4 Equation (2) can be solved for R_2 directly. This yields

Answer

$$R_2 = \frac{5F}{16} \quad (3)$$

Next, substituting R_2 into Eqs. (1) completes the solution, giving

Answer

$$R_1 = \frac{11F}{16} \quad M_1 = \frac{3Fl}{16} \quad (4)$$

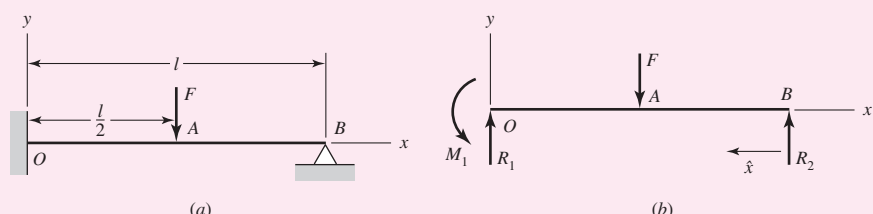
Note that the solution agrees with what is given for beam 11 in Table A-9.

Solution 2

- 1 Choose M_1 at O to be the redundant reaction.
- 2 Using static equilibrium equations solve for R_1 and R_2 in terms of F and M_1 . This results in

$$R_1 = \frac{F}{2} + \frac{M_1}{l} \quad R_2 = \frac{F}{2} - \frac{M_1}{l} \quad (5)$$

| **Figure 4-16**



- 3** Since M_1 is the redundant reaction at O , write the equation for the angular deflection at point O . From Castiglano's theorem this is

$$\theta_O = \frac{\partial U}{\partial M_1} \quad (6)$$

We can apply Eq. (4–31), using the variable x as shown in Fig. 4–16b. However, simpler terms can be found by using a variable \hat{x} that starts at B and is positive to the left. With this and the expression for R_2 from Eq. (5) the moment equations are

$$M = \left(\frac{F}{2} - \frac{M_1}{l} \right) \hat{x} \quad 0 \leq \hat{x} \leq \frac{l}{2} \quad (7)$$

$$M = \left(\frac{F}{2} - \frac{M_1}{l} \right) \hat{x} - F \left(\hat{x} - \frac{l}{2} \right) \quad \frac{l}{2} \leq \hat{x} \leq l \quad (8)$$

For both equations

$$\frac{\partial M}{\partial M_1} = -\frac{\hat{x}}{l} \quad (9)$$

Substituting Eqs. (7) to (9) in Eq. (6), using the form of Eq. (4–31) where $F_i = M_1$, gives

$$\begin{aligned} \theta_O = \frac{\partial U}{\partial M_1} &= \frac{1}{EI} \left\{ \int_0^{l/2} \left(\frac{F}{2} - \frac{M_1}{l} \right) \hat{x} \left(-\frac{\hat{x}}{l} \right) d\hat{x} + \int_{l/2}^l \left[\left(\frac{F}{2} - \frac{M_1}{l} \right) \hat{x} \right. \right. \\ &\quad \left. \left. - F \left(\hat{x} - \frac{l}{2} \right) \right] \left(-\frac{\hat{x}}{l} \right) d\hat{x} \right\} = 0 \end{aligned}$$

Canceling $1/EI$, and combining the first two integrals, simplifies this quite readily to

$$\left(\frac{F}{2} - \frac{M_1}{l} \right) \int_0^l \hat{x}^2 d\hat{x} - F \int_{l/2}^l \left(\hat{x} - \frac{l}{2} \right) \hat{x} d\hat{x} = 0$$

Integrating gives

$$\left(\frac{F}{2} - \frac{M_1}{l} \right) \frac{l^3}{3} - \frac{F}{3} \left[l^3 - \left(\frac{l}{2} \right)^3 \right] + \frac{Fl}{4} \left[l^2 - \left(\frac{l}{2} \right)^2 \right] = 0$$

which reduces to

$$M_1 = \frac{3Fl}{16} \quad (10)$$

- 4** Substituting Eq. (10) into (5) results in

$$R_1 = \frac{11F}{16} \quad R_2 = \frac{5F}{16} \quad (11)$$

which again agrees with beam 11 of Table A–9.

For some problems even procedure 1 can be a task. Procedure 2 eliminates some tricky geometric problems that would complicate procedure 1. We will describe the procedure for a beam problem.

Procedure 2

- 1 Write the equations of static equilibrium for the beam in terms of the applied loads and unknown restraint reactions.
- 2 Write the deflection equation for the beam in terms of the applied loads and unknown restraint reactions.
- 3 Apply boundary conditions to the deflection equation of step 2 consistent with the restraints.
- 4 Solve the equations from steps 1 and 3.

EXAMPLE 4-15

The rods AD and CE shown in Fig. 4-17a each have a diameter of 10 mm. The second-area moment of beam ABC is $I = 62.5(10^3) \text{ mm}^4$. The modulus of elasticity of the material used for the rods and beam is $E = 200 \text{ GPa}$. The threads at the ends of the rods are single-threaded with a pitch of 1.5 mm. The nuts are first snugly fit with bar ABC horizontal. Next the nut at A is tightened one full turn. Determine the resulting tension in each rod and the deflections of points A and C .

Solution

There is a lot going on in this problem; a rod shortens, the rods stretch in tension, and the beam bends. Let's try the procedure!

- 1 The free-body diagram of the beam is shown in Fig. 4-17b. Summing forces, and moments about B , gives

$$F_B - F_A - F_C = 0 \quad (1)$$

$$4F_A - 3F_C = 0 \quad (2)$$

- 2 Using singularity functions, we find the moment equation for the beam is

$$M = -F_Ax + F_B(x - 0.2)^1$$

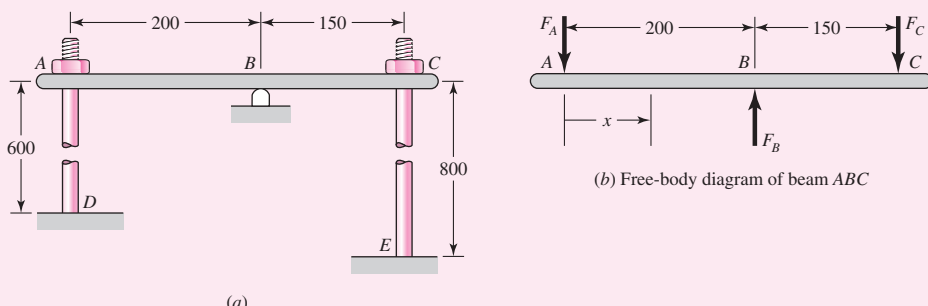
where x is in meters. Integration yields

$$\begin{aligned} EI \frac{dy}{dx} &= -\frac{F_A}{2}x^2 + \frac{F_B}{2}(x - 0.2)^2 + C_1 \\ EIy &= -\frac{F_A}{6}x^3 + \frac{F_B}{6}(x - 0.2)^3 + C_1x + C_2 \end{aligned} \quad (3)$$

The term $EI = 200(10^9) 62.5(10^{-9}) = 1.25(10^4) \text{ N} \cdot \text{m}^2$.

Figure 4-17

Dimensions in mm.



- 3** The upward deflection of point A is $(Fl/AE)_{AD} - Np$, where the first term is the elastic stretch of AD , N is the number of turns of the nut, and p is the pitch of the thread. Thus, the deflection of A in meters is

$$\begin{aligned} y_A &= \frac{F_A(0.6)}{\frac{\pi}{4}(0.010)^2(200)(10^9)} - (1)(0.0015) \\ &= 3.8197(10^{-8})F_A - 1.5(10^{-3}) \end{aligned} \quad (4)$$

The upward deflection of point C is $(Fl/AE)_{CE}$, or

$$y_C = \frac{F_C(0.8)}{\frac{\pi}{4}(0.010)^2(200)(10^9)} = 5.093(10^{-8})F_C \quad (5)$$

Equations (4) and (5) will now serve as the boundary conditions for Eq. (3). At $x = 0$, $y = y_A$. Substituting Eq. (4) into (3) with $x = 0$ and $EI = 1.25(10^4)$, noting that the singularity function is zero for $x = 0$, gives

$$-4.7746(10^{-4})F_A + C_2 = -18.75 \quad (6)$$

At $x = 0.2$ m, $y = 0$, and Eq. (3) yields

$$-1.3333(10^{-3})F_A + 0.2C_1 + C_2 = 0 \quad (7)$$

At $x = 0.35$ m, $y = y_C$. Substituting Eq. (5) into (3) with $x = 0.35$ m and $EI = 1.25(10^4)$ gives

$$-7.1458(10^{-3})F_A + 5.625(10^{-4})F_B - 6.3662(10^{-4})F_C + 0.35C_1 + C_2 = 0 \quad (8)$$

Equations (1), (2), (6), (7), and (8) are five equations in F_A , F_B , F_C , C_1 , and C_2 . Written in matrix form, they are

$$\begin{bmatrix} -1 & 1 & -1 & 0 & 0 \\ 4 & 0 & -3 & 0 & 0 \\ -4.7746(10^{-4}) & 0 & 0 & 0 & 1 \\ -1.3333(10^{-3}) & 0 & 0 & 0.2 & 1 \\ -7.1458(10^{-3}) & 5.625(10^{-4}) & -6.3662(10^{-4}) & 0.35 & 1 \end{bmatrix} \begin{Bmatrix} F_A \\ F_B \\ F_C \\ C_1 \\ C_2 \end{Bmatrix} = \begin{Bmatrix} 0 \\ 0 \\ -18.75 \\ 0 \\ 0 \end{Bmatrix}$$

Solving these equations yields

Answer	$F_A = 2988$ N	$F_B = 6971$ N	$F_C = 3983$ N
	$C_1 = 106.54$ N · m ²	$C_2 = -17.324$ N · m ³	

Equation (3) can be reduced to

$$y = -(39.84x^3 - 92.95(x - 0.2)^3 - 8.523x + 1.386)(10^{-3})$$

Answer At $x = 0$, $y = y_A = -1.386(10^{-3})$ m = -1.386 mm.

Answer At $x = 0.35$ m, $y = y_C = -[39.84(0.35)^3 - 92.95(0.35 - 0.2)^3 - 8.523(0.35) + 1.386](10^{-3}) = 0.203(10^{-3})$ m = 0.203 mm

Note that we could have easily incorporated the stiffness of the support at B if we were given a spring constant.

4-11 Compression Members—General

The analysis and design of compression members can differ significantly from that of members loaded in tension or in torsion. If you were to take a long rod or pole, such as a meterstick, and apply gradually increasing compressive forces at each end, nothing would happen at first, but then the stick would bend (buckle), and finally bend so much as to fracture. Try it. The other extreme would occur if you were to saw off, say, a 5-mm length of the meterstick and perform the same experiment on the short piece. You would then observe that the failure exhibits itself as a mashing of the specimen, that is, a simple compressive failure. For these reasons it is convenient to classify compression members according to their length and according to whether the loading is central or eccentric. The term *column* is applied to all such members except those in which failure would be by simple or pure compression. Columns can be categorized then as:

- 1 Long columns with central loading
- 2 Intermediate-length columns with central loading
- 3 Columns with eccentric loading
- 4 Struts or short columns with eccentric loading

Classifying columns as above makes it possible to develop methods of analysis and design specific to each category. Furthermore, these methods will also reveal whether or not you have selected the category appropriate to your particular problem. The four sections that follow correspond, respectively, to the four categories of columns listed above.

4-12 Long Columns with Central Loading

Figure 4–18 shows long columns with differing end (boundary) conditions. If the axial force P shown acts along the centroidal axis of the column, simple compression of the member occurs for low values of the force. However, under certain conditions, when P reaches a specific value, the column becomes *unstable* and bending as shown in Fig. 4–18 develops rapidly. This force is determined by writing the bending deflection equation for the column, resulting in a differential equation where when the boundary conditions are applied, results in the *critical load* for unstable bending.⁹ The critical force for the pin-ended column of Fig. 4–18a is given by

$$P_{\text{cr}} = \frac{\pi^2 EI}{l^2} \quad (4-42)$$

which is called the *Euler column formula*. Equation (4–42) can be extended to apply to other end-conditions by writing

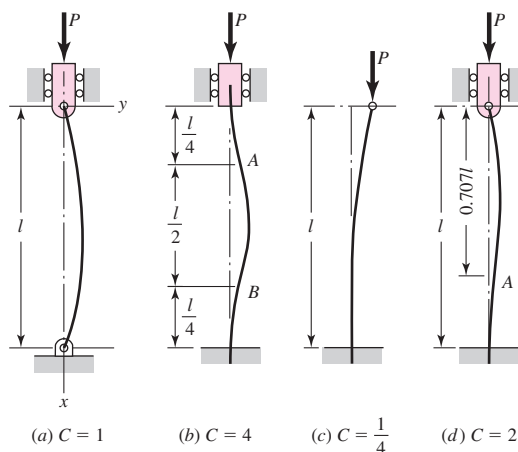
$$P_{\text{cr}} = \frac{C\pi^2 EI}{l^2} \quad (4-43)$$

where the constant C depends on the end conditions as shown in Fig. 4–18.

⁹See F. P. Beer, E. R. Johnston, Jr., and J. T. DeWolf, *Mechanics of Materials*, 5th ed., McGraw-Hill, New York, 2009, pp. 610–613.

Figure 4-18

- (a) Both ends rounded or pivoted; (b) both ends fixed; (c) one end free and one end fixed; (d) one end rounded and pivoted, and one end fixed.



Using the relation $I = Ak^2$, where A is the area and k the radius of gyration, enables us to rearrange Eq. (4-43) into the more convenient form

$$\frac{P_{\text{cr}}}{A} = \frac{C\pi^2 E}{(l/k)^2} \quad (4-44)$$

where l/k is called the *slenderness ratio*. This ratio, rather than the actual column length, will be used in classifying columns according to length categories.

The quantity P_{cr}/A in Eq. (4-44) is the *critical unit load*. It is the load per unit area necessary to place the column in a condition of *unstable equilibrium*. In this state any small crookedness of the member, or slight movement of the support or load, will cause the column to begin to collapse. The unit load has the same units as strength, but this is the strength of a specific column, not of the column material. Doubling the length of a member, for example, will have a drastic effect on the value of P_{cr}/A but no effect at all on, say, the yield strength S_y of the column material itself.

Equation (4-44) shows that the critical unit load depends only upon the end conditions, the modulus of elasticity, and the slenderness ratio. Thus a column obeying the Euler formula made of high-strength alloy steel is *no stronger* than one made of low-carbon steel, since E is the same for both.

The factor C is called the *end-condition constant*, and it may have any one of the theoretical values $\frac{1}{4}$, 1, 2, and 4, depending upon the manner in which the load is applied. In practice it is difficult, if not impossible, to fix the column ends so that the factor $C = 2$ or $C = 4$ would apply. Even if the ends are welded, some deflection will occur. Because of this, some designers never use a value of C greater than unity. However, if liberal factors of safety are employed, and if the column load is accurately known, then a value of C not exceeding 1.2 for both ends fixed, or for one end rounded and one end fixed, is not unreasonable, since it supposes only partial fixation. Of course, the value $C = \frac{1}{4}$ must always be used for a column having one end fixed and one end free. These recommendations are summarized in Table 4-2.

When Eq. (4-44) is solved for various values of the unit load P_{cr}/A in terms of the slenderness ratio l/k , we obtain the curve PQR shown in Fig. 4-19. Since the yield strength of the material has the same units as the unit load, the horizontal line through S_y and Q has been added to the figure. This would appear to make the figure $S_y QR$ cover the entire range of compression problems from the shortest to the longest

Table 4-2

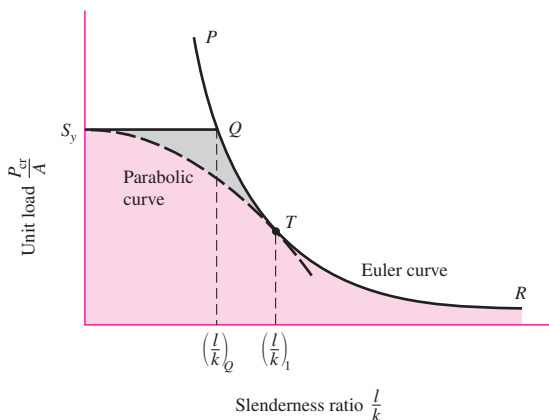
End-Condition Constants for Euler Columns [to Be Used with Eq. (4-43)]

Column End Conditions	Theoretical Value	Conservative Value	Recommended Value*
Fixed-free	$\frac{1}{4}$	$\frac{1}{4}$	$\frac{1}{4}$
Rounded-rounded	1	1	1
Fixed-rounded	2	1	1.2
Fixed-fixed	4	1	1.2

*To be used only with liberal factors of safety when the column load is accurately known.

Figure 4-19

Euler curve plotted using Eq. (4-43) with $C = 1$.



compression member. Thus it would appear that any compression member having an l/k value less than $(l/k)_Q$ should be treated as a pure compression member while all others are to be treated as Euler columns. Unfortunately, this is not true.

In the actual design of a member that functions as a column, the designer will be aware of the end conditions shown in Fig. 4-18, and will endeavor to configure the ends, using bolts, welds, or pins, for example, so as to achieve the required ideal end conditions. In spite of these precautions, the result, following manufacture, is likely to contain defects such as initial crookedness or load eccentricities. The existence of such defects and the methods of accounting for them will usually involve a factor-of-safety approach or a stochastic analysis. These methods work well for long columns and for simple compression members. However, tests show numerous failures for columns with slenderness ratios below and in the vicinity of point Q , as shown in the shaded area in Fig. 4-19. These have been reported as occurring even when near-perfect geometric specimens were used in the testing procedure.

A column failure is always sudden, total, unexpected, and hence dangerous. There is no advance warning. A beam will bend and give visual warning that it is overloaded, but not so for a column. For this reason neither simple compression methods nor the Euler column equation should be used when the slenderness ratio is near $(l/k)_Q$. Then what should we do? The usual approach is to choose some point T on the Euler curve of Fig. 4-19. If the slenderness ratio is specified as $(l/k)_1$ corresponding to point T , then use the Euler equation only when the actual slenderness ratio is

greater than $(l/k)_1$. Otherwise, use one of the methods in the sections that follow. See Examples 4–17 and 4–18.

Most designers select point T such that $P_{\text{cr}}/A = S_y/2$. Using Eq. (4–43), we find the corresponding value of $(l/k)_1$ to be

$$\left(\frac{l}{k}\right)_1 = \left(\frac{2\pi^2 CE}{S_y}\right)^{1/2} \quad (4-45)$$

4-13 Intermediate-Length Columns with Central Loading

Over the years there have been a number of column formulas proposed and used for the range of l/k values for which the Euler formula is not suitable. Many of these are based on the use of a single material; others, on a so-called safe unit load rather than the critical value. Most of these formulas are based on the use of a linear relationship between the slenderness ratio and the unit load. The *parabolic* or *J. B. Johnson formula* now seems to be the preferred one among designers in the machine, automotive, aircraft, and structural-steel construction fields.

The general form of the parabolic formula is

$$\frac{P_{\text{cr}}}{A} = a - b \left(\frac{l}{k}\right)^2 \quad (a)$$

where a and b are constants that are evaluated by fitting a parabola to the Euler curve of Fig. 4–19 as shown by the dashed line ending at T . If the parabola is begun at S_y , then $a = S_y$. If point T is selected as previously noted, then Eq. (4–42) gives the value of $(l/k)_1$ and the constant b is found to be

$$b = \left(\frac{S_y}{2\pi}\right)^2 \frac{1}{CE} \quad (b)$$

Upon substituting the known values of a and b into Eq. (a), we obtain, for the parabolic equation,

$$\frac{P_{\text{cr}}}{A} = S_y - \left(\frac{S_y}{2\pi} \frac{l}{k}\right)^2 \frac{1}{CE} \quad \frac{l}{k} \leq \left(\frac{l}{k}\right)_1 \quad (4-46)$$

4-14 Columns with Eccentric Loading

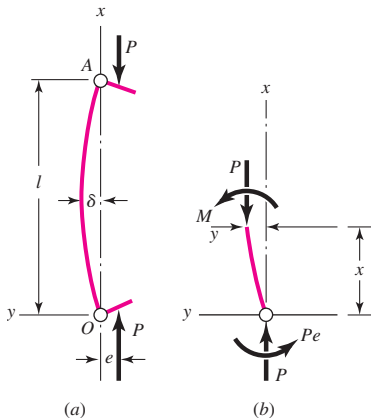
We have noted before that deviations from an ideal column, such as load eccentricities or crookedness, are likely to occur during manufacture and assembly. Though these deviations are often quite small, it is still convenient to have a method of dealing with them. Frequently, too, problems occur in which load eccentricities are unavoidable.

Figure 4–20a shows a column in which the line of action of the column forces is separated from the centroidal axis of the column by the eccentricity e . From Fig. 4–20b, $M = -P(e + y)$. Substituting this into Eq. (4–12), $d^2y/dx^2 = M/EI$, results in the differential equation

$$\frac{d^2y}{dx^2} + \frac{P}{EI}y = -\frac{Pe}{EI} \quad (a)$$

Figure 4-20

Notation for an eccentrically loaded column.



The solution of Eq. (a), for the boundary conditions that $y = 0$ at $x = 0, l$ is

$$y = e \left[\tan \left(\frac{l}{2} \sqrt{\frac{P}{EI}} \right) \sin \left(\sqrt{\frac{P}{EI}} x \right) + \cos \left(\sqrt{\frac{P}{EI}} x \right) - 1 \right] \quad (b)$$

By substituting $x = l/2$ in Eq. (b) and using a trigonometric identity, we obtain

$$\delta = e \left[\sec \left(\sqrt{\frac{P}{EI}} \frac{l}{2} \right) - 1 \right] \quad (4-47)$$

The magnitude of the maximum bending moment also occurs at midspan and is

$$M_{\max} = P(e + \delta) = Pe \sec \left(\frac{l}{2} \sqrt{\frac{P}{EI}} \right) \quad (4-48)$$

The magnitude of the maximum *compressive* stress at midspan is found by superposing the axial component and the bending component. This gives

$$\sigma_c = \frac{P}{A} + \frac{Mc}{I} = \frac{P}{A} + \frac{Mc}{Ak^2} \quad (c)$$

Substituting M_{\max} from Eq. (4-48) yields

$$\sigma_c = \frac{P}{A} \left[1 + \frac{ec}{k^2} \sec \left(\frac{l}{2k} \sqrt{\frac{P}{EA}} \right) \right] \quad (4-49)$$

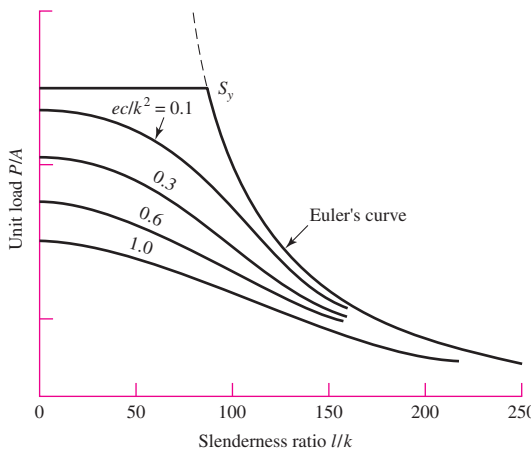
By imposing the compressive yield strength S_{yc} as the maximum value of σ_c , we can write Eq. (4-49) in the form

$$\frac{P}{A} = \frac{S_{yc}}{1 + (ec/k^2) \sec[(l/2k)\sqrt{P/AE}]} \quad (4-50)$$

This is called the *secant column formula*. The term ec/k^2 is called the *eccentricity ratio*. Figure 4-21 is a plot of Eq. (4-50) for a steel having a compressive (and tensile)

Figure 4-21

Comparison of secant and Euler equations for steel with $S_y = 40$ kpsi.



yield strength of 40 kpsi. Note how the P/A contours asymptotically approach the Euler curve as l/k increases.

Equation (4-50) cannot be solved explicitly for the load P . Design charts, in the fashion of Fig. 4-21, can be prepared for a single material if much column design is to be done. Otherwise, a root-finding technique using numerical methods must be used.

EXAMPLE 4-16

Develop specific Euler equations for the sizes of columns having

- Round cross sections
- Rectangular cross sections

Solution

(a) Using $A = \pi d^2/4$ and $k = \sqrt{I/A} = [(\pi d^4/64)/(\pi d^2/4)]^{1/2} = d/4$ with Eq. (4-44) gives

Answer

$$d = \left(\frac{64P_{\text{cr}}l^2}{\pi^3 CE} \right)^{1/4} \quad (4-51)$$

(b) For the rectangular column, we specify a cross section $h \times b$ with the restriction that $h \leq b$. If the end conditions are the same for buckling in both directions, then buckling will occur in the direction of the least thickness. Therefore

$$I = \frac{bh^3}{12} \quad A = bh \quad k^2 = I/A = \frac{h^2}{12}$$

Substituting these in Eq. (4-44) gives

Answer

$$b = \frac{12P_{\text{cr}}l^2}{\pi^2 CEh^3} \quad h \leq b \quad (4-52)$$

Note, however, that rectangular columns do not generally have the same end conditions in both directions.

EXAMPLE 4-17

Specify the diameter of a round column 1.5 m long that is to carry a maximum load estimated to be 22 kN. Use a design factor $n_d = 4$ and consider the ends as pinned (rounded). The column material selected has a minimum yield strength of 500 MPa and a modulus of elasticity of 207 GPa.

Solution

We shall design the column for a critical load of

$$P_{\text{cr}} = n_d P = 4(22) = 88 \text{ kN}$$

Then, using Eq. (4-51) with $C = 1$ (see Table 4-2) gives

$$d = \left(\frac{64P_{\text{cr}}l^2}{\pi^3 CE} \right)^{1/4} = \left[\frac{64(88)(1.5)^2}{\pi^3(1)(207)} \right]^{1/4} \left(\frac{10^3}{10^9} \right)^{1/4} (10^3) = 37.48 \text{ mm}$$

Table A-17 shows that the preferred size is 40 mm. The slenderness ratio for this size is

$$\frac{l}{k} = \frac{l}{d/4} = \frac{1.5(10^3)}{40/4} = 150$$

To be sure that this is an Euler column, we use Eq. (5-51) and obtain

$$\left(\frac{l}{k} \right)_1 = \left(\frac{2\pi^2 CE}{S_y} \right)^{1/2} = \left[\frac{2\pi^2(1)(207)}{500} \right]^{1/2} \left(\frac{10^9}{10^6} \right)^{1/2} = 90.4$$

which indicates that it is indeed an Euler column. So select

Answer

$$d = 40 \text{ mm}$$

EXAMPLE 4-18

Repeat Ex. 4-16 for J. B. Johnson columns.

Solution

(a) For round columns, Eq. (4-46) yields

$$\text{Answer} \quad d = 2 \left(\frac{P_{\text{cr}}}{\pi S_y} + \frac{S_y l^2}{\pi^2 C E} \right)^{1/2} \quad (4-53)$$

(b) For a rectangular section with dimensions $h \leq b$, we find

$$\text{Answer} \quad b = \frac{P_{\text{cr}}}{h S_y \left(1 - \frac{3l^2 S_y}{\pi^2 C E h^2} \right)} \quad h \leq b \quad (4-54)$$

EXAMPLE 4-19

Choose a set of dimensions for a rectangular link that is to carry a maximum compressive load of 5000 lbf. The material selected has a minimum yield strength of 75 ksi and a modulus of elasticity $E = 30$ Mpsi. Use a design factor of 4 and an end condition constant $C = 1$ for buckling in the weakest direction, and design for (a) a length of 15 in, and (b) a length of 8 in with a minimum thickness of $\frac{1}{2}$ in.

Solution

(a) Using Eq. (4–44), we find the limiting slenderness ratio to be

$$\left(\frac{l}{k}\right)_1 = \left(\frac{2\pi^2 CE}{S_y}\right)^{1/2} = \left[\frac{2\pi^2(1)(30)(10^6)}{75(10)^3}\right]^{1/2} = 88.9$$

By using $P_{cr} = n_d P = 4(5000) = 20000$ lbf, Eqs. (4–52) and (4–54) are solved, using various values of h , to form Table 4–3. The table shows that a cross section of $\frac{5}{8}$ by $\frac{3}{4}$ in, which is marginally suitable, gives the least area.

(b) An approach similar to that in part (a) is used with $l = 8$ in. All trial computations are found to be in the J. B. Johnson region of l/k values. A minimum area occurs when the section is a near square. Thus a cross section of $\frac{1}{2}$ by $\frac{3}{4}$ in is found to be suitable and safe.

Table 4–3

Table Generated to Solve
Ex. 4–19, part (a)

	<i>h</i>	<i>b</i>	<i>A</i>	<i>l/k</i>	Type	Eq. No.
	0.375	3.46	1.298	139	Euler	(4–52)
	0.500	1.46	0.730	104	Euler	(4–52)
	0.625	0.76	0.475	83	Johnson	(4–54)
	0.5625	1.03	0.579	92	Euler	(4–52)

4–15**Struts or Short Compression Members**

A short bar loaded in pure compression by a force P acting along the centroidal axis will shorten in accordance with Hooke's law, until the stress reaches the elastic limit of the material. At this point, permanent set is introduced and usefulness as a machine member may be at an end. If the force P is increased still more, the material either becomes "barrel-like" or fractures. When there is eccentricity in the loading, the elastic limit is encountered at smaller loads.

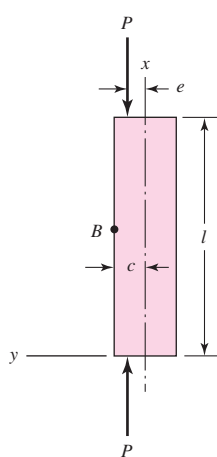
A *strut* is a *short compression member* such as the one shown in Fig. 4–22. The magnitude of the maximum compressive stress in the x direction at point B in an intermediate section is the sum of a simple component P/A and a flexural component Mc/I ; that is,

$$\sigma_c = \frac{P}{A} + \frac{Mc}{I} = \frac{P}{A} + \frac{PecA}{IA} = \frac{P}{A} \left(1 + \frac{ec}{k^2}\right) \quad (4-55)$$

where $k = (I/A)^{1/2}$ and is the radius of gyration, c is the coordinate of point B , and e is the eccentricity of loading.

Note that the length of the strut does not appear in Eq. (4–55). In order to use the equation for design or analysis, we ought, therefore, to know the range of lengths for which the equation is valid. In other words, how long is a short member?

The difference between the secant formula Eq. (4–50) and Eq. (4–55) is that the secant equation, unlike Eq. (4–55), accounts for an increased bending moment due to bending deflection. Thus the secant equation shows the eccentricity to be magnified by the bending deflection. This difference between the two formulas suggests that one way

**Figure 4–22**

Eccentrically loaded strut.

of differentiating between a “secant column” and a strut, or short compression member, is to say that in a strut, the effect of bending deflection must be limited to a certain small percentage of the eccentricity. If we decide that the limiting percentage is to be 1 percent of e , then, from Eq. (4–44), the limiting slenderness ratio turns out to be

$$\left(\frac{l}{k}\right)_2 = 0.282 \left(\frac{AE}{P}\right)^{1/2} \quad (4-56)$$

This equation then gives the limiting slenderness ratio for using Eq. (4–55). If the actual slenderness ratio is greater than $(l/k)_2$, then use the secant formula; otherwise, use Eq. (4–55).

EXAMPLE 4-20

Figure 4–23a shows a workpiece clamped to a milling machine table by a bolt tightened to a tension of 2000 lbf. The clamp contact is offset from the centroidal axis of the strut by a distance $e = 0.10$ in, as shown in part b of the figure. The strut, or block, is steel, 1 in square and 4 in long, as shown. Determine the maximum compressive stress in the block.

Solution

First we find $A = bh = 1(1) = 1$ in 2 , $I = bh^3/12 = 1(1)^3/12 = 0.0833$ in 4 , $k^2 = I/A = 0.0833/1 = 0.0833$ in 2 , and $l/k = 4/(0.0833)^{1/2} = 13.9$. Equation (4–56) gives the limiting slenderness ratio as

$$\left(\frac{l}{k}\right)_2 = 0.282 \left(\frac{AE}{P}\right)^{1/2} = 0.282 \left[\frac{1(30)(10^6)}{1000}\right]^{1/2} = 48.8$$

Thus the block could be as long as

$$l = 48.8k = 48.8(0.0833)^{1/2} = 14.1 \text{ in}$$

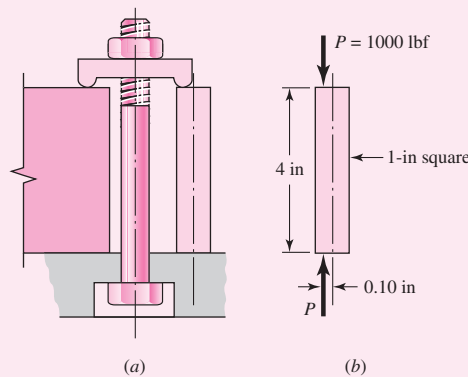
before it need be treated by using the secant formula. So Eq. (4–55) applies and the maximum compressive stress is

Answer

$$\sigma_c = \frac{P}{A} \left(1 + \frac{ec}{k^2}\right) = \frac{1000}{1} \left[1 + \frac{0.1(0.5)}{0.0833}\right] = 1600 \text{ psi}$$

Figure 4-23

A strut that is part of a workpiece clamping assembly.



4-16 Elastic Stability

Section 4-12 presented the conditions for the unstable behavior of long, slender columns. *Elastic instability* can also occur in structural members other than columns. *Compressive loads/stresses within any long, thin structure can cause structural instabilities* (buckling). The compressive stress may be elastic or inelastic and the instability may be global or local. Global instabilities can cause *catastrophic* failure, whereas local instabilities may cause permanent deformation and function failure but not a catastrophic failure. The buckling discussed in Sec. 4-12 was global instability. However, consider a wide flange beam in bending. One flange will be in compression, and if thin enough, can develop localized buckling in a region where the bending moment is a maximum. Localized buckling can also occur in the web of the beam, where transverse shear stresses are present at the beam centroid. Recall, for the case of pure shear stress τ , a stress transformation will show that at 45° , a compressive stress of $\sigma = -\tau$ exists. If the web is sufficiently thin where the shear force V is a maximum, localized buckling of the web can occur. For this reason, additional support in the form of bracing is typically applied at locations of high shear forces.¹⁰

Thin-walled beams in bending can buckle in a torsional mode as illustrated in Fig. 4-24. Here a cantilever beam is loaded with a lateral force, F . As F increases from zero, the end of the beam will deflect in the negative y direction normally according to the bending equation, $y = -FL^3/(3EI)$. However, if the beam is long enough and the ratio of b/h is sufficiently small, there is a critical value of F for which the beam will collapse in a twisting mode as shown. This is due to the *compression* in the bottom fibers of the beam which cause the fibers to buckle sideways (z direction).

There are a great many other examples of unstable structural behavior, such as thin-walled pressure vessels in compression or with outer pressure or inner vacuum, thin-walled open or closed members in torsion, thin arches in compression, frames in compression, and shear panels. Because of the vast array of applications and the complexity of their analyses, further elaboration is beyond the scope of this book. The intent of this section is to make the reader aware of the possibilities and potential safety issues. The key issue is that the designer should be aware that if any *unbraced* part of a structural member is *thin*, and/or *long*, and in *compression* (directly or *indirectly*), the possibility of buckling should be investigated.¹¹

For unique applications, the designer may need to revert to a numerical solution such as using finite elements. Depending on the application and the finite-element code available, an analysis can be performed to determine the critical loading (see Fig. 4-25).

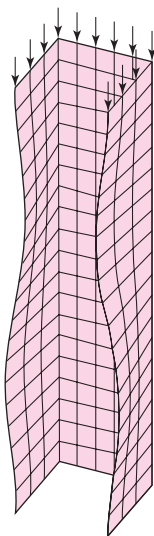


Figure 4-24

Torsional buckling of a thin-walled beam in bending.

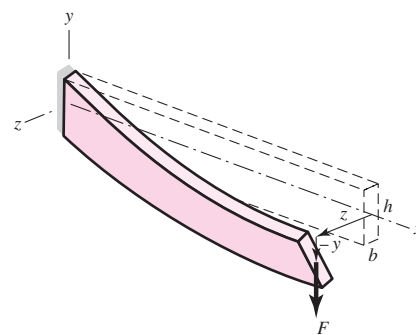


Figure 4-25

Finite-element representation of flange buckling of a channel in compression.

¹⁰See C. G. Salmon, J. E. Johnson, and F. A. Malhas, *Steel Structures: Design and Behavior*, 5th ed., Prentice Hall, Upper Saddle River, NJ, 2009.

¹¹See S. P. Timoshenko and J. M. Gere, *Theory of Elastic Stability*, 2nd ed., McGraw-Hill, New York, 1961. See also, Z. P. Bazant and L. Cedolin, *Stability of Structures*, Oxford University Press, New York, 1991.

4-17 Shock and Impact

Impact refers to the collision of two masses with initial relative velocity. In some cases it is desirable to achieve a known impact in design; for example, this is the case in the design of coining, stamping, and forming presses. In other cases, impact occurs because of excessive deflections, or because of clearances between parts, and in these cases it is desirable to minimize the effects. The rattling of mating gear teeth in their tooth spaces is an impact problem caused by shaft deflection and the clearance between the teeth. This impact causes gear noise and fatigue failure of the tooth surfaces. The clearance space between a cam and follower or between a journal and its bearing may result in crossover impact and also cause excessive noise and rapid fatigue failure.

Shock is a more general term that is used to describe any suddenly applied force or disturbance. Thus the study of shock includes impact as a special case.

Figure 4-26 represents a highly simplified mathematical model of an automobile in collision with a rigid obstruction. Here m_1 is the lumped mass of the engine. The displacement, velocity, and acceleration are described by the coordinate x_1 and its time derivatives. The lumped mass of the vehicle less the engine is denoted by m_2 , and its motion by the coordinate x_2 and its derivatives. Springs k_1 , k_2 , and k_3 represent the linear and nonlinear stiffnesses of the various structural elements that compose the vehicle. Friction and damping can and should be included, but is not shown in this model. The determination of the spring rates for such a complex structure will almost certainly have to be performed experimentally. Once these values—the k 's, m 's, damping and frictional coefficients—are obtained, a set of nonlinear differential equations can be written and a computer solution obtained for any impact velocity. For sake of illustration, assuming the springs to be linear, isolate each mass and write their equations of motion. This results in

$$\begin{aligned} m\ddot{x}_1 + k_1x_1 + k_2(x_1 - x_2) &= 0 \\ m\ddot{x}_2 + k_3x_2 - k_2(x_1 - x_2) &= 0 \end{aligned} \quad (4-57)$$

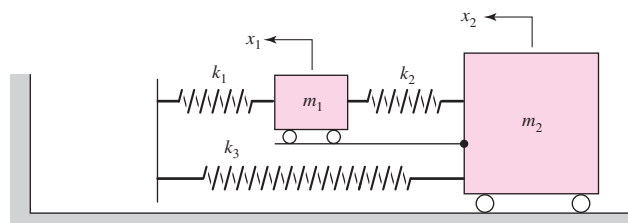
The analytical solution of the Eq. (4-57) pair is harmonic and is studied in a course on mechanical vibrations.¹² If the values of the m 's and k 's are known, the solution can be obtained easily using a program such as MATLAB.

Suddenly Applied Loading

A simple case of impact is illustrated in Fig. 4-27a. Here a weight W falls a distance h and impacts a cantilever of stiffness EI and length l . We want to find the maximum deflection and the maximum force exerted on the beam due to the impact.

Figure 4-26

Two-degree-of-freedom mathematical model of an automobile in collision with a rigid obstruction.



¹²See William T. Thomson and Marie Dillon Dahleh, *Theory of Vibrations with Applications*, 5th ed., Prentice Hall, Upper Saddle River, NJ, 1998.

Figure 4-27

(a) A weight free to fall a distance h to free end of a beam. (b) Equivalent spring model.

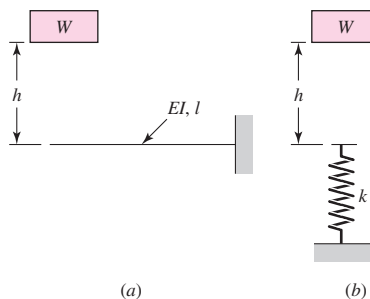


Figure 4–27b shows an abstract model of the system considering the beam as a simple spring. For beam 1 of Table A–9, we find the spring rate to be $k = F/y = 3EI/l^3$. The beam mass and damping can be accounted for, but for this example will be considered negligible. If the beam is considered massless, there is no momentum transfer, only energy. If the maximum deflection of the spring (beam) is considered to be δ , the drop of the weight is $h + \delta$, and the loss of potential energy is $W(h + \delta)$. The resulting increase in potential (strain) energy of the spring is $\frac{1}{2}k\delta^2$. Thus, for energy conservation, $\frac{1}{2}k\delta^2 = W(h + \delta)$. Rearranging this gives

$$\delta^2 - 2\frac{W}{k}\delta - 2\frac{W}{k}h = 0 \quad (a)$$

Solving for δ yields

$$\delta = \frac{W}{k} \pm \frac{W}{k} \left(1 + \frac{2hk}{W} \right)^{1/2} \quad (b)$$

The negative solution is possible only if the weight “sticks” to the beam and vibrates between the limits of Eq. (b). Thus, the maximum deflection is

$$\delta = \frac{W}{k} + \frac{W}{k} \left(1 + \frac{2hk}{W} \right)^{1/2} \quad (4-58)$$

The maximum force acting on the beam is now found to be

$$F = k\delta = W + W \left(1 + \frac{2hk}{W} \right)^{1/2} \quad (4-59)$$

Note, in this equation, that if $h = 0$, then $F = 2W$. This says that when the weight is released while in contact with the spring but is not exerting any force on the spring, the largest force is double the weight.

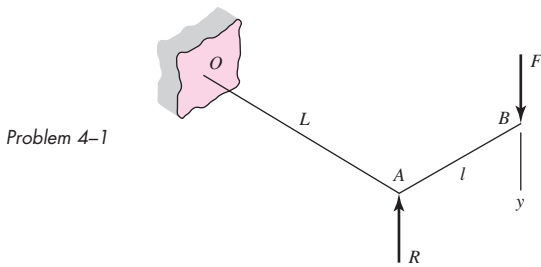
Most systems are not as ideal as those explored here, so be wary about using these relations for nonideal systems.

PROBLEMS

Problems marked with an asterisk (*) are linked to problems in other chapters, as summarized in Table 1–1 of Sec. 1–16, p. 24.

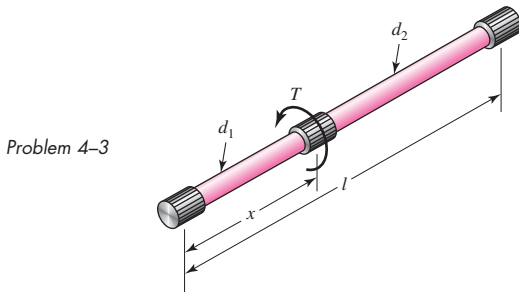
4-1

The figure shows a torsion bar OA fixed at O , simply supported at A , and connected to a cantilever AB . The spring rate of the torsion bar is k_T , in newton-meters per radian, and that of the cantilever is k_l , in newtons per meter. What is the overall spring rate based on the deflection y at point B ?



- 4-2** For Prob. 4-1, if the simple support at point A were eliminated and the cantilever spring rate of OA is given by k_L , determine the overall spring rate of the bar based on the deflection of point B.

- 4-3** A torsion-bar spring consists of a prismatic bar, usually of round cross section, that is twisted at one end and held fast at the other to form a stiff spring. An engineer needs a stiffer one than usual and so considers building in both ends and applying the torque somewhere in the central portion of the span, as shown in the figure. This effectively creates two springs in parallel. If the bar is uniform in diameter, that is, if $d = d_1 = d_2$, (a) determine how the spring rate and the end reactions depend on the location x at which the torque is applied, (b) determine the spring rate, the end reactions, and the maximum shear stress, if $d = 0.5$ in, $x = 5$ in, $l = 10$ in, $T = 1500$ lbf · in, and $G = 11.5$ Mpsi.



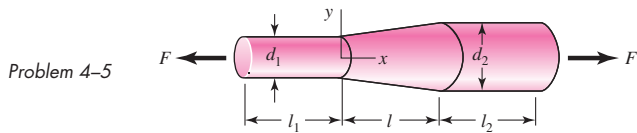
- 4-4** An engineer is forced by geometric considerations to apply the torque on the spring of Prob. 4-3 at the location $x = 0.4l$. For a uniform-diameter spring, this would cause one leg of the span to be underutilized when both legs have the same diameter. For optimal design the diameter of each leg should be designed such that the maximum shear stress in each leg is the same. This problem is to redesign the spring of part (b) of Prob. 4-3. Using $x = 0.4l$, $l = 10$ in, $T = 1500$ lbf · in, and $G = 11.5$ Mpsi, design the spring such that the maximum shear stresses in each leg are equal and the spring has the same spring rate (angle of twist) as part (b) of Prob. 4-3. Specify d_1 , d_2 , the spring rate k , and the torque and the maximum shear stress in each leg.

- 4-5** A bar in tension has a circular cross section and includes a tapered portion of length l , as shown.

(a) For the tapered portion, use Eq. (4-3) in the form of $\delta = \int_0^l [F/(AE)] dx$ to show that

$$\delta = \frac{4}{\pi} \frac{Fl}{d_1 d_2 E}$$

(b) Determine the elongation of each portion if $d_1 = 0.5$ in, $d_2 = 0.75$ in, $l = l_1 = l_2 = 2.0$ in, $E = 30$ Mpsi, and $F = 1000$ lbf.

**4-6**

Instead of a tensile force, consider the bar in Prob. 4-5 to be loaded by a torque T .

- (a) Use Eq. (4-5) in the form of $\theta = \int_0^l [T/(GJ)] dx$ to show that the angle of twist of the tapered portion is

$$\theta = \frac{32}{3\pi} \frac{Tl(d_1^2 + d_1d_2 + d_2^2)}{Gd_1^3d_2^3}$$

- (b) Using the same geometry as in Prob. 4-5b with $T = 1500$ lbf · in and $G = 11.5$ Mpsi, determine the angle of twist in degrees for each portion.

4-7

When a vertically suspended hoisting cable is long, the weight of the cable itself contributes to the elongation. If a 500-ft steel cable has an effective diameter of 0.5 in and lifts a load of 5000 lbf, determine the total elongation and the percent of the total elongation due to the cable's own weight.

4-8

Derive the equations given for beam 2 in Table A-9 using statics and the double-integration method.

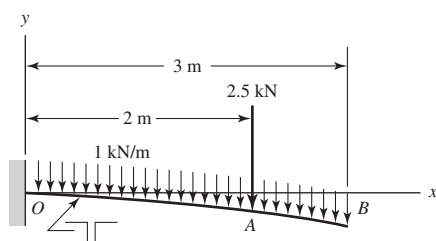
4-9

Derive the equations given for beam 5 in Table A-9 using statics and the double-integration method.

4-10

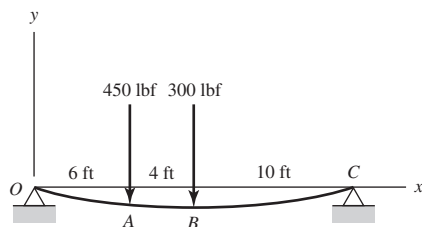
The figure shows a cantilever consisting of steel angles size $100 \times 100 \times 12$ mm mounted back to back. Using superposition, find the deflection at B and the maximum stress in the beam.

Problem 4-10

**4-11**

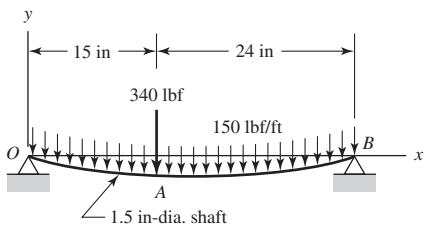
A simply supported beam loaded by two forces is shown in the figure. Select a pair of structural steel channels mounted back to back to support the loads in such a way that the deflection at midspan will not exceed $\frac{1}{2}$ in and the maximum stress will not exceed 15 kpsi. Use superposition.

Problem 4-11



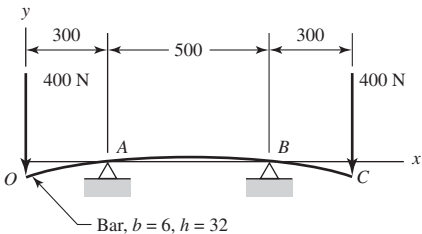
- 4-12** Using superposition, find the deflection of the steel shaft at *A* in the figure. Find the deflection at midspan. By what percentage do these two values differ?

Problem 4-12
Dimensions in inches.



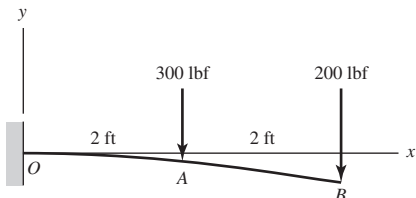
- 4-13** A rectangular steel bar supports the two overhanging loads shown in the figure. Using superposition, find the deflection at the ends and at the center.

Problem 4-13
Dimensions in millimeters.



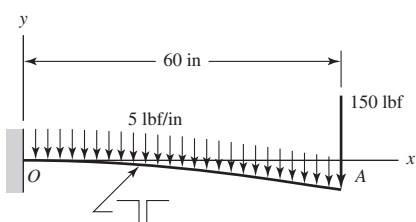
- 4-14** An aluminum tube with outside diameter of 2 in and inside diameter of 1.5 in is cantilevered and loaded as shown. Using the formulas in Appendix Table A-9 and superposition, find the deflection at *B*.

Problem 4-14



- 4-15** The cantilever shown in the figure consists of two structural-steel channels size 3 in, 5.0 lbf/in. Using superposition, find the deflection at *A*. Include the weight of the channels.

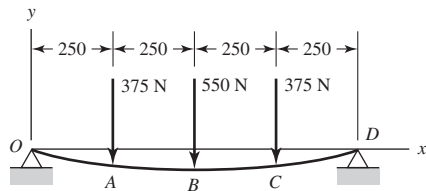
Problem 4-15



4-16

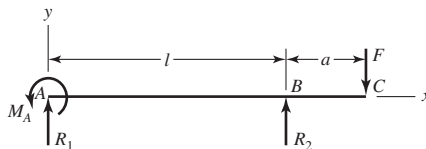
Using superposition for the bar shown, determine the minimum diameter of a steel shaft for which the maximum deflection is 2 mm.

Problem 4-16
Dimensions in millimeters.

**4-17**

A simply supported beam has a concentrated moment M_A applied at the left support and a concentrated force F applied at the free end of the overhang on the right. Using superposition, determine the deflection equations in regions AB and BC.

Problem 4-17

**4-18**

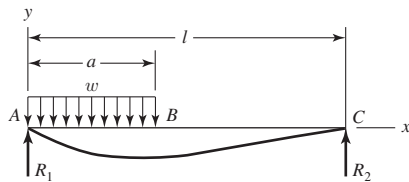
Calculating beam deflections using superposition is quite convenient provided you have a comprehensive table to refer to. Because of space limitations, this book provides a table that covers a great deal of applications, but not all possibilities. Take for example, Prob. 4-19, which follows this problem. Problem 4-19 is not directly solvable from Table A-9, but with the addition of the results of this problem, it is. For the beam shown, using statics and double integration, show that

$$R_1 = \frac{wa}{2l}(2l - a) \quad R_2 = \frac{wa^2}{2l} \quad V_{AB} = \frac{w}{2l}[2l(a - x) - a^2] \quad V_{BC} = -\frac{wa^2}{2l}$$

$$M_{AB} = \frac{wx}{2l}(2al - a^2 - lx) \quad M_{BC} = \frac{wa^2}{2l}(l - x)$$

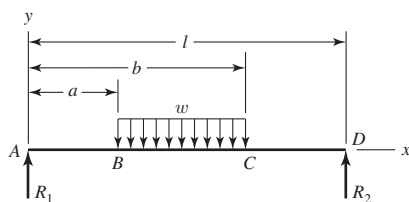
$$y_{AB} = \frac{wx}{24EI} [2ax^2(2l - a) - lx^3 - a^2(2l - a)^2] \quad y_{BC} = y_{AB} + \frac{w}{24EI}(x - a)^4$$

Problem 4-18

**4-19**

Using the results of Prob. 4-18, use superposition to determine the deflection equations for the three regions of the beam shown.

Problem 4-19

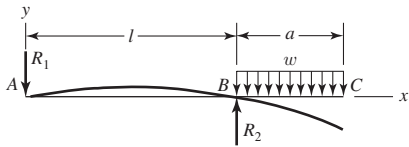


4-20

Like Prob. 4-18, this problem provides another beam to add to Table A-9. For the simply supported beam shown with an overhanging uniform load, use statics and double integration to show that

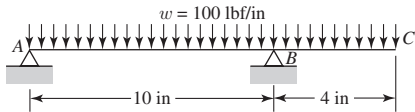
$$\begin{aligned} R_1 &= \frac{wa^2}{2l} & R_2 &= \frac{wa}{2l}(2l+a) & V_{AB} &= -\frac{wa^2}{2l} & V_{BC} &= w(l+a-x) \\ M_{AB} &= -\frac{wa^2}{2l}x & M_{BC} &= -\frac{w}{2}(l+a-x)^2 \\ y_{AB} &= \frac{wa^2x}{12EI} (l^2 - x^2) & y_{BC} &= -\frac{w}{24EI} [(l+a-x)^4 - 4a^2(l-x)(l+a) - a^4] \end{aligned}$$

Problem 4-20

**4-21**

Consider the uniformly loaded simply supported steel beam with an overhang as shown. The second-area moment of the beam is $I = 0.05 \text{ in}^4$. Use superposition (with Table A-9 and the results of Prob. 4-20) to determine the reactions and the deflection equations of the beam. Plot the deflections.

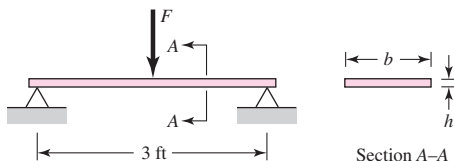
Problem 4-21

**4-22**

Illustrated is a rectangular steel bar with simple supports at the ends and loaded by a force F at the middle; the bar is to act as a spring. The ratio of the width to the thickness is to be about $b = 10h$, and the desired spring scale is 1800 lbf/in.

- (a) Find a set of cross-section dimensions, using preferred fractional sizes from Table A-17.
- (b) What deflection would cause a permanent set in the spring if this is estimated to occur at a normal stress of 60 ksi?

Problem 4-22

**4-23* to
4-28***

For the steel countershaft specified in the table, find the deflection and slope of the shaft at point A. Use superposition with the deflection equations in Table A-9. Assume the bearings constitute simple supports.

Problem Number	Problem, Page Number Defining Shaft
4-23*	3-68, 137
4-24*	3-69, 137
4-25*	3-70, 137
4-26*	3-71, 137
4-27*	3-72, 138
4-28*	3-73, 138

**4-29* to
4-34***

For the steel countershaft specified in the table, find the slope of the shaft at each bearing. Use superposition with the deflection equations in Table A-9. Assume the bearings constitute simple supports.

Problem Number	Problem, Page Number Defining Shaft
4-29*	3-68, 137
4-30*	3-69, 137
4-31*	3-70, 137
4-32*	3-71, 137
4-33*	3-72, 138
4-34*	3-73, 138

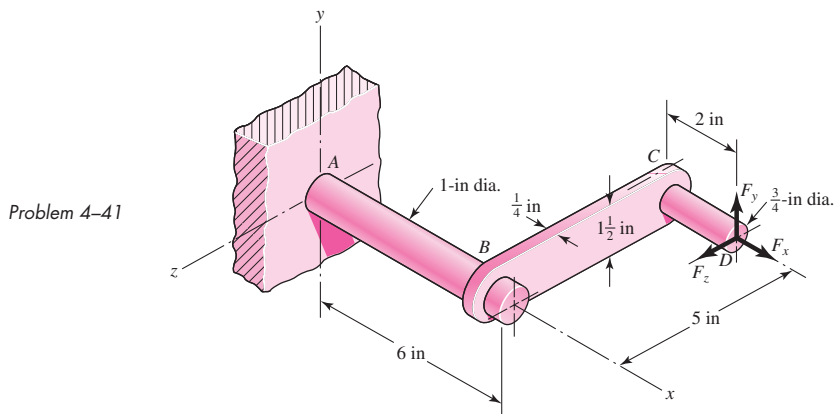
**4-35* to
4-40***

For the steel countershaft specified in the table, assume the bearings have a maximum slope specification of 0.06° for good bearing life. Determine the minimum shaft diameter.

Problem Number	Problem, Page Number Defining Shaft
4-35*	3-68, 137
4-36*	3-69, 137
4-37*	3-70, 137
4-38*	3-71, 137
4-39*	3-72, 138
4-40*	3-73, 138

4-41*

The cantilevered handle in the figure is made from mild steel that has been welded at the joints. For $F_y = 200 \text{ lbf}$, $F_x = F_z = 0$, determine the vertical deflection (along the y axis) at the tip. Use superposition. See the discussion on p. 102 for the twist in the rectangular cross section in section BC .

**4-42**

For the cantilevered handle in Prob. 4-41, let $F_x = -150$ lbf, $F_y = 0$ lbf, $F_z = -100$ lbf. Find the deflection at the tip along the x axis.

4-43*

The cantilevered handle in Prob. 3-84, p. 140, is made from mild steel. Let $F_y = 250$ lbf, $F_x = F_z = 0$. Determine the angle of twist in bar OC , ignoring the fillets but including the changes in diameter along the 13-in effective length. Compare the angle of twist if the bar OC is simplified to be all of uniform 1-in diameter. Use superposition to determine the vertical deflection (along the y axis) at the tip, using the simplified bar OC .

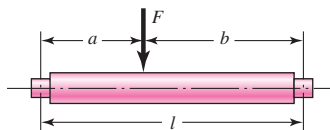
4-44

A flat-bed trailer is to be designed with a curvature such that when loaded to capacity the trailer bed is flat. The load capacity is to be 3000 lbf/ft between the axles, which are 25 ft apart, and the second-area moment of the steel structure of the bed is $I = 485 \text{ in}^4$. Determine the equation for the curvature of the unloaded bed and the maximum height of the bed relative to the axles.

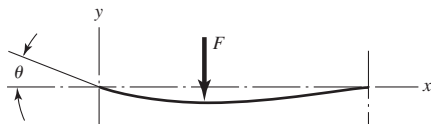
4-45

The designer of a shaft usually has a slope constraint imposed by the bearings used. This limit will be denoted as ξ . If the shaft shown in the figure is to have a uniform diameter d except in the locality of the bearing mounting, it can be approximated as a uniform beam with simple supports. Show that the minimum diameters to meet the slope constraints at the left and right bearings are, respectively,

$$d_L = \left| \frac{32Fb(l^2 - b^2)}{3\pi El\xi} \right|^{1/4} \quad d_R = \left| \frac{32Fa(l^2 - a^2)}{3\pi El\xi} \right|^{1/4}$$



Problem 4-45

**4-46**

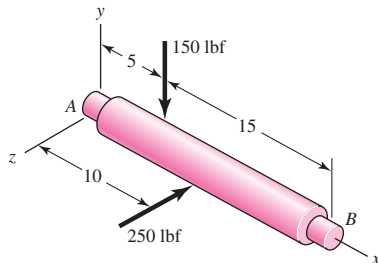
A steel shaft is to be designed so that it is supported by roller bearings. The basic geometry is shown in the figure from Prob. 4-45, with $l = 300$ mm, $a = 100$ mm, and $F = 3$ kN. The allowable slope at the bearings is 0.001 mm/mm without bearing life penalty. For a design factor

of 1.28, what uniform-diameter shaft will support the load without penalty? Determine the maximum deflection of the shaft.

4-47

If the diameter of the steel beam shown is 1.25 in, determine the deflection of the beam at $x = 8$ in.

Problem 4-47
Dimensions in inches.

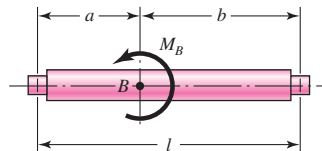
**4-48**

For the beam of Prob. 4-47, plot the *magnitude* of the displacement of the beam in 0.1-in increments. Approximate the maximum displacement and the value of x where it occurs.

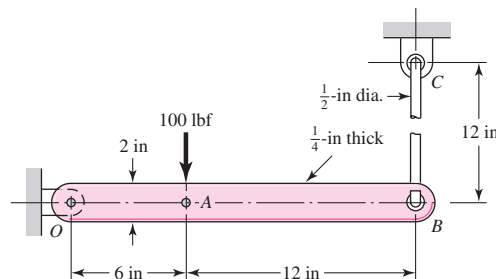
4-49

Shown in the figure is a uniform-diameter shaft with bearing shoulders at the ends; the shaft is subjected to a concentrated moment $M = 1000 \text{ lbf} \cdot \text{in}$. The shaft is of carbon steel and has $a = 4$ in and $l = 10$ in. The slope at the ends must be limited to 0.002 rad. Find a suitable diameter d .

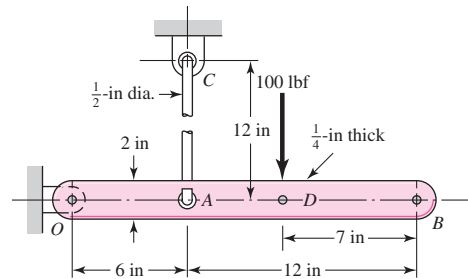
Problem 4-49

**4-50* and
4-51**

The figure shows a rectangular member OB, made from $\frac{1}{4}$ -in-thick aluminum plate, pinned to the ground at one end and supported by a $\frac{1}{2}$ -in-diameter round steel rod with hooks formed on the ends. A load of 100 lbf is applied as shown. Use superposition to determine the vertical deflection at point B.



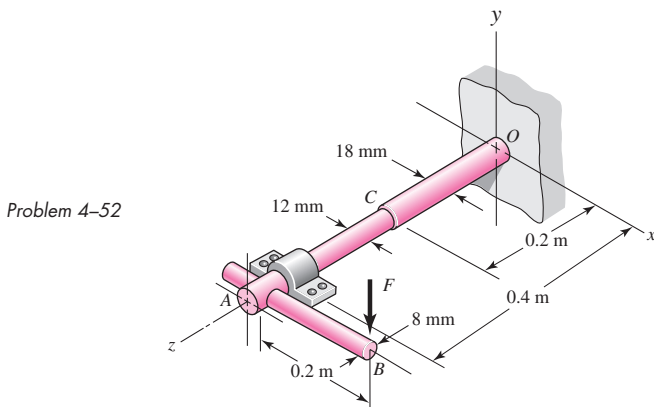
*Problem 4-50**



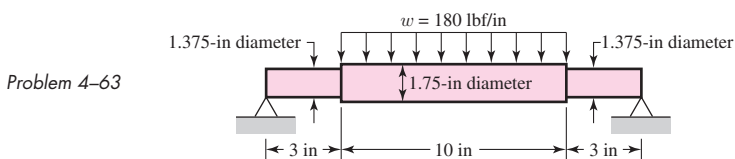
Problem 4-51

4-52

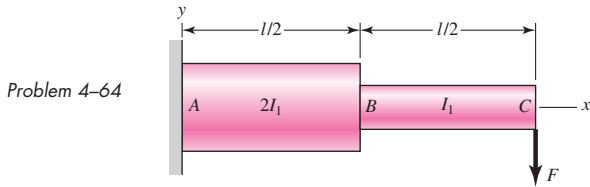
The figure illustrates a stepped torsion-bar spring OA with an actuating cantilever AB. Both parts are of carbon steel. Use superposition and find the spring rate k corresponding to a force F acting at B.



- 4-53** Consider the simply supported beam 5 with a center load in Appendix A-9. Determine the deflection equation if the stiffness of the left and right supports are k_1 and k_2 , respectively.
- 4-54** Consider the simply supported beam 10 with an overhanging load in Appendix A-9. Determine the deflection equation if the stiffness of the left and right supports are k_1 and k_2 , respectively.
- 4-55** Prove that for a uniform-cross-section beam with simple supports at the ends loaded by a single concentrated load, the location of the maximum deflection will never be outside the range of $0.423l \leq x \leq 0.577l$ regardless of the location of the load along the beam. The importance of this is that you can always get a quick estimate of y_{\max} by using $x = l/2$.
- 4-56** Solve Prob. 4-10 using singularity functions. Use statics to determine the reactions.
- 4-57** Solve Prob. 4-11 using singularity functions. Use statics to determine the reactions.
- 4-58** Solve Prob. 4-12 using singularity functions. Use statics to determine the reactions.
- 4-59** Solve Prob. 4-21 using singularity functions to determine the deflection equation of the beam. Use statics to determine the reactions.
- 4-60** Solve Prob. 4-13 using singularity functions. Since the beam is symmetric, only write the equation for half the beam and use the slope at the beam center as a boundary condition. Use statics to determine the reactions.
- 4-61** Solve Prob. 4-17 using singularity functions. Use statics to determine the reactions.
- 4-62** Solve Prob. 4-19 using singularity functions to determine the deflection equation of the beam. Use statics to determine the reactions.
- 4-63** Using singularity functions, write the deflection equation for the steel beam shown. Since the beam is symmetric, write the equation for only half the beam and use the slope at the beam center as a boundary condition. Plot your results and determine the maximum deflection.



- 4-64** Determine the deflection equation for the cantilever beam shown using singularity functions. Evaluate the deflections at B and C and compare your results with Example 4-10.



4-65 Use Castigliano's theorem to verify the maximum deflection for the uniformly loaded beam 7 of Appendix Table A-9. Neglect shear.

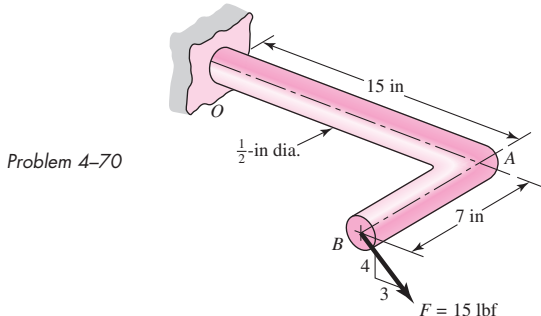
4-66 Use Castigliano's theorem to verify the maximum deflection for the uniformly loaded cantilever beam 3 of Appendix Table A-9. Neglect shear.

4-67 Solve Prob. 4-15 using Castigliano's theorem.

4-68 Solve Prob. 4-52 using Castigliano's theorem.

4-69 Determine the deflection at midspan for the beam of Prob. 4-63 using Castigliano's theorem.

4-70 Using Castigliano's theorem, determine the deflection of point B in the direction of the force F for the steel bar shown.



4-71* Solve Prob. 4-41 using Castigliano's theorem. Since Eq. (4-18) for torsional strain energy was derived from the angular displacement for circular cross sections, it is not applicable for section BC. You will need to obtain a new strain energy equation for the rectangular cross section from Eqs. (4-15) and (3-41).

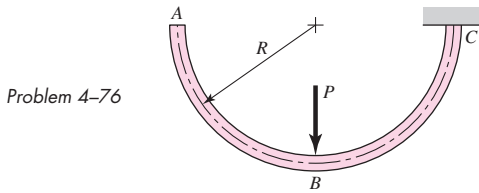
4-72 Solve Prob. 4-42 using Castigliano's theorem.

4-73* The cantilevered handle in Prob. 3-84 is made from mild steel. Let $F_y = 250$ lbf and $F_x = F_z = 0$. Using Castigliano's theorem, determine the vertical deflection (along the y axis) at the tip. Repeat the problem with shaft OC simplified to a uniform diameter of 1 in for its entire length. What is the percent error from this simplification?

4-74* Solve Prob. 4-50 using Castigliano's theorem.

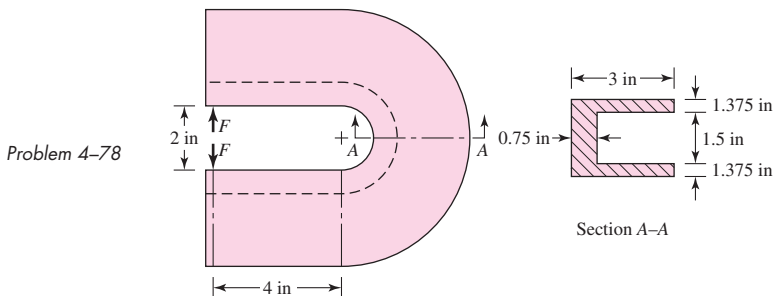
4-75 Solve Prob. 4-51 using Castigliano's theorem.

4-76 The steel curved bar shown has a rectangular cross section with a radial height $h = 6$ mm, and a thickness $b = 4$ mm. The radius of the centroidal axis is $R = 40$ mm. A force $P = 10$ N is applied as shown. Find the vertical deflection at B. Use Castigliano's method for a curved flexural member, and since $R/h < 10$, do not neglect any of the terms.

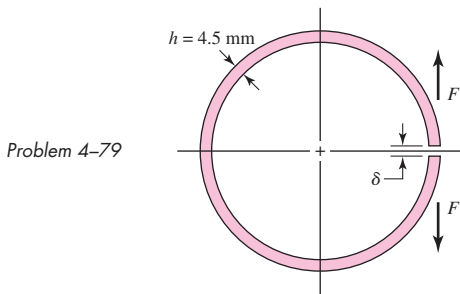


4-77 Repeat Prob. 4-76 to find the vertical deflection at A .

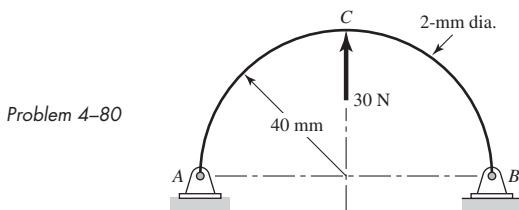
4-78 For the curved steel beam shown, $F = 6.7$ kips. Determine the relative deflection of the applied forces.



4-79 A steel piston ring has a mean diameter of 70 mm, a radial height $h = 4.5$ mm, and a thickness $b = 3$ mm. The ring is assembled using an expansion tool that separates the split ends a distance δ by applying a force F as shown. Use Castigiano's theorem and determine the force F needed to expand the split ends a distance $\delta = 1$ mm.

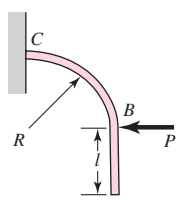


4-80 For the steel wire form shown, use Castigiano's method to determine the horizontal reaction forces at A and B and the deflection at C .

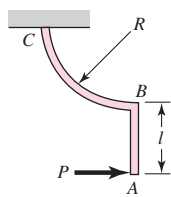


**4-81 and
4-82**

The part shown is formed from a $\frac{1}{8}$ -in diameter steel wire, with $R = 5$ in and $l = 4$ in. A force is applied with $P = 1$ lbf. Use Castigiano's method to estimate the horizontal deflection at point A. Justify any components of strain energy that you choose to neglect.



Problem 4-81



Problem 4-82

4-83

Repeat Prob. 4-81 for the vertical deflection at point A.

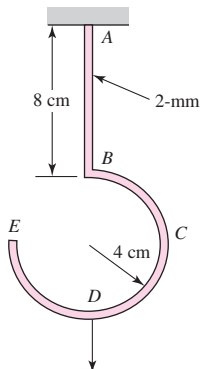
4-84

Repeat Prob. 4-82 for the vertical deflection at point A.

4-85

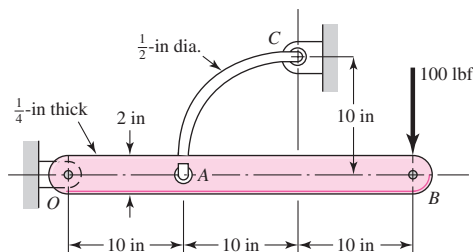
A hook is formed from a 2-mm-diameter steel wire and fixed firmly into the ceiling as shown. A 1-kg mass is hung from the hook at point D. Use Castigiano's theorem to determine the vertical deflection of point D.

Problem 4-85

**4-86**

The figure shows a rectangular member OB, made from $\frac{1}{4}$ -in-thick aluminum plate, pinned to the ground at one end, and supported by a $\frac{1}{2}$ -in-diameter round steel rod that is formed into an arc and pinned to the ground at C. A load of 100 lbf is applied at B. Use Castigiano's theorem to determine the vertical deflection at point B. Justify any choices to neglect any components of strain energy.

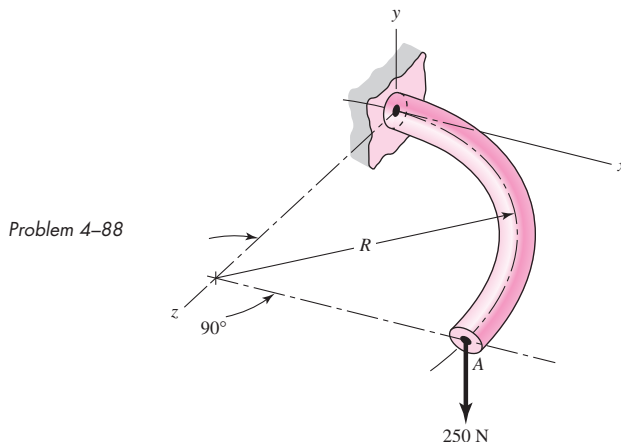
Problem 4-86

**4-87**

Repeat Prob. 4-86 for the vertical deflection at point A.

4-88

For the wire form shown, determine the deflection of point A in the y direction. Assume $R/h > 10$ and consider the effects of bending and torsion only. The wire is steel with $E = 200 \text{ GPa}$, $\nu = 0.29$, and has a diameter of 6 mm. Before application of the 250-N force the wire form is in the xz plane where the radius R is 80 mm.

**4-89**

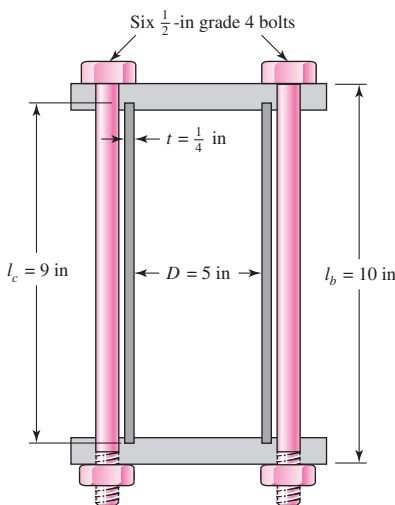
A 100-ft cable is made using a 12-gauge (0.1055-in) steel wire and three strands of 10-gauge (0.1019-in) copper wire. Find the deflection of the cable and the stress in each wire if the cable is subjected to a tension of 400 lbf.

4-90

The figure shows a steel pressure cylinder of diameter 5 in that uses six SAE grade 4 steel bolts having a grip of 10 in. These bolts have a proof strength (see Chap. 8) of 65 kpsi. Suppose the bolts are tightened to 75 percent of this strength.

(a) Find the tensile stress in the bolts and the compressive stress in the cylinder walls.

(b) Repeat part (a), but assume now that a fluid under a pressure of 500 psi is introduced into the cylinder.

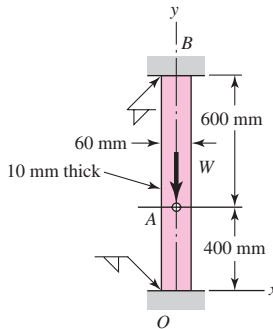
Problem 4-90**4-91**

A torsion bar of length L consists of a round core of stiffness $(GJ)_c$ and a shell of stiffness $(GJ)_s$. If a torque T is applied to this composite bar, what percentage of the total torque is carried by the shell?

4-92

A rectangular aluminum bar 10 mm thick and 60 mm wide is welded to fixed supports at the ends, and the bar supports a load $W = 4 \text{ kN}$, acting through a pin as shown. Find the reactions at the supports and the deflection of point A.

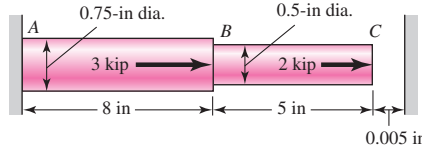
Problem 4-92

**4-93**

Solve Prob. 4-92 using Castiglano's method and procedure 1 from Sec. 4-10.

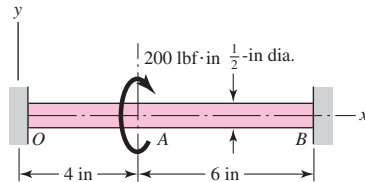
4-94

An aluminum step bar is loaded as shown. (a) Verify that end C deflects to the rigid wall, and (b) determine the wall reaction forces, the stresses in each member, and the deflection of B.

Problem 4-94
(Not drawn to scale)**4-95**

The steel shaft shown in the figure is subjected to a torque of 200 lbf · in applied at point A. Find the torque reactions at O and B; the angle of twist at A, in degrees; and the shear stress in sections OA and AB.

Problem 4-95

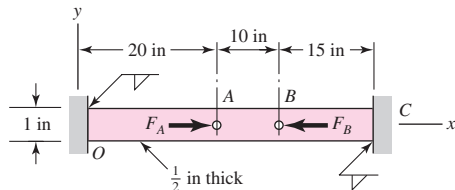
**4-96**

Repeat Prob. 4-95 with the diameters of section OA being 0.5 in and section AB being 0.75 in.

4-97

The figure shows a $\frac{1}{2}$ - by 1-in rectangular steel bar welded to fixed supports at each end. The bar is axially loaded by the forces $F_A = 12 \text{ kip}$ and $F_B = 6 \text{ kip}$ acting on pins at A and B. Assuming that the bar will not buckle laterally, find the reactions at the fixed supports, the stress in section AB, and the deflection of point A. Use procedure 1 from Sec. 4-10.

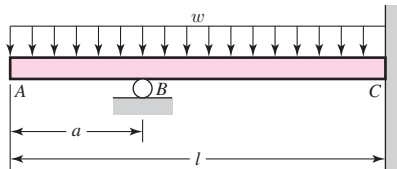
Problem 4-97



4-98

For the beam shown, determine the support reactions using superposition and procedure 1 from Sec. 4-10.

Problem 4-98
A C

**4-99**

Solve Prob. 4-98 using Castigliano's theorem and procedure 1 from Sec. 4-10.

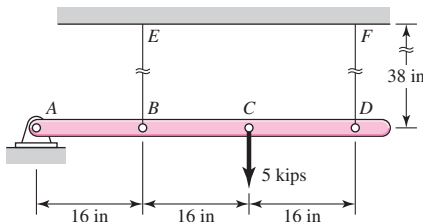
4-100

Consider beam 13 in Table A-9, but with flexible supports. Let $w = 500 \text{ lbf/ft}$, $l = 2 \text{ ft}$, $E = 30 \text{ Mpsi}$, and $I = 0.85 \text{ in}^4$. The support at the left end has a translational spring constant of $k_1 = 1.5(10^6) \text{ lbf/in}$ and a rotational spring constant of $k_2 = 2.5(10^6) \text{ lbf} \cdot \text{in}$. The right support has a translational spring constant of $k_3 = 2.0(10^6) \text{ lbf/in}$. Using procedure 2 of Sec. 4-10, determine the reactions at the supports and the deflection at the midpoint of the beam.

4-101

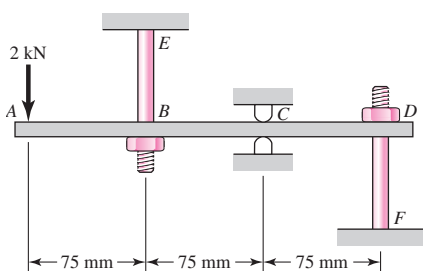
The steel beam $ABCD$ shown is simply supported at A and supported at B and D by steel cables, each having an effective diameter of 0.5 in. The second area moment of the beam is $I = 1.2 \text{ in}^4$. A force of 5 kips is applied at point C . Using procedure 2 of Sec. 4-10 determine the stresses in the cables and the deflections of B , C , and D .

Problem 4-101

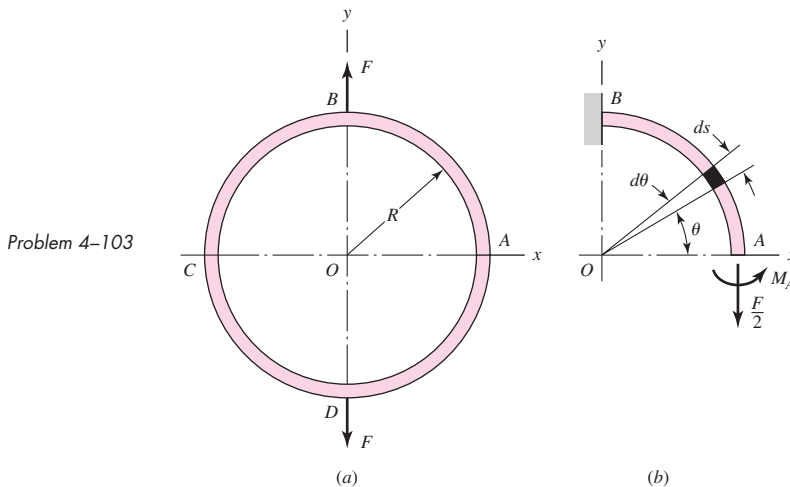
**4-102**

The steel beam $ABCD$ shown is supported at C as shown and supported at B and D by shoulder steel bolts, each having a diameter of 8 mm. The lengths of BE and DF are 50 mm and 65 mm, respectively. The beam has a second area moment of $21(10^3) \text{ mm}^4$. Prior to loading, the members are stress-free. A force of 2 kN is then applied at point A . Using procedure 2 of Sec. 4-10, determine the stresses in the bolts and the deflections of points A , B , and D .

Problem 4-102

**4-103**

A thin ring is loaded by two equal and opposite forces F in part a of the figure. A free-body diagram of one quadrant is shown in part b . This is a statically indeterminate problem, because the moment M_A cannot be found by statics. (a) Find the maximum bending moment in the ring due to the forces F , and (b) find the increase in the diameter of the ring along the y axis. Assume that the radius of the ring is large so that Eq. (4-41) can be used.

**4-104**

A round tubular column has outside and inside diameters of D and d , respectively, and a diametral ratio of $K = d/D$. Show that buckling will occur when the outside diameter is

$$D = \left[\frac{64P_{cr}l^2}{\pi^3 CE(1 - K^4)} \right]^{1/4}$$

4-105

For the conditions of Prob. 4-104, show that buckling according to the parabolic formula will occur when the outside diameter is

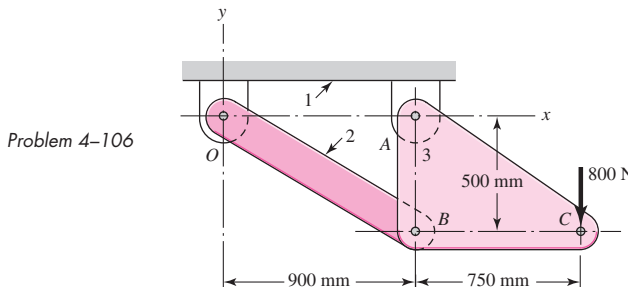
$$D = 2 \left[\frac{P_{cr}}{\pi S_y(1 - K^2)} + \frac{S_y l^2}{\pi^2 CE(1 + K^2)} \right]^{1/2}$$

4-106

Link 2, shown in the figure, is 25 mm wide, has 12-mm-diameter bearings at the ends, and is cut from low-carbon steel bar stock having a minimum yield strength of 165 MPa. The end-condition constants are $C = 1$ and $C = 1.2$ for buckling in and out of the plane of the drawing, respectively.

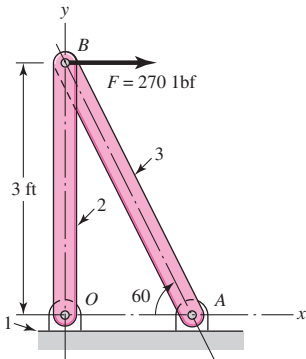
(a) Using a design factor $n_d = 4$, find a suitable thickness for the link.

(b) Are the bearing stresses at O and B of any significance?

**4-107**

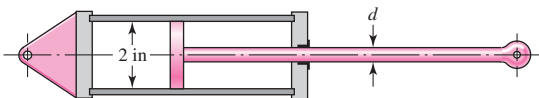
Link 3, shown schematically in the figure, acts as a brace to support the 270-lbf load. For buckling in the plane of the figure, the link may be regarded as pinned at both ends. For out-of-plane buckling, the ends are fixed. Select a suitable material and a method of manufacture, such as forging, casting, stamping, or machining, for casual applications of the brace in oil-field machinery. Specify the dimensions of the cross section as well as the ends so as to obtain a strong, safe, well-made, and economical brace.

Problem 4-107

**4-108**

The hydraulic cylinder shown in the figure has a 2-in bore and is to operate at a pressure of 1500 psi. With the clevis mount shown, the piston rod should be sized as a column with both ends rounded for any plane of buckling. The rod is to be made of forged AISI 1030 steel without further heat treatment.

Problem 4-108

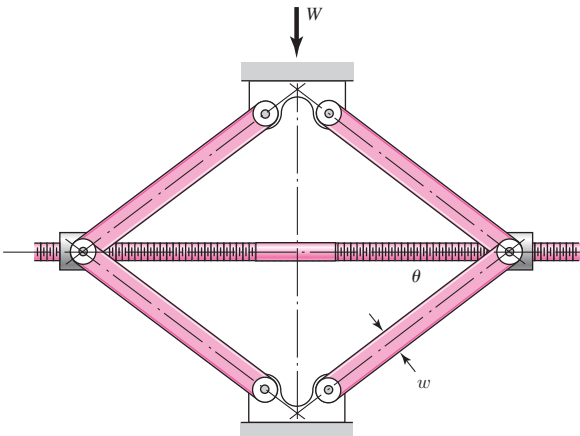


- (a) Use a design factor $n_d = 2.5$ and select a preferred size for the rod diameter if the column length is 50 in.
- (b) Repeat part (a) but for a column length of 16 in.
- (c) What factor of safety actually results for each of the cases above?

4-109

The figure shows a schematic drawing of a vehicular jack that is to be designed to support a maximum mass of 300 kg based on the use of a design factor $n_d = 3.50$. The opposite-handed threads on the two ends of the screw are cut to allow the link angle θ to vary from 15 to 70° . The links are to be machined from AISI 1010 hot-rolled steel bars. Each of the four links is to consist of two bars, one on each side of the central bearings. The bars are to be 350 mm long and have a bar width of $w = 30$ mm. The pinned ends are to be designed to secure an end-condition constant of at least $C = 1.4$ for out-of-plane buckling. Find a suitable preferred thickness and the resulting factor of safety for this thickness.

Problem 4-109

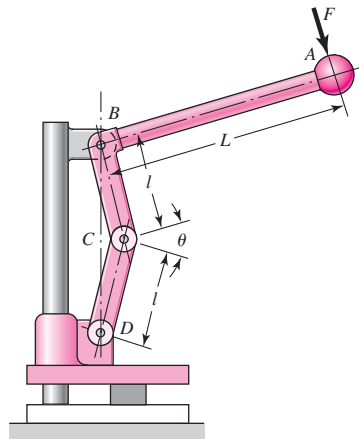


4-110

If drawn, a figure for this problem would resemble that for Prob. 4-90. A strut that is a standard hollow right circular cylinder has an outside diameter of 3 in and a wall thickness of $\frac{1}{4}$ in and is compressed between two circular end plates held by four bolts equally spaced on a bolt circle of 4.5-in diameter. All four bolts are hand-tightened, and then bolt A is tightened to a tension of 1500 lbf and bolt C, diagonally opposite, is tightened to a tension of 9000 lbf. The strut axis of symmetry is coincident with the center of the bolt circles. Find the maximum compressive load, the eccentricity of loading, and the largest compressive stress in the strut.

4-111

Design link CD of the hand-operated toggle press shown in the figure. Specify the cross-section dimensions, the bearing size and rod-end dimensions, the material, and the method of processing.

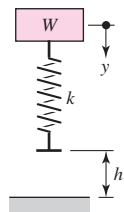


Problem 4-111

$$L = 9 \text{ in}, l = 3 \text{ in}, \theta_{\min} = 0^\circ.$$

4-112

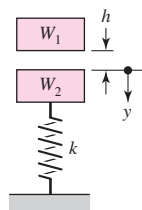
Find the maximum values of the spring force and deflection of the impact system shown in the figure if $W = 30 \text{ lbf}$, $k = 100 \text{ lbf/in}$, and $h = 2 \text{ in}$. Ignore the mass of the spring and solve using energy conservation.



Problem 4-112

4-113

As shown in the figure, the weight W_1 strikes W_2 from a height h . If $W_1 = 40 \text{ N}$, $W_2 = 400 \text{ N}$, $h = 200 \text{ mm}$, and $k = 32 \text{ kN/m}$, find the maximum values of the spring force and the deflection of W_2 . Assume that the impact between W_1 and W_2 is *inelastic*, ignore the mass of the spring, and solve using energy conservation.

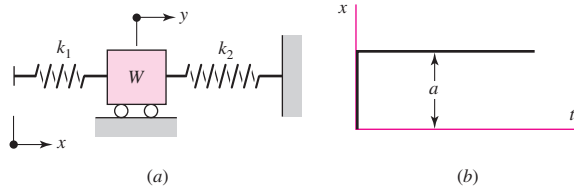


Problem 4-113

4-114

Part *a* of the figure shows a weight *W* mounted between two springs. If the free end of spring k_1 is suddenly displaced through the distance $x = a$, as shown in part *b*, determine the maximum displacement y of the weight. Let $W = 5 \text{ lbf}$, $k_1 = 10 \text{ lbf/in}$, $k_2 = 20 \text{ lbf/in}$, and $a = 0.25 \text{ in}$. Ignore the mass of each spring and solve using energy conservation.

Problem 4-114



PART

2

Failure Prevention

5

Failures Resulting from Static Loading

Chapter Outline

5-1	Static Strength	216
5-2	Stress Concentration	217
5-3	Failure Theories	219
5-4	Maximum-Shear-Stress Theory for Ductile Materials	219
5-5	Distortion-Energy Theory for Ductile Materials	221
5-6	Coulomb-Mohr Theory for Ductile Materials	228
5-7	Failure of Ductile Materials Summary	231
5-8	Maximum-Normal-Stress Theory for Brittle Materials	235
5-9	Modifications of the Mohr Theory for Brittle Materials	235
5-10	Failure of Brittle Materials Summary	238
5-11	Selection of Failure Criteria	239
5-12	Introduction to Fracture Mechanics	239
5-13	Stochastic Analysis	248
5-14	Important Design Equations	259

In Chap. 1 we learned that *strength is a property or characteristic of a mechanical element*. This property results from the material identity, the treatment and processing incidental to creating its geometry, and the loading, and it is at the controlling or critical location.

In addition to considering the strength of a single part, we must be cognizant that the strengths of the mass-produced parts will all be somewhat different from the others in the collection or ensemble because of variations in dimensions, machining, forming, and composition. Descriptors of strength are necessarily statistical in nature, involving parameters such as mean, standard deviations, and distributional identification.

A *static load* is a stationary force or couple applied to a member. To be stationary, the force or couple must be unchanging in magnitude, point or points of application, and direction. A static load can produce axial tension or compression, a shear load, a bending load, a torsional load, or any combination of these. To be considered static, the load cannot change in any manner.

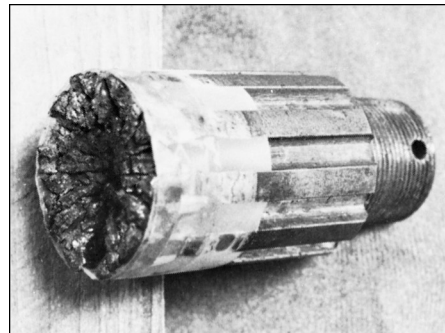
In this chapter we consider the relations between strength and static loading in order to make the decisions concerning material and its treatment, fabrication, and geometry for satisfying the requirements of functionality, safety, reliability, competitiveness, usability, manufacturability, and marketability. How far we go down this list is related to the scope of the examples.

“Failure” is the first word in the chapter title. Failure can mean a part has separated into two or more pieces; has become permanently distorted, thus ruining its geometry; has had its reliability downgraded; or has had its function compromised, whatever the reason. A designer speaking of failure can mean any or all of these possibilities. In this chapter our attention is focused on the predictability of permanent distortion or separation. In strength-sensitive situations the designer must separate mean stress and mean strength at the critical location sufficiently to accomplish his or her purposes.

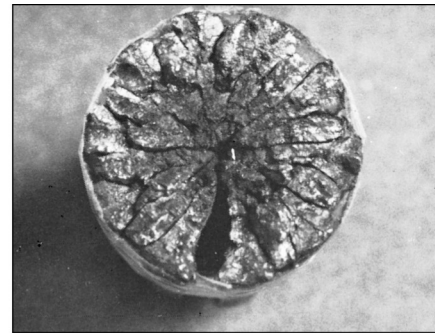
Figures 5–1 to 5–5 are photographs of several failed parts. The photographs exemplify the need of the designer to be well-versed in failure prevention. Toward this end we shall consider one-, two-, and three-dimensional stress states, with and without stress concentrations, for both ductile and brittle materials.

Figure 5–1

- (a) Failure of a truck drive-shaft spline due to corrosion fatigue. Note that it was necessary to use clear tape to hold the pieces in place.
- (b) Direct end view of failure.



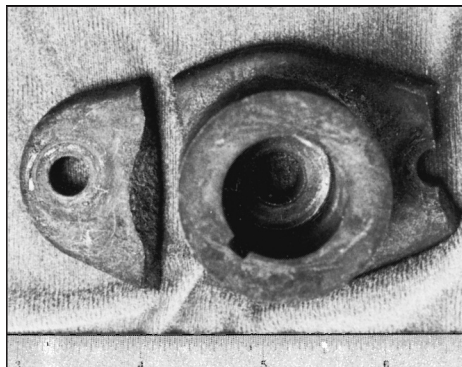
(a)



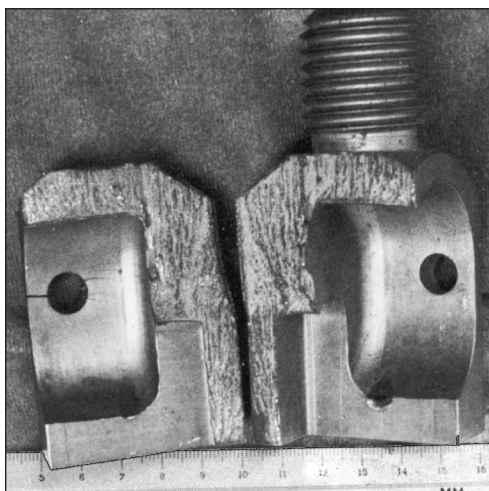
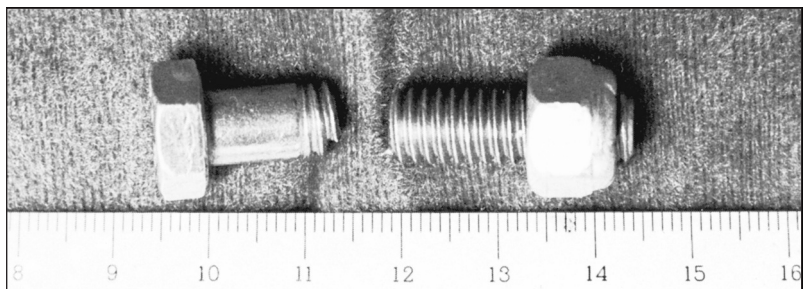
(b)

Figure 5–2

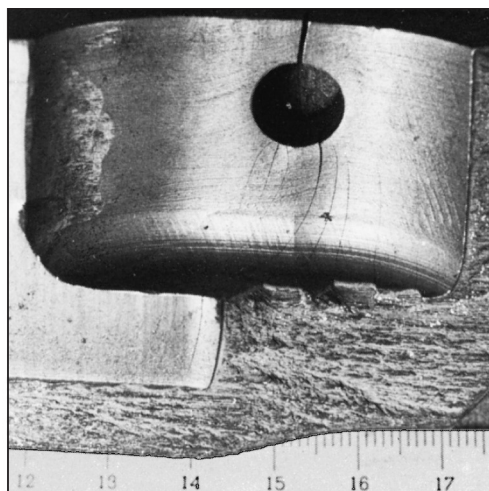
Impact failure of a lawn-mower blade driver hub. The blade impacted a surveying pipe marker.

**Figure 5–3**

Failure of an overhead-pulley retaining bolt on a weightlifting machine. A manufacturing error caused a gap that forced the bolt to take the entire moment load.



(a)



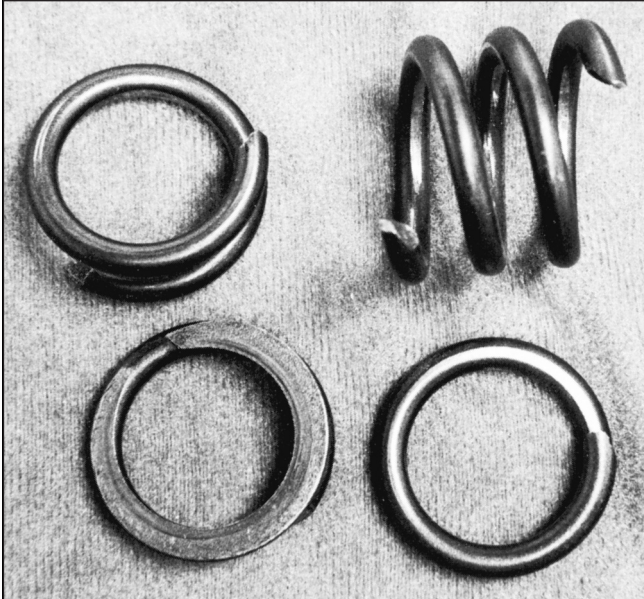
(b)

Figure 5–4

Chain test fixture that failed in one cycle. To alleviate complaints of excessive wear, the manufacturer decided to case-harden the material. (a) Two halves showing fracture; this is an excellent example of brittle fracture initiated by stress concentration. (b) Enlarged view of one portion to show cracks induced by stress concentration at the support-pin holes.

Figure 5–5

Valve-spring failure caused by spring surge in an oversped engine. The fractures exhibit the classic 45° shear failure.



5–1 Static Strength

Ideally, in designing any machine element, the engineer should have available the results of a great many strength tests of the particular material chosen. These tests should be made on specimens having the same heat treatment, surface finish, and size as the element the engineer proposes to design; and the tests should be made under exactly the same loading conditions as the part will experience in service. This means that if the part is to experience a bending load, it should be tested with a bending load. If it is to be subjected to combined bending and torsion, it should be tested under combined bending and torsion. If it is made of heat-treated AISI 1040 steel drawn at 500°C with a ground finish, the specimens tested should be of the same material prepared in the same manner. Such tests will provide very useful and precise information. Whenever such data are available for design purposes, the engineer can be assured of doing the best possible job of engineering.

The cost of gathering such extensive data prior to design is justified if failure of the part may endanger human life or if the part is manufactured in sufficiently large quantities. Refrigerators and other appliances, for example, have very good reliabilities because the parts are made in such large quantities that they can be thoroughly tested in advance of manufacture. The cost of making these tests is very low when it is divided by the total number of parts manufactured.

You can now appreciate the following four design categories:

- 1 Failure of the part would endanger human life, or the part is made in extremely large quantities; consequently, an elaborate testing program is justified during design.
- 2 The part is made in large enough quantities that a moderate series of tests is feasible.
- 3 The part is made in such small quantities that testing is not justified at all; or the design must be completed so rapidly that there is not enough time for testing.
- 4 The part has already been designed, manufactured, and tested and found to be unsatisfactory. Analysis is required to understand why the part is unsatisfactory and what to do to improve it.

More often than not it is necessary to design using only published values of yield strength, ultimate strength, percentage reduction in area, and percentage elongation, such as those listed in Appendix A. How can one use such meager data to design against both static and dynamic loads, two- and three-dimensional stress states, high and low temperatures, and very large and very small parts? These and similar questions will be addressed in this chapter and those to follow, but think how much better it would be to have data available that duplicate the actual design situation.

5–2

Stress Concentration

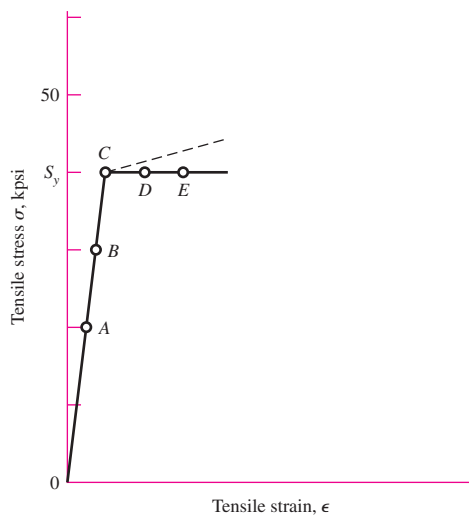
Stress concentration (see Sec. 3–13) is a highly localized effect. In some instances it may be due to a surface scratch. If the material is ductile and the load static, the design load may cause yielding in the critical location in the notch. This yielding can involve strain strengthening of the material and an increase in yield strength at the small critical notch location. Since the loads are static and the material is ductile, that part can carry the loads satisfactorily with no general yielding. In these cases the designer sets the geometric (theoretical) stress-concentration factor K_t to unity.

The rationale can be expressed as follows. The worst-case scenario is that of an idealized non-strain-strengthening material shown in Fig. 5–6. The stress-strain curve rises linearly to the yield strength S_y , then proceeds at constant stress, which is equal to S_y . Consider a filleted rectangular bar as depicted in Fig. A–15–5, where the cross-section area of the small shank is 1 in². If the material is ductile, with a yield point of 40 kpsi, and the theoretical *stress-concentration factor* (SCF) K_t is 2,

- A load of 20 kip induces a nominal tensile stress of 20 kpsi in the shank as depicted at point A in Fig. 5–6. At the critical location in the fillet the stress is 40 kpsi, and the SCF is $K = \sigma_{\max}/\sigma_{\text{nom}} = 40/20 = 2$.
- A load of 30 kip induces a nominal tensile stress of 30 kpsi in the shank at point B. The fillet stress is still 40 kpsi (point D), and the SCF $K = \sigma_{\max}/\sigma_{\text{nom}} = S_y/\sigma = 40/30 = 1.33$.
- At a load of 40 kip the induced tensile stress (point C) is 40 kpsi in the shank. At the critical location in the fillet, the stress (at point E) is 40 kpsi. The SCF $K = \sigma_{\max}/\sigma_{\text{nom}} = S_y/\sigma = 40/40 = 1$.

Figure 5–6

An idealized stress-strain curve. The dashed line depicts a strain-strengthening material.



For materials that strain-strengthen, the critical location in the notch has a higher S_y . The shank area is at a stress level a little below 40 kpsi, is carrying load, and is very near its failure-by-general-yielding condition. This is the reason designers do not apply K_t in *static loading* of a *ductile material* loaded elastically, instead setting $K_t = 1$.

When using this rule for ductile materials with static loads, be careful to assure yourself that the material is not susceptible to brittle fracture (see Sec. 5–12) in the environment of use. The usual definition of geometric (theoretical) stress-concentration factor for normal stress K_t and shear stress K_{ts} is given by Eq. pair (3–48) as

$$\sigma_{\max} = K_t \sigma_{\text{nom}} \quad (a)$$

$$\tau_{\max} = K_{ts} \tau_{\text{nom}} \quad (b)$$

Since your attention is on the stress-concentration factor, and the definition of σ_{nom} or τ_{nom} is given in the graph caption or from a computer program, be sure the value of nominal stress is appropriate for the section carrying the load.

As shown in Fig. 2–2b, p. 33, brittle materials do not exhibit a plastic range. The stress-concentration factor given by Eq. (a) or (b) could raise the stress to a level to cause fracture to initiate at the stress raiser, and initiate a catastrophic failure of the member.

An exception to this rule is a brittle material that inherently contains microdiscontinuity stress concentration, worse than the macrodiscontinuity that the designer has in mind. Sand molding introduces sand particles, air, and water vapor bubbles. The grain structure of cast iron contains graphite flakes (with little strength), which are literally cracks introduced during the solidification process. When a tensile test on a cast iron is performed, the strength reported in the literature *includes* this stress concentration. In such cases K_t or K_{ts} need not be applied.

An important source of stress-concentration factors is R. E. Peterson, who compiled them from his own work and that of others.¹ Peterson developed the style of presentation in which the stress-concentration factor K_t is multiplied by the nominal stress σ_{nom} to estimate the magnitude of the largest stress in the locality. His approximations were based on photoelastic studies of two-dimensional strips (Hartman and Levan, 1951; Wilson and White, 1973), with some limited data from three-dimensional photoelastic tests of Hartman and Levan. A contoured graph was included in the presentation of each case. Filleted shafts in tension were based on two-dimensional strips. Table A–15 provides many charts for the theoretical stress-concentration factors for several fundamental load conditions and geometry. Additional charts are also available from Peterson.²

Finite element analysis (FEA) can also be applied to obtain stress-concentration factors. Improvements on K_t and K_{ts} for filleted shafts were reported by Tipton, Sorem, and Rolovic.³

¹R. E. Peterson, “Design Factors for Stress Concentration,” *Machine Design*, vol. 23, no. 2, February 1951; no. 3, March 1951; no. 5, May 1951; no. 6, June 1951; no. 7, July 1951.

²Walter D. Pilkey and Deborah Pilkey, *Peterson's Stress-Concentration Factors*, 3rd ed, John Wiley & Sons, New York, 2008.

³S. M. Tipton, J. R. Sorem Jr., and R. D. Rolovic, “Updated Stress-Concentration Factors for Filleted Shafts in Bending and Tension,” *Trans. ASME, Journal of Mechanical Design*, vol. 118, September 1996, pp. 321–327.

5–3 Failure Theories

Section 5–1 illustrated some ways that loss of function is manifested. Events such as distortion, permanent set, cracking, and rupturing are among the ways that a machine element fails. Testing machines appeared in the 1700s, and specimens were pulled, bent, and twisted in simple loading processes.

If the failure mechanism is simple, then simple tests can give clues. Just what is simple? The tension test is uniaxial (that's simple) and elongations are largest in the axial direction, so strains can be measured and stresses inferred up to "failure." Just what is important: a critical stress, a critical strain, a critical energy? In the next several sections, we shall show failure theories that have helped answer some of these questions.

Unfortunately, there is no universal theory of failure for the general case of material properties and stress state. Instead, over the years several hypotheses have been formulated and tested, leading to today's accepted practices. Being accepted, we will characterize these "practices" as *theories* as most designers do.

Structural metal behavior is typically classified as being ductile or brittle, although under special situations, a material normally considered ductile can fail in a brittle manner (see Sec. 5–12). Ductile materials are normally classified such that $\varepsilon_f \geq 0.05$ and have an identifiable yield strength that is often the same in compression as in tension ($S_{yt} = S_{yc} = S_y$). Brittle materials, $\varepsilon_f < 0.05$, do not exhibit an identifiable yield strength, and are typically classified by ultimate tensile and compressive strengths, S_{ut} and S_{uc} , respectively (where S_{uc} is given as a positive quantity). The generally accepted theories are:

Ductile materials (yield criteria)

- Maximum shear stress (MSS), Sec. 5–4
- Distortion energy (DE), Sec. 5–5
- Ductile Coulomb-Mohr (DCM), Sec. 5–6

Brittle materials (fracture criteria)

- Maximum normal stress (MNS), Sec. 5–8
- Brittle Coulomb-Mohr (BCM), Sec. 5–9
- Modified Mohr (MM), Sec. 5–9

It would be inviting if we had one universally accepted theory for each material type, but for one reason or another, they are all used. Later, we will provide rationales for selecting a particular theory. First, we will describe the bases of these theories and apply them to some examples.

5–4 Maximum-Shear-Stress Theory for Ductile Materials

The *maximum-shear-stress* (MSS) theory predicts that *yielding begins whenever the maximum shear stress in any element equals or exceeds the maximum shear stress in a tension-test specimen of the same material when that specimen begins to yield*. The MSS theory is also referred to as the *Tresca* or *Guest* theory.

Many theories are postulated on the basis of the consequences seen from tensile tests. As a strip of a ductile material is subjected to tension, slip lines (called *Lüder lines*) form at approximately 45° with the axis of the strip. These slip lines are the

beginning of yield, and when loaded to fracture, fracture lines are also seen at angles approximately 45° with the axis of tension. Since the shear stress is maximum at 45° from the axis of tension, it makes sense to think that this is the mechanism of failure. It will be shown in the next section, that there is a little more going on than this. However, it turns out the MSS theory is an acceptable but conservative predictor of failure; and since engineers are conservative by nature, it is quite often used.

Recall that for simple tensile stress, $\sigma = P/A$, and the maximum shear stress occurs on a surface 45° from the tensile surface with a magnitude of $\tau_{\max} = \sigma/2$. So the maximum shear stress at yield is $\tau_{\max} = S_y/2$. For a general state of stress, three principal stresses can be determined and ordered such that $\sigma_1 \geq \sigma_2 \geq \sigma_3$. The maximum shear stress is then $\tau_{\max} = (\sigma_1 - \sigma_3)/2$ (see Fig. 3–12). Thus, for a general state of stress, the maximum-shear-stress theory predicts yielding when

$$\tau_{\max} = \frac{\sigma_1 - \sigma_3}{2} \geq \frac{S_y}{2} \quad \text{or} \quad \sigma_1 - \sigma_3 \geq S_y \quad (5-1)$$

Note that this implies that the yield strength in shear is given by

$$S_{sy} = 0.5S_y \quad (5-2)$$

which, as we will see later is about 15 percent low (conservative).

For design purposes, Eq. (5–1) can be modified to incorporate a factor of safety, n . Thus,

$$\tau_{\max} = \frac{S_y}{2n} \quad \text{or} \quad \sigma_1 - \sigma_3 = \frac{S_y}{n} \quad (5-3)$$

Plane stress is a very common state of stress in design. However, it is extremely important to realize that plane stress is a *three-dimensional* state of stress. Plane stress transformations in Sec. 3–6 are restricted to the in-plane stresses only, where the in-plane principal stresses are given by Eq. (3–13) and labeled as σ_1 and σ_2 . It is true that these are the principal stresses in the *plane of analysis*, but out of plane there is a third principal stress and it is *always zero* for plane stress. This means that if we are going to use the convention of ordering $\sigma_1 \geq \sigma_2 \geq \sigma_3$ for three-dimensional analysis, upon which Eq. (5–1) is based, we cannot arbitrarily call the in-plane principal stresses σ_1 and σ_2 until we relate them with the third principal stress of zero. To illustrate the MSS theory graphically for plane stress, we will first label the principal stresses given by Eq. (3–13) as σ_A and σ_B , and then order them with the zero principal stress according to the convention $\sigma_1 \geq \sigma_2 \geq \sigma_3$. Assuming that $\sigma_A \geq \sigma_B$, there are three cases to consider when using Eq. (5–1) for plane stress:

Case 1: $\sigma_A \geq \sigma_B \geq 0$. For this case, $\sigma_1 = \sigma_A$ and $\sigma_3 = 0$. Equation (5–1) reduces to a yield condition of

$$\sigma_A \geq S_y \quad (5-4)$$

Case 2: $\sigma_A \geq 0 \geq \sigma_B$. Here, $\sigma_1 = \sigma_A$ and $\sigma_3 = \sigma_B$, and Eq. (5–1) becomes

$$\sigma_A - \sigma_B \geq S_y \quad (5-5)$$

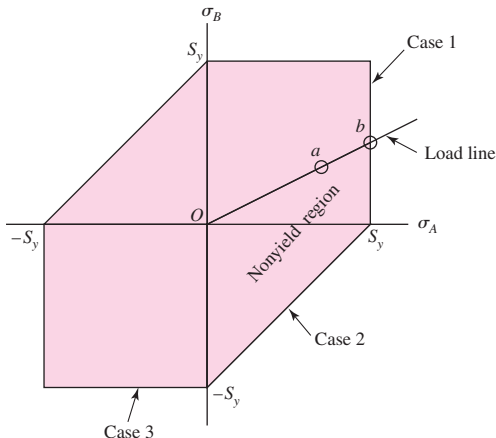
Case 3: $0 \geq \sigma_A \geq \sigma_B$. For this case, $\sigma_1 = 0$ and $\sigma_3 = \sigma_B$, and Eq. (5–1) gives

$$\sigma_B \leq -S_y \quad (5-6)$$

Equations (5–4) to (5–6) are represented in Fig. 5–7 by the three lines indicated in the σ_A, σ_B plane. The remaining unmarked lines are cases for $\sigma_B \geq \sigma_A$, which completes the *stress yield envelope* but are not normally used. The maximum-shear-stress theory predicts yield if a stress state is outside the shaded region bordered by the stress yield envelope. In Fig. 5–7, suppose point a represents the stress state of a critical stress element

Figure 5–7

The maximum-shear-stress (MSS) theory yield envelope for plane stress, where σ_A and σ_B are the two nonzero principal stresses.



of a member. If the load is increased, it is typical to assume that the principal stresses will increase proportionally along the line from the origin through point *a*. Such a *load line* is shown. If the stress situation increases along the load line until it crosses the stress failure envelope, such as at point *b*, the MSS theory predicts that the stress element will yield. The factor of safety guarding against yield at point *a* is given by the ratio of strength (distance to failure at point *b*) to stress (distance to stress at point *a*), that is $n = Ob/Oa$.

Note that the first part of Eq. (5–3), $\tau_{\max} = S_y/2n$, is sufficient for design purposes provided the designer is careful in determining τ_{\max} . For plane stress, Eq. (3–14) does not always predict τ_{\max} . However, consider the special case when one normal stress is zero in the plane, say σ_x and τ_{xy} have values and $\sigma_y = 0$. It can be easily shown that this is a Case 2 problem, and the shear stress determined by Eq. (3–14) is τ_{\max} . Shaft design problems typically fall into this category where a normal stress exists from bending and/or axial loading, and a shear stress arises from torsion.

5–5

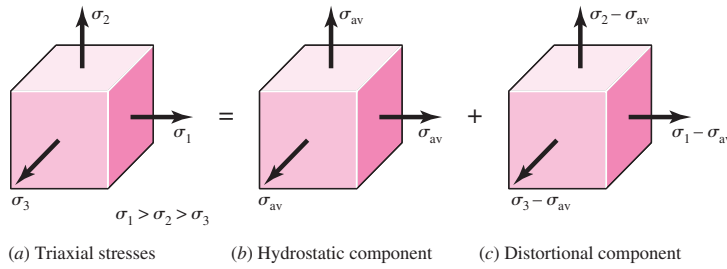
Distortion-Energy Theory for Ductile Materials

The *distortion-energy theory* predicts that yielding occurs when the distortion strain energy per unit volume reaches or exceeds the distortion strain energy per unit volume for yield in simple tension or compression of the same material.

The distortion-energy (DE) theory originated from the observation that ductile materials stressed hydrostatically (equal principal stresses) exhibited yield strengths greatly in excess of the values given by the simple tension test. Therefore it was postulated that yielding was not a simple tensile or compressive phenomenon at all, but, rather, that it was related somehow to the angular distortion of the stressed element. To develop the theory, note, in Fig. 5–8a, the unit volume subjected to any three-dimensional stress state designated by the stresses σ_1 , σ_2 , and σ_3 . The stress state shown in Fig. 5–8b is one of hydrostatic normal stresses due to the stresses σ_{av} acting in each of the same principal directions as in Fig. 5–8a. The formula for σ_{av} is simply

$$\sigma_{av} = \frac{\sigma_1 + \sigma_2 + \sigma_3}{3} \quad (a)$$

Thus the element in Fig. 5–8b undergoes pure volume change, that is, no angular distortion. If we regard σ_{av} as a component of σ_1 , σ_2 , and σ_3 , then this component can be subtracted from them, resulting in the stress state shown in Fig. 5–8c. This element is subjected to pure angular distortion, that is, no volume change.



(a) Triaxial stresses

(b) Hydrostatic component

(c) Distortional component

Figure 5-8

(a) Element with triaxial stresses; this element undergoes both volume change and angular distortion. (b) Element under hydrostatic normal stresses undergoes only volume change. (c) Element has angular distortion without volume change.

The strain energy per unit volume for simple tension is $u = \frac{1}{2}\epsilon\sigma$. For the element of Fig. 5-8a the strain energy per unit volume is $u = \frac{1}{2}[\epsilon_1\sigma_1 + \epsilon_2\sigma_2 + \epsilon_3\sigma_3]$. Substituting Eq. (3-19) for the principal strains gives

$$u = \frac{1}{2E} [\sigma_1^2 + \sigma_2^2 + \sigma_3^2 - 2\nu(\sigma_1\sigma_2 + \sigma_2\sigma_3 + \sigma_3\sigma_1)] \quad (b)$$

The strain energy for producing only volume change u_v can be obtained by substituting σ_{av} for σ_1 , σ_2 , and σ_3 in Eq. (b). The result is

$$u_v = \frac{3\sigma_{av}^2}{2E}(1 - 2\nu) \quad (c)$$

If we now substitute the square of Eq. (a) in Eq. (c) and simplify the expression, we get

$$u_v = \frac{1 - 2\nu}{6E} (\sigma_1^2 + \sigma_2^2 + \sigma_3^2 + 2\sigma_1\sigma_2 + 2\sigma_2\sigma_3 + 2\sigma_3\sigma_1) \quad (5-7)$$

Then the distortion energy is obtained by subtracting Eq. (5-7) from Eq. (b). This gives

$$u_d = u - u_v = \frac{1 + \nu}{3E} \left[\frac{(\sigma_1 - \sigma_2)^2 + (\sigma_2 - \sigma_3)^2 + (\sigma_3 - \sigma_1)^2}{2} \right] \quad (5-8)$$

Note that the distortion energy is zero if $\sigma_1 = \sigma_2 = \sigma_3$.

For the simple tensile test, at yield, $\sigma_1 = S_y$ and $\sigma_2 = \sigma_3 = 0$, and from Eq. (5-8) the distortion energy is

$$u_d = \frac{1 + \nu}{3E} S_y^2 \quad (5-9)$$

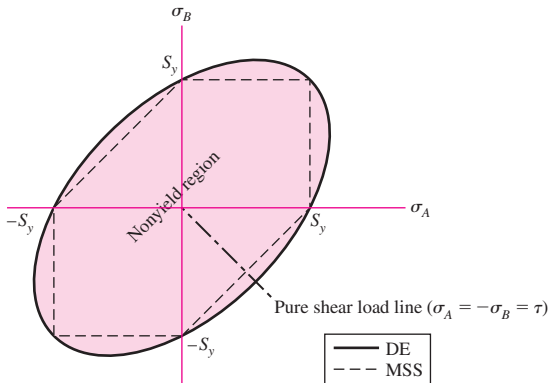
So for the general state of stress given by Eq. (5-8), yield is predicted if Eq. (5-8) equals or exceeds Eq. (5-9). This gives

$$\left[\frac{(\sigma_1 - \sigma_2)^2 + (\sigma_2 - \sigma_3)^2 + (\sigma_3 - \sigma_1)^2}{2} \right]^{1/2} \geq S_y \quad (5-10)$$

If we had a simple case of tension σ , then yield would occur when $\sigma \geq S_y$. Thus, the left of Eq. (5-10) can be thought of as a *single, equivalent, or effective stress* for the entire general state of stress given by σ_1 , σ_2 , and σ_3 . This effective stress is usually

Figure 5–9

The distortion-energy (DE) theory yield envelope for plane stress states. This is a plot of points obtained from Eq. (5–13) with $\sigma' = S_y$.



called the *von Mises stress*, σ' , named after Dr. R. von Mises, who contributed to the theory. Thus Eq. (5–10), for yield, can be written as

$$\sigma' \geq S_y \quad (5-11)$$

where the von Mises stress is

$$\sigma' = \left[\frac{(\sigma_1 - \sigma_2)^2 + (\sigma_2 - \sigma_3)^2 + (\sigma_3 - \sigma_1)^2}{2} \right]^{1/2} \quad (5-12)$$

For plane stress, the von Mises stress can be represented by the principal stresses σ_A , σ_B , and zero. Then from Eq. (5–12), we get

$$\sigma' = (\sigma_A^2 - \sigma_A \sigma_B + \sigma_B^2)^{1/2} \quad (5-13)$$

Equation (5–13) is a rotated ellipse in the σ_A , σ_B plane, as shown in Fig. 5–9 with $\sigma' = S_y$. The dotted lines in the figure represent the MSS theory, which can be seen to be more restrictive, hence, more conservative.⁴

Using xyz components of three-dimensional stress, the von Mises stress can be written as

$$\sigma' = \frac{1}{\sqrt{2}} [(\sigma_x - \sigma_y)^2 + (\sigma_y - \sigma_z)^2 + (\sigma_z - \sigma_x)^2 + 6(\tau_{xy}^2 + \tau_{yz}^2 + \tau_{zx}^2)]^{1/2} \quad (5-14)$$

and for plane stress,

$$\sigma' = (\sigma_x^2 - \sigma_x \sigma_y + \sigma_y^2 + 3\tau_{xy}^2)^{1/2} \quad (5-15)$$

The distortion-energy theory is also called:

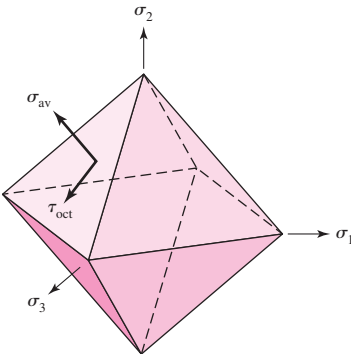
- The von Mises or von Mises–Hencky theory
- The shear-energy theory
- The octahedral-shear-stress theory

Understanding octahedral shear stress will shed some light on why the MSS is conservative. Consider an isolated element in which the normal stresses on each surface are

⁴The three-dimensional equations for DE and MSS can be plotted relative to three-dimensional σ_1 , σ_2 , σ_3 , coordinate axes. The failure surface for DE is a circular cylinder with an axis inclined at 45° from each principal stress axis, whereas the surface for MSS is a hexagon inscribed within the cylinder. See Arthur P. Boresi and Richard J. Schmidt, *Advanced Mechanics of Materials*, 6th ed., John Wiley & Sons, New York, 2003, Sec. 4.4.

Figure 5-10

Octahedral surfaces.



equal to the hydrostatic stress σ_{av} . There are eight surfaces symmetric to the principal directions that contain this stress. This forms an octahedron as shown in Fig. 5-10. The shear stresses on these surfaces are equal and are called the *octahedral shear stresses* (Fig. 5-10 has only one of the octahedral surfaces labeled). Through coordinate transformations the octahedral shear stress is given by⁵

$$\tau_{oct} = \frac{1}{3} [(\sigma_1 - \sigma_2)^2 + (\sigma_2 - \sigma_3)^2 + (\sigma_3 - \sigma_1)^2]^{1/2} \quad (5-16)$$

Under the name of the octahedral-shear-stress theory, *failure is assumed to occur whenever the octahedral shear stress for any stress state equals or exceeds the octahedral shear stress for the simple tension-test specimen at failure.*

As before, on the basis of the tensile test results, yield occurs when $\sigma_1 = S_y$ and $\sigma_2 = \sigma_3 = 0$. From Eq. (5-16) the octahedral shear stress under this condition is

$$\tau_{oct} = \frac{\sqrt{2}}{3} S_y \quad (5-17)$$

When, for the general stress case, Eq. (5-16) is equal or greater than Eq. (5-17), yield is predicted. This reduces to

$$\left[\frac{(\sigma_1 - \sigma_2)^2 + (\sigma_2 - \sigma_3)^2 + (\sigma_3 - \sigma_1)^2}{2} \right]^{1/2} \geq S_y \quad (5-18)$$

which is identical to Eq. (5-10), verifying that the maximum-octahedral-shear-stress theory is equivalent to the distortion-energy theory.

The model for the MSS theory ignores the contribution of the normal stresses on the 45° surfaces of the tensile specimen. However, these stresses are $P/2A$, and *not* the hydrostatic stresses which are $P/3A$. Herein lies the difference between the MSS and DE theories.

The mathematical manipulation involved in describing the DE theory might tend to obscure the real value and usefulness of the result. The equations given allow the most complicated stress situation to be represented by a single quantity, the von Mises stress, which then can be compared against the yield strength of the material through Eq. (5-11). This equation can be expressed as a design equation by

$$\sigma' = \frac{S_y}{n} \quad (5-19)$$

⁵For a derivation, see Arthur P. Boresi, op. cit., pp. 36–37.

The distortion-energy theory predicts no failure under hydrostatic stress and agrees well with all data for ductile behavior. Hence, it is the most widely used theory for ductile materials and is recommended for design problems unless otherwise specified.

One final note concerns the shear yield strength. Consider a case of pure shear τ_{xy} , where for plane stress $\sigma_x = \sigma_y = 0$. For yield, Eq. (5-11) with Eq. (5-15) gives

$$(3\tau_{xy}^2)^{1/2} = S_y \quad \text{or} \quad \tau_{xy} = \frac{S_y}{\sqrt{3}} = 0.577S_y \quad (5-20)$$

Thus, the shear yield strength predicted by the distortion-energy theory is

$$S_{sy} = 0.577S_y \quad (5-21)$$

which as stated earlier, is about 15 percent greater than the $0.5 S_y$ predicted by the MSS theory. For pure shear, τ_{xy} the principal stresses from Eq. (3-13) are $\sigma_A = -\sigma_B = \tau_{xy}$. The load line for this case is in the third quadrant at an angle of 45° from the σ_A, σ_B axes shown in Fig. 5-9.

EXAMPLE 5-1

A hot-rolled steel has a yield strength of $S_{yt} = S_{yc} = 100$ kpsi and a true strain at fracture of $\varepsilon_f = 0.55$. Estimate the factor of safety for the following principal stress states:

- (a) $\sigma_x = 70$ kpsi, $\sigma_y = 70$ kpsi, $\tau_{xy} = 0$ kpsi
- (b) $\sigma_x = 60$ kpsi, $\sigma_y = 40$ kpsi, $\tau_{xy} = -15$ kpsi
- (c) $\sigma_x = 0$ kpsi, $\sigma_y = 40$ kpsi, $\tau_{xy} = 45$ kpsi
- (d) $\sigma_x = -40$ kpsi, $\sigma_y = -60$ kpsi, $\tau_{xy} = 15$ kpsi
- (e) $\sigma_1 = 30$ kpsi, $\sigma_2 = 30$ kpsi, $\sigma_3 = 30$ kpsi

Solution

Since $\varepsilon_f > 0.05$ and S_{yt} and S_{yc} are equal, the material is ductile and both the distortion-energy (DE) theory and maximum-shear-stress (MSS) theory apply. Both will be used for comparison. Note that cases *a* to *d* are plane stress states.

(a) Since there is no shear stress on this stress element, the normal stresses are equal to the principal stresses. The ordered principal stresses are $\sigma_A = \sigma_1 = 70$, $\sigma_B = \sigma_2 = 70$, $\sigma_3 = 0$ kpsi.

DE From Eq. (5-13),

$$\sigma' = [70^2 - 70(70) + 70^2]^{1/2} = 70 \text{ kpsi}$$

From Eq. (5-19),

$$\text{Answer} \quad n = \frac{S_y}{\sigma'} = \frac{100}{70} = 1.43$$

MSS Noting that the two nonzero principal stresses are equal, τ_{max} will be from the largest Mohr's circle, which will incorporate the third principal stress at zero. From Eq. (3-16),

$$\tau_{max} = \frac{\sigma_1 - \sigma_3}{2} = \frac{70 - 0}{2} = 35 \text{ kpsi}$$

From Eq. (5-3),

$$\text{Answer} \quad n = \frac{S_y/2}{\tau_{max}} = \frac{100/2}{35} = 1.43$$

(b) From Eq. (3–13), the nonzero principal stresses are

$$\sigma_A, \sigma_B = \frac{60+40}{2} \pm \sqrt{\left(\frac{60-40}{2}\right)^2 + (-15)^2} = 68.0, 32.0 \text{ kpsi}$$

The ordered principal stresses are $\sigma_A = \sigma_1 = 68.0$, $\sigma_B = \sigma_2 = 32.0$, $\sigma_3 = 0$ kpsi.

DE $\sigma' = [68^2 - 68(32) + 68^2]^{1/2} = 59.0 \text{ kpsi}$

Answer

$$n = \frac{S_y}{\sigma'} = \frac{100}{59.0} = 1.70$$

MSS Noting that the two nonzero principal stresses are both positive, τ_{\max} will be from the largest Mohr's circle which will incorporate the third principle stress at zero. From Eq. (3–16),

$$\tau_{\max} = \frac{\sigma_1 - \sigma_3}{2} = \frac{68.0 - 0}{2} = 34.0 \text{ kpsi}$$

Answer

$$n = \frac{S_y/2}{\tau_{\max}} = \frac{100/2}{34.0} = 1.47$$

(c) This time, we shall obtain the factors of safety directly from the xy components of stress.

DE From Eq. (5–15),

$$\sigma' = (\sigma_x^2 - \sigma_x \sigma_y + \sigma_y^2 + 3\tau_{xy}^2)^{1/2} = [(40^2 + 3(45)^2)]^{1/2} = 87.6 \text{ kpsi}$$

Answer

$$n = \frac{S_y}{\sigma'} = \frac{100}{87.6} = 1.14$$

MSS Taking care to note from a quick sketch of Mohr's circle that one nonzero principal stress will be positive while the other one will be negative, τ_{\max} can be obtained from the extreme-value shear stress given by Eq. (3–14) without finding the principal stresses.

$$\tau_{\max} = \sqrt{\left(\frac{\sigma_x - \sigma_y}{2}\right)^2 + \tau_{xy}^2} = \sqrt{\left(\frac{0 - 40}{2}\right)^2 + 45^2} = 49.2 \text{ kpsi}$$

Answer

$$n = \frac{S_y/2}{\tau_{\max}} = \frac{100/2}{49.2} = 1.02$$

For comparison purposes later in this problem, the nonzero principal stresses can be obtained from Eq. (3–13) to be 70.0 kpsi and –30 kpsi.

(d) From Eq. (3–13), the nonzero principal stresses are

$$\sigma_A, \sigma_B = \frac{-40 + (-60)}{2} \pm \sqrt{\left(\frac{-40 - (-60)}{2}\right)^2 + (15)^2} = -32.0, -68.0 \text{ kpsi}$$

The ordered principal stresses are $\sigma_1 = 0$, $\sigma_A = \sigma_2 = -32.0$, $\sigma_B = \sigma_3 = -68.0$ kpsi.

DE $\sigma' = [(-32)^2 - (-32)(-68) + (-68)^2]^{1/2} = 59.0 \text{ kpsi}$

Answer

$$n = \frac{S_y}{\sigma'} = \frac{100}{59.0} = 1.70$$

MSS From Eq. (3–16),

$$\tau_{\max} = \frac{\sigma_1 - \sigma_3}{2} = \frac{0 - (-68.0)}{2} = 34.0 \text{ kpsi}$$

Answer

$$n = \frac{S_y/2}{\tau_{\max}} = \frac{100/2}{34.0} = 1.47$$

(e) The ordered principal stresses are $\sigma_1 = 30$, $\sigma_2 = 30$, $\sigma_3 = 30$ kpsi

DE From Eq. (5–12),

$$\sigma' = \left[\frac{(30 - 30)^2 + (30 - 30)^2 + (30 - 30)^2}{2} \right]^{1/2} = 0 \text{ kpsi}$$

Answer

$$n = \frac{S_y}{\sigma'} = \frac{100}{0} \rightarrow \infty$$

MSS From Eq. (5–3),

Answer

$$n = \frac{S_y}{\sigma_1 - \sigma_3} = \frac{100}{30 - 30} \rightarrow \infty$$

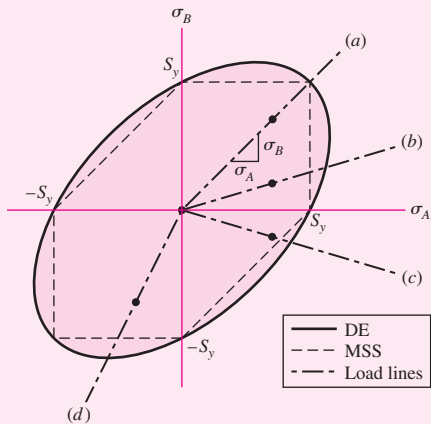
A tabular summary of the factors of safety is included for comparisons.

	(a)	(b)	(c)	(d)	(e)
DE	1.43	1.70	1.14	1.70	∞
MSS	1.43	1.47	1.02	1.47	∞

Since the MSS theory is on or within the boundary of the DE theory, it will always predict a factor of safety equal to or less than the DE theory, as can be seen in the table. For each case, except case (e), the coordinates and load lines in the σ_A , σ_B plane are shown in Fig. 5–11. Case (e) is not plane stress. Note that the load line for case (a) is the only plane stress case given in which the two theories agree, thus giving the same factor of safety.

Figure 5–11

Load lines for Example 5–1.



5-6 Coulomb-Mohr Theory for Ductile Materials

Not all materials have compressive strengths equal to their corresponding tensile values. For example, the yield strength of magnesium alloys in compression may be as little as 50 percent of their yield strength in tension. The ultimate strength of gray cast irons in compression varies from 3 to 4 times greater than the ultimate tensile strength. So, in this section, we are primarily interested in those theories that can be used to predict failure for materials whose strengths in tension and compression are not equal.

Historically, the Mohr theory of failure dates to 1900, a date that is relevant to its presentation. There were no computers, just slide rules, compasses, and French curves. Graphical procedures, common then, are still useful today for visualization. The idea of Mohr is based on three “simple” tests: tension, compression, and shear, to yielding if the material can yield, or to rupture. It is easier to define shear yield strength as S_{sy} than it is to test for it.

The practical difficulties aside, Mohr’s hypothesis was to use the results of tensile, compressive, and torsional shear tests to construct the three circles of Fig. 5–12 defining a failure envelope tangent to the three circles, depicted as curve $ABCDE$ in the figure. The argument amounted to the three Mohr circles describing the stress state in a body (see Fig. 3–12) growing during loading until one of them became tangent to the failure envelope, thereby defining failure. Was the form of the failure envelope straight, circular, or quadratic? A compass or a French curve defined the failure envelope.

A variation of Mohr’s theory, called the *Coulomb-Mohr theory* or the *internal-friction theory*, assumes that the boundary BCD in Fig. 5–12 is straight. With this assumption only the tensile and compressive strengths are necessary. Consider the conventional ordering of the principal stresses such that $\sigma_1 \geq \sigma_2 \geq \sigma_3$. The largest circle connects σ_1 and σ_3 , as shown in Fig. 5–13. The centers of the circles in Fig. 5–13 are C_1 , C_2 , and C_3 . Triangles OB_iC_i are similar, therefore

$$\frac{B_2C_2 - B_1C_1}{OC_2 - OC_1} = \frac{B_3C_3 - B_1C_1}{OC_3 - OC_1}$$

or,

$$\frac{B_2C_2 - B_1C_1}{C_1C_2} = \frac{B_3C_3 - B_1C_1}{C_1C_3}$$

Figure 5–12

Three Mohr circles, one for the uniaxial compression test, one for the test in pure shear, and one for the uniaxial tension test, are used to define failure by the Mohr hypothesis. The strengths S_c and S_t are the compressive and tensile strengths, respectively; they can be used for yield or ultimate strength.

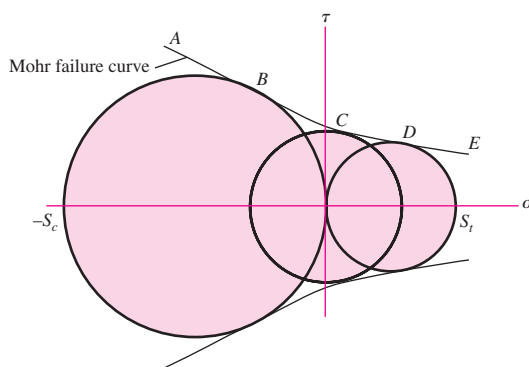
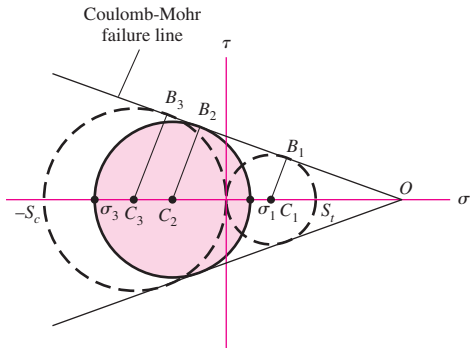


Figure 5-13

Mohr's largest circle for a general state of stress.



where $B_1C_1 = S_t/2$, $B_2C_2 = (\sigma_1 - \sigma_3)/2$, and $B_3C_3 = S_c/2$, are the radii of the right, center, and left circles, respectively. The distance from the origin to C_1 is $S_t/2$, to C_3 is $S_c/2$, and to C_2 (in the positive σ direction) is $(\sigma_1 + \sigma_3)/2$. Thus

$$\frac{\frac{\sigma_1 - \sigma_3}{2} - \frac{S_t}{2}}{\frac{S_t}{2} - \frac{\sigma_1 + \sigma_3}{2}} = \frac{\frac{S_c}{2} - \frac{S_t}{2}}{\frac{S_t}{2} + \frac{S_c}{2}}$$

Cancelling the 2 in each term, cross-multiplying, and simplifying reduces this equation to

$$\frac{\sigma_1}{S_t} - \frac{\sigma_3}{S_c} = 1 \quad (5-22)$$

where either yield strength or ultimate strength can be used.

For plane stress, when the two nonzero principal stresses are $\sigma_A \geq \sigma_B$, we have a situation similar to the three cases given for the MSS theory, Eqs. (5-4) to (5-6). That is, the failure conditions are

Case 1: $\sigma_A \geq \sigma_B \geq 0$. For this case, $\sigma_1 = \sigma_A$ and $\sigma_3 = 0$. Equation (5-22) reduces to

$$\sigma_A \geq S_t \quad (5-23)$$

Case 2: $\sigma_A \geq 0 \geq \sigma_B$. Here, $\sigma_1 = \sigma_A$ and $\sigma_3 = \sigma_B$, and Eq. (5-22) becomes

$$\frac{\sigma_A}{S_t} - \frac{\sigma_B}{S_c} \geq 1 \quad (5-24)$$

Case 3: $0 \geq \sigma_A \geq \sigma_B$. For this case, $\sigma_1 = 0$ and $\sigma_3 = \sigma_B$, and Eq. (5-22) gives

$$\sigma_B \leq -S_c \quad (5-25)$$

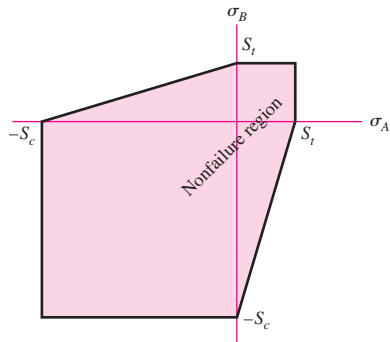
A plot of these cases, together with the normally unused cases corresponding to $\sigma_B \geq \sigma_A$, is shown in Fig. 5-14.

For design equations, incorporating the factor of safety n , divide all strengths by n . For example, Eq. (5-22) as a design equation can be written as

$$\frac{\sigma_1}{S_t} - \frac{\sigma_3}{S_c} = \frac{1}{n} \quad (5-26)$$

Figure 5-14

Plot of the Coulomb-Mohr theory failure envelope for plane stress states.



Since for the Coulomb-Mohr theory we do not need the torsional shear strength circle we can deduce it from Eq. (5-22). For pure shear τ , $\sigma_1 = -\sigma_3 = \tau$. The torsional yield strength occurs when $\tau_{\max} = S_{sy}$. Substituting $\sigma_1 = -\sigma_3 = S_{sy}$ into Eq. (5-22) and simplifying gives

$$S_{sy} = \frac{S_{yt} S_{yc}}{S_{yt} + S_{yc}} \quad (5-27)$$

EXAMPLE 5-2

A 25-mm-diameter shaft is statically torqued to 230 N · m. It is made of cast 195-T6 aluminum, with a yield strength in tension of 160 MPa and a yield strength in compression of 170 MPa. It is machined to final diameter. Estimate the factor of safety of the shaft.

Solution The maximum shear stress is given by

$$\tau = \frac{16T}{\pi d^3} = \frac{16(230)}{\pi [25(10^{-3})]^3} = 75(10^6) \text{ N/m}^2 = 75 \text{ MPa}$$

The two nonzero principal stresses are 75 and -75 MPa, making the ordered principal stresses $\sigma_1 = 75$, $\sigma_2 = 0$, and $\sigma_3 = -75$ MPa. From Eq. (5-26), for yield,

Answer $n = \frac{1}{\sigma_1/S_{yt} - \sigma_3/S_{yc}} = \frac{1}{75/160 - (-75)/170} = 1.10$

Alternatively, from Eq. (5-27),

$$S_{sy} = \frac{S_{yt} S_{yc}}{S_{yt} + S_{yc}} = \frac{160(170)}{160 + 170} = 82.4 \text{ MPa}$$

and $\tau_{\max} = 75$ MPa. Thus,

Answer $n = \frac{S_{sy}}{\tau_{\max}} = \frac{82.4}{75} = 1.10$

5-7 Failure of Ductile Materials Summary

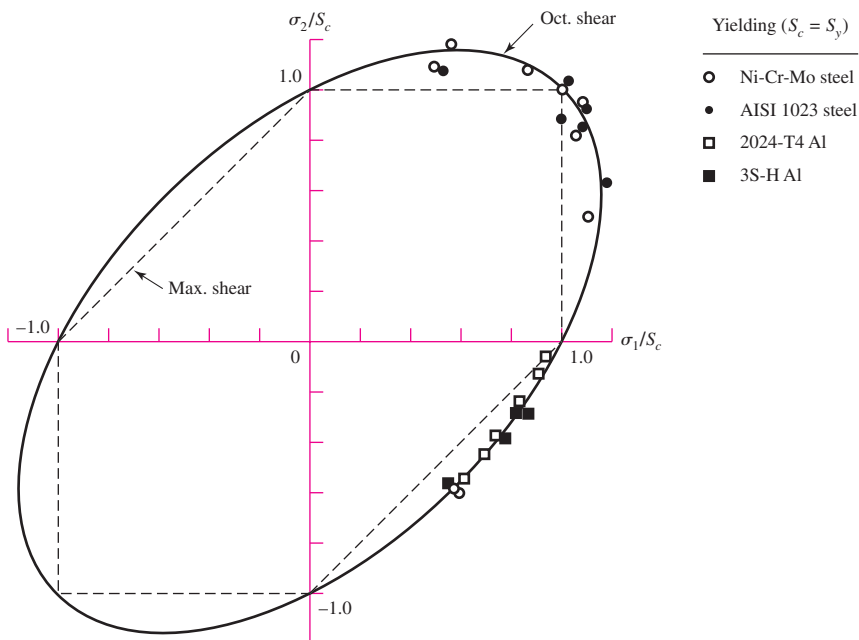
Having studied some of the various theories of failure, we shall now evaluate them and show how they are applied in design and analysis. In this section we limit our studies to materials and parts that are known to fail in a ductile manner. Materials that fail in a brittle manner will be considered separately because these require different failure theories.

To help decide on appropriate and workable theories of failure, Marin⁶ collected data from many sources. Some of the data points used to select failure theories for ductile materials are shown in Fig. 5-15.⁷ Mann also collected many data for copper and nickel alloys; if shown, the data points for these would be mingled with those already diagrammed. Figure 5-15 shows that either the maximum-shear-stress theory or the distortion-energy theory is acceptable for design and analysis of materials that would fail in a ductile manner.

The selection of one or the other of these two theories is something that you, the engineer, must decide. For design purposes the maximum-shear-stress theory is easy, quick to use, and conservative. If the problem is to learn *why* a part failed, then the distortion-energy theory may be the best to use; Fig. 5-15 shows that the plot of the distortion-energy theory passes closer to the central area of the data points, and thus is generally a better predictor of failure. However, keep in mind that though a failure curve passing through the center of the experimental data is *typical* of the data, its *reliability* from a statistical standpoint is about 50 percent. For design purposes, a larger factor of safety may be warranted when using such a failure theory.

Figure 5-15

Experimental data superposed on failure theories. (From Fig. 7.11, p. 257, Mechanical Behavior of Materials, 2nd ed., N. E. Dowling, Prentice Hall, Englewood Cliffs, N.J., 1999. Modified to show only ductile failures.)



⁶Joseph Marin was one of the pioneers in the collection, development, and dissemination of material on the failure of engineering elements. He has published many books and papers on the subject. Here the reference used is Joseph Marin, *Engineering Materials*, Prentice-Hall, Englewood Cliffs, N.J., 1952. (See pp. 156 and 157 for some data points used here.)

⁷Note that some data in Fig. 5-15 are displayed along the top horizontal boundary where $\sigma_B \geq \sigma_A$. This is often done with failure data to thin out congested data points by plotting on the mirror image of the line $\sigma_B = \sigma_A$.

For ductile materials with unequal yield strengths, S_{yt} in tension and S_{yc} in compression, the Mohr theory is the best available. However, the theory requires the results from three separate modes of tests, graphical construction of the failure locus, and fitting the largest Mohr's circle to the failure locus. The alternative to this is to use the Coulomb-Mohr theory, which requires only the tensile and compressive yield strengths and is easily dealt with in equation form.

EXAMPLE 5-3

This example illustrates the use of a failure theory to determine the strength of a mechanical element or component. The example may also clear up any confusion existing between the phrases *strength of a machine part*, *strength of a material*, and *strength of a part at a point*.

A certain force F applied at D near the end of the 15-in lever shown in Fig. 5-16, which is quite similar to a socket wrench, results in certain stresses in the cantilevered bar $OABC$. This bar ($OABC$) is of AISI 1035 steel, forged and heat-treated so that it has a minimum (ASTM) yield strength of 81 kpsi. We presume that this component would be of no value after yielding. Thus the force F required to initiate yielding can be regarded as the strength of the component part. Find this force.

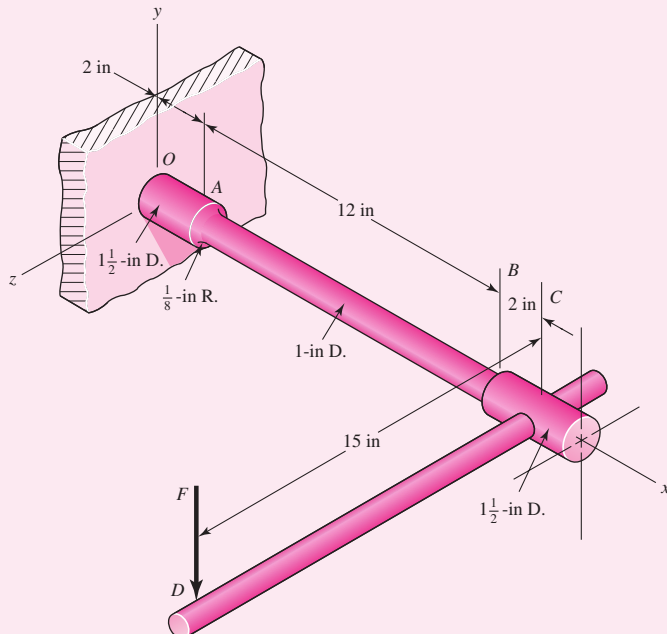
Solution

We will assume that lever DC is strong enough and hence not a part of the problem. A 1035 steel, heat-treated, will have a reduction in area of 50 percent or more and hence is a ductile material at normal temperatures. This also means that stress concentration at shoulder A need not be considered. A stress element at A on the top surface will be subjected to a tensile bending stress and a torsional stress. This point, on the 1-in-diameter section, is the weakest section, and governs the strength of the assembly. The two stresses are

$$\sigma_x = \frac{M}{I/c} = \frac{32M}{\pi d^3} = \frac{32(14F)}{\pi(1^3)} = 142.6F$$

$$\tau_{zx} = \frac{Tr}{J} = \frac{16T}{\pi d^3} = \frac{16(15F)}{\pi(1^3)} = 76.4F$$

| Figure 5-16



Employing the distortion-energy theory, we find, from Eq. (5–15), that

$$\sigma' = (\sigma_x^2 + 3\tau_{zx}^2)^{1/2} = [(142.6F)^2 + 3(76.4F)^2]^{1/2} = 194.5F$$

Equating the von Mises stress to S_y , we solve for F and get

Answer

$$F = \frac{S_y}{194.5} = \frac{81\ 000}{194.5} = 416 \text{ lbf}$$

In this example the strength of the material at point A is $S_y = 81$ kpsi. The strength of the assembly or component is $F = 416$ lbf.

Let us apply the MSS theory for comparison. For a point undergoing plane stress with only one nonzero normal stress and one shear stress, the two nonzero principal stresses will have opposite signs, and hence the maximum shear stress is obtained from the Mohr's circle between them. From Eq. (3–14)

$$\tau_{\max} = \sqrt{\left(\frac{\sigma_x}{2}\right)^2 + \tau_{zx}^2} = \sqrt{\left(\frac{142.6F}{2}\right)^2 + (76.4F)^2} = 104.5F$$

Setting this equal to $S_y/2$, from Eq. (5–3) with $n = 1$, and solving for F , we get

$$F = \frac{81\ 000/2}{104.5} = 388 \text{ lbf}$$

which is about 7 percent less than found for the DE theory. As stated earlier, the MSS theory is more conservative than the DE theory.

EXAMPLE 5–4

The cantilevered tube shown in Fig. 5–17 is to be made of 2014 aluminum alloy treated to obtain a specified minimum yield strength of 276 MPa. We wish to select a stock-size tube from Table A–8 using a design factor $n_d = 4$. The bending load is $F = 1.75$ kN, the axial tension is $P = 9.0$ kN, and the torsion is $T = 72$ N · m. What is the realized factor of safety?

Solution

The critical stress element is at point A on the top surface at the wall, where the bending moment is the largest, and the bending and torsional stresses are at their maximum values. The critical stress element is shown in Fig. 5–17b. Since the axial stress and bending stress are both in tension along the x axis, they are additive for the normal stress, giving

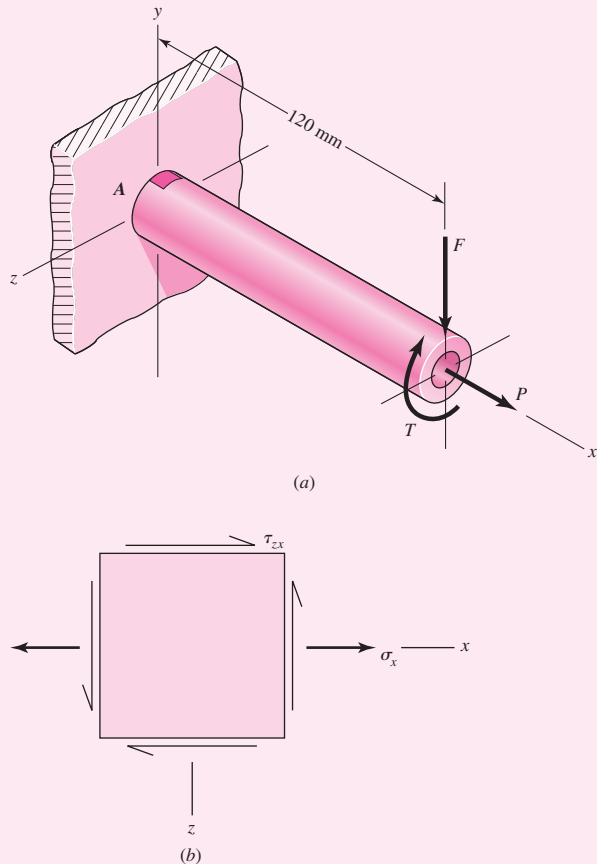
$$\sigma_x = \frac{P}{A} + \frac{Mc}{I} = \frac{9}{A} + \frac{120(1.75)(d_o/2)}{I} = \frac{9}{A} + \frac{105d_o}{I} \quad (1)$$

where, if millimeters are used for the area properties, the stress is in gigapascals.

The torsional stress at the same point is

$$\tau_{zx} = \frac{Tr}{J} = \frac{72(d_o/2)}{J} = \frac{36d_o}{J} \quad (2)$$

| Figure 5-17



For accuracy, we choose the distortion-energy theory as the design basis. The von Mises stress from Eq. (5-15), is

$$\sigma' = (\sigma_x^2 + 3\tau_{zx}^2)^{1/2} \quad (3)$$

On the basis of the given design factor, the goal for σ' is

$$\sigma' \leq \frac{S_y}{n_d} = \frac{0.276}{4} = 0.0690 \text{ GPa} \quad (4)$$

where we have used gigapascals in this relation to agree with Eqs. (1) and (2).

Programming Eqs. (1) to (3) on a spreadsheet and entering metric sizes from Table A-8 reveals that a 42×5 -mm tube is satisfactory. The von Mises stress is found to be $\sigma' = 0.06043$ GPa for this size. Thus the realized factor of safety is

Answer

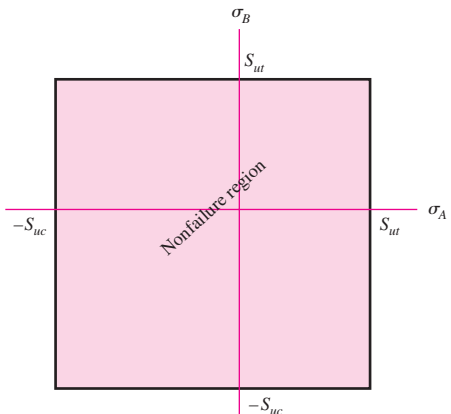
$$n = \frac{S_y}{\sigma'} = \frac{0.276}{0.06043} = 4.57$$

For the next size smaller, a 42×4 -mm tube, $\sigma' = 0.07105$ GPa giving a factor of safety of

$$n = \frac{S_y}{\sigma'} = \frac{0.276}{0.07105} = 3.88$$

Figure 5–18

Graph of maximum-normal-stress (MNS) theory failure envelope for plane stress states.



5–8

Maximum-Normal-Stress Theory for Brittle Materials

The maximum-normal-stress (MNS) theory states that *failure occurs whenever one of the three principal stresses equals or exceeds the strength*. Again we arrange the principal stresses for a general stress state in the ordered form $\sigma_1 \geq \sigma_2 \geq \sigma_3$. This theory then predicts that failure occurs whenever

$$\sigma_1 \geq S_{ut} \quad \text{or} \quad \sigma_3 \leq -S_{uc} \quad (5-28)$$

where S_{ut} and S_{uc} are the ultimate tensile and compressive strengths, respectively, given as positive quantities.

For plane stress, with the principal stresses given by Eq. (3–13), with $\sigma_A \geq \sigma_B$, Eq. (5–28) can be written as

$$\sigma_A \geq S_{ut} \quad \text{or} \quad \sigma_B \leq -S_{uc} \quad (5-29)$$

which is plotted in Fig. 5–18.

As before, the failure criteria equations can be converted to design equations. We can consider two sets of equations where $\sigma_A \geq \sigma_B$ as

$$\sigma_A = \frac{S_{ut}}{n} \quad \text{or} \quad \sigma_B = -\frac{S_{uc}}{n} \quad (5-30)$$

As will be seen later, the maximum-normal-stress theory is not very good at predicting failure in the fourth quadrant of the σ_A , σ_B plane. Thus, we will not recommend the theory for use. It has been included here mainly for historical reasons.

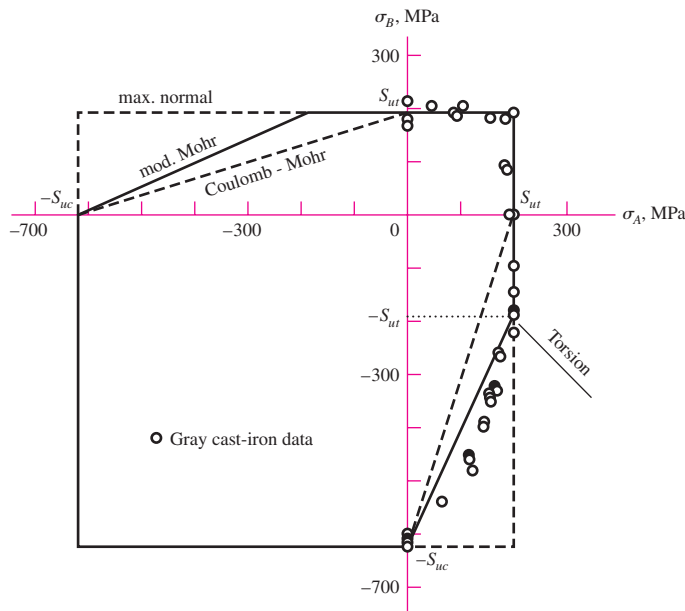
5–9

Modifications of the Mohr Theory for Brittle Materials

We will discuss two modifications of the Mohr theory for brittle materials: the Brittle-Coulomb-Mohr (BCM) theory and the modified Mohr (MM) theory. The equations provided for the theories will be restricted to plane stress and be of the design type incorporating the factor of safety.

Figure 5-19

Biaxial fracture data of gray cast iron compared with various failure criteria.
(Dowling, N. E., Mechanical Behavior of Materials, 2nd ed., 1999, p. 261. Reprinted by permission of Pearson Education, Inc., Upper Saddle River, New Jersey.)



The Coulomb-Mohr theory was discussed earlier in Sec. 5-6 with Eqs. (5-23) to (5-25). Written as design equations for a brittle material, they are:

Brittle-Coulomb-Mohr

$$\sigma_A = \frac{S_{ut}}{n} \quad \sigma_A \geq \sigma_B \geq 0 \quad (5-31a)$$

$$\frac{\sigma_A}{S_{ut}} - \frac{\sigma_B}{S_{uc}} = \frac{1}{n} \quad \sigma_A \geq 0 \geq \sigma_B \quad (5-31b)$$

$$\sigma_B = -\frac{S_{uc}}{n} \quad 0 \geq \sigma_A \geq \sigma_B \quad (5-31c)$$

On the basis of observed data for the fourth quadrant, the modified Mohr theory expands the fourth quadrant with the solid lines shown in the second and fourth quadrants of Fig. 5-19.

Modified Mohr

$$\sigma_A = \frac{S_{ut}}{n} \quad \sigma_A \geq \sigma_B \geq 0$$

$$\sigma_A \geq 0 \geq \sigma_B \quad \text{and} \quad \left| \frac{\sigma_B}{\sigma_A} \right| \leq 1 \quad (5-32a)$$

$$\frac{(S_{uc} - S_{ut}) \sigma_A}{S_{uc} S_{ut}} - \frac{\sigma_B}{S_{uc}} = \frac{1}{n} \quad \sigma_A \geq 0 \geq \sigma_B \quad \text{and} \quad \left| \frac{\sigma_B}{\sigma_A} \right| > 1 \quad (5-32b)$$

$$\sigma_B = -\frac{S_{uc}}{n} \quad 0 \geq \sigma_A \geq \sigma_B \quad (5-32c)$$

Data are still outside this extended region. The straight line introduced by the modified Mohr theory, for $\sigma_A \geq 0 \geq \sigma_B$ and $|\sigma_B/\sigma_A| > 1$, can be replaced by a parabolic relation

which can more closely represent some of the data.⁸ However, this introduces a nonlinear equation for the sake of a minor correction, and will not be presented here.

EXAMPLE 5-5

Consider the wrench in Ex. 5-3, Fig. 5-16, as made of cast iron, machined to dimension. The force F required to fracture this part can be regarded as the strength of the component part. If the material is ASTM grade 30 cast iron, find the force F with
 (a) Coulomb-Mohr failure model.
 (b) Modified Mohr failure model.

Solution

We assume that the lever DC is strong enough, and not part of the problem. Since grade 30 cast iron is a brittle material *and* cast iron, the stress-concentration factors K_t and K_{ts} are set to unity. From Table A-24, the tensile ultimate strength is 31 kpsi and the compressive ultimate strength is 109 kpsi. The stress element at A on the top surface will be subjected to a tensile bending stress and a torsional stress. This location, on the 1-in-diameter section fillet, is the weakest location, and it governs the strength of the assembly. The normal stress σ_x and the shear stress at A are given by

$$\sigma_x = K_t \frac{M}{I/c} = K_t \frac{32M}{\pi d^3} = (1) \frac{32(14F)}{\pi(1)^3} = 142.6F$$

$$\tau_{xy} = K_{ts} \frac{Tr}{J} = K_{ts} \frac{16T}{\pi d^3} = (1) \frac{16(15F)}{\pi(1)^3} = 76.4F$$

From Eq. (3-13) the nonzero principal stresses σ_A and σ_B are

$$\sigma_A, \sigma_B = \frac{142.6F + 0}{2} \pm \sqrt{\left(\frac{142.6F - 0}{2}\right)^2 + (76.4F)^2} = 175.8F, -33.2F$$

This puts us in the fourth-quadrant of the σ_A, σ_B plane.

(a) For BCM, Eq. (5-31b) applies with $n = 1$ for failure.

$$\frac{\sigma_A}{S_{ut}} - \frac{\sigma_B}{S_{uc}} = \frac{175.8F}{31(10^3)} - \frac{(-33.2F)}{109(10^3)} = 1$$

Solving for F yields

Answer

$$F = 167 \text{ lbf}$$

(b) For MM, the slope of the load line is $|\sigma_B/\sigma_A| = 33.2/175.8 = 0.189 < 1$. Obviously, Eq. (5-32a) applies.

$$\frac{\sigma_A}{S_{ut}} = \frac{175.8F}{31(10^3)} = 1$$

Answer

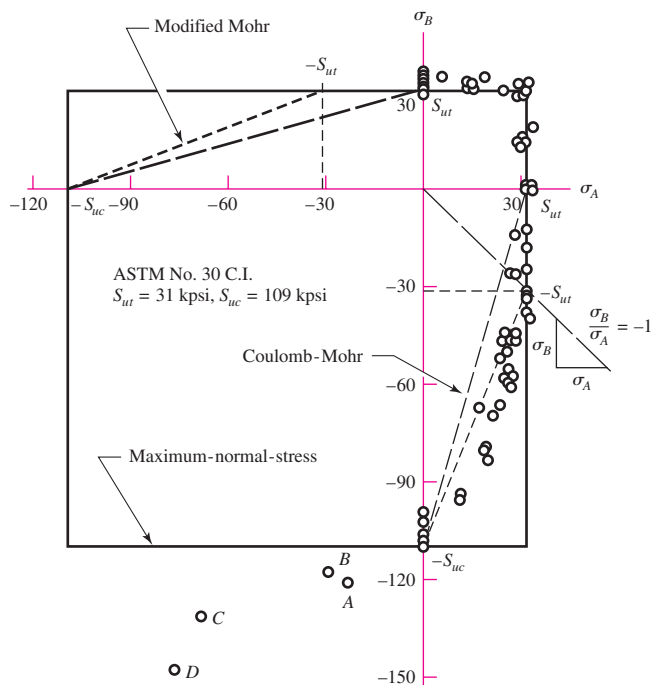
$$F = 176 \text{ lbf}$$

As one would expect from inspection of Fig. 5-19, Coulomb-Mohr is more conservative.

⁸See J. E. Shigley, C. R. Mischke, R. G. Budynas, *Mechanical Engineering Design*, 7th ed., McGraw-Hill, New York, 2004, p. 275.

Figure 5–20

A plot of experimental data points obtained from tests on cast iron. Shown also are the graphs of three failure theories of possible usefulness for brittle materials. Note points *A*, *B*, *C*, and *D*. To avoid congestion in the first quadrant, points have been plotted for $\sigma_A > \sigma_B$ as well as for the opposite sense. (Source of data: Charles F. Walton (ed.), Iron Castings Handbook, Iron Founders' Society, 1971, pp. 215, 216, Cleveland, Ohio.)



5-10 Failure of Brittle Materials Summary

We have identified failure or strength of brittle materials that conform to the usual meaning of the word *brittle*, relating to those materials whose true strain at fracture is 0.05 or less. We also have to be aware of normally ductile materials that for some reason may develop a brittle fracture or crack if used below the transition temperature. Figure 5–20 shows data for a nominal grade 30 cast iron taken under biaxial stress conditions, with several brittle failure hypotheses shown, superposed. We note the following:

- In the first quadrant the data appear on both sides and along the failure curves of maximum-normal-stress, Coulomb-Mohr, and modified Mohr. All failure curves are the same, and data fit well.
- In the fourth quadrant the modified Mohr theory represents the data best, whereas the maximum-normal-stress theory does not.
- In the third quadrant the points *A*, *B*, *C*, and *D* are too few to make any suggestion concerning a fracture locus.

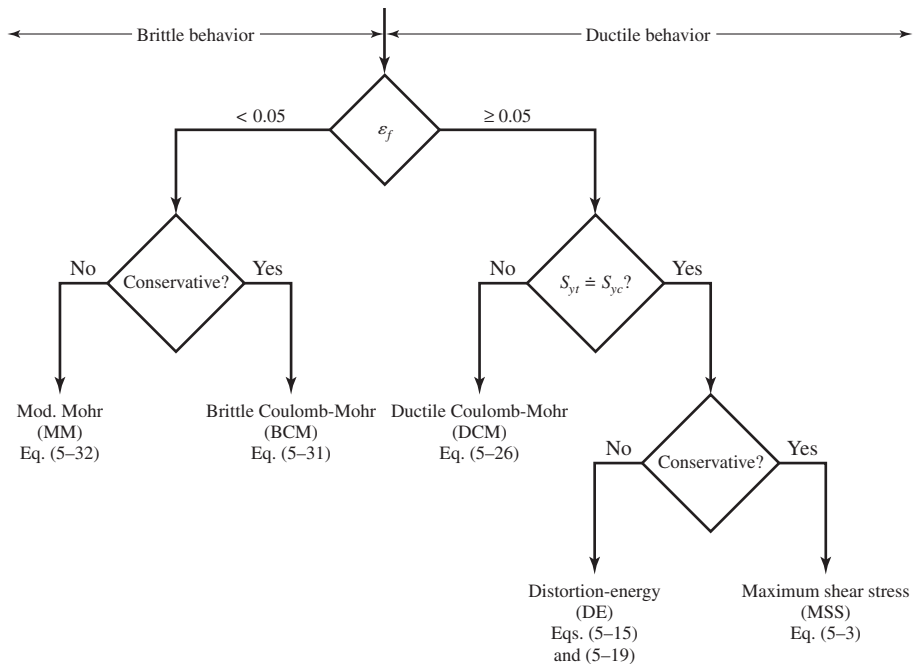
5-11 Selection of Failure Criteria

For ductile behavior the preferred criterion is the distortion-energy theory, although some designers also apply the maximum-shear-stress theory because of its simplicity and conservative nature. In the rare case when $S_{yt} \neq S_{yc}$, the ductile Coulomb-Mohr method is employed.

For brittle behavior, the original Mohr hypothesis, constructed with tensile, compression, and torsion tests, with a curved failure locus is the best hypothesis we have. However, the difficulty of applying it without a computer leads engineers to choose modifications,

Figure 5–21

Failure theory selection flowchart.



namely, Coulomb Mohr, or modified Mohr. Figure 5–21 provides a summary flowchart for the selection of an effective procedure for analyzing or predicting failures from static loading for brittle or ductile behavior. Note that the maximum-normal-stress theory is excluded from Fig. 5–21 as the other theories better represent the experimental data.

5–12

Introduction to Fracture Mechanics

The idea that cracks exist in parts even before service begins, and that cracks can grow during service, has led to the descriptive phrase “damage-tolerant design.” The focus of this philosophy is on crack growth until it becomes critical, and the part is removed from service. The analysis tool is *linear elastic fracture mechanics* (LEFM). Inspection and maintenance are essential in the decision to retire parts before cracks reach catastrophic size. Where human safety is concerned, periodic inspections for cracks are mandated by codes and government ordinance.

We shall now briefly examine some of the basic ideas and vocabulary needed for the potential of the approach to be appreciated. The intent here is to make the reader aware of the dangers associated with the sudden brittle fracture of so-called ductile materials. The topic is much too extensive to include in detail here and the reader is urged to read further on this complex subject.⁹

⁹References on brittle fracture include:

H. Tada, P. C. Paris, and G. R. Irwin, *The Stress Analysis of Cracks Handbook*, 3rd ed., ASME Press, New York, 2000.

D. Broek, *Elementary Engineering Fracture Mechanics*, 4th ed., Martinus Nijhoff, London, 1985.

D. Broek, *The Practical Use of Fracture Mechanics*, Kluwar Academic Pub., London, 1988.

David K. Felbeck and Anthony G. Atkins, *Strength and Fracture of Engineering Solids*, 2nd ed., Prentice-Hall, Englewood Cliffs, N.J., 1995.

Kåre Hellan, *Introduction to Fracture Mechanics*, McGraw-Hill, New York, 1984.

The use of elastic stress-concentration factors provides an indication of the average load required on a part for the onset of plastic deformation, or yielding; these factors are also useful for analysis of the loads on a part that will cause fatigue fracture. However, stress-concentration factors are limited to structures for which all dimensions are precisely known, particularly the radius of curvature in regions of high stress concentration. When there exists a crack, flaw, inclusion, or defect of unknown small radius in a part, the elastic stress-concentration factor approaches infinity as the root radius approaches zero, thus rendering the stress-concentration factor approach useless. Furthermore, even if the radius of curvature of the flaw tip is known, the high local stresses there will lead to local plastic deformation surrounded by a region of elastic deformation. Elastic stress-concentration factors are no longer valid for this situation, so analysis from the point of view of stress-concentration factors does not lead to criteria useful for design when very sharp cracks are present.

By combining analysis of the gross elastic changes in a structure or part that occur as a sharp brittle crack grows with measurements of the energy required to produce new fracture surfaces, it is possible to calculate the average stress (if no crack were present) that will cause crack growth in a part. Such calculation is possible only for parts with cracks for which the elastic analysis has been completed, and for materials that crack in a relatively brittle manner and for which the fracture energy has been carefully measured. The term *relatively brittle* is rigorously defined in the test procedures,¹⁰ but it means, roughly, *fracture without yielding occurring throughout the fractured cross section*.

Thus glass, hard steels, strong aluminum alloys, and even low-carbon steel below the ductile-to-brittle transition temperature can be analyzed in this way. Fortunately, ductile materials blunt sharp cracks, as we have previously discovered, so that fracture occurs at average stresses of the order of the yield strength, and the designer is prepared for this condition. The middle ground of materials that lie between “relatively brittle” and “ductile” is now being actively analyzed, but exact design criteria for these materials are not yet available.

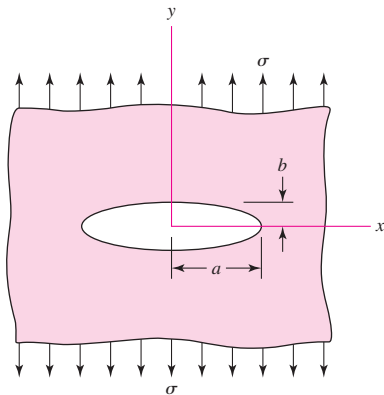
Quasi-Static Fracture

Many of us have had the experience of observing brittle fracture, whether it is the breaking of a cast-iron specimen in a tensile test or the twist fracture of a piece of blackboard chalk. It happens so rapidly that we think of it as instantaneous, that is, the cross section simply parting. Fewer of us have skated on a frozen pond in the spring, with no one near us, heard a cracking noise, and stopped to observe. The noise is due to cracking. The cracks move slowly enough for us to see them run. The phenomenon is not instantaneous, since some time is necessary to feed the crack energy from the stress field to the crack for propagation. Quantifying these things is important to understanding the phenomenon “in the small.” In the large, a static crack may be stable and will not propagate. Some level of loading can render the crack unstable, and the crack propagates to fracture.

The foundation of fracture mechanics was first established by Griffith in 1921 using the stress field calculations for an elliptical flaw in a plate developed by Inglis in 1913. For the infinite plate loaded by an applied uniaxial stress σ in Fig. 5–22, the maximum stress occurs at $(\pm a, 0)$ and is given by

$$(\sigma_y)_{\max} = \left(1 + 2\frac{a}{b}\right)\sigma \quad (5-33)$$

¹⁰BS 5447:1977 and ASTM E399-78.

| Figure 5–22

Note that when $a = b$, the ellipse becomes a circle and Eq. (5–33) gives a stress-concentration factor of 3. This agrees with the well-known result for an infinite plate with a circular hole (see Table A–15–1). For a fine crack, $b/a \rightarrow 0$, and Eq. (5–34) predicts that $(\sigma_y)_{\max} \rightarrow \infty$. However, on a microscopic level, an infinitely sharp crack is a hypothetical abstraction that is physically impossible, and when plastic deformation occurs, the stress will be finite at the crack tip.

Griffith showed that the crack growth occurs when the energy release rate from applied loading is greater than the rate of energy for crack growth. Crack growth can be stable or unstable. Unstable crack growth occurs when the *rate* of change of the energy release rate relative to the crack length is equal to or greater than the *rate* of change of the crack growth rate of energy. Griffith's experimental work was restricted to brittle materials, namely glass, which pretty much confirmed his surface energy hypothesis. However, for ductile materials, the energy needed to perform plastic work at the crack tip is found to be much more crucial than surface energy.

Crack Modes and the Stress Intensity Factor

Three distinct modes of crack propagation exist, as shown in Fig. 5–23. A tensile stress field gives rise to mode I, the *opening crack propagation mode*, as shown in Fig. 5–23a. This mode is the most common in practice. Mode II is the *sliding mode*, is due to in-plane shear, and can be seen in Fig. 5–23b. Mode III is the *tearing mode*, which arises from out-of-plane shear, as shown in Fig. 5–23c. Combinations of these modes can also occur. Since mode I is the most common and important mode, the remainder of this section will consider only this mode.

| Figure 5–23

Crack propagation modes.

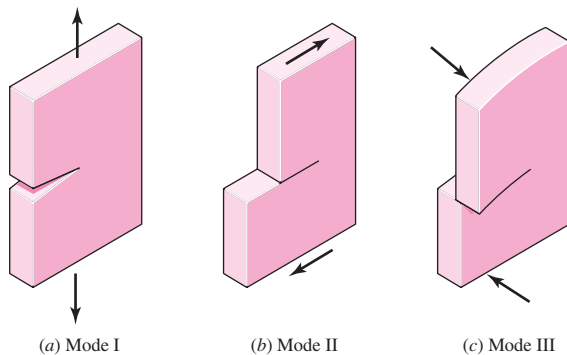
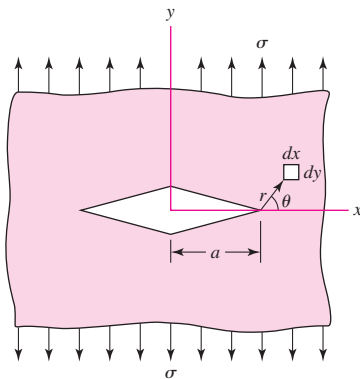


Figure 5-24

Mode I crack model.



Consider a mode I crack of length $2a$ in the infinite plate of Fig. 5-24. By using complex stress functions, it has been shown that the stress field on a $dx\ dy$ element in the vicinity of the crack tip is given by

$$\sigma_x = \sigma \sqrt{\frac{a}{2r}} \cos \frac{\theta}{2} \left(1 - \sin \frac{\theta}{2} \sin \frac{3\theta}{2} \right) \quad (5-34a)$$

$$\sigma_y = \sigma \sqrt{\frac{a}{2r}} \cos \frac{\theta}{2} \left(1 + \sin \frac{\theta}{2} \sin \frac{3\theta}{2} \right) \quad (5-34b)$$

$$\tau_{xy} = \sigma \sqrt{\frac{a}{2r}} \sin \frac{\theta}{2} \cos \frac{\theta}{2} \cos \frac{3\theta}{2} \quad (5-34c)$$

$$\sigma_z = \begin{cases} 0 & \text{(for plane stress)} \\ v(\sigma_x + \sigma_y) & \text{(for plane strain)} \end{cases} \quad (5-34d)$$

The stress σ_y near the tip, with $\theta = 0$, is

$$\sigma_y|_{\theta=0} = \sigma \sqrt{\frac{a}{2r}} \quad (a)$$

As with the elliptical crack, we see that $\sigma_y|_{\theta=0} \rightarrow \infty$ as $r \rightarrow 0$, and again the concept of an infinite stress concentration at the crack tip is inappropriate. The quantity $\sigma_y|_{\theta=0}\sqrt{2r} = \sigma\sqrt{a}$, however, does remain constant as $r \rightarrow 0$. It is common practice to define a factor K called the *stress intensity factor* given by

$$K = \sigma \sqrt{\pi a} \quad (b)$$

where the units are MPa $\sqrt{\text{m}}$ or kpsi $\sqrt{\text{in}}$. Since we are dealing with a mode I crack, Eq. (b) is written as

$$K_I = \sigma \sqrt{\pi a} \quad (5-35)$$

The stress intensity factor is *not* to be confused with the static stress-concentration factors K_t and K_{ts} defined in Secs. 3-13 and 5-2.

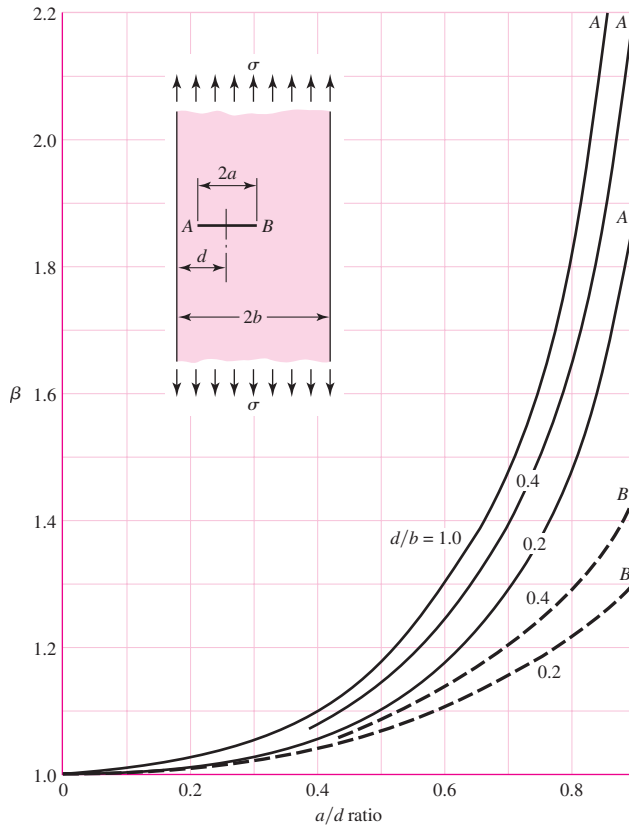
Thus Eqs. (5-34) can be rewritten as

$$\sigma_x = \frac{K_I}{\sqrt{2\pi r}} \cos \frac{\theta}{2} \left(1 - \sin \frac{\theta}{2} \sin \frac{3\theta}{2} \right) \quad (5-36a)$$

$$\sigma_y = \frac{K_I}{\sqrt{2\pi r}} \cos \frac{\theta}{2} \left(1 + \sin \frac{\theta}{2} \sin \frac{3\theta}{2} \right) \quad (5-36b)$$

Figure 5–25

Off-center crack in a plate in longitudinal tension; solid curves are for the crack tip at A; dashed curves are for the tip at B.



$$\tau_{xy} = \frac{K_I}{\sqrt{2\pi r}} \sin \frac{\theta}{2} \cos \frac{\theta}{2} \cos \frac{3\theta}{2} \quad (5-36c)$$

$$\sigma_z = \begin{cases} 0 & \text{(for plane stress)} \\ v(\sigma_x + \sigma_y) & \text{(for plane strain)} \end{cases} \quad (5-36d)$$

The stress intensity factor is a function of geometry, size and shape of the crack, and the type of loading. For various load and geometric configurations, Eq. (5–35) can be written as

$$K_I = \beta \sigma \sqrt{\pi a} \quad (5-37)$$

where β is the *stress intensity modification factor*. Tables for β are available in the literature for basic configurations.¹¹ Figures 5–25 to 5–30 present a few examples of β for mode I crack propagation.

¹¹See, for example:

H. Tada, P. C. Paris, and G. R. Irwin, *The Stress Analysis of Cracks Handbook*, 3rd ed., ASME Press, New York, 2000.

G. C. Sib, *Handbook of Stress Intensity Factors for Researchers and Engineers*, Institute of Fracture and Solid Mechanics, Lehigh University, Bethlehem, Pa., 1973.

Y. Murakami, ed., *Stress Intensity Factors Handbook*, Pergamon Press, Oxford, U.K., 1987.

W. D. Pilkey, *Formulas for Stress, Strain, and Structural Matrices*, 2nd ed. John Wiley & Sons, New York, 2005.

Figure 5-26

Plate loaded in longitudinal tension with a crack at the edge; for the solid curve there are no constraints to bending; the dashed curve was obtained with bending constraints added.

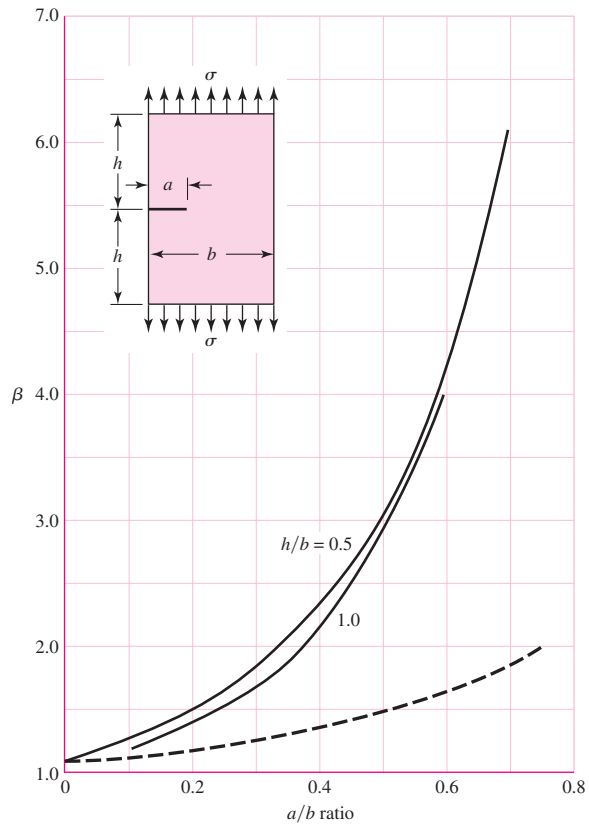


Figure 5-27

Beams of rectangular cross section having an edge crack.

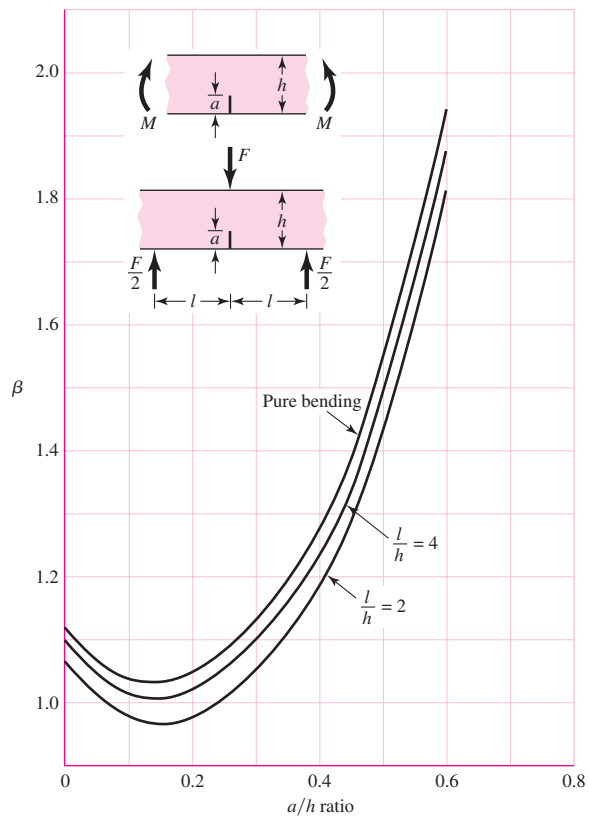
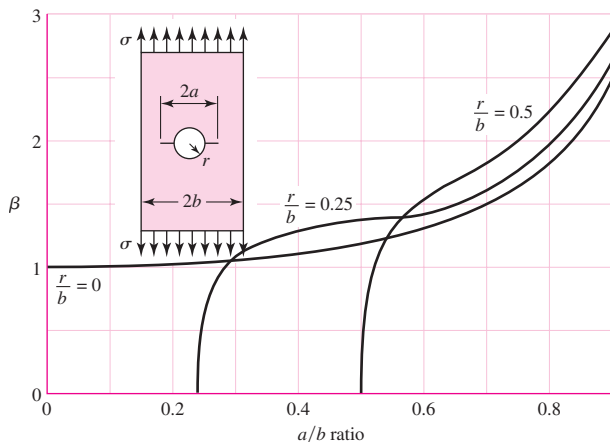
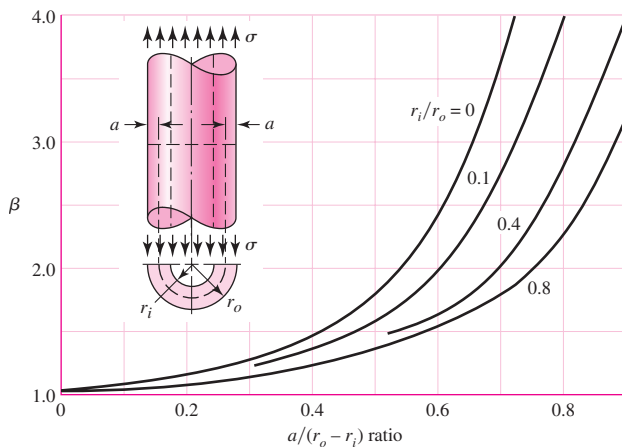


Figure 5–28

Plate in tension containing a circular hole with two cracks.

**Figure 5–29**

A cylinder loading in axial tension having a radial crack of depth a extending completely around the circumference of the cylinder.



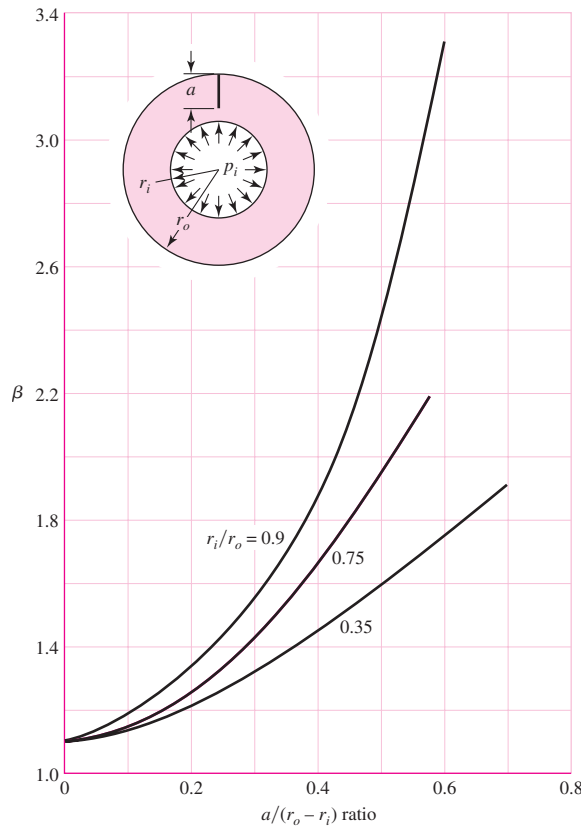
Fracture Toughness

When the magnitude of the mode I stress intensity factor reaches a critical value, K_{Ic} , crack propagation initiates. The *critical stress intensity factor* K_{Ic} is a material property that depends on the material, crack mode, processing of the material, temperature, loading rate, and the state of stress at the crack site (such as plane stress versus plane strain). The critical stress intensity factor K_{Ic} is also called the *fracture toughness* of the material. The fracture toughness for plane strain is normally lower than that for plane stress. For this reason, the term K_{Ic} is typically defined as the *mode I, plane strain fracture toughness*. Fracture toughness K_{Ic} for engineering metals lies in the range $20 \leq K_{Ic} \leq 200 \text{ MPa} \cdot \sqrt{\text{m}}$; for engineering polymers and ceramics, $1 \leq K_{Ic} \leq 5 \text{ MPa} \cdot \sqrt{\text{m}}$. For a 4340 steel, where the yield strength due to heat treatment ranges from 800 to 1600 MPa, K_{Ic} decreases from 190 to 40 $\text{MPa} \cdot \sqrt{\text{m}}$.

Table 5–1 gives some approximate typical room-temperature values of K_{Ic} for several materials. As previously noted, the fracture toughness depends on many factors and the table is meant only to convey some typical magnitudes of K_{Ic} . For an actual application, it is recommended that the material specified for the application be certified using standard test procedures [see the American Society for Testing and Materials (ASTM) standard E399].

Figure 5-30

Cylinder subjected to internal pressure p , having a radial crack in the longitudinal direction of depth a . Use Eq. (4-51) for the tangential stress at $r = r_0$.



One of the first problems facing the designer is that of deciding whether the conditions exist, or not, for a brittle fracture. Low-temperature operation, that is, operation below room temperature, is a key indicator that brittle fracture is a possible failure mode. Tables of transition temperatures for various materials have not been published, possibly because of the wide variation in values, even for a single material. Thus, in many situations, laboratory testing may give the only clue to the possibility of a brittle fracture. Another key indicator of the possibility of fracture is the ratio of the yield strength to the ultimate strength. A high ratio of S_y/S_u indicates there is only a small

Table 5-1

Values of K_{Ic} for Some Engineering Materials at Room Temperature

Material	K_{Ic} , MPa $\sqrt{\text{m}}$	S_y , MPa
Aluminum		
2024	26	455
7075	24	495
7178	33	490
Titanium		
Ti-6AL-4V	115	910
Ti-6AL-4V	55	1035
Steel		
4340	99	860
4340	60	1515
52100	14	2070

ability to absorb energy in the plastic region and hence there is a likelihood of brittle fracture.

The strength-to-stress ratio K_{Ic}/K_I can be used as a factor of safety as

$$n = \frac{K_{Ic}}{K_I} \quad (5-38)$$

EXAMPLE 5-6

A steel ship deck plate is 30 mm thick and 12 m wide. It is loaded with a nominal uniaxial tensile stress of 50 MPa. It is operated below its ductile-to-brittle transition temperature with K_{Ic} equal to 28.3 MPa. If a 65-mm-long central transverse crack is present, estimate the tensile stress at which catastrophic failure will occur. Compare this stress with the yield strength of 240 MPa for this steel.

Solution

For Fig. 5-25, with $d = b$, $2a = 65$ mm and $2b = 12$ m, so that $d/b = 1$ and $a/d = 65/12(10^3) = 0.00542$. Since a/d is so small, $\beta = 1$, so that

$$K_I = \sigma \sqrt{\pi a} = 50\sqrt{\pi(32.5 \times 10^{-3})} = 16.0 \text{ MPa } \sqrt{\text{m}}$$

From Eq. (5-38),

$$n = \frac{K_{Ic}}{K_I} = \frac{28.3}{16.0} = 1.77$$

The stress at which catastrophic failure occurs is

Answer

$$\sigma_c = \frac{K_{Ic}}{K_I} \sigma = \frac{28.3}{16.0}(50) = 88.4 \text{ MPa}$$

The yield strength is 240 MPa, and catastrophic failure occurs at $88.4/240 = 0.37$, or at 37 percent of yield. The factor of safety in this circumstance is $K_{Ic}/K_I = 28.3/16 = 1.77$ and *not* $240/50 = 4.8$.

EXAMPLE 5-7

A plate of width 1.4 m and length 2.8 m is required to support a tensile force in the 2.8-m direction of 4.0 MN. Inspection procedures will detect only through-thickness edge cracks larger than 2.7 mm. The two Ti-6AL-4V alloys in Table 5-1 are being considered for this application, for which the safety factor must be 1.3 and minimum weight is important. Which alloy should be used?

Solution

(a) We elect first to estimate the thickness required to resist yielding. Since $\sigma = P/wt$, we have $t = P/w\sigma$. For the weaker alloy, we have, from Table 5-1, $S_y = 910$ MPa. Thus,

$$\sigma_{\text{all}} = \frac{S_y}{n} = \frac{910}{1.3} = 700 \text{ MPa}$$

Thus

$$t = \frac{P}{w\sigma_{\text{all}}} = \frac{4.0(10)^3}{1.4(700)} = 4.08 \text{ mm or greater}$$

For the stronger alloy, we have, from Table 5–1,

$$\sigma_{\text{all}} = \frac{1035}{1.3} = 796 \text{ MPa}$$

and so the thickness is

Answer

$$t = \frac{P}{w\sigma_{\text{all}}} = \frac{4.0(10)^3}{1.4(796)} = 3.59 \text{ mm or greater}$$

(b) Now let us find the thickness required to prevent crack growth. Using Fig. 5–26, we have

$$\frac{h}{b} = \frac{2.8/2}{1.4} = 1 \quad \frac{a}{b} = \frac{2.7}{1.4(10^3)} = 0.00193$$

Corresponding to these ratios we find from Fig. 5–26 that $\beta \doteq 1.1$, and $K_I = 1.1\sigma\sqrt{\pi a}$.

$$n = \frac{K_{Ic}}{K_I} = \frac{115\sqrt{10^3}}{1.1\sigma\sqrt{\pi a}}, \quad \sigma = \frac{K_{Ic}}{1.1n\sqrt{\pi a}}$$

From Table 5–1, $K_{Ic} = 115 \text{ MPa}\sqrt{m}$ for the weaker of the two alloys. Solving for σ with $n = 1$ gives the fracture stress

$$\sigma = \frac{115}{1.1\sqrt{\pi(2.7 \times 10^{-3})}} = 1135 \text{ MPa}$$

which is greater than the yield strength of 910 MPa, and so yield strength is the basis for the geometry decision. For the stronger alloy $S_y = 1035 \text{ MPa}$, with $n = 1$ the fracture stress is

$$\sigma = \frac{K_{Ic}}{nK_I} = \frac{55}{1(1.1)\sqrt{\pi(2.7 \times 10^{-3})}} = 542.9 \text{ MPa}$$

which is less than the yield strength of 1035 MPa. The thickness t is

$$t = \frac{P}{w\sigma_{\text{all}}} = \frac{4.0(10^3)}{1.4(542.9/1.3)} = 6.84 \text{ mm or greater}$$

This example shows that the fracture toughness K_{Ic} limits the geometry when the stronger alloy is used, and so a thickness of 6.84 mm or larger is required. When the weaker alloy is used the geometry is limited by the yield strength, giving a thickness of only 4.08 mm or greater. Thus the weaker alloy leads to a thinner and lighter weight choice since the failure modes differ.

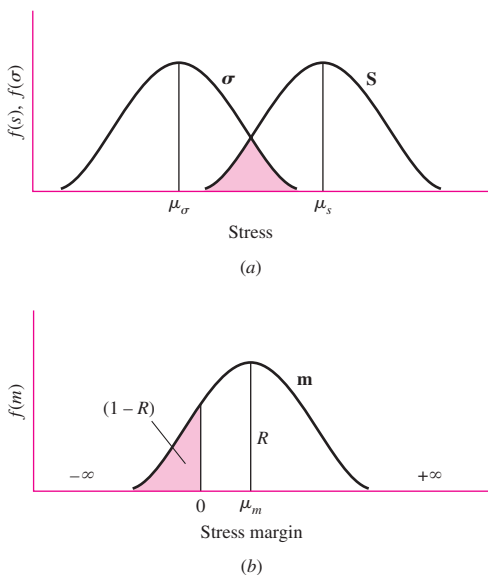
5–13 Stochastic Analysis¹²

Reliability is the probability that machine systems and components will perform their intended function satisfactorily without failure. Up to this point, discussion in this chapter has been restricted to deterministic relations between static stress, strength, and the design factor. Stress and strength, however, are statistical in nature and very much tied to the reliability of the stressed component. Consider the probability density functions

¹²Review Chap. 20 before reading this section.

Figure 5–31

Plot of density functions showing how the interference of S and σ is used to obtain the stress margin m . (a) Stress and strength distributions. (b) Distribution of interference; the reliability R is the area of the density function for m greater than zero; the interference is the area $(1 - R)$.



for stress and strength, σ and S , shown in Fig. 5–31a. The mean values of stress and strength are μ_σ and μ_S , respectively. Here, the “average” factor of safety is

$$\bar{n} = \frac{\mu_S}{\mu_\sigma} \quad (a)$$

The *margin of safety* for any value of stress σ and strength S is defined as

$$m = S - \sigma \quad (b)$$

The average part will have a margin of safety of $\bar{m} = \mu_S - \mu_\sigma$. However, for the overlap of the distributions shown by the shaded area in Fig. 5–31a, the stress exceeds the strength, the margin of safety is negative, and these parts are expected to fail. This shaded area is called the *interference* of σ and S .

Figure 5–31b shows the distribution of m , which obviously depends on the distributions of stress and strength. The reliability that a part will perform without failure, R , is the area of the margin of safety distribution for $m > 0$. The interference is the area $1 - R$ where parts are expected to fail. We next consider some typical cases involving stress-strength interference.

Normal-Normal Case

Consider the normal distributions, $S = N(\mu_S, \hat{\sigma}_S^2)$ and $\sigma = N(\mu_\sigma, \hat{\sigma}_\sigma^2)$. The stress margin is $m = S - \sigma$, and will be normally distributed because the addition or subtraction of normals is normal. Thus $m = N(\mu_m, \hat{\sigma}_m^2)$. Reliability is the probability p that $m > 0$. That is,

$$R = p(S > \sigma) = p(S - \sigma > 0) = p(m > 0) \quad (5-39)$$

To find the chance that $m > 0$ we form the z variable of m and substitute $m = 0$ [See Eq. (20–16)]. Noting that $\mu_m = \mu_S - \mu_\sigma$ and $\hat{\sigma}_m = (\hat{\sigma}_S^2 + \hat{\sigma}_\sigma^2)^{1/2}$, we write

$$z = \frac{m - \mu_m}{\hat{\sigma}_m} = \frac{0 - \mu_m}{\hat{\sigma}_m} = -\frac{\mu_m}{\hat{\sigma}_m} = -\frac{\mu_S - \mu_\sigma}{(\hat{\sigma}_S^2 + \hat{\sigma}_\sigma^2)^{1/2}} \quad (5-40)$$

Equation (5–40) is called the *normal coupling equation*. The reliability associated with z is given by

$$R = \int_x^\infty \frac{1}{\sqrt{2\pi}} \exp\left(-\frac{u^2}{2}\right) du = 1 - F = 1 - \Phi(z) \quad (5-41)$$

The body of Table A–10 gives R when $z > 0$ and $(1 - R = F)$ when $z \leq 0$. Noting that $\bar{n} = \mu_S/\mu_\sigma$, square both sides of Eq. (5–40), and introduce C_S and C_σ where $C_S = \hat{\sigma}_S/\mu_S$ and $C_\sigma = \hat{\sigma}_\sigma/\mu_\sigma$. Solve the resulting quadratic for \bar{n} to obtain

$$\bar{n} = \frac{1 \pm \sqrt{1 - (1 - z^2 C_S^2)(1 - z^2 C_\sigma^2)}}{1 - z^2 C_S^2} \quad (5-42)$$

The plus sign is associated with $R > 0.5$, and the minus sign with $R < 0.5$.

Lognormal-Lognormal Case

Consider the lognormal distributions $\mathbf{S} = \mathbf{LN}(\mu_S, \hat{\sigma}_S)$ and $\boldsymbol{\sigma} = \mathbf{LN}(\mu_\sigma, \hat{\sigma}_\sigma)$. If we interfere their companion normals using Eqs. (20–18) and (20–19), we obtain

$$\begin{aligned} \mu_{\ln S} &= \ln \mu_S - \ln \sqrt{1 + C_S^2} && \text{(strength)} \\ \hat{\sigma}_{\ln S} &= \sqrt{\ln(1 + C_S^2)} \end{aligned}$$

and

$$\begin{aligned} \mu_{\ln \sigma} &= \ln \mu_\sigma - \ln \sqrt{1 + C_\sigma^2} && \text{(stress)} \\ \hat{\sigma}_{\ln \sigma} &= \sqrt{\ln(1 + C_\sigma^2)} \end{aligned}$$

Using Eq. (5–40) for interfering normal distributions gives

$$z = -\frac{\mu_{\ln S} - \mu_{\ln \sigma}}{(\hat{\sigma}_{\ln S}^2 + \hat{\sigma}_{\ln \sigma}^2)^{1/2}} = -\frac{\ln\left(\frac{\mu_S}{\mu_\sigma} \sqrt{\frac{1 + C_\sigma^2}{1 + C_S^2}}\right)}{\sqrt{\ln[(1 + C_S^2)(1 + C_\sigma^2)]}} \quad (5-43)$$

The reliability R is expressed by Eq. (5–41). The design factor \mathbf{n} is the random variable that is the quotient of $\mathbf{S}/\boldsymbol{\sigma}$. The quotient of lognormals is lognormal, so pursuing the z variable of the lognormal \mathbf{n} , we note

$$\mu_n = \frac{\mu_S}{\mu_\sigma} \quad C_n = \sqrt{\frac{C_S^2 + C_\sigma^2}{1 + C_\sigma^2}} \quad \hat{\sigma}_n = C_n \mu_n$$

The companion normal to $\mathbf{n} = \mathbf{LN}(\mu_n, \hat{\sigma}_n)$, from Eqs. (20–18) and (20–19), has a mean and standard deviation of

$$\mu_y = \ln \mu_n - \ln \sqrt{1 + C_n^2} \quad \hat{\sigma}_y = \sqrt{\ln(1 + C_n^2)}$$

The z variable for the companion normal y distribution is

$$z = \frac{y - \mu_y}{\hat{\sigma}_y}$$

Failure will occur when the stress is greater than the strength, when $\bar{n} < 1$, or when $y < 0$.

$$z = \frac{0 - \mu_y}{\hat{\sigma}_y} = -\frac{\mu_y}{\sigma_y} = -\frac{\ln \mu_n - \ln \sqrt{1 + C_n^2}}{\sqrt{\ln(1 + C_n^2)}} \doteq -\frac{\ln(\mu_n / \sqrt{1 + C_n^2})}{\sqrt{\ln(1 + C_n^2)}} \quad (5-44)$$

Solving for μ_n gives

$$\mu_n = \bar{n} = \exp \left[-z \sqrt{\ln(1 + C_n^2)} + \ln \sqrt{1 + C_n^2} \right] \doteq \exp \left[C_n \left(-z + \frac{C_n}{2} \right) \right] \quad (5-45)$$

Equations (5-42) and (5-45) are remarkable for several reasons:

- They relate design factor \bar{n} to the reliability goal (through z) and the coefficients of variation of strength and stress.
- They are *not* functions of the means of stress and strength.
- They estimate the design factor necessary to achieve the reliability goal before decisions involving means are made. The C_S depends slightly on the particular material. The C_σ has the coefficient of variation (COV) of the load, and that is generally given.

EXAMPLE 5-8

A round cold-drawn 1018 steel rod has an 0.2 percent yield strength $S_y = N(78.4, 5.90)$ kpsi and is to be subjected to a static axial load of $P = N(50, 4.1)$ kip. What value of the design factor \bar{n} corresponds to a reliability of 0.999 against yielding ($z = -3.09$)? Determine the corresponding diameter of the rod.

Solution $C_S = 5.90/78.4 = 0.0753$, and

$$\sigma = \frac{P}{A} = \frac{4P}{\pi d^2}$$

Since the COV of the diameter is an order of magnitude less than the COV of the load or strength, the diameter is treated deterministically:

$$C_\sigma = C_P = \frac{4.1}{50} = 0.082$$

From Eq. (5-42),

$$\bar{n} = \frac{1 + \sqrt{1 - [1 - (-3.09)^2(0.0753^2)][1 - (-3.09)^2(0.082^2)]}}{1 - (-3.09)^2(0.0753^2)} = 1.416$$

The diameter is found deterministically:

Answer

$$d = \sqrt{\frac{4\bar{P}}{\pi \bar{S}_y / \bar{n}}} = \sqrt{\frac{4(50\,000)}{\pi(78\,400)/1.416}} = 1.072 \text{ in}$$

Check $S_y = N(78.4, 5.90)$ kpsi, $P = N(50, 4.1)$ kip, and $d = 1.072$ in. Then

$$A = \frac{\pi d^2}{4} = \frac{\pi (1.072^2)}{4} = 0.9026 \text{ in}^2$$

$$\bar{\sigma} = \frac{\bar{P}}{A} = \frac{(50\ 000)}{0.9026} = 55\ 400 \text{ psi}$$

$$C_P = C_\sigma = \frac{4.1}{50} = 0.082$$

$$\hat{\sigma}_\sigma = C_\sigma \bar{\sigma} = 0.082(55\ 400) = 4540 \text{ psi}$$

$$\hat{\sigma}_S = 5.90 \text{ kpsi}$$

From Eq. (5-40)

$$z = -\frac{78.4 - 55.4}{(5.90^2 + 4.54^2)^{1/2}} = -3.09$$

From Appendix Table A-10, $R = \Phi(-3.09) = 0.999$.

EXAMPLE 5-9

Rework Ex. 5-8 with lognormally distributed stress and strength.

Solution

$C_S = 5.90/78.4 = 0.0753$, and $C_\sigma = C_P = 4.1/50 = 0.082$. Then

$$\sigma = \frac{P}{A} = \frac{4P}{\pi d^2}$$

$$C_n = \sqrt{\frac{C_S^2 + C_\sigma^2}{1 + C_\sigma^2}} = \sqrt{\frac{0.0753^2 + 0.082^2}{1 + 0.082^2}} = 0.1110$$

From Table A-10, $z = -3.09$. From Eq. (5-45),

$$\bar{n} = \exp \left[-(-3.09) \sqrt{\ln(1 + 0.111^2)} + \ln \sqrt{1 + 0.111^2} \right] = 1.416$$

$$d = \sqrt{\frac{4\bar{P}}{\pi \bar{S}_y / \bar{n}}} = \sqrt{\frac{4(50\ 000)}{\pi (78\ 400) / 1.416}} = 1.0723 \text{ in}$$

Check

$S_y = LN(78.4, 5.90)$, $P = LN(50, 4.1)$ kip. Then

$$A = \frac{\pi d^2}{4} = \frac{\pi (1.0723^2)}{4} = 0.9031$$

$$\bar{\sigma} = \frac{\bar{P}}{A} = \frac{50\ 000}{0.9031} = 55\ 365 \text{ psi}$$

$$C_\sigma = C_P = \frac{4.1}{50} = 0.082$$

$$\hat{\sigma}_\sigma = C_\sigma \mu_\sigma = 0.082(55\ 367) = 4540 \text{ psi}$$

From Eq. (5-43),

$$z = -\frac{\ln \left(\frac{78.4}{55.365} \sqrt{\frac{1 + 0.082^2}{1 + 0.0753^2}} \right)}{\sqrt{\ln[(1 + 0.0753^2)(1 + 0.082^2)]}} = -3.1343$$

Appendix Table A-10 gives $R = 0.99950$.

Interference—General

In the previous segments, we employed interference theory to estimate reliability when the distributions are both normal and when they are both lognormal. Sometimes, however, it turns out that the strength has, say, a Weibull distribution while the stress is distributed lognormally. In fact, stresses are quite likely to have a lognormal distribution, because the multiplication of variates that are normally distributed produces a result that approaches lognormal. What all this means is that we must expect to encounter interference problems involving mixed distributions and we need a general method to handle the problem.

It is quite likely that we will use interference theory for problems involving distributions other than strength and stress. For this reason we employ the subscript 1 to designate the strength distribution and the subscript 2 to designate the stress distribution. Figure 5–32 shows these two distributions aligned so that a single cursor x can be used to identify points on both distributions. We can now write

$$\left(\begin{array}{l} \text{Probability that} \\ \text{stress is less} \\ \text{than strength} \end{array} \right) = dP(\sigma < x) = dR = F_2(x) dF_1(x)$$

By substituting $1 - R_2$ for F_2 and $-dR_1$ for dF_1 , we have

$$dR = -[1 - R_2(x)] dR_1(x)$$

The reliability for all possible locations of the cursor is obtained by integrating x from $-\infty$ to ∞ ; but this corresponds to an integration from 1 to 0 on the reliability R_1 . Therefore

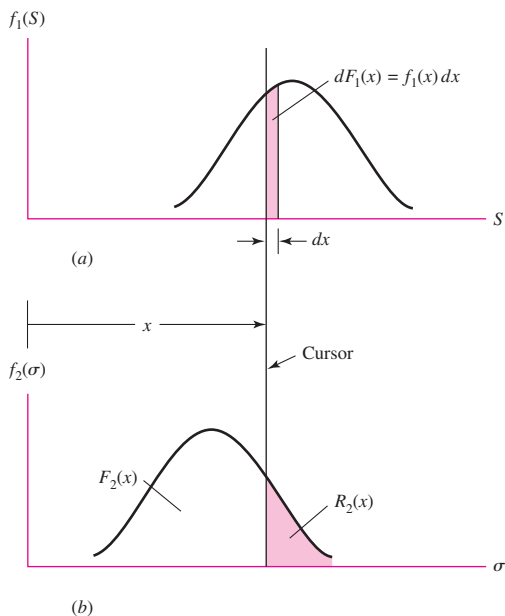
$$R = - \int_1^0 [1 - R_2(x)] dR_1(x)$$

which can be written

$$R = 1 - \int_0^1 R_2 dR_1 \quad (5-46)$$

Figure 5–32

(a) PDF of the strength distribution; (b) PDF of the load-induced stress distribution.



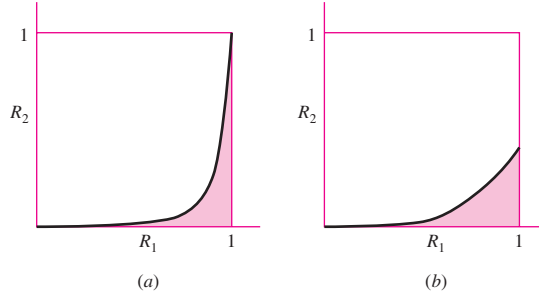


Figure 5-33

Curve shapes of the $R_1 R_2$ plot. In each case the shaded area is equal to $1 - R$ and is obtained by numerical integration.
 (a) Typical curve for asymptotic distributions; (b) curve shape obtained from lower truncated distributions such as the Weibull.

where

$$R_1(x) = \int_x^{\infty} f_1(S) dS \quad (5-47)$$

$$R_2(x) = \int_x^{\infty} f_2(\sigma) d\sigma \quad (5-48)$$

For the usual distributions encountered, plots of R_1 versus R_2 appear as shown in Fig. 5-33. Both of the cases shown are amenable to numerical integration and computer solution. When the reliability is high, the bulk of the integration area is under the right-hand spike of Fig. 5-33a.

5-14 Important Design Equations

The following equations and their locations are provided as a summary. *Note for plane stress:* The principal stresses in the following equations that are labeled σ_A and σ_B represent the principal stresses determined from the *two-dimensional* Eq. (3-13).

Maximum Shear Theory

p. 220 $\tau_{\max} = \frac{\sigma_1 - \sigma_3}{2} = \frac{S_y}{2n}$ (5-3)

Distortion-Energy Theory

Von Mises stress, p. 223

$$\sigma' = \left[\frac{(\sigma_1 - \sigma_2)^2 + (\sigma_2 - \sigma_3)^2 + (\sigma_3 - \sigma_1)^2}{2} \right]^{1/2} \quad (5-12)$$

$$p. 223 \quad \sigma' = \frac{1}{\sqrt{2}} [(\sigma_x - \sigma_y)^2 + (\sigma_y - \sigma_z)^2 + (\sigma_z - \sigma_x)^2 + 6(\tau_{xy}^2 + \tau_{yz}^2 + \tau_{zx}^2)]^{1/2} \quad (5-14)$$

Plane stress, p. 223

$$\sigma' = (\sigma_A^2 - \sigma_A \sigma_B + \sigma_B^2)^{1/2} \quad (5-13)$$

$$\sigma' = (\sigma_x^2 - \sigma_x \sigma_y + \sigma_y^2 + 3\tau_{xy}^2)^{1/2} \quad (5-15)$$

Yield design equation, p. 224

$$\sigma' = \frac{S_y}{n} \quad (5-19)$$

Shear yield strength, p. 225

$$S_{sy} = 0.577 S_y \quad (5-21)$$

Coulomb-Mohr Theory

p. 225

$$\frac{\sigma_1}{S_t} - \frac{\sigma_3}{S_c} = \frac{1}{n} \quad (5-26)$$

where S_t is tensile yield (ductile) or ultimate tensile (brittle), and S_c is compressive yield (ductile) or ultimate compressive (brittle) strengths.

Modified Mohr (Plane Stress)

$$\sigma_A = \frac{S_{ut}}{n} \quad \sigma_A \geq \sigma_B \geq 0 \quad (5-32a)$$

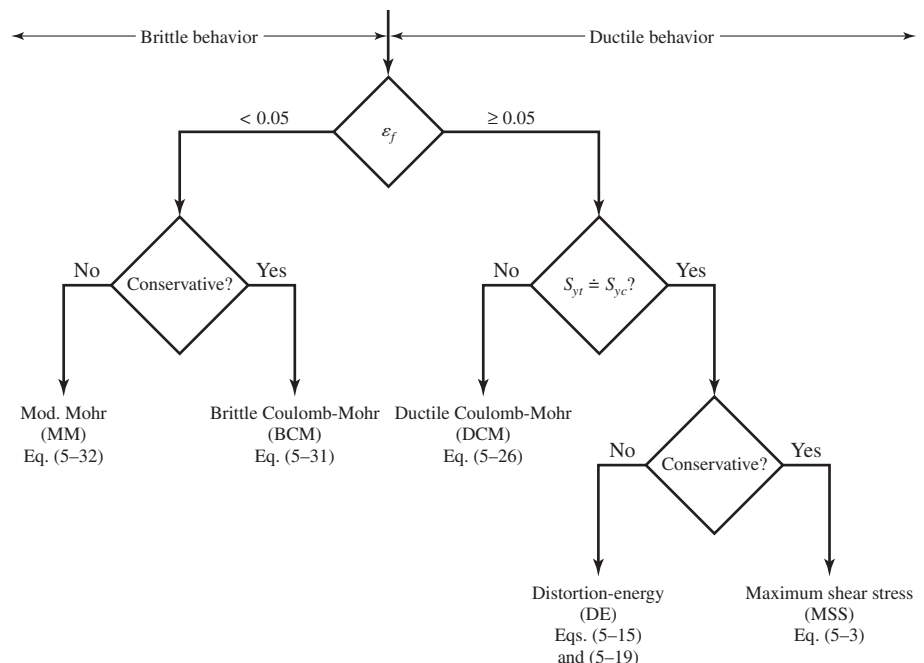
$$\sigma_A \geq 0 \geq \sigma_B \quad \text{and} \quad \left| \frac{\sigma_B}{\sigma_A} \right| \leq 1$$

$$\text{p. 236} \quad \frac{(S_{uc} - S_{ut})\sigma_A}{S_{uc}S_{ut}} - \frac{\sigma_B}{S_{uc}} = \frac{1}{n} \quad \sigma_A \geq 0 \geq \sigma_B \quad \text{and} \quad \left| \frac{\sigma_B}{\sigma_A} \right| > 1 \quad (5-32b)$$

$$\sigma_B = -\frac{S_{uc}}{n} \quad 0 \geq \sigma_A \geq \sigma_B \quad (5-32c)$$

Failure Theory Flowchart

Fig. 5-21, p. 239



Fracture Mechanics

p. 243

$$K_I = \beta \sigma \sqrt{\pi a}$$

(5-37)

where β is found in Figs. 5–25 to 5–30 (pp. 243 to 246)

p. 247

$$n = \frac{K_{Ic}}{K_I}$$

(5-38)

where K_{Ic} is found in Table 5–1 (p. 246)

Stochastic Analysis

Mean factor of safety defined as $\bar{n} = \mu_S/\mu_\sigma$ (μ_S and μ_σ are mean strength and stress, respectively)

Normal-Normal Case

p. 250

$$\bar{n} = \frac{1 \pm \sqrt{1 - (1 - z^2 C_S^2)(1 - z^2 C_\sigma^2)}}{1 - z^2 C_S^2}$$

where z can be found in Table A–10, $C_S = \hat{\sigma}_S/\mu_S$, and $C_\sigma = \hat{\sigma}_\sigma/\mu_\sigma$.

Lognormal-Lognormal Case

p. 251

$$\bar{n} = \exp \left[-z \sqrt{\ln(1 + C_n^2)} + \ln \sqrt{1 + C_n^2} \right] \doteq \exp \left[C_n \left(-z + \frac{C_n}{2} \right) \right]$$

where

$$C_n = \sqrt{\frac{C_S^2 + C_\sigma^2}{1 + C_\sigma^2}}$$

(See other definitions in normal-normal case.)

PROBLEMS

Problems marked with an asterisk (*) are linked to problems in other chapters, as summarized in Table 1–1 of Sec. 1–16, p. 24.

5–1

A ductile hot-rolled steel bar has a minimum yield strength in tension and compression of 350 MPa. Using the distortion-energy and maximum-shear-stress theories determine the factors of safety for the following plane stress states:

- (a) $\sigma_x = 100$ MPa, $\sigma_y = 100$ MPa
- (b) $\sigma_x = 100$ MPa, $\sigma_y = 50$ MPa
- (c) $\sigma_x = 100$ MPa, $\tau_{xy} = -75$ MPa
- (d) $\sigma_x = -50$ MPa, $\sigma_y = -75$ MPa, $\tau_{xy} = -50$ MPa
- (e) $\sigma_x = 100$ MPa, $\sigma_y = 20$ MPa, $\tau_{xy} = -20$ MPa

5–2

Repeat Prob. 5–1 with the following principal stresses obtained from Eq. (3–13):

- (a) $\sigma_A = 100$ MPa, $\sigma_B = 100$ MPa
- (b) $\sigma_A = 100$ MPa, $\sigma_B = -100$ MPa
- (c) $\sigma_A = 100$ MPa, $\sigma_B = 50$ MPa
- (d) $\sigma_A = 100$ MPa, $\sigma_B = -50$ MPa
- (e) $\sigma_A = -50$ MPa, $\sigma_B = -100$ MPa

- 5-3** Repeat Prob. 5-1 for a bar of AISI 1030 hot-rolled steel and:
 (a) $\sigma_x = 25$ kpsi, $\sigma_y = 15$ kpsi
 (b) $\sigma_x = 15$ kpsi, $\sigma_y = -15$ kpsi
 (c) $\sigma_x = 20$ kpsi, $\tau_{xy} = -10$ kpsi
 (d) $\sigma_x = -12$ kpsi, $\sigma_y = 15$ kpsi, $\tau_{xy} = -9$ kpsi
 (e) $\sigma_x = -24$ kpsi, $\sigma_y = -24$ kpsi, $\tau_{xy} = -15$ kpsi
- 5-4** Repeat Prob. 5-1 for a bar of AISI 1015 cold-drawn steel with the following principal stresses obtained from Eq. (3-13):
 (a) $\sigma_A = 30$ kpsi, $\sigma_B = 30$ kpsi
 (b) $\sigma_A = 30$ kpsi, $\sigma_B = -30$ kpsi
 (c) $\sigma_A = 30$ kpsi, $\sigma_B = 15$ kpsi
 (d) $\sigma_A = -30$ kpsi, $\sigma_B = -15$ kpsi
 (e) $\sigma_A = -50$ kpsi, $\sigma_B = 10$ kpsi
- 5-5** Repeat Prob. 5-1 by first plotting the failure loci in the σ_A , σ_B plane to scale; then, for each stress state, plot the load line and by graphical measurement estimate the factors of safety.
- 5-6** Repeat Prob. 5-3 by first plotting the failure loci in the σ_A , σ_B plane to scale; then, for each stress state, plot the load line and by graphical measurement estimate the factors of safety.
- 5-7 to 5-11** An AISI 1018 steel has a yield strength, $S_y = 295$ MPa. Using the distortion-energy theory for the given state of plane stress, (a) determine the factor of safety, (b) plot the failure locus, the load line, and estimate the factor of safety by graphical measurement.

Problem Number	σ_x (MPa)	σ_y (MPa)	τ_{xy} (MPa)
5-7	75	-35	0
5-8	-100	30	0
5-9	100	0	-25
5-10	-30	-65	40
5-11	-80	30	-10

- 5-12** A ductile material has the properties $S_{yt} = 60$ kpsi and $S_{yc} = 75$ kpsi. Using the ductile Coulomb-Mohr theory, determine the factor of safety for the states of plane stress given in Prob. 5-3.
- 5-13** Repeat Prob. 5-12 by first plotting the failure loci in the σ_A , σ_B plane to scale; then for each stress state, plot the load line and by graphical measurement estimate the factor of safety.
- 5-14 to 5-18** An AISI 4142 steel Q&T at 800°F exhibits $S_{yt} = 235$ kpsi, $S_{yc} = 285$ kpsi, and $\varepsilon_f = 0.07$. For the given state of plane stress, (a) determine the factor of safety, (b) plot the failure locus and the load line, and estimate the factor of safety by graphical measurement.

Problem Number	σ_x (kpsi)	σ_y (kpsi)	τ_{xy} (kpsi)
5-14	150	-50	0
5-15	-150	50	0
5-16	125	0	-75
5-17	-80	-125	50
5-18	125	80	-75

5-19

A brittle material has the properties $S_{ut} = 30$ kpsi and $S_{uc} = 90$ kpsi. Using the brittle Coulomb-Mohr and modified-Mohr theories, determine the factor of safety for the following states of plane stress.

- (a) $\sigma_x = 25$ kpsi, $\sigma_y = 15$ kpsi
- (b) $\sigma_x = 15$ kpsi, $\sigma_y = -15$ kpsi
- (c) $\sigma_x = 20$ kpsi, $\tau_{xy} = -10$ kpsi
- (d) $\sigma_x = -15$ kpsi, $\sigma_y = 10$ kpsi, $\tau_{xy} = -15$ kpsi
- (e) $\sigma_x = -20$ kpsi, $\sigma_y = -20$ kpsi, $\tau_{xy} = -15$ kpsi

5-20

Repeat Prob. 5-19 by first plotting the failure loci in the σ_A , σ_B plane to scale; then for each stress state, plot the load line and by graphical measurement estimate the factor of safety.

5-21 to**5-25**

For an ASTM 30 cast iron, (a) find the factors of safety using the BCM and MM theories, (b) plot the failure diagrams in the σ_A , σ_B plane to scale and locate the coordinates of the stress state, and (c) estimate the factors of safety from the two theories by graphical measurements along the load line.

Problem Number	σ_x (kpsi)	σ_y (kpsi)	τ_{xy} (kpsi)
5-21	15	10	0
5-22	15	-50	0
5-23	15	0	-10
5-24	-10	-25	-10
5-25	-35	13	-10

5-26 to**5-30**

A cast aluminum 195-T6 exhibits $S_{ut} = 36$ kpsi, $S_{uc} = 35$ kpsi, and $\varepsilon_f = 0.045$. For the given state of plane stress, (a) using the Coulomb-Mohr theory, determine the factor of safety, (b) plot the failure locus and the load line, and estimate the factor of safety by graphical measurement.

Problem Number	σ_x (kpsi)	σ_y (kpsi)	τ_{xy} (kpsi)
5-26	15	-10	0
5-27	-15	10	0
5-28	12	0	-8
5-29	-10	-15	10
5-30	15	8	-8

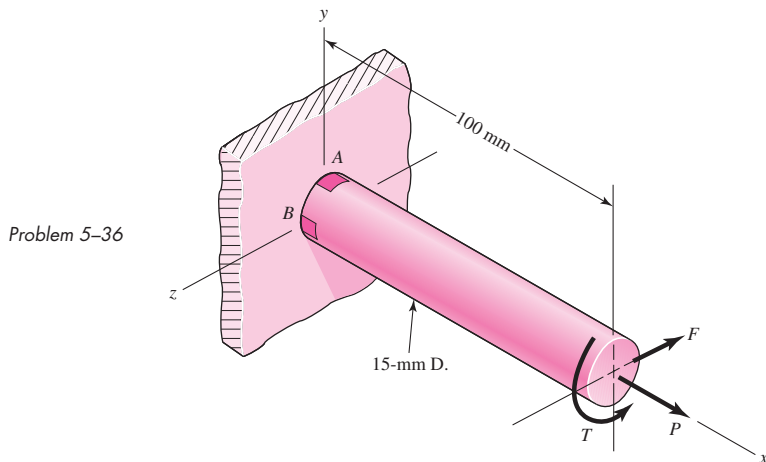
5-31 to**5-35**

Repeat Probs. 5-26 to 5-30 using the modified-Mohr theory.

Problem number	5-31	5-32	5-33	5-34	5-35
Repeat problem	5-26	5-27	5-28	5-29	5-30

5-36

This problem illustrates that the factor of safety for a machine element depends on the particular point selected for analysis. Here you are to compute factors of safety, based upon the distortion-energy theory, for stress elements at A and B of the member shown in the figure. This bar is made of AISI 1006 cold-drawn steel and is loaded by the forces $F = 0.55$ kN, $P = 4.0$ kN, and $T = 25$ N · m.



5-37 For the beam in Prob. 3-44, p. 133, determine the minimum yield strength that should be considered to obtain a minimum factor of safety of 2 based on the distortion-energy theory.

5-38 A 1020 CD steel shaft is to transmit 20 hp while rotating at 1750 rpm. Determine the minimum diameter for the shaft to provide a minimum factor of safety of 3 based on the maximum-shear-stress theory.

**5-39* to
5-55*** For the problem specified in the table, build upon the results of the original problem to determine the minimum factor of safety for yielding. Use both the maximum-shear-stress theory and the distortion-energy theory, and compare the results. The material is 1018 CD steel.

Problem Number	Original Problem, Page Number
5-39*	3-68, 137
5-40*	3-69, 137
5-41*	3-70, 137
5-42*	3-71, 137
5-43*	3-72, 138
5-44*	3-73, 138
5-45*	3-74, 138
5-46*	3-76, 139
5-47*	3-77, 139
5-48*	3-79, 139
5-49*	3-80, 139
5-50*	3-81, 140
5-51*	3-82, 140
5-52*	3-83, 140
5-53*	3-84, 140
5-54*	3-85, 141
5-55*	3-86, 141

5-56* Build upon the results of Probs. 3–84 and 3–87 to compare the use of a low-strength, ductile material (1018 CD) in which the stress-concentration factor can be ignored to a high-strength but more brittle material (4140 Q&T @ 400°F) in which the stress-concentration factor should be included. For each case, determine the factor of safety for yielding using the distortion-energy theory.

5-57 Design the lever arm *CD* of Fig. 5–16 by specifying a suitable size and material.

5-58 A spherical pressure vessel is formed of 16-gauge (0.0625-in) cold-drawn AISI 1020 sheet steel. If the vessel has a diameter of 15 in, use the distortion-energy theory to estimate the pressure necessary to initiate yielding. What is the estimated bursting pressure?

5-59 This problem illustrates that the strength of a machine part can sometimes be measured in units other than those of force or moment. For example, the maximum speed that a flywheel can reach without yielding or fracturing is a measure of its strength. In this problem you have a rotating ring made of hot-forged AISI 1020 steel; the ring has a 6-in inside diameter and a 10-in outside diameter and is 1.5 in thick. Using the distortion-energy theory, determine the speed in revolutions per minute that would cause the ring to yield. At what radius would yielding begin? [Note: The maximum radial stress occurs at $r = (r_o r_i)^{1/2}$; see Eq. (3–55).]

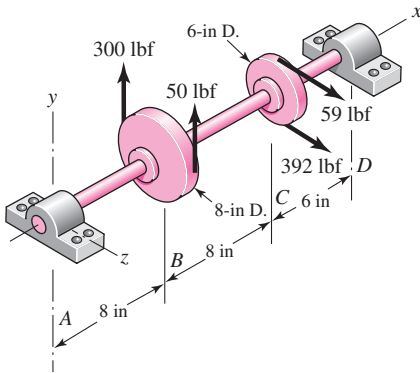
5-60 A light pressure vessel is made of 2024-T3 aluminum alloy tubing with suitable end closures. This cylinder has a $3\frac{1}{2}$ -in OD, a 0.065-in wall thickness, and $\nu = 0.334$. The purchase order specifies a minimum yield strength of 46 ksi. Using the distortion-energy theory, determine the factor of safety if the pressure-release valve is set at 500 psi.

5-61 A cold-drawn AISI 1015 steel tube is 300 mm OD by 200 mm ID and is to be subjected to an external pressure caused by a shrink fit. Using the distortion-energy theory, determine the maximum pressure that would cause the material of the tube to yield.

5-62 What speed would cause fracture of the ring of Prob. 5–59 if it were made of grade 30 cast iron?

5-63 The figure shows a shaft mounted in bearings at *A* and *D* and having pulleys at *B* and *C*. The forces shown acting on the pulley surfaces represent the belt tensions. The shaft is to be made of AISI 1035 CD steel. Using a conservative failure theory with a design factor of 2, determine the minimum shaft diameter to avoid yielding.

Problem 5–63



5-64 By modern standards, the shaft design of Prob. 5–63 is poor because it is so long. Suppose it is redesigned by halving the length dimensions. Using the same material and design factor as in Prob. 5–63, find the new shaft diameter.

5-65* Build upon the results of Prob. 3–40, p. 132, to determine the factor of safety for yielding based on the distortion-energy theory for each of the simplified models in parts *c*, *d*, and *e* of the figure

for Prob. 3–40. The pin is machined from AISI 1018 hot-rolled steel. Compare the three models from a designer's perspective in terms of accuracy, safety, and modeling time.

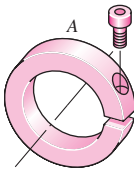
5–66*

For the clevis pin of Prob. 3–40, p. 132, redesign the pin diameter to provide a factor of safety of 2.5 based on a conservative yielding failure theory, and the most conservative loading model from parts *c*, *d*, and *e* of the figure for Prob. 3–40. The pin is machined from AISI 1018 hot-rolled steel.

5–67

A split-ring clamp-type shaft collar is shown in the figure. The collar is 50 mm OD by 25 mm ID by 12 mm wide. The screw is designated as M 6 × 1. The relation between the screw tightening torque T , the nominal screw diameter d , and the tension in the screw F_t is approximately $T = 0.2 F_t d$. The shaft is sized to obtain a close running fit. Find the axial holding force F_x of the collar as a function of the coefficient of friction and the screw torque.

Problem 5–67



5–68

Suppose the collar of Prob. 5–67 is tightened by using a screw torque of 20 N · m. The collar material is AISI 1035 steel heat-treated to a minimum tensile yield strength of 450 MPa.

- Estimate the tension in the screw.
- By relating the tangential stress to the hoop tension, find the internal pressure of the shaft on the ring.
- Find the tangential and radial stresses in the ring at the inner surface.
- Determine the maximum shear stress and the von Mises stress.
- What are the factors of safety based on the maximum-shear-stress and the distortion-energy theories?

5–69

In Prob. 5–67, the role of the screw was to induce the hoop tension that produces the clamping. The screw should be placed so that no moment is induced in the ring. Just where should the screw be located?

5–70

A tube has another tube shrunk over it. The specifications are:

	Inner Member	Outer Member
ID	1.250 ± 0.003 in	2.001 ± 0.0004 in
OD	2.002 ± 0.0004 in	3.000 ± 0.004 in

Both tubes are made of a plain carbon steel.

- Find the nominal shrink-fit pressure and the von Mises stresses at the fit surface.
- If the inner tube is changed to solid shafting with the same outside dimensions, find the nominal shrink-fit pressure and the von Mises stresses at the fit surface.

5–71

Two steel tubes have the specifications:

	Inner Tube	Outer Tube
ID	20 ± 0.050 mm	39.98 ± 0.008 mm
OD	40 ± 0.008 mm	65 ± 0.10 mm

These are shrink-fitted together. Find the nominal shrink-fit pressure and the von Mises stress in each body at the fit surface.

5-72 Repeat Prob. 5-71 for maximum shrink-fit conditions.

5-73 A solid steel shaft has a gear with ASTM grade 20 cast-iron hub ($E = 14.5 \text{ GPa}$) shrink-fitted to it. The shaft diameter is $2.001 \pm 0.0004 \text{ in}$. The specifications for the gear hub are

$$\begin{array}{rcc} 2.000 & + 0.0004 & \text{in} \\ & - 0.0000 & \end{array}$$

ID with an OD of $4.00 \pm \frac{1}{32} \text{ in}$. Using the midrange values and the modified Mohr theory, estimate the factor of safety guarding against fracture in the gear hub due to the shrink fit.

5-74 Two steel tubes are shrink-fitted together where the nominal diameters are 40, 45, and 50 mm. Careful measurement before fitting determined the diametral interference between the tubes to be 0.062 mm. After the fit, the assembly is subjected to a torque of 900 N · m and a bending-moment of 675 N · m. Assuming no slipping between the cylinders, analyze the outer cylinder at the inner and outer radius. Determine the factor of safety using distortion energy with $S_y = 415 \text{ MPa}$.

5-75 Repeat Prob. 5-74 for the inner tube.

**5-76 to
5-81** For the problem given in the table, the specifications for the press fit of two cylinders are given in the original problem from Chap. 3. If both cylinders are hot-rolled AISI 1040 steel, determine the minimum factor of safety for the outer cylinder based on the distortion-energy theory.

Problem Number	Original Problem, Page Number
5-76	3-110, 143
5-77	3-111, 143
5-78	3-112, 143
5-79	3-113, 143
5-80	3-114, 143
5-81	3-115, 143

5-82 For Eqs. (5-36) show that the principal stresses are given by

$$\sigma_1 = \frac{K_I}{\sqrt{2\pi r}} \cos \frac{\theta}{2} \left(1 + \sin \frac{\theta}{2} \right)$$

$$\sigma_2 = \frac{K_I}{\sqrt{2\pi r}} \cos \frac{\theta}{2} \left(1 - \sin \frac{\theta}{2} \right)$$

$$\sigma_3 = \begin{cases} 0 & \text{(plane stress)} \\ \sqrt{\frac{2}{\pi r}} v K_I \cos \frac{\theta}{2} & \text{(plane strain)} \end{cases}$$

5-83 Use the results of Prob. 5-82 for plane strain near the tip with $\theta = 0$ and $v = \frac{1}{3}$. If the yield strength of the plate is S_y , what is σ_1 when yield occurs?

(a) Use the distortion-energy theory.

(b) Use the maximum-shear-stress theory. Using Mohr's circles, explain your answer.

5-84 A plate 100 mm wide, 200 mm long, and 12 mm thick is loaded in tension in the direction of the length. The plate contains a crack as shown in Fig. 5-26 with the crack length of 16 mm. The material is steel with $K_{Ic} = 80 \text{ MPa} \cdot \sqrt{\text{m}}$, and $S_y = 950 \text{ MPa}$. Determine the maximum possible load that can be applied before the plate (a) yields, and (b) has uncontrollable crack growth.

5-85 A cylinder subjected to internal pressure p_i has an outer diameter of 14 in and a 1-in wall thickness. For the cylinder material, $K_{Ic} = 72 \text{ kpsi} \cdot \sqrt{\text{in}}$, $S_y = 170 \text{ kpsi}$, and $S_{ut} = 192 \text{ kpsi}$. If the cylinder contains a radial crack in the longitudinal direction of depth 0.5 in determine the pressure that will cause uncontrollable crack growth.

5-86 A carbon steel collar of length 1 in is to be machined to inside and outside diameters, respectively, of

$$D_i = 0.750 \pm 0.0004 \text{ in} \quad D_o = 1.125 \pm 0.002 \text{ in}$$

This collar is to be shrink-fitted to a hollow steel shaft having inside and outside diameters, respectively, of

$$d_i = 0.375 \pm 0.002 \text{ in} \quad d_o = 0.752 \pm 0.0004 \text{ in}$$

These tolerances are assumed to have a normal distribution, to be centered in the spread interval, and to have a total spread of ± 4 standard deviations. Determine the means and the standard deviations of the tangential stress components for both cylinders at the interface.

5-87 Suppose the collar of Prob. 5-44 has a yield strength of $S_y = N(95.5, 6.59)$ kpsi. What is the probability that the material will not yield?

5-88 A carbon steel tube has an outside diameter of 75 mm and a wall thickness of 3 mm. The tube is to carry an internal hydraulic pressure given as $p = N(40, 2)$ MPa. The material of the tube has a yield strength of $S_y = N(350, 29)$ MPa. Find the reliability using thin-wall theory.

This page intentionally left blank

6

Fatigue Failure Resulting from Variable Loading

Chapter Outline

6-1	Introduction to Fatigue in Metals	266
6-2	Approach to Fatigue Failure in Analysis and Design	272
6-3	Fatigue-Life Methods	273
6-4	The Stress-Life Method	273
6-5	The Strain-Life Method	276
6-6	The Linear-Elastic Fracture Mechanics Method	278
6-7	The Endurance Limit	282
6-8	Fatigue Strength	283
6-9	Endurance Limit Modifying Factors	286
6-10	Stress Concentration and Notch Sensitivity	295
6-11	Characterizing Fluctuating Stresses	300
6-12	Fatigue Failure Criteria for Fluctuating Stress	303
6-13	Torsional Fatigue Strength under Fluctuating Stresses	317
6-14	Combinations of Loading Modes	317
6-15	Varying, Fluctuating Stresses; Cumulative Fatigue Damage	321
6-16	Surface Fatigue Strength	327
6-17	Stochastic Analysis	330
6-18	Road Maps and Important Design Equations for the Stress-Life Method	344

In Chap. 5 we considered the analysis and design of parts subjected to static loading. The behavior of machine parts is entirely different when they are subjected to time-varying loading. In this chapter we shall examine how parts fail under variable loading and how to proportion them to successfully resist such conditions.

6-1

Introduction to Fatigue in Metals

In most testing of those properties of materials that relate to the stress-strain diagram, the load is applied gradually, to give sufficient time for the strain to fully develop. Furthermore, the specimen is tested to destruction, and so the stresses are applied only once. Testing of this kind is applicable, to what are known as *static conditions*; such conditions closely approximate the actual conditions to which many structural and machine members are subjected.

The condition frequently arises, however, in which the stresses vary with time or they fluctuate between different levels. For example, a particular fiber on the surface of a rotating shaft subjected to the action of bending loads undergoes both tension and compression for each revolution of the shaft. If the shaft is part of an electric motor rotating at 1725 rev/min, the fiber is stressed in tension and compression 1725 times each minute. If, in addition, the shaft is also axially loaded (as it would be, for example, by a helical or worm gear), an axial component of stress is superposed upon the bending component. In this case, some stress is always present in any one fiber, but now the *level* of stress is fluctuating. These and other kinds of loading occurring in machine members produce stresses that are called *variable, repeated, alternating, or fluctuating stresses*.

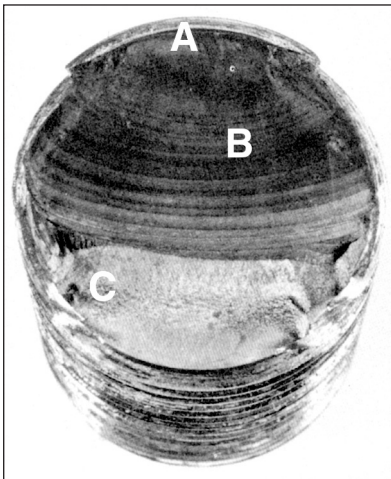
Often, machine members are found to have failed under the action of repeated or fluctuating stresses; yet the most careful analysis reveals that the actual maximum stresses were well below the ultimate strength of the material, and quite frequently even below the yield strength. The most distinguishing characteristic of these failures is that the stresses have been repeated a very large number of times. Hence the failure is called a *fatigue failure*.

When machine parts fail statically, they usually develop a very large deflection, because the stress has exceeded the yield strength, and the part is replaced before fracture actually occurs. Thus many static failures give visible warning in advance. But a fatigue failure gives no warning! It is sudden and total, and hence dangerous. It is relatively simple to design against a static failure, because our knowledge is comprehensive. Fatigue is a much more complicated phenomenon, only partially understood, and the engineer seeking competence must acquire as much knowledge of the subject as possible.

A fatigue failure has an appearance similar to a brittle fracture, as the fracture surfaces are flat and perpendicular to the stress axis with the absence of necking. The fracture features of a fatigue failure, however, are quite different from a static brittle fracture arising from three stages of development. *Stage I* is the initiation of one or more micro-cracks due to cyclic plastic deformation followed by crystallographic propagation extending from two to five grains about the origin. Stage I cracks are not normally discernible to the naked eye. *Stage II* progresses from microcracks to macrocracks forming parallel plateau-like fracture surfaces separated by longitudinal ridges. The plateaus are generally smooth and normal to the direction of maximum tensile stress. These surfaces can be wavy dark and light bands referred to as *beach marks* or *clamshell marks*, as seen in Fig. 6-1. During cyclic loading, these cracked surfaces open and close, rubbing together, and the beach mark appearance depends on the changes in the level or frequency of loading and the corrosive nature of the environment. *Stage III* occurs during the final stress cycle when the remaining material cannot support the loads, resulting in

Figure 6-1

Fatigue failure of a bolt due to repeated unidirectional bending. The failure started at the thread root at A, propagated across most of the cross section shown by the beach marks at B, before final fast fracture at C. (From ASM Handbook, Vol. 12: Fractography, 2nd printing, 1992, ASM International, Materials Park, OH 44073-0002, fig 50, p. 120. Reprinted by permission of ASM International®, www.asminternational.org.)



a sudden, fast fracture. A stage III fracture can be brittle, ductile, or a combination of both. Quite often the beach marks, if they exist, and possible patterns in the stage III fracture called *chevron lines*, point toward the origins of the initial cracks.

There is a good deal to be learned from the fracture patterns of a fatigue failure.¹ Figure 6-2 shows representations of failure surfaces of various part geometries under differing load conditions and levels of stress concentration. Note that, in the case of rotational bending, even the direction of rotation influences the failure pattern.

Fatigue failure is due to crack formation and propagation. A fatigue crack will typically initiate at a discontinuity in the material where the cyclic stress is a maximum. Discontinuities can arise because of:

- Design of rapid changes in cross section, keyways, holes, etc. where stress concentrations occur as discussed in Secs. 3-13 and 5-2.
- Elements that roll and/or slide against each other (bearings, gears, cams, etc.) under high contact pressure, developing concentrated subsurface contact stresses (Sec. 3-19) that can cause surface pitting or spalling after many cycles of the load.
- Carelessness in locations of stamp marks, tool marks, scratches, and burrs; poor joint design; improper assembly; and other fabrication faults.
- Composition of the material itself as processed by rolling, forging, casting, extrusion, drawing, heat treatment, etc. Microscopic and submicroscopic surface and subsurface discontinuities arise, such as inclusions of foreign material, alloy segregation, voids, hard precipitated particles, and crystal discontinuities.

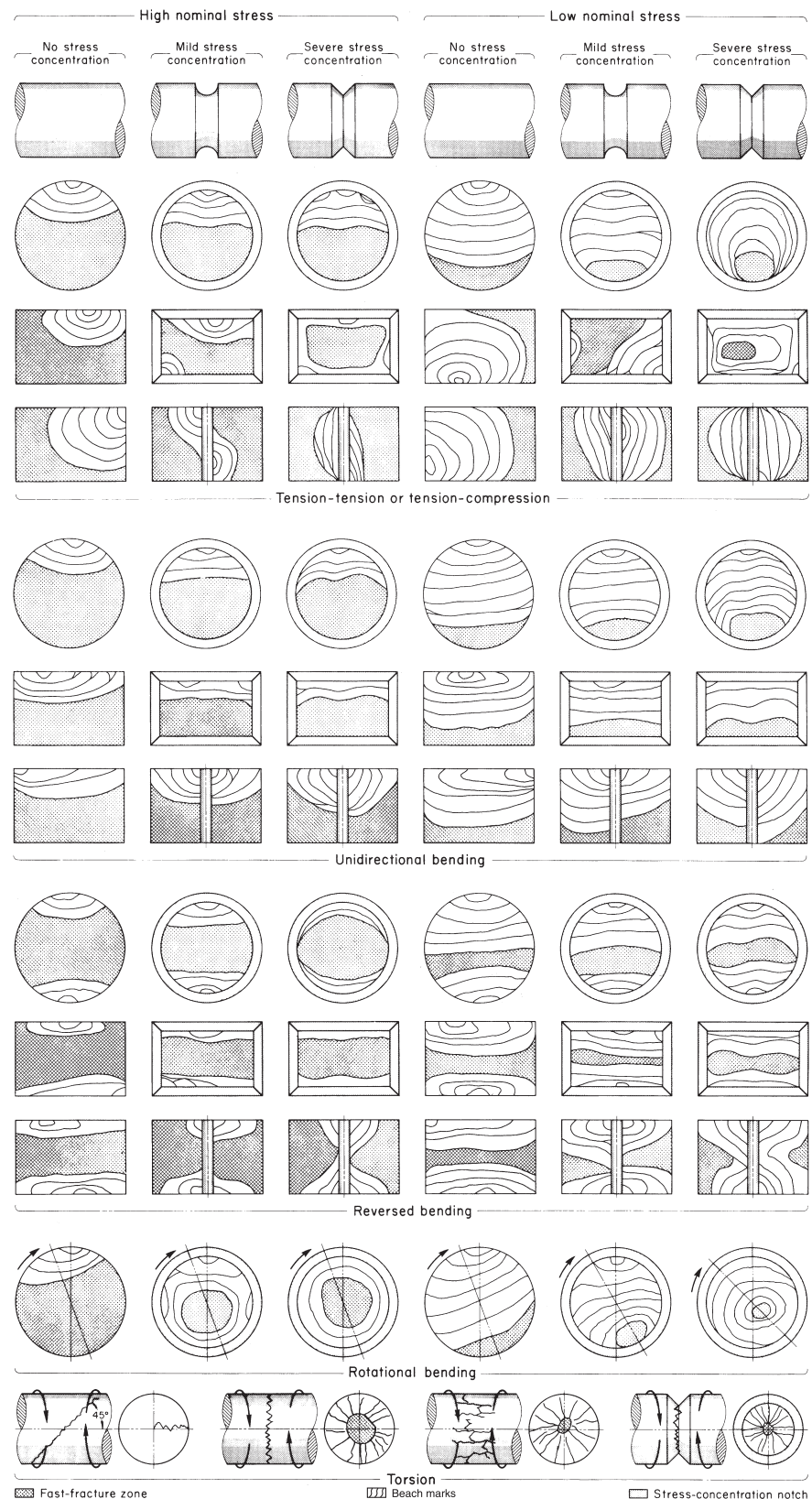
Various conditions that can accelerate crack initiation include residual tensile stresses, elevated temperatures, temperature cycling, a corrosive environment, and high-frequency cycling.

The rate and direction of fatigue crack propagation is primarily controlled by localized stresses and by the structure of the material at the crack. However, as with crack formation, other factors may exert a significant influence, such as environment, temperature, and frequency. As stated earlier, cracks will grow along planes normal to the

¹See the ASM Handbook, *Fractography*, ASM International, Metals Park, Ohio, vol. 12, 9th ed., 1987.

Figure 6-2

Schematics of fatigue fracture surfaces produced in smooth and notched components with round and rectangular cross sections under various loading conditions and nominal stress levels. (From *ASM Metals Handbook, Vol. 11: Failure Analysis and Prevention, 1986, ASM International, Materials Park, OH 44073-0002, fig 18, p. 111*. Reprinted by permission of ASM International®, www.asminternational.org.)



maximum tensile stresses. The crack growth process can be explained by fracture mechanics (see Sec. 6–6).

A major reference source in the study of fatigue failure is the 21-volume *ASM Metals Handbook*. Figures 6–1 to 6–8, reproduced with permission from ASM International, are but a minuscule sample of examples of fatigue failures for a great variety of conditions included in the handbook. Comparing Fig. 6–3 with Fig. 6–2, we see that failure occurred by rotating bending stresses, with the direction of rotation being clockwise with respect to the view and with a mild stress concentration and low nominal stress.

Figure 6–3

Fatigue fracture of an AISI 4320 drive shaft. The fatigue failure initiated at the end of the keyway at points *B* and progressed to final rupture at *C*. The final rupture zone is small, indicating that loads were low.
(From *ASM Handbook*, Vol. 12: Fractography, 2nd printing, 1992, *ASM International*, Materials Park, OH 44073-0002, fig 51, p. 120. Reprinted by permission of *ASM International*®, www.asminternational.org.)



Figure 6–4

Fatigue fracture surface of an AISI 8640 pin. Sharp corners of the mismatched grease holes provided stress concentrations that initiated two fatigue cracks indicated by the arrows.
(From *ASM Handbook*, Vol. 12: Fractography, 2nd printing, 1992, *ASM International*, Materials Park, OH 44073-0002, fig 520, p. 331. Reprinted by permission of *ASM International*®, www.asminternational.org.)

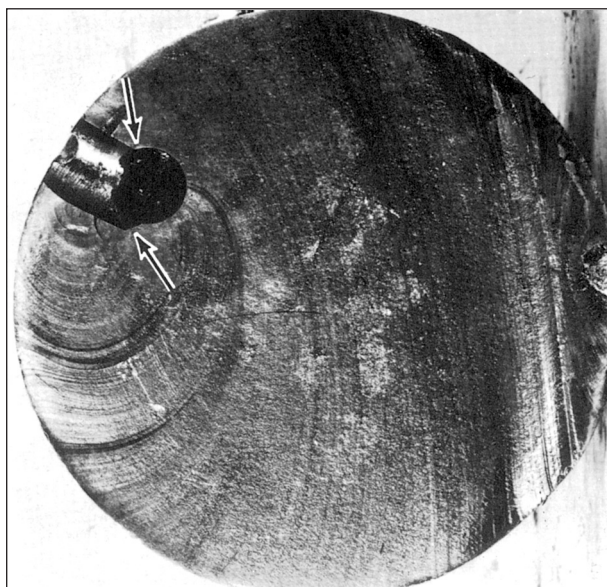
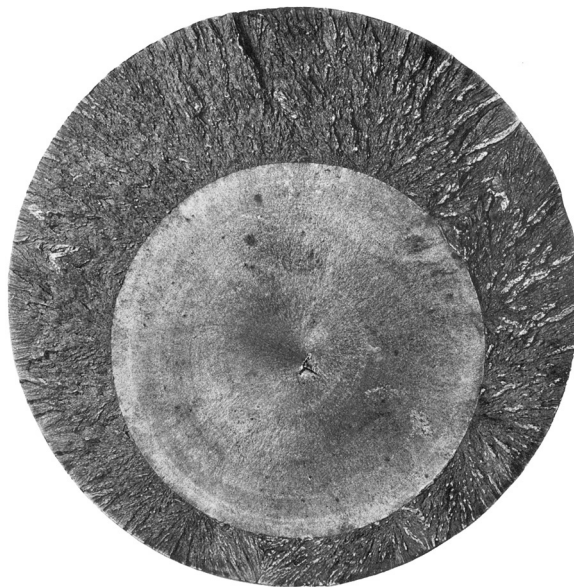
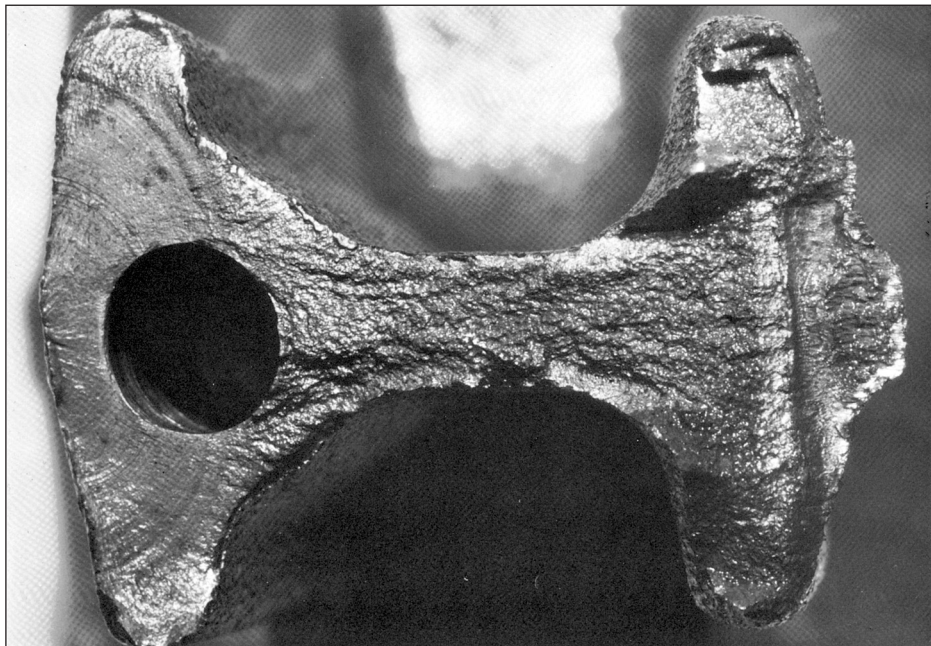


Figure 6-5

Fatigue fracture surface of a forged connecting rod of AISI 8640 steel. The fatigue crack origin is at the left edge, at the flash line of the forging, but no unusual roughness of the flash trim was indicated. The fatigue crack progressed halfway around the oil hole at the left, indicated by the beach marks, before final fast fracture occurred. Note the pronounced shear lip in the final fracture at the right edge. (From ASM Handbook, Vol. 12: Fractography, 2nd printing, 1992, ASM International, Materials Park, OH 44073-0002, fig 523, p. 332. Reprinted by permission of ASM International®, www.asminternational.org.)

**Figure 6-6**

Fatigue fracture surface of a 200-mm (8-in) diameter piston rod of an alloy steel steam hammer used for forging. This is an example of a fatigue fracture caused by pure tension where surface stress concentrations are absent and a crack may initiate anywhere in the cross section. In this instance, the initial crack formed at a forging flake slightly below center, grew outward symmetrically, and ultimately produced a brittle fracture without warning. (From ASM Handbook, Vol. 12: Fractography, 2nd printing, 1992, ASM International, Materials Park, OH 44073-0002, fig 570, p. 342. Reprinted by permission of ASM International®, www.asminternational.org.)

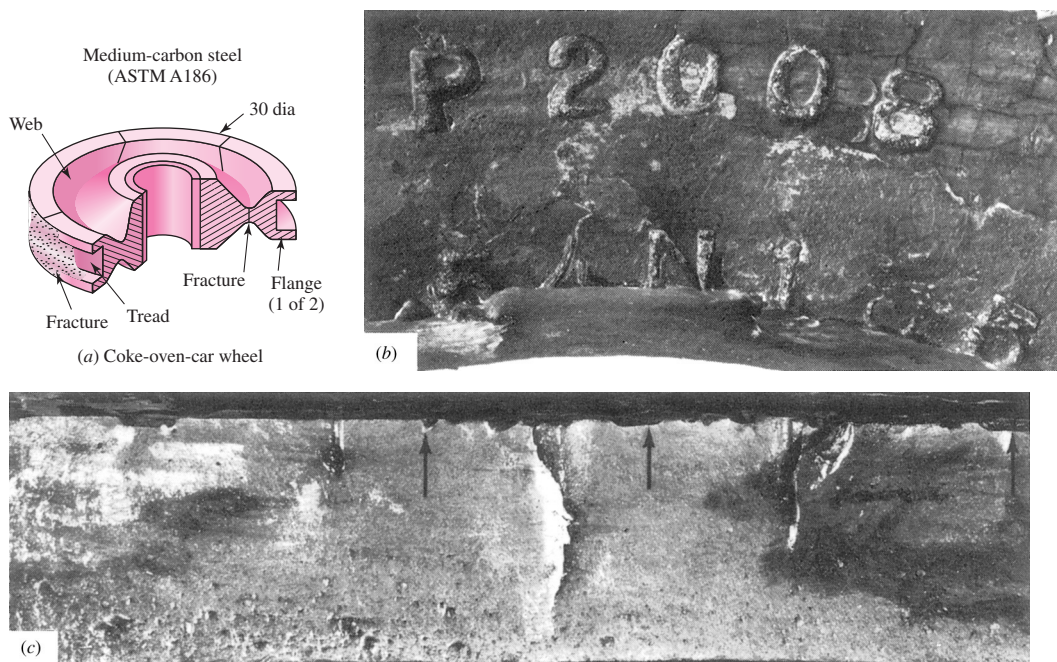
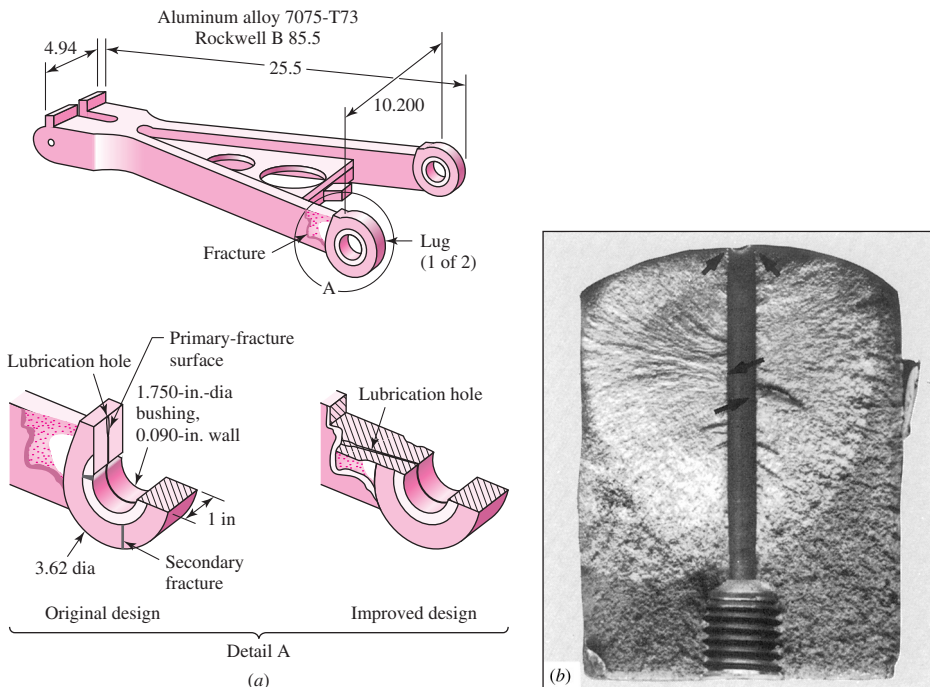


Figure 6-7

Fatigue failure of an ASTM A186 steel double-flange trailer wheel caused by stamp marks. (a) Coke-oven car wheel showing position of stamp marks and fractures in the rib and web. (b) Stamp mark showing heavy impression and fracture extending along the base of the lower row of numbers. (c) Notches, indicated by arrows, created from the heavily indented stamp marks from which cracks initiated along the top at the fracture surface. (From *ASM Metals Handbook*, Vol. 11: Failure Analysis and Prevention, 1986, ASM International, Materials Park, OH 44073-0002, fig 51, p. 130. Reprinted by permission of ASM International®, www.asminternational.org.)

Figure 6-8

Aluminum alloy 7075-T73 landing-gear torque-arm assembly redesign to eliminate fatigue fracture at a lubrication hole. (a) Arm configuration, original and improved design (dimensions given in inches). (b) Fracture surface where arrows indicate multiple crack origins. (From *ASM Metals Handbook*, Vol. 11: Failure Analysis and Prevention, 1986, ASM International, Materials Park, OH 44073-0002, fig 23, p. 114. Reprinted by permission of ASM International®, www.asminternational.org.)



6-2 Approach to Fatigue Failure in Analysis and Design

As noted in the previous section, there are a great many factors to be considered, even for very simple load cases. The methods of fatigue failure analysis represent a combination of engineering and science. Often science fails to provide the complete answers that are needed. But the airplane must still be made to fly—safely. And the automobile must be manufactured with a reliability that will ensure a long and troublefree life and at the same time produce profits for the stockholders of the industry. Thus, while science has not yet completely explained the complete mechanism of fatigue, the engineer must still design things that will not fail. In a sense this is a classic example of the true meaning of engineering as contrasted with science. Engineers use science to solve their problems if the science is available. But available or not, the problem must be solved, and whatever form the solution takes under these conditions is called *engineering*.

In this chapter, we will take a structured approach in the design against fatigue failure. As with static failure, we will attempt to relate to test results performed on simply loaded specimens. However, because of the complex nature of fatigue, there is much more to account for. From this point, we will proceed methodically, and in stages. In an attempt to provide some insight as to what follows in this chapter, a brief description of the remaining sections will be given here.

Fatigue-Life Methods (Secs. 6-3 to 6-6)

Three major approaches used in design and analysis to predict when, if ever, a cyclically loaded machine component will fail in fatigue over a period of time are presented. The premises of each approach are quite different but each adds to our understanding of the mechanisms associated with fatigue. The application, advantages, and disadvantages of each method are indicated. Beyond Sec. 6-6, only one of the methods, the stress-life method, will be pursued for further design applications.

Fatigue Strength and the Endurance Limit (Secs. 6-7 and 6-8)

The strength-life (*S-N*) diagram provides the fatigue strength S_f versus cycle life N of a material. The results are generated from tests using a simple loading of standard laboratory-controlled specimens. The loading often is that of sinusoidally reversing pure bending. The laboratory-controlled specimens are polished without geometric stress concentration at the region of minimum area.

For steel and iron, the *S-N* diagram becomes horizontal at some point. The strength at this point is called the *endurance limit* S'_e and occurs somewhere between 10^6 and 10^7 cycles. The prime mark on S'_e refers to the endurance limit of the *controlled laboratory specimen*. For nonferrous materials that do not exhibit an endurance limit, a fatigue strength at a specific number of cycles, S'_f , may be given, where again, the prime denotes the fatigue strength of the laboratory-controlled specimen.

The strength data are based on many controlled conditions that will not be the same as that for an actual machine part. What follows are practices used to account for the differences between the loading and physical conditions of the specimen and the actual machine part.

Endurance Limit Modifying Factors (Sec. 6-9)

Modifying factors are defined and used to account for differences between the specimen and the actual machine part with regard to surface conditions, size, loading, temperature, reliability, and miscellaneous factors. Loading is still considered to be simple and reversing.

Stress Concentration and Notch Sensitivity (Sec. 6-10)

The actual part may have a geometric stress concentration by which the fatigue behavior depends on the static stress-concentration factor and the component material's sensitivity to fatigue damage.

Fluctuating Stresses (Secs. 6-11 to 6-13)

These sections account for simple stress states from fluctuating load conditions that are not purely sinusoidally reversing axial, bending, or torsional stresses.

Combinations of Loading Modes (Sec. 6-14)

Here a procedure based on the distortion-energy theory is presented for analyzing combined fluctuating stress states, such as combined bending and torsion. Here it is assumed that the levels of the fluctuating stresses are in phase and not time varying.

Varying, Fluctuating Stresses; Cumulative Fatigue Damage (Sec. 6-15)

The fluctuating stress levels on a machine part may be time varying. Methods are provided to assess the fatigue damage on a cumulative basis.

Remaining Sections

The remaining three sections of the chapter pertain to the special topics of surface fatigue strength, stochastic analysis, and road maps with important equations.

6-3 Fatigue-Life Methods

The three major fatigue life methods used in design and analysis are the *stress-life method*, the *strain-life method*, and the *linear-elastic fracture mechanics method*. These methods attempt to predict the life in number of cycles to failure, N , for a specific level of loading. Life of $1 \leq N \leq 10^3$ cycles is generally classified as *low-cycle fatigue*, whereas *high-cycle fatigue* is considered to be $N > 10^3$ cycles.

The stress-life method, based on stress levels only, is the least accurate approach, especially for low-cycle applications. However, it is the most traditional method, since it is the easiest to implement for a wide range of design applications, has ample supporting data, and represents high-cycle applications adequately.

The strain-life method involves more detailed analysis of the plastic deformation at localized regions where the stresses and strains are considered for life estimates. This method is especially good for low-cycle fatigue applications. In applying this method, several idealizations must be compounded, and so some uncertainties will exist in the results. For this reason, it will be discussed only because of its value in adding to the understanding of the nature of fatigue.

The fracture mechanics method assumes a crack is already present and detected. It is then employed to predict crack growth with respect to stress intensity. It is most practical when applied to large structures in conjunction with computer codes and a periodic inspection program.

6-4 The Stress-Life Method

To determine the strength of materials under the action of fatigue loads, specimens are subjected to repeated or varying forces of specified magnitudes while the cycles or stress reversals are counted to destruction. The most widely used fatigue-testing device

is the R. R. Moore high-speed rotating-beam machine. This machine subjects the specimen to pure bending (no transverse shear) by means of weights. The specimen, shown in Fig. 6-9, is very carefully machined and polished, with a final polishing in an axial direction to avoid circumferential scratches. Other fatigue-testing machines are available for applying fluctuating or reversed axial stresses, torsional stresses, or combined stresses to the test specimens.

To establish the fatigue strength of a material, quite a number of tests are necessary because of the statistical nature of fatigue. For the rotating-beam test, a constant bending load is applied, and the number of revolutions (stress reversals) of the beam required for failure is recorded. The first test is made at a stress that is somewhat under the ultimate strength of the material. The second test is made at a stress that is less than that used in the first. This process is continued, and the results are plotted as an *S-N* diagram (Fig. 6-10). This chart may be plotted on semilog paper or on log-log paper. In the case of ferrous metals and alloys, the graph becomes horizontal after the material has been stressed for a certain number of cycles. Plotting on log paper emphasizes the bend in the curve, which might not be apparent if the results were plotted by using Cartesian coordinates.

The ordinate of the *S-N* diagram is called the *fatigue strength* S_f ; a statement of this strength value must always be accompanied by a statement of the number of cycles N to which it corresponds.

Figure 6-9

Test-specimen geometry for the R. R. Moore rotating-beam machine. The bending moment is uniform, $M = Fa$, over the curved length and at the highest-stressed section at the mid-point of the beam.

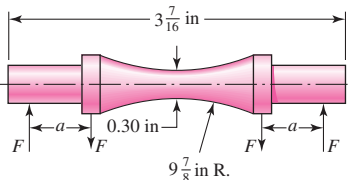


Figure 6-10

An *S-N* diagram plotted from the results of completely reversed axial fatigue tests. Material: UNS G41300 steel, normalized; $S_{ut} = 116$ kpsi; maximum $S_{ut} = 125$ kpsi. (Data from NACA Tech. Note 3866, December 1966.)

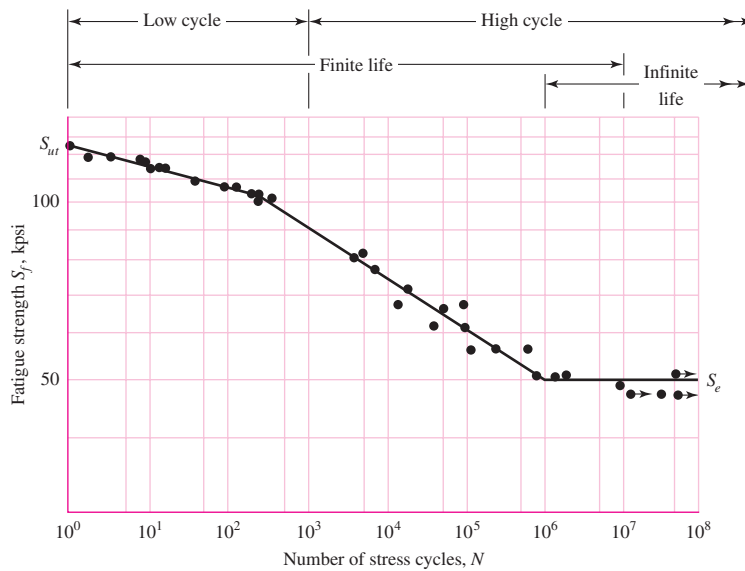
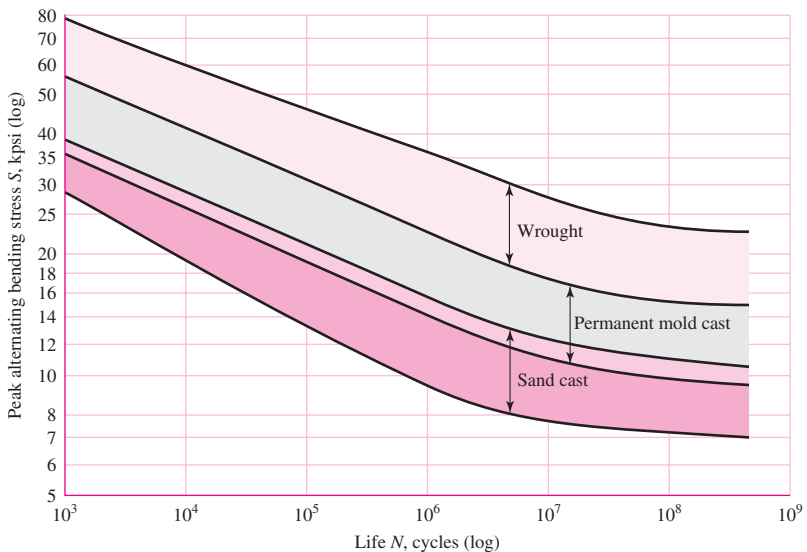


Figure 6-11

S-N bands for representative aluminum alloys, excluding wrought alloys with $S_{ut} < 38$ kpsi. (From R. C. Juvinall, Engineering Considerations of Stress, Strain and Strength. Copyright © 1967 by The McGraw-Hill Companies, Inc. Reprinted by permission.)



Soon we shall learn that S-N diagrams can be determined either for a test specimen or for an actual mechanical element. Even when the material of the test specimen and that of the mechanical element are identical, there will be significant differences between the diagrams for the two.

In the case of the steels, a knee occurs in the graph, and beyond this knee failure will not occur, no matter how great the number of cycles. The strength corresponding to the knee is called the *endurance limit* S_e , or the fatigue limit. The graph of Fig. 6-10 never does become horizontal for nonferrous metals and alloys, and hence these materials do not have an endurance limit. Figure 6-11 shows scatter bands indicating the S-N curves for most common aluminum alloys excluding wrought alloys having a tensile strength below 38 kpsi. Since aluminum does not have an endurance limit, normally the fatigue strength S_f is reported at a specific number of cycles, normally $N = 5(10^8)$ cycles of reversed stress (see Table A-24).

The S-N diagram is usually obtained by *completely reversed* stress cycles, in which the stress level alternates between equal magnitudes of tension and compression. We note that a stress cycle ($N = 1$) constitutes a single application and removal of a load and then another application and removal of the load in the opposite direction. Thus $N = \frac{1}{2}$ means the load is applied once and then removed, which is the case with the simple tension test.

The body of knowledge available on fatigue failure from $N = 1$ to $N = 1000$ cycles is generally classified as *low-cycle fatigue*, as indicated in Fig. 6-10. *High-cycle fatigue*, then, is concerned with failure corresponding to stress cycles greater than 10^3 cycles.

We also distinguish a *finite-life region* and an *infinite-life region* in Fig. 6-10. The boundary between these regions cannot be clearly defined except for a specific material; but it lies somewhere between 10^6 and 10^7 cycles for steels, as shown in Fig. 6-10.

As noted previously, it is always good engineering practice to conduct a testing program on the materials to be employed in design and manufacture. This, in fact, is a requirement, not an option, in guarding against the possibility of a fatigue failure.

Because of this necessity for testing, it would really be unnecessary for us to proceed any further in the study of fatigue failure except for one important reason: the desire to know why fatigue failures occur so that the most effective method or methods can be used to improve fatigue strength. Thus our primary purpose in studying fatigue is to understand why failures occur so that we can guard against them in an optimum manner. For this reason, the analytical design approaches presented in this book, or in any other book, for that matter, do not yield absolutely precise results. The results should be taken as a guide, as something that indicates what is important and what is not important in designing against fatigue failure.

As stated earlier, the stress-life method is the least accurate approach especially for low-cycle applications. However, it is the most traditional method, with much published data available. It is the easiest to implement for a wide range of design applications and represents high-cycle applications adequately. For these reasons the stress-life method will be emphasized in subsequent sections of this chapter. However, care should be exercised when applying the method for low-cycle applications, as the method does not account for the true stress-strain behavior when localized yielding occurs.

6-5 The Strain-Life Method

The best approach yet advanced to explain the nature of fatigue failure is called by some the *strain-life* method. The approach can be used to estimate fatigue strengths, but when it is so used it is necessary to compound several idealizations, and so some uncertainties will exist in the results. For this reason, the method is presented here only because of its value in explaining the nature of fatigue.

A fatigue failure almost always begins at a local discontinuity such as a notch, crack, or other area of stress concentration. When the stress at the discontinuity exceeds the elastic limit, plastic strain occurs. If a fatigue fracture is to occur, there must exist cyclic plastic strains. Thus we shall need to investigate the behavior of materials subject to cyclic deformation.

In 1910, Bairstow verified by experiment Bauschinger's theory that the elastic limits of iron and steel can be changed, either up or down, by the cyclic variations of stress.² In general, the elastic limits of annealed steels are likely to increase when subjected to cycles of stress reversals, while cold-drawn steels exhibit a decreasing elastic limit.

R. W. Landgraf has investigated the low-cycle fatigue behavior of a large number of very high-strength steels, and during his research he made many cyclic stress-strain plots.³ Figure 6-12 has been constructed to show the general appearance of these plots for the first few cycles of controlled cyclic strain. In this case the strength decreases with stress repetitions, as evidenced by the fact that the reversals occur at ever-smaller stress levels. As previously noted, other materials may be strengthened, instead, by cyclic stress reversals.

The SAE Fatigue Design and Evaluation Steering Committee released a report in 1975 in which the life in reversals to failure is related to the strain amplitude $\Delta\varepsilon/2$.⁴

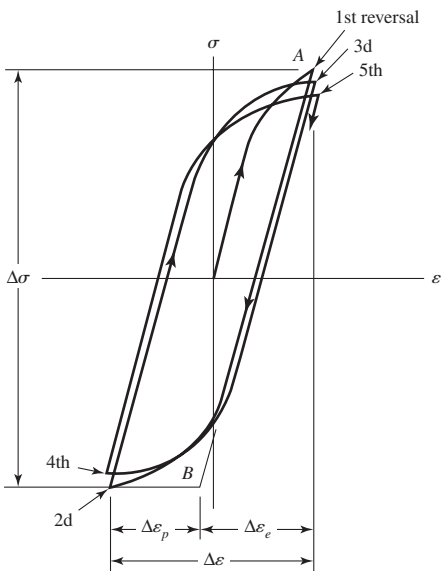
²L. Bairstow, "The Elastic Limits of Iron and Steel under Cyclic Variations of Stress," *Philosophical Transactions, Series A*, vol. 210, Royal Society of London, 1910, pp. 35–55.

³R. W. Landgraf, *Cyclic Deformation and Fatigue Behavior of Hardened Steels*, Report no. 320, Department of Theoretical and Applied Mechanics, University of Illinois, Urbana, 1968, pp. 84–90.

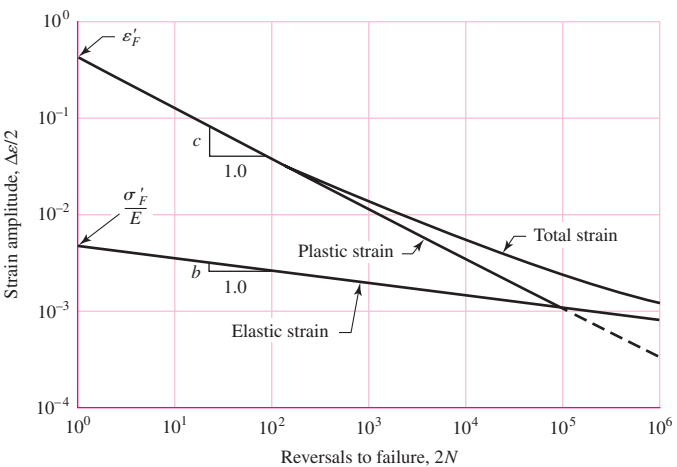
⁴*Technical Report on Fatigue Properties*, SAE J1099, 1975.

Figure 6-12

True stress–true strain hysteresis loops showing the first five stress reversals of a cyclic-softening material. The graph is slightly exaggerated for clarity. Note that the slope of the line AB is the modulus of elasticity E . The stress range is $\Delta\sigma$, $\Delta\varepsilon_p$ is the plastic-strain range, and $\Delta\varepsilon_e$ is the elastic strain range. The total-strain range is $\Delta\varepsilon = \Delta\varepsilon_p + \Delta\varepsilon_e$.

**Figure 6-13**

A log-log plot showing how the fatigue life is related to the true-strain amplitude for hot-rolled SAE 1020 steel. (Reprinted with permission from SAE J1099_200208 © 2002 SAE International.)



The report contains a plot of this relationship for SAE 1020 hot-rolled steel; the graph has been reproduced as Fig. 6-13. To explain the graph, we first define the following terms:

- *Fatigue ductility coefficient* ε'_F is the true strain corresponding to fracture in one reversal (point A in Fig. 6-12). The plastic-strain line begins at this point in Fig. 6-13.
- *Fatigue strength coefficient* σ'_F is the true stress corresponding to fracture in one reversal (point A in Fig. 6-12). Note in Fig. 6-13 that the elastic-strain line begins at σ'_F/E .
- *Fatigue ductility exponent* c is the slope of the plastic-strain line in Fig. 6-13 and is the power to which the life $2N$ must be raised to be proportional to the true plastic-strain amplitude. If the number of stress reversals is $2N$, then N is the number of cycles.

- Fatigue strength exponent b is the slope of the elastic-strain line, and is the power to which the life $2N$ must be raised to be proportional to the true-stress amplitude.

Now, from Fig. 6–12, we see that the total strain is the sum of the elastic and plastic components. Therefore the total strain amplitude is half the total strain range

$$\frac{\Delta\epsilon}{2} = \frac{\Delta\epsilon_e}{2} + \frac{\Delta\epsilon_p}{2} \quad (a)$$

The equation of the plastic-strain line in Fig. 6–13 is

$$\frac{\Delta\epsilon_p}{2} = \epsilon'_F(2N)^c \quad (6-1)$$

The equation of the elastic strain line is

$$\frac{\Delta\epsilon_e}{2} = \frac{\sigma'_F}{E}(2N)^b \quad (6-2)$$

Therefore, from Eq. (a), we have for the total-strain amplitude

$$\frac{\Delta\epsilon}{2} = \frac{\sigma'_F}{E}(2N)^b + \epsilon'_F(2N)^c \quad (6-3)$$

which is the Manson-Coffin relationship between fatigue life and total strain.⁵ Some values of the coefficients and exponents are listed in Table A–23. Many more are included in the SAE J1099 report.⁶

Though Eq. (6–3) is a perfectly legitimate equation for obtaining the fatigue life of a part when the strain and other cyclic characteristics are given, it appears to be of little use to the designer. The question of how to determine the total strain at the bottom of a notch or discontinuity has not been answered. There are no tables or charts of strain-concentration factors in the literature. It is possible that strain-concentration factors will become available in research literature very soon because of the increase in the use of finite-element analysis. Moreover, finite element analysis can of itself approximate the strains that will occur at all points in the subject structure.⁷

6–6

The Linear-Elastic Fracture Mechanics Method

The first phase of fatigue cracking is designated as stage I fatigue. Crystal slip that extends through several contiguous grains, inclusions, and surface imperfections is presumed to play a role. Since most of this is invisible to the observer, we just say that stage I involves several grains. The second phase, that of crack extension, is called stage II fatigue. The advance of the crack (that is, new crack area is created) does produce evidence that can be observed on micrographs from an electron microscope. The growth of

⁵J. F. Tavernelli and L. F. Coffin, Jr., “Experimental Support for Generalized Equation Predicting Low Cycle Fatigue,” and S. S. Manson, discussion, *Trans. ASME, J. Basic Eng.*, vol. 84, no. 4, pp. 533–537.

⁶See also, Landgraf, *Ibid.*

⁷For further discussion of the strain-life method see N. E. Dowling, *Mechanical Behavior of Materials*, 2nd ed., Prentice-Hall, Englewood Cliffs, N.J., 1999, Chap. 14.

the crack is orderly. Final fracture occurs during stage III fatigue, although fatigue is not involved. When the crack is sufficiently long that $K_I = K_{Ic}$ for the stress amplitude involved, where K_{Ic} is the critical stress intensity for the undamaged metal, then there is sudden, catastrophic failure of the remaining cross section in tensile overload (see Sec. 5-12). Stage III fatigue is associated with rapid acceleration of crack growth then fracture.

Crack Growth

Fatigue cracks nucleate and grow when stresses vary and there is some tension in each stress cycle. Consider the stress to be fluctuating between the limits of σ_{\min} and σ_{\max} , where the stress range is defined as $\Delta\sigma = \sigma_{\max} - \sigma_{\min}$. From Eq. (5-37) the stress intensity is given by $K_I = \beta\sigma\sqrt{\pi a}$. Thus, for $\Delta\sigma$, the stress intensity range per cycle is

$$\Delta K_I = \beta(\sigma_{\max} - \sigma_{\min})\sqrt{\pi a} = \beta\Delta\sigma\sqrt{\pi a} \quad (6-4)$$

To develop fatigue strength data, a number of specimens of the same material are tested at various levels of $\Delta\sigma$. Cracks nucleate at or very near a free surface or large discontinuity. Assuming an initial crack length of a_i , crack growth as a function of the number of stress cycles N will depend on $\Delta\sigma$, that is, ΔK_I . For ΔK_I below some threshold value $(\Delta K_I)_{\text{th}}$ a crack will not grow. Figure 6-14 represents the crack length a as a function of N for three stress levels $(\Delta\sigma)_3 > (\Delta\sigma)_2 > (\Delta\sigma)_1$, where $(\Delta K_I)_3 > (\Delta K_I)_2 > (\Delta K_I)_1$ for a given crack size. Notice the effect of the higher stress range in Fig. 6-14 in the production of longer cracks at a particular cycle count.

When the rate of crack growth per cycle, da/dN in Fig. 6-14, is plotted as shown in Fig. 6-15, the data from all three stress range levels superpose to give a sigmoidal curve. The three stages of crack development are observable, and the stage II data are linear on log-log coordinates, within the domain of linear elastic fracture mechanics (LEFM) validity. A group of similar curves can be generated by changing the stress ratio $R = \sigma_{\min}/\sigma_{\max}$ of the experiment.

Here we present a simplified procedure for estimating the remaining life of a cyclically stressed part after discovery of a crack. This requires the assumption that plane strain

Figure 6-14

The increase in crack length a from an initial length of a_i as a function of cycle count for three stress ranges, $(\Delta\sigma)_3 > (\Delta\sigma)_2 > (\Delta\sigma)_1$.

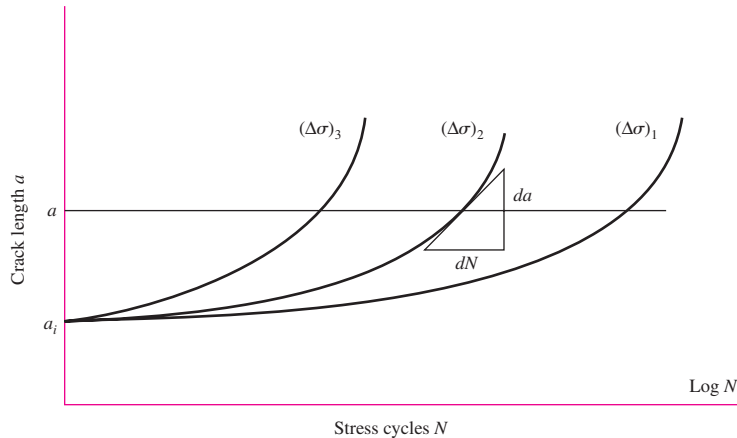
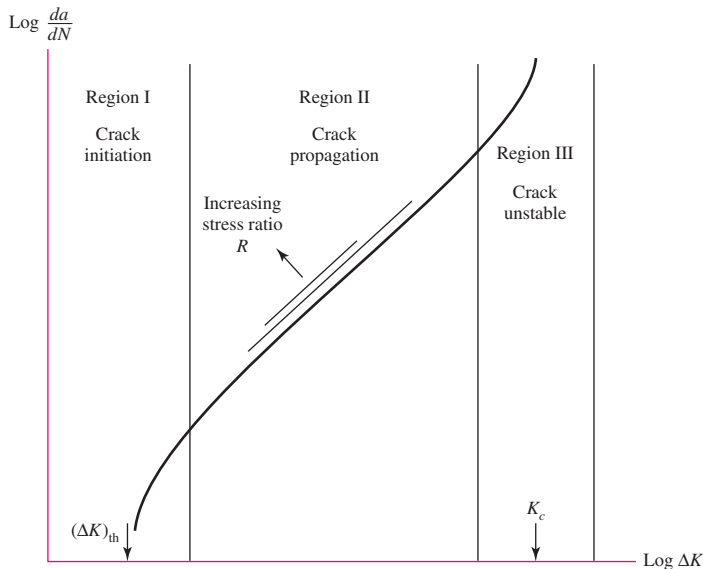


Figure 6-15

When da/dN is measured in Fig. 6-14 and plotted on log-log coordinates, the data for different stress ranges superpose, giving rise to a sigmoid curve as shown. $(\Delta K_1)_{th}$ is the threshold value of ΔK_1 , below which a crack does not grow. From threshold to rupture an aluminum alloy will spend 85–90 percent of life in region I, 5–8 percent in region II, and 1–2 percent in region III.

**Table 6-1**

Conservative Values of Factor C and Exponent m in Eq. (6-5) for Various Forms of Steel ($R = \sigma_{max}/\sigma_{min} \doteq 0$)

Material	$C, \frac{\text{m/cycle}}{(\text{MPa}\sqrt{\text{m}})^m}$	$C, \frac{\text{in/cycle}}{(\text{kpsi}\sqrt{\text{in}})^m}$	m
Ferritic-pearlitic steels	$6.89(10^{-12})$	$3.60(10^{-10})$	3.00
Martensitic steels	$1.36(10^{-10})$	$6.60(10^{-9})$	2.25
Austenitic stainless steels	$5.61(10^{-12})$	$3.00(10^{-10})$	3.25

From J. M. Barsom and S. T. Rolfe, *Fatigue and Fracture Control in Structures*, 2nd ed., Prentice Hall, Upper Saddle River, NJ, 1987, pp. 288–291, Copyright ASTM International. Reprinted with permission.

conditions prevail.⁸ Assuming a crack is discovered early in stage II, the crack growth in region II of Fig. 6-15 can be approximated by the *Paris equation*, which is of the form

$$\frac{da}{dN} = C(\Delta K_1)^m \quad (6-5)$$

where C and m are empirical material constants and ΔK_1 is given by Eq. (6-4). Representative, but conservative, values of C and m for various classes of steels are listed in Table 6-1. Substituting Eq. (6-4) and integrating gives

$$\int_0^{N_f} dN = N_f = \frac{1}{C} \int_{a_i}^{a_f} \frac{da}{(\beta \Delta \sigma \sqrt{\pi a})^m} \quad (6-6)$$

Here a_i is the initial crack length, a_f is the final crack length corresponding to failure, and N_f is the estimated number of cycles to produce a failure after the initial crack is formed. Note that β may vary in the integration variable (e.g., see Figs. 5-25 to 5-30).

⁸Recommended references are: Dowling, op. cit.; J. A. Collins, *Failure of Materials in Mechanical Design*, John Wiley & Sons, New York, 1981; H. O. Fuchs and R. I. Stephens, *Metal Fatigue in Engineering*, John Wiley & Sons, New York, 1980; and Harold S. Reemsnyder, "Constant Amplitude Fatigue Life Assessment Models," *SAE Trans.* 820688, vol. 91, Nov. 1983.

If this should happen, then Reemsnyder⁹ suggests the use of numerical integration employing the algorithm

$$\begin{aligned}\delta a_j &= C(\Delta K_I)_j^m (\delta N)_j \\ a_{j+1} &= a_j + \delta a_j \\ N_{j+1} &= N_j + \delta N_j \\ N_f &= \sum \delta N_j\end{aligned}\quad (6-7)$$

Here δa_j and δN_j are increments of the crack length and the number of cycles. The procedure is to select a value of δN_j , using a_i determine β and compute ΔK_I , determine δa_j , and then find the next value of a . Repeat the procedure until $a = a_f$.

The following example is highly simplified with β constant in order to give some understanding of the procedure. Normally, one uses fatigue crack growth computer programs such as NASA/FLAGRO 2.0 with more comprehensive theoretical models to solve these problems.

EXAMPLE 6-1

The bar shown in Fig. 6-16 is subjected to a repeated moment $0 \leq M \leq 1200 \text{ lbf} \cdot \text{in}$. The bar is AISI 4430 steel with $S_{ut} = 185 \text{ ksi}$, $S_y = 170 \text{ ksi}$, and $K_{Ic} = 73 \text{ ksi}\sqrt{\text{in}}$. Material tests on various specimens of this material with identical heat treatment indicate worst-case constants of $C = 3.8(10^{-11})(\text{in}/\text{cycle})/(\text{ksi}\sqrt{\text{in}})^m$ and $m = 3.0$. As shown, a nick of size 0.004 in has been discovered on the bottom of the bar. Estimate the number of cycles of life remaining.

Solution

The stress range $\Delta\sigma$ is always computed by using the nominal (uncracked) area. Thus

$$\frac{I}{c} = \frac{bh^2}{6} = \frac{0.25(0.5)^2}{6} = 0.01042 \text{ in}^3$$

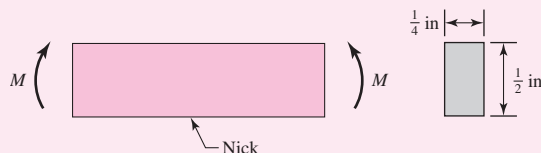
Therefore, before the crack initiates, the stress range is

$$\Delta\sigma = \frac{\Delta M}{I/c} = \frac{1200}{0.01042} = 115.2(10^3) \text{ psi} = 115.2 \text{ ksi}$$

which is below the yield strength. As the crack grows, it will eventually become long enough such that the bar will completely yield or undergo a brittle fracture. For the ratio of S_y/S_{ut} it is highly unlikely that the bar will reach complete yield. For brittle fracture, designate the crack length as a_f . If $\beta = 1$, then from Eq. (5-37) with $K_I = K_{Ic}$, we approximate a_f as

$$a_f = \frac{1}{\pi} \left(\frac{K_{Ic}}{\beta \sigma_{max}} \right)^2 \doteq \frac{1}{\pi} \left(\frac{73}{115.2} \right)^2 = 0.1278 \text{ in}$$

| Figure 6-16



⁹Op. cit.

From Fig. 5–27, we compute the ratio a_f/h as

$$\frac{a_f}{h} = \frac{0.1278}{0.5} = 0.256$$

Thus a_f/h varies from near zero to approximately 0.256. From Fig. 5–27, for this range β is nearly constant at approximately 1.07. We will assume it to be so, and re-evaluate a_f as

$$a_f = \frac{1}{\pi} \left(\frac{73}{1.07(115.2)} \right)^2 = 0.112 \text{ in}$$

Thus, from Eq. (6–6), the estimated remaining life is

Answer

$$N_f = \frac{1}{C} \int_{a_i}^{a_f} \frac{da}{(\beta \Delta \sigma \sqrt{\pi a})^m} = \frac{1}{3.8(10^{-11})} \int_{0.004}^{0.112} \frac{da}{[1.07(115.2)\sqrt{\pi a}]^3}$$

$$= -\frac{5.047(10^3)}{\sqrt{a}} \Big|_{0.004}^{0.112} = 64.7 (10^3) \text{ cycles}$$

6–7 The Endurance Limit

The determination of endurance limits by fatigue testing is now routine, though a lengthy procedure. Generally, stress testing is preferred to strain testing for endurance limits.

For preliminary and prototype design and for some failure analysis as well, a quick method of estimating endurance limits is needed. There are great quantities of data in the literature on the results of rotating-beam tests and simple tension tests of specimens taken from the same bar or ingot. By plotting these as in Fig. 6–17, it is possible to see whether there is any correlation between the two sets of results. The graph appears to suggest that the endurance limit ranges from about 40 to 60 percent of the tensile strength for steels up to about 210 kpsi (1450 MPa). Beginning at about $S_{ut} = 210$ kpsi (1450 MPa), the scatter appears to increase, but the trend seems to level off, as suggested by the dashed horizontal line at $S'_e = 105$ kpsi.

We wish now to present a method for estimating endurance limits. Note that estimates obtained from quantities of data obtained from many sources probably have a large spread and might deviate significantly from the results of actual laboratory tests of the mechanical properties of specimens obtained through strict purchase-order specifications. Since the area of uncertainty is greater, compensation must be made by employing larger design factors than would be used for static design.

For steels, simplifying our observation of Fig. 6–17, we will estimate the endurance limit as

$$S'_e = \begin{cases} 0.5S_{ut} & S_{ut} \leq 200 \text{ kpsi (1400 MPa)} \\ 100 \text{ kpsi} & S_{ut} > 200 \text{ kpsi} \\ 700 \text{ MPa} & S_{ut} > 1400 \text{ MPa} \end{cases} \quad (6-8)$$

where S_{ut} is the *minimum* tensile strength. The prime mark on S'_e in this equation refers to the *rotating-beam specimen* itself. We wish to reserve the unprimed symbol S_e for the endurance limit of an actual machine element subjected to any kind of loading. Soon we shall learn that the two strengths may be quite different.

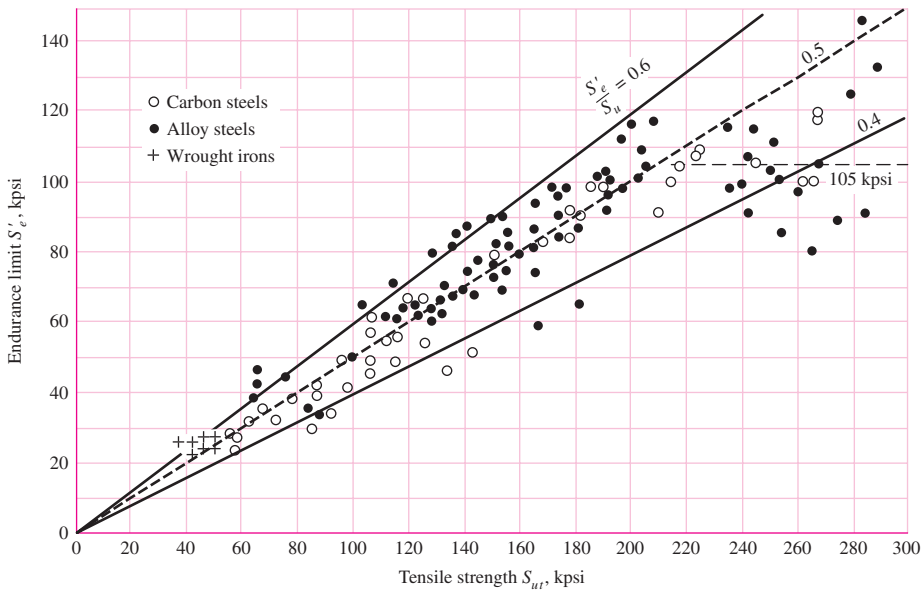


Figure 6-17

Graph of endurance limits versus tensile strengths from actual test results for a large number of wrought irons and steels. Ratios of S'_e/S_{ut} of 0.60, 0.50, and 0.40 are shown by the solid and dashed lines. Note also the horizontal dashed line for $S'_e = 105$ kpsi. Points shown having a tensile strength greater than 210 kpsi have a mean endurance limit of $S'_e = 105$ kpsi and a standard deviation of 13.5 kpsi. (Collated from data compiled by H. J. Grover, S. A. Gordon, and L. R. Jackson in Fatigue of Metals and Structures, Bureau of Naval Weapons Document NAVWEPS 00-25-534, 1960; and from Fatigue Design Handbook, SAE, 1968, p. 42.)

Steels treated to give different microstructures have different S'_e/S_{ut} ratios. It appears that the more ductile microstructures have a higher ratio. Martensite has a very brittle nature and is highly susceptible to fatigue-induced cracking; thus the ratio is low. When designs include detailed heat-treating specifications to obtain specific microstructures, it is possible to use an estimate of the endurance limit based on test data for the particular microstructure; such estimates are much more reliable and indeed should be used.

The endurance limits for various classes of cast irons, polished or machined, are given in Table A-24. Aluminum alloys do not have an endurance limit. The fatigue strengths of some aluminum alloys at $5(10^8)$ cycles of reversed stress are given in Table A-24.

6-8 Fatigue Strength

As shown in Fig. 6-10, a region of low-cycle fatigue extends from $N = 1$ to about 10^3 cycles. In this region the fatigue strength S_f is only slightly smaller than the tensile strength S_{ut} . An analytical approach has been given by Shigley, Mischke, and Brown¹⁰

¹⁰J. E. Shigley, C. R. Mischke, and T. H. Brown, Jr., *Standard Handbook of Machine Design*, 3rd ed., McGraw-Hill, New York, 2004, pp. 29.25–29.27.

for both high-cycle and low-cycle regions, requiring the parameters of the Manson-Coffin equation plus the strain-strengthening exponent m . Engineers often have to work with less information.

Figure 6–10 indicates that the high-cycle fatigue domain extends from 10^3 cycles for steels to the endurance limit life N_e , which is about 10^6 to 10^7 cycles. The purpose of this section is to develop methods of approximation of the S - N diagram in the high-cycle region, when information may be as sparse as the results of a simple tension test. Experience has shown high-cycle fatigue data are rectified by a logarithmic transform to both stress and cycles-to-failure. Equation (6–2) can be used to determine the fatigue strength at 10^3 cycles. Defining the specimen fatigue strength at a specific number of cycles as $(S'_f)_N = E\Delta\varepsilon_e/2$, write Eq. (6–2) as

$$(S'_f)_N = \sigma'_F(2N)^b \quad (6-9)$$

At 10^3 cycles,

$$(S'_f)_{10^3} = \sigma'_F(2 \cdot 10^3)^b = f S_{ut}$$

where f is the fraction of S_{ut} represented by $(S'_f)_{10^3}$ cycles. Solving for f gives

$$f = \frac{\sigma'_F}{S_{ut}}(2 \cdot 10^3)^b \quad (6-10)$$

Now, from Eq. (2–15), $\sigma'_F = \sigma_0\varepsilon^m$, with $\varepsilon = \varepsilon'_F$. If this true-stress–true-strain equation is not known, the SAE approximation¹¹ for steels with $H_B \leq 500$ may be used:

$$\sigma'_F = S_{ut} + 50 \text{ kpsi} \quad \text{or} \quad \sigma'_F = S_{ut} + 345 \text{ MPa} \quad (6-11)$$

To find b , substitute the endurance strength and corresponding cycles, S'_e and N_e , respectively into Eq. (6–9) and solving for b

$$b = -\frac{\log(\sigma'_F/S'_e)}{\log(2N_e)} \quad (6-12)$$

Thus, the equation $S'_f = \sigma'_F(2N)^b$ is known. For example, if $S_{ut} = 105$ kpsi and $S'_e = 52.5$ kpsi with $N_e = 10^6$ cycles,

$$\text{Eq. (6-11)} \quad \sigma'_F = 105 + 50 = 155 \text{ kpsi}$$

$$\text{Eq. (6-12)} \quad b = -\frac{\log(155/52.5)}{\log(2 \cdot 10^6)} = -0.0746$$

$$\text{Eq. (6-10)} \quad f = \frac{155}{105} (2 \cdot 10^3)^{-0.0746} = 0.837$$

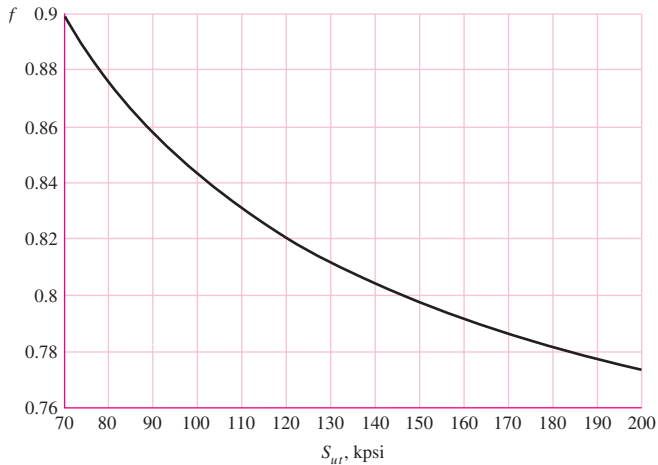
and for Eq. (6–9), with $S'_f = (S'_f)_N$,

$$S'_f = 155(2N)^{-0.0746} = 147 N^{-0.0746} \quad (a)$$

¹¹*Fatigue Design Handbook*, vol. 4, Society of Automotive Engineers, New York, 1958, p. 27.

Figure 6-18

Fatigue strength fraction, f ,
of S_{ut} at 10^3 cycles for
 $S_e = S'_e = 0.5S_{ut}$ at 10^6 cycles.



The process given for finding f can be repeated for various ultimate strengths. Figure 6-18 is a plot of f for $70 \leq S_{ut} \leq 200$ kpsi. To be conservative, for $S_{ut} < 70$ kpsi, let $f = 0.9$.

For an actual mechanical component, S'_e is reduced to S_e (see Sec. 6-9) which is less than $0.5 S_{ut}$. However, unless actual data is available, we recommend using the value of f found from Fig. 6-18. Equation (a), for the actual mechanical component, can be written in the form

$$S_f = a N^b \quad (6-13)$$

where N is cycles to failure and the constants a and b are defined by the points 10^3 , $(S_f)_{10^3}$ and 10^6 , S_e with $(S_f)_{10^3} = f S_{ut}$. Substituting these two points in Eq. (6-13) gives

$$a = \frac{(f S_{ut})^2}{S_e} \quad (6-14)$$

$$b = -\frac{1}{3} \log \left(\frac{f S_{ut}}{S_e} \right) \quad (6-15)$$

If a *completely reversed* stress σ_{rev} is given, setting $S_f = \sigma_{rev}$ in Eq. (6-13), the number of cycles-to-failure can be expressed as

$$N = \left(\frac{\sigma_{rev}}{a} \right)^{1/b} \quad (6-16)$$

Note that the typical $S-N$ diagram, and thus Eq. (6-16), is only applicable for completely reversed loading. For general fluctuating loading situations, it is necessary to obtain a completely reversed stress that may be considered to be equivalent in fatigue damage as the actual fluctuating stress (see Ex. 6-12, p. 313).

Low-cycle fatigue is often defined (see Fig. 6-10) as failure that occurs in a range of $1 \leq N \leq 10^3$ cycles. On a log-log plot such as Fig. 6-10 the failure locus in this range is nearly linear below 10^3 cycles. A straight line between 10^3 , $f S_{ut}$ and 1 , S_{ut} (transformed) is conservative, and it is given by

$$S_f \geq S_{ut} N^{(\log f)/3} \quad 1 \leq N \leq 10^3 \quad (6-17)$$

EXAMPLE 6-2

Given a 1050 HR steel, *estimate*

- the rotating-beam endurance limit at 10^6 cycles.
- the endurance strength of a polished rotating-beam specimen corresponding to 10^4 cycles to failure
- the expected life of a polished rotating-beam specimen under a completely reversed stress of 55 kpsi.

Solution

(a) From Table A-20, $S_{ut} = 90$ kpsi. From Eq. (6-8),

Answer

$$S'_e = 0.5(90) = 45 \text{ kpsi}$$

(b) From Fig. 6-18, for $S_{ut} = 90$ kpsi, $f = 0.86$. From Eq. (6-14),

$$a = \frac{[0.86(90)]^2}{45} = 133.1 \text{ kpsi}$$

From Eq. (6-15),

$$b = -\frac{1}{3} \log \left[\frac{0.86(90)}{45} \right] = -0.0785$$

Thus, Eq. (6-13) is

$$S'_f = 133.1 N^{-0.0785}$$

Answer

For 10^4 cycles to failure, $S'_f = 133.1(10^4)^{-0.0785} = 64.6$ kpsi

(c) From Eq. (6-16), with $\sigma_{rev} = 55$ kpsi,

Answer

$$N = \left(\frac{55}{133.1} \right)^{1/-0.0785} = 77\,500 = 7.75(10^4) \text{ cycles}$$

Keep in mind that these are only *estimates*. So expressing the answers using three-place accuracy is a little misleading.

6-9

Endurance Limit Modifying Factors

We have seen that the rotating-beam specimen used in the laboratory to determine endurance limits is prepared very carefully and tested under closely controlled conditions. It is unrealistic to expect the endurance limit of a mechanical or structural member to match the values obtained in the laboratory. Some differences include

- *Material*: composition, basis of failure, variability
- *Manufacturing*: method, heat treatment, fretting corrosion, surface condition, stress concentration
- *Environment*: corrosion, temperature, stress state, relaxation times
- *Design*: size, shape, life, stress state, speed, fretting, galling

Marin¹² identified factors that quantified the effects of surface condition, size, loading, temperature, and miscellaneous items. The question of whether to adjust the endurance limit by subtractive corrections or multiplicative corrections was resolved by an extensive statistical analysis of a 4340 (electric furnace, aircraft quality) steel, in which a correlation coefficient of 0.85 was found for the multiplicative form and 0.40 for the additive form. A Marin equation is therefore written as

$$S_e = k_a k_b k_c k_d k_e k_f S'_e \quad (6-18)$$

where k_a = surface condition modification factor
 k_b = size modification factor
 k_c = load modification factor
 k_d = temperature modification factor
 k_e = reliability factor¹³
 k_f = miscellaneous-effects modification factor
 S'_e = rotary-beam test specimen endurance limit
 S_e = endurance limit at the critical location of a machine part in the geometry and condition of use

When endurance tests of parts are not available, estimations are made by applying Marin factors to the endurance limit.

Surface Factor k_a

The surface of a rotating-beam specimen is highly polished, with a final polishing in the axial direction to smooth out any circumferential scratches. The surface modification factor depends on the quality of the finish of the actual part surface and on the tensile strength of the part material. To find quantitative expressions for common finishes of machine parts (ground, machined, or cold-drawn, hot-rolled, and as-forged), the coordinates of data points were recaptured from a plot of endurance limit versus ultimate tensile strength of data gathered by Lipson and Noll and reproduced by Horger.¹⁴ The data can be represented by

$$k_a = a S_{ut}^b \quad (6-19)$$

where S_{ut} is the minimum tensile strength and a and b are to be found in Table 6-2.

¹²Joseph Marin, *Mechanical Behavior of Engineering Materials*, Prentice-Hall, Englewood Cliffs, N.J., 1962, p. 224.

¹³Complete stochastic analysis is presented in Sec. 6-17. Until that point the presentation here is one of a deterministic nature. However, we must take care of the known scatter in the fatigue data. This means that we will not carry out a true reliability analysis at this time but will attempt to answer the question: What is the probability that a *known* (assumed) stress will exceed the strength of a randomly selected component made from this material population?

¹⁴C. J. Noll and C. Lipson, "Allowable Working Stresses," *Society for Experimental Stress Analysis*, vol. 3, no. 2, 1946, p. 29. Reproduced by O. J. Horger (ed.), *Metals Engineering Design ASME Handbook*, McGraw-Hill, New York, 1953, p. 102.

Table 6-2

Parameters for Marin Surface Modification Factor, Eq. (6-19)

Surface Finish	Factor <i>a</i> <i>S_{ut}</i> , kpsi	Exponent <i>b</i> <i>S_{ut}</i> , MPa
Ground	1.34	1.58 −0.085
Machined or cold-drawn	2.70	4.51 −0.265
Hot-rolled	14.4	57.7 −0.718
As-forged	39.9	272. −0.995

From C.J. Noll and C. Lipson, "Allowable Working Stresses," *Society for Experimental Stress Analysis*, vol. 3, no. 2, 1946 p. 29. Reproduced by O.J. Horger (ed.) *Metals Engineering Design ASME Handbook*, McGraw-Hill, New York. Copyright © 1953 by The McGraw-Hill Companies, Inc. Reprinted by permission.

EXAMPLE 6-3

A steel has a minimum ultimate strength of 520 MPa and a machined surface. Estimate *k_a*.

Solution

From Table 6-2, *a* = 4.51 and *b* = −0.265. Then, from Eq. (6-19)

Answer

$$k_a = 4.51(520)^{-0.265} = 0.860$$

Again, it is important to note that this is an approximation as the data is typically quite scattered. Furthermore, this is not a correction to take lightly. For example, if in the previous example the steel was forged, the correction factor would be 0.540, a significant reduction of strength.

Size Factor *k_b*

The size factor has been evaluated using 133 sets of data points.¹⁵ The results for bending and torsion may be expressed as

$$k_b = \begin{cases} (d/0.3)^{-0.107} = 0.879d^{-0.107} & 0.11 \leq d \leq 2 \text{ in} \\ 0.91d^{-0.157} & 2 < d \leq 10 \text{ in} \\ (d/7.62)^{-0.107} = 1.24d^{-0.107} & 2.79 \leq d \leq 51 \text{ mm} \\ 1.51d^{-0.157} & 51 < d \leq 254 \text{ mm} \end{cases} \quad (6-20)$$

For axial loading there is no size effect, so

$$k_b = 1 \quad (6-21)$$

but see *k_c*.

One of the problems that arises in using Eq. (6-20) is what to do when a round bar in bending is not rotating, or when a noncircular cross section is used. For example, what is the size factor for a bar 6 mm thick and 40 mm wide? The approach to be used

¹⁵Charles R. Mischke, "Prediction of Stochastic Endurance Strength," *Trans. of ASME, Journal of Vibration, Acoustics, Stress, and Reliability in Design*, vol. 109, no. 1, January 1987, Table 3.

here employs an *equivalent diameter* d_e obtained by equating the volume of material stressed at and above 95 percent of the maximum stress to the same volume in the rotating-beam specimen.¹⁶ It turns out that when these two volumes are equated, the lengths cancel, and so we need only consider the areas. For a rotating round section, the 95 percent stress area is the area in a ring having an outside diameter d and an inside diameter of $0.95d$. So, designating the 95 percent stress area $A_{0.95\sigma}$, we have

$$A_{0.95\sigma} = \frac{\pi}{4}[d^2 - (0.95d)^2] = 0.0766d^2 \quad (6-22)$$

This equation is also valid for a rotating hollow round. For nonrotating solid or hollow rounds, the 95 percent stress area is twice the area outside of two parallel chords having a spacing of $0.95d$, where d is the diameter. Using an exact computation, this is

$$A_{0.95\sigma} = 0.01046d^2 \quad (6-23)$$

With d_e in Eq. (6-22), setting Eqs. (6-22) and (6-23) equal to each other enables us to solve for the effective diameter. This gives

$$d_e = 0.370d \quad (6-24)$$

as the effective size of a round corresponding to a nonrotating solid or hollow round.

A rectangular section of dimensions $h \times b$ has $A_{0.95\sigma} = 0.05hb$. Using the same approach as before,

$$d_e = 0.808(hb)^{1/2} \quad (6-25)$$

Table 6-3 provides $A_{0.95\sigma}$ areas of common structural shapes undergoing non-rotating bending.

EXAMPLE 6-4

A steel shaft loaded in bending is 32 mm in diameter, abutting a filleted shoulder 38 mm in diameter. The shaft material has a mean ultimate tensile strength of 690 MPa. Estimate the Marin size factor k_b if the shaft is used in

- (a) A rotating mode.
- (b) A nonrotating mode.

Solution

- (a) From Eq. (6-20)

Answer

$$k_b = \left(\frac{d}{7.62} \right)^{-0.107} = \left(\frac{32}{7.62} \right)^{-0.107} = 0.858$$

- (b) From Table 6-3,

$$d_e = 0.37d = 0.37(32) = 11.84 \text{ mm}$$

From Eq. (6-20),

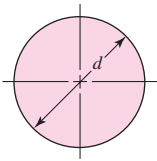
Answer

$$k_b = \left(\frac{11.84}{7.62} \right)^{-0.107} = 0.954$$

¹⁶See R. Kuguel, "A Relation between Theoretical Stress-Concentration Factor and Fatigue Notch Factor Deduced from the Concept of Highly Stressed Volume," *Proc. ASTM*, vol. 61, 1961, pp. 732-748.

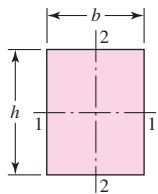
Table 6-3

$A_{0.95\sigma}$ Areas of Common Nonrotating Structural Shapes



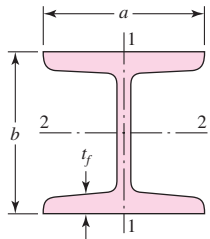
$$A_{0.95\sigma} = 0.01046d^2$$

$$d_e = 0.370d$$



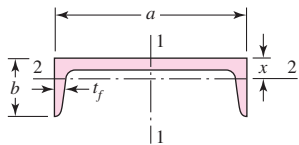
$$A_{0.95\sigma} = 0.05hb$$

$$d_e = 0.808\sqrt{hb}$$



$$A_{0.95\sigma} = \begin{cases} 0.10at_f & \text{axis 1-1} \\ 0.05ba & \text{axis 2-2} \end{cases}$$

$$t_f > 0.025a$$



$$A_{0.95\sigma} = \begin{cases} 0.05ab & \text{axis 1-1} \\ 0.052xa + 0.1t_f(b-x) & \text{axis 2-2} \end{cases}$$

Loading Factor k_c

When fatigue tests are carried out with rotating bending, axial (push-pull), and torsional loading, the endurance limits differ with S_{ut} . This is discussed further in Sec. 6-17. Here, we will specify average values of the load factor as

$$k_c = \begin{cases} 1 & \text{bending} \\ 0.85 & \text{axial} \\ 0.59 & \text{torsion}^{17} \end{cases} \quad (6-26)$$

Temperature Factor k_d

When operating temperatures are below room temperature, brittle fracture is a strong possibility and should be investigated first. When the operating temperatures are higher than room temperature, yielding should be investigated first because the yield strength drops off so rapidly with temperature; see Fig. 2-9. Any stress will induce creep in a material operating at high temperatures; so this factor must be considered too.

¹⁷Use this only for pure torsional fatigue loading. When torsion is combined with other stresses, such as bending, $k_c = 1$ and the combined loading is managed by using the effective von Mises stress as in Sec. 5-5.

Note: For pure torsion, the distortion energy predicts that $(k_c)_{\text{torsion}} = 0.577$.

Table 6-4

	Temperature, °C	S_T/S_{RT}	Temperature, °F	S_T/S_{RT}
Effect of Operating Temperature on the Tensile Strength of Steel.* (S_T = tensile strength at operating temperature; S_{RT} = tensile strength at room temperature; $0.099 \leq \hat{\sigma} \leq 0.110$)	20	1.000	70	1.000
	50	1.010	100	1.008
	100	1.020	200	1.020
	150	1.025	300	1.024
	200	1.020	400	1.018
	250	1.000	500	0.995
	300	0.975	600	0.963
	350	0.943	700	0.927
	400	0.900	800	0.872
	450	0.843	900	0.797
	500	0.768	1000	0.698
	550	0.672	1100	0.567
	600	0.549		

*Data source: Fig. 2-9.

Finally, it may be true that there is no fatigue limit for materials operating at high temperatures. Because of the reduced fatigue resistance, the failure process is, to some extent, dependent on time.

The limited amount of data available show that the endurance limit for steels increases slightly as the temperature rises and then begins to fall off in the 400 to 700°F range, not unlike the behavior of the tensile strength shown in Fig. 2-9. For this reason it is probably true that the endurance limit is related to tensile strength at elevated temperatures in the same manner as at room temperature.¹⁸ It seems quite logical, therefore, to employ the same relations to predict endurance limit at elevated temperatures as are used at room temperature, at least until more comprehensive data become available. At the very least, this practice will provide a useful standard against which the performance of various materials can be compared.

Table 6-4 has been obtained from Fig. 2-9 by using only the tensile-strength data. Note that the table represents 145 tests of 21 different carbon and alloy steels. A fourth-order polynomial curve fit to the data underlying Fig. 2-9 gives

$$k_d = 0.975 + 0.432(10^{-3})T_F - 0.115(10^{-5})T_F^2 + 0.104(10^{-8})T_F^3 - 0.595(10^{-12})T_F^4 \quad (6-27)$$

where $70 \leq T_F \leq 1000^\circ\text{F}$.

Two types of problems arise when temperature is a consideration. If the rotating-beam endurance limit is known at room temperature, then use

$$k_d = \frac{S_T}{S_{RT}} \quad (6-28)$$

¹⁸For more, see Table 2 of ANSI/ASME B106. 1M-1985 shaft standard, and E. A. Brandes (ed.), *Smithell's Metals Reference Book*, 6th ed., Butterworth, London, 1983, pp. 22-134 to 22-136, where endurance limits from 100 to 650°C are tabulated.

from Table 6–4 or Eq. (6–27) and proceed as usual. If the rotating-beam endurance limit is not given, then compute it using Eq. (6–8) and the temperature-corrected tensile strength obtained by using the factor from Table 6–4. Then use $k_d = 1$.

EXAMPLE 6–5

A 1035 steel has a tensile strength of 70 kpsi and is to be used for a part that sees 450°F in service. Estimate the Marin temperature modification factor and $(S_e)_{450^\circ}$ if

- The room-temperature endurance limit by test is $(S'_e)_{70^\circ} = 39.0$ kpsi.
- Only the tensile strength at room temperature is known.

Solution

(a) First, from Eq. (6–27),

$$\begin{aligned} k_d &= 0.975 + 0.432(10^{-3})(450) - 0.115(10^{-5})(450^2) \\ &\quad + 0.104(10^{-8})(450^3) - 0.595(10^{-12})(450^4) = 1.007 \end{aligned}$$

Thus,

Answer

$$(S_e)_{450^\circ} = k_d(S'_e)_{70^\circ} = 1.007(39.0) = 39.3 \text{ kpsi}$$

(b) Interpolating from Table 6–4 gives

$$(S_T/S_{RT})_{450^\circ} = 1.018 + (0.995 - 1.018) \frac{450 - 400}{500 - 400} = 1.007$$

Thus, the tensile strength at 450°F is estimated as

$$(S_{ut})_{450^\circ} = (S_T/S_{RT})_{450^\circ} (S_{ut})_{70^\circ} = 1.007(70) = 70.5 \text{ kpsi}$$

From Eq. (6–8) then,

Answer

$$(S_e)_{450^\circ} = 0.5(S_{ut})_{450^\circ} = 0.5(70.5) = 35.2 \text{ kpsi}$$

Part *a* gives the better estimate due to actual testing of the particular material.

Reliability Factor k_e

The discussion presented here accounts for the scatter of data such as shown in Fig. 6–17 where the mean endurance limit is shown to be $S'_e/S_{ut} \doteq 0.5$, or as given by Eq. (6–8). Most endurance strength data are reported as mean values. Data presented by Haugen and Wirsching¹⁹ show standard deviations of endurance strengths of less than 8 percent. Thus the reliability modification factor to account for this can be written as

$$k_e = 1 - 0.08 z_a \quad (6-29)$$

where z_a is defined by Eq. (20–16) and values for any desired reliability can be determined from Table A–10. Table 6–5 gives reliability factors for some standard specified reliabilities.

For a more comprehensive approach to reliability, see Sec. 6–17.

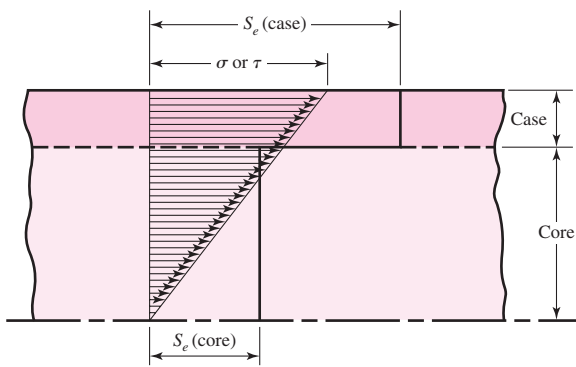
¹⁹E. B. Haugen and P. H. Wirsching, "Probabilistic Design," *Machine Design*, vol. 47, no. 12, 1975, pp. 10–14.

Table 6–5

	Reliability, %	Transformation Variate z_α	Reliability Factor k_e
Reliability Factors k_e	50	0	1.000
Corresponding to 8 Percent Standard Deviation of the Endurance Limit	90	1.288	0.897
	95	1.645	0.868
	99	2.326	0.814
	99.9	3.091	0.753
	99.99	3.719	0.702
	99.999	4.265	0.659
	99.9999	4.753	0.620

Figure 6–19

The failure of a case-hardened part in bending or torsion. In this example, failure occurs in the core.



Miscellaneous-Effects Factor k_f

Though the factor k_f is intended to account for the reduction in endurance limit due to all other effects, it is really intended as a reminder that these must be accounted for, because actual values of k_f are not always available.

Residual stresses may either improve the endurance limit or affect it adversely. Generally, if the residual stress in the surface of the part is compression, the endurance limit is improved. Fatigue failures appear to be tensile failures, or at least to be caused by tensile stress, and so anything that reduces tensile stress will also reduce the possibility of a fatigue failure. Operations such as shot peening, hammering, and cold rolling build compressive stresses into the surface of the part and improve the endurance limit significantly. Of course, the material must not be worked to exhaustion.

The endurance limits of parts that are made from rolled or drawn sheets or bars, as well as parts that are forged, may be affected by the so-called *directional characteristics* of the operation. Rolled or drawn parts, for example, have an endurance limit in the transverse direction that may be 10 to 20 percent less than the endurance limit in the longitudinal direction.

Parts that are case-hardened may fail at the surface or at the maximum core radius, depending upon the stress gradient. Figure 6–19 shows the typical triangular stress distribution of a bar under bending or torsion. Also plotted as a heavy line in this figure are the endurance limits S_e for the case and core. For this example the endurance limit of the core rules the design because the figure shows that the stress σ or τ , whichever applies, at the outer core radius, is appreciably larger than the core endurance limit.

Corrosion

It is to be expected that parts that operate in a corrosive atmosphere will have a lowered fatigue resistance. This is, of course, true, and it is due to the roughening or pitting of the surface by the corrosive material. But the problem is not so simple as the one of finding the endurance limit of a specimen that has been corroded. The reason for this is that the corrosion and the stressing occur at the same time. Basically, this means that in time any part will fail when subjected to repeated stressing in a corrosive atmosphere. There is no fatigue limit. Thus the designer's problem is to attempt to minimize the factors that affect the fatigue life; these are:

- Mean or static stress
- Alternating stress
- Electrolyte concentration
- Dissolved oxygen in electrolyte
- Material properties and composition
- Temperature
- Cyclic frequency
- Fluid flow rate around specimen
- Local crevices

Electrolytic Plating

Metallic coatings, such as chromium plating, nickel plating, or cadmium plating, reduce the endurance limit by as much as 50 percent. In some cases the reduction by coatings has been so severe that it has been necessary to eliminate the plating process. Zinc plating does not affect the fatigue strength. Anodic oxidation of light alloys reduces bending endurance limits by as much as 39 percent but has no effect on the torsional endurance limit.

Metal Spraying

Metal spraying results in surface imperfections that can initiate cracks. Limited tests show reductions of 14 percent in the fatigue strength.

Cyclic Frequency

If, for any reason, the fatigue process becomes time-dependent, then it also becomes frequency-dependent. Under normal conditions, fatigue failure is independent of frequency. But when corrosion or high temperatures, or both, are encountered, the cyclic rate becomes important. The slower the frequency and the higher the temperature, the higher the crack propagation rate and the shorter the life at a given stress level.

Fretage Corrosion

The phenomenon of fretage corrosion is the result of microscopic motions of tightly fitting parts or structures. Bolted joints, bearing-race fits, wheel hubs, and any set of tightly fitted parts are examples. The process involves surface discoloration, pitting, and eventual fatigue. The fretage factor k_f depends upon the material of the mating pairs and ranges from 0.24 to 0.90.

6-10

Stress Concentration and Notch Sensitivity

In Sec. 3-13 it was pointed out that the existence of irregularities or discontinuities, such as holes, grooves, or notches, in a part increases the theoretical stresses significantly in the immediate vicinity of the discontinuity. Equation (3-48) defined a stress-concentration factor K_t (or K_{ts}), which is used with the nominal stress to obtain the maximum resulting stress due to the irregularity or defect. It turns out that some materials are not fully sensitive to the presence of notches and hence, for these, a reduced value of K_t can be used. For these materials, the effective maximum stress in fatigue is,

$$\sigma_{\max} = K_f \sigma_0 \quad \text{or} \quad \tau_{\max} = K_{fs} \tau_0 \quad (6-30)$$

where K_f is a reduced value of K_t and σ_0 is the nominal stress. The factor K_f is commonly called a *fatigue stress-concentration factor*, and hence the subscript *f*. So it is convenient to think of K_f as a stress-concentration factor reduced from K_t because of lessened sensitivity to notches. The resulting factor is defined by the equation

$$K_f = \frac{\text{maximum stress in notched specimen}}{\text{stress in notch-free specimen}} \quad (a)$$

Notch sensitivity q is defined by the equation

$$q = \frac{K_f - 1}{K_t - 1} \quad \text{or} \quad q_{\text{shear}} = \frac{K_{fs} - 1}{K_{ts} - 1} \quad (6-31)$$

where q is usually between zero and unity. Equation (6-31) shows that if $q = 0$, then $K_f = 1$, and the material has no sensitivity to notches at all. On the other hand, if $q = 1$, then $K_f = K_t$, and the material has full notch sensitivity. In analysis or design work, find K_t first, from the geometry of the part. Then specify the material, find q , and solve for K_f from the equation

$$K_f = 1 + q(K_t - 1) \quad \text{or} \quad K_{fs} = 1 + q_{\text{shear}}(K_{ts} - 1) \quad (6-32)$$

Notch sensitivities for specific materials are obtained experimentally. Published experimental values are limited, but some values are available for steels and aluminum. Trends for notch sensitivity as a function of notch radius and ultimate strength are shown in Fig. 6-20 for reversed bending or axial loading, and Fig. 6-21 for reversed

Figure 6-20

Notch-sensitivity charts for steels and UNS A92024-T wrought aluminum alloys subjected to reversed bending or reversed axial loads. For larger notch radii, use the values of q corresponding to the $r = 0.16$ -in (4-mm) ordinate. (From George Sines and J. L. Waisman (eds.), Metal Fatigue, McGraw-Hill, New York. Copyright © 1969 by The McGraw-Hill Companies, Inc. Reprinted by permission.)

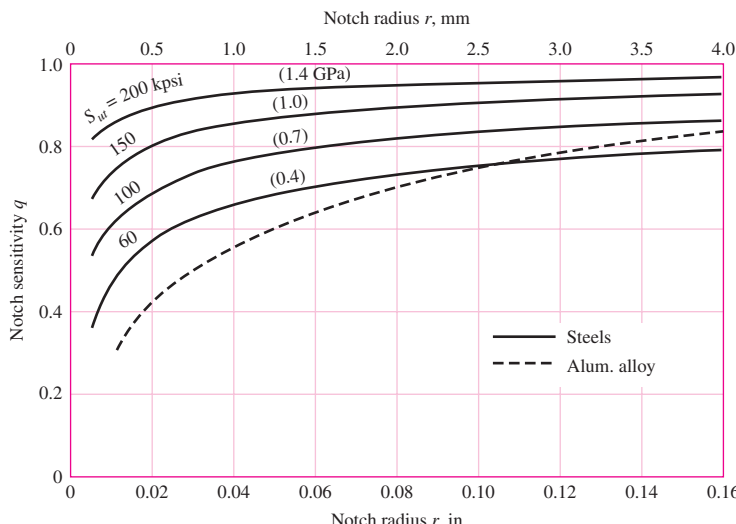
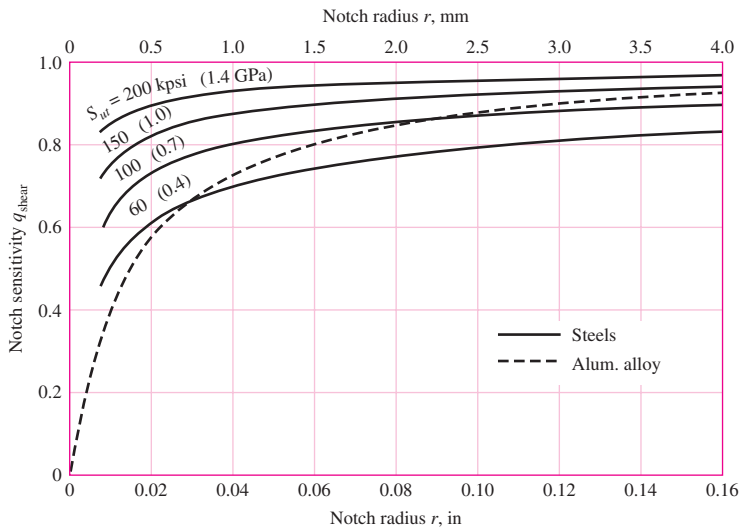


Figure 6-21

Notch-sensitivity curves for materials in reversed torsion. For larger notch radii, use the values of q_{shear} corresponding to $r = 0.16$ in (4 mm).



torsion. In using these charts it is well to know that the actual test results from which the curves were derived exhibit a large amount of scatter. Because of this scatter it is always safe to use $K_f = K_t$ if there is any doubt about the true value of q . Also, note that q is not far from unity for large notch radii.

Figure 6-20 has as its basis the *Neuber equation*, which is given by

$$K_f = 1 + \frac{K_t - 1}{1 + \sqrt{a}/r} \quad (6-33)$$

where \sqrt{a} is defined as the *Neuber constant* and is a material constant. Equating Eqs. (6-31) and (6-33) yields the notch sensitivity equation

$$q = \frac{1}{1 + \frac{\sqrt{a}}{\sqrt{r}}} \quad (6-34)$$

correlating with Figs. 6-20 and 6-21 as

$$\text{Bending or axial: } \sqrt{a} = 0.246 - 3.08(10^{-3})S_{ut} + 1.51(10^{-5})S_{ut}^2 - 2.67(10^{-8})S_{ut}^3 \quad (6-35a)$$

$$\text{Torsion: } \sqrt{a} = 0.190 - 2.51(10^{-3})S_{ut} + 1.35(10^{-5})S_{ut}^2 - 2.67(10^{-8})S_{ut}^3 \quad (6-35b)$$

where the equations apply to steel and S_{ut} is in ksi. Equation (6-34) used in conjunction with Eq. pair (6-35) is equivalent to Figs. (6-20) and (6-21). As with the graphs, the results from the curve fit equations provide only approximations to the experimental data.

The notch sensitivity of cast irons is very low, varying from 0 to about 0.20, depending upon the tensile strength. To be on the conservative side, it is recommended that the value $q = 0.20$ be used for all grades of cast iron.

EXAMPLE 6-6

A steel shaft in bending has an ultimate strength of 690 MPa and a shoulder with a fillet radius of 3 mm connecting a 32-mm diameter with a 38-mm diameter. Estimate K_f using:

- Figure 6-20.
- Equations (6-33) and (6-35).

Solution From Fig. A-15-9, using $D/d = 38/32 = 1.1875$, $r/d = 3/32 = 0.09375$, we read the graph to find $K_t \doteq 1.65$.
 (a) From Fig. 6-20, for $S_{ut} = 690$ MPa and $r = 3$ mm, $q \doteq 0.84$. Thus, from Eq. (6-32)

Answer

$$K_f = 1 + q(K_t - 1) \doteq 1 + 0.84(1.65 - 1) = 1.55$$

(b) From Eq. (6-35a) with $S_{ut} = 690$ MPa = 100 kpsi, $\sqrt{a} = 0.0622\sqrt{\text{in}} = 0.313\sqrt{\text{mm}}$. Substituting this into Eq. (6-33) with $r = 3$ mm gives

Answer

$$K_f = 1 + \frac{K_t - 1}{1 + \sqrt{a/r}} \doteq 1 + \frac{1.65 - 1}{1 + \frac{0.313}{\sqrt{3}}} = 1.55$$

Some designers use $1/K_f$ as a Marin factor to reduce S_e . For simple loading, infinite life problems, it makes no difference whether S_e is reduced by dividing it by K_f or the nominal stress is multiplied by K_f . However, for *finite life*, since the *S-N* diagram is nonlinear, the two approaches yield differing results. There is no clear evidence pointing to which method is better. Furthermore, in Sec. 6-14, when we consider combining loads, there generally are multiple fatigue stress-concentration factors occurring at a point (e.g. K_f for bending and K_{fs} for torsion). Here, it is only practical to modify the nominal stresses. To be consistent in this text, we will exclusively use the fatigue stress-concentration factor as a multiplier of the nominal stress.

EXAMPLE 6-7

For the step-shaft of Ex. 6-6, it is determined that the fully corrected endurance limit is $S_e = 280$ MPa. Consider the shaft undergoes a fully reversing nominal stress in the fillet of $(\sigma_{rev})_{nom} = 260$ MPa. Estimate the number of cycles to failure.

Solution

From Ex. 6-6, $K_f = 1.55$, and the ultimate strength is $S_{ut} = 690$ MPa = 100 kpsi. The maximum reversing stress is

$$(\sigma_{rev})_{max} = K_f(\sigma_{rev})_{nom} = 1.55(260) = 403 \text{ MPa}$$

From Fig. 6-18, $f = 0.845$. From Eqs. (6-14), (6-15), and (6-16)

$$a = \frac{(f S_{ut})^2}{S_e} = \frac{[0.845(690)]^2}{280} = 1214 \text{ MPa}$$

$$b = -\frac{1}{3} \log \frac{f S_{ut}}{S_e} = -\frac{1}{3} \log \left[\frac{0.845(690)}{280} \right] = -0.1062$$

Answer

$$N = \left(\frac{\sigma_{rev}}{a} \right)^{1/b} = \left(\frac{403}{1214} \right)^{1/-0.1062} = 32.3(10^3) \text{ cycles}$$

Up to this point, examples illustrated each factor in Marin's equation and stress concentrations alone. Let us consider a number of factors occurring simultaneously.

EXAMPLE 6-8

A 1015 hot-rolled steel bar has been machined to a diameter of 1 in. It is to be placed in reversed axial loading for 70 000 cycles to failure in an operating environment of 550°F. Using ASTM minimum properties, and a reliability of 99 percent, estimate the endurance limit and fatigue strength at 70 000 cycles.

Solution

From Table A-20, $S_{ut} = 50$ kpsi at 70°F. Since the rotating-beam specimen endurance limit is not known at room temperature, we determine the ultimate strength at the elevated temperature first, using Table 6-4. From Table 6-4,

$$\left(\frac{S_T}{S_{RT}} \right)_{550^\circ} = \frac{0.995 + 0.963}{2} = 0.979$$

The ultimate strength at 550°F is then

$$(S_{ut})_{550^\circ} = (S_T/S_{RT})_{550^\circ} (S_{ut})_{70^\circ} = 0.979(50) = 49.0 \text{ kpsi}$$

The rotating-beam specimen endurance limit at 550°F is then estimated from Eq. (6-8) as

$$S'_e = 0.5(49) = 24.5 \text{ kpsi}$$

Next, we determine the Marin factors. For the machined surface, Eq. (6-19) with Table 6-2 gives

$$k_a = a S_{ut}^b = 2.70(49^{-0.265}) = 0.963$$

For axial loading, from Eq. (6-21), the size factor $k_b = 1$, and from Eq. (6-26) the loading factor is $k_c = 0.85$. The temperature factor $k_d = 1$, since we accounted for the temperature in modifying the ultimate strength and consequently the endurance limit. For 99 percent reliability, from Table 6-5, $k_e = 0.814$. Finally, since no other conditions were given, the miscellaneous factor is $k_f = 1$. The endurance limit for the part is estimated by Eq. (6-18) as

$$\begin{aligned} S_e &= k_a k_b k_c k_d k_e k_f S'_e \\ &= 0.963(1)(0.85)(1)(0.814)(1)24.5 = 16.3 \text{ kpsi} \end{aligned}$$

Answer

For the fatigue strength at 70 000 cycles we need to construct the $S-N$ equation. From p. 285, since $S_{ut} = 49 < 70$ kpsi, then $f = 0.9$. From Eq. (6-14)

$$a = \frac{(f S_{ut})^2}{S_e} = \frac{[0.9(49)]^2}{16.3} = 119.3 \text{ kpsi}$$

and Eq. (6-15)

$$b = -\frac{1}{3} \log \left(\frac{f S_{ut}}{S_e} \right) = -\frac{1}{3} \log \left[\frac{0.9(49)}{16.3} \right] = -0.1441$$

Finally, for the fatigue strength at 70 000 cycles, Eq. (6-13) gives

Answer

$$S_f = a N^b = 119.3(70\,000)^{-0.1441} = 23.9 \text{ kpsi}$$

EXAMPLE 6-9

Figure 6-22a shows a rotating shaft simply supported in ball bearings at *A* and *D* and loaded by a nonrotating force *F* of 6.8 kN. Using ASTM “minimum” strengths, estimate the life of the part.

Solution

From Fig. 6-22b we learn that failure will probably occur at *B* rather than at *C* or at the point of maximum moment. Point *B* has a smaller cross section, a higher bending moment, and a higher stress-concentration factor than *C*, and the location of maximum moment has a larger size and no stress-concentration factor.

We shall solve the problem by first estimating the strength at point *B*, since the strength will be different elsewhere, and comparing this strength with the stress at the same point.

From Table A-20 we find $S_{ut} = 690$ MPa and $S_y = 580$ MPa. The endurance limit S'_e is estimated as

$$S'_e = 0.5(690) = 345 \text{ MPa}$$

From Eq. (6-19) and Table 6-2,

$$k_a = 4.51(690)^{-0.265} = 0.798$$

From Eq. (6-20),

$$k_b = (32/7.62)^{-0.107} = 0.858$$

Since $k_c = k_d = k_e = k_f = 1$,

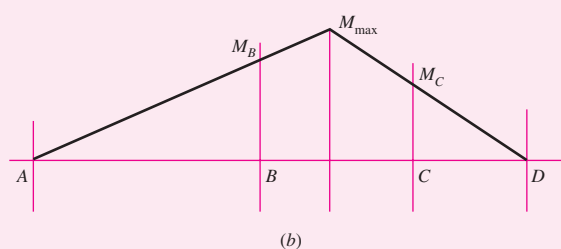
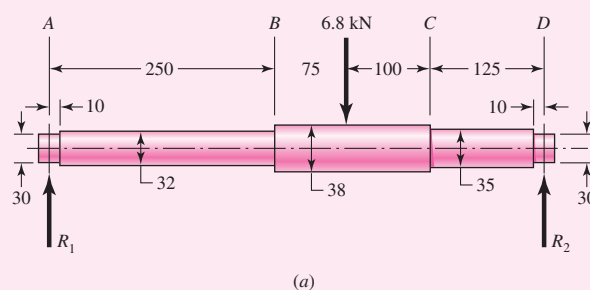
$$S_e = 0.798(0.858)345 = 236 \text{ MPa}$$

To find the geometric stress-concentration factor K_t we enter Fig. A-15-9 with $D/d = 38/32 = 1.1875$ and $r/d = 3/32 = 0.09375$ and read $K_t \doteq 1.65$. Substituting $S_{ut} = 690/6.89 = 100$ ksi into Eq. (6-35a) yields $\sqrt{a} = 0.0622 \sqrt{\text{in}} = 0.313 \sqrt{\text{mm}}$. Substituting this into Eq. (6-33) gives

$$K_f = 1 + \frac{K_t - 1}{1 + \sqrt{a/r}} = 1 + \frac{1.65 - 1}{1 + 0.313/\sqrt{3}} = 1.55$$

Figure 6-22

(a) Shaft drawing showing all dimensions in millimeters; all fillets 3-mm radius. The shaft rotates and the load is stationary; material is machined from AISI 1050 cold-drawn steel. (b) Bending-moment diagram.



The next step is to estimate the bending stress at point *B*. The bending moment is

$$M_B = R_1 x = \frac{225F}{550} 250 = \frac{225(6.8)}{550} 250 = 695.5 \text{ N} \cdot \text{m}$$

Just to the left of *B* the section modulus is $I/c = \pi d^3/32 = \pi 32^3/32 = 3.217 (10^3) \text{ mm}^3$. The reversing bending stress is, assuming infinite life,

$$\sigma_{\text{rev}} = K_f \frac{M_B}{I/c} = 1.55 \frac{695.5}{3.217} (10)^{-6} = 335.1(10^6) \text{ Pa} = 335.1 \text{ MPa}$$

This stress is greater than S_e and less than S_y . This means we have both finite life and no yielding on the first cycle.

For finite life, we will need to use Eq. (6–16). The ultimate strength, $S_{ut} = 690 \text{ MPa} = 100 \text{ ksi}$. From Fig. 6–18, $f = 0.844$. From Eq. (6–14)

$$a = \frac{(f S_{ut})^2}{S_e} = \frac{[0.844(690)]^2}{236} = 1437 \text{ MPa}$$

and from Eq. (6–15)

$$b = -\frac{1}{3} \log \left(\frac{f S_{ut}}{S_e} \right) = -\frac{1}{3} \log \left[\frac{0.844(690)}{236} \right] = -0.1308$$

From Eq. (6–16),

Answer

$$N = \left(\frac{\sigma_{\text{rev}}}{a} \right)^{1/b} = \left(\frac{335.1}{1437} \right)^{-1/0.1308} = 68(10^3) \text{ cycles}$$

6-11

Characterizing Fluctuating Stresses

Fluctuating stresses in machinery often take the form of a sinusoidal pattern because of the nature of some rotating machinery. However, other patterns, some quite irregular, do occur. It has been found that in periodic patterns exhibiting a single maximum and a single minimum of force, the shape of the wave is not important, but the peaks on both the high side (maximum) and the low side (minimum) are important. Thus F_{\max} and F_{\min} in a cycle of force can be used to characterize the force pattern. It is also true that ranging above and below some baseline can be equally effective in characterizing the force pattern. If the largest force is F_{\max} and the smallest force is F_{\min} , then a steady component and an alternating component can be constructed as follows:

$$F_m = \frac{F_{\max} + F_{\min}}{2} \quad F_a = \left| \frac{F_{\max} - F_{\min}}{2} \right|$$

where F_m is the midrange steady component of force, and F_a is the amplitude of the alternating component of force.

Figure 6–23

Some stress-time relations:
 (a) fluctuating stress with high-frequency ripple; (b and c) nonsinusoidal fluctuating stress; (d) sinusoidal fluctuating stress; (e) repeated stress; (f) completely reversed sinusoidal stress.

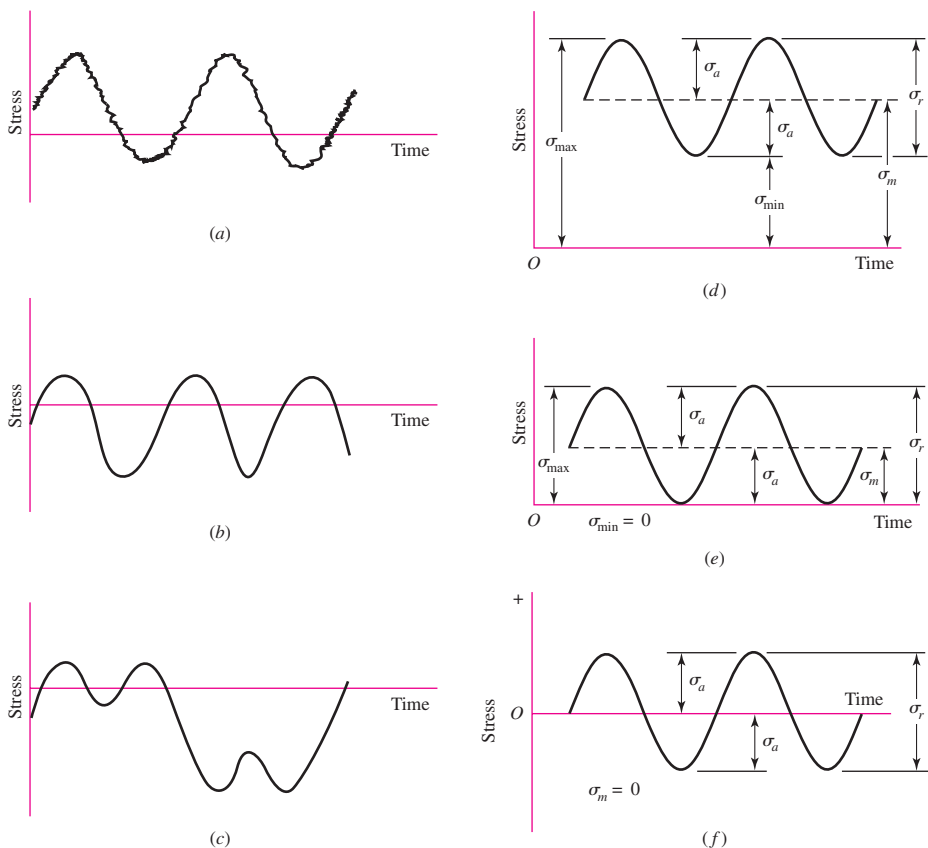


Figure 6–23 illustrates some of the various stress-time traces that occur. The components of stress, some of which are shown in Fig. 6–23d, are

$$\sigma_{min} = \text{minimum stress}$$

$$\sigma_m = \text{midrange component}$$

$$\sigma_{max} = \text{maximum stress}$$

$$\sigma_r = \text{range of stress}$$

$$\sigma_a = \text{amplitude component}$$

$$\sigma_s = \text{static or steady stress}$$

The steady, or static, stress is *not* the same as the midrange stress; in fact, it may have any value between σ_{min} and σ_{max} . The steady stress exists because of a fixed load or preload applied to the part, and it is usually independent of the varying portion of the load. A helical compression spring, for example, is always loaded into a space shorter than the free length of the spring. The stress created by this initial compression is called the steady, or static, component of the stress. It is not the same as the midrange stress.

We shall have occasion to apply the subscripts of these components to shear stresses as well as normal stresses.

The following relations are evident from Fig. 6–23:

$$\sigma_m = \frac{\sigma_{max} + \sigma_{min}}{2} \quad (6-36)$$

$$\sigma_a = \left| \frac{\sigma_{max} - \sigma_{min}}{2} \right|$$

In addition to Eq. (6–36), the *stress ratio*

$$R = \frac{\sigma_{\min}}{\sigma_{\max}} \quad (6-37)$$

and the *amplitude ratio*

$$A = \frac{\sigma_a}{\sigma_m} \quad (6-38)$$

are also defined and used in connection with fluctuating stresses.

Equations (6–36) utilize symbols σ_a and σ_m as the stress components at the location under scrutiny. This means, in the absence of a notch, σ_a and σ_m are equal to the nominal stresses σ_{ao} and σ_{mo} induced by loads F_a and F_m , respectively; in the presence of a notch they are $K_f\sigma_{ao}$ and $K_f\sigma_{mo}$, respectively, as long as the material remains without plastic strain. In other words, the fatigue stress-concentration factor K_f is applied to *both* components.

When the steady stress component is high enough to induce localized notch yielding, the designer has a problem. The first-cycle local yielding produces plastic strain and strain-strengthening. This is occurring at the location where fatigue crack nucleation and growth are most likely. The material properties (S_y and S_{ut}) are new and difficult to quantify. The prudent engineer controls the concept, material and condition of use, and geometry so that no plastic strain occurs. There are discussions concerning possible ways of quantifying what is occurring under localized and general yielding in the presence of a notch, referred to as the *nominal mean stress* method, *residual stress* method, and the like.²⁰ The nominal mean stress method (set $\sigma_a = K_f\sigma_{ao}$ and $\sigma_m = \sigma_{mo}$) gives roughly comparable results to the residual stress method, but both are *approximations*.

There is the method of Dowling²¹ for ductile materials, which, for materials with a pronounced yield point and approximated by an elastic–perfectly plastic behavior model, quantitatively expresses the steady stress component stress-concentration factor K_{fm} as

$$\begin{aligned} K_{fm} &= K_f & K_f |\sigma_{\max,o}| < S_y \\ K_{fm} &= \frac{S_y - K_f \sigma_{ao}}{|\sigma_{mo}|} & K_f |\sigma_{\max,o}| > S_y \\ K_{fm} &= 0 & K_f |\sigma_{\max,o} - \sigma_{\min,o}| > 2S_y \end{aligned} \quad (6-39)$$

For the purposes of this book, for ductile materials in fatigue,

- Avoid localized plastic strain at a notch. Set $\sigma_a = K_f\sigma_{ao}$ and $\sigma_m = K_f\sigma_{mo}$.
- When plastic strain at a notch cannot be avoided, use Eqs. (6–39); or conservatively, set $\sigma_a = K_f\sigma_{ao}$ and use $K_{fm} = 1$, that is, $\sigma_m = \sigma_{mo}$.

²⁰R. C. Juvinall, *Stress, Strain, and Strength*, McGraw-Hill, New York, 1967, articles 14.9–14.12; R. C. Juvinall and K. M. Marshek, *Fundamentals of Machine Component Design*, 4th ed., Wiley, New York, 2006, Sec. 8.11; M. E. Dowling, *Mechanical Behavior of Materials*, 2nd ed., Prentice Hall, Englewood Cliffs, N.J., 1999, Secs. 10.3–10.5.

²¹Dowling, op. cit., pp. 437–438.

6-12 Fatigue Failure Criteria for Fluctuating Stress

Now that we have defined the various components of stress associated with a part subjected to fluctuating stress, we want to vary both the midrange stress and the stress amplitude, or alternating component, to learn something about the fatigue resistance of parts when subjected to such situations. Three methods of plotting the results of such tests are in general use and are shown in Figs. 6-24, 6-25, and 6-26.

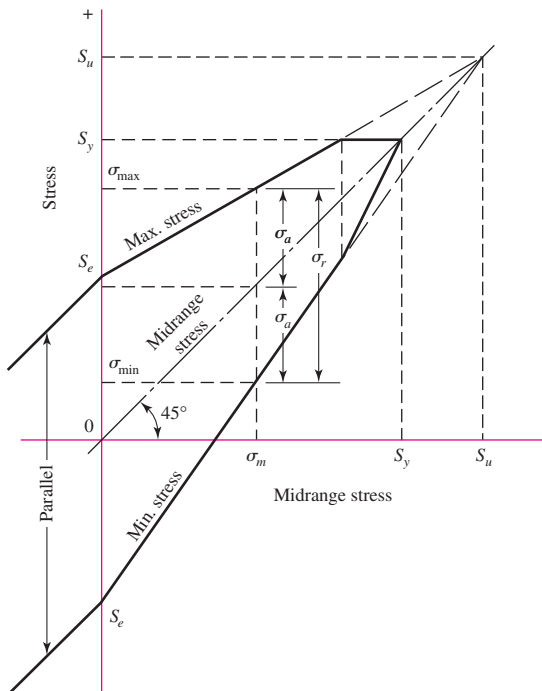
The *modified Goodman diagram* of Fig. 6-24 has the midrange stress plotted along the abscissa and all other components of stress plotted on the ordinate, with tension in the positive direction. The endurance limit, fatigue strength, or finite-life strength, whichever applies, is plotted on the ordinate above and below the origin. The midrange-stress line is a 45° line from the origin to the tensile strength of the part. The modified Goodman diagram consists of the lines constructed to S_e (or S_f) above and below the origin. Note that the yield strength is also plotted on both axes, because yielding would be the criterion of failure if σ_{\max} exceeded S_y .

Another way to display test results is shown in Fig. 6-25. Here the abscissa represents the ratio of the midrange strength S_m to the ultimate strength, with tension plotted to the right and compression to the left. The ordinate is the ratio of the alternating strength to the endurance limit. The line BC then represents the modified Goodman criterion of failure. Note that the existence of midrange stress in the compressive region has little effect on the endurance limit.

The very clever diagram of Fig. 6-26 is unique in that it displays four of the stress components as well as the two stress ratios. A curve representing the endurance limit for values of R beginning at $R = -1$ and ending with $R = 1$ begins at S_e on the σ_a axis and ends at S_{ut} on the σ_m axis. Constant-life curves for $N = 10^5$ and $N = 10^4$ cycles

Figure 6-24

Modified Goodman diagram showing all the strengths and the limiting values of all the stress components for a particular midrange stress.



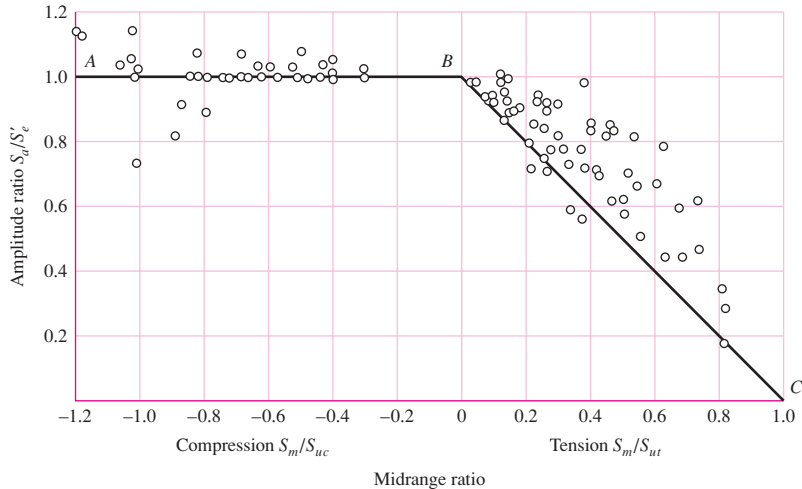
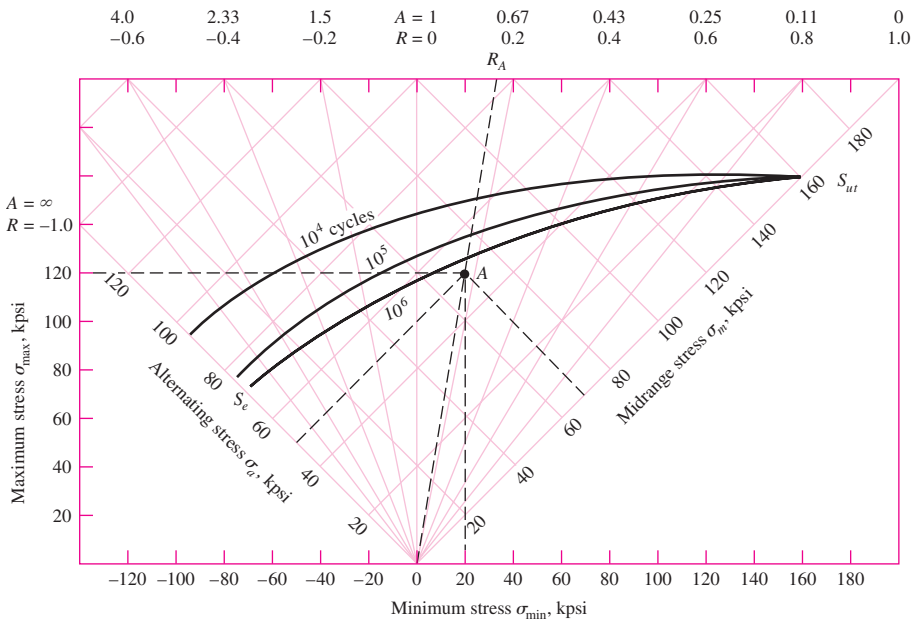


Figure 6-25

Plot of fatigue failures for midrange stresses in both tensile and compressive regions. Normalizing the data by using the ratio of steady strength component to tensile strength S_m/S_{ut} , steady strength component to compressive strength S_m/S_{uc} and strength amplitude component to endurance limit S_a/S'_e enables a plot of experimental results for a variety of steels. [Data source: Thomas J. Dolan, "Stress Range," Sec. 6.2 in O. J. Horger (ed.), ASME Handbook—Metals Engineering Design, McGraw-Hill, New York, 1953.]

Figure 6-26

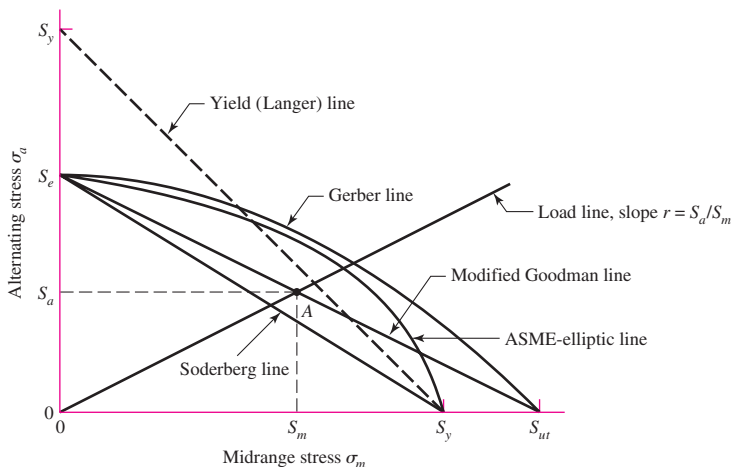
Master fatigue diagram created for AISI 4340 steel having $S_{ut} = 158$ and $S_y = 147$ kpsi. The stress components at A are $\sigma_{\min} = 20$, $\sigma_{\max} = 120$, $\sigma_m = 70$, and $\sigma_a = 50$, all in kpsi. (Source: H. J. Grover, Fatigue of Aircraft Structures, U.S. Government Printing Office, Washington, D.C., 1966, pp. 317, 322. See also J. A. Collins, Failure of Materials in Mechanical Design, Wiley, New York, 1981, p. 216.)



have been drawn too. Any stress state, such as the one at A, can be described by the minimum and maximum components, or by the midrange and alternating components. And safety is indicated whenever the point described by the stress components lies below the constant-life line.

Figure 6–27

Fatigue diagram showing various criteria of failure. For each criterion, points on or “above” the respective line indicate failure. Some point A on the Goodman line, for example, gives the strength S_m as the limiting value of σ_m corresponding to the strength S_a , which, paired with σ_m , is the limiting value of σ_a .



When the midrange stress is compression, failure occurs whenever $\sigma_a = S_e$ or whenever $\sigma_{\max} = S_{yc}$, as indicated by the left-hand side of Fig. 6–25. Neither a fatigue diagram nor any other failure criteria need be developed.

In Fig. 6–27, the tensile side of Fig. 6–25 has been redrawn in terms of strengths, instead of strength ratios, with the same modified Goodman criterion together with four additional criteria of failure. Such diagrams are often constructed for analysis and design purposes; they are easy to use and the results can be scaled off directly.

The early viewpoint expressed on a σ_m , σ_a diagram was that there existed a locus which divided safe from unsafe combinations of σ_m and σ_a . Ensuing proposals included the parabola of Gerber (1874), the Goodman (1890)²² (straight) line, and the Soderberg (1930) (straight) line. As more data were generated it became clear that a fatigue criterion, rather than being a “fence,” was more like a zone or band wherein the probability of failure could be estimated. We include the failure criterion of Goodman because

- It is a straight line and the algebra is linear and easy.
- It is easily graphed, every time for every problem.
- It reveals subtleties of insight into fatigue problems.
- Answers can be scaled from the diagrams as a check on the algebra.

We also caution that it is deterministic and the phenomenon is not. It is biased and we cannot quantify the bias. It is not conservative. It is a stepping-stone to understanding; it is history; and to read the work of other engineers and to have meaningful oral exchanges with them, it is necessary that you understand the Goodman approach should it arise.

Either the fatigue limit S_e or the finite-life strength S_f is plotted on the ordinate of Fig. 6–27. These values will have already been corrected using the Marin factors of Eq. (6–18). Note that the yield strength S_y is plotted on the ordinate too. This serves as a reminder that first-cycle yielding rather than fatigue might be the criterion of failure.

The midrange-stress axis of Fig. 6–27 has the yield strength S_y and the tensile strength S_{ut} plotted along it.

²²It is difficult to date Goodman's work because it went through several modifications and was never published.

Five criteria of failure are diagrammed in Fig. 6–27: the Soderberg, the modified Goodman, the Gerber, the ASME-elliptic, and yielding. The diagram shows that only the Soderberg criterion guards against any yielding, but is biased low.

Considering the modified Goodman line as a criterion, point A represents a limiting point with an alternating strength S_a and midrange strength S_m . The slope of the load line shown is defined as $r = S_a/S_m$.

The criterion equation for the Soderberg line is

$$\frac{S_a}{S_e} + \frac{S_m}{S_y} = 1 \quad (6-40)$$

Similarly, we find the modified Goodman relation to be

$$\frac{S_a}{S_e} + \frac{S_m}{S_{ut}} = 1 \quad (6-41)$$

Examination of Fig. 6–25 shows that both a parabola and an ellipse have a better opportunity to pass among the midrange tension data and to permit quantification of the probability of failure. The Gerber failure criterion is written as

$$\frac{S_a}{S_e} + \left(\frac{S_m}{S_{ut}} \right)^2 = 1 \quad (6-42)$$

and the ASME-elliptic is written as

$$\left(\frac{S_a}{S_e} \right)^2 + \left(\frac{S_m}{S_y} \right)^2 = 1 \quad (6-43)$$

The *Langer* first-cycle-yielding criterion is used in connection with the fatigue curve:

$$S_a + S_m = S_y \quad (6-44)$$

The stresses $n\sigma_a$ and $n\sigma_m$ can replace S_a and S_m , where n is the design factor or factor of safety. Then, Eq. (6–40), the Soderberg line, becomes

$$\text{Soderberg} \quad \frac{\sigma_a}{S_e} + \frac{\sigma_m}{S_y} = \frac{1}{n} \quad (6-45)$$

Equation (6–41), the modified Goodman line, becomes

$$\text{mod-Goodman} \quad \frac{\sigma_a}{S_e} + \frac{\sigma_m}{S_{ut}} = \frac{1}{n} \quad (6-46)$$

Equation (6–42), the Gerber line, becomes

$$\text{Gerber} \quad \frac{n\sigma_a}{S_e} + \left(\frac{n\sigma_m}{S_{ut}} \right)^2 = 1 \quad (6-47)$$

Equation (6–43), the ASME-elliptic line, becomes

$$\text{ASME-elliptic} \quad \left(\frac{n\sigma_a}{S_e} \right)^2 + \left(\frac{n\sigma_m}{S_y} \right)^2 = 1 \quad (6-48)$$

We will emphasize the Gerber and ASME-elliptic for fatigue failure criterion and the Langer for first-cycle yielding. However, conservative designers often use the modified Goodman criterion, so we will continue to include it in our discussions. The design equation for the Langer first-cycle-yielding is

$$\text{Langer static yield} \quad \sigma_a + \sigma_m = \frac{S_y}{n} \quad (6-49)$$

The failure criteria are used in conjunction with a load line, $r = S_a/S_m = \sigma_a/\sigma_m$. Principal intersections are tabulated in Tables 6–6 to 6–8. Formal expressions for fatigue factor of safety are given in the lower panel of Tables 6–6 to 6–8. The first row of each table corresponds to the fatigue criterion, the second row is the static Langer criterion, and the third row corresponds to the intersection of the static and fatigue

Table 6–6

Amplitude and Steady Coordinates of Strength and Important Intersections in First Quadrant for Modified Goodman and Langer Failure Criteria

Intersecting Equations	Intersection Coordinates
$\frac{S_a}{S_e} + \frac{S_m}{S_{ut}} = 1$	$S_a = \frac{r S_e S_{ut}}{r S_{ut} + S_e}$
Load line $r = \frac{S_a}{S_m}$	$S_m = \frac{S_a}{r}$
$\frac{S_a}{S_y} + \frac{S_m}{S_y} = 1$	$S_a = \frac{r S_y}{1+r}$
Load line $r = \frac{S_a}{S_m}$	$S_m = \frac{S_y}{1+r}$
$\frac{S_a}{S_e} + \frac{S_m}{S_{ut}} = 1$	$S_m = \frac{(S_y - S_e) S_{ut}}{S_{ut} - S_e}$
$\frac{S_a}{S_y} + \frac{S_m}{S_y} = 1$	$S_a = S_y - S_m, r_{crit} = S_a/S_m$

Fatigue factor of safety

$$n_f = \frac{1}{\frac{\sigma_a}{S_e} + \frac{\sigma_m}{S_{ut}}}$$

Table 6–7

Amplitude and Steady Coordinates of Strength and Important Intersections in First Quadrant for Gerber and Langer Failure Criteria

Intersecting Equations	Intersection Coordinates
$\frac{S_a}{S_e} + \left(\frac{S_m}{S_{ut}}\right)^2 = 1$	$S_a = \frac{r^2 S_{ut}^2}{2S_e} \left[-1 + \sqrt{1 + \left(\frac{2S_e}{rS_{ut}}\right)^2} \right]$
Load line $r = \frac{S_a}{S_m}$	$S_m = \frac{S_a}{r}$
$\frac{S_a}{S_y} + \frac{S_m}{S_y} = 1$	$S_a = \frac{r S_y}{1+r}$
Load line $r = \frac{S_a}{S_m}$	$S_m = \frac{S_y}{1+r}$
$\frac{S_a}{S_e} + \left(\frac{S_m}{S_{ut}}\right)^2 = 1$	$S_m = \frac{S_{ut}^2}{2S_e} \left[1 - \sqrt{1 + \left(\frac{2S_e}{S_{ut}}\right)^2 \left(1 - \frac{S_y}{S_e}\right)} \right]$
$\frac{S_a}{S_y} + \frac{S_m}{S_y} = 1$	$S_a = S_y - S_m, r_{crit} = S_a/S_m$

Fatigue factor of safety

$$n_f = \frac{1}{2} \left(\frac{S_{ut}}{\sigma_m} \right)^2 \frac{\sigma_a}{S_e} \left[-1 + \sqrt{1 + \left(\frac{2\sigma_m S_e}{S_{ut} \sigma_a} \right)^2} \right] \quad \sigma_m > 0$$

Table 6-8

	Intersecting Equations	Intersection Coordinates
Amplitude and Steady Coordinates of Strength and Important	$\left(\frac{S_a}{S_e}\right)^2 + \left(\frac{S_m}{S_y}\right)^2 = 1$	$S_a = \sqrt{\frac{r^2 S_e^2 S_y^2}{S_e^2 + r^2 S_y^2}}$
Intersections in First Quadrant for ASME-Elliptic and Langer Failure Criteria	Load line $r = S_a/S_m$	$S_m = \frac{S_a}{r}$
	$\frac{S_a}{S_y} + \frac{S_m}{S_y} = 1$	$S_a = \frac{r S_y}{1+r}$
	Load line $r = S_a/S_m$	$S_m = \frac{S_y}{1+r}$
	$\left(\frac{S_a}{S_e}\right)^2 + \left(\frac{S_m}{S_y}\right)^2 = 1$	$S_a = 0, \frac{2 S_y S_e^2}{S_e^2 + S_y^2}$
	$\frac{S_a}{S_y} + \frac{S_m}{S_y} = 1$	$S_m = S_y - S_a, r_{\text{crit}} = S_a/S_m$
Fatigue factor of safety	$n_f = \sqrt{\frac{1}{(\sigma_a/S_e)^2 + (\sigma_m/S_y)^2}}$	

criteria. The first column gives the intersecting equations and the second column the intersection coordinates.

There are two ways to proceed with a typical analysis. One method is to assume that fatigue occurs first and use one of Eqs. (6-45) to (6-48) to determine n or size, depending on the task. Most often fatigue is the governing failure mode. Then follow with a static check. If static failure governs then the analysis is repeated using Eq. (6-49).

Alternatively, one could use the tables. Determine the load line and establish which criterion the load line intersects first and use the corresponding equations in the tables.

Some examples will help solidify the ideas just discussed.

EXAMPLE 6-10

A 1.5-in-diameter bar has been machined from an AISI 1050 cold-drawn bar. This part is to withstand a fluctuating tensile load varying from 0 to 16 kip. Because of the ends, and the fillet radius, a fatigue stress-concentration factor K_f is 1.85 for 10^6 or larger life. Find S_a and S_m and the factor of safety guarding against fatigue and first-cycle yielding, using (a) the Gerber fatigue line and (b) the ASME-elliptic fatigue line.

Solution

We begin with some preliminaries. From Table A-20, $S_{ut} = 100$ ksi and $S_y = 84$ ksi. Note that $F_a = F_m = 8$ kip. The Marin factors are, deterministically,

$$k_a = 2.70(100)^{-0.265} = 0.797: \text{Eq. (6-19), Table 6-2, p. 288}$$

$k_b = 1$ (axial loading, see k_c)

$$k_c = 0.85: \text{Eq. (6-26), p. 290}$$

$$k_d = k_e = k_f = 1$$

$$S_e = 0.797(1)0.850(1)(1)0.5(100) = 33.9 \text{ kpsi: Eqs. (6-8), (6-18), p. 282, p. 287}$$

The nominal axial stress components σ_{ao} and σ_{mo} are

$$\sigma_{ao} = \frac{4F_a}{\pi d^2} = \frac{4(8)}{\pi 1.5^2} = 4.53 \text{ kpsi} \quad \sigma_{mo} = \frac{4F_m}{\pi d^2} = \frac{4(8)}{\pi 1.5^2} = 4.53 \text{ kpsi}$$

Applying K_f to both components σ_{ao} and σ_{mo} constitutes a prescription of no notch yielding:

$$\sigma_a = K_f \sigma_{ao} = 1.85(4.53) = 8.38 \text{ kpsi} = \sigma_m$$

(a) Let us calculate the factors of safety first. From the bottom panel from Table 6-7 the factor of safety for fatigue is

Answer

$$n_f = \frac{1}{2} \left(\frac{100}{8.38} \right)^2 \left(\frac{8.38}{33.9} \right) \left\{ -1 + \sqrt{1 + \left[\frac{2(8.38)33.9}{100(8.38)} \right]^2} \right\} = 3.66$$

From Eq. (6-49) the factor of safety guarding against first-cycle yield is

Answer

$$n_y = \frac{S_y}{\sigma_a + \sigma_m} = \frac{84}{8.38 + 8.38} = 5.01$$

Thus, we see that fatigue will occur first and the factor of safety is 3.68. This can be seen in Fig. 6-28 where the load line intersects the Gerber fatigue curve first at point *B*. If the plots are created to true scale it would be seen that $n_f = OB/OA$.

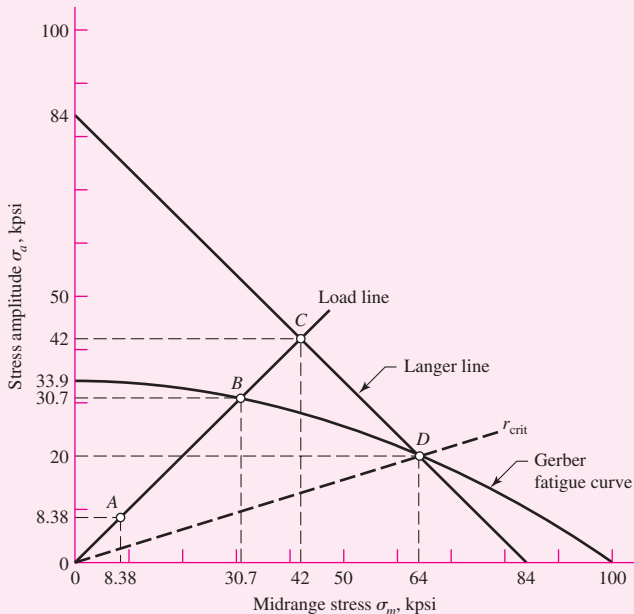
From the first panel of Table 6-7, $r = \sigma_a/\sigma_m = 1$,

Answer

$$S_a = \frac{(1)^2 100^2}{2(33.9)} \left\{ -1 + \sqrt{1 + \left[\frac{2(33.9)}{(1)100} \right]^2} \right\} = 30.7 \text{ kpsi}$$

Figure 6-28

Principal points *A*, *B*, *C*, and *D* on the designer's diagram drawn for Gerber, Langer, and load line.



Answer

$$S_m = \frac{S_a}{r} = \frac{30.7}{1} = 30.7 \text{ kpsi}$$

As a check on the previous result, $n_f = OB/OA = S_a/\sigma_a = S_m/\sigma_m = 30.7/8.38 = 3.66$ and we see total agreement.

We could have detected that fatigue failure would occur first without drawing Fig. 6-28 by calculating r_{crit} . From the third row third column panel of Table 6-7, the intersection point between fatigue and first-cycle yield is

$$S_m = \frac{100^2}{2(33.9)} \left[1 - \sqrt{1 + \left(\frac{2(33.9)}{100} \right)^2 \left(1 - \frac{84}{33.9} \right)} \right] = 64.0 \text{ kpsi}$$

$$S_a = S_y - S_m = 84 - 64 = 20 \text{ kpsi}$$

The critical slope is thus

$$r_{crit} = \frac{S_a}{S_m} = \frac{20}{64} = 0.312$$

which is less than the actual load line of $r = 1$. This indicates that fatigue occurs before first-cycle-yield.

(b) Repeating the same procedure for the ASME-elliptic line, for fatigue

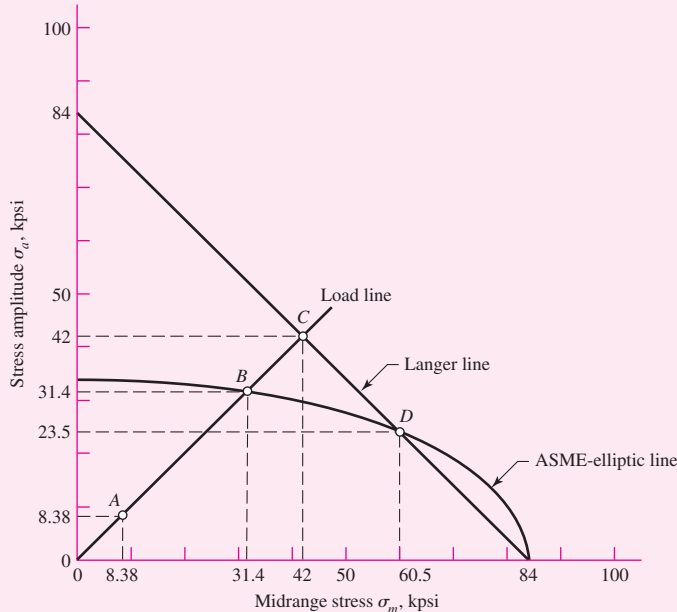
Answer

$$n_f = \sqrt{\frac{1}{(8.38/33.9)^2 + (8.38/84)^2}} = 3.75$$

Again, this is less than $n_y = 5.01$ and fatigue is predicted to occur first. From the first row second column panel of Table 6-8, with $r = 1$, we obtain the coordinates S_a and S_m of point B in Fig. 6-29 as

Figure 6-29

Principal points A , B , C , and D on the designer's diagram drawn for ASME-elliptic, Langer, and load lines.



Answer

$$S_a = \sqrt{\frac{(1)^2 33.9^2 (84)^2}{33.9^2 + (1)^2 84^2}} = 31.4 \text{ kpsi}, \quad S_m = \frac{S_a}{r} = \frac{31.4}{1} = 31.4 \text{ kpsi}$$

To verify the fatigue factor of safety, $n_f = S_a/\sigma_a = 31.4/8.38 = 3.75$.

As before, let us calculate r_{crit} . From the third row second column panel of Table 6–8,

$$S_a = \frac{2(84)33.9^2}{33.9^2 + 84^2} = 23.5 \text{ kpsi}, \quad S_m = S_y - S_a = 84 - 23.5 = 60.5 \text{ kpsi}$$

$$r_{\text{crit}} = \frac{S_a}{S_m} = \frac{23.5}{60.5} = 0.388$$

which again is less than $r = 1$, verifying that fatigue occurs first with $n_f = 3.75$.

The Gerber and the ASME-elliptic fatigue failure criteria are very close to each other and are used interchangeably. The ANSI/ASME Standard B106.1M–1985 uses ASME-elliptic for shafting.

EXAMPLE 6–11

A flat-leaf spring is used to retain an oscillating flat-faced follower in contact with a plate cam. The follower range of motion is 2 in and fixed, so the alternating component of force, bending moment, and stress is fixed, too. The spring is preloaded to adjust to various cam speeds. The preload must be increased to prevent follower float or jump. For lower speeds the preload should be decreased to obtain longer life of cam and follower surfaces. The spring is a steel cantilever 32 in long, 2 in wide, and $\frac{1}{4}$ in thick, as seen in Fig. 6–30a. The spring strengths are $S_{ut} = 150$ kpsi, $S_y = 127$ kpsi, and $S_e = 28$ kpsi fully corrected. The total cam motion is 2 in. The designer wishes to preload the spring by deflecting it 2 in for low speed and 5 in for high speed.

(a) Plot the Gerber-Langer failure lines with the load line.

(b) What are the strength factors of safety corresponding to 2 in and 5 in preload?

Solution

We begin with preliminaries. The second area moment of the cantilever cross section is

$$I = \frac{bh^3}{12} = \frac{2(0.25)^3}{12} = 0.00260 \text{ in}^4$$

Since, from Table A–9, beam 1, force F and deflection y in a cantilever are related by $F = 3EIy/l^3$, then stress σ and deflection y are related by

$$\sigma = \frac{Mc}{I} = \frac{32Fc}{I} = \frac{32(3EIy)c}{l^3 I} = \frac{96Ecy}{l^3} = Ky$$

$$\text{where } K = \frac{96Ec}{l^3} = \frac{96(30 \cdot 10^6)0.125}{32^3} = 10.99(10^3) \text{ psi/in} = 10.99 \text{ kpsi/in}$$

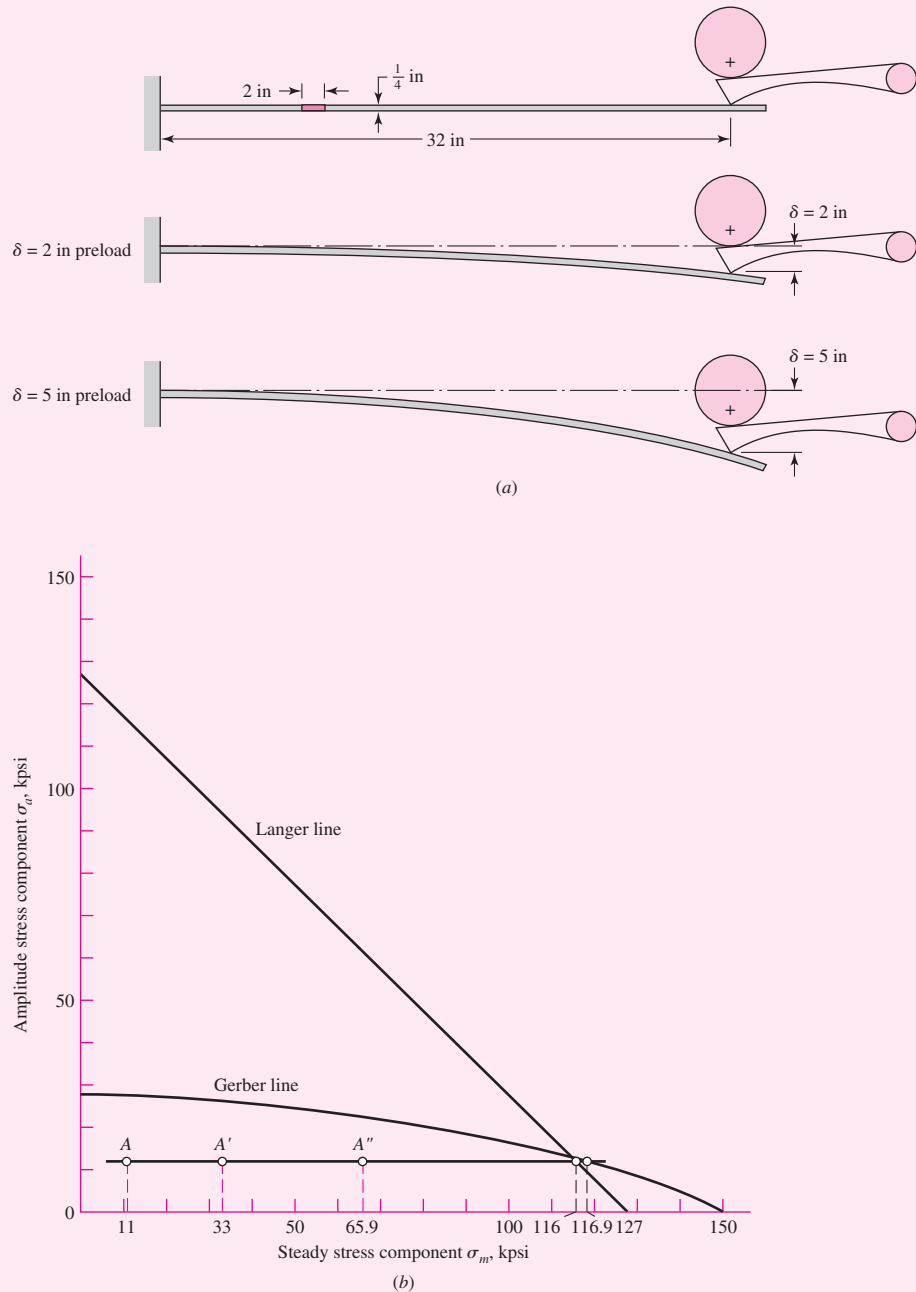
Now the minimums and maximums of y and σ can be defined by

$$y_{\min} = \delta \quad y_{\max} = 2 + \delta$$

$$\sigma_{\min} = K\delta \quad \sigma_{\max} = K(2 + \delta)$$

Figure 6-30

Cam follower retaining spring.
(a) Geometry; (b) designer's fatigue diagram for Ex. 6-11.



The stress components are thus

$$\sigma_a = \frac{K(2 + \delta) - K\delta}{2} = K = 10.99 \text{ kpsi}$$

$$\sigma_m = \frac{K(2 + \delta) + K\delta}{2} = K(1 + \delta) = 10.99(1 + \delta)$$

$$\text{For } \delta = 0, \quad \sigma_a = \sigma_m = 10.99 = 11 \text{ kpsi}$$

$$\text{For } \delta = 2 \text{ in}, \quad \sigma_a = 11 \text{ kpsi}, \quad \sigma_m = 10.99(1+2) = 33 \text{ kpsi}$$

$$\text{For } \delta = 5 \text{ in}, \quad \sigma_a = 11 \text{ kpsi}, \quad \sigma_m = 10.99(1+5) = 65.9 \text{ kpsi}$$

(a) A plot of the Gerber and Langer criteria is shown in Fig. 6–30b. The three preload deflections of 0, 2, and 5 in are shown as points A, A', and A''. Note that since σ_a is constant at 11 kpsi, the load line is horizontal and does not contain the origin. The intersection between the Gerber line and the load line is found from solving Eq. (6–42) for S_m and substituting 11 kpsi for S_a :

$$S_m = S_{ut} \sqrt{1 - \frac{S_a}{S_e}} = 150 \sqrt{1 - \frac{11}{28}} = 116.9 \text{ kpsi}$$

The intersection of the Langer line and the load line is found from solving Eq. (6–44) for S_m and substituting 11 kpsi for S_a :

$$S_m = S_y - S_a = 127 - 11 = 116 \text{ kpsi}$$

The threats from fatigue and first-cycle yielding are approximately equal.

(b) For $\delta = 2$ in,

Answer $n_f = \frac{S_m}{\sigma_m} = \frac{116.9}{33} = 3.54 \quad n_y = \frac{116}{33} = 3.52$

and for $\delta = 5$ in,

Answer $n_f = \frac{116.9}{65.9} = 1.77 \quad n_y = \frac{116}{65.9} = 1.76$

EXAMPLE 6-12

A steel bar undergoes cyclic loading such that $\sigma_{\max} = 60$ kpsi and $\sigma_{\min} = -20$ kpsi. For the material, $S_{ut} = 80$ kpsi, $S_y = 65$ kpsi, a fully corrected endurance limit of $S_e = 40$ kpsi, and $f = 0.9$. Estimate the number of cycles to a fatigue failure using:

- (a) Modified Goodman criterion.
- (b) Gerber criterion.

Solution From the given stresses,

$$\sigma_a = \frac{60 - (-20)}{2} = 40 \text{ kpsi} \quad \sigma_m = \frac{60 + (-20)}{2} = 20 \text{ kpsi}$$

(a) For the modified Goodman criterion, Eq. (6–46), the fatigue factor of safety based on infinite life is

$$n_f = \frac{1}{\frac{\sigma_a}{S_e} + \frac{\sigma_m}{S_{ut}}} = \frac{1}{\frac{40}{40} + \frac{20}{80}} = 0.8$$

This indicates a finite life is predicted. The $S-N$ diagram is only applicable for completely reversed stresses. To estimate the finite life for a fluctuating stress, we will obtain an equivalent completely reversed stress that is expected to be as damaging as the fluctuating stress. A commonly used approach is to assume that since the modified Goodman line represents all stress situations with a constant life of 10^6 cycles, other constant-life lines can be generated by passing a line through $(S_{ut}, 0)$ and a fluctuating stress point (σ_m, σ_a) . The point where this line intersects the σ_a axis represents a completely reversed stress (since at this point $\sigma_m = 0$), which predicts the same life as the fluctuating stress.

This completely reversed stress can be obtained by replacing S_e with σ_{rev} in Eq. (6-46) for the modified Goodman line resulting in

$$\sigma_{rev} = \frac{\sigma_a}{1 - \frac{\sigma_m}{S_{ut}}} = \frac{40}{1 - \frac{20}{80}} = 53.3 \text{ kpsi}$$

From the material properties, Eqs. (6-14) to (6-16), p. 285, give

$$a = \frac{(f S_{ut})^2}{S_e} = \frac{[0.9(80)]^2}{40} = 129.6 \text{ kpsi}$$

$$b = -\frac{1}{3} \log \left(\frac{f S_{ut}}{S_e} \right) = -\frac{1}{3} \log \left[\frac{0.9(80)}{40} \right] = -0.0851$$

$$N = \left(\frac{\sigma_{rev}}{a} \right)^{1/b} = \left(\frac{\sigma_{rev}}{129.6} \right)^{-1/0.0851} \quad (1)$$

Substituting σ_{rev} into Eq. (1) yields

Answer $N = \left(\frac{53.3}{129.6} \right)^{-1/0.0851} \doteq 3.4(10^4) \text{ cycles}$

(b) For Gerber, similar to part (a), from Eq. (6-47),

$$\sigma_{rev} = \frac{\sigma_a}{1 - \left(\frac{\sigma_m}{S_{ut}} \right)^2} = \frac{40}{1 - \left(\frac{20}{80} \right)^2} = 42.7 \text{ kpsi}$$

Again, from Eq. (1),

Answer $N = \left(\frac{42.7}{129.6} \right)^{-1/0.0851} \doteq 4.6(10^5) \text{ cycles}$

Comparing the answers, we see a large difference in the results. Again, the modified Goodman criterion is conservative as compared to Gerber for which the moderate difference in S_f is then magnified by a logarithmic S, N relationship.

For many *brittle* materials, the first quadrant fatigue failure criteria follows a concave upward Smith-Dolan locus represented by

$$\frac{S_a}{S_e} = \frac{1 - S_m/S_{ut}}{1 + S_m/S_{ut}} \quad (6-50)$$

or as a design equation,

$$\frac{n\sigma_a}{S_e} = \frac{1 - n\sigma_m/S_{ut}}{1 + n\sigma_m/S_{ut}} \quad (6-51)$$

For a radial load line of slope r , we substitute S_a/r for S_m in Eq. (6-50) and solve for S_a , obtaining the intersect

$$S_a = \frac{r S_{ut} + S_e}{2} \left[-1 + \sqrt{1 + \frac{4r S_{ut} S_e}{(r S_{ut} + S_e)^2}} \right] \quad (6-52)$$

The fatigue diagram for a brittle material differs markedly from that of a ductile material because:

- Yielding is not involved since the material may not have a yield strength.
- Characteristically, the compressive ultimate strength exceeds the ultimate tensile strength severalfold.

- First-quadrant fatigue failure locus is concave-upward (Smith-Dolan), for example, and as flat as Goodman. Brittle materials are more sensitive to midrange stress, being lowered, but compressive midrange stresses are beneficial.
- Not enough work has been done on brittle fatigue to discover insightful generalities, so we stay in the first and a bit of the second quadrant.

The most likely domain of designer use is in the range from $-S_{ut} \leq \sigma_m \leq S_{ut}$. The locus in the first quadrant is Goodman, Smith-Dolan, or something in between. The portion of the second quadrant that is used is represented by a straight line between the points $-S_{ut}$, S_{ut} and 0 , S_e , which has the equation

$$S_a = S_e + \left(\frac{S_e}{S_{ut}} - 1 \right) S_m \quad -S_{ut} \leq S_m \leq 0 \quad (\text{for cast iron}) \quad (6-53)$$

Table A-24 gives properties of gray cast iron. The endurance limit stated is really $k_a k_b S'_e$ and only corrections k_c , k_d , k_e , and k_f need be made. The average k_c for axial and torsional loading is 0.9.

EXAMPLE 6-13

A grade 30 gray cast iron is subjected to a load F applied to a 1 by $\frac{3}{8}$ -in cross-section link with a $\frac{1}{4}$ -in-diameter hole drilled in the center as depicted in Fig. 6-31a. The surfaces are machined. In the neighborhood of the hole, what is the factor of safety guarding against failure under the following conditions:

- The load $F = 1000$ lbf tensile, steady.
 - The load is 1000 lbf repeatedly applied.
 - The load fluctuates between -1000 lbf and 300 lbf without column action.
- Use the Smith-Dolan fatigue locus.

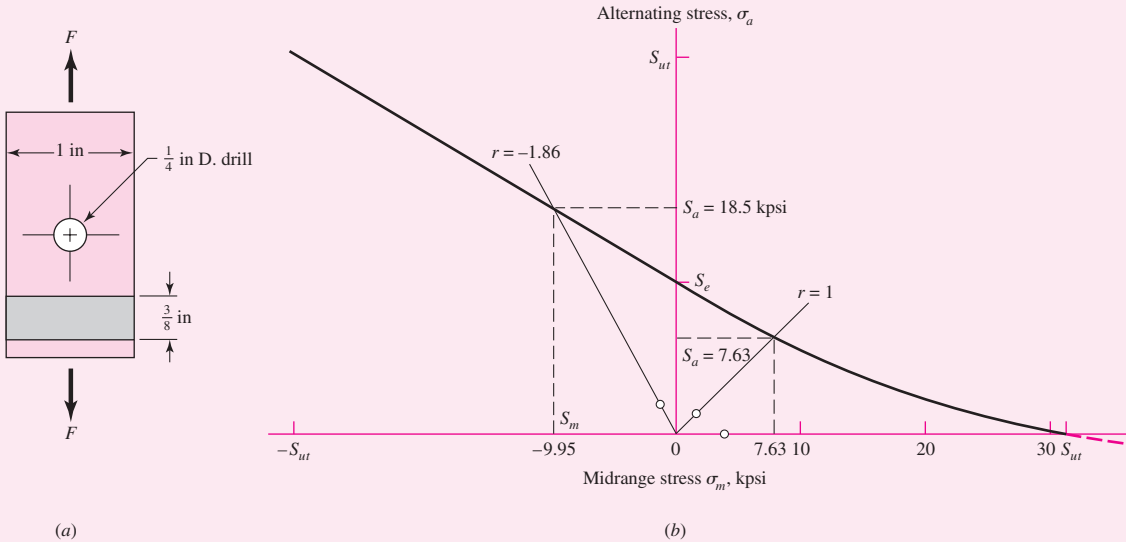


Figure 6-31

The grade 30 cast-iron part in axial fatigue with (a) its geometry displayed and (b) its designer's fatigue diagram for the circumstances of Ex. 6-13.

Solution

Some preparatory work is needed. From Table A-24, $S_{ut} = 31$ kpsi, $S_{uc} = 109$ kpsi, $k_a k_b S'_e = 14$ kpsi. Since k_c for axial loading is 0.9, then $S_e = (k_a k_b S'_e) k_c = 14(0.9) = 12.6$ kpsi. From Table A-15-1, $A = t(w - d) = 0.375(1 - 0.25) = 0.281 \text{ in}^2$, $d/w = 0.25/1 = 0.25$, and $K_t = 2.45$. The notch sensitivity for cast iron is 0.20 (see p. 296), so

$$K_f = 1 + q(K_t - 1) = 1 + 0.20(2.45 - 1) = 1.29$$

$$(a) \sigma_a = \frac{K_f F_a}{A} = \frac{1.29(0)}{0.281} = 0 \quad \sigma_m = \frac{K_f F_m}{A} = \frac{1.29(1000)}{0.281}(10^{-3}) = 4.59 \text{ kpsi}$$

and

Answer

$$n = \frac{S_{ut}}{\sigma_m} = \frac{31.0}{4.59} = 6.75$$

$$(b) F_a = F_m = \frac{F}{2} = \frac{1000}{2} = 500 \text{ lbf}$$

$$\sigma_a = \sigma_m = \frac{K_f F_a}{A} = \frac{1.29(500)}{0.281}(10^{-3}) = 2.30 \text{ kpsi}$$

$$r = \frac{\sigma_a}{\sigma_m} = 1$$

From Eq. (6-52),

$$S_a = \frac{(1)31 + 12.6}{2} \left[-1 + \sqrt{1 + \frac{4(1)31(12.6)}{[(1)31 + 12.6]^2}} \right] = 7.63 \text{ kpsi}$$

Answer

$$n = \frac{S_a}{\sigma_a} = \frac{7.63}{2.30} = 3.32$$

$$(c) F_a = \frac{1}{2}|300 - (-1000)| = 650 \text{ lbf} \quad \sigma_a = \frac{1.29(650)}{0.281}(10^{-3}) = 2.98 \text{ kpsi}$$

$$F_m = \frac{1}{2}[300 + (-1000)] = -350 \text{ lbf} \quad \sigma_m = \frac{1.29(-350)}{0.281}(10^{-3}) = -1.61 \text{ kpsi}$$

$$r = \frac{\sigma_a}{\sigma_m} = \frac{3.0}{-1.61} = -1.86$$

From Eq. (6-53), $S_a = S_e + (S_e/S_{ut} - 1)S_m$ and $S_m = S_a/r$. It follows that

$$S_a = \frac{S_e}{1 - \frac{1}{r} \left(\frac{S_e}{S_{ut}} - 1 \right)} = \frac{12.6}{1 - \frac{1}{-1.86} \left(\frac{12.6}{31} - 1 \right)} = 18.5 \text{ kpsi}$$

Answer

$$n = \frac{S_a}{\sigma_a} = \frac{18.5}{2.98} = 6.20$$

Figure 6-31b shows the portion of the designer's fatigue diagram that was constructed.

6-13 Torsional Fatigue Strength under Fluctuating Stresses

Extensive tests by Smith²³ provide some very interesting results on pulsating torsional fatigue. Smith's first result, based on 72 tests, shows that the existence of a torsional steady-stress component not more than the torsional yield strength has no effect on the torsional endurance limit, provided the material is *ductile, polished, notch-free, and cylindrical*.

Smith's second result applies to materials with stress concentration, notches, or surface imperfections. In this case, he finds that the torsional fatigue limit decreases monotonically with torsional steady stress. Since the great majority of parts will have surfaces that are less than perfect, this result indicates Gerber, ASME-elliptic, and other approximations are useful. Jorres of Associated Spring-Barnes Group, confirms Smith's results and recommends the use of the modified Goodman relation for pulsating torsion. In constructing the Goodman diagram, Jorres uses

$$S_{su} = 0.67 S_{ut} \quad (6-54)$$

Also, from Chap. 5, $S_{sy} = 0.577 S_{yt}$ from distortion-energy theory, and the mean load factor k_c is given by Eq. (6-26), or 0.577. This is discussed further in Chap. 10.

6-14 Combinations of Loading Modes

It may be helpful to think of fatigue problems as being in three categories:

- Completely reversing simple loads
- Fluctuating simple loads
- *Combinations of loading modes*

The simplest category is that of a completely reversed single stress which is handled with the *S-N* diagram, relating the alternating stress to a life. Only one type of loading is allowed here, and the midrange stress must be zero. The next category incorporates general fluctuating loads, using a criterion to relate midrange and alternating stresses (modified Goodman, Gerber, ASME-elliptic, or Soderberg). Again, only *one* type of loading is allowed at a time. The third category, which we will develop in this section, involves cases where there are combinations of different types of loading, such as combined bending, torsion, and axial.

In Sec. 6-9 we learned that a load factor k_c is used to obtain the endurance limit, and hence the result is dependent on whether the loading is axial, bending, or torsion. In this section we want to answer the question, "How do we proceed when the loading is a *mixture* of, say, axial, bending, and torsional loads?" This type of loading introduces a few complications in that there may now exist combined normal and shear stresses, each with alternating and midrange values, and several of the factors used in determining the endurance limit depend on the type of loading. There may also be multiple stress-concentration factors, one for each mode of loading. The problem of how to deal with combined stresses was encountered when developing static failure theories. The distortion energy failure theory proved to be a satisfactory method of combining the

²³James O. Smith, "The Effect of Range of Stress on the Fatigue Strength of Metals," *Univ. of Ill. Eng. Exp. Sta. Bull.* 334, 1942.

multiple stresses on a stress element of a ductile material into a single equivalent von Mises stress. The same approach will be used here.

The first step is to generate *two* stress elements—one for the alternating stresses and one for the midrange stresses. Apply the appropriate fatigue stress-concentration factors to each of the stresses; i.e., apply $(K_f)_{\text{bending}}$ for the bending stresses, $(K_{fs})_{\text{torsion}}$ for the torsional stresses, and $(K_f)_{\text{axial}}$ for the axial stresses. Next, calculate an equivalent von Mises stress for each of these two stress elements, σ'_a and σ'_m . Finally, select a fatigue failure criterion (modified Goodman, Gerber, ASME-elliptic, or Soderberg) to complete the fatigue analysis. For the endurance limit, S_e , use the endurance limit modifiers, k_a , k_b , and k_c , for bending. The torsional load factor, $k_c = 0.59$ should not be applied as it is already accounted for in the von Mises stress calculation (see footnote 17 on p. 290). The load factor for the axial load can be accounted for by dividing the alternating axial stress by the axial load factor of 0.85. For example, consider the common case of a shaft with bending stresses, torsional shear stresses, and axial stresses. For this case, the von Mises stress is of the form $\sigma' = (\sigma_x^2 + 3\tau_{xy}^2)^{1/2}$. Considering that the bending, torsional, and axial stresses have alternating and midrange components, the von Mises stresses for the two stress elements can be written as

$$\sigma'_a = \left\{ \left[(K_f)_{\text{bending}}(\sigma_a)_{\text{bending}} + (K_f)_{\text{axial}} \frac{(\sigma_a)_{\text{axial}}}{0.85} \right]^2 + 3 [(K_{fs})_{\text{torsion}}(\tau_a)_{\text{torsion}}]^2 \right\}^{1/2} \quad (6-55)$$

$$\sigma'_m = \left\{ \left[(K_f)_{\text{bending}}(\sigma_m)_{\text{bending}} + (K_f)_{\text{axial}}(\sigma_m)_{\text{axial}} \right]^2 + 3 [(K_{fs})_{\text{torsion}}(\tau_m)_{\text{torsion}}]^2 \right\}^{1/2} \quad (6-56)$$

For first-cycle localized yielding, the maximum von Mises stress is calculated. This would be done by first adding the axial and bending alternating and midrange stresses to obtain σ_{\max} and adding the alternating and midrange shear stresses to obtain τ_{\max} . Then substitute σ_{\max} and τ_{\max} into the equation for the von Mises stress. A simpler and more conservative method is to add Eq. (6-55) and Eq. (6-56). That is, let $\sigma'_{\max} = \sigma'_a + \sigma'_m$.

If the stress components are not in phase but have the same frequency, the maxima can be found by expressing each component in trigonometric terms, using phase angles, and then finding the sum. If two or more stress components have differing frequencies, the problem is difficult; one solution is to assume that the two (or more) components often reach an in-phase condition, so that their magnitudes are additive.

EXAMPLE 6-14

A rotating shaft is made of 42- × 4-mm AISI 1018 cold-drawn steel tubing and has a 6-mm-diameter hole drilled transversely through it. Estimate the factor of safety guarding against fatigue and static failures using the Gerber and Langer failure criteria for the following loading conditions:

- (a) The shaft is subjected to a completely reversed torque of 120 N · m in phase with a completely reversed bending moment of 150 N · m.
- (b) The shaft is subjected to a pulsating torque fluctuating from 20 to 160 N · m and a steady bending moment of 150 N · m.

Solution

Here we follow the procedure of estimating the strengths and then the stresses, followed by relating the two.

From Table A-20 we find the minimum strengths to be $S_{ut} = 440$ MPa and $S_y = 370$ MPa. The endurance limit of the rotating-beam specimen is $0.5(440) = 220$ MPa. The surface factor, obtained from Eq. (6-19) and Table 6-2, p. 287, is

$$k_a = 4.51 S_{ut}^{-0.265} = 4.51(440)^{-0.265} = 0.899$$

From Eq. (6-20) the size factor is

$$k_b = \left(\frac{d}{7.62} \right)^{-0.107} = \left(\frac{42}{7.62} \right)^{-0.107} = 0.833$$

The remaining Marin factors are all unity, so the modified endurance strength S_e is

$$S_e = 0.899(0.833)220 = 165 \text{ MPa}$$

(a) Theoretical stress-concentration factors are found from Table A-16. Using $a/D = 6/42 = 0.143$ and $d/D = 34/42 = 0.810$, and using linear interpolation, we obtain $A = 0.798$ and $K_t = 2.366$ for bending; and $A = 0.89$ and $K_{ts} = 1.75$ for torsion. Thus, for bending,

$$Z_{\text{net}} = \frac{\pi A}{32D}(D^4 - d^4) = \frac{\pi(0.798)}{32(42)}[(42)^4 - (34)^4] = 3.31(10^3) \text{ mm}^3$$

and for torsion

$$J_{\text{net}} = \frac{\pi A}{32}(D^4 - d^4) = \frac{\pi(0.89)}{32}[(42)^4 - (34)^4] = 155(10^3) \text{ mm}^4$$

Next, using Figs. 6-20 and 6-21, pp. 295-296, with a notch radius of 3 mm we find the notch sensitivities to be 0.78 for bending and 0.81 for torsion. The two corresponding fatigue stress-concentration factors are obtained from Eq. (6-32) as

$$K_f = 1 + q(K_t - 1) = 1 + 0.78(2.366 - 1) = 2.07$$

$$K_{fs} = 1 + 0.81(1.75 - 1) = 1.61$$

The alternating bending stress is now found to be

$$\sigma_{xa} = K_f \frac{M}{Z_{\text{net}}} = 2.07 \frac{150}{3.31(10^{-6})} = 93.8(10^6) \text{ Pa} = 93.8 \text{ MPa}$$

and the alternating torsional stress is

$$\tau_{xya} = K_{fs} \frac{TD}{2J_{\text{net}}} = 1.61 \frac{120(42)(10^{-3})}{2(155)(10^{-9})} = 26.2(10^6) \text{ Pa} = 26.2 \text{ MPa}$$

The midrange von Mises component σ'_m is zero. The alternating component σ'_a is given by

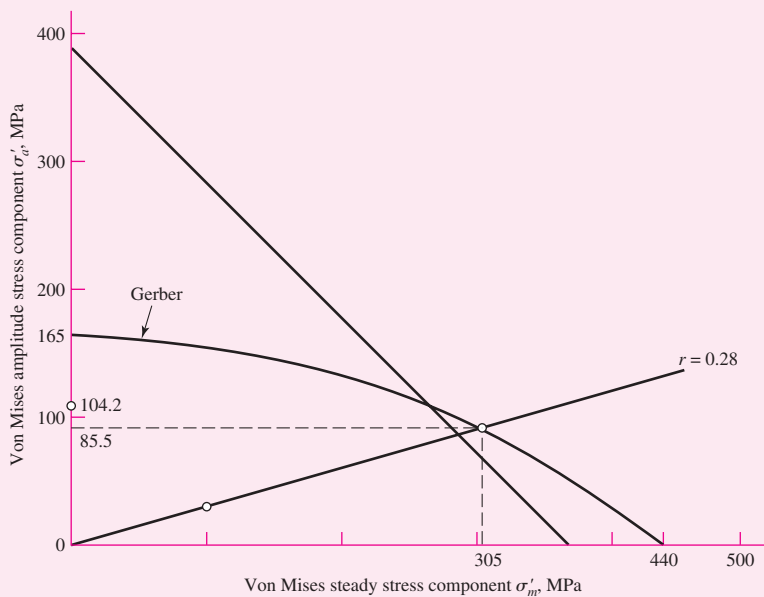
$$\sigma'_a = (\sigma_{xa}^2 + 3\tau_{xya}^2)^{1/2} = [93.8^2 + 3(26.2^2)]^{1/2} = 104.2 \text{ MPa}$$

Since $S_e = S_a$, the fatigue factor of safety n_f is

$$\text{Answer} \quad n_f = \frac{S_a}{\sigma'_a} = \frac{165}{104.2} = 1.58$$

Figure 6-32

Designer's fatigue diagram for Ex. 6-14.



The first-cycle yield factor of safety is

Answer

$$n_y = \frac{S_y}{\sigma'_a} = \frac{370}{105.6} = 3.50$$

There is no localized yielding; the threat is from fatigue. See Fig. 6-32.

(b) This part asks us to find the factors of safety when the alternating component is due to pulsating torsion, and a steady component is due to both torsion and bending. We have $T_a = (160 - 20)/2 = 70 \text{ N} \cdot \text{m}$ and $T_m = (160 + 20)/2 = 90 \text{ N} \cdot \text{m}$. The corresponding amplitude and steady-stress components are

$$\tau_{xya} = K_{fs} \frac{T_a D}{2J_{\text{net}}} = 1.61 \frac{70(42)(10^{-3})}{2(155)(10^{-9})} = 15.3(10^6) \text{ Pa} = 15.3 \text{ MPa}$$

$$\tau_{xym} = K_{fs} \frac{T_m D}{2J_{\text{net}}} = 1.61 \frac{90(42)(10^{-3})}{2(155)(10^{-9})} = 19.7(10^6) \text{ Pa} = 19.7 \text{ MPa}$$

The steady bending stress component σ_{xm} is

$$\sigma_{xm} = K_f \frac{M_m}{Z_{\text{net}}} = 2.07 \frac{150}{3.31(10^{-6})} = 93.8(10^6) \text{ Pa} = 93.8 \text{ MPa}$$

The von Mises components σ'_a and σ'_m are

$$\sigma'_a = [3(15.3)^2]^{1/2} = 26.5 \text{ MPa}$$

$$\sigma'_m = [93.8^2 + 3(19.7)^2]^{1/2} = 99.8 \text{ MPa}$$

From Table 6-7, p. 307, the fatigue factor of safety is

Answer

$$n_f = \frac{1}{2} \left(\frac{440}{99.8} \right)^2 \frac{26.5}{165} \left\{ -1 + \sqrt{1 + \left[\frac{2(99.8)165}{440(26.5)} \right]^2} \right\} = 3.12$$

From the same table, with $r = \sigma'_a/\sigma'_m = 26.5/99.8 = 0.28$, the strengths can be shown to be $S_a = 85.5$ MPa and $S_m = 305$ MPa. See the plot in Fig. 6–32.

The first-cycle yield factor of safety n_y is

Answer

$$n_y = \frac{S_y}{\sigma'_a + \sigma'_m} = \frac{370}{26.5 + 99.8} = 2.93$$

There is no notch yielding. The likelihood of failure may first come from first-cycle yielding at the notch. See the plot in Fig. 6–32.

6–15

Varying, Fluctuating Stresses; Cumulative Fatigue Damage

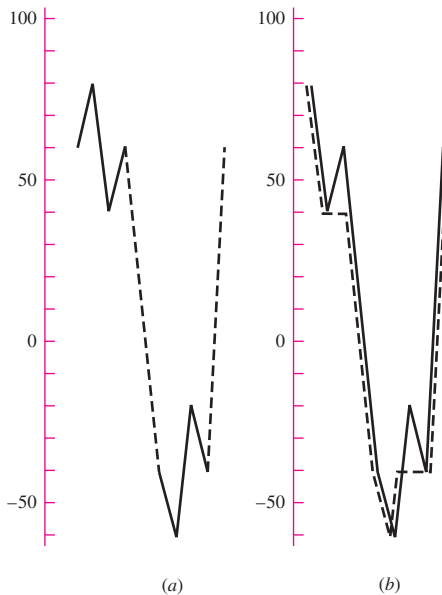
Instead of a single fully reversed stress history block composed of n cycles, suppose a machine part, at a critical location, is subjected to

- A fully reversed stress σ_1 for n_1 cycles, σ_2 for n_2 cycles, . . . , or
- A “wiggly” time line of stress exhibiting many and different peaks and valleys.

What stresses are significant, what counts as a cycle, and what is the measure of damage incurred? Consider a fully reversed cycle with stresses varying 60, 80, 40, and 60 kpsi and a second fully reversed cycle –40, –60, –20, and –40 kpsi as depicted in Fig. 6–33a. First, it is clear that to impose the pattern of stress in Fig. 6–33a on a part it is necessary that the time trace look like the solid lines plus the dashed lines in Fig. 6–33a. Figure 6–33b moves the snapshot to exist beginning with 80 kpsi and ending with 80 kpsi. Acknowledging the existence of a single stress-time trace is to discover a “hidden” cycle shown as the dashed line in Fig. 6–33b. If there are 100 applications of the all-positive stress cycle, then 100 applications of the all-negative stress cycle, the

Figure 6–33

Variable stress diagram prepared for assessing cumulative damage.



hidden cycle is applied but once. If the all-positive stress cycle is applied alternately with the all-negative stress cycle, the hidden cycle is applied 100 times.

To ensure that the hidden cycle is not lost, begin on the snapshot with the largest (or smallest) stress and add previous history to the right side, as was done in Fig. 6-33b. Characterization of a cycle takes on a max–min–same max (or min–max–same min) form. We identify the hidden cycle first by moving along the dashed-line trace in Fig. 6-33b identifying a cycle with an 80-kpsi max, a 60-kpsi min, and returning to 80 kpsi. Mentally deleting the used part of the trace (the dashed line) leaves a 40, 60, 40 cycle and a –40, –20, –40 cycle. Since failure loci are expressed in terms of stress amplitude component σ_a and steady component σ_m , we use Eq. (6-36) to construct the table below:

Cycle Number	σ_{\max}	σ_{\min}	σ_a	σ_m
1	80	–60	70	10
2	60	40	10	50
3	–20	–40	10	–30

The most damaging cycle is number 1. It could have been lost.

Methods for counting cycles include:

- Number of tensile peaks to failure.
- All maxima above the waveform mean, all minima below.
- The global maxima between crossings above the mean and the global minima between crossings below the mean.
- All positive slope crossings of levels above the mean, and all negative slope crossings of levels below the mean.
- A modification of the preceding method with only one count made between successive crossings of a level associated with each counting level.
- Each local max–min excursion is counted as a half-cycle, and the associated amplitude is half-range.
- The preceding method plus consideration of the local mean.
- Rain-flow counting technique.

The method used here amounts to a variation of the *rain-flow counting technique*.

The *Palmgren-Miner*²⁴ *cycle-ratio summation rule*, also called *Miner's rule*, is written

$$\sum \frac{n_i}{N_i} = c \quad (6-57)$$

where n_i is the number of cycles at stress level σ_i and N_i is the number of cycles to failure at stress level σ_i . The parameter c has been determined by experiment; it is usually found in the range $0.7 < c < 2.2$ with an average value near unity.

²⁴A. Palmgren, "Die Lebensdauer von Kugellagern," *ZVDI*, vol. 68, pp. 339–341, 1924; M. A. Miner, "Cumulative Damage in Fatigue," *J. Appl. Mech.*, vol. 12, *Trans. ASME*, vol. 67, pp. A159–A164, 1945.

Using the deterministic formulation as a linear damage rule we write

$$D = \sum \frac{n_i}{N_i} \quad (6-58)$$

where D is the accumulated damage. When $D = c = 1$, failure ensues.

EXAMPLE 6-15

Given a part with $S_{ut} = 151$ kpsi and at the critical location of the part, $S_e = 67.5$ kpsi. For the loading of Fig. 6-33, estimate the number of repetitions of the stress-time block in Fig. 6-33 that can be made before failure.

Solution

From Fig. 6-18, p. 285, for $S_{ut} = 151$ kpsi, $f = 0.795$. From Eq. (6-14),

$$a = \frac{(fS_{ut})^2}{S_e} = \frac{[0.795(151)]^2}{67.5} = 213.5 \text{ kpsi}$$

From Eq. (6-15),

$$b = -\frac{1}{3} \log \left(\frac{fS_{ut}}{S_e} \right) = -\frac{1}{3} \log \left[\frac{0.795(151)}{67.5} \right] = -0.0833$$

So,

$$S_f = 213.5 N^{-0.0833} \quad N = \left(\frac{S_f}{213.5} \right)^{-1/0.0833} \quad (1), (2)$$

We prepare to add two columns to the previous table. Using the Gerber fatigue criterion, Eq. (6-47), p. 306, with $S_e = S_f$, and $n = 1$, we can write

$$S_f = \begin{cases} \frac{\sigma_a}{1 - (\sigma_m/S_{ut})^2} & \sigma_m > 0 \\ S_e & \sigma_m \leq 0 \end{cases} \quad (3)$$

where S_f is the fatigue strength associated with a completely reversed stress, σ_{rev} , equivalent to the fluctuating stresses [see Ex. 6-12, part (b)].

Cycle 1: $r = \sigma_a/\sigma_m = 70/10 = 7$, and the strength amplitude from Table 6-7, p. 307, is

$$S_a = \frac{7^2 151^2}{2(67.5)} \left\{ -1 + \sqrt{1 + \left[\frac{2(67.5)}{7(151)} \right]^2} \right\} = 67.2 \text{ kpsi}$$

Since $\sigma_a > S_a$, that is, $70 > 67.2$, life is reduced. From Eq. (3),

$$S_f = \frac{70}{1 - (10/151)^2} = 70.3 \text{ kpsi}$$

and from Eq. (2)

$$N = \left(\frac{70.3}{213.5} \right)^{-1/0.0833} = 619(10^3) \text{ cycles}$$

Cycle 2: $r = 10/50 = 0.2$, and the strength amplitude is

$$S_a = \frac{0.2^2 151^2}{2(67.5)} \left\{ -1 + \sqrt{1 + \left[\frac{2(67.5)}{0.2(151)} \right]^2} \right\} = 24.2 \text{ kpsi}$$

Since $\sigma_a < S_a$, that is $10 < 24.2$, then $S_f = S_e$ and indefinite life follows. Thus, $N \rightarrow \infty$.

Cycle 3: $r = 10/-30 = -0.333$, and since $\sigma_m < 0$, $S_f = S_e$, indefinite life follows and $N \rightarrow \infty$

Cycle Number	S_f , kpsi	N , cycles
1	70.3	$619(10^3)$
2	67.5	∞
3	67.5	∞

From Eq. (6-58) the damage per block is

$$D = \sum \frac{n_i}{N_i} = N \left[\frac{1}{619(10^3)} + \frac{1}{\infty} + \frac{1}{\infty} \right] = \frac{N}{619(10^3)}$$

Answer Setting $D = 1$ yields $N = 619(10^3)$ cycles.

To further illustrate the use of the Miner rule, let us consider a steel having the properties $S_{ut} = 80$ kpsi, $S'_{e,0} = 40$ kpsi, and $f = 0.9$, where we have used the designation $S'_{e,0}$ instead of the more usual S'_e to indicate the endurance limit of the *virgin*, or *undamaged*, material. The log S -log N diagram for this material is shown in Fig. 6-34 by the heavy solid line. From Eqs. (6-14) and (6-15), p. 285, we find that $a = 129.6$ kpsi and $b = -0.085\ 091$. Now apply, say, a reversed stress $\sigma_1 = 60$ kpsi for $n_1 = 3000$ cycles. Since $\sigma_1 > S'_{e,0}$, the endurance limit will be damaged, and we wish to find the new endurance limit $S'_{e,1}$ of the damaged material using the Miner rule. The equation of the virgin material failure line in Fig. 6-34 in the 10^3 to 10^6 cycle range is

$$S_f = aN^b = 129.6N^{-0.085\ 091}$$

The cycles to failure at stress level $\sigma_1 = 60$ kpsi are

$$N_1 = \left(\frac{\sigma_1}{129.6} \right)^{-1/0.085\ 091} = \left(\frac{60}{129.6} \right)^{-1/0.085\ 091} = 8520 \text{ cycles}$$

Figure 6-34

Use of the Miner rule to predict the endurance limit of a material that has been overstressed for a finite number of cycles.

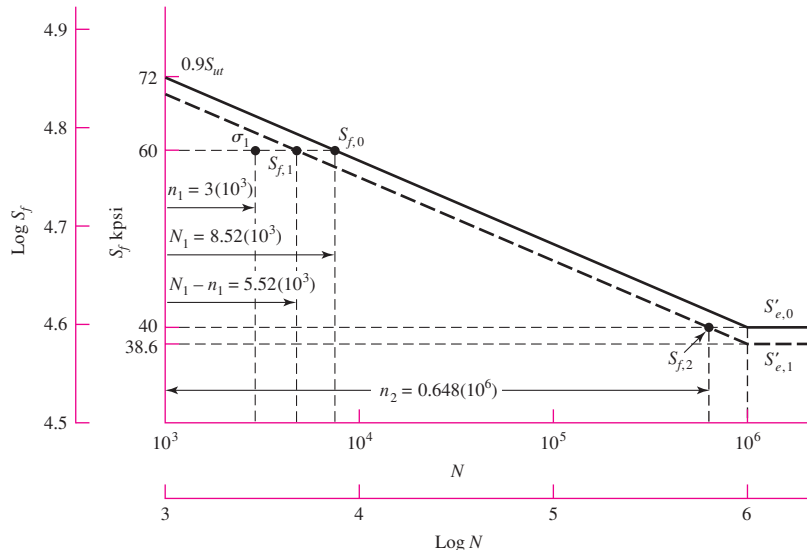


Figure 6–34 shows that the material has a life $N_1 = 8520$ cycles at 60 kpsi, and consequently, after the application of σ_1 for 3000 cycles, there are $N_1 - n_1 = 5520$ cycles of life remaining at σ_1 . This locates the finite-life strength $S_{f,1}$ of the damaged material, as shown in Fig. 6–34. To get a second point, we ask the question: With n_1 and N_1 given, how many cycles of stress $\sigma_2 = S'_{e,0}$ can be applied before the damaged material fails? This corresponds to n_2 cycles of stress reversal, and hence, from Eq. (6–58), we have

$$\frac{n_1}{N_1} + \frac{n_2}{N_2} = 1 \quad (a)$$

Solving for n_2 gives

$$n_2 = (N_1 - n_1) \frac{N_2}{N_1} \quad (b)$$

Then

$$n_2 = [8.52(10^3) - 3(10^3)] \frac{10^6}{8.52(10^3)} = 0.648(10^6) \text{ cycles}$$

This corresponds to the finite-life strength $S_{f,2}$ in Fig. 6–34. A line through $S_{f,1}$ and $S_{f,2}$ is the log S –log N diagram of the damaged material according to the Miner rule. Two points, $(N_1 - n_1, \sigma_1)$ and (n_2, σ_2) , determine the new equation for the line, $S_f = a'N^{b'}$. Thus, $\sigma_1 = a'(N_1 - n_1)^{b'}$, and $\sigma_2 = a'n_2^{b'}$. Dividing the two equations, taking the logarithm of the results, and solving for b' gives

$$b' = \frac{\log(\sigma_1/\sigma_2)}{\log\left(\frac{N_1 - n_1}{n_2}\right)}$$

Substituting n_2 from Eq. (b) and simplifying gives

$$b' = \frac{\log(\sigma_1/\sigma_2)}{\log(N_1/N_2)}$$

For the undamaged material, $N_1 = (\sigma_1/a)^{1/b}$ and $N_2 = (\sigma_2/a)^{1/b}$, then

$$b' = \frac{\log(\sigma_1/\sigma_2)}{\log[(\sigma_1/a)^{1/b}/(\sigma_2/a)^{1/b}]} = \frac{\log(\sigma_1/\sigma_2)}{(1/b)\log(\sigma_1/\sigma_2)} = b$$

This means that the damaged material line has the same slope as the virgin material line, and the two lines are parallel. The value of a' is then found from $a' = S_f/N^b$.

For the case we are illustrating, $a' = 60/[5.52(10)^3]^{-0.085091} = 124.898$ kpsi, and thus the new endurance limit is $S'_{e,1} = a'N_e^b = 124.898[(10)^6]^{-0.085091} = 38.6$ kpsi.

Though the Miner rule is quite generally used, it fails in two ways to agree with experiment. First, note that this theory states that the static strength S_{ut} is damaged, that is, decreased, because of the application of σ_1 ; see Fig. 6–34 at $N = 10^3$ cycles. Experiments fail to verify this prediction.

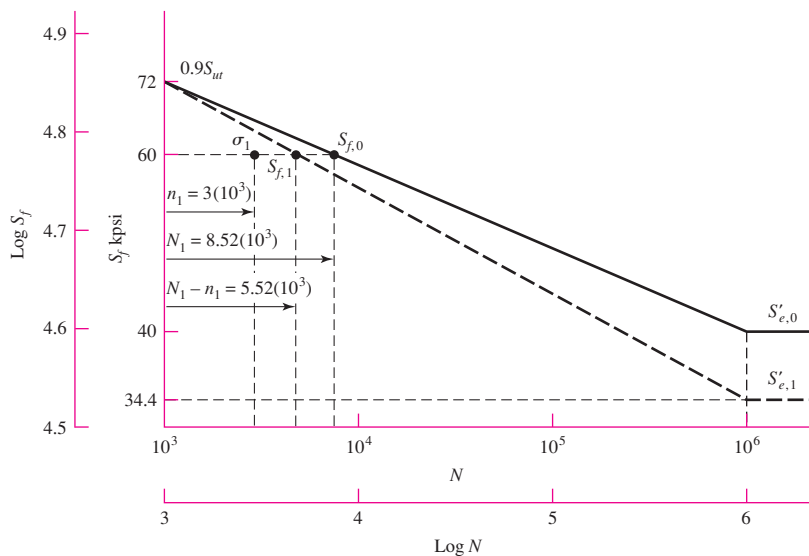
The Miner rule, as given by Eq. (6–58), does not account for the order in which the stresses are applied, and hence ignores any stresses less than $S'_{e,0}$. But it can be seen in Fig. 6–34 that a stress σ_3 in the range $S'_{e,1} < \sigma_3 < S'_{e,0}$ would cause damage if applied after the endurance limit had been damaged by the application of σ_1 .

Manson's²⁵ approach overcomes both of the deficiencies noted for the Palmgren-Miner method; historically it is a much more recent approach, and it is just as easy to

²⁵S. S. Manson, A. J. Nachtigall, C. R. Ensign, and J. C. Fresche, "Further Investigation of a Relation for Cumulative Fatigue Damage in Bending," *Trans. ASME, J. Eng. Ind.*, ser. B, vol. 87, No. 1, pp. 25–35, February 1965.

Figure 6-35

Use of the Manson method to predict the endurance limit of a material that has been overstressed for a finite number of cycles.



use. Except for a slight change, we shall use and recommend the Manson method in this book. Manson plotted the S -log N diagram instead of a log S -log N plot as is recommended here. Manson also resorted to experiment to find the point of convergence of the S -log N lines corresponding to the static strength, instead of arbitrarily selecting the intersection of $N = 10^3$ cycles with $S = 0.9S_{ut}$ as is done here. Of course, it is always better to use experiment, but our purpose in this book has been to use the simple test data to learn as much as possible about fatigue failure.

The method of Manson, as presented here, consists in having all log S -log N lines, that is, lines for both the damaged and the virgin material, converge to the same point, $0.9S_{ut}$ at 10^3 cycles. In addition, the log S -log N lines must be constructed in the same historical order in which the stresses occur.

The data from the preceding example are used for illustrative purposes. The results are shown in Fig. 6-35. Note that the strength $S_{f,1}$ corresponding to $N_1 - n_1 = 5.52(10^3)$ cycles is found in the same manner as before. Through this point and through $0.9S_{ut}$ at 10^3 cycles, draw the heavy dashed line to meet $N = 10^6$ cycles and define the endurance limit $S'_{e,1}$ of the damaged material. Again, with two points on the line, $b' = [\log(72/60)]/\log[(10^3)/5.52(10^3)] = -0.106722$, and $a' = 60/[5.52(10^3)]^{-0.106722} = 150.487$ kpsi. In this case, the new endurance limit is $S'_{e,1} = a'N_e^{b'} = 150.487(10^6)^{-0.106722} = 34.4$ kpsi, which is somewhat less than that found by the Miner method.

It is now easy to see from Fig. 6-35 that a reversed stress $\sigma = 36$ kpsi, say, would not harm the endurance limit of the virgin material, no matter how many cycles it might be applied. However, if $\sigma = 36$ kpsi should be applied *after* the material was damaged by $\sigma_1 = 60$ kpsi, then additional damage would be done.

Both these rules involve a number of computations, which are repeated every time damage is estimated. For complicated stress-time traces, this might be every cycle. Clearly a computer program is useful to perform the tasks, including scanning the trace and identifying the cycles.

Collins said it well: "In spite of all the problems cited, the Palmgren linear damage rule is frequently used because of its simplicity and the experimental fact that other more complex damage theories do not always yield a significant improvement in failure prediction reliability."²⁶

6-16

Surface Fatigue Strength

The surface fatigue mechanism is not definitively understood. The contact-affected zone, in the absence of surface shearing tractions, entertains compressive principal stresses. Rotary fatigue has its cracks grown at or near the surface in the presence of tensile stresses that are associated with crack propagation, to catastrophic failure. There are shear stresses in the zone, which are largest just below the surface. Cracks seem to grow from this stratum until small pieces of material are expelled, leaving pits on the surface. Because engineers had to design durable machinery before the surface fatigue phenomenon was understood in detail, they had taken the posture of conducting tests, observing pits on the surface, and declaring failure at an arbitrary projected area of hole, and they related this to the Hertzian contact pressure. This compressive stress did not produce the failure directly, but whatever the failure mechanism, whatever the stress type that was instrumental in the failure, the contact stress was an *index* to its magnitude.

Buckingham²⁷ conducted a number of tests relating the fatigue at 10^8 cycles to endurance strength (Hertzian contact pressure). While there is evidence of an endurance limit at about $3(10^7)$ cycles for cast materials, hardened steel rollers showed no endurance limit up to $4(10^8)$ cycles. Subsequent testing on hard steel shows no endurance limit. Hardened steel exhibits such high fatigue strengths that its use in resisting surface fatigue is widespread.

Our studies thus far have dealt with the failure of a machine element by yielding, by fracture, and by fatigue. The endurance limit obtained by the rotating-beam test is frequently called the *flexural endurance limit*, because it is a test of a rotating beam. In this section we shall study a property of *mating materials* called the *surface endurance shear*. The design engineer must frequently solve problems in which two machine elements mate with one another by rolling, sliding, or a combination of rolling and sliding contact. Obvious examples of such combinations are the mating teeth of a pair of gears, a cam and follower, a wheel and rail, and a chain and sprocket. A knowledge of the surface strength of materials is necessary if the designer is to create machines having a long and satisfactory life.

When two surfaces roll or roll and slide against one another with sufficient force, a pitting failure will occur after a certain number of cycles of operation. Authorities are not in complete agreement on the exact mechanism of the pitting; although the subject is quite complicated, they do agree that the Hertz stresses, the number of cycles, the surface finish, the hardness, the degree of lubrication, and the temperature all influence the strength. In Sec. 3-19 it was learned that, when two surfaces are pressed together, a maximum shear stress is developed slightly below the contacting surface. It is postulated by some authorities that a surface fatigue failure is initiated by this maximum shear stress and then is propagated rapidly to the surface. The lubricant then enters the crack that is formed and, under pressure, eventually wedges the chip loose.

²⁶J. A. Collins, *Failure of Materials in Mechanical Design*, John Wiley & Sons, New York, 1981, p. 243.

²⁷Earle Buckingham, *Analytical Mechanics of Gears*, McGraw-Hill, New York, 1949.

To determine the surface fatigue strength of mating materials, Buckingham designed a simple machine for testing a pair of contacting rolling surfaces in connection with his investigation of the wear of gear teeth. Buckingham and, later, Talbourdet gathered large numbers of data from many tests so that considerable design information is now available. To make the results useful for designers, Buckingham defined a *load-stress factor*, also called a *wear factor*, which is derived from the Hertz equations. Equations (3–73) and (3–74), p. 124, for contacting cylinders are found to be

$$b = \sqrt{\frac{2F}{\pi l} \frac{(1 - v_1^2)/E_1 + (1 - v_2^2)/E_2}{(1/d_1) + (1/d_2)}} \quad (6-59)$$

$$p_{\max} = \frac{2F}{\pi b l} \quad (6-60)$$

where b = half width of rectangular contact area

F = contact force

l = length of cylinders

v = Poisson's ratio

E = modulus of elasticity

d = cylinder diameter

It is more convenient to use the cylinder radius, so let $2r = d$. If we then designate the length of the cylinders as w (for width of gear, bearing, cam, etc.) instead of l and remove the square root sign, Eq. (6–59) becomes

$$b^2 = \frac{4F}{\pi w} \frac{(1 - v_1^2)/E_1 + (1 - v_2^2)/E_2}{1/r_1 + 1/r_2} \quad (6-61)$$

We can define a *surface endurance strength* S_C using

$$p_{\max} = \frac{2F}{\pi b w} \quad (6-62)$$

as

$$S_C = \frac{2F}{\pi b w} \quad (6-63)$$

which may also be called *contact strength*, the *contact fatigue strength*, or the *Hertzian endurance strength*. The strength is the contacting pressure which, after a specified number of cycles, will cause failure of the surface. Such failures are often called *wear* because they occur over a very long time. They should not be confused with abrasive wear, however. By squaring Eq. (6–63), substituting b^2 from Eq. (6–61), and rearranging, we obtain

$$\frac{F}{w} \left(\frac{1}{r_1} + \frac{1}{r_2} \right) = \pi S_C^2 \left[\frac{1 - v_1^2}{E_1} + \frac{1 - v_2^2}{E_2} \right] = K_1 \quad (6-64)$$

The left expression consists of parameters a designer may seek to control independently. The central expression consists of material properties that come with the material and condition specification. The third expression is the parameter K_1 , Buckingham's load-stress factor, determined by a test fixture with values F , w , r_1 , r_2 and the number of

cycles associated with the first tangible evidence of fatigue. In gear studies a similar K factor is used:

$$K_g = \frac{K_1}{4} \sin \phi \quad (6-65)$$

where ϕ is the tooth pressure angle, and the term $[(1 - v_1^2)/E_1 + (1 - v_2^2)/E_2]$ is defined as $1/(\pi C_P^2)$, so that

$$S_C = C_P \sqrt{\frac{F}{w} \left(\frac{1}{r_1} + \frac{1}{r_2} \right)} \quad (6-66)$$

Buckingham and others reported K_1 for 10^8 cycles and nothing else. This gives only one point on the $S_C N$ curve. For cast metals this may be sufficient, but for wrought steels, heat-treated, some idea of the slope is useful in meeting design goals of other than 10^8 cycles.

Experiments show that K_1 versus N , K_g versus N , and S_C versus N data are rectified by log-log transformation. This suggests that

$$K_1 = \alpha_1 N^{\beta_1} \quad K_g = a N^b \quad S_C = \alpha N^\beta$$

The three exponents are given by

$$\beta_1 = \frac{\log(K_1/K_2)}{\log(N_1/N_2)} \quad b = \frac{\log(K_{g1}/K_{g2})}{\log(N_1/N_2)} \quad \beta = \frac{\log(S_{C1}/S_{C2})}{\log(N_1/N_2)} \quad (6-67)$$

Data on induction-hardened steel on steel give $(S_C)_{10^7} = 271$ kpsi and $(S_C)_{10^8} = 239$ kpsi, so β , from Eq. (6-67), is

$$\beta = \frac{\log(271/239)}{\log(10^7/10^8)} = -0.055$$

It may be of interest that the American Gear Manufacturers Association (AGMA) uses $\beta = -0.056$ between $10^4 < N < 10^{10}$ if the designer has no data to the contrary beyond 10^7 cycles.

A longstanding correlation in steels between S_C and H_B at 10^8 cycles is

$$(S_C)_{10^8} = \begin{cases} 0.4H_B - 10 \text{ kpsi} \\ 2.76H_B - 70 \text{ MPa} \end{cases} \quad (6-68)$$

AGMA uses

$$0.99(S_C)_{10^7} = 0.327H_B + 26 \text{ kpsi} \quad (6-69)$$

Equation (6-66) can be used in design to find an allowable surface stress by using a design factor. Since this equation is nonlinear in its stress-load transformation, the designer must decide if loss of function denotes inability to carry the load. If so, then to find the allowable stress, one divides the load F by the design factor n_d :

$$\sigma_C = C_P \sqrt{\frac{F}{wn_d} \left(\frac{1}{r_1} + \frac{1}{r_2} \right)} = \frac{C_P}{\sqrt{n_d}} \sqrt{\frac{F}{w} \left(\frac{1}{r_1} + \frac{1}{r_2} \right)} = \frac{S_C}{\sqrt{n_d}}$$

and $n_d = (S_C/\sigma_C)^2$. If the loss of function is focused on stress, then $n_d = S_C/\sigma_C$. It is recommended that an engineer

- Decide whether loss of function is failure to carry load or stress.
- Define the design factor and factor of safety accordingly.
- Announce what he or she is using and why.
- Be prepared to defend his or her position.

In this way everyone who is party to the communication knows what a design factor (or factor of safety) of 2 means and adjusts, if necessary, the judgmental perspective.

6-17 Stochastic Analysis²⁸

As already demonstrated in this chapter, there are a great many factors to consider in a fatigue analysis, much more so than in a static analysis. So far, each factor has been treated in a deterministic manner, and if not obvious, these factors are subject to variability and control the overall reliability of the results. When reliability is important, then fatigue testing must certainly be undertaken. There is no other way. Consequently, the methods of stochastic analysis presented here and in other sections of this book constitute guidelines that enable the designer to obtain a good understanding of the various issues involved and help in the development of a safe and reliable design.

In this section, key stochastic modifications to the deterministic features and equations described in earlier sections are provided in the same order of presentation.

Endurance Limit

To begin, a method for estimating endurance limits, the *tensile strength correlation method*, is presented. The ratio $\Phi = S'_e / \bar{S}_{ut}$ is called the *fatigue ratio*.²⁹ For ferrous metals, most of which exhibit an endurance limit, the endurance limit is used as a numerator. For materials that do not show an endurance limit, an endurance strength at a specified number of cycles to failure is used and noted. Gough³⁰ reported the stochastic nature of the fatigue ratio Φ for several classes of metals, and this is shown in Fig. 6-36. The first item to note is that the coefficient of variation is of the order 0.10 to 0.15, and the distribution varies for classes of metals. The second item to note is that Gough's data include materials of no interest to engineers. In the absence of testing, engineers use the correlation that Φ represents to estimate the endurance limit S'_e from the mean ultimate strength \bar{S}_{ut} .

Gough's data are for ensembles of metals, some chosen for metallurgical interest, and include materials that are not commonly selected for machine parts. Mischke³¹ analyzed data for 133 common steels and treatments in varying diameters in rotating bending,³² and the result was

$$\Phi = 0.445d^{-0.107}\text{LN}(1, 0.138)$$

where d is the specimen diameter in inches and $\text{LN}(1, 0.138)$ is a unit lognormal variate with a mean of 1 and a standard deviation (and coefficient of variation) of 0.138. For the standard R. R. Moore specimen,

$$\Phi_{0.30} = 0.445(0.30)^{-0.107}\text{LN}(1, 0.138) = 0.506\text{LN}(1, 0.138)$$

²⁸Review Chap. 20 before reading this section.

²⁹From this point, since we will be dealing with statistical distributions in terms of means, standard deviations, etc. A key quantity, the ultimate strength, will here be presented by its mean value, \bar{S}_{ut} . This means that certain terms that were defined earlier in terms of the minimum value of S_{ut} will change slightly.

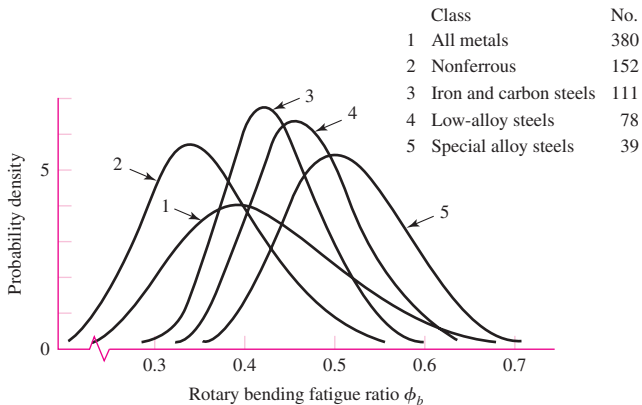
³⁰In J. A. Pope, *Metal Fatigue*, Chapman and Hall, London, 1959.

³¹Charles R. Mischke, "Prediction of Stochastic Endurance Strength," *Trans. ASME, Journal of Vibration, Acoustics, Stress, and Reliability in Design*, vol. 109, no. 1, January 1987, pp. 113–122.

³²Data from H. J. Grover, S. A. Gordon, and L. R. Jackson, *Fatigue of Metals and Structures*, Bureau of Naval Weapons, Document NAVWEPS 00-2500435, 1960.

Figure 6-36

The lognormal probability density PDF of the fatigue ratio ϕ_b of Gough.



Also, 25 plain carbon and low-alloy steels with $S_{ut} > 212$ kpsi are described by

$$S'_e = 107 \text{LN}(1, 0.139) \text{ kpsi}$$

In summary, for the rotating-beam specimen,

$$S'_e = \begin{cases} 0.506\bar{S}_{ut} \text{LN}(1, 0.138) \text{ kpsi or MPa} & \bar{S}_{ut} \leq 212 \text{ kpsi (1460 MPa)} \\ 107 \text{LN}(1, 0.139) \text{ kpsi} & \bar{S}_{ut} > 212 \text{ kpsi} \\ 740 \text{LN}(1, 0.139) \text{ MPa} & \bar{S}_{ut} > 1460 \text{ MPa} \end{cases} \quad (6-70)$$

where \bar{S}_{ut} is the *mean* ultimate tensile strength.

Equations (6-70) represent the state of information before an engineer has chosen a material. In choosing, the designer has made a random choice from the ensemble of possibilities, and the statistics can give the odds of disappointment. If the testing is limited to finding an estimate of the ultimate tensile strength mean \bar{S}_{ut} with the chosen material, Eqs. (6-70) are directly helpful. If there is to be rotary-beam fatigue testing, then statistical information on the endurance limit is gathered and there is no need for the correlation above.

Table 6-9 compares approximate mean values of the fatigue ratio $\bar{\phi}_{0.30}$ for several classes of ferrous materials.

Endurance Limit Modifying Factors

A Marin equation can be written as

$$S_e = k_a k_b k_c k_d k_f S'_e \quad (6-71)$$

where the size factor k_b is deterministic and remains unchanged from that given in Sec. 6-9. Also, since we are performing a stochastic analysis, the “reliability factor” k_e is unnecessary here.

The surface factor k_a cited earlier in deterministic form as Eq. (6-20), p. 288, is now given in stochastic form by

$$k_a = a \bar{S}_{ut}^b \text{LN}(1, C) \quad (\bar{S}_{ut} \text{ in kpsi or MPa}) \quad (6-72)$$

where Table 6-10 gives values of a , b , and C for various surface conditions.

Table 6-9

Comparison of Approximate Values of Mean Fatigue Ratio for Some Classes of Metals	Material Class	$\bar{\phi}_{0.30}$
Wrought steels	0.50	
Cast steels	0.40	
Powdered steels	0.38	
Gray cast iron	0.35	
Malleable cast iron	0.40	
Normalized nodular cast iron	0.33	

Table 6-10

Parameters in Marin Surface Condition Factor

Surface Finish	$k_a = a S_{ut}^b \text{LN}(1, C)$			Coefficient of Variation, C
	a	kpsi	MPa	
Ground*	1.34	1.58	-0.086	0.120
Machined or Cold-rolled	2.67	4.45	-0.265	0.058
Hot-rolled	14.5	58.1	-0.719	0.110
As-forged	39.8	271	-0.995	0.145

*Due to the wide scatter in ground surface data, an alternate function is $k_a = 0.878\text{LN}(1, 0.120)$.

Note: S_{ut} in kpsi or MPa.

EXAMPLE 6-16

A steel has a mean ultimate strength of 520 MPa and a machined surface. Estimate k_a .

Solution From Table 6-10,

$$k_a = 4.45(520)^{-0.265}\text{LN}(1, 0.058)$$

$$\bar{k}_a = 4.45(520)^{-0.265}(1) = 0.848$$

$$\hat{\sigma}_{ka} = C\bar{k}_a = (0.058)4.45(520)^{-0.265} = 0.049$$

Answer so $k_a = \text{LN}(0.848, 0.049)$.

The load factor k_c for axial and torsional loading is given by

$$(k_c)_{\text{axial}} = 1.23\bar{S}_{ut}^{-0.0778}\text{LN}(1, 0.125) \quad (6-73)$$

$$(k_c)_{\text{torsion}} = 0.328\bar{S}_{ut}^{0.125}\text{LN}(1, 0.125) \quad (6-74)$$

where \bar{S}_{ut} is in kpsi. There are fewer data to study for axial fatigue. Equation (6-73) was deduced from the data of Landgraf and of Grover, Gordon, and Jackson (as cited earlier).

Torsional data are sparser, and Eq. (6-74) is deduced from data in Grover et al. Notice the mild sensitivity to strength in the axial and torsional load factor, so k_c in these cases is not constant. Average values are shown in the last column of Table 6-11, and as footnotes to Tables 6-12 and 6-13. Table 6-14 shows the influence of material classes on the load factor k_c . Distortion energy theory predicts $(k_c)_{\text{torsion}} = 0.577$ for materials to which the distortion-energy theory applies. For bending, $k_c = \text{LN}(1, 0)$.

Table 6-11

Parameters in Marin Loading Factor

Mode of Loading	kpsi	α	$k_c = \alpha \bar{S}_{ut}^{-\beta} \ln(1, C)$			Average k_c
			MPa	β	C	
Bending	1	1	1	0	0	1
Axial	1.23	1.43	-0.0778	0.125	0.125	0.85
Torsion	0.328	0.258	0.125	0.125	0.125	0.59

Table 6-12

Average Marin Loading Factor for Axial Load

\bar{S}_{ut} , kpsi	k_c^*
50	0.907
100	0.860
150	0.832
200	0.814

*Average entry 0.85.

Table 6-13

Average Marin Loading Factor for Torsional Load

\bar{S}_{ut} , kpsi	k_c^*
50	0.535
100	0.583
150	0.614
200	0.636

*Average entry 0.59.

Table 6-14

Average Marin Torsional Loading Factor k_c for Several Materials

Material	Range	n	\bar{k}_c	σ_{kc}
Wrought steels	0.52–0.69	31	0.60	0.03
Wrought Al	0.43–0.74	13	0.55	0.09
Wrought Cu and alloy	0.41–0.67	7	0.56	0.10
Wrought Mg and alloy	0.49–0.60	2	0.54	0.08
Titanium	0.37–0.57	3	0.48	0.12
Cast iron	0.79–1.01	9	0.90	0.07
Cast Al, Mg, and alloy	0.71–0.91	5	0.85	0.09

Source: The table is an extension of P. G. Forrest, *Fatigue of Metals*, Pergamon Press, London, 1962, Table 17, p. 110, with standard deviations estimated from range and sample size using Table A-1 in J. B. Kennedy and A. M. Neville, *Basic Statistical Methods for Engineers and Scientists*, 3rd ed., Harper & Row, New York, 1986, pp. 54–55.

EXAMPLE 6-17

Estimate the Marin loading factor \mathbf{k}_c for a 1-in-diameter bar that is used as follows.

- (a) In bending. It is made of steel with $S_{ut} = 100\text{LN}(1, 0.035)$ kpsi, and the designer intends to use the correlation $S'_e = \Phi_{0.30}\bar{S}_{ut}$ to predict S'_e .
- (b) In bending, but endurance testing gave $S'_e = 55\text{LN}(1, 0.081)$ kpsi.
- (c) In push-pull (axial) fatigue, $S_{ut} = \text{LN}(86.2, 3.92)$ kpsi, and the designer intended to use the correlation $S'_e = \Phi_{0.30}\bar{S}_{ut}$.
- (d) In torsional fatigue. The material is cast iron, and S'_e is known by test.

Solution

- (a) Since the bar is in bending,

Answer

$$\mathbf{k}_c = (1, 0)$$

- (b) Since the test is in bending and use is in bending,

Answer

$$\mathbf{k}_c = (1, 0)$$

- (c) From Eq. (6-73),

Answer

$$(\mathbf{k}_c)_{ax} = 1.23(86.2)^{-0.0778}\text{LN}(1, 0.125)$$

$$\bar{k}_c = 1.23(86.2)^{-0.0778}(1) = 0.870$$

$$\hat{\sigma}_{kc} = C\bar{k}_c = 0.125(0.870) = 0.109$$

- (d) From Table 6-15, $\bar{k}_c = 0.90$, $\hat{\sigma}_{kc} = 0.07$, and

Answer

$$C_{kc} = \frac{0.07}{0.90} = 0.08$$

The temperature factor \mathbf{k}_d is

$$\mathbf{k}_d = \bar{k}_d \text{LN}(1, 0.11) \quad (6-75)$$

where $\bar{k}_d = k_d$, given by Eq. (6-27), p. 291.

Finally, \mathbf{k}_f is, as before, the miscellaneous factor that can come about from a great many considerations, as discussed in Sec. 6-9, where now statistical distributions, possibly from testing, are considered.

Stress Concentration and Notch Sensitivity

Notch sensitivity q was defined by Eq. (6-31), p. 295. The stochastic equivalent is

$$\mathbf{q} = \frac{\mathbf{K}_f - 1}{K_t - 1} \quad (6-76)$$

where K_t is the theoretical (or geometric) stress-concentration factor, a deterministic quantity. A study of lines 3 and 4 of Table 20-6, will reveal that adding a scalar to (or subtracting one from) a variate \mathbf{x} will affect only the mean. Also, multiplying (or dividing) by a scalar affects both the mean and standard deviation. With this in mind, we can

Table 6–15

Heywood's Parameter
 \sqrt{a} and coefficients of
variation C_{Kf} for steels

Notch Type	$\sqrt{a}(\sqrt{\text{in}}), S_{ut} \text{ in kpsi}$	$\sqrt{a}(\sqrt{\text{mm}}), S_{ut} \text{ in MPa}$	Coefficient of Variation C_{Kf}
Transverse hole	$5/S_{ut}$	$174/S_{ut}$	0.10
Shoulder	$4/S_{ut}$	$139/S_{ut}$	0.11
Groove	$3/S_{ut}$	$104/S_{ut}$	0.15

relate the statistical parameters of the fatigue stress-concentration factor K_f to those of notch sensitivity q . It follows that

$$q = \text{LN} \left(\frac{\bar{K}_f - 1}{K_t - 1}, \frac{C\bar{K}_f}{K_t - 1} \right)$$

where $C = C_{Kf}$ and

$$\begin{aligned} \bar{q} &= \frac{\bar{K}_f - 1}{K_t - 1} \\ \hat{\sigma}_q &= \frac{C\bar{K}_f}{K_t - 1} \\ C_q &= \frac{C\bar{K}_f}{\bar{K}_f - 1} \end{aligned} \quad (6-77)$$

The fatigue stress-concentration factor K_f has been investigated more in England than in the United States. For \bar{K}_f , consider a modified Neuber equation (after Heywood³³), where the fatigue stress-concentration factor is given by

$$\bar{K}_f = \frac{K_t}{1 + \frac{2(K_t - 1)}{K_t} \frac{\sqrt{a}}{\sqrt{r}}} \quad (6-78)$$

where Table 6–15 gives values of \sqrt{a} and C_{Kf} for steels with transverse holes, shoulders, or grooves. Once K_f is described, q can also be quantified using the set Eqs. (6–77).

The modified Neuber equation gives the fatigue stress-concentration factor as

$$K_f = \bar{K}_f \text{LN}(1, C_{Kf}) \quad (6-79)$$

EXAMPLE 6–18

Estimate K_f and q for the steel shaft given in Ex. 6–6, p. 296.

Solution

From Ex. 6–6, a steel shaft with $S_{ut} = 690$ MPa and a shoulder with a fillet of 3 mm was found to have a theoretical stress-concentration factor of $K_t \doteq 1.65$. From Table 6–15,

$$\sqrt{a} = \frac{139}{S_{ut}} = \frac{139}{690} = 0.2014\sqrt{\text{mm}}$$

³³R. B. Heywood, *Designing Against Fatigue*, Chapman & Hall, London, 1962.

From Eq. (6-78),

$$K_f = \frac{K_t}{1 + \frac{2(K_t - 1)}{K_t} \frac{\sqrt{a}}{\sqrt{r}}} = \frac{1.65}{1 + \frac{2(1.65 - 1)}{1.65} \frac{0.2014}{\sqrt{3}}} = 1.51$$

which is 2.5 percent lower than what was found in Ex. 6-6.

From Table 6-15, $C_{Kf} = 0.11$. Thus from Eq. (6-79),

Answer

$$K_f = 1.51 \text{ LN}(1, 0.11)$$

From Eq. (6-77), with $K_t = 1.65$

$$\bar{q} = \frac{1.51 - 1}{1.65 - 1} = 0.785$$

$$C_q = \frac{C_{Kf} \bar{K}_f}{\bar{K}_f - 1} = \frac{0.11(1.51)}{1.51 - 1} = 0.326$$

$$\hat{\sigma}_q = C_q \bar{q} = 0.326(0.785) = 0.256$$

So,

Answer

$$\mathbf{q} = \text{LN}(0.785, 0.256)$$

EXAMPLE 6-19

The bar shown in Fig. 6-37 is machined from a cold-rolled flat having an ultimate strength of $S_{ut} = \text{LN}(87.6, 5.74)$ kpsi. The axial load shown is completely reversed. The load amplitude is $\mathbf{F}_a = \text{LN}(1000, 120)$ lbf.

(a) Estimate the reliability.

(b) Reestimate the reliability when a rotating bending endurance test shows that $\mathbf{S}'_e = \text{LN}(40, 2)$ kpsi.

Solution

$$(a) \text{ From Eq. (6-70), } \mathbf{S}'_e = 0.506 \bar{S}_{ut} \text{LN}(1, 0.138) = 0.506(87.6) \text{LN}(1, 0.138) \\ = 44.3 \text{LN}(1, 0.138) \text{ kpsi}$$

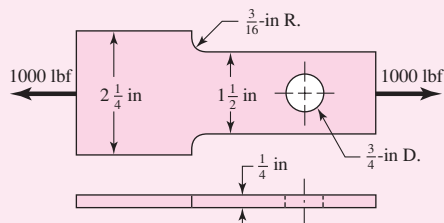
From Eq. (6-72) and Table 6-10,

$$\mathbf{k}_a = 2.67 \bar{S}_{ut}^{-0.265} \text{LN}(1, 0.058) = 2.67(87.6)^{-0.265} \text{LN}(1, 0.058)$$

$$= 0.816 \text{LN}(1, 0.058)$$

$$k_b = 1 \quad (\text{axial loading})$$

| **Figure 6-37**



From Eq. (6–73),

$$\begin{aligned}\mathbf{k}_c &= 1.23 \bar{S}_{ut}^{-0.0778} \mathbf{LN}(1, 0.125) = 1.23(87.6)^{-0.0778} \mathbf{LN}(1, 0.125) \\ &= 0.869 \mathbf{LN}(1, 0.125) \\ \mathbf{k}_d &= \mathbf{k}_f = (1, 0)\end{aligned}$$

The endurance strength, from Eq. (6–71), is

$$\begin{aligned}\mathbf{S}_e &= \mathbf{k}_a \mathbf{k}_b \mathbf{k}_c \mathbf{k}_d \mathbf{k}_f \mathbf{S}'_e \\ \mathbf{S}_e &= 0.816 \mathbf{LN}(1, 0.058)(1) 0.869 \mathbf{LN}(1, 0.125)(1)(1) 44.3 \mathbf{LN}(1, 0.138)\end{aligned}$$

The parameters of \mathbf{S}_e are

$$\begin{aligned}\bar{S}_e &= 0.816(0.869)44.3 = 31.4 \text{ kpsi} \\ C_{Se} &= (0.058^2 + 0.125^2 + 0.138^2)^{1/2} = 0.195\end{aligned}$$

so $\mathbf{S}_e = 31.4 \mathbf{LN}(1, 0.195)$ kpsi.

In computing the stress, the section at the hole governs. Using the terminology of Table A–15–1 we find $d/w = 0.50$, therefore $K_t \doteq 2.18$. From Table 6–15, $\sqrt{a} = 5/S_{ut} = 5/87.6 = 0.0571$ and $C_{kf} = 0.10$. From Eqs. (6–78) and (6–79) with $r = 0.375$ in,

$$\begin{aligned}\mathbf{K}_f &= \frac{K_t}{1 + \frac{2(K_t - 1)}{K_t} \frac{\sqrt{a}}{\sqrt{r}}} \mathbf{LN}(1, C_{K_f}) = \frac{2.18}{1 + \frac{2(2.18 - 1)}{2.18} \frac{0.0571}{\sqrt{0.375}}} \mathbf{LN}(1, 0.10) \\ &= 1.98 \mathbf{LN}(1, 0.10)\end{aligned}$$

The stress at the hole is

$$\begin{aligned}\boldsymbol{\sigma} &= \mathbf{K}_f \frac{\mathbf{F}}{A} = 1.98 \mathbf{LN}(1, 0.10) \frac{1000 \mathbf{LN}(1, 0.12)}{0.25(0.75)} \\ \bar{\sigma} &= 1.98 \frac{1000}{0.25(0.75)} 10^{-3} = 10.56 \text{ kpsi} \\ C_\sigma &= (0.10^2 + 0.12^2)^{1/2} = 0.156\end{aligned}$$

so stress can be expressed as $\boldsymbol{\sigma} = 10.56 \mathbf{LN}(1, 0.156)$ kpsi.³⁴

The endurance limit is considerably greater than the load-induced stress, indicating that finite life is not a problem. For interfering lognormal-lognormal distributions, Eq. (5–43), p. 250, gives

$$z = -\frac{\ln \left(\frac{\bar{S}_e}{\bar{\sigma}} \sqrt{\frac{1+C_\sigma^2}{1+C_{Se}^2}} \right)}{\sqrt{\ln[(1+C_{Se}^2)(1+C_\sigma^2)]}} = -\frac{\ln \left(\frac{31.4}{10.56} \sqrt{\frac{1+0.156^2}{1+0.195^2}} \right)}{\sqrt{\ln[(1+0.195^2)(1+0.156^2)]}} = -4.37$$

From Table A–10 the probability of failure $p_f = \Phi(-4.37) = .000\ 006\ 35$, and the reliability is

Answer

$$R = 1 - 0.000\ 006\ 35 = 0.999\ 993\ 65$$

³⁴Note that there is a simplification here. The area is *not* a deterministic quantity. It will have a statistical distribution also. However no information was given here, and so it was treated as being deterministic.

(b) The rotary endurance tests are described by $S'_e = 40\text{LN}(1, 0.05)$ kpsi whose mean is less than the predicted mean in part *a*. The mean endurance strength \bar{S}_e is

$$\bar{S}_e = 0.816(0.869)40 = 28.4 \text{ kpsi}$$

$$C_{Se} = (0.058^2 + 0.125^2 + 0.05^2)^{1/2} = 0.147$$

so the endurance strength can be expressed as $S_e = 28.3\text{LN}(1, 0.147)$ kpsi. From Eq. (5–43),

$$z = -\frac{\ln\left(\frac{28.4}{10.56}\sqrt{\frac{1+0.156^2}{1+0.147^2}}\right)}{\sqrt{\ln[(1+0.147^2)(1+0.156^2)]}} = -4.65$$

Using Table A–10, we see the probability of failure $p_f = \Phi(-4.65) = 0.000\ 001\ 71$, and

$$R = 1 - 0.000\ 001\ 71 = 0.999\ 998\ 29$$

an increase! The reduction in the probability of failure is $(0.000\ 001\ 71 - 0.000\ 006\ 35)/0.000\ 006\ 35 = -0.73$, a reduction of 73 percent. We are analyzing an existing design, so in part (*a*) the factor of safety was $\bar{n} = \bar{S}/\bar{\sigma} = 31.4/10.56 = 2.97$. In part (*b*) $\bar{n} = 28.4/10.56 = 2.69$, a *decrease*. This example gives you the opportunity to see the role of the design factor. Given knowledge of \bar{S} , C_S , $\bar{\sigma}$, C_σ , and reliability (through z), the mean factor of safety (as a design factor) separates \bar{S} and $\bar{\sigma}$ so that the reliability goal is achieved. Knowing \bar{n} alone *says nothing about the probability of failure*. Looking at $\bar{n} = 2.97$ and $\bar{n} = 2.69$ says nothing about the respective probabilities of failure. The tests did not reduce \bar{S}_e significantly, but reduced the variation C_S such that the reliability was *increased*.

When a mean design factor (or mean factor of safety) defined as $\bar{S}_e/\bar{\sigma}$ is said to be *silent* on matters of frequency of failures, it means that a scalar factor of safety by itself does not offer any information about probability of failure. Nevertheless, some engineers let the factor of safety speak up, and they can be wrong in their conclusions.

As revealing as Ex. 6–19 is concerning the meaning (and lack of meaning) of a design factor or factor of safety, let us remember that the rotary testing associated with part (*b*) changed *nothing* about the part, but only our knowledge about the part. The mean endurance limit was 40 kpsi all the time, and our adequacy assessment had to move with what was known.

Fluctuating Stresses

Deterministic failure curves that lie among the data are candidates for regression models. Included among these are the Gerber and ASME-elliptic for ductile materials, and, for brittle materials, Smith-Dolan models, which use mean values in their presentation. Just as the deterministic failure curves are located by endurance strength and ultimate tensile (or yield) strength, so too are stochastic failure curves located by S_e and by S_{ut} or S_y . Figure 6–32, p. 320, shows a parabolic Gerber mean curve. We also need to establish a contour located one standard deviation from the mean. Since stochastic

curves are most likely to be used with a radial load line we will use the equation given in Table 6–7, p. 307, expressed in terms of the strength means as

$$\bar{S}_a = \frac{r^2 \bar{S}_{ut}^2}{2\bar{S}_e} \left[-1 + \sqrt{1 + \left(\frac{2\bar{S}_e}{r\bar{S}_{ut}} \right)^2} \right] \quad (6-80)$$

Because of the positive correlation between S_e and S_{ut} , we increment \bar{S}_e by $C_{Se}\bar{S}_e$, \bar{S}_{ut} by $C_{Sut}\bar{S}_{ut}$, and \bar{S}_a by $C_{Sa}\bar{S}_a$, substitute into Eq. (6–80), and solve for C_{Sa} to obtain

$$C_{Sa} = \frac{(1 + C_{Sut})^2}{1 + C_{Se}} \frac{\left\{ -1 + \sqrt{1 + \left[\frac{2\bar{S}_e(1 + C_{Se})}{r\bar{S}_{ut}(1 + C_{Sut})} \right]^2} \right\}}{\left[-1 + \sqrt{1 + \left(\frac{2\bar{S}_e}{r\bar{S}_{ut}} \right)^2} \right]} - 1 \quad (6-81)$$

Equation (6–81) can be viewed as an interpolation formula for C_{Sa} , which falls between C_{Se} and C_{Sut} depending on load line slope r . Note that $S_a = \bar{S}_a \text{LN}(1, C_{Sa})$.

Similarly, the ASME-elliptic criterion of Table 6–8, p. 308, expressed in terms of its means is

$$\bar{S}_a = \frac{r\bar{S}_y\bar{S}_e}{\sqrt{r^2\bar{S}_y^2 + \bar{S}_e^2}} \quad (6-82)$$

Similarly, we increment \bar{S}_e by $C_{Se}\bar{S}_e$, \bar{S}_y by $C_{Sy}\bar{S}_y$, and \bar{S}_a by $C_{Sa}\bar{S}_a$, substitute into Eq. (6–82), and solve for C_{Sa} :

$$C_{Sa} = (1 + C_{Sy})(1 + C_{Se}) \sqrt{\frac{r^2\bar{S}_y^2 + \bar{S}_e^2}{r^2\bar{S}_y^2(1 + C_{Sy})^2 + \bar{S}_e^2(1 + C_{Se})^2}} - 1 \quad (6-83)$$

Many *brittle* materials follow a Smith-Dolan failure criterion, written deterministically as

$$\frac{n\sigma_a}{S_e} = \frac{1 - n\sigma_m/S_{ut}}{1 + n\sigma_m/S_{ut}} \quad (6-84)$$

Expressed in terms of its means,

$$\frac{\bar{S}_a}{\bar{S}_e} = \frac{1 - \bar{S}_m/\bar{S}_{ut}}{1 + \bar{S}_m/\bar{S}_{ut}} \quad (6-85)$$

For a radial load line slope of r , we substitute \bar{S}_a/r for \bar{S}_m and solve for \bar{S}_a , obtaining

$$\bar{S}_a = \frac{r\bar{S}_{ut} + \bar{S}_e}{2} \left[-1 + \sqrt{1 + \frac{4r\bar{S}_{ut}\bar{S}_e}{(r\bar{S}_{ut} + \bar{S}_e)^2}} \right] \quad (6-86)$$

and the expression for C_{Sa} is

$$C_{Sa} = \frac{r\bar{S}_{ut}(1 + C_{Sut}) + \bar{S}_e(1 + C_{Se})}{2\bar{S}_a} \cdot \left\{ -1 + \sqrt{1 + \frac{4r\bar{S}_{ut}\bar{S}_e(1 + C_{Se})(1 + C_{Sut})}{[r\bar{S}_{ut}(1 + C_{Sut}) + \bar{S}_e(1 + C_{Se})]^2}} \right\} - 1 \quad (6-87)$$

EXAMPLE 6-20

A rotating shaft experiences a steady torque $\mathbf{T} = 1360\mathbf{LN}(1, 0.05)$ lbf · in, and at a shoulder with a 1.1-in small diameter, a fatigue stress-concentration factor $\mathbf{K}_f = 1.50\mathbf{LN}(1, 0.11)$, $\mathbf{K}_{fs} = 1.28\mathbf{LN}(1, 0.11)$, and at that location a bending moment of $\mathbf{M} = 1260\mathbf{LN}(1, 0.05)$ lbf · in. The material of which the shaft is machined is hot-rolled 1035 with $\mathbf{S}_{ut} = 86.2\mathbf{LN}(1, 0.045)$ kpsi and $\mathbf{S}_y = 56.0\mathbf{LN}(1, 0.077)$ kpsi. Estimate the reliability using a stochastic Gerber failure zone.

Solution

Establish the endurance strength. From Eqs. (6-70) to (6-72) and Eq. (6-20), p. 288,

$$\mathbf{S}'_e = 0.506(86.2)\mathbf{LN}(1, 0.138) = 43.6\mathbf{LN}(1, 0.138) \text{ kpsi}$$

$$\mathbf{k}_a = 2.67(86.2)^{-0.265}\mathbf{LN}(1, 0.058) = 0.820\mathbf{LN}(1, 0.058)$$

$$k_b = (1.1/0.30)^{-0.107} = 0.870$$

$$\mathbf{k}_c = \mathbf{k}_d = \mathbf{k}_f = \mathbf{LN}(1, 0)$$

$$\mathbf{S}_e = 0.820\mathbf{LN}(1, 0.058)0.870(43.6)\mathbf{LN}(1, 0.138)$$

$$\bar{\mathbf{S}}_e = 0.820(0.870)43.6 = 31.1 \text{ kpsi}$$

$$C_{Se} = (0.058^2 + 0.138^2)^{1/2} = 0.150$$

and so $\mathbf{S}_e = 31.1\mathbf{LN}(1, 0.150)$ kpsi.

Stress (in kpsi):

$$\sigma_a = \frac{32\mathbf{K}_f\mathbf{M}_a}{\pi d^3} = \frac{32(1.50)\mathbf{LN}(1, 0.11)1.26\mathbf{LN}(1, 0.05)}{\pi(1.1)^3}$$

$$\bar{\sigma}_a = \frac{32(1.50)1.26}{\pi(1.1)^3} = 14.5 \text{ kpsi}$$

$$C_{\sigma a} = (0.11^2 + 0.05^2)^{1/2} = 0.121$$

$$\tau_m = \frac{16\mathbf{K}_{fs}\mathbf{T}_m}{\pi d^3} = \frac{16(1.28)\mathbf{LN}(1, 0.11)1.36\mathbf{LN}(1, 0.05)}{\pi(1.1)^3}$$

$$\bar{\tau}_m = \frac{16(1.28)1.36}{\pi(1.1)^3} = 6.66 \text{ kpsi}$$

$$C_{\tau m} = (0.11^2 + 0.05^2)^{1/2} = 0.121$$

$$\bar{\sigma}'_a = (\bar{\sigma}_a^2 + 3\bar{\tau}_m^2)^{1/2} = [14.5^2 + 3(0)^2]^{1/2} = 14.5 \text{ kpsi}$$

$$\bar{\sigma}'_m = (\bar{\sigma}_m^2 + 3\bar{\tau}_m^2)^{1/2} = [0 + 3(6.66)^2]^{1/2} = 11.54 \text{ kpsi}$$

$$r = \frac{\bar{\sigma}'_a}{\bar{\sigma}'_m} = \frac{14.5}{11.54} = 1.26$$

Strength: From Eqs. (6-80) and (6-81),

$$\bar{\mathbf{S}}_a = \frac{1.26^2 86.2^2}{2(31.1)} \left\{ -1 + \sqrt{1 + \left[\frac{2(31.1)}{1.26(86.2)} \right]^2} \right\} = 28.9 \text{ kpsi}$$

$$C_{Sa} = \frac{(1 + 0.045)^2}{1 + 0.150} \frac{-1 + \sqrt{1 + \left[\frac{2(31.1)(1 + 0.15)}{1.26(86.2)(1 + 0.045)} \right]^2}}{-1 + \sqrt{1 + \left[\frac{2(31.1)}{1.26(86.2)} \right]^2}} - 1 = 0.134$$

Reliability: Since $S_a = 28.9\text{LN}(1, 0.134)$ kpsi and $\sigma'_a = 14.5\text{LN}(1, 0.121)$ kpsi, Eq. (5–43), p. 250, gives

$$z = -\frac{\ln \left(\frac{\bar{S}_a}{\bar{\sigma}_a} \sqrt{\frac{1 + C_{\sigma_a}^2}{1 + C_{S_a}^2}} \right)}{\sqrt{\ln[(1 + C_{S_a}^2)(1 + C_{\sigma_a}^2)]}} = -\frac{\ln \left(\frac{28.9}{14.5} \sqrt{\frac{1 + 0.121^2}{1 + 0.134^2}} \right)}{\sqrt{\ln[(1 + 0.134^2)(1 + 0.121^2)]}} = -3.83$$

From Table A–10 the probability of failure is $p_f = 0.000\ 065$, and the reliability is, against fatigue,

Answer

$$R = 1 - p_f = 1 - 0.000\ 065 = 0.999\ 935$$

The chance of first-cycle yielding is estimated by interfering S_y with σ'_{\max} . The quantity σ'_{\max} is formed from $\sigma'_a + \sigma'_m$. The mean of σ'_{\max} is $\bar{\sigma}'_a + \bar{\sigma}'_m = 14.5 + 11.54 = 26.04$ kpsi. The coefficient of variation of the sum is 0.121, since both COVs are 0.121, thus $C_{\sigma_{\max}} = 0.121$. We interfere $S_y = 56\text{LN}(1, 0.077)$ kpsi with $\sigma'_{\max} = 26.04\text{LN}(1, 0.121)$ kpsi. The corresponding z variable is

$$z = -\frac{\ln \left(\frac{56}{26.04} \sqrt{\frac{1 + 0.121^2}{1 + 0.077^2}} \right)}{\sqrt{\ln[(1 + 0.077^2)(1 + 0.121^2)]}} = -5.39$$

which represents, from Table A–10, a probability of failure of approximately $0.0^{7}358$ [which represents $3.58(10^{-8})$] of first-cycle yield in the fillet.

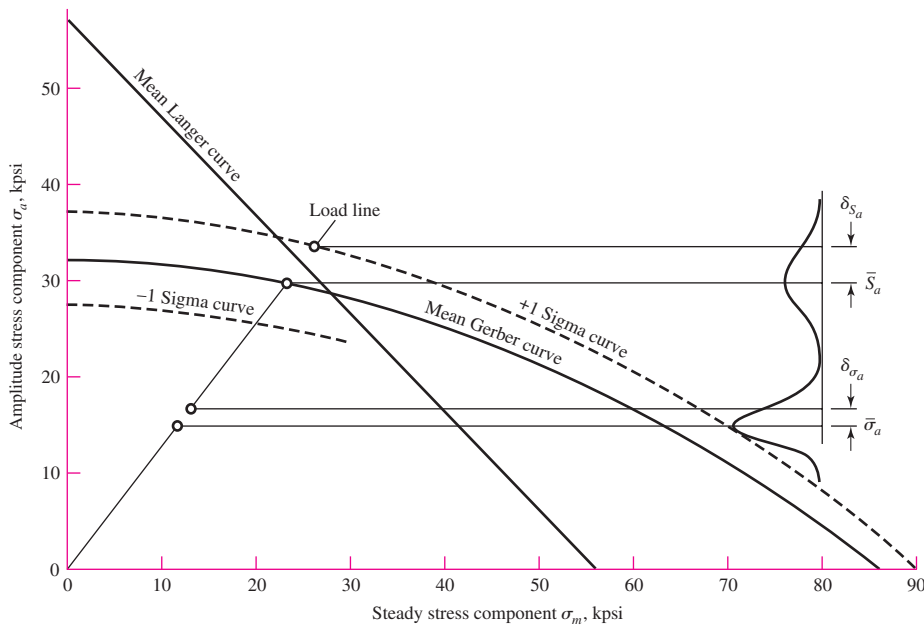
The probability of observing a fatigue failure exceeds the probability of a yield failure, something a deterministic analysis does not foresee and in fact could lead one to expect a yield failure should a failure occur. Look at the $\sigma'_a S_a$ interference and the $\sigma'_{\max} S_y$ interference and examine the z expressions. These control the relative probabilities. A deterministic analysis is oblivious to this and can mislead. Check your statistics text for events that are not mutually exclusive, but are independent, to quantify the probability of failure:

$$\begin{aligned} p_f &= p(\text{yield}) + p(\text{fatigue}) - p(\text{yield and fatigue}) \\ &= p(\text{yield}) + p(\text{fatigue}) - p(\text{yield})p(\text{fatigue}) \\ &= 0.358(10^{-7}) + 0.65(10^{-4}) - 0.358(10^{-7})0.65(10^{-4}) = 0.650(10^{-4}) \\ R &= 1 - 0.650(10^{-4}) = 0.999\ 935 \end{aligned}$$

against either or both modes of failure.

Figure 6-38

Designer's fatigue diagram for Ex. 6-20.



Examine Fig. 6-38, which depicts the results of Ex. 6-20. The problem distribution of \mathbf{S}_e was compounded of historical experience with \mathbf{S}'_e and the uncertainty manifestations due to features requiring Marin considerations. The Gerber "failure zone" displays this. The interference with load-induced stress predicts the risk of failure. If additional information is known (R. R. Moore testing, with or without Marin features), the stochastic Gerber can accommodate to the information. Usually, the accommodation to additional test information is movement and contraction of the failure zone. In its own way the stochastic failure model accomplishes more precisely what the deterministic models and conservative postures intend. Additionally, stochastic models can estimate the probability of failure, something a deterministic approach cannot address.

The Design Factor in Fatigue

The designer, in envisioning how to execute the geometry of a part subject to the imposed constraints, can begin making a priori decisions without realizing the impact on the design task. Now is the time to note how these things are related to the reliability goal.

The mean value of the design factor is given by Eq. (5-45), repeated here as

$$\bar{n} = \exp \left[-z \sqrt{\ln(1 + C_n^2)} + \ln \sqrt{1 + C_n^2} \right] \doteq \exp[C_n(-z + C_n/2)] \quad (6-88)$$

in which, from Table 20-6 for the quotient $\mathbf{n} = \mathbf{S}/\sigma$,

$$C_n = \sqrt{\frac{C_S^2 + C_\sigma^2}{1 + C_\sigma^2}}$$

where C_S is the COV of the significant strength and C_σ is the COV of the significant stress at the critical location. Note that \bar{n} is a function of the reliability goal (through z) and the COVs of the strength and stress. There are no means present, just measures of variability. The nature of C_S in a fatigue situation may be C_{Se} for fully reversed loading, or C_{Sa} otherwise. Also, experience shows $C_{Se} > C_{Sa} > C_{Sut}$, so C_{Se} can be used as a conservative estimate of C_{Sa} . If the loading is bending or axial, the form of

σ'_a might be

$$\sigma'_a = K_f \frac{M_{ac}}{I} \quad \text{or} \quad \sigma'_a = K_f \frac{\bar{F}}{A}$$

respectively. This makes the COV of σ'_a , namely $C_{\sigma'_a}$, expressible as

$$C_{\sigma'_a} = (C_{Kf}^2 + C_F^2)^{1/2}$$

again a function of variabilities. The COV of S_e , namely C_{Se} , is

$$C_{Se} = (C_{ka}^2 + C_{kc}^2 + C_{kd}^2 + C_{kf}^2 + C_{Se'}^2)^{1/2}$$

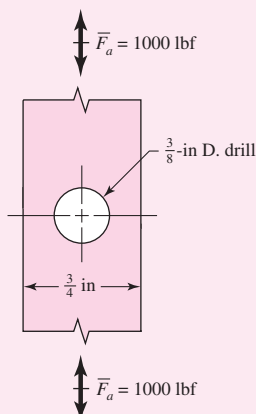
again, a function of variabilities. An example will be useful.

EXAMPLE 6-21

A strap to be made from a cold-drawn steel strip workpiece is to carry a fully reversed axial load $\bar{F} = \text{LN}(1000, 120)$ lbf as shown in Fig. 6-39. Consideration of adjacent parts established the geometry as shown in the figure, except for the thickness t . Make a decision as to the magnitude of the design factor if the reliability goal is to be 0.999 95, then make a decision as to the workpiece thickness t .

Solution

Let us take each a priori decision and note the consequence:



A Priori Decision	Consequence
Use 1018 CD steel	$\bar{S}_{ut} = 87.6 \text{ kpsi}$, $C_{Sut} = 0.0655$
Function:	
Carry axial load	$C_F = 0.12$, $C_{kc} = 0.125$
$R \geq 0.999\ 95$	$z = -3.891$
Machined surfaces	$C_{ka} = 0.058$
Hole critical	$C_{Kf} = 0.10$, $C_{\sigma'_a} = (0.10^2 + 0.12^2)^{1/2} = 0.156$
Ambient temperature	$C_{kd} = 0$
Correlation method	$C_{Se'} = 0.138$
Hole drilled	$C_{Se} = (0.058^2 + 0.125^2 + 0.138^2)^{1/2} = 0.195$
$C_n = \sqrt{\frac{C_{Se}^2 + C_{\sigma'_a}^2}{1 + C_{\sigma'_a}^2}} = \sqrt{\frac{0.195^2 + 0.156^2}{1 + 0.156^2}} = 0.2467$	
$\bar{n} = \exp \left[-(-3.891) \sqrt{\ln(1 + 0.2467^2)} + \ln \sqrt{1 + 0.2467^2} \right] = 2.65$	

Figure 6-39

A strap with a thickness t is subjected to a fully reversed axial load of 1000 lbf.

Example 6-21 considers the thickness necessary to attain a reliability of 0.999 95 against a fatigue failure.

These eight a priori decisions have quantified the mean design factor as $\bar{n} = 2.65$. Proceeding deterministically hereafter we write

$$\sigma'_a = \frac{\bar{S}_e}{\bar{n}} = \bar{K}_f \frac{\bar{F}}{(w - d)t}$$

from which

$$t = \frac{\bar{K}_f \bar{n} \bar{F}}{(w - d) \bar{S}_e} \quad (1)$$

To evaluate the preceding equation we need \bar{S}_e and \bar{K}_f . The Marin factors are

$$\mathbf{k}_a = 2.67 \bar{S}_{ut}^{-0.265} \text{LN}(1, 0.058) = 2.67(87.6)^{-0.265} \text{LN}(1, 0.058)$$

$$\bar{k}_a = 0.816$$

$$k_b = 1$$

$$\mathbf{k}_c = 1.23 \bar{S}_{ut}^{-0.078} \text{LN}(1, 0.125) = 0.868 \text{LN}(1, 0.125)$$

$$\bar{k}_c = 0.868$$

$$\bar{k}_d = \bar{k}_f = 1$$

and the endurance strength is

$$\bar{S}_e = 0.816(1)(0.868)(1)(1)0.506(87.6) = 31.4 \text{ kpsi}$$

The hole governs. From Table A-15-1 we find $d/w = 0.50$, therefore $K_t = 2.18$. From Table 6-15 $\sqrt{a} = 5/\bar{S}_{ut} = 5/87.6 = 0.0571$, $r = 0.1875$ in. From Eq. (6-78) the fatigue stress-concentration factor is

$$\bar{K}_f = \frac{2.18}{1 + \frac{2(2.18 - 1)}{2.18} \frac{0.0571}{\sqrt{0.1875}}} = 1.91$$

The thickness t can now be determined from Eq. (1)

$$t \geq \frac{\bar{K}_f \bar{n} \bar{F}}{(w - d) S_e} = \frac{1.91(2.65)1000}{(0.75 - 0.375)31400} = 0.430 \text{ in}$$

Use $\frac{1}{2}$ -in-thick strap for the workpiece. The $\frac{1}{2}$ -in thickness attains and, in the rounding to available nominal size, exceeds the reliability goal.

The example demonstrates that, for a given reliability goal, the fatigue design factor that facilitates its attainment is decided by the variabilities of the situation. Furthermore, the necessary design factor is not a constant independent of the way the concept unfolds. Rather, it is a function of a number of seemingly unrelated a priori decisions that are made in giving definition to the concept. The involvement of stochastic methodology can be limited to defining the necessary design factor. In particular, in the example, the design factor is not a function of the design variable t ; rather, t follows from the design factor.

6-18 Road Maps and Important Design Equations for the Stress-Life Method

As stated in Sec. 6-15, there are three categories of fatigue problems. The important procedures and equations for deterministic stress-life problems are presented here.

Completely Reversing Simple Loading

- 1 Determine S'_e either from test data or

p. 282

$$S'_e = \begin{cases} 0.5 S_{ut} & S_{ut} \leq 200 \text{ kpsi (1400 MPa)} \\ 100 \text{ kpsi} & S_{ut} > 200 \text{ kpsi} \\ 700 \text{ MPa} & S_{ut} > 1400 \text{ MPa} \end{cases} \quad (6-8)$$